



**PHYTOMEDICINAL STUDIES ON
THE AMAZONIAN TRADITIONAL
MEDICINE "CHUCHUGUASA"
(*Maytenus laevis* Reissek)**

Thesis submitted by

HAZAR ABDUL RAZZAQ MOUAD

For the degree of Doctor of Philosophy

2016

Natural Products Research Laboratories
Strathclyde Institute of Pharmacy and Biomedical Sciences
University of Strathclyde
27 Taylor Street
Glasgow G4 0NR
UK

Copyright

‘This thesis is the result of author's original research. It has been composed by the author and has not been previously submitted for examination which has led to the award of a degree.’

‘The copy of this thesis belongs to the author under the terms of the United Kingdom Copyright Acts as qualified by University of Strathclyde Regulation 3.50.

Due acknowledgement must always be made of the use of any material contained in, or derived from this thesis.’

Signed:

Date:

By the name of Allah

Dedicated to Syria and my family

Acknowledgments

I acknowledge with deep gratitude the expert supervision, the tremendous tolerance and the guidance I received from my supervisor *Prof. Alexander Gray* throughout the course of this study. His father-like affection encouraged me to carry on with my work despite all the complications and challenges I have as a Syrian student in the UK during the fierce war and the horrific circumstances that my country is suffering from. I also offer my special thanks to my second supervisor *Dr. Valerie Ferro* who introduced me to the biological world which was totally a new discipline for me. Her kind supervision and guidance were invaluable attributes to my overall PhD experience.

I am grateful to *Dr. Ann Simpson* (and again to my supervisor *Prof. Alexander Gray*) for providing the plant material with the help and full permission of the Amazonian sabedores of Caquetá Medio in Colombia *Eusebio Mendoza* (Uitoto ethnia) and *Noé Rodríguez Jujuborre* (Muinane ethnia). I also would like to thank the anthropologist *Blanca de Corredor*, *Simon Román Enokayai* and his father *Oscar Román Enokayai* for sharing their ethnobotanical knowledge of the plant.

I would like to express my sincere thanks to *Dr. John Igoli* for his kind support, knowledge and care he offered during my work in the lab. I also thank *Mrs. Carol Clements* for carrying out the anti-trpanosomal assays.

I am grateful to *Mr. Craig Irving* for helping me out with NMR experiments. I am also obliged to *Ms. Patricia Keating* and *Dr. Tong Zhang* (Alex) for their assistance in MS experiments, and *Mr. Gavin Bain* for his help in Optical Rotation measurements. Great thanks to *Dr. Amit Delori* for carrying out the X-Ray crystallography of one of the novel compounds isolated in this study. I also thank *Dr. Ibrahim Khadra* and *Dr. Ticiano Gomes do Nascimento* for their help in the Semi-prep HPLC separation technique.

I will never forget my colleagues for their support, humorous moments and useful time sharing information and experiences.

I extend my heartfelt gratitude to my family for their prayerful concern and thoughtfulness all these years I have been away from home. My special thank to my dear *Adnan*, who has been to me a true dependable husband, friend and companion during my most difficult moments, and to my beloved son *Faris* who brings the joy to my life.

Finally, I am more than grateful for the award of a scholarship by Damascus University, Syria, without which this study would not have been possible.

Abstract

The importance of natural products and medicinal plants has continued to grow due to their significant role in the search for new drugs or precursors of potent drugs with minimal side effects for the treatment of numerous illnesses. The Amazonian Rainforest represents the most extensive resource of natural diversity remaining on the planet. The unsurpassed knowledge, culture and medicinal practices, created by its indigenous people over thousands of years, have formed rich foundations for ethnobotanical studies about traditional medicinal plants which might be potential sources of biologically active phytochemicals. Regrettably, this may not be so for very much longer, due to the rate of deforestation and the effects of westernisation on these native societies.

From the Amazonian basin, Resguardo Monochoa area of Caquetá-Medio in Colombia, a plant locally named "Chuchuguasa" was collected (root and stem bark) by well known Amazonian sabedores from the indigenous Uitoto and Muinane communities who identified the tree as a *Maytenus laevis* Reissek (Celastraceae). Following a strict collecting methodology, the plant material (the roots in particular) was chosen from the side of the tree that receives the first rays of sun at 5 am. This plant is used in traditional medicine for several purposes mainly in the form of an alcoholic extract (aguardiente).

A considerable amount of phytochemical investigation had already been performed on the *Maytenus* species associated with Chuchuguasa (mainly the stem bark), however, there is little information so far about the chemistry of *M. laevis*, particularly that involving the root bark. This project aimed to carry out further phytochemical work on the root and stem barks of *M. laevis* in an attempt to isolate constituents, which may possess biological activities that could be exploited.

Twenty compounds were isolated from solvent extracts of the two plant materials of *M. laevis*, in addition to a polymer which was characterised as *trans*-1, 4-polyisoprene (Gutta-percha). Six compounds were identified as novel and were given the names 22(β)-hydroxycelastrol, 22(α)-hydroxynetzahualcoyene, 2,22-dihydroxy-

3-methoxy-15, 12-dioxo-5, 8-oxa-24, 30-dinor-5, 6-seco-friedelan-1,3,5(10)-trien-6-al (trivial name jujuborreal^{*}), methyl 2, 3, 22 α -trihydroxy-24, 25-dinorfriedelan-1,3,5(10),6,8,14-hexaen-29-oate, 15(β)-acetoxymfriedelane-1,3-dione, and (4R, 4aR, 6aR, 7aS, 8aR, 12aR, 12bS, 14aR, 14bS)- 4, 4a, 8a, 11, 11, 12b, 14a-heptamethyl-7-methyleneoctadecahydrobenzo[a]naphtho[2,1-f]azulene-1, 3(2H,14bH)-dione (trivial name 1,3-dioxocorredor-14,26-ene^{**}).

The remaining fourteen compounds were not novel and composed of nine triterpenoids of friedelane, norfriedelane and aromatic-types including canophyllol, friedelane-1,3-dione, 28-hydroxyfriedelane-1,3-dione, netzahualcoyondiol, netzahualcoyone, pristimerin, celastrol, salaquinone A, regeol A, two steroids (stigmast-4-en-3-one and β -sitosterol), two simple phenolics (*p*-hydroxybenzaldehyde and 3,4-dihydroxybenzoic acid) and one isocoumarin (\pm mellein). Nevertheless, 8 of them are reported for the first time from *M. laevis* and from those other related species that are often referred to as Chuchuguasa.

The structures of the new and known compounds were all elucidated by spectroscopic methods. The novel compound, 1,3-dioxocorredor-14,26-ene, was identified with the aid of X-ray crystallography and was shown to be the first of a new skeletal class of triterpenes for which the name corredorane^{**} is suggested.

A preliminary *in vitro* cytotoxicity assessment of the crude extracts and most of the isolated compounds was carried out against the cancer cell line A375 (human, malignant melanoma cell line) and the normal cell line Hs27 (human, skin fibroblast cell line) using a resazurin assay. The n-hexane and ethyl acetate extracts of both parts of the plant showed selective activity on the cancer cells, but those of the root barks were the most potent with an EC₅₀ of 2.9 μ g/ml. This effect was linked in part to the extracts' contents of triterpenoids of quinonemethides and nor-friedelanes types. The compounds under the aforementioned classifications were major components of the root bark extracts, but minor in those of the stem bark; hence, this reflected the potency of the effects exerted by these extracts.

* These are named in memory of sabedor Noé Rodríguez Jujuborre (died in 2015) and ** the anthropologist Blanca de Corredor (died in 2011).

All the isolated quinonemethides displayed high toxicity to both cell lines, however, netzahualcoyondiol, celastrol, and the new compound 22(β)-hydroxycelastrol exerted selective toxicity to the cancer cells at the lowest tested concentration (3.125 $\mu\text{g/ml}$) with EC_{50} values of 3.5, 5.1 and 4.4 μM , respectively. The two nor-friedelanes (salaquinone A and jujuborreal), along with the new aromatic triterpene [methyl 2, 3, 22 α -trihydroxy-24,25-dinorfriedelan-1,3,5(10),6,8,14-hexaen-29-oate] also showed selective toxicity to the cancer cells, with salaquinone A being the most potent (EC_{50} 1.4 μM). All the friedelane triterpenoids, isolated mainly from the stem bark, were either not active or weakly active with $\text{EC}_{50} > 100 \mu\text{g/ml}$. These findings provide some scientific support for the traditional use of the plant (root bark) as an anti-tumour therapy in skin cancer and appear to confirm some of the knowledge shared by the Amazonian sabedores.

The crude extracts and some of the isolated compounds were also screened *in vitro* for anti-trypanosomal activity against *Trypanosoma brucei brucei* (S427) blood stream forms using an Alamar BlueTM microplate assay. Suramin and dimethylsulfoxide (DMSO) were used as positive and solvent controls, respectively. Preliminary screening of the crude extracts showed very potent activity at a concentration of 20 $\mu\text{g/ml}$, with the exception of the methanol extracts. All the screened quinonemethides, salaquinone A, regeol A and protocatechuic acid (PA) displayed high activity at 20 μM with cell viability values less than 10% of the control value. These compounds were then tested at a lower concentration of 5 μM and they all maintained their efficacies except regeol A and PA. These findings, although preliminary, propose a new potential therapeutic use of *M. laevis* (the root and stem barks), which could lead to the discovery of potent agents for the treatment of related parasitic diseases that are considered endemic in its habitat, such as Chagas disease (*Trypanosoma cruzi* Chagas).

Table of Contents

<i>List of Figures</i>	<i>VI</i>
<i>List of Table</i>	<i>XIV</i>
<i>List of Schemes</i>	<i>XVI</i>
<i>List of abbreviations</i>	<i>XVII</i>
1. Introduction	1
1.1 The importance of medicinal plants; A glance from a historical view.....	1
1.2 Traditional medicine in Amazonia	2
1.3 The family Celastraceae R. Brown.....	4
1.4 The genus <i>Maytenus</i>	5
1.5 Chuchuguasa	6
1.5.1 General morphological description of Chuchuguasa	6
1.5.2 Traditional uses of Chuchuguasa	7
1.5.3 Previous phytochemical studies on Chuchuguasa	8
1.5.4 Previous pharmacological reports on Chuchuguasa	36
1.5.4.1 <i>M. laevis</i>	36
1.5.4.2 <i>M. chuchuhuasca</i>	38
1.5.4.3 <i>M. krukovii</i>	38
1.5.4.4 <i>M. macrocarpa</i>	39
1.6 Aims and objectives	41
2. Materials and Methods	43
2.1 Materials	43
2.1.1 Solvents	43
2.1.2 Reagents and chemicals	43
2.1.3 Equipment	44
2.1.4 Plant material	45

2.2	Methods	47
2.2.1	Extraction of Plant Material	47
2.2.2	Analytical and Chromatographic techniques	47
2.2.2.1	<i>Thin Layer Chromatography</i>	47
2.2.2.2	<i>Vacuum Liquid Chromatography</i>	48
2.2.2.3	<i>Column Chromatography</i>	49
2.2.2.4	<i>Size-Exclusion Chromatography</i>	49
2.2.2.5	<i>Preparative thin layer chromatography</i>	49
2.2.2.6	<i>Semi-Preparative High-Performance Liquid Chromatography</i> ...	50
2.2.2.7	<i>Flash chromatography</i>	50
2.2.3	Structure Elucidation.....	51
2.2.3.1	<i>Nuclear Magnetic Resonance</i>	51
2.2.3.1.1	<i>One-Dimensional NMR experiments</i>	52
2.2.3.1.2	<i>Two-Dimensional NMR experiments</i>	53
2.2.3.2	<i>Mass Spectroscopy</i>	53
2.2.3.3	<i>X-Ray crystallography</i>	54
2.2.3.4	<i>Optical Rotation</i>	55
2.2.3.5	<i>Infrared spectroscopy</i>	55
2.2.4	Bioassays.....	56
2.2.4.1	<i>Tissue Culture and Cytotoxicity Assessment</i>	56
2.2.4.1.1	<i>Preparation of Complete Medium</i>	56
2.2.4.1.2	<i>Maintenance of cell lines</i>	56
2.2.4.1.3	<i>Passaging adherent cells</i>	56
2.2.4.1.4	<i>Cell storage</i>	57
2.2.4.1.5	<i>Plant sample preparation</i>	57
2.2.4.1.6	<i>Resazurin solution preparation</i>	57

2.2.4.1.7	<i>Resazurin cytotoxicity assay</i>	57
2.2.4.1.8	<i>Statistical analysis</i>	59
2.2.4.2	<i>Anti-tyrpanosomal assay</i>	59
2.2.4.2.1	<i>Sample preparation</i>	59
2.2.4.2.2	<i>Assay protocol</i>	59
3.	Results and Discussion	61
	Part I: Phytochemical studies	61
	Preface.....	61
3.1	Solvent Extraction and Yields.....	61
3.2	Polymers.....	62
3.2.1	Characterisation of HM-1 as trans-1,4-polyisoprene.....	62
3.3	Terpenoids.....	67
3.3.1	Friedelane-type triterpenes.....	67
3.3.1.1	<i>Characterisation of HM-2 as canophyllol</i>	68
3.3.1.2	<i>Characterisation of HM-3 as friedelan-1,3-dione</i>	79
3.3.1.3	<i>Characterisation of HM-4 as the novel triterpene (15(β)-acetoxfriedelan-1,3-dione)</i>	90
3.3.1.4	<i>Characterisation of HM-5 as a 28-Hydroxyfriedelan-1,3-dione</i>	100
3.3.1.5	<i>Characterisation of HM-6 as the novel corredorane-type triterpene 1,3-dioxocorredor-14,26-ene</i>	112
3.3.2	Quinonemethide-type triterpenes (celastroloids).....	126
3.3.2.1	<i>Characterisation of HM-7 as netzahualcoyondiol</i>	126
3.3.2.2	<i>Characterisation of HM-8 as netzahualcoyone</i>	136
3.3.2.3	<i>Characterisation of HM-9 as the new celastrolid, 22(α)-hydroxynetzahualcoyene</i>	145
3.3.2.4	<i>Characterisation of HM-10 as pristimerin</i>	156
3.3.2.5	<i>Characterisation of HM-11 as celastrol</i>	165

3.3.2.6	<i>Characterisation of HM-12 as the new celastroid, 22(β)-hydroxycelastrol.....</i>	173
3.3.3	Norfriedelane-type triterpenes and aromatic triterpenes.....	183
3.3.3.1	<i>Characterisation of HM-13 as salaquinone A.....</i>	183
3.3.3.2	<i>Characterisation of HM-14 as regeol A.....</i>	194
3.3.3.3	<i>Characterisation of HM-15 as the new aromatic triterpene, methyl 2,3,22α-trihydroxy-24,25-dinorfriedelan-1,3,5(10),6,8,14-hexaen-29-oate.....</i>	205
3.3.3.4	<i>Characterisation of HM-16 as the new triterpene, 2,22-dihydroxy-3-methoxy-15,12-dioxo-5,8-oxa-24,30-dinor-5,6-seco-friedelan-1,3,5(10)-trien-6-al (j juborreal).....</i>	217
3.4	Steroids.....	230
3.4.1	Characterisation of HM-17 as β-sitosterol.....	230
3.4.2	Characterisation of HM-18 as stigmast-4-en-3-one.....	233
3.5	Simple phenolics.....	239
3.5.1	Characterisation of benzoic acid derivatives.....	239
3.5.1.1	<i>Characterisation of HM-19 as 3, 4-dihydroxybenzoic acid.....</i>	239
3.5.2	Characterisation of benzaldehyde derivatives.....	243
3.5.2.1	<i>Characterisation of HM-20 as p-hydroxybenzaldehyde (HBA)..</i>	243
3.6	Isocoumarin.....	247
3.6.1	Characterisation of HM-21 as (±) mellein.....	247
3.7	General illustrative and supportive findings and overall conclusion.....	253
4.	Results and Discussion.....	255
	Part II: Biological Studies.....	255
4.1	<i>In vitro</i> cytotoxicity assessment.....	255
4.1.1	Effects of crude extracts from the root bark of <i>M. laevis</i> on cell viability.....	255

4.1.1.1	<i>Effects of constituents from the n-hexane extract (MLH) on cell viability</i>	257
4.1.1.2	<i>Effects of constituents from the EtOAc extract (MLEt) on cell viability</i>	260
4.1.2	Effects of crude extracts from the stem bark of <i>M. laevis</i> on cell viability	263
4.1.2.1	<i>Effects of constituents from the n-hexane extract (MLHs) on cell viability</i>	265
4.1.2.2	<i>Effects of constituents from the EtOAc extract (MLEts) on cell viability</i>	270
4.2	<i>In vitro</i> anti-trypanosomal activity assessment	274
4.2.1	Anti-trypanosomal activity of crude extracts of <i>M. laevis</i>	274
4.2.2	Anti-trypanosomal activity of some isolated compounds/ fractions	276
4.2.3	Overall evaluation of the anti-trypanosomal activity of the crude extracts	281
5.	Conclusions and Future Work	283
5.1	Summary of key findings	283
5.2	Recommendations for future work	285
5.3	Overall conclusion	287
	Appendices	288
	References	298

List of Figures

Figure 1.1	A; <i>M. laevis</i> (Chuchuguasa) tree, B; the leaves.....	7
Figure 1.2	Structures of dihydro- β -agarofuran sesquiterpene pyridine alkaloids previously isolated from Chuchuguasa.....	11
Figure 1.3	Structures of dihydro- β -agarofuran sesquiterpene polyol esters previously isolated from Chuchuguasa	13
Figure 1.4	Structures of triterpenoids and sterols previously isolated from Chuchuguasa.....	17
Figure 1.5	Structures of dammarane triterpenes previously isolated from Chuchuguasa.....	23
Figure 1.6	Structures of the triterpene dimers previously isolated from Chuchuguasa.....	27
Figure 1.7	Structures of iridoids previously isolated from Chuchuguasa.....	32
Figure 1.8	Structures of phenolics previously isolated from Chuchuguasa.....	33
Figure 1.9	Structures of miscellaneous compounds previously isolated from Chuchuguasa.....	35
Figure 2.1	(A); <i>Eusebio Mendoza</i> collecting Chuchuguasa root, (B); Alexander I. Gray with Chuchuguasa root in 25/1/1993	46
Figure 2.2	<i>M. Laevis</i> ; (A) Root bark, (B) Stem bark	46
Figure 2.3	Reduction of resazurin to resorufin in living cells	58
Figure 2.4	Assay plate template.....	59
Figure 3.1	Structure of HM-1	63
Figure 3.2	Full and selected expansion of ^1H NMR spectrum (400 MHz) of HM-1 in CDCl_3	64
Figure 3.3	DEPTq135 ^{13}C NMR spectrum (100 MHz) of HM-1 in CDCl_3	64
Figure 3.4	Full HSQC spectrum (400 MHz) of HM-1 in CDCl_3	65
Figure 3.5	Full HMBC spectrum (400 MHz) of HM-1 in CDCl_3	65
Figure 3.6	Full ^1H - ^1H COSY spectrum (400 MHz) of HM-1 in CDCl_3	66
Figure 3.7	1D NOE experiments (400 MHz) showing the NOE effects between the olefinic proton (H-3) and the methyl group (Me-5).....	66

Figure 3.8	Comparison between (A & B); Random-noise, proton-decoupled 15.08 MHz ^{13}C NMR spectra of the natural <i>cis</i> and <i>trans</i> -1,4-polyisoprenes and (C); The DEPTq 135 ^{13}C NMR spectrum (400 MHz) of HM-1 in CDCl_3	67
Figure 3.9	Full structure of HM-2 with HMBC correlations.....	71
Figure 3.10	3D structure of HM-2 with important NOESY correlations	71
Figure 3.11	Full ^1H NMR spectrum with selected expansions (400 MHz) of HM-2 in CDCl_3	73
Figure 3.12	Full DEPTq 135 ^{13}C NMR spectrum (100 MHz) of HM-2 in CDCl_3	74
Figure 3.13	HSQC spectrum (400 MHz) of HM-2 in CDCl_3	75
Figure 3.14	HMBC spectrum (400 MHz) of HM-2 in CDCl_3	76
Figure 3.15	Full ^1H - ^1H COSY spectrum (400 MHz) of HM-2 in CDCl_3	78
Figure 3.16	Full NOESY spectrum (400 MHz) of HM-2 in CDCl_3	78
Figure 3.17	Full structure of HM-3 with key HMBC correlations	82
Figure 3.18	Energy minimised 3D structure of HM-3 using ChemDraw Ultra-11.0 showing the key NOE correlations	82
Figure 3.19	Full ^1H NMR spectrum with selected expansion (400 MHz) of HM-3 in CDCl_3	84
Figure 3.20	DEPTq 135 ^{13}C NMR spectrum (100 MHz) of HM-3 in CDCl_3	85
Figure 3.21	HSQC spectrum (400 MHz) of HM-3 in CDCl_3	86
Figure 3.22	HMBC spectrum (400 MHz) of HM-3 in CDCl_3	87
Figure 3.23	^1H - ^1H COSY spectrum (400 MHz) of HM-3 in CDCl_3	88
Figure 3.24	NOESY spectrum (400 MHz) of HM-3 in CDCl_3	89
Figure 3.25	Structure of HM-4 with HMBC correlations.....	92
Figure 3.26	Energy minimised 3D structure of HM-4 with important NOE correlations	92
Figure 3.27	^1H NMR spectrum with selected expansions (400 MHz) of HM-4 in CDCl_3	94
Figure 3.28	DEPTq 135 ^{13}C NMR spectrum (100 MHz) of HM-4 in CDCl_3	95
Figure 3.29	HSQC spectrum (400 MHz) of HM-4 in CDCl_3	96
Figure 3.30	HMBC spectrum (400 MHz) of HM-4 in CDCl_3	97
Figure 3.31	Full ^1H - ^1H COSY spectrum (400 MHz) of HM-4 in CDCl_3	98

Figure 3.32	Full NOESY spectrum (400 MHz) of HM-4 in CDCl ₃	99
Figure 3.33	Full structure of HM-5 with key HMBC correlations	103
Figure 3.34	3D structure of HM-5 with important NOESY correlations	103
Figure 3.35	Full ¹ H NMR spectrum with selected expansion (400 MHz) of HM-5 in CDCl ₃	106
Figure 3.36	DEPTq 135 ¹³ C NMR spectrum (100 MHz) of HM-5 in CDCl ₃	107
Figure 3.37	HSQC spectrum (400 MHz) of HM-5 in CDCl ₃	108
Figure 3.38	HMBC spectrum (400 MHz) of HM-5 in CDCl ₃	109
Figure 3.39	¹ H- ¹ H COSY spectrum (400 MHz) of HM-5 in CDCl ₃	110
Figure 3.40	Full NOESY spectrum (400 MHz) of HM-5 in CDCl ₃	111
Figure 3.41	Selected NOESY expansion of the (-CH ₂ OH) group;.....	111
Figure 3.42	Part structures of HM-6 with key HMBC correlations	114
Figure 3.43	Solvated (in CDCl ₃) “sticks” format taken from crystal structure of HM-6	114
Figure 3.44	The Oak Ridge Thermal Ellipsoid Plot (ORTEP) of the crystal structure of HM-6 with atoms labelling.....	115
Figure 3.45	Full structure of HM-6 showing the non-systematic numbering and the key HMBC correlations of Me-27	116
Figure 3.46	Putative bioconversion of HM-3 into HM-6	117
Figure 3.47	3D structure of HM-6 with important NOESY correlations	118
Figure 3.48	Full ¹ H NMR spectrum with selected expansion (400 MHz) of HM-6 in CDCl ₃	120
Figure 3.49	Stacked DEPTq135 ¹³ C spectrum (100MHz) showing the differences at two temperature settings	121
Figure 3.50	DEPTq 135 ¹³ C NMR spectrum (100 MHz) of HM-6 in CDCl ₃	121
Figure 3.51	HSQC spectrum (400 MHz) of HM-6 in CDCl ₃	122
Figure 3.52	HMBC spectrum (400 MHz) of HM-6 in CDCl ₃	123
Figure 3.53	Full NOESY spectrum (400 MHz) of HM-6 in CDCl ₃	124
Figure 3.54	Full ¹ H- ¹ H COSY spectrum (400 MHz) of HM-6 in CDCl ₃	125
Figure 3.55	Structure of HM-7 with the HMBC correlations.....	129
Figure 3.56	¹ H NMR spectrum with selected expansions (400 MHz) of HM-7 in CDCl ₃	131

Figure 3.57	DEPTq 135 ¹³ C NMR spectrum (100 MHz) of HM-7 in CDCl ₃	132
Figure 3.58	HSQC spectrum (400 MHz) of HM-7 in CDCl ₃	133
Figure 3.59	HMBC spectrum (400 MHz) of HM-7 in CDCl ₃	134
Figure 3.60	Full ¹ H- ¹ H COSY spectrum (400 MHz) of HM-7 in CDCl ₃	135
Figure 3.61	Structure of HM-8 with the key HMBC correlations.....	139
Figure 3.62	X-Ray model of Netzahualcoyone with selected NOESY correlations observed in this study on HM-8	139
Figure 3.63	¹ H NMR spectrum (400 MHz) of HM-8 in CDCl ₃	140
Figure 3.64	DEPTq 135 ¹³ C NMR spectrum (100 MHz) of HM-8 in CDCl ₃	141
Figure 3.65	HSQC spectrum (400 MHz) of HM-8 in CDCl ₃	142
Figure 3.66	HMBC spectrum (400 MHz) of HM-8 in CDCl ₃	143
Figure 3.67	Full ¹ H- ¹ H COSY spectrum (400 MHz) of HM-8 in CDCl ₃	144
Figure 3.68	Full NOESY spectrum (400 MHz) of HM-8 in CDCl ₃	144
Figure 3.69	Structure of netzahualcoyonol as reported by Jeller <i>et al.</i> , (2004)...	147
Figure 3.70	Structure of HM-9 with the key HMBC correlations.....	148
Figure 3.71	Energy minimised 3D structure of HM-9 by ChemDraw Ultra 11.0 software with the key NOE correlations	148
Figure 3.72	¹ H NMR spectrum (400 MHz) of HM-9 in CDCl ₃	150
Figure 3.73	DEPTq 135 ¹³ C NMR spectrum (100 MHz) of HM-9 in CDCl ₃	151
Figure 3.74	HSQC spectrum (400 MHz) of HM-9 in CDCl ₃	152
Figure 3.75	HMBC spectrum (400 MHz) of HM-9 in CDCl ₃	153
Figure 3.76	Full ¹ H- ¹ H COSY spectrum (400 MHz) of HM-9 in CDCl ₃	154
Figure 3.77	NOESY spectrum (400 MHz) of HM-9 in CDCl ₃	155
Figure 3.78	Possible biosynthetic scheme for the conversion of pristimerin to netzahualcoyondiol	157
Figure 3.79	Structure of HM-10 with the key HMBC correlations.....	158
Figure 3.80	¹ H NMR spectrum (400 MHz) of HM-10 in CDCl ₃	160
Figure 3.81	DEPTq 135 ¹³ C NMR spectrum (100 MHz) of HM-10 in CDCl ₃ ...	161
Figure 3.82	HSQC spectrum (400 MHz) of HM-10 in CDCl ₃	162
Figure 3.83	HMBC spectrum (400 MHz) of HM-10 in CDCl ₃	163
Figure 3.84	Full ¹ H- ¹ H COSY spectrum (400 MHz) of HM-10 in CDCl ₃	164
Figure 3.85	Structure of HM-11 with the key HMBC correlations.....	167

Figure 3.86	^1H NMR spectrum (400 MHz) of HM-11 in CDCl_3	168
Figure 3.87	DEPTq ^{13}C NMR spectrum (100 MHz) of HM-11 in CDCl_3 ...	169
Figure 3.88	HSQC spectrum (400 MHz) of HM-11 in CDCl_3	170
Figure 3.89	HMBC spectrum (400 MHz) of HM-11 in CDCl_3	171
Figure 3.90	Full ^1H - ^1H COSY spectrum (400 MHz) of HM-11 in CDCl_3	172
Figure 3.91	Structure of HM-12 with the key HMBC correlations	175
Figure 3.92	^1H NMR spectrum (400 MHz) of HM-12 in CDCl_3	177
Figure 3.93	DEPTq ^{13}C NMR spectrum (100 MHz) of HM-12 in CDCl_3 ...	178
Figure 3.94	HSQC spectrum (400 MHz) of HM-12 in CDCl_3	179
Figure 3.95	HMBC spectrum (400 MHz) of HM-12 in CDCl_3	180
Figure 3.96	NOESY spectrum (400 MHz) of HM-8 in CDCl_3	181
Figure 3.97	^1H - ^1H COSY spectrum (400 MHz) of HM-12 in CDCl_3	182
Figure 3.98	Structure of HM-13 with the HMBC correlations	186
Figure 3.99	Energy minimised 3D structure of HM-13 showing NOESY correlations	186
Figure 3.100	^1H NMR spectrum (400 MHz) of HM-13 in CDCl_3	188
Figure 3.101	DEPTq ^{13}C NMR spectrum (100 MHz) of HM-13 in CDCl_3 ...	189
Figure 3.102	HSQC spectrum (400 MHz) of HM-13 in CDCl_3	190
Figure 3.103	HMBC spectrum (400 MHz) of HM-13 in CDCl_3	191
Figure 3.104	Full ^1H - ^1H COSY spectrum (400 MHz) of HM-13 in CDCl_3	192
Figure 3.105	NOESY spectrum (400 MHz) of HM-13 in CDCl_3	193
Figure 3.106	Structure of HM-14 with the HMBC correlations	197
Figure 3.107	^1H NMR spectrum (400 MHz) of HM-14 in CDCl_3 in mixture	199
Figure 3.108	Full ^{13}C NMR (A) and DEPT 135 (B) spectra (100 MHz) of HM-14 in CDCl_3	200
Figure 3.109	Selected expansion in the aliphatic region of ^{13}C NMR (A) and DEPT 135 (B) spectra (100 MHz) of HM-14 in CDCl_3	200
Figure 3.110	HSQC spectrum (400 MHz) of HM-14 in CDCl_3	201
Figure 3.111	HMBC spectrum (400 MHz) of HM-14 in CDCl_3	202
Figure 3.112	Full ^1H - ^1H COSY spectrum (400 MHz) of HM-14 in CDCl_3	203
Figure 3.113	NOESY spectrum (400 MHz) of HM-14 in CDCl_3	203

Figure 3.114	Energy minimised 3D structure of HM-14 showing NOESY correlations	204
Figure 3.115	Structure of HM-15 by two numbering systems	208
Figure 3.116	^1H NMR spectrum (400 MHz) of HM-15 in $(\text{CD}_3)_2\text{CO}$	210
Figure 3.117	DEPTq ^{13}C NMR spectrum (100 MHz) of HM-15 in $(\text{CD}_3)_2\text{CO}$	211
Figure 3.118	HSQC spectrum (400 MHz) of HM-15 in $(\text{CD}_3)_2\text{CO}$	212
Figure 3.119	HMBC spectrum (400 MHz) of HM-15 in $(\text{CD}_3)_2\text{CO}$	213
Figure 3.120	Full ^1H - ^1H COSY spectrum (400 MHz) of HM-15 in $(\text{CD}_3)_2\text{CO}$	214
Figure 3.121	NOESY spectrum (400 MHz) of HM-15 in $(\text{CD}_3)_2\text{CO}$	215
Figure 3.122	(A & B) show the energy minimised 3D structure of HM-15 from two different sides using ChemDraw Ultra-11.0 software and the important NOESY correlations.....	216
Figure 3.123	Partial structure of HM-16.....	219
Figure 3.124	Structure of HM-16 by two numbering systems	221
Figure 3.125	^1H NMR spectrum (400 MHz) of HM-16 in CDCl_3	223
Figure 3.126	DEPTq ^{13}C NMR spectrum (100 MHz) of HM-16 in CDCl_3 ...	224
Figure 3.127	^1H - ^1H COSY spectrum (400 MHz) of HM-16 in CDCl_3	225
Figure 3.128	HSQC spectrum (400 MHz) of HM-16 in CDCl_3	226
Figure 3.129	HMBC spectrum (400 MHz) of HM-16 in CDCl_3	227
Figure 3.130	NOESY spectrum (400 MHz) of HM-16 in CDCl_3	228
Figure 3.131	Energy minimised 3D structure of HM-16 showing NOESY correlations	229
Figure 3.132	Full structure of HM-17.....	231
Figure 3.133	Full ^1H NMR spectrum (400 MHz) of HM-17 in CDCl_3	232
Figure 3.134	DEPTq ^{13}C NMR spectrum (100 MHz) of HM-17 in CDCl_3 ...	232
Figure 3.135	Full structure of HM-18 with the key HMBC correlations	234
Figure 3.136	Full ^1H NMR spectrum (400 MHz) of HM-18 in CDCl_3	236
Figure 3.137	DEPTq ^{13}C NMR spectrum (100 MHz) of HM-18 in CDCl_3	236
Figure 3.138	HSQC spectrum (400 MHz) of HM-18 in CDCl_3	237
Figure 3.139	Full COSY spectrum (400 MHz) of HM-18 in CDCl_3	237
Figure 3.140	HMBC spectrum (400 MHz) of HM-18 in CDCl_3	238

Figure 3.141	Structure of HM-19	241
Figure 3.142	Full ^1H NMR spectrum (400 MHz) of HM-19 in $(\text{CD}_3)_2\text{CO}$	241
Figure 3.143	Full DEPTq ^{13}C NMR spectrum (100 MHz) of HM-19 in $(\text{CD}_3)_2\text{CO}$	242
Figure 3.144	HMBC spectrum (400 MHz) of HM-19 in $(\text{CD}_3)_2\text{CO}$	242
Figure 3.145	Structure of HM-20 with key HMBC correlations.....	244
Figure 3.146	^1H NMR spectrum (400 MHz) of HM-20 in CDCl_3 in mixture.....	245
Figure 3.147	Full ^{13}C NMR (A) and DEPT 135 (B) spectra (100 MHz) of HM-20 in CDCl_3 in mixture.....	245
Figure 3.148	HMBC spectrum (400 MHz) of HM-20 in CDCl_3	246
Figure 3.149	Structure of (R)-HM-21 with important HMBC correlations	249
Figure 3.150	Full ^1H NMR spectrum (400 MHz) of HM-21 in CDCl_3	250
Figure 3.151	Full DEPTq ^{13}C 135 spectrum (100 MHz) of HM-21 in CDCl_3	250
Figure 3.152	Full HSQC spectrum (400 MHz) of HM-21 in CDCl_3	251
Figure 3.153	Full HMBC spectrum (400 MHz) of HM-21 in CDCl_3	251
Figure 3.154	^1H - ^1H COSY spectrum (400 MHz) of HM-21 in CDCl_3	252
Figure 3.155	Full NOESY spectrum (400 MHz) in CDCl_3 and key NOE correlations of HM-21	252
Figure 3.156	Comparison between root and stem bark extracts (A & C) and (B &D), respectively, on TLC.	254
Figure 4.1	The cytotoxicity effect of n-hexane (A) and EtOAc (B) crude extracts from the root bark of <i>M. laevis</i> on A375 and Hs27 cell lines using a resazurin assay.....	256
Figure 4.2	The cytotoxicity effect of netzahualcoyondiol (HM-7) on A375 and Hs27 cell lines using resazurin assay.....	257
Figure 4.3	Cytotoxicity of isolated compounds from an EtOAc extract of the root bark of <i>M. laevis</i> on A375 and Hs27 cell lines using a resazurin assay	261
Figure 4.4	The cytotoxicity effect of n-hexane (A) and EtOAc (B) crude extracts from the stem bark of <i>M. laevis</i> on A375 and Hs27 cell lines using a resazurin assay.....	264

Figure 4.5	Cytotoxicity of some isolated compounds from n-hexane extract of the stem bark of <i>M. laevis</i> on A375 and Hs27 cell lines using a resazurin assay.....	269
Figure 4.6	Cytotoxicity of some isolated compounds from an EtOAC extract of the stem bark of <i>M. laevis</i> on A375 and Hs27 cell lines using a resazurin assay	271
Figure 4.7	Preliminary screening results of the crude extracts from of the root and stem barks of <i>M. laevis</i> against <i>Trypanosoma b. brucei</i> (S427) blood stream forms using an Alamar blue assay	275
Figure 4.8	Preliminary screening of some isolated compounds from the extracts of the root and stem barks of <i>M. laevis</i> against <i>Trypanosoma b. brucei</i> (S427) blood stream forms at two concentrations (20 and 5 μ M) using an Alamar blue assay.....	278

List of Tables

Table 1.1	Dihydro- β -agarofuran sesquiterpene pyridine alkaloids previously isolated from Chuchuguasa	10
Table 1.2	Dihydro- β -agarofuran sesquiterpene polyol esters previously isolated from Chuchuguasa	13
Table 1.3	Triterpenoids and sterols previously isolated from Chuchuguasa.....	14
Table 1.4	Dammarane triterpenes previously isolated from Chuchuguasa	22
Table 1.5	Triterpene dimers previously isolated from Chuchuguasa.....	25
Table 1.6	Iridoids previously isolated from Chuchuguasa.....	32
Table 1.7	Phenolics previously isolated from Chuchuguasa.....	33
Table 1.8	Miscellaneous compounds previously isolated from Chuchuguasa...	35
Table 2.1	Key parameters for the separation method by Reveleris FC.....	51
Table 2.2	Deuterated solvents used for NMR analysis	52
Table 2.3	Main parameters for the HRESI Mass spectral analysis.....	54
Table 3.1	Amounts and yields of the crude extracts of ML root and stem barks	61
Table 3.2	^1H (400 MHz) and ^{13}C (100 MHz) NMR data of HM-2 in CDCl_3	72
Table 3.3	^1H (400 MHz) and ^{13}C (100 MHz) NMR data of HM-3 in CDCl_3	83
Table 3.4	^1H (400 MHz) and ^{13}C (100 MHz) NMR data of HM-4 in CDCl_3	93
Table 3.5	Comparison of the HSQC data in CDCl_3 of HM-5 and a similarly 28-hydroxyfriedelane-1.3-dione.....	104
Table 3.6	Some selected HMBC correlations for HM-5 in CDCl_3	105
Table 3.7	^1H (400 MHz) and ^{13}C (100 MHz) NMR data of HM-6 in CDCl_3 ..	119
Table 3.8	^1H (400 MHz) and ^{13}C (100 MHz) NMR data of HM-7 in CDCl_3 ..	130
Table 3.9	^1H (400 MHz) and ^{13}C (100 MHz) NMR data of HM-8 and HM-9 in CDCl_3	149
Table 3.10	^1H (400 MHz) and ^{13}C (100 MHz) NMR data of HM-10 in CDCl_3	159
Table 3.11	^1H (400 MHz) and ^{13}C (100 MHz) NMR data of HM-11 and HM-12.....	176

Table 3.12	^1H (400 MHz) and ^{13}C (100 MHz) NMR data of HM-13 in CDCl_3	187
Table 3.13	^1H (400 MHz) and ^{13}C (100 MHz) NMR data of HM-14 in CDCl_3	198
Table 3.14	^1H (400 MHz) and ^{13}C (100 MHz) NMR data of HM-15 in acetone- d_6	209
Table 3.15	^1H (400 MHz) and ^{13}C (100 MHz) NMR data of HM-16 in CDCl_3	222
Table 3.16	^1H (400 MHz) and ^{13}C (100 MHz) NMR data of HM-18 in CDCl_3	235
Table 3.17	^1H (400 MHz) and ^{13}C (100 MHz) NMR data of the isolated simple phenolics.....	246
Table 3.18	Comparison of ^1H (400 MHz) and ^{13}C (100 MHz) NMR data of HM-21 and ^1H (300 MHz) and ^{13}C (75 MHz) of (\pm) Mellein in CDCl_3	249
Table 4.1	Cytotoxic activity of pristimerin on human tumour cell lines.....	259
Table 4.2	Summary of the cytotoxicity effects (EC_{50} values) of crude extracts and their constituents from the root and stem bark of <i>M. laevis</i>	273
Table 4.3	Anti-trypanosomal activities of the crude extracts and some fractions/ sub-fractions from the root and stem barks of <i>M. laevis</i> against <i>T. b. brucei</i> (S427)	275
Table 4.4	Preliminary screening of some isolated compounds from the root and stem barks of <i>M. laevis</i> against <i>T. b. brucei</i> (S427).....	279

List of Schemes

- Scheme 1.1 Conversion of oxidosqualene to friedelane triterpenes and their involvement as the biosynthetic precursors to the quinonemethides ... 9
- Scheme 3.1 Some major classes of celastroloids and their structural (biogenetic) interrelationship 254

List of Abbreviations

Acetone- d_6	Deuterated acetone
AR	Aldose reductase
ATCC	American Type Cell Culture
<i>brs</i>	Broad singlet
CC	Column chromatography
$CDCl_3$	Deuterated Chloroform
CNS	Central Nervous System
Col.	Colombia
COSY	Correlation Spectroscopy
d.	Died
<i>d</i>	Doublet
<i>dd</i>	Doublet of a doublet
DBE	Double bond equivalence
DCM	Dichloromethane
DEPTq	Distortionless Enhancement by Polarisation Transfer including the detection of quaternary nuclei.
DMEM	Dulbecco's Modified Eagle Medium
DMSO	Dimethyl sulfoxide
DMSO- d_6	Deuterated dimethyl sulfoxide
EC ₅₀	50% Effective concentration
EtOAc	Ethyl acetate
FC	Flash Chromatography
FBS	Fatal Bovine solution
HAT	Human African Trypanosomiasis
HIV	Human immunodeficiency virus
HMBC	Heteronuclear Multiple Bond Coherence
HRESI-MS	High-resolution Electrospray Ionisation Mass Spectroscopy
HSQC	Heteronuclear Multiple Quantum Coherence
IC ₅₀	50% Inhibitory concentration
IR	InfraRed spectroscopy
<i>m</i>	Multiplet
MeOH	Methanol

MHz	Megahertz
MIC	Minimum inhibitory concentration
ML	<i>Maytenus laevis</i>
MM-ES+APCI	Multimode-Electrospray + Atmospheric-Pressure Chemical Ionisation
NMR	Nuclear Magnetic Resonance
NOE	Nuclear Overhauser effect
NOESY	Nuclear Overhauser Enhancement Spectroscopy
OR	Optical Rotation
PTLC	Preparative thin layer chromatography
R _f	Retardation Factor
<i>s</i>	Singlet
SC	Sephadex Chromatography
SC ₅₀	Concentration required for 50% reduction of 40µM DPPH radical (Scavenging activity)
SEC	Size-Exclusion Chromatography
<i>t</i>	Triplet
TLC	Thin layer Chromatography
TM	Traditional Medicine
T&CM	Traditional and Complementary Medicine
TMS	Tetramethylsilane
UV	Ultraviolet light
VLC	Vacuum Liquid Chromatography
WHO	World Health Organization

CHAPTER I

1. INTRODUCTION

1.1 The importance of medicinal plants; A glance from a historical view

The relationship between man and nature goes back to time immemorial. Primitive man became aware of his environment, and by noticing the great diversity of plants available to him, tried to benefit from them as much as possible. Subsequently, plants became part of man's daily life as sources of food, clothing, shelter, poisons and medicine. Fossil records date human use of plants as medicines to at least the Middle Paleolithic age; some 60,000 years ago (Solecki, 1975). Since then, the use of plants as traditional medicines (TM) has developed. Herbs have been used by native healers especially in rural regions of the developing countries of Asia, Africa and Latin America as therapies for many diseases as they have been the only affordable and accessible form of health care in many of these areas, and indeed they have managed to save lives on uncountable occasions. In Africa up to 80% of the population uses TM to help meet their health care needs, while in China, TM accounts for around 40% of all health care delivered (WHO, 2002).

For example, the bark of many species of *Cinchona* from S. America has been used since 1630 for the treatment of malaria (Evans, 2009), and *Digitalis purpurea* leaf was used successfully to treat congestive heart failure according to William Withering's book, 1785, (Bessen, 1986). *Ephedra* species such as *E. sinica* and *E. equisetina* have been used in Traditional Chinese Medicine and Kampo medicine (Japan) from ancient times mainly in mixtures of different herbal formulae as therapy for various respiratory disorders such as asthma, coughs, nasal congestion and influenza (Kitani *et al.*, 2009). These are a few of the hundreds of medicinal plants which have been used for their properties as anti-inflammatory, hypotensive, hypoglycaemic, amoebicidal, antifertility, antiprotozoal agents, and more.

In the last 30 years, significant changes in the attitude of members of the public and researchers towards herbal medicines has occurred, leading to a growing tendency for people in developed countries to use TM to complement existing synthetic drug treatments. Over 100 million Europeans are currently traditional and complementary medicine (T&CM) users, with one fifth regularly using T&CM and the same number preferring health care which includes T&CM (WHO, 2013). In fact, between 1981-2006, 24 natural compounds formed the core of marketed drugs in this time period, 19 of them were isolated from soil microbes and 5 were of plant

origin such as Taxol® (paclitaxel) from *Taxus brevifolia* as an anticancer agent and Artemisinin from *Artemisia annua* as an anti-malarial drug, (Ganesan, 2008). Furthermore, biologically active natural products from plants and their analogues formed up to 57% of the top 150 brand names prescribed in the United States in 1993 (Newman *et al.*, 1997; Newman and Cragg, 2012).

Nature has served as a source of healing agents for thousands of years and it will continue to be the largest reservoir of novel chemicals in years to come since more than 250,000 species of flowering plants exist on our planet and barely a small fraction, 5-10%, of these plants have been mined exhaustively to date (Sarker *et al.*, 2006).

1.2 Traditional medicine in Amazonia

The Amazonian Rainforest represents the most extensive resource of natural diversity remaining on the planet and it symbolises the mystery, power, and sacred intimate relationship between humans and their ambient nature. This connectivity over centuries has created unsurpassed knowledge which accumulated via experimentation with plants and other healing materials by the indigenous people living in unity with their surrounding environment and who have learned how to adapt for their physical, cultural and spiritual well being. They have transmitted their treasured ancestral heritage as their own vegetal pharmacopoeia from generation to generation which became a specific trait of each of their societies (Schultes and Raffauf, 1992). This knowledge has been passed on in tribes such as the Uitoto in the form of the great "*historia*" by the true traditional healers "*sabedores* or true shamans" who follow disciplines/careers of more than 45 years (Mitchell *et al.*, 2010).

By understanding the importance of this invaluable knowledge and by the curiosity of science, the rainforest medicines have offered western medicine a rich foundation of a variety of phytochemicals and active constituents, which then have evolved to their current forms. For example; revealing the secret of Curare, the powerful arrow poison which is prepared from the bark of different species of *Chondrodendron* lianas by various Indian tribes of South America (such as Uitoto and Tikunas) for the purpose of hunting, caused a scientific revolution in surgical anaesthesia when the active component, d-tubocurarine, was isolated and identified

(Lee, 2005). Quinine, isolated from the bark of *Cinchona* tree commonly from *Cinchona officinalis* (Rubiaceae), has been a very effective drug for the treatment of malaria and also for "night cramps" in muscles of the elderly (Mandal *et al.*, 1995), and was originally used for thousands of years by the Indians of S. America (Plotkin, 1993).

Obtaining these benefits from jungle exploration was not cost free. The interference from outsiders such as colonists, migrants and others has had significant impact on the indigenous people, their languages, cultures, habits and beliefs. The encroachment of westernisation on these native societies via missionary activities, wars, road development, travel and tourism, has spoiled their lore and their knowledge of the plants properties, uses and their hidden secrets (Corredor de and Simpson, 2009).

On the bright side, some of these local communities, such as those in the Colombian Amazon, by whom the plant of this study was collected, have managed to keep their empirical plant knowledge while being introduced to western medicines and beliefs (Schultes and Raffauf, 1992). However, other factors have played a negative effect regarding transferring this heritage smoothly through generations. The Colombian State education system encourages the indigenous children to follow a national curriculum in schools away from their elders, hence, preventing them from learning their lore and secrets by those who present the repositories of tribal knowledge (Corredor de and Simpson, 2009). By interrupting this link, the threat of losing such a wealth of knowledge is becoming alarming and due to being passed down mainly by oral tradition is in danger of being lost to humanity before we even have the opportunity to reveal all its aspects. Furthermore, much of what has been written so far may not be fully "translated" as the attitudes in the past were largely "the informed + the informant", i.e. some of what has been "written down" may be inaccurate.

In parallel, the accelerated intentional destruction of the rainforests worldwide and the consequent extinction of several plant and animal species, which were yet to be discovered, as well as the loss of knowledge of their native dwellers "sabedores" who know how to manage them is taking away the indigenous methods of survival including their TM. This makes us pay dearly, as what could be our greatest chance

of searching for powerful, safe and new medicines to conquer those health crises that humanity is suffering from, is being blown away.

These facts are now being realised more than ever and scientists have become aware that Mother Nature is our sanctuary for a brighter future regarding our way of treating diseases. To get benefits from this rich reservoir of the earth's healing agents, there is a need to protect those indigenous people in their habitat and help them to conserve their folklore record from disintegrating. Moreover, it is well known that those Amerindian people are wholly dependent on their land and ecosystem to survive, to procure their daily necessities, and to find therapies to combat diseases for being the only affordable way of health care (Caufield, 1986). Therefore, intensive studies on these TM to evaluate their safety and efficacy and to identify their bio-active components "the positive energy" would generate many benefits to them, in particular, and consequently to those who rely mainly on medicinal plants as curative sources and who are estimated to be about 3.5 to 4 billion people in the world (Farnsworth, 1988).

1.3 The family Celastraceae R. Brown

Celastraceae or the bittersweet family has been estimated to include 800 species in about 50 genera (Schultes and Raffauf, 1992) or even up to 94 genera with some 1300 species (Mabberley, 1993) of woody vines, trees and shrubs widely spread in both hemispheres. The differences in the previous estimations were attributed to the shortening in the taxonomic work on the family as well as to the controversial issue regarding the identification of Celastraceae and Hippocrateaceae as two distinctive families (Simmons *et al.*, 2001). *Maytenus*, *Euonymus*, *Cassine*, and *Celastrus* are the largest genera in the family (Heywood, 1993) as cited by Gunatilaka (1996).

Intensive research has been conducted on different species of this family which has proven to be of great ethnobotanical interest (González *et al.*, 2000). This considerable attention was due to the wide-range of chemical distribution in many species of this family, in which a number of interesting and characteristic bioactive compounds have been reported via benefiting from the ethnobotanical data in indicating plants with specific TM uses. The sesquiterpene polyesters and pyridine-sesquiterpene alkaloids with a dihydro- β -agarofuran skeleton along with the quinonemethide triterpenes "celastrolids", are the most widespread secondary

metabolites isolated from Celastraceae and are considered as chemotaxonomic indicators of this family (Reyes *et al.*, 2007; Jeller *et al.*, 2004) in addition to dulcitol and *trans*-polyisoprene (gutta-percha) (Hegnauer, 1966).

1.4 The genus *Maytenus*

The genus *Maytenus* contains about 200 species of evergreen trees and shrubs found throughout temperate and tropical regions (Schultes and Raffauf, 1992). They are widely used in folk medicine in North Africa, South and Central America and Southeast Asia to treat a variety of illnesses (Sagwan *et al.*, 2011; Da Silva *et al.*, 2011). A wide array of biologically-active compounds has been identified from different species of *Maytenus* which justify the potential therapeutic uses of these plants in TM through preparations of their constituents. Cytotoxic quinoid triterpenes have been shown to exhibit anti-mitotic properties (Morita *et al.*, 2008) as well as anti-microbial and anti-protozoal activities (Moujir *et al.*, 1991; Dos Santos *et al.*, 2013). The anti-inflammatory properties of the root extracts of a *Maytenus* species was observed when used topically (Sosa *et al.*, 2007). A biological evaluation of the leaf extracts of other *Maytenus* species indicated their potential anti-ulcerogenic, anti-inflammatory and anti-nociceptive properties (Jorge *et al.*, 2004; Souza-Formigoni *et al.*, 1991). Anti-tumour activity and insecticidal properties were attributed to the presence of maytansinoids in different species of this genus (Kupchan *et al.*, 1972; Madrigal *et al.*, 1985). Sesquiterpene polyesters and sesquiterpene pyridine alkaloids isolated from *Maytenus* species also proved to possess antifeedant or insecticidal activity (Núñez *et al.*, 2004). Moreover, these compounds with their complex structures were found to have immunosuppressive and anti-HIV activities as well as antitumor-promoting activity (Hussein *et al.*, 1999; Duan *et al.*, 1999; González *et al.*, 2000). A number of dimeric celastrols were encountered exclusively from Celastraceae plants, mainly from *Maytenus* species, which showed some cytotoxic activities (Shirota *et al.*, 1997a).

In spite of significant progress in research, the phytochemical and potential pharmacological activities of most of the plants belonging to the genus *Maytenus* have presented challenges due to difficulties with proper botanical classification of some of these species as the taxonomic differences between them seem to be very slight. Thus, it is suspected that additional compounds have yet to be discovered

which may substantiate traditional use or may indicate other potential therapeutic uses of these plants.

1.5 Chuchuguasa (*Maytenus laevis*, *M. krukovii*, *M. chuchuhuasha*, *M. macrocarpa* and *M. colasii*)

Common Names: Chuchuhuasi, chuchuguache, chuchuguaza, chuchuhuasca (Col., Peru).

There has been a certain amount of confusion about the actual plants, which are referred to in their locality as "Chuchuguasa". However, it is agreed that these plants belong to the genus *Maytenus* (Colas, 1937) as cited by Gonzalez *et al.* (1982). The main *Maytenus* species associated with "Chuchuguasa" are *M. laevis* Reissek, *M. krukovii* A.C. Smith, *M. chuchuhuasha* Raymond-Hamet and Colas and *M. colasii* Benoist (*Salacia colasii*) as reported by Gonzalez *et al.* (1982) in addition to *M. macrocarpa* Briquet. *M. ebenifolia*, is another *Maytenus* species which is considered as a synonym for the aforementioned species by the Tropical Plant Database. However, when searching its name in "The International Plant Names Index", it was found that Siegfried Reissek, the author who identified this plant, is the same author who identified *M. laevis*, hence, this species should be different and not associated with Chuchuguasa. Therefore, this literature search will focus on the five former species as they are thought to be botanically the same and the most widely accepted species for "Chuchuguasa" in the tropical rainforests.

1.5.1 General morphological description of Chuchuguasa

Commonly known as "Chuchuguasa", it is an enormous canopy tree found in several areas of the sub-Andean rainforest in the Amazonian basin, mainly in Bolivia, Colombia, Ecuador and Peru (Martinod *et al.*, 1976; Gonzalez *et al.*, 1982). *M. laevis*, the species under study, grows up to 25 m, with a trunk diameter of up to 0.6 m, straight and well branched in the upper half (Figure 1.1; A). Yellowish grey dead bark, living bark reddish and uneven, wood very hard but "milky" and reddish heartwood, delicate textured light green foliage, leaves narrowly elliptic, apex abruptly acuminate, simple, alternate, glabrous undersides, barely visible secondary nerves, 9-11.5 cm long, 3.5-4 cm wide, petiole 7-10mm long (Figure 1.1; B), axillary unisexual flowers, small with orange tinted petals, five yellow stamens and green

calyx (Duarte, 1979; García-Barriga, 1974). The roots are thick and covered with a reddish-orange outer corky layer.



**Figure 1.1: A; *M. laevis* (Chuchuguasa) tree, B; the leaves
Identified by sabedores Noé Rodríguez Jujuborre and Eusebio Mendoza**

1.5.2 Traditional uses of Chuchuguasa

The plant has been used by indigenous people in the Amazon remote communities for the treatment of a number of ailments for centuries. It is also collected by indigenous and non-indigenous communities to be sent to urban societies to be sold in herbal markets alone or as herbal blends with other plants in different pharmaceutical preparations such as creams, drops/ liquid extracts and powder (SunfoodTM Superfoods, San Diego). In the Amazonian cities, the bark extract is used as a tonic, anti-anaemic, for treatment of rheumatism and arthritis, stimulant, anti-diarrhoea, antispasmodic, anticancer, anti-inflammatory and as a sexual stimulant (López *et al.*, 2006).

The Uitoto and Muinane tribes, of Caquetá Medio region, Colombia, by whom the plant of this study was collected (section 2.1.4), use the Chuchuguasa (*M. laevis*) mainly for the treatment of arthritis, rheumatism and back pain. It is believed that the time of collection, the part and orientation of the plant are essential for the healing power and the positive energy to be at their highest levels (Corredor de and Simpson, 2009). The curative prescription is prepared by soaking the root bark overnight in the local sugarcane rum (aguardiente), which is then taken in a small cupful as a tonic

(personal communication with Ann Simpson who was given this information by the Amazonian sabedores Eusebio Mendoza, 1993; Simón Román Enokayai, 1992 (d. 2009); and his father, Oscar Román Enokayai). A one litre concentrated aqueous decoction of a 5 cm piece of the trunk is used as a one-week course for the treatment of rheumatism and arthritis by the Sionas tribes, another ethnic group of the Mocoa region in Colombia. This decoction is taken twice a day as one small cupful each time (García-Barriga, 1974) as cited by (Schultes and Raffauf, 1992). The alcoholic aguardiente infusion of the powdered red root bark is also used throughout the Amazonian river basin of South America as a tonic and stimulant, and even as an aphrodisiac, while it is used topically for the treatment of sores and as an anti-tumour agent in skin cancer in Ecuador (Gonzalez *et al.*, 1982; Martinod *et al.*, 1976).

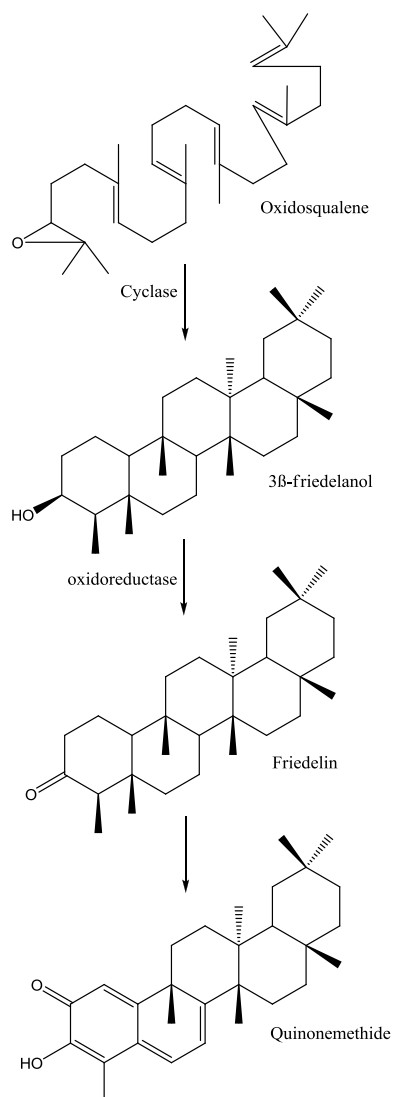
In Peru, the bark maceration of Chuchuguasa (*M. macrocarpa*) is used to regulate menstrual periods, for an upset stomach and considered as anti-diarrheic and anti-arthritic agents, while its decoction is used for dysentery (Duke & Vasquez, 1994, P.114). In Bolivia it is frequently used as a diuretic and to control rheumatism, gout and yellow fever (López *et al.*, 2006)

Preparations of Chuchuguasa mixed with aguardiente and honey were commonly given as a tonic to eco-tourists on their jungle treks (Sanz-Biset *et al.*, 2009), and also sold in the local airports of Amazonas such as Alfredo Vásquez Cobo International airport, Leticia, Colombia (personal communication with Ann Simpson and Alexander I. Gray).

1.5.3 Previous phytochemical studies on Chuchuguasa

This section reviews the phytochemicals isolated previously from the plants of *Maytenus* species which are referred to as Chuchuguasa. These include: dihydro- β -agarofuran sesquiterpene pyridine alkaloids, dihydro- β -agarofuran sesquiterpene polyol esters, quinonemethide, friedelane, olean-12-ene, urs-12-ene and lupane-type triterpenes, dammarane triterpenes, sterols, triterpene dimers which consist of one quinoid unit and one aromatic unit derived from pristimerin, tingenone and/ or their derivatives; in addition to iridoids and polyphenols (see Table 1.1 to Table 1.8 and Figure 1.2 to Figure 1.9).

The co-occurrence of triterpenes of different classes in these plants, particularly, celastroloids and friedelanes, has led to the assumption of the presence of a biogenetic relationship between them (Gunatilaka, 1996). The postulated biosynthetic pathway implicated oxidosqualene as a premiere step. Oxidosqualene is originated initially from joining six isoprene units (Wang *et al.*, 2011). Next, it is cyclised in a highly regio/ stereo-specific way to produce intermediates which in turn are transformed to various skeletal types of triterpenes by different enzyme systems (Abe, 2007). Scheme 1.1 depicts the conversion of oxidosqualene to friedelane products which in turn form the putative precursors of quinonemethide triterpenes as reported by Corsino *et al.* (2000).



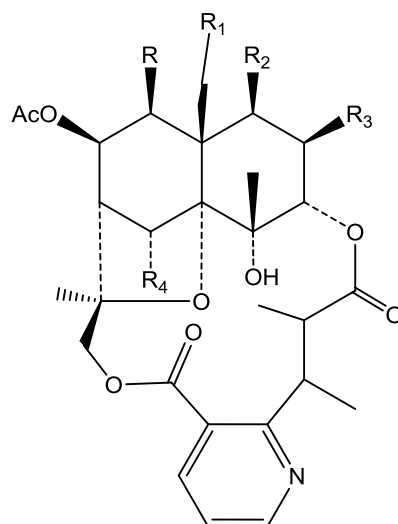
Scheme 1.1: Conversion of oxidosqualene to friedelane triterpenes and their involvement as the biosynthetic precursors to the quinonemethides (Corsino *et al.*, 2000)

Table 1.1: Dihydro- β -agarofuran sesquiterpene pyridine alkaloids previously isolated from Chuchuguasa

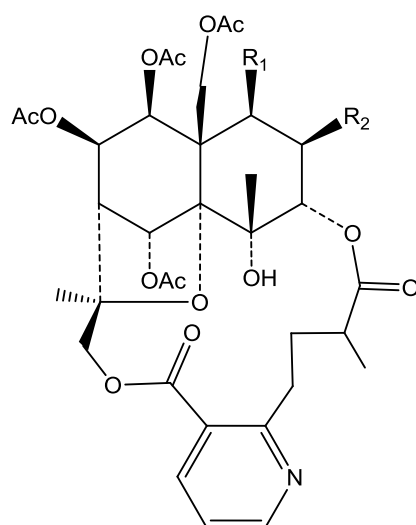
Compounds isolated	Plant species (*)	Reference
Laevisine A (1) Ebenifoline E-I (2) Euojaponine I (3) Euonymine (4)	<i>M. laevis</i> (b)	(Piacente <i>et al.</i> , 1999)
Mayteine (5)	<i>M. laevis</i> (b) <i>M. laevis</i> (b) <i>M. krukovii</i> (Sb)	(Piacente <i>et al.</i> , 1999)/ (Nakagawa <i>et al.</i> , 2004)/ (Sekar <i>et al.</i> , 1995)
7-(acetyloxy)- O^{11} -benzoyl- $O^{2,11}$ - deacetyl-7-deoxoevonine (6)	<i>M. laevis</i> (b)	(Nakagawa <i>et al.</i> , 2004)
Ebenifoline E-III (7)	<i>M. laevis</i> (b) <i>M. ebenifolia</i>	(Nakagawa <i>et al.</i> , 2004)/ (Itokawa <i>et al.</i> , 1993)
Ebenifoline E-II = 6-benzoyl-6- deacetylmayteine (8)	<i>M. laevis</i> (b) <i>M. ebenifolia</i> <i>M. krukovii</i> (Sb)	(Nakagawa <i>et al.</i> , 2004)/ (Itokawa <i>et al.</i> , 1993)/ (Sekar <i>et al.</i> , 1995)
Laevisine B (9) Euojaponine F (10) Euonine (11) Wilforine (12)	<i>M. laevis</i> (b)	(Piacente <i>et al.</i> , 1999)
Chuchuhuanine W-I (13) Chuchuhuanine E-I (14) Chuchuhuanine E-II (15) Chuchuhuanine E-III (16) Chuchuhuanine E-IV (17) Chuchuhuanine E-V (18)	<i>M. chuchuhuasca</i> (Rb)	(Shirota <i>et al.</i> , 1994b)/ (Cordell, 2003) [†]
Chuchuhuanine E-VI (19) Chuchuhuanine E-VII (20)	<i>M. chuchuhuasca</i> (Rb)	(Shirota <i>et al.</i> , 2004a)/ (Cordell, 2003) [†]
4-Deoxyeuonymine (21)	<i>M. chuchuhuasca</i> (Rb)	(Shirota <i>et al.</i> , 1994b)/ (Cordell, 2003) [†]

* Studied plant parts; (b): bark, (Sb): Stem bark, (Rb): Root bark

† Structure's reference

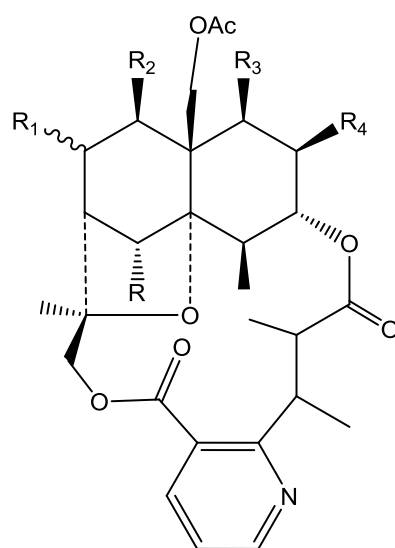
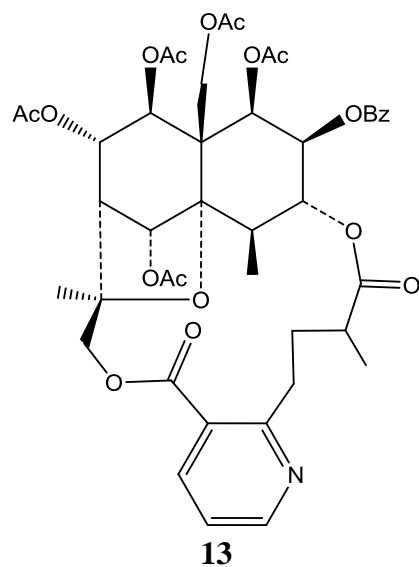


Compound	R	R ₁	R ₂	R ₃	R ₄
1	OAc	OAc	OCOC(CH ₃)=CHCH ₃	OAc	OAc
2	OAc	OAc	OBz	OH	OAc
3	OAc	OAc	ONic	OAc	OAc
4	OAc	OAc	OAc	OAc	OAc
5	OAc	OAc	OBz	OAc	OAc
6	OAc	OBz	OAc	OH	OAc
7	OBz	OAc	OBz	OAc	OAc
8	OAc	OAc	OBz	OAc	OBz



Compound	R ₁	R ₂
9	ONic	OAc
10	OBz	OAc
11	OAc	OAc
12	OAc	OBz

Figure 1.2: Structures of dihydro- β -agarofuran sesquiterpene pyridine alkaloids previously isolated from Chuchuguasa



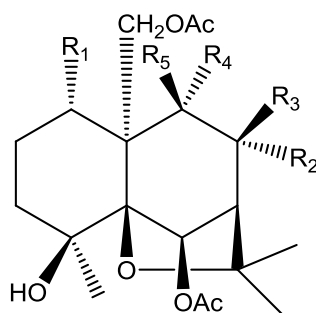
Compound	R	R ₁	R ₂	R ₃	R ₄
14	OAc	α -OAc	OAc	OAc	OAc
15	OAc	α -OAc	OAc	OBz	OAc
16	OAc	α -OAc	OAc	OAc	OBz
17	OH	α -OAc	OAc	OAc	OAc
18	OAc	α -OAc	OAc	OAc	OH
19	OAc	α -OAc	OAc	OBz	OBz
20	OAc	α -OBz	OAc	OBz	OAc
21	OAc	β -OAc	OAc	OAc	OAc

Figure 1.2 (cont.): Structures of dihydro- β -agarofuran sesquiterpene pyridine alkaloids previously isolated from Chuchuguasa

Table 1.2: Dihydro- β -agarofuran sesquiterpene polyol esters previously isolated from Chuchuguasa

Compounds isolated	Plant species (*)	Reference
6 β ,8 β ,15-triacetoxy-1 α ,9 α -dibenzoyloxy-4 β -hydroxy- β -dihydroagarofuran (22)	<i>M. macrocarpa</i> (leaves)	(Chávez <i>et al.</i> , 1999)
1 α ,6 β ,8 β ,15-tetraacetoxy-9 α -benzoyloxy-4 β -hydroxy- β -dihydroagarofuran (23)		
(1S,4S,6R,7R,8R,9R)-1,6,15-triacetoxy-8,9-dibenzoyloxy-4-hydroxy- β -dihydroagarofuran (24)		

* Studied plant part



Compound	R ₁	R ₂	R ₃	R ₄	R ₅
22	OBz	H	OAc	OBz	H
23	OAc	H	OAc	OBz	H
24	OAc	OBz	H	H	OBz

Figure 1.3: Structures of dihydro- β -agarofuran sesquiterpene polyol esters previously isolated from Chuchuguasa

Table 1.3: Triterpenoids and sterols previously isolated from Chuchuguasa

Compounds isolated	Plant species (*)	Reference
3 α ,22 β -dihydroxyolean-12-en-29-oic acid (25)	<i>M. laevis</i> (b)	(Nakagawa <i>et al.</i> , 2004)
3 β ,22 β -dihydroxyolean-12-en-29-oic acid or (22- <i>epi</i> -maytenfolic acid) (26)	<i>M. laevis</i> (b)	(Nakagawa <i>et al.</i> , 2004)/ (Kutney <i>et al.</i> , 1992)/ (Piacente <i>et al.</i> , 2006)
Maytenfolic acid (27)	<i>M. macrocarpa</i> (b) <i>M. laevis</i> (b)/ <i>M. macrocarpa</i> (b)	(Nakagawa <i>et al.</i> , 2004)/ (Nozaki <i>et al.</i> , 1986)/ (Piacente <i>et al.</i> , 2006)
Triptocallic acid D (28) Triptocallic acid A (29)	<i>M. laevis</i> (b)	(Nakagawa <i>et al.</i> , 2004)/ (Nakano <i>et al.</i> , 1997)
3 β ,22 α -dihydroxy-olean-12-en-30-oic acid (Macrocarpoic acid A) (30)	<i>M. macrocarpa</i> (b)	(Piacente <i>et al.</i> , 2006)
Epikatonic acid (31)	<i>M. laevis</i> (b)	(Nakagawa <i>et al.</i> , 2004)/ (Fujita <i>et al.</i> , 2000)
22 β -hydroxy-3-oxoolean-12-en-oic acid or (22- <i>epi</i> -triptotriterpenonic acid A) (32)	<i>M. laevis</i> (b) <i>M. macrocarpa</i> (b)	(Nakagawa <i>et al.</i> , 2004)/ (Kutney <i>et al.</i> , 1992)/ (Piacente <i>et al.</i> , 2006)
3-oxoolean-12-en-oic acid (33)	<i>M. laevis</i> (b)	(Nakagawa <i>et al.</i> , 2004)/ (Sousa <i>et al.</i> , 1990)
22 α -hydroxy-olean-12-en-3-oxo-30-oic acid (Macrocarpoic acid B) (34) 22 α -hydroxy-12-en-3-oxo-29-oic acid (Triptotriterpenonic acid A) (35)	<i>M. macrocarpa</i> (b)	(Piacente <i>et al.</i> , 2006)
3-Oxo-6 β -hydroxyolean-12-ene (daturaolone) (36)	<i>M. macrocarpa</i> (Sb exudate)	(Chávez <i>et al.</i> , 1997)/ (Kocór <i>et al.</i> , 1973)
Abruslactone A (37)	<i>M. laevis</i> (b)	(Nakagawa <i>et al.</i> , 2004)/ (Nozaki <i>et al.</i> , 1986)
3- <i>epi</i> abruslactone A (38)	<i>M. laevis</i> (b)	(Nakagawa <i>et al.</i> , 2004)/ (Silva <i>et al.</i> , 1998)
28-hydroxy-12-ursene-3 β -yl-caffeate (3-(<i>E</i>)-caffeoyluvaol) (39)	<i>M. laevis</i> (b) <i>M. macrocarpa</i> (b)	Nakagawa <i>et al.</i> , 2004/ (Piacente <i>et al.</i> , 2006)
3-(<i>E</i>)- <i>p</i> -coumaroyluvaol (Macrocarpol A) (40)	<i>M. macrocarpa</i> (b)	(Piacente <i>et al.</i> , 2006)
Krukovine A (41) Krukovine B (42) Krukovine C (43) Krukovine D (44) Krukovine E (45)	<i>M. krukovii</i> (Sb)	(Shirota <i>et al.</i> , 1996)

* Studied plant parts; (b): bark, (Sb): Stem bark, (Rb): Root bark

Table 1.3 (Cont.): Triterpenoids and sterols previously isolated from *Chuchuguasa*

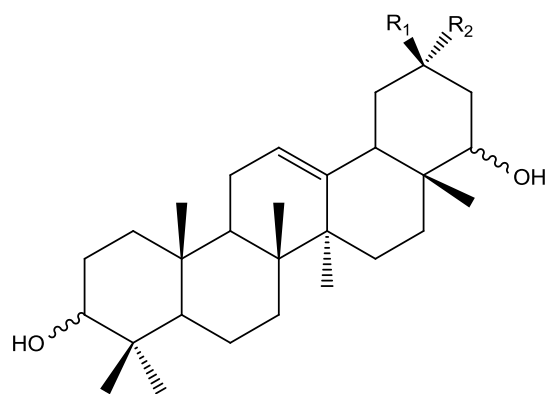
Compounds isolated	Plant species (*)	Reference
Wilforlide B (46)	<i>M. laevis</i> (b)	(Nakagawa <i>et al.</i> , 2004)/ (Luo <i>et al.</i> , 2007)
Macrocarpins A (47)	<i>M. macrocarpa</i> (R)	(Chávez <i>et al.</i> , 2000)
Macrocarpins B (48)		
Macrocarpins C (49)		
Macrocarpins D (50)		
Lupeol (51)	<i>M. macrocarpa</i> (leaves)	(Chávez <i>et al.</i> , 1999)/ (Magalhães <i>et al.</i> , 2011)
3-(<i>E</i>)- <i>p</i> -coumaroylbetulin (52)	<i>M. macrocarpa</i> (b)	(Piacente <i>et al.</i> , 2006)
3-(<i>Z</i>)- <i>p</i> -coumaroylbetulin (53)		
3-(<i>E</i>)-caffeoylbetulin (54)		
Nepeticin (55)		
Canophyllol (56)	<i>M. laevis</i> (b)	(Nakagawa <i>et al.</i> , 2004)/ (Nozaki <i>et al.</i> , 1986)/
	<i>M. macrocarpa</i> (Sb exudate)	(Chávez <i>et al.</i> , 1997)/ (Chávez <i>et al.</i> , 1998)
Friedelin (57)	<i>M. macrocarpa</i> (Sb exudate)/ (leaves)	(Chávez <i>et al.</i> , 1997)/ (Chávez <i>et al.</i> , 1999)
Epifriedelinol (58)	<i>M. macrocarpa</i> (leaves)	(Chávez <i>et al.</i> , 1999)/ (Betancor <i>et al.</i> , 1980)
3-Oxo-29-hydroxyfriedelane (59)	<i>M. macrocarpa</i> (Sb exudate)	(Chávez <i>et al.</i> , 1997)/ (Chávez <i>et al.</i> , 1998)
3-Oxofriedelan-25-al (60)		(Chávez <i>et al.</i> , 1998)/ (Anjaneyulu and Narayanarao, 1980)
28-Hydroxyfriedelane-1,3-dione (61)	<i>M. macrocarpa</i> (Sb exudate)	(Chávez <i>et al.</i> , 1998)
Salaspermic acid (62)	<i>M. laevis</i> (b)	(Nakagawa <i>et al.</i> , 2004)/ (Viswanathan, 1979)
Orthosphenic acid (63)	<i>M. macrocarpa</i> (b)	(Piacente <i>et al.</i> , 2006)
3 β ,29-dihydroxyglutin-5-ene (64)	<i>M. macrocarpa</i> (Sb exudate)	(Chávez <i>et al.</i> , 1997)/ (González <i>et al.</i> , 1987)

* Studied plant parts; (b): bark, (Sb): Stem bark, (Rb): Root bark

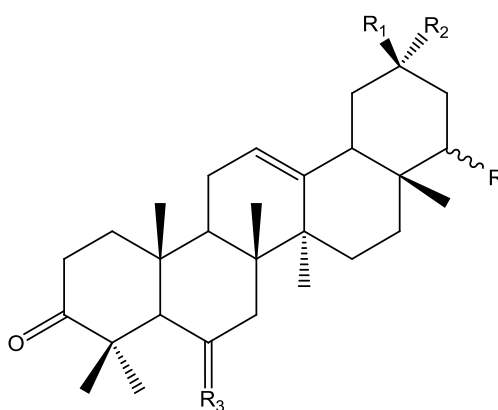
Table 1.3 (Cont.): Triterpenoids and sterols previously isolated from *Chuchuguasa*

Compounds isolated	Plant species (*)	Reference
Tingenone (65)	<i>M. laevis</i> (Rb) <i>M. chuchuhuasca</i> <i>M. chuchuhuasca</i> (b) <i>M. chuchuhuasca</i> (Sb) <i>M. macrocarpa</i> (Sb exudate)	(Gonzalez <i>et al.</i> , 1982)/ (Martinod <i>et al.</i> , 1976)/ (Morita <i>et al.</i> , 2008)/ (Shirota <i>et al.</i> , 1994a)/ (Chávez <i>et al.</i> , 1997)
22 β -hydroxytingenone (66)	<i>M. laevis</i> (Rb) <i>M. chuchuhuasca</i> (Sb) <i>M. chuchuhuasca</i> (b)	(Gonzalez <i>et al.</i> , 1982)/ (Shirota <i>et al.</i> , 1994a)/ (Morita <i>et al.</i> , 2008)
Pristimerin (67)	<i>M. chuchuhuasca</i> <i>M. chuchuhuasca</i> (b) <i>M. chuchuhuasca</i> (Sb) <i>M. macrocarpa</i> (Sb exudate)	(Martinod <i>et al.</i> , 1976)/ (Morita <i>et al.</i> , 2008)/ (Shirota <i>et al.</i> , 1994a)/ (Chávez <i>et al.</i> , 1997)/
Celastrol (68)	<i>M. chuchuhuasca</i> (b) <i>M. macrocarpa</i> (Sb exudate)	(Morita <i>et al.</i> , 2008)/ (Chávez <i>et al.</i> , 1997)
Netzahualcoyene (Vitideasin) (69)	<i>M. macrocarpa</i> (Sb exudate)	(Chávez <i>et al.</i> , 1997)
Scutione (70)	<i>M. macrocarpa</i> (Sb exudate)	(Chávez <i>et al.</i> , 1997)/ (González <i>et al.</i> , 1996)
6-oxopristimerol (71)	<i>M. chuchuhuasca</i> (Sb)	(Shirota <i>et al.</i> , 1994a)
3-methyl-6-oxotingenol (72)		
3-methyl-22 β ,23-dihydroxy-6-oxotingenol (73)		
β -sitosterol (74)	<i>M. laevis</i> (b)	(Nakagawa <i>et al.</i> , 2004)/ (Sousa <i>et al.</i> , 1990)

* Studied plant parts; (b): bark, (Sb): Stem bark, (Rb): Root bark

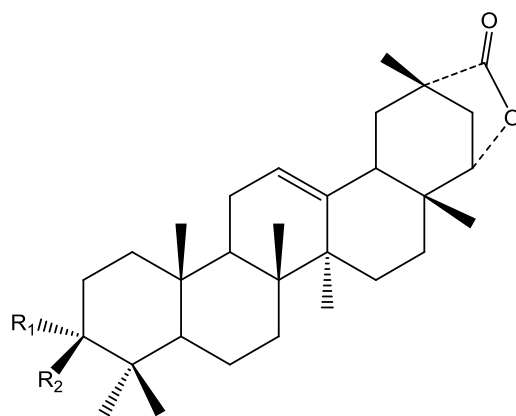


Compound	R ₁	R ₂	3-OH	22-OH
25	Me	COOH	α	β
26	Me	COOH	β	β
27	Me	COOH	β	α
28	Me	COOH	α	α
29	H	COOH	α	α
30	COOH	Me	β	α
31	Me	COOH	β	-



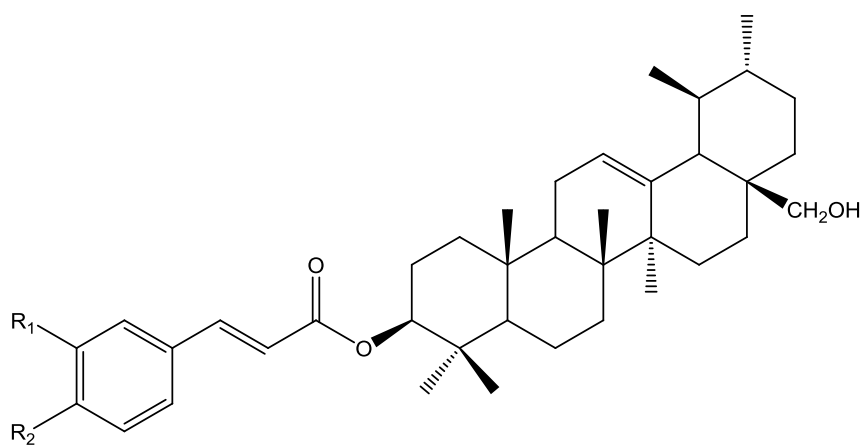
Compound	R	R ₁	R ₂	R ₃
32	β-OH	Me	COOH	2H
33	H	Me	COOH	2H
34	α-OH	COOH	Me	2H
35	α-OH	Me	COOH	2H
36	H	Me	Me	β-OH, H

Figure 1.4: Structures of triterpenoids and sterols previously isolated from Chuchuguasa



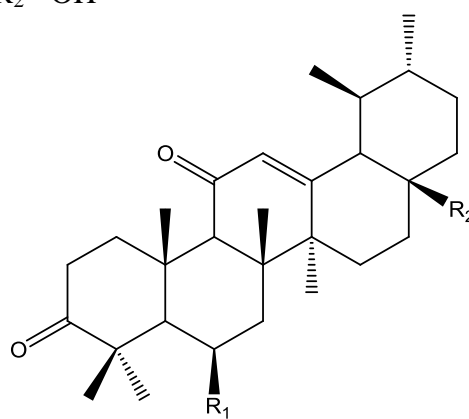
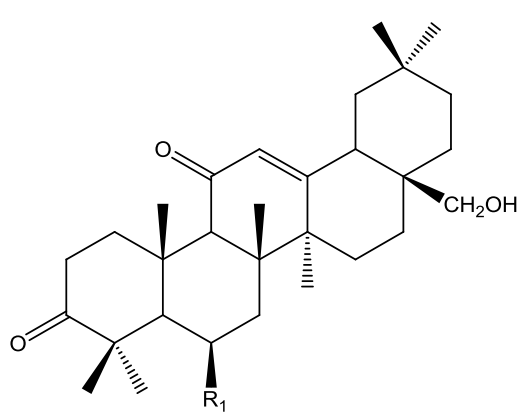
37 R₁= H, R₂= OH

38 R₁= OH, R₂= H



39 R₁= OH, R₂= OH

40 R₁= H, R₂= OH



Compound	R ₁
41	H
43	OH

Compound	R ₁	R ₂
42	H	CH ₂ OH
44	OH	CH ₂ OH
45	H	OH

Figure 1.4 (Cont.): Structures of triterpenoids and sterols previously isolated from Chuchuguasa

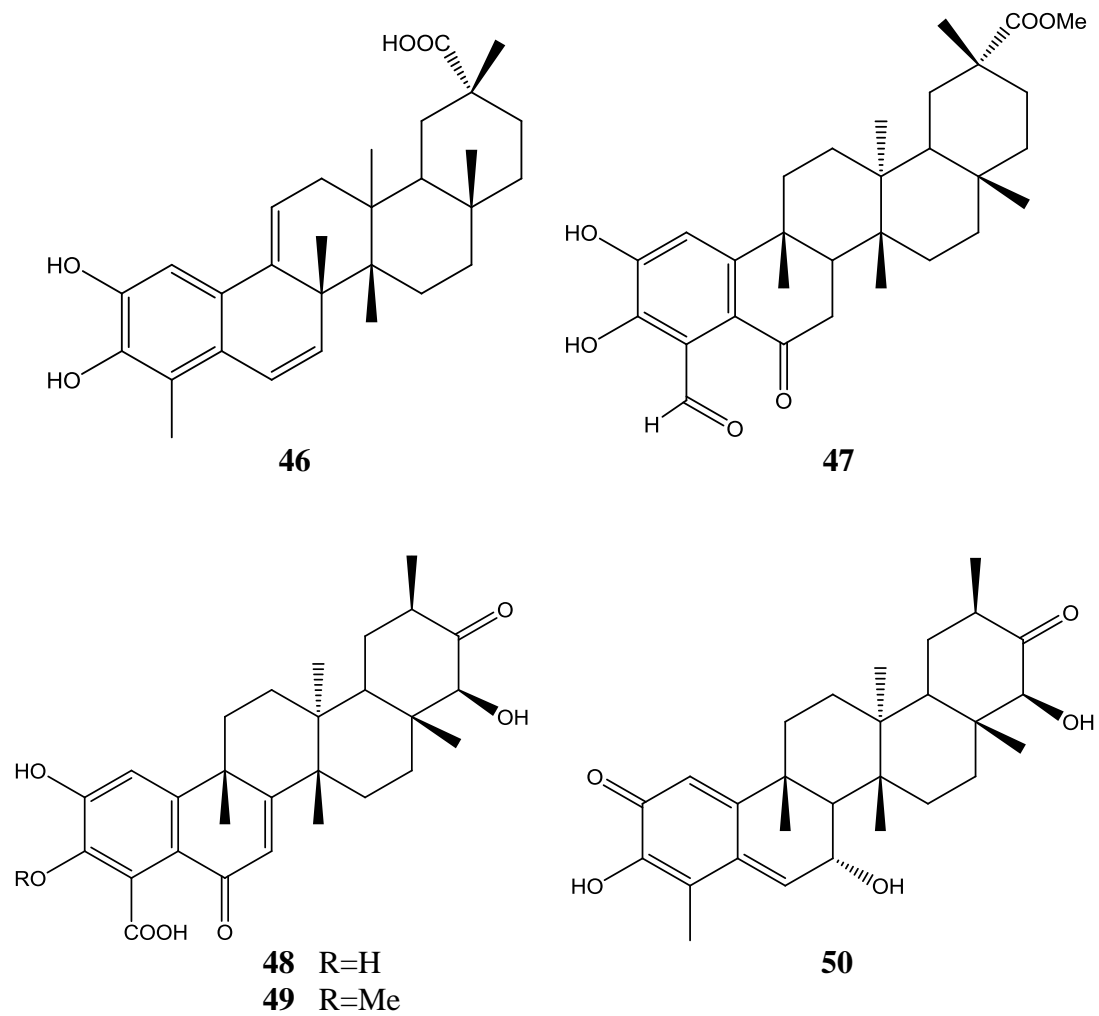
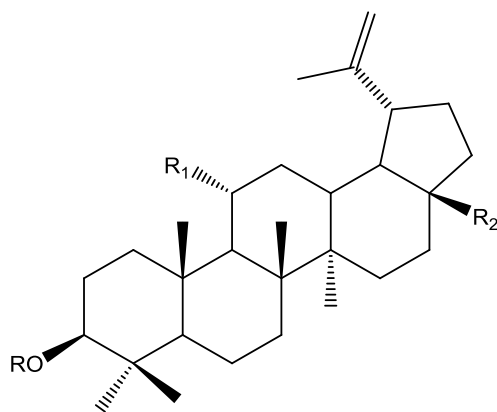
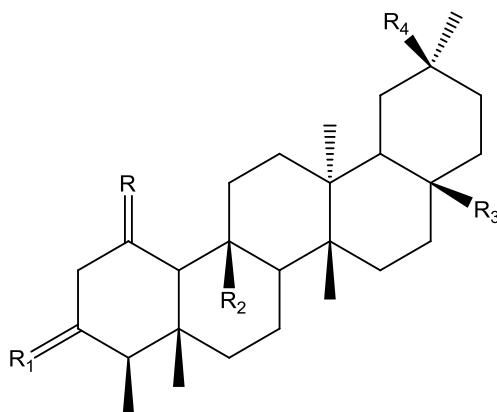


Figure 1.4 (Cont.): Structures of triterpenoids and sterols previously isolated from Chuchuguasa



Compound	R	R ₁	R ₂
51	H	H	Me
52		H	CH ₂ OH
53		H	CH ₂ OH
54		H	CH ₂ OH
55	H	OH	Me



Compound	R	R ₁	R ₂	R ₃	R ₄
56	2H	O	Me	CH ₂ OH	Me
57	2H	O	Me	Me	Me
58	2H	β-OH, H	Me	Me	Me
59	2H	O	Me	Me	CH ₂ OH
60	2H	O	CHO	Me	Me
61	O	O	Me	CH ₂ OH	Me

Figure 1.4 (Cont.): Structures of triterpenoids and sterols previously isolated from Chuchuguasa

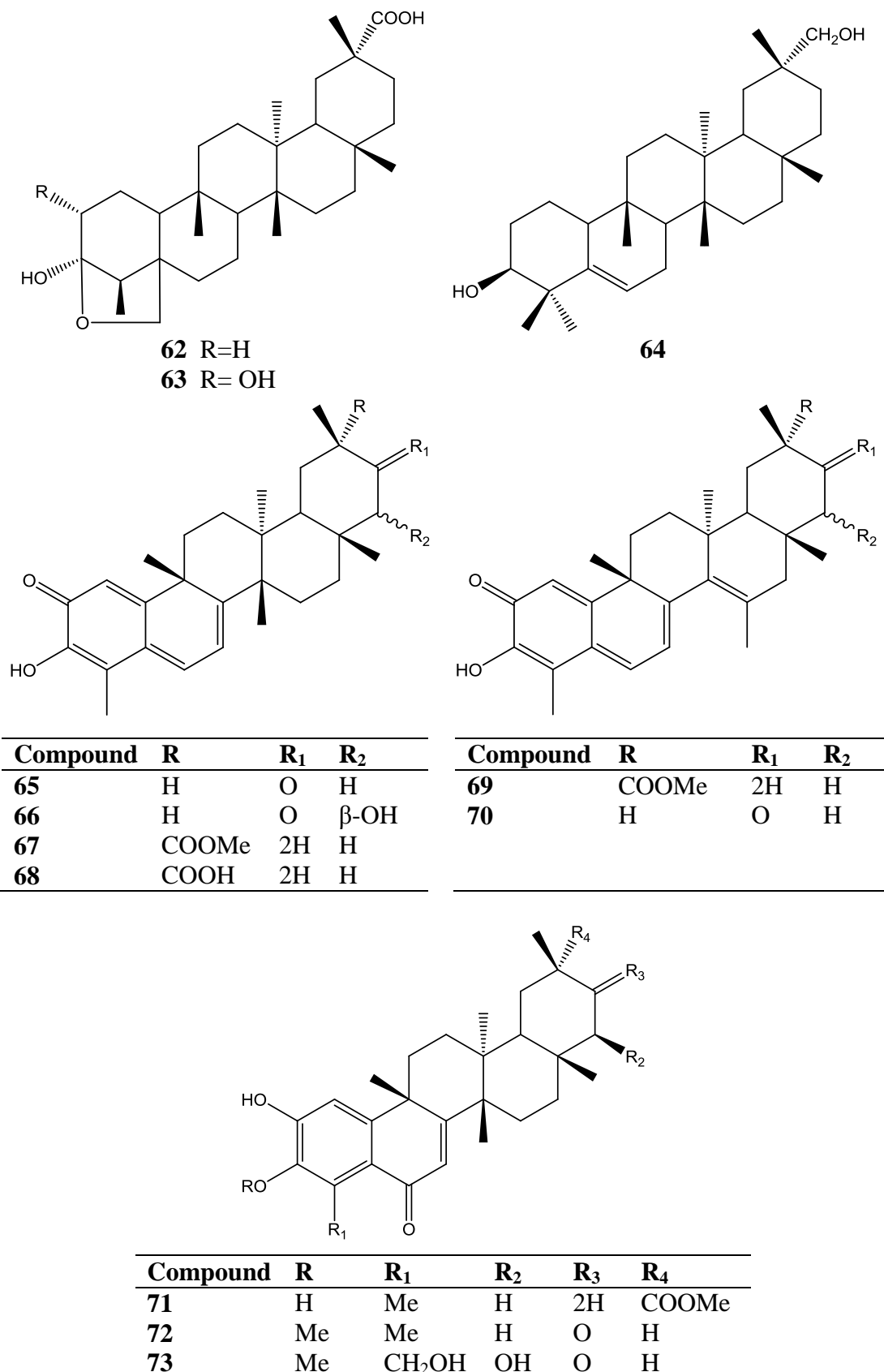


Figure 1.4 (Cont.): Structures of triterpenoids and sterols previously isolated from Chuchuguasa

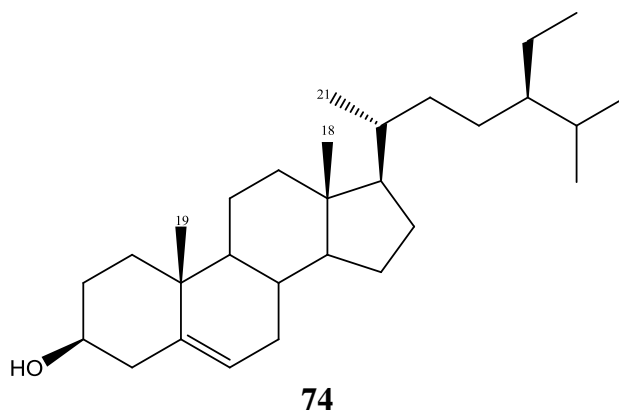
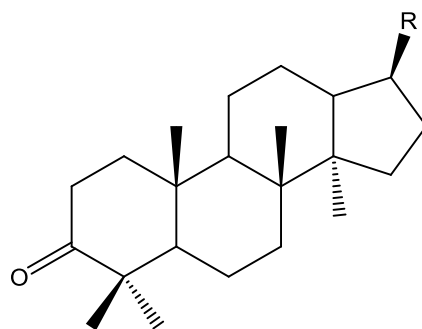


Figure 1.4 (Cont.): Structures of triterpenoids and sterols previously isolated from Chuchuguasa

Table 1.4: Dammarane triterpenes previously isolated from Chuchuguasa

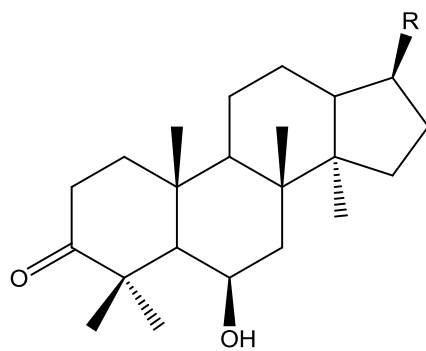
Compounds isolated	Plant species (*)	Reference
24-(<i>E</i>)-3-oxo-dammara-20,24-dien-26-al (75)	<i>M. macrocarpa</i> (Sb exudate)	(Chávez <i>et al.</i> , 1997)
24-(<i>Z</i>)-3-oxo-dammara-20,24-dien-26-al (76)		
24-(<i>E</i>)-3-oxo-dammara-20,24-dien-26-ol (77)		
24-(<i>E</i>)-3-oxo-dammara-23 α -hydroxy-20,24-dien-26-al (78)		
24-(<i>E</i>)-3-oxo-dammara-23 β -hydroxy-20,24-dien-26-al (79)		
23-(<i>Z</i>)-3,25-dioxo-25-nor-dammara-20,24-diene (80)		
24-(<i>E</i>)-3-oxo-23-methylene-dammara-20,24-dien-26-oico (81)		
24-(<i>Z</i>)-3-oxodammara-20(21),24-dien-27-oic acid (82)	<i>M. macrocarpa</i> (Sb exudate)	(Torpocco <i>et al.</i> , 2007)
24-(<i>E</i>)-3-oxo-dammara-6 β -hydroxy-20,24-dien-26-al (83)	<i>M. macrocarpa</i> (Sb exudate)	(Chávez <i>et al.</i> , 1997)
24-(<i>E</i>)-3-oxo-dammara-6 β -hydroxy-20,24-dien-26-ol (84)		
Octa- <i>nor</i> -13-hydroxydammara-1-en-3,17-dione (85)	<i>M. macrocarpa</i> (Sb exudate)	(Torpocco <i>et al.</i> , 2007)

* Studied plant parts:(Sb): Stem bark



Compound	R
75 24-E 76 24-Z	
77	
78 23(α)-OH 79 23-(β)-OH	
80	
81	
82	

Figure 1.5: Structures of dammarane triterpenes previously isolated from Chuchuguasa



Compound	R
83	
84	

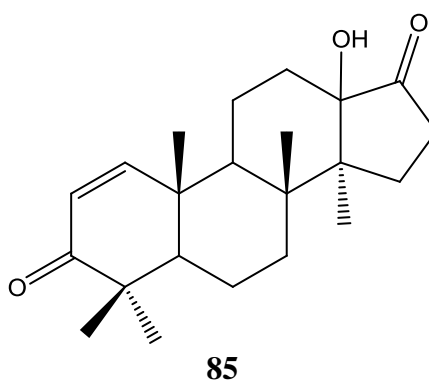


Figure 1.5 (Cont.): Structures of dammarane triterpenes previously isolated from Chuchuguasa

Table 1.5: Triterpene dimers previously isolated from Chuchuguasa

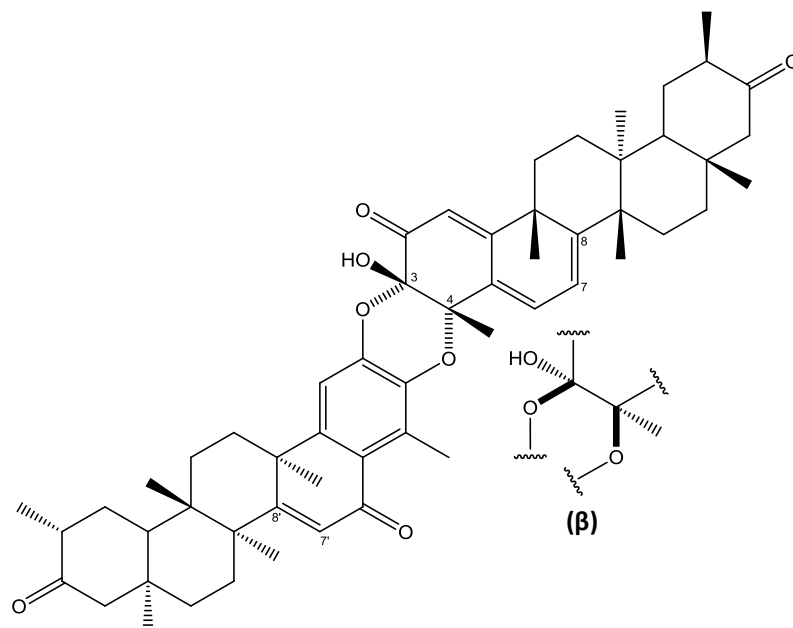
Compounds isolated	Plant species (*)	Reference
Xuxuarine A α (86) Xuxuarine A β (87)	<i>M. chuchhuasca</i> (Sb)	(Shirota <i>et al.</i> , 1995)
7',8'-dihydroxuxuarine A α (88)	<i>M. chuchhuasca</i> (Sb)	(Shirota <i>et al.</i> , 2004b)
7',8'-dihydroxuxuarine A β (89)	<i>M. chuchhuasca</i> (Sb)	(Shirota <i>et al.</i> , 1995)
7,8-dihydroxuxuarine A α (90)	<i>M. chuchhuasca</i> (Sb)	(Shirota <i>et al.</i> , 1997b)
Xuxuarine B α (91) Xuxuarine B β (92) Xuxuarine C α (93) Xuxuarine C β (94) Xuxuarine D α (95) Xuxuarine D β (96)	<i>M. chuchhuasca</i> (Sb)	(Shirota <i>et al.</i> , 1995)
7',8'-dihydroxuxuarine D β (97)	<i>M. chuchhuasca</i> (Sb)	(Shirota <i>et al.</i> , 2004b)
Xuxuarine E β (98)	<i>M. chuchhuasca</i> (Sb)	(Shirota <i>et al.</i> , 1997b)
Xuxuarine F α (99)	<i>M. chuchhuasca</i> (Sb)	(Shirota <i>et al.</i> , 2004b)
Xuxuarine F β (100) Xuxuarine G α (101) Xuxuarine G β (102)	<i>M. chuchhuasca</i> (Sb)	(Shirota <i>et al.</i> , 1998)

* Studied plant parts; (Sb): Stem bark

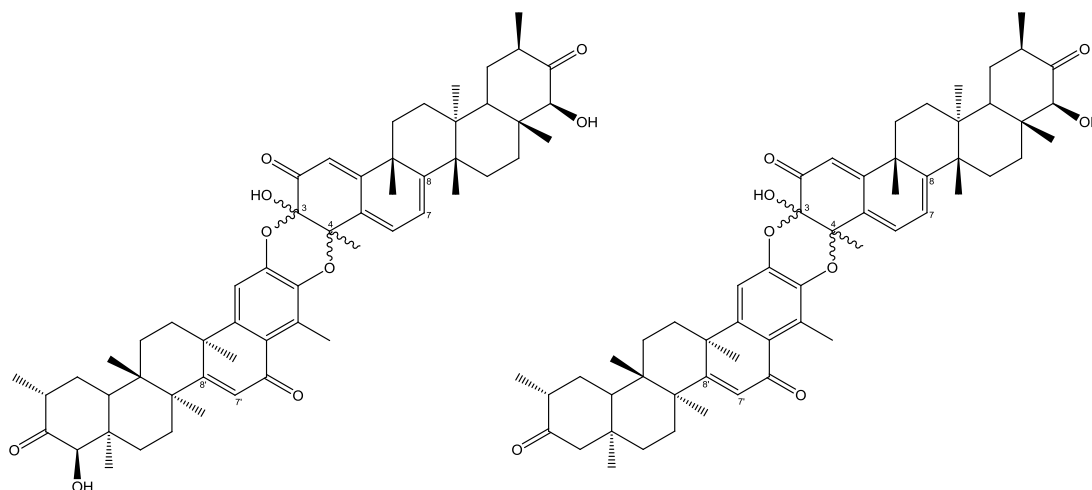
Table 1.5 (Cont.): Triterpene dimers previously isolated from Chuchuguasa

Compounds isolated	Plant species (*)	Reference
Isoxuxuarine A α (103) Isoxuxuarine A β (104) 7,8-dihydroisoxuxuarine A α (105)	<i>M. chuchhuasca</i> (Sb)	(Shirota <i>et al.</i> , 1997b)
Isoxuxuarine B α (106) Isoxuxuarine B β (107) 7,8-dihydroisoxuxuarine B α (108) Isoxuxuarine C α (109) Isoxuxuarine C β (110) 7,8-dihydroisoxuxuarine C α (111) Isoxuxuarine D α (112) Isoxuxuarine D β (113) 7,8-dihydroisoxuxuarine D α (114)	<i>M. chuchhuasca</i> (Sb)	(Shirota <i>et al.</i> , 2004c)
Scutidin α A (115)	<i>M. chuchhuasca</i> (Sb)	(Shirota <i>et al.</i> , 1998)
Isoxuxuarine E β (116)	<i>M. chuchhuasca</i> (Sb)	(Shirota <i>et al.</i> , 2004b)
7,8-dihydroisoxuxuarine E α (117)	<i>M. chuchhuasca</i> (Sb)	(Shirota <i>et al.</i> , 1998)
7 α -hydroxyisoxuxuarine E α (118) Isoxuxuarine F α (Cangorosin B) (119) 7,8-dihydroisoxuxuarine F α (120) Isoxuxuarine G β (121) 7,8-dihydroisoxuxuarine G α (122)	<i>M. chuchhuasca</i> (Sb)	(Shirota <i>et al.</i> , 2004b)
Xuxuasin A (123)	<i>M. chuchhuasca</i> (Sb)	(Shirota <i>et al.</i> , 2004d)
Xuxuasin B (124)	<i>M. chuchhuasca</i> (Sb)	(Shirota <i>et al.</i> , 2004d)

* Studied plant parts; (Sb): Stem bark

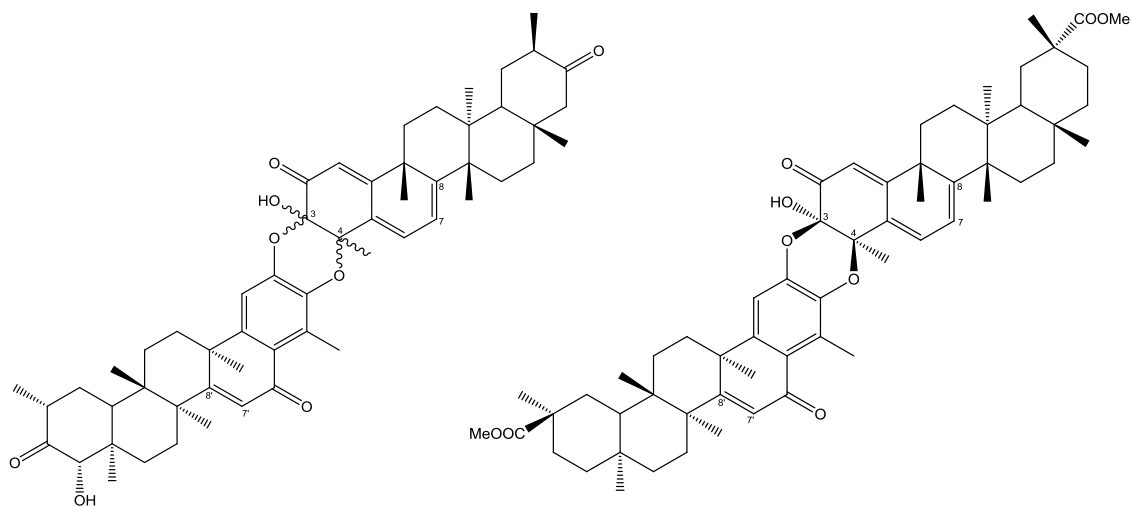


Compound	
86	<i>cis</i> -3,4-dioxy bond = α
87	<i>cis</i> -3,4-dioxy bond = β
88	7',8'-dihydro derivative of 86
89	7',8'-dihydro derivative of 87
90	7,8-dihydro derivative of 86

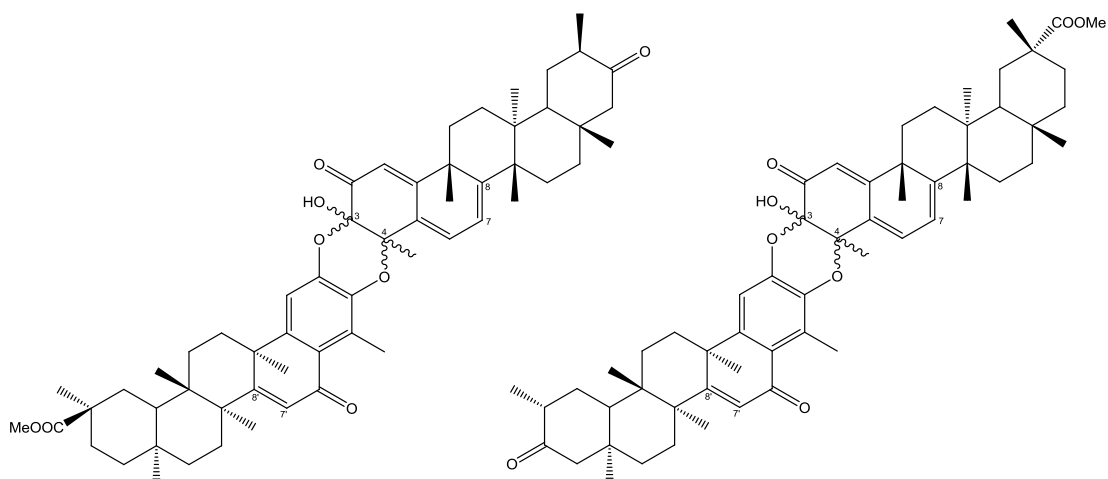


Compound		Compound	
91	<i>cis</i> -3,4-dioxy bond = α	93	<i>cis</i> -3,4-dioxy bond = α
92	<i>cis</i> -3,4-dioxy bond = β	94	<i>cis</i> -3,4-dioxy bond = β

Figure 1.6: Structures of the triterpene dimers previously isolated from Chuchuguasa

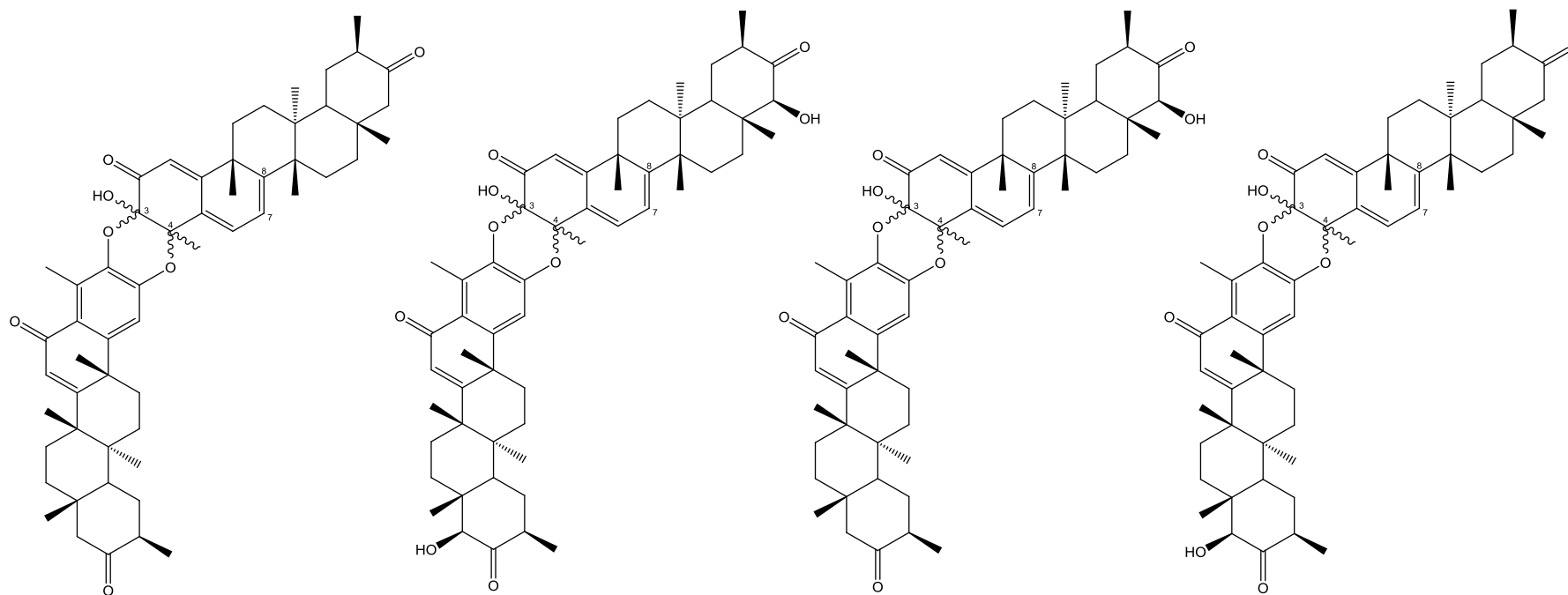


Compound	Compound
95 <i>cis</i> -3,4-dioxy bond = α	98 <i>cis</i> -3,4-dioxy bond = β
96 <i>cis</i> -3,4-dioxy bond = β	
97 7',8'-dihydro derivative of 96	



Compound	Compound
99 <i>cis</i> -3,4-dioxy bond = α	101 <i>cis</i> -3,4-dioxy bond = α
100 <i>cis</i> -3,4-dioxy bond = β	102 <i>cis</i> -3,4-dioxy bond = β

Figure 1.6 (Cont.): Structures of the triterpene dimers previously isolated from Chuchuguasa



Compound	Compound	Compound	Compound
103 <i>cis</i> -3,4-dioxy bond = α	106 <i>cis</i> -3,4-dioxy bond = α	109 <i>cis</i> -3,4-dioxy bond = α	112 <i>cis</i> -3,4-dioxy bond = α
104 <i>cis</i> -3,4-dioxy bond = β	107 <i>cis</i> -3,4-dioxy bond = β	110 <i>cis</i> -3,4-dioxy bond = β	113 <i>cis</i> -3,4-dioxy bond = β
105 7,8-dihydro deriv. of 103	108 7,8-dihydro deriv. of 106	111 7,8-dihydro deriv. of 109	114 7,8-dihydro deriv. of 112

Figure 1.6 (Cont.): Structures of the triterpene dimers previously isolated from Chuchuguasa

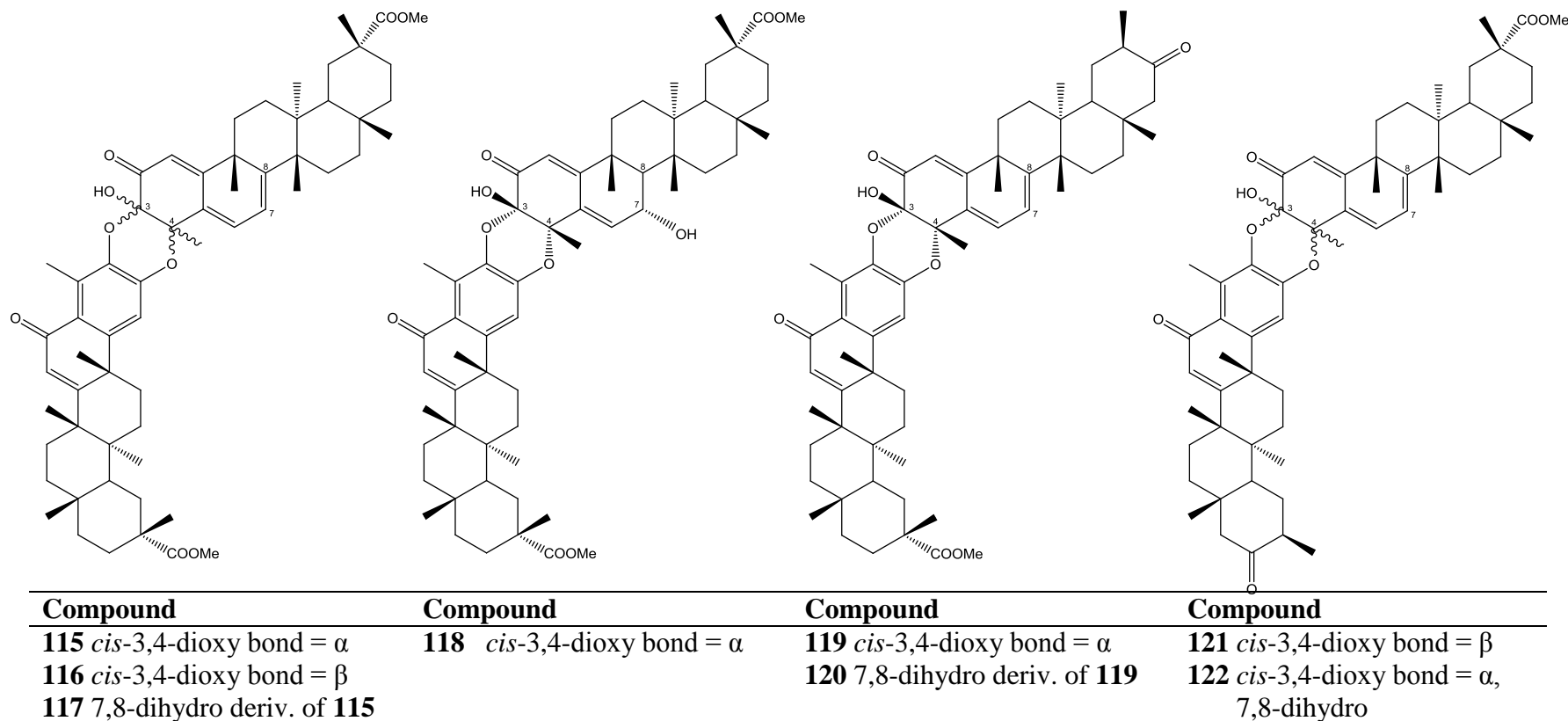


Figure 1.6 (Cont.): Structures of the triterpene dimers previously isolated from Chuchuguasa

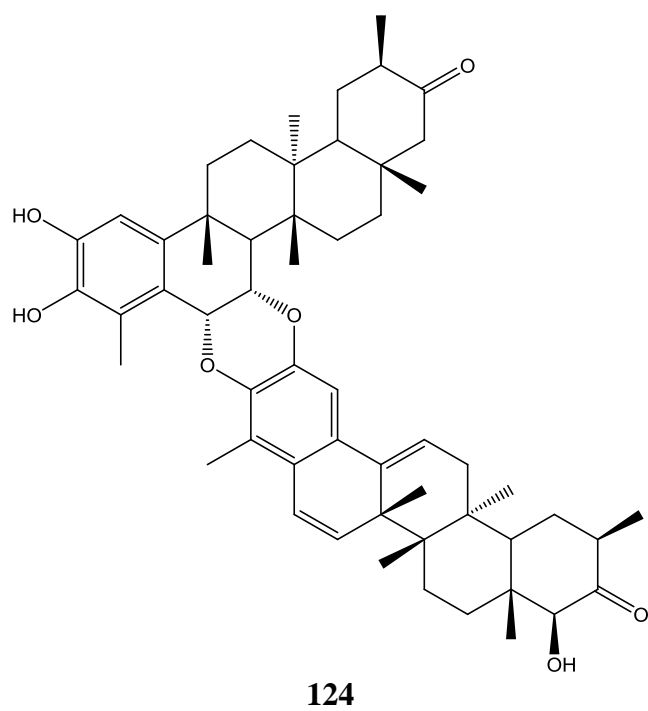
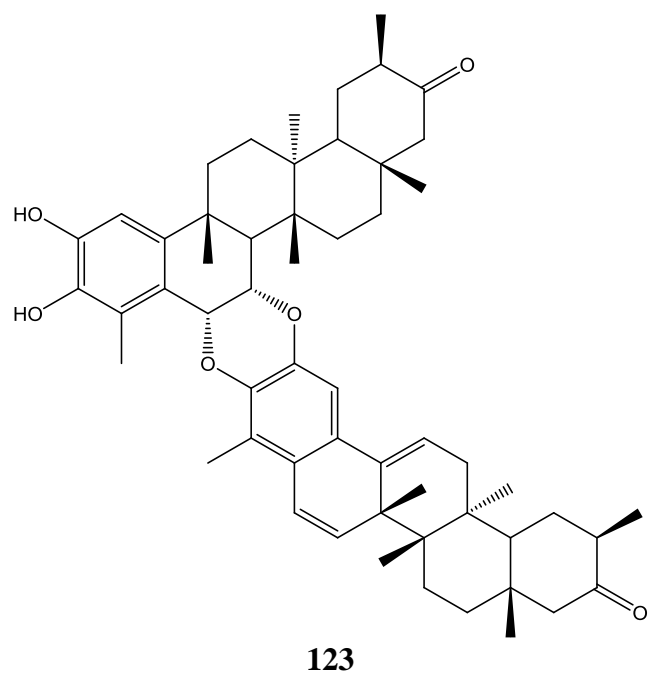
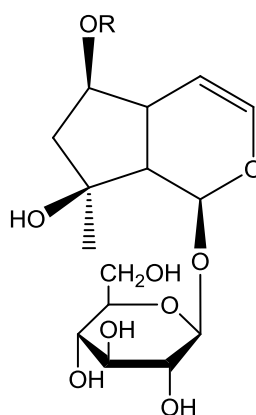


Figure 1.6 (Cont.): Structures of the triterpene dimers previously isolated from Chuchuguasa

Table 1.6: Iridoids previously isolated from Chuchuguasa

Compounds isolated	Plant species (*)	Reference
Ajugol (125)	<i>M. laevis</i> (b)	(Nakagawa <i>et al.</i> , 2004)/ (Nishimura <i>et al.</i> , 1989)
6- <i>O</i> -(3',4',5'-trimethoxybenzoyl) ajugol (126)	<i>M. laevis</i> (b)	(Nakagawa <i>et al.</i> , 2004)
6- <i>O</i> -(3',4'-dimethoxybenzoyl) ajugol (127)	<i>M. laevis</i> (b)	(Nakagawa <i>et al.</i> , 2004)/ (Nakano <i>et al.</i> , 1993)
6- <i>O</i> -(<i>p</i> -hydroxybenzoyl) ajugol (128)		
6- <i>O</i> -(4'-hydroxy-3'-methoxybenzoyl) ajugol (129)	<i>M. laevis</i> (b)	(Nakagawa <i>et al.</i> , 2004)/ (Iwagawa <i>et al.</i> , 1990)

* Studied plant parts; (b): bark



Compound	R
125	H
126	3',4',5'-trimethoxybenzoyl
127	3',4' – dimethoxybenzoyl
128	<i>p</i> -hydroxybenzoyl
129	4'-hydroxy-3'-methoxybenzoyl

Figure 1.7: Structures of iridoids previously isolated from Chuchuguasa

Table 1.7: Phenolics previously isolated from Chuchuguasa

Compounds isolated	Plant species (*)	Reference
<i>p</i> -Hydroxybenzaldehyde (130)	<i>M. macrocarpa</i> (Rb)	(Tizkova <i>et al.</i> , 2013)
<i>p</i> -Hydroxybenzoic acid (131)	<i>M. laevis</i> (b)	(Nakagawa <i>et al.</i> , 2004)/
	<i>M. macrocarpa</i> (Rb)	(Tizkova <i>et al.</i> , 2013)
<i>p</i> -Hydroxybenzoic acid methyl ester (132)	<i>M. macrocarpa</i> (Rb)	(Tizkova <i>et al.</i> , 2013)
<i>p</i> -Hydroxybenzoic acid ethyl ester (133)		
3,4,5-Trimethoxybenzyl alcohol (134)		
Noreugenin (135)		
(2 <i>R</i> ,3 <i>S</i>)-4'- <i>O</i> -Methyl-2,3-dihydromyricetin (136)	<i>M. laevis</i> (b)	(Nakagawa <i>et al.</i> , 2004)
Mearnsetin (137)	<i>M. laevis</i> (b)	(Nakagawa <i>et al.</i> , 2004)/ (Sadasivam and Kumaresan, 2011)
(-)-4'- <i>O</i> -Methylepigallocatechin (Ourateacatechin) (138)	<i>M. laevis</i> (b)	(Nakagawa <i>et al.</i> , 2004)/ (Hussein <i>et al.</i> , 1999)/ <i>M. laevis</i> (Rb) (Gonzalez <i>et al.</i> , 1982)
3',4'-Di- <i>O</i> -methyl(-)-epicatechin (139)	<i>M. laevis</i> (b)	(Nakagawa <i>et al.</i> , 2004)/ (Morimoto <i>et al.</i> , 1985)
Ourateproanthocyanidin A (140)	<i>M. laevis</i> (b)	(Nakagawa <i>et al.</i> , 2004)/ (Weeratunga <i>et al.</i> , 1985)/ <i>M. laevis</i> (Rb) (Gonzalez <i>et al.</i> , 1982)
Ourateproanthocyanidin B	<i>M. laevis</i> (Rb)	(Gonzalez <i>et al.</i> , 1982)

* Studied plant parts; (Rb): Stem bark, (b): bark

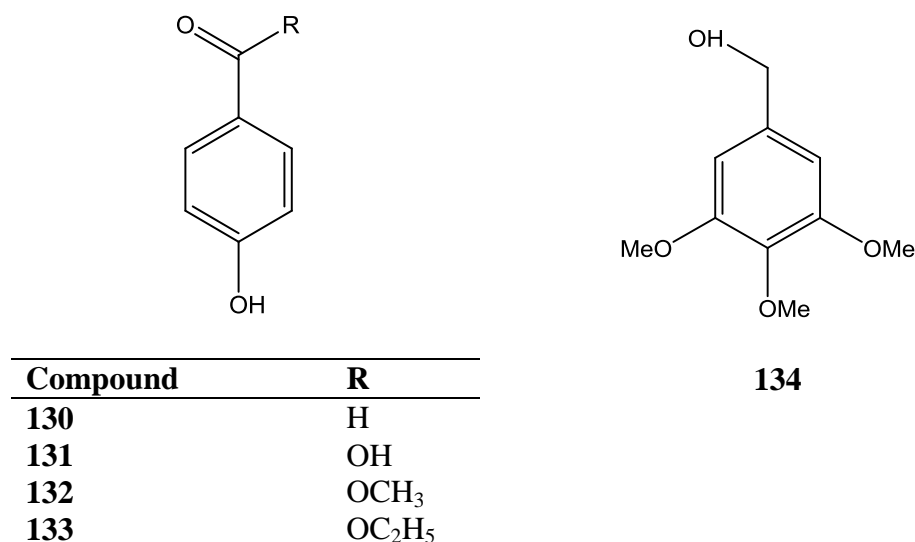
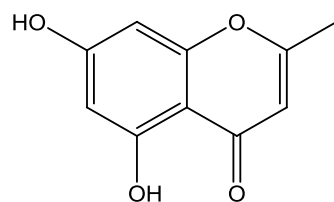
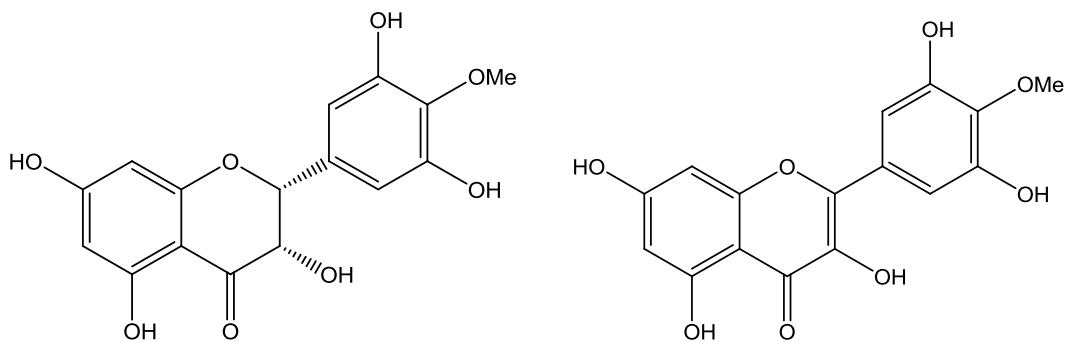


Figure 1.8: Structures of phenolics previously isolated from Chuchuguasa

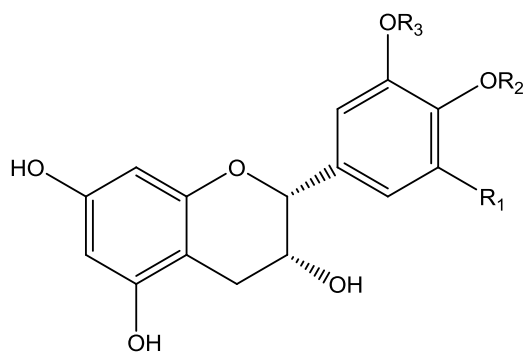


135

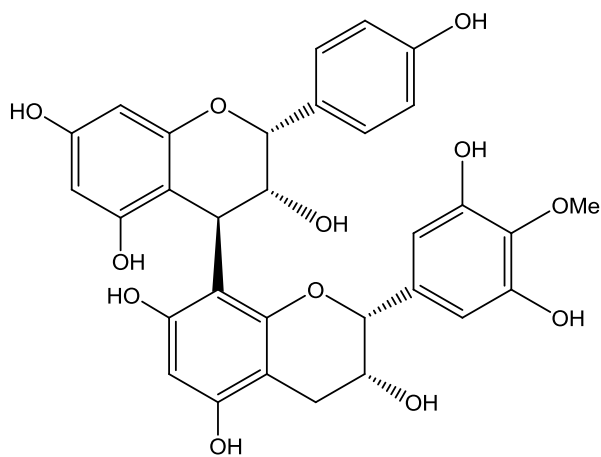


136

137



Compound	R ₁	R ₂	R ₃
138	OH	Me	H
139	H	Me	Me



140

Figure 1.8 (Cont.): Structures of phenolics previously isolated from Chuchuguasa

Table 1.8: Miscellaneous compounds previously isolated from Chuchuguasa

Compounds isolated	Plant species (*)	Reference
Lambertic acid (141)	<i>M. laevis</i> (b)	(Nakagawa <i>et al.</i> , 2004)/ (Campello <i>et al.</i> , 1975)
<i>Ent</i> -isolariciresinol (142)	<i>M. laevis</i> (b)	(Nakagawa <i>et al.</i> , 2004)/ (Urones <i>et al.</i> , 1987)
(-)-secoisolariciresinol,4- <i>O</i> - β -D-(6- <i>O</i> -veratroyl) glucopyranoside (143)	<i>M. laevis</i> (b)	(Nakagawa <i>et al.</i> , 2004)
Isoverbascoside (144)	<i>M. laevis</i> (b)	(Nakagawa <i>et al.</i> , 2004)/ (Kanchanapoom <i>et al.</i> , 2002)
Lutein (145)	<i>M. macrocarpa</i> (leaves)	(Chávez <i>et al.</i> , 1999)

* Studied plant parts; (b): bark

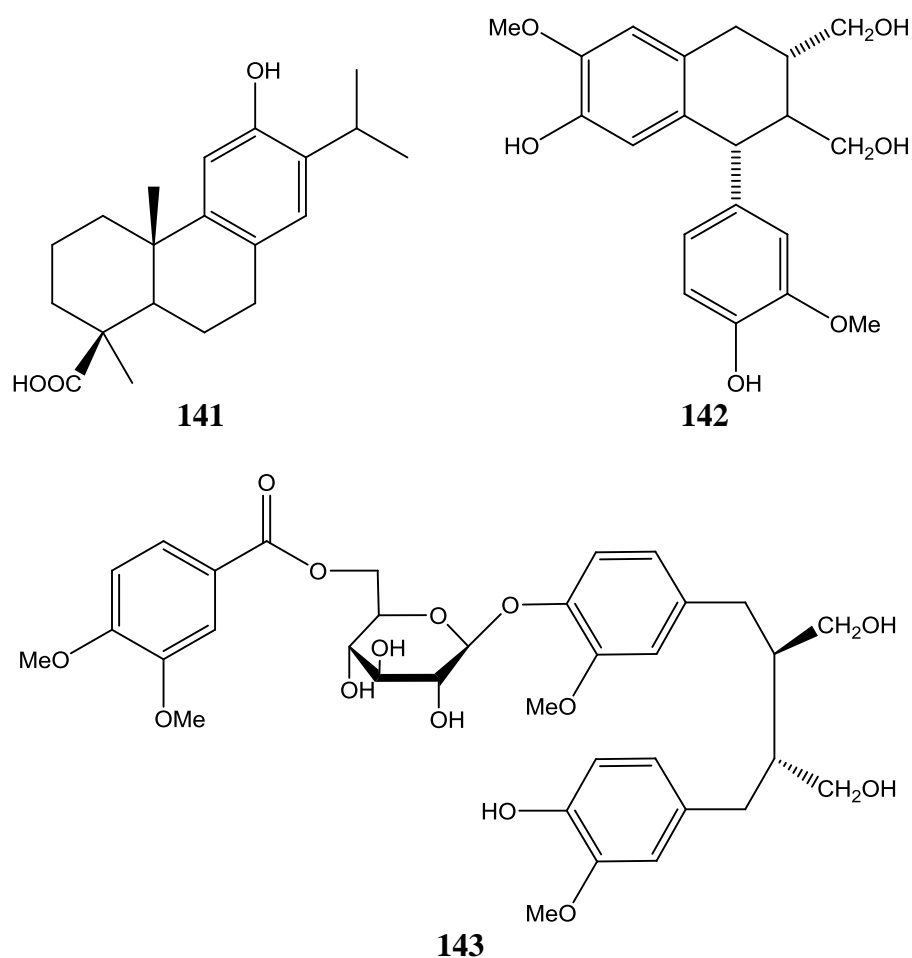


Figure 1.9: Structures of miscellaneous compounds previously isolated from Chuchuguasa

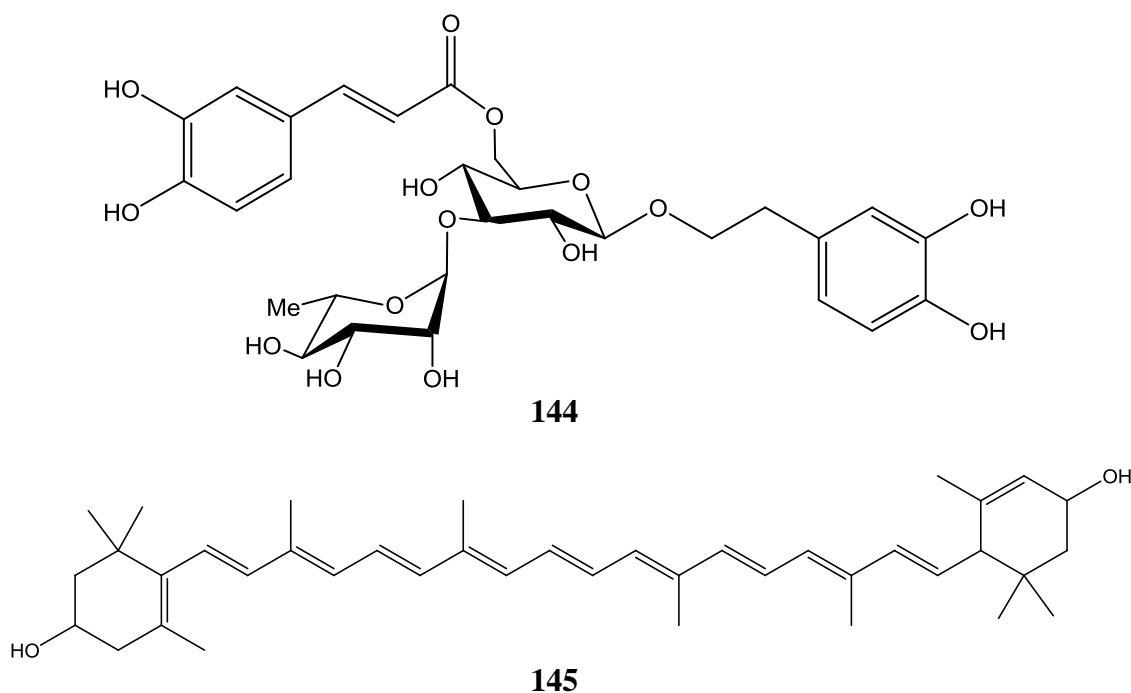


Figure 1.9 (Cont.): Structures of miscellaneous compounds previously isolated from Chuchuguasa

1.5.4 Previous pharmacological reports on Chuchuguasa

The majority of the aforementioned compounds and/ or crude extracts were tested for their activities in various biological domains. This section will encompass these studies by addressing them according to each plant species studied.

1.5.4.1 *M. laevis*

The intravenous administration of a suspension of pulverised leaves of *M. laevis* in physiological saline (15 mg/kg) to mice subsequently challenged with Gram positive pathogenic microorganisms, *Staphylococcus aureus* Smith and β -hemolytic *Streptococcus pyogenes*, induced prophylactic activity by increasing phagocytosis of the reticuloendothelial system (RES) (DiCarlo *et al.*, 1964).

Some compounds isolated from the methanol extract of the bark have been shown to have cytokine-inducing activity (Nakagawa *et al.*, 2004). To investigate the anti-tumour or anti-inflammatory effects, human peripheral blood mononuclear cells (PBMCs) were stimulated with the isolated compounds (1 or 10 μ g/ml) for 48 h at 37°C. The secreted cytokines (IL-6, IL-12 and TNF- α) in the supernatants of these

cultures were measured against a positive control OK-432 [a *Streptococcus pyogenes*-derived immunopotentiator, which was found to evoke antitumor effects by stimulating a number of immunocompetent cells and to induce various cytokines including IL-1, IL-2, IL-6, TNF- α and IFN- γ]. Only two compounds, the friedelane triterpene canophyllol **56** and the agarofuran pyridine alkaloid mayteine **5** were found to significantly cause induction of the three anti-inflammatory cytokines with the former being the most potent.

Gonzalez *et al.* (1982) reported that the presence of tingenone **65** and 22 β -hydroxytingenone **66** in the root bark could account for the traditional use of the tree in skin cancer, having shown antitumor activity (Melo *et al.*, 1974) as cited by them and further confirmed by later studies such as by Elhag *et al.* (1999). Moreover, the Gonzalez *et al.* (1982) report supported the findings of previous studies where the aqueous extract of the trunk bark showed anti-inflammatory activity (Olarde, 1976) and the leaves exhibited radio protective action (Flemming *et al.*, 1967) as cited by them. They attributed these properties to the isolated antioxidant polyphenolic compounds, ourateacatechin (**138**) and proanthocyanidins (**140**). The former compound was also reported to exhibit antiulcerogenic gastric activity (Pereira *et al.*, 1993) as cited by Mossi *et al.* (2004).

The isolated dihydro- β -agarofuran sesquiterpene pyridine alkaloids (**2**, **4**, **5** and **11**) from the bark by Piacente *et al.* (1999) were found to possess insecticidal and antifeedant activities as reported by Núñez *et al.* (2004), while ebenifoline E-II **8** showed a significant immunosuppressive activity (Duan *et al.*, 2001). The iridoid, ajugol **125**, showed antimicrobial activity (Akcos *et al.*, 1998).

The isolated compounds, maytenfolic acid **27**, lambertic acid **141** and ourateacatechin **138** showed inhibitory activity on rat lens aldose reductase which implied their potential anti-diabetic effect (Matsuda *et al.*, 1999). In the Chen *et al.*, (2002) study, the phenylpropanoid glycoside, isoverbascoside **144**, exhibited anti-proliferating activity and caused differentiation in the human gastric cancer cell line MGC803.

1.5.4.2 *M. chuchhuasca*

The quinonemethides, tingenone **65**, 22 β -hydroxytingenone **66**, pristimerin **67** and celastrol **68**, isolated from the bark of *M. chuchhuasca* by Morita *et al.* (2008) were found to possess cytotoxic effects on melanoma RPMI8226 cells, acting as mitotic inhibitors by disrupting the polymerisation of tubulin protein where the latter was the most potent. On the other hand, the aromatic triterpene derivatives, **71**, **72** and **73** showed moderate cytotoxic activity against a number of tumour cell lines and Shirota *et al.* (1994a) proposed the importance of the diosphenol function in ring A to elicit potent activity. Also, the two quinonemethides, **65** and **67**, demonstrated insecticidal effects on larvae of the codling moth (*Cydia pomonella*, Lepidoptera: Tortricidae) presented by their antifeedant activity together with molt effect suppression, with the latter compound being the most active (Avilla *et al.*, 2000). Moreover, pristimerin **67** and celastrol **68** exhibited an *in vitro* activity against both chloroquine-sensitive and multidrug-resistant *Plasmodium falciparum* strains, and when combined at fixed ratios (1:1, 1:3 and 3:1) they possessed an additive antimalarial effect (Figueiredo *et al.*, 1998).

The triterpene dimers, xuxuarines, **86**, **87**, **89** and **91-96** isolated from the stem bark by Shirota *et al.* (1995) were screened for their cytotoxic activity against some cancer cell lines and only the α -type xuxuarines exhibited weak to moderate activities. So far, there are no studies on the biological activities of the isoxuxuarines in literature.

1.5.4.3 *M. krukovii*

Bruni *et al.* (2006) outlined several biological activities of a 20% EtOH extract of the bark. It was found that it provided a mutagenic protection against the indirectly acting mutagen 2-aminoanthracene on the *Salmonella typhimurium* strains TA98 and TA100, and it possessed antioxidant and radical scavenging activity in a dose-dependent manner using different assays. However, it did not show antibacterial activity against both Gram positive and negative bacteria, and it was weakly active against tested fungi strains with the exception of the phytopathogen *Pithyium ultimum*. The antimutagenic activity was suggested to be attributable to the

synergistic interaction of polyphenolic compounds, which have been shown to exist in the extract.

In a study by Sekar *et al.* (1995), the EtOH extract of the stem bark showed a significant protein kinase C (PKC) inhibitory activity with an IC₅₀ value of 10 µg/ml. The subsequently isolated dihydro-β-agarofuran sesquiterpene pyridine alkaloids, **5** and **8**, did not possess the same activity; however, they exhibited toxicity in a brine shrimp lethality assay with a LC₅₀ < 10 µg/ml.

1.5.4.4 *M. macrocarpa*

While the EtOH extract of the stem bark showed no antibacterial activity (Kloucek *et al.*, 2005), the EtOH extract of the root bark demonstrated a broad spectrum of activity against a series of Gram positive and negative bacterial strains along with one yeast, *Candida albicans* ATCC 10231, using a broth microdilution method. The MIC values ranged from 125-250 µg/ml (Kloucek *et al.*, 2007). Recently, the antibacterial activity was further confirmed by Ulloa-Urizar *et al.*, (2015) against *Pseudomonas aeruginosa* with a MIC of 25 mg/ml.

The dihydro-β-agarofuran sesquiterpene polyol esters, **22-24**, isolated from the leaves were tested for some biological activities by Chávez *et al.* (1999). While **22** and **23** showed marginal antitumour activity against P-388 lymphoid neoplasm, A-549 human lung carcinoma, HT-29 human colon carcinoma, and MEL-28 human melanoma cell lines, none of them demonstrated aldose reductase (AR) inhibitory activity (the enzyme which catalyzes the reduction of glucose to sorbitol in the polyol pathway leading to several complications in diabetic patients such as initiating cataract problems and nephropathy).

Similarly, Chávez *et al.* (1998) showed that the isolated friedelane triterpenes **56**, **57** and **59-61** from the stem bark exudates were inactive when tested against the cancer cell lines above, and the latter compound, 28-hydroxyfriedelane-1,3-dione **61**, showed weak inhibitory activity against AR with an IC₅₀ of 12 mg/ml.

A later study by Chávez *et al.* (2000) on the macrocarpin triterpenes A-D (**47-50**), isolated from the roots, reported antitumour activity with IC₅₀ values ranging from 1-5.2 µM, with the exception of macrocarpin C **49**, which demonstrated low activity

that was assumed to be possibly due to the presence of a methoxy group at C-3 instead of OH compared to macrocarpin B **48**.

The olean-12-ene triterpene derivatives, **26**, **27**, **30**, **32**, **34** and **35**, along with the urs-12-ene derivatives, **39** and **40**, the lupane-type triterpenes, **52-55**, and the friedelane triterpene, **63**, isolated from the bark, were tested for their anti- HIV activity by Piacente *et al.* (2006) in C8166 cells infected with HIV-1_{MN}. Triptotriterpenonic acid A **35** showed the strongest activity with an EC₅₀ of 1 µg/ml. For the same activity in H9 lymphocyte cells, salaspermic acid **62** (*M. laevis*) was more potent (IC₅₀ of 25 µg/ml) than its derivative orthosphenic acid **63** (IC₅₀ 31 µg/ml), where the latter only differs by the presence of an extra α-OH group at C-2 (Chen *et al.*, 1992). Maytenfolic acid **27** was also reported as an antileukemic agent in Nozaki *et al.*, (1986) study.

The lupane-type triterpenes, lupeol **51**, 3-(*E*)-caffeoylbetulin **54** and nepeticin (**55**) were found to elicit anti-inflammatory activity via inhibiting the production of prostaglandin E₂ (PGE₂) and less preferably nitric oxide (NO) in mouse macrophages RAW 264.7 stimulated with lipopolysaccharide (LPS) (Reyes *et al.*, 2006).

The nor-quinonemethide triterpene, scutione **70**, isolated from the stem bark exudate by Chávez *et al.*, (1997), displayed strong antibiotic activity against a series of Gram positive bacteria with MIC values ranging from 0.1-2 µg/ml, while it was inactive against the tested Gram negative organisms (González *et al.*, 1996). A mild cytotoxic activity against three carcinoma cell lines was also reported.

The two dammarane triterpenes, **82** and **85**, isolated from the stem bark exudate were evaluated for their cytotoxic activity against a series of yeast strains by Torpocco *et al.* (2007). None of them demonstrated any antifungal activity even at the highest tested concentration 100 µg/ml, and they were both considered non genotoxic. The biological activity of the rest of the isolated dammarane triterpenes by Chávez *et al.* (1997) was not evaluated, however, other similar compounds were shown to possess cytotoxic activities (Smith-Kielland *et al.*, 1996; Wang *et al.*, 2006).

The friedelane-type triterpenes, friedelin **57** and epifriedelinol **58**, were reported to demonstrate antiulcerogenic gastric activity (Pereira *et al.*, 1993) as cited by Mossi *et al.* (2004).

1.6 Aims and objectives

The present work aimed to carry out a phytochemical investigation on a well known Amazonian medicinal plant, *M. laevis* "Chuchuguasa" (Celastraceae). Although a large ethnobotanical literature has flourished on "Chuchuguasa" and an extensive phytochemical work has been accomplished on the *Maytenus* species associated with "Chuchuguasa" and which are considered to be botanically similar, the preliminary findings carried out in a previous project on this plant within our group (Igoli *et al.*, 2011) have prompted further investigation of different parts of this plant in an attempt to isolate new constituents which may possess interesting biological activities. This follows the fact that research on the chemical composition of these species and other similar ones have proved the presence of a diverse range of secondary metabolites.

The objectives of this work included:

- Extraction of plant material with solvents of increasing polarity using a Soxhlet apparatus.
- Fractionation of the resulting extracts and subsequent purification of the naturally-occurring compounds using different chromatographic techniques such as Thin Layer Chromatography (TLC), Vacuum Liquid Chromatography (VLC), High-Performance Liquid Chromatography (HPLC) and Flash Chromatography.
- Structure elucidation of the isolates using Nuclear Magnetic Resonance (NMR) and other spectroscopic techniques such as Infrared Spectroscopy (IR), optical rotation (OR) and Mass spectroscopy.
- *In vitro* screening of the crude extracts, fractions and isolated pure compounds for some biological activities in the light of the traditional use of this plant. These tests included:
 - Cytotoxicity assessment against the cancer cell line A375 (ATCC[®] CRL1619[™]) (human, malignant melanoma cell line) compared with the normal cell line Hs27 (ATCC[®] CRL-1634[™]) (human, skin fibroblast cell line), for the purpose of examining the reported traditional use for skin cancer.

- *In vitro* anti-trypanosomal activity against the blood stream forms of *Trypanosoma brucei brucei* Plimmer & Bradford (*T. b. brucei*) (S427).
- Search for scientific evidence to back up the traditional collecting and use of the plant by Uitoto sabedores of Caquetá-Medio, Colombia.

CHAPTER II

2. MATERIALS AND METHODS

2.1 Materials

2.1.1 Solvents

Solvents listed below were obtained from Fisher Scientific UK Ltd, VWR International, Belgium and Sigma Aldrich, Germany. These solvents were used during different processes of extraction, chromatographic separation, analytical thin layer chromatography (TLCs).

- Acetic acid (Analytical grade)
- Acetone (Analytical grade)
- Acetonitrile (HPLC grade)
- CHCl_3 , $\geq 99.8\%$, spectrophotometric grade (Sigma-Aldrich, USA)
- Chloroform (HPLC grade)
- Dichloromethane (HPLC grade)
- Ethyl acetate (HPLC grade)
- Methanol (HPLC grade)
- n-Hexane (HPLC grade)
- n-Pentane (HPLC grade)
- Water (HPLC grade)

Solvents for NMR analysis: Below is the list of deuterated (99.9%) solvents obtained from VWR International, Belgium.

- Acetone- d_6
- Chloroform D (CDCl_3)
- Dimethylsulphoxide- d_6 (DMSO- d_6)

2.1.2 Reagents and chemicals

- Anti-bumping granules (Fisher Scientific, UK)
- Celite[®] S (Sigma-Aldrich, Mexico)
- Cotton wool (Fisher Scientific, UK)
- Filter paper 240 mm, 5-13 μm (VWR International, France)
- *p*-Anisaldehyde (Sigma-Aldrich, Germany)
- Sephadex LH-20 (GE Healthcare, Sweden)

- Silica gel 60 (0.063-0.200 mm) for column chromatography (Merck, Germany)
- Sulphuric acid (Sigma-Aldrich, Germany)
- TLC grade silica gel (60H, Merck, Germany)
- TLC silica gel 60 F₂₅₄ pre-coated aluminium sheet (Merck, Germany)
- Vanillin (BDH, UK)
- 0.22µm filter (Millex[®] GP, Ireland)
- 15 ml centrifuge tube (Corning[®], Mexico)
- 5 ml bijou (Sigma-Aldrich, UK)
- 75 cm² and 150 cm² flasks (Corning[®], USA)
- 96-well clear plate (TPP[®], Switzerland) and (Nunc[™], UK)
- Alamar blue[®] BUF 012B (AbD Serotec[®], UK)
- Cryogenic tubes (Nunc[®] Cryotubes)
- DMSO (Sigma-Aldrich, USA)
- Dulbecco's Modified Eagle's Medium (DMEM) (Gibco[®], UK)
- Foetal bovine serum (FBS) (Biosera, South America)
- Hank's saline solution (Sigma-Aldrich, UK)
- HMI-9 medium (Invitrogen, UK)
- Kanamycin sulphate (Gibco[®], UK)
- L-glutamine (Sigma-Aldrich, UK)
- MEM Non-essential amino acid solution (Sigma-Aldrich, UK)
- Penicillin/ Streptomycin (Cambrex, UK).
- Resazurin sodium salt (Sigma-Aldrich, USA)
- RPMI 1640 medium (Lonza Biowhittaker, Belgium)
- Sodium pyruvate (Gibco, Invitrogen, UK)
- Suramin S2671 (Sigma-Aldrich, UK)
- TripLETM Express (Gibco[®], Denmark)

2.1.3 *Equipment*

- 341 Polarimeter (PerkinElmer Inc, USA)
- -80°C freezer (Sanyo Electric Biomedical Co., Japan)

- ACE, C18 (10×250 mm, 5µm particle size, Hichrom, UK)
- Bruker Apex II diffractometer (Bruker Corporation, UK)
- Bruker Avance-III (400 and 600 MHz) NMR (Bruker, Germany)
- CL2 centrifuge, 263 Aerocarrier rotor (Thermo Scientific, UK)
- Column: ACE 5 C18 150x4.6 mm (Hichrom Ltd, UK)
- Exactive mass spectrometer (Thermo Fisher Scientific, Germany)
- Hammer mill (MSE, Atomix, UK)
- JEOL JNM LA400 NMR spectrophotometer (JEOL, UK).
- LC-MS Agilent 6130 multimode source mass spectrometer (Agilent Technologies, Inc., USA)
- Nicolet™ iS™10 FT-IR Spectrometer (Thermo Scientific, UK)
- NMR tubes (5mm x178 mm, Sigma-Aldrich Ltd, UK)
- Reveleris® Flash Forward system of Grace Davison Discovery Sciences (Illinois, USA)
- Rotary evaporator (Büchi, Switzerland)
- Semi-preparative HPLC (Gilson Scientific Ltd, UK)
- Shigemi NMR tubes (Sigma-Aldrich Ltd, UK)
- Soxhlet apparatus (Quickfit, UK)
- SpectraMax M5 micro-plate reader (Molecular Devices Corporation, USA)
- UV-Lamp 254 nm and 364 nm UVGL-58 (UVP, USA)

2.1.4 Plant material

The root and stem barks of *Maytenus laevis* "Chuchuguasa" (Celastraceae) were collected in the Resguardo Monochoa area of Caquetá Medio in Colombia. The collection of the plant materials was carried out by the Amazonian sabedores from the indigenous Uitoto tribe, Eusebio Mendoza, and from Muinane tribe, Noé Rodríguez Jujuborre, who identified the tree as a *M. laevis* species (Figure 2.1). The root bark was collected from the side of the tree that receives the first rays of sun at 5 am, following a strict collecting methodology based on the Uitoto's beliefs about the importance of the collection time and the plant orientation (section 1.5.2). A voucher specimen has been kept in SIPBS herbarium.



(A)



(B)

Figure 2.1: (A); *Eusebio Mendoza* collecting Chuchuguasa root, (B); *Alexander I. Gray* with Chuchuguasa root in 25/1/1993; [The collections were done with the full permission from sabedores for academic research]



(A)



(B)

Figure 2.2: *M. Laevis*; (A) Root bark, (B) Stem bark

2.2 Methods

2.2.1 *Extraction of Plant Material*

The dried plant materials were ground into a fine powder using a Hammer mill. The extraction of the plant material was performed successively with solvents of increasing polarity (n-hexane, ethyl acetate, and methanol) using a Soxhlet apparatus. The extraction process was carried out for 2-4 days with each solvent (or until the solvents ran clear in the Soxhlet chamber).

The extracts were filtered through filter paper and concentrated by evaporation under reduced pressure (using a rotary evaporator) at a temperature of 40°C.

2.2.2 *Analytical and Chromatographic techniques*

A number of classical and modern chromatographic techniques were used in this work for isolation and purification of compounds from the crude extracts as follows.

2.2.2.1 *Thin Layer Chromatography (TLC)*

TLC was used to select the appropriate solvent system for further chromatographic methods such as column chromatography (CC), gel filtration chromatography (GF) and preparative thin layer chromatography (PTLC). This technique was performed on normal phase pre-coated silica gel 60 aluminium plates to detect and monitor the compounds through the separation processes. Each sample (crude extract, fractions, and pure compounds) was dissolved in an appropriate solvent and applied as a spot or thin line on to the silica about 1-2 cm above the base of the plate (origin). The plate was placed into a glass tank with a suitable solvent mixture at a level to just wet the lower edge of the plate. A filter paper was previously placed inside the tank to assist the saturation of the TLC chamber with solvent vapours. When the solvent reached about 1 cm below the top of the plate, the plate was removed and the solvent front was marked with a pencil line. The developed TLC plate was air dried and the spots were detected as follows:

Detection by UV light: The plates were firstly examined using a non-destructive ultraviolet detection. The spots were observed under UV light either at λ 254 nm as dark bands on a green background due to quenching fluorescence of a fluorescent

indicator in the silica gel F₂₅₄ plates or at λ 366 nm where they fluoresced as coloured bands. The visible bands were marked with a pencil outline.

Detection by spray reagent: The TLC plates were sprayed with chemical reagents such as *p*-anisaldehyde-sulphuric acid or vanillin-sulphuric acid (VAS), followed by heating (120°C) using a hand-held heater to assist the colour development. The R_f values were calculated and enabled fractions with similar profiles to be pooled for spectroscopic analysis.

Modified anisaldehyde-sulphuric acid reagent:

P-anisaldehyde (0.5 ml) was mixed with a mixture of 10 ml glacial acetic acid and 85 ml methanol. Then, 5 ml concentrated (97%) sulphuric acid was added slowly (Waldi, 1965).

Vanillin-sulphuric acid reagent:

Vanillin (1 g) was dissolved in 80 ml absolute ethanol, followed by a slow addition of 20 ml concentrated (97%) sulphuric acid (Waldi, 1965).

2.2.2.2 Vacuum Liquid Chromatography (VLC)

A straight-sided sintered glass Büchner funnel [13 cm (diameter) × 10 cm (height)] was dry-packed with TLC grade silica (Silica gel 60H) under vacuum applied via a water vacuum pump. This chromatographic technique was chosen for initial rapid fractionation of the crude extracts (Sarker *et al.*, 2006, p. 7). To inspect the consistency of the column, a non-polar solvent was allowed to pass through the column under vacuum. Plant samples were dissolved in a small amount of an appropriate solvent and adsorbed on to a small amount of silica gel 60 (CC-grade silica gel). The silica gel with the adsorbed sample was dried and transferred to the top of the column bed as a narrow layer. Elution was carried out with solvents of increasing polarity starting with n-hexane, n-hexane/EtOAc and EtOAc/MeOH. A specific volume of each solvent system was added each time while the vacuum was applied until the column dried up. The fractions were collected manually into a vacuum flask and were evaporated to dryness by rotary evaporation. Finally the fractions were examined by TLC to enable pooling according to their similarities (Coll and Bowden, 1986).

2.2.2.3 Column Chromatography (CC)

CC enables separation of compounds from crude extracts or less complicated mixtures/ fractions. A glass column (different sizes) was plugged with cotton wool and packed to 2/3 the length with a slurry of silica gel 60 in the least polar system (usually n-hexane). The solvent was allowed to flow through the column, leaving a packed bed of silica gel. The sample was dissolved in a minimum amount of a suitable solvent and pre-adsorbed onto silica gel 60 and was left in a fume cupboard to dry, before loading on the top of the column. A cotton plug was applied to the top to avoid distortion. Elution was carried out using a range of mobile phases composed of polar/ non-polar solvents of varying ratios of increasing polarity (the amount of consumed solvents varied depending on TLC observations). The collected fractions were then examined by TLC and combined according to similar chemical profiles (Megalla, 1983).

2.2.2.4 Size-Exclusion Chromatography (SEC)

This technique, also known as gel filtration chromatography, enables separation of molecules according to their size and shape as there is little or no interaction between the solute and the stationary phase. The largest molecules elute from the column first followed by the smallest which tend to diffuse into the porous gel particles. A glass column of a proper size [2 cm (diameter) × 100 cm (height)] plugged with cotton wool was packed with a slurry of Sephadex LH-20, prepared by suspending the stationary phase in 50:50 dichloromethane/methanol or 100% methanol overnight for non-polar or polar fractions, respectively. Once the packed bed was settled, and the level of the solvent was just above the top of the bed, the sample to be fractionated was applied carefully using a Pasteur pipette after dissolving it in a minimum amount of the same solvent that was used to pack the column. Elution was carried out isocratically, and the fractions were collected in small vials (about 1 ml per fraction) (Kremmer and Boross, 1979).

2.2.2.5 Preparative thin layer chromatography (PTLC)

PTLC was used to separate and purify some fractions containing simple mixtures. TLC silica gel 60 F₂₅₄ pre-coated aluminium sheets were used firstly on a small-scale

to determine the best solvent system to achieve optimum separation. Larger TLC plates (20×20 cm) were then used to separate more quantity of the sample. The samples were dissolved in a minimum volume of an appropriate solvent and were then applied 2cm from the bottom as a thin band across the entire width of the plate using a Pasteur pipette. The plates were developed as in section 2.2.2.1. The plates were observed under UV light (sometimes sprayed at one side with a suitable reagent if they were invisible), and the bands of interest were cut into strips along with the absorbent. The strips attributed to each separate component were cut into small pieces and soaked in a polar solvent overnight for maximum recovery. After filtration and evaporation, the recovered components were analysed by NMR spectroscopy.

2.2.2.6 *Semi-Preparative High-Performance Liquid Chromatography (Semi-preparative HPLC)*

Semi-preparative HPLC was used to separate a mixture of two triterpene type compounds found as major components in a VLC fraction of the n-hexane extract of the root bark of *M. laevis*. The experiment was performed with the help of Dr. Ticiano Gomes do Nascimento on a Gilson system equipped with a multiple wavelength UV detector (monitoring at λ 210, 265, 290 and 320 nm). The column was ACE, C18 (10×250 mm, 5 μ m particle size) and the loop volume was 5 ml. An isocratic solvent system of acetonitrile-water (60%:40% v/v) was used as the mobile phase (determined after a number of optimisation trials on an analytical HPLC). The flow rate was 5 ml/ min and the column temperature was 25°C. The sample concentration was 100 mg/ml and the injection volume for each run was 200 μ l.

2.2.2.7 *Flash chromatography (FC)*

FC is a separation technique that is similar in principle to conventional CC, but using air pressure to elute the sample through an optimized medium or short column at a faster rate and to obtain higher resolution (Still *et al.*, 1978).

The Reveleris[®] Flash Forward system of Grace Davison Discovery Sciences is a modern flash chromatographic system which is linked to two detectors, a UV detector (wavelength range: 200-500 nm) and an evaporative light scattering detector (ELSD). This has the advantage of giving a greater sensitivity by detecting all the

compounds within the sample and not just the UV-active compounds. The system allows for up to four solvent mixtures that can be used in a single run. The pump flow rate can range from 4 to 200 ml/ min and can be automatically adjusted at high pressure. The fraction collector is built into the system with auto-tray recognition.

This technique was used to separate a mixture of very similar two triterpene type compounds found as major components in a 60 mg sample obtained by PTLC of a VLC fraction of the n-hexane extract of the stem bark of *M. laevis*. The sample was dissolved in a minimum volume of a mixture of DCM: EtOAc and mixed thoroughly with a sufficient amount of Celite[®] S and placed in the fume hood to dry. The Celite[®] mixture was then packed into the sample loader which was then connected to the system. The conditions of the separation method are listed in Table 2.1. Eighty peaks were collected and TLC was performed to pool similar fractions, resulting in 17 sub-fractions.

Table 2.1: Key parameters for the separation method by Reveleris FC

Attribute	Conditions
Column	Reveleris [®] C18 40 µm 12g
Solvent system	Water, Acetonitrile
Flow rate	10 ml/ min
Gradient	0 min 90% Acetonitrile to 68.4 min 90% Acetonitrile 78.4 min 100% Acetonitrile to 109.3 min 100% Acetonitrile 110.3 min 90% Acetonitrile to 115.1 min 90% Acetonitrile
ELSD threshold	5 mV
UV threshold	0.05 AU
UV wavelengths	290 and 320 nm
Volume per-vial	20 ml

2.2.3 Structure Elucidation

2.2.3.1 Nuclear Magnetic Resonance (NMR)

NMR is the main technique used for structure elucidation. One and two dimensional (1D and 2D, respectively) experiments were used to detect the type of compounds in fractions and to identify the structure of pure compounds. The NMR data were

obtained on a JEOL (JNM LA400) spectrometer (400 MHz) at SIPBS and on Bruker Avance 300 (400MHz) spectrometer at the Department of Pure and Applied Chemistry using tetramethylsilane (TMS) as an internal standard. Deuterated solvents such as CDCl_3 , $(\text{CD}_3)_2\text{CO}$ and $\text{DMSO-}d_6$ (Table 2.2) were used to prepare sample solutions depending on the solubility of the compounds. Approximately, 10 mg of each sample was dissolved in 500-600 μl of the appropriate solvent and placed into a standard NMR tube (5mm x 178mm) to give about 4.0 cm depth. NMR experiments of samples with low yield were carried out using Shigemi NMR tubes. Samples were dissolved in 300 μl of CDCl_3 or $\text{DMSO-}d_6$ and placed into a Shigemi tube that matched with the respective solvent.

Table 2.2: Deuterated solvents used for NMR analysis

Solvent	Chemical formula	^1H shift(s) in ppm	^{13}C shift(s) in ppm
Deuterated chloroform	CDCl_3	7.27	77.2
Deuterated DMSO	$(\text{CD}_3)_2\text{SO}$	2.50	39.5
Deuterated acetone	$(\text{CD}_3)_2\text{CO}$	2.05	29.8 206.2

(Gottlieb *et al.*, 1997)

2.2.3.1.1 One-Dimensional NMR experiments (1D)

1D ^1H NMR experiment was executed as the initial step to identify the type of the components in a given sample or to assess its purity. It provides information about the type and the number of protons in the molecule (by the chemical shifts and integration) as well as their multiplicity (coupling constant) which gives an idea of the adjacent protons. The ^1H NMR was also valuable in determining the relative molar ratio of the components present in a mixture. The 1D ^{13}C NMR experiment was useful in providing information about the kind and the number of carbon atoms in a molecule. The Distortionless Enhancement through Polarisation Transfer (DEPTq-135) experiment differentiates different types of carbon atoms according to their proton attachments. The CH_3 and CH carbon atoms give signals in one direction while the CH_2 and fully substituted carbons give signals in the other. Finally, the Nuclear Overhauser effect (NOE) Difference experiment was used for determining

the relative stereochemistry of a selected proton. The NOE effect is revealed when the irradiation of one proton at its resonance frequency leads to the increase in the intensity of the other proton signal(s) which is/are away from each other over short distances through space (Williams & Fleming, 2008).

2.2.3.1.2 Two-Dimensional NMR experiments (2D)

Further 2D experiments were carried out for accurate assignments of the proton and carbon chemical shifts as well as for determining the relative stereochemistry. The Correlation Spectroscopy (COSY) experiment was used to indicate the connectivity between neighbouring protons. The ^1H - ^1H correlations due to germinal (2J) and vicinal (3J) coupling appeared as cross-peaks symmetrically arranged about the diagonal. The ^1H -detected Heteronuclear Single Quantum Coherence (HSQC) experiment was used to identify the 1J ^1H - ^{13}C correlations, while the Heteronuclear Multiple Bond Coherence (HMBC) experiment was valuable for determining the ^1H - ^{13}C correlations via long range couplings ($^3J_{\text{CH}}$ and $^2J_{\text{CH}}$). In the present study, the HMBC experiments were performed using a delay time $1/(2J)$ in the pulse sequence of 0.0714 s (*i.e.* long range $J_{\text{CH}} = 7$ Hz). The Nuclear Overhauser Enhancement spectroscopy (NOESY) experiment was useful to establish the relative stereochemistry of the pure compounds. The spectrum obtained is similar to a COSY spectrum; however, the cross-peaks represent ^1H - ^1H interactions arising from through space dipolar coupling rather than through-bond coupling (Claridge, 2008; Williams & Fleming, 2008). A mixing time of 0.5s was set for all the NOESY experiments.

2.2.3.2 Mass Spectroscopy

This spectroscopic technique complements NMR spectroscopy as it provides valuable structural information such as the molecular weight and molecular formula of the compounds under investigation. It is a very sensitive method which can be carried out with a few micrograms of sample. It is usually coupled with a separation technique such as liquid chromatography (LC), which provides a quick and economical general idea of the compounds present in a mixture. Samples containing the purified compounds were dissolved in methanol to get a concentration of 100 $\mu\text{g/ml}$.

LC-MS experiments were carried out in both ESI positive and negative modes on either the UltiMate-3000 HPLC instrument or the Accela HPLC system which were connected to an Exactive mass spectrometer. The sample solution (10-20 μl) was injected into an ACE 5 C18 column along with the mobile phase of A 0.1% (v/v) formic acid in water and B 0.1% (v/v) formic acid in acetonitrile (10% to 100% in 30 min) at a flow rate of 300 $\mu\text{l}/\text{min}$. Some of the pure samples were directly injected to the Exactive mass spectrometer to confirm their exact mass from the MS spectrum generated. Key parameters for mass spectral analysis are presented in Table 2.3 which may vary slightly for different experiments. All HRESI-MS experiments were carried out by Dr. Tong Zhang (Alex), SIPBS, Strathclyde University.

Some samples were analysed on the LC-MS Agilent 6130 multimode source mass spectrometer using both positive and negative MM-ES+APCI ionisation modes. The sample solution (10 μl) was injected into an Agilent Zorbax Eclipse C18 Column (4.6 \times 150 mm, 5 μm) along with the mobile phase (water 5mM ammonium acetate: acetonitrile 5mM ammonium acetate) using a gradient method 5% to 100% over 30 min at a flow rate of 1 ml/ min. These experiments were carried out at the Department of Pure and Applied Chemistry, Strathclyde University by Ms. Patricia Keating.

Table 2.3: Main parameters for the HRESI Mass spectral analysis

Attribute	Positive mode	Negative mode
Capillary Temp ($^{\circ}\text{C}$)		320.00
Sheath Gas flow (bar)		50.00
Auxiliary Gas flow (bar)		17.00
Spray voltage (kV)	4.50	4.0
Spray current (μA)		100.00

2.2.3.3 X-Ray crystallography

This technique was used as a complementary and supportive method to the NMR experiments to elucidate the chemical structure of the novel compound HM-6. Good quality single crystals were obtained from CDCl_3 . A single crystal was chosen after being viewed under a microscope and X-ray diffraction data was collected using a Bruker Apex II diffractometer with an IncoTec $\text{I}\mu\text{S}$ microsource ($\lambda=0.71073 \text{ \AA}$). The

data collection was smooth and without any complications and the crystal was stable throughout the data collection period. The intensity data were processed using a Bruker SAINT suite of programs, followed by absorption correction with Siemens Area Detector Absorption Correction Program (SADABS). The structures were solved using SHELXS program and refined by least-square methods using SHELXL. All non-hydrogen atoms were refined by anisotropical methods and hydrogen atoms were either refined or placed in calculated positions. Crystal structural refinement converged to good R factors, as listed in Appendix I. The molecular diagram was generated using Diamond version 3.1f. The crystal structure determination was carried out by Dr. Amit Delori, SIPBS, Strathclyde University.

2.2.3.4 Optical Rotation (OR)

The optical rotation of some isolated compounds was measured using a 341 polarimeter at the Department of Pure and Applied Chemistry, Strathclyde University by Mr. Gavin Bain. Variable concentrations of these compounds were prepared by dissolving them in a suitable solvent (CHCl₃ spectrophotometric grade) to give 2 ml test solutions in volumetric flasks. Ten readings from the machine were averaged and the optical rotation was calculated using the following equation:

$$[\alpha]_{\lambda}^T = \frac{100 \times \alpha}{l \times c}$$

Where α is the average of the measured rotation ($^{\circ}$), l is the path length in decimetres, c is the concentration of the solution in g/ 100ml, T is the temperature at which the measurement was taken (20°C), and λ is the wavelength in nanometres ($D=589$ nm).

2.2.3.5 Infrared (IR) spectroscopy

The IR spectra of some isolated compounds were recorded on the Nicolet™ iS™10 FT-IR Spectrometer. A very small amount of the dry sample was loaded and the spectrum was generated as a plot of absorbance against wave numbers (500-4000 cm⁻¹ range) using the OMNIC computer software.

2.2.4 Bioassays

2.2.4.1 Tissue Culture and Cytotoxicity Assessment

Crude extracts and isolated pure compounds were tested for their effect on the viability of two cell lines; the normal cell line Hs27 (ATCC[®] CRL-1634[™]) (human, skin fibroblast cell line) and the cancer cell line A375 (ATCC[®] CRL1619[™]) (human, malignant melanoma cell line) using a resazurin-based cytotoxicity assay. The cells were kindly donated by Mrs Louise Young, SIPBS, Strathclyde University.

2.2.4.1.1 Preparation of Complete Medium

The growth medium (known as Complete Medium) for both cell lines was prepared in a sterile flow hood and stored at 4°C until required.

Hs27 cells were grown in Dulbecco's Modified Eagle's Medium (DMEM) supplemented with 10% (v/v) foetal bovine serum (FBS) and 1% (v/v) penicillin/streptomycin. While A375 cells were grown in RPMI 1640 medium supplemented with 10% (v/v) FBS, 1% (v/v) kanamycin sulphate, 1% (v/v) L-glutamine, 1% (v/v) sodium pyruvate and 1% (v/v) MEM non-essential amino acid solution.

2.2.4.1.2 Maintenance of cell lines

Both cell lines were cultured in the appropriate complete medium and incubated in a humidified atmosphere at 37°C in the presence of 5% CO₂. The growth medium was replaced every three days and the cells were passaged at 70-80% confluence.

A vial of cells stored in liquid nitrogen (-210°C) was thawed rapidly in a water bath at 37°C and transferred into 10 ml of warm growth medium in a 15 ml centrifuge tube and centrifuged at 1000 rpm (56 ×g) for 5 min. The supernatant was removed and the cells resuspended in 10 ml complete medium. The suspension was then transferred into 75 cm² flask containing 5 ml complete medium and incubated in a humidified air at 37°C containing 5% CO₂.

2.2.4.1.3 Passaging adherent cells

The cells were passaged when they were approximately 70-80% confluent. The growth medium was completely removed from the flask and the cells were washed

with 5 ml Hank's saline solution. The cells were detached from the flask with 2 ml TripLE™ Express incubated for 5-6 minutes at 37°C. Complete medium (8 ml) was added to the cells to inactivate the trypsin. The cells were counted using a haemocytometer for seeding at a specific density in a clear and sterile (75 or 150 cm²) flask in 15 ml or 30 ml of complete medium as applicable, and incubated in a humidified atmosphere at 37°C in the presence of 5% CO₂ for 3-4 days, depending on cell growth.

2.2.4.1.4 Cell storage

Both cell lines were stored at a cell density of 1x10⁶ cell/ml. A 1 ml cryopreservation medium was prepared as 5% (v/v) DMSO in complete DMEM for the Hs27 cell line and as 10% (v/v) DMSO in FBS for the A375 cell line. The cells were aliquoted in cryogenic tubes and kept for a few days in a -80°C freezer before being transferred into liquid nitrogen when longer storage was required.

2.2.4.1.5 Plant sample preparation

Crude extracts and pure compounds were dissolved in DMSO to give a stock solution of 20 mg/ml and were kept at -20°C. Further dilution to the required starting concentration was carried out using cell growth medium.

2.2.4.1.6 Resazurin solution preparation

Resazurin sodium salt (5mg) was dissolved in 50 ml deionised water. The solution was filtered sterilised using a 0.22µm filter unit and aliquoted into 5 ml bijou and stored in the fridge, occluded from light until required.

2.2.4.1.7 Resazurin cytotoxicity assay

The assay incorporates a colorimetric/ fluorometric growth indicator, based on the detection of metabolic activity. Resazurin is an oxidation-reduction (REDOX) indicator that allows monitoring of metabolic activity by both fluorescent and colorimetric detection.

The REDOX indicator is reduced in the mitochondria of living cells in the presence of nicotinamide adenine dinucleotide (NADH) dehydrogenase which causes the indicator to change from resazurin, the oxidized, non-fluorescent, blue form to resorufin, the reduced, fluorescent, red form (Figure 2.3). The fluorescence is

measured at the excitation and emission wavelengths of 560 nm and 590 nm, respectively.

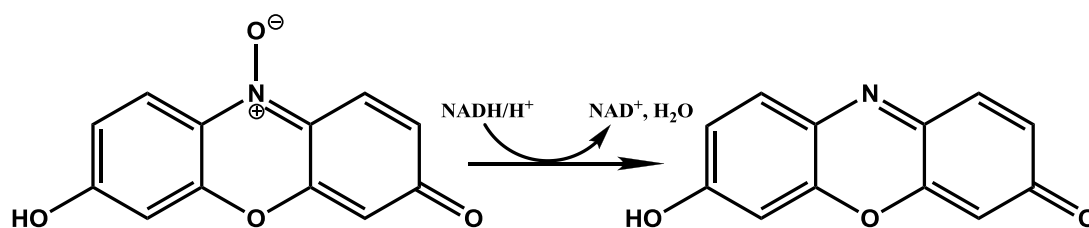


Figure 2.3: Reduction of resazurin to resorufin in living cells

The cell lines were seeded in 96-well tissue culture plates at 1×10^5 cell/ml and 5×10^4 cell/ml for Hs27 and A375 cell lines, respectively and allowed to adhere for 24 h in a humidified incubator at 37°C in the presence of 5% CO_2 .

A 1:1 serial dilution of each sample was performed in a dilution plate to give a concentration range from 200 $\mu\text{g/ml}$ to 6.25 $\mu\text{g/ml}$. The diluted test sample (100 μl) was transferred to the corresponding assay well in the cell plate to give a final assay volume of 200 μl . Controls (serial dilutions of 0.5% and 10% DMSO as solvent controls) were added to the appropriate control wells (Figure 2.4). The plate was then incubated for 24 h at 37°C in a humidified atmosphere containing 5% CO_2 . On day 3, 10% (v/v) resazurin solution was added to each well and the assay plate was wrapped with tin foil and returned to the incubator under the previous conditions. Fluorescence intensity was measured after 5 and 24 h using a SpectraMax M5 microplate reader at the excitation and emission wavelengths of 560 nm and 590 nm, respectively). Additional background plates were always prepared following the same protocol containing samples alone without cells.

The cell viability was determined as a percentage of the mean cell viability of each concentration to the mean cell viability of the untreated cells (blank control) after subtracting the background (i.e. the effect of the coloured compounds on the fluorescence) and the 0.5% DMSO (the vehicle) readings. The untreated control cells had a viability of 100%. The EC_{50} values were calculated for the concentration response data using GraphPad Prism software version 4.0 and the results were confirmed microscopically. The cytotoxicity assays were performed in replicate (n=3 or 6) depending on the cell's availability, cell growth rate, the experiment's complications and time limitation.

	1	2	3	4	5	6	7	8	9	10	11	12
A	Sample 1						Sample 3					
B												
C												
D	Sample 2						Sample 4					
E												
F												
G	0.5% DMSO						10% DMSO					
H							Cell control			Medium		

Figure 2.4: Assay plate template

2.2.4.1.8 Statistical analysis

Statistically significant differences were determined using Prism software version 4.0 by one-way ANOVA analysis of variance followed by Dunnett post-test to compare each concentration versus control where appropriate, and two-way ANOVA with Bonferroni post-test to compare between both cell lines at each tested concentration.

2.2.4.2 Anti-trypanosomal assay

The anti-trypanosomal activity of the crude extracts along with some fractions and the majority of the isolated pure compounds was determined using an Alamar blue™ 96 well microplate assay (Ráz *et al.*, 1997), performed by Ms. Carol Clements, SIPBS, Strathclyde University.

2.2.4.2.1 Sample preparation

The samples were prepared as a stock solution of 10 mg/ml (1 mg/100µl) for the crude extracts/ fractions and 10 mM for the pure compounds in 100% DMSO.

A trypanosome suspension containing the bloodstream form of *Trypanosoma brucei brucei* S427 was prepared by counting and diluting the trypanosomes to a concentration of 3×10^4 trypanosomes/ml.

2.2.4.2.2 Assay protocol

The samples were initially tested in duplicate (n=2) at a single concentration of 20µg/ml or 20µM to determine their *in vitro* activity. The stock solutions (10mg/ml) were diluted to 1 mg/ml using HMI-9 medium. The test sample (4 µl) followed by 96 µl HMI-9 medium were pipetted into the assay well in 96- well plates. The plates

were arranged as follows; Controls such as sterility and DMSO controls (at a concentration of 1 to 0.002%) in column 1 as negative controls, test samples in columns 2-11 and a concentration range (1.0 μM - 0.008 μM) of suramin S2671 as a positive control in column 12. The trypanosome suspension (100 μl) was added to each well of the assay plate with the exception of well A1 (sterility control) to give the final assay concentration of the samples 20 $\mu\text{g}/\text{ml}$. The plate was then incubated at 37°C, 5% CO_2 in a humidified atmosphere for 48 h. After which 20 μl of Alamar blue[®] BUF 012B was added and the incubation continued under the previous conditions for another 24 h. Fluorescence was then determined using a Wallac 1420 Victor2 microplate reader (Excitation and Emission wavelengths of 560 nm and 590 nm, respectively). The results were calculated as percentages of the DMSO control values. Later on, the active samples (with less than 10% of control values, i.e. >90% inhibition) were further tested in duplicate to determine their MIC values.

The template of a clear flat-bottomed 96-well plate was arranged as follows: In column 2, 200 $\mu\text{g}/\text{ml}$ test solutions were prepared by pipetting 4 μl of (10 mg/ml) test stock solution and adding 196 μl HMI-9 medium into each well. In column 1 and 3-12, 100 μl of HMI-9 medium was pipetted into each well, while a concentration range of 1.0 to 0.008 μM of suramin (10 μM) was prepared in column 12. Serial 1:1 dilutions were carried out from columns 2 to 11 using a multi-channel pipette. After which, 100 μl of the trypanosomes suspension at a concentration of $3 \times 10^4/\text{ml}$ was added to each well of the assay plate to give the final assay concentration of the samples ranged from 100 $\mu\text{g}/\text{ml}$ to 0.19 $\mu\text{g}/\text{ml}$. The plate was then incubated at 37°C, 5% CO_2 in a humidified atmosphere for 48 h, and the protocol was continued as previously described. The MIC values were determined as the lowest concentrations of the active samples that had given less than 5% cell growth comparing to the control values.

CHAPTER III

3. RESULTS AND DISCUSSION

PART I: PHYTOCHEMICAL STUDIES

Preface

In this chapter, Part I (phytochemical studies) explains the structural elucidation process of the compounds identified in some of the fractions which were obtained from the n-hexane and EtOAc extracts of the root and stem barks of *M. laevis*, and arranged according to their chemical classifications. It also highlights some of the biological effects of these compounds as published in the literature.

Part II (biological studies) illustrates the results of the biological activities which were addressed in this work on the isolated compounds in comparison with those reported in the literature.

3.1 Solvent Extraction and Yields

Ground dried root and stem barks of *M. laevis* were successively extracted with n-hexane, EtOAc and MeOH using a Soxhlet apparatus. A rubber-like substance (polymer), produced while evaporating the extracts by rotary evaporator, was separated from the liquid part by filtration. The yields of the crude extracts are listed in the table below.

Table 3.1: Amounts and yields of the crude extracts of ML root and stem barks.

Part used	Weight of plant material g	n-Hexane extract g (%)		EtOAc extract g (%)		MeOH extract g (%)
		Liquid	Polymer	Liquid	Polymer	
Root bark	550	14 (2.5%)	36 (6.5%)	10 (1.8%)	4 (0.7%)	56 (10.2%)
Stem bark	600	10 (1.7%)	3.5 (0.6%)	5 (0.8%)	-	35 (5.8%)

All the extracts were initially fractionated by VLC. The columns were eluted with gradient solvent systems and the collected and combined fractions were analysed by ¹H NMR experiments. The patterns of the proton spectra of most of these fractions indicated the presence of triterpene-type compounds, sterols, phenolics as well as fats and tannins. A series of separation and purification processes were further carried out to isolate the pure compounds generally using Sephadex LH20, CC and PTLC, in addition to Semi-Prep HPLC and Grace Reveleris flash chromatography in special cases.

3.2 Polymers

3.2.1 Characterisation of HM-1 as *trans*-1,4-polyisoprene (rubber-like substance)

HM-1 was separated from the root and stem barks during the rotary evaporation process of the n-hexane and EtOAc extracts. On TLC, a pink spot appeared after spraying with *p*-anisaldehyde-sulphuric acid reagent followed by heating.

The ^1H NMR spectrum (400 MHz, CDCl_3 , Figure 3.2) showed one methyl singlet at δ_{H} 1.61 (3H, *s*), two allylic methylenes at δ_{H} 1.99 and 2.07 (*m*) and one olefinic methine at δ_{H} 5.13 (1H, *td*, $J = 7.0, 1.7$ Hz).

The DEPTq135 ^{13}C NMR spectrum (100 MHz, Figure 3.3) showed only five carbon signals including one methyl, two methylenes, one olefinic methine and one olefinic quaternary carbon at δ_{C} 16.1, 26.7, 39.7, 124.2 and 134.9, respectively.

From the complete analysis of the 2D NMR spectra including HSQC, HMBC and COSY (Figure 3.4, Figure 3.5, Figure 3.6), and by comparison with the literature, this compound was suggested to be a polymer consisting of a chain of the monomeric isoprene unit $[\text{C}_5\text{H}_8]^*$ (Figure 3.1).

The stereo-chemical configuration of the double bond in the monomeric unit was determined as *trans* due to the following facts;

- It has long been established that the *trans*-1,4-polyisoprene possesses hard, tough and brittle properties, which apply on the material isolated from this plant, comparing to the *cis*-1,4-polyisoprene which has an elasticity (rubbery) property at room temperature (Goodman, 1967; Miller, 1966).
- From the COSY spectrum, the long-rang coupling or the (W correlation) between the olefinic proton at δ_{H} 5.13 and the methyl at δ_{H} 1.61 was observed, indicating the *trans* configuration.
- The 1D NOE difference experiment (Figure 3.7; A) showed that irradiating the signal at δ_{H} 5.13 (H-3) caused an NOE effect to the methylene protons at δ_{H} 1.99 and 2.07, but showed no NOE effect to the methyl at δ_{H} 1.61 (3H-5) and vice versa in the NOE diff. experiment (Figure 3.7; B). This indicated that the methine H-3 and the methyl at δ_{H} 1.61 are located on the opposite sides of the double bond in the monomeric unit (i.e. in *trans* position).

- The comparison between the DEPTq ^{13}C NMR spectrum of HM-1 and ^{13}C NMR spectra of the natural *cis* and *trans*-1,4-polyisoprenes, as represented in the Duch and Grant, (1970) report (Figure 3.8), showed that the difference between the chemical shift values of the methylene carbon (C-1) and the methyl carbon (C-5) was about 24 ppm in the *trans*-polymer, while it was about 10 ppm in the *cis*-polymer.
- Finally, the pattern of the ^1H NMR spectrum of HM-1 was identical to that obtained for the pure *trans*-1,4-polyisoprene (TPI) in CDCl_3 as mentioned in the Chen *et al.*, (2015) report. However, there was about 0.045 ppm difference in the chemical shift values of the five proton signals of the TPI comparing to those of the HM-1 as they were reported at δ_{H} 1.95 (2H-1), 2.03 (2H-4), 5.07 (H-3) and 1.56 (3H-5). This might be due to a difference in solvent calibration.

This is the first report of the isolation of this polymer (Gutta-percha) from *M. laevis*, however, it has been reported that some plants from *Maytenus* species such as *M. oleioides* and *M. acuminatus* have a reasonably high content of rubber-like materials, (i.e. balata 2.67% from the latter) (Paterson-Jones, 1983). When Gutta-percha was first introduced to the western world, it was used for insulation of underwater cables (Prakash *et al.*, 2005).

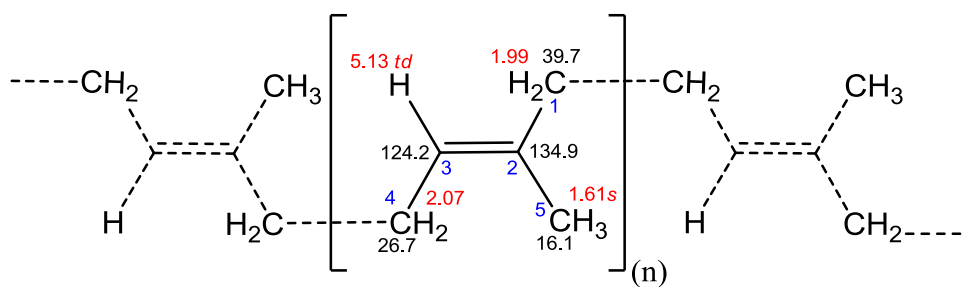


Figure 3.1: Structure of HM-1

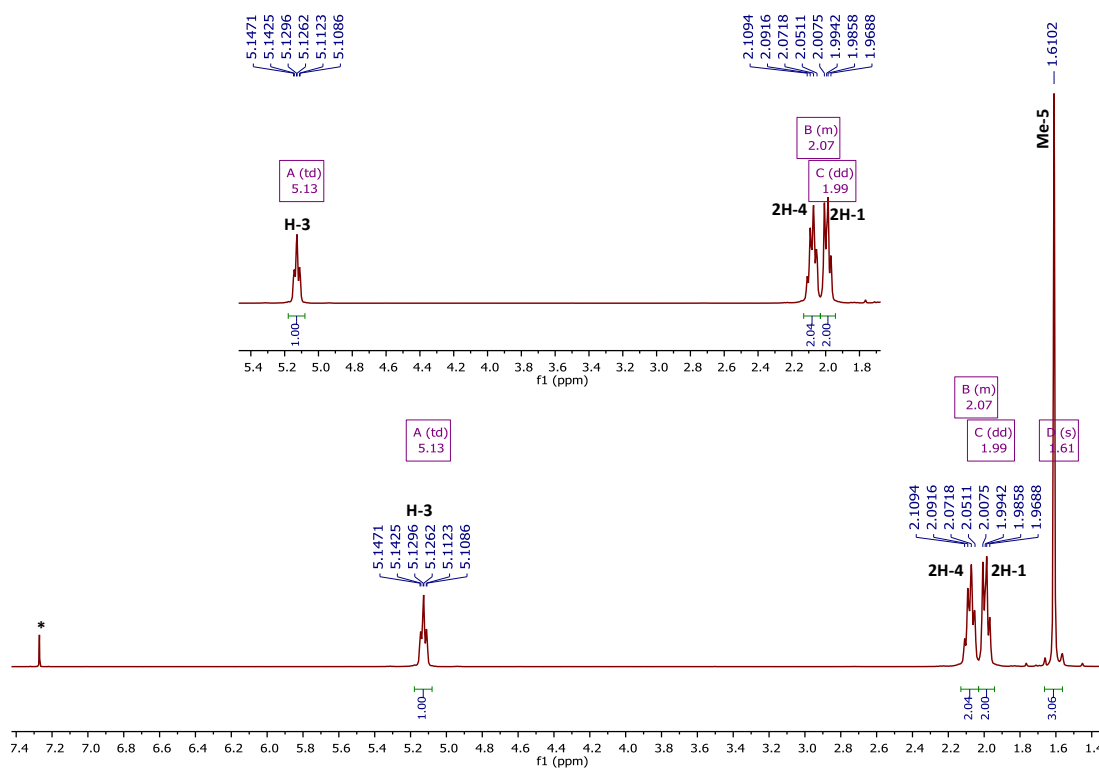


Figure 3.2: Full and selected expansion of ^1H NMR spectrum (400 MHz) of HM-1 in CDCl_3 ; (*) CHCl_3 0.01% residue in CDCl_3

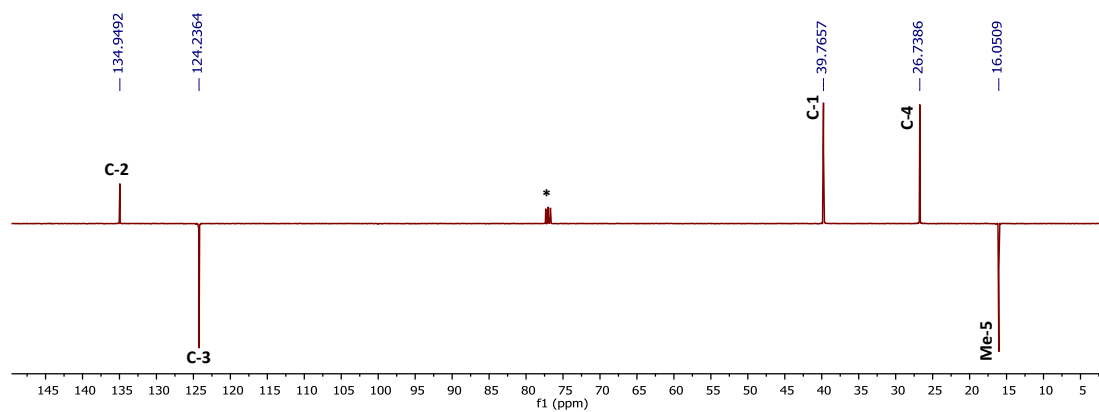


Figure 3.3: DEPTq135 ^{13}C NMR spectrum (100 MHz) of HM-1 in CDCl_3 (*)

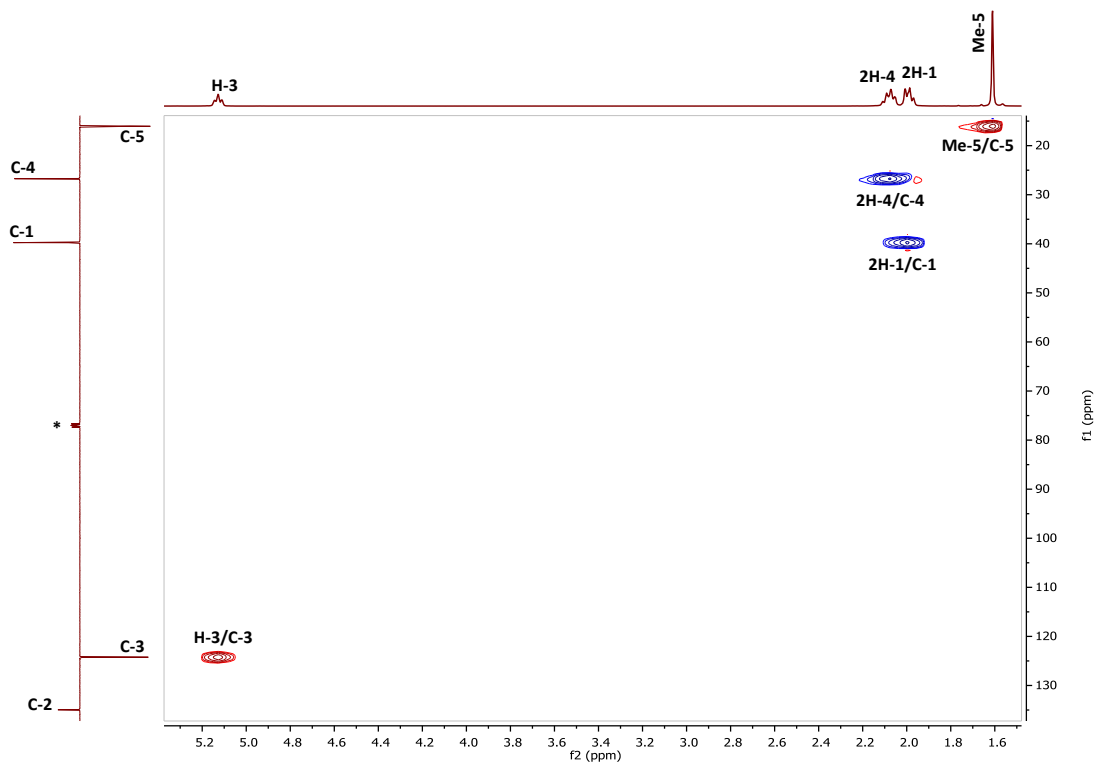


Figure 3.4: Full HSQC spectrum (400 MHz) of HM-1 in CDCl_3 (*)

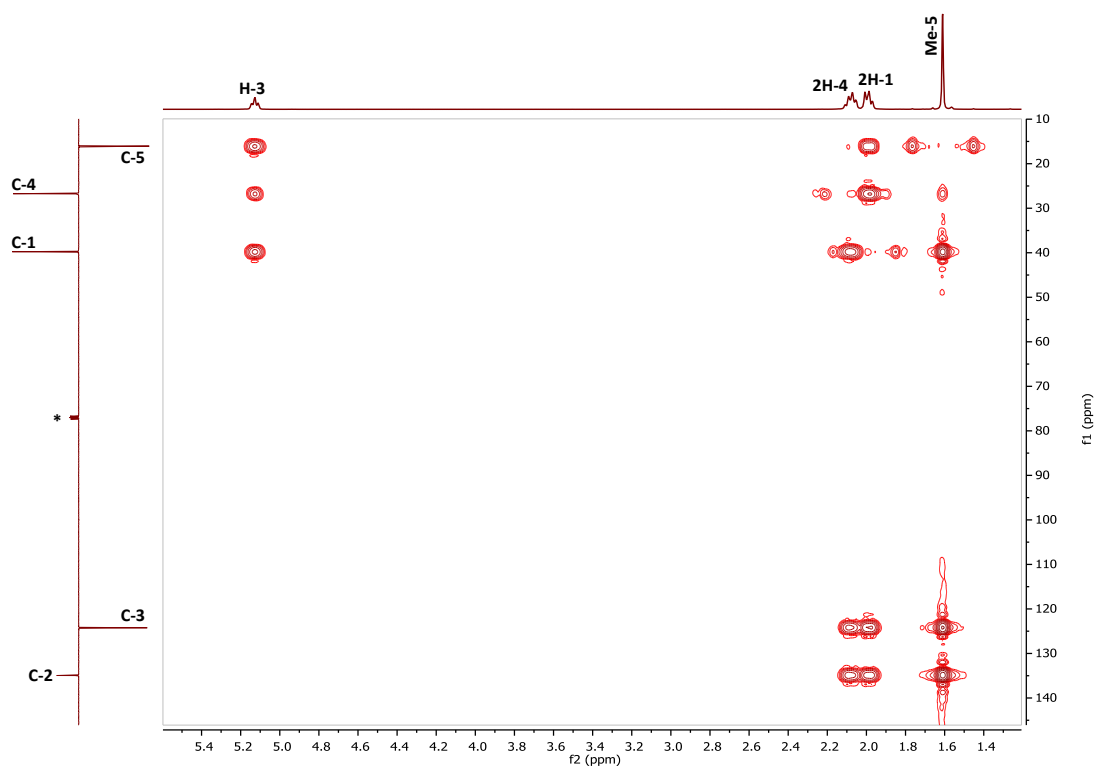


Figure 3.5: Full HMBC spectrum (400 MHz) of HM-1 in CDCl_3 (*)

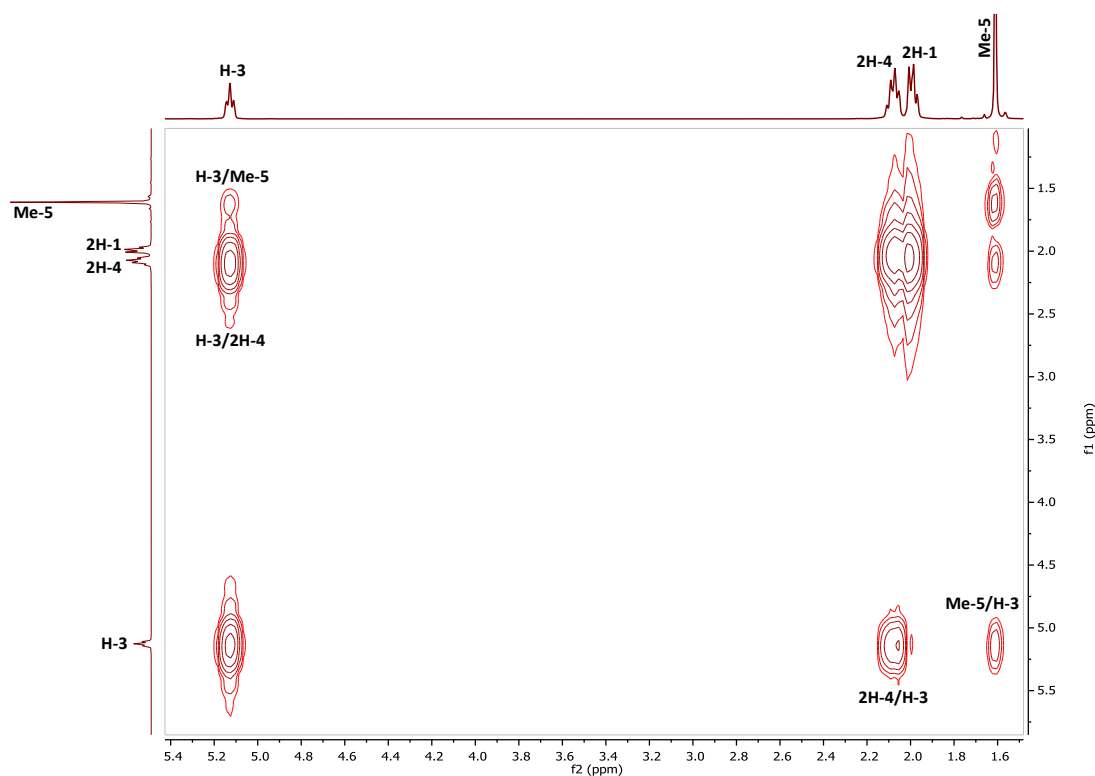


Figure 3.6: Full ^1H - ^1H COSY spectrum (400 MHz) of HM-1 in CDCl_3

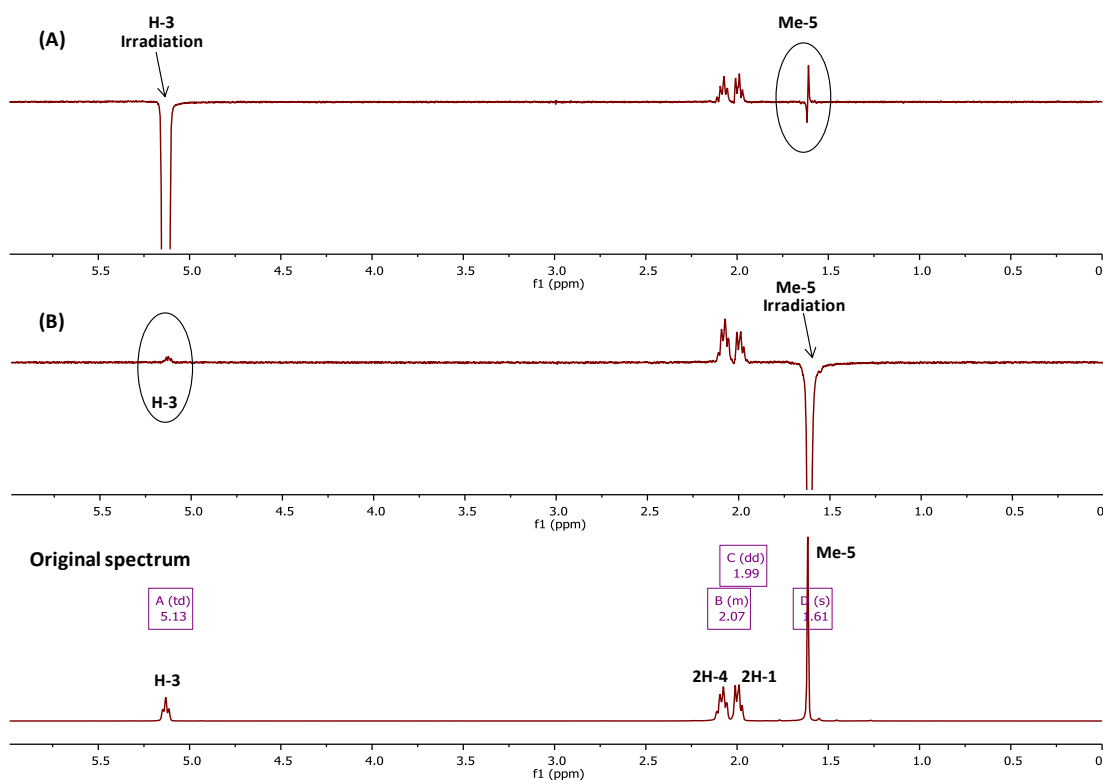


Figure 3.7: 1D NOE experiments (400 MHz) showing the NOE effects between the olefinic proton (H-3) and the methyl group (Me-5)

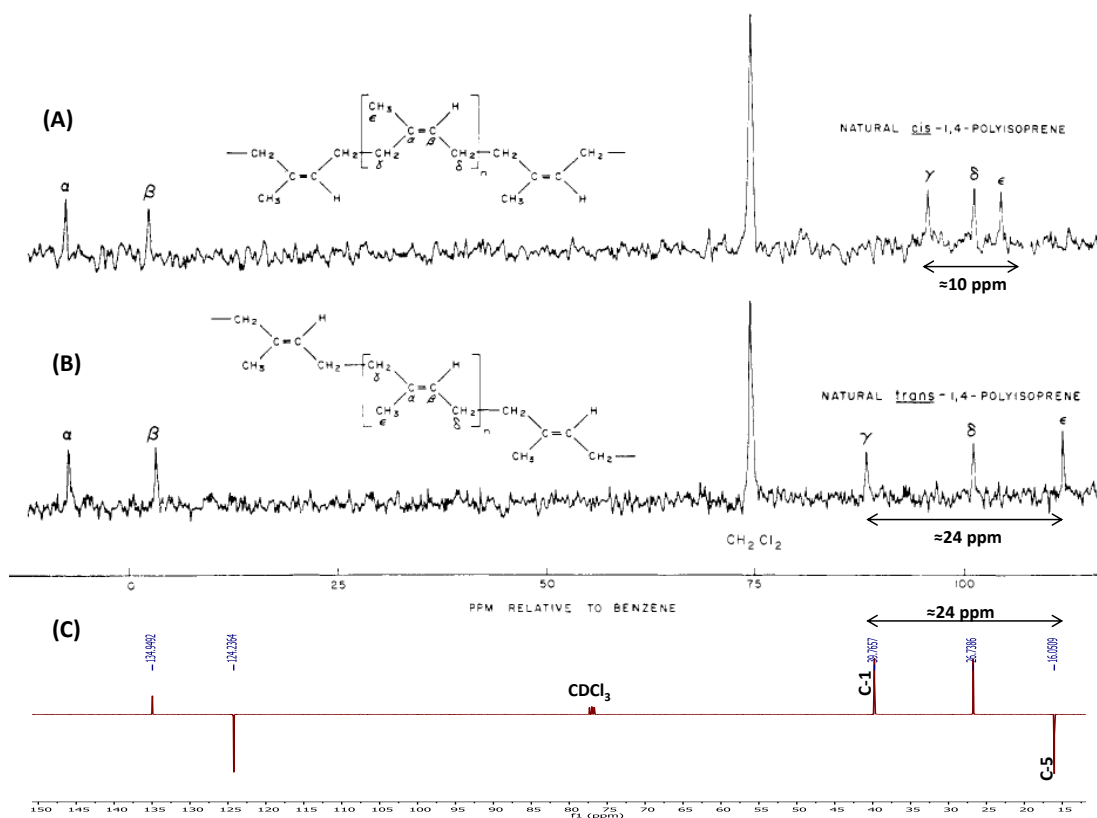


Figure 3.8: Comparison between (A & B); Random-noise, proton-decoupled 15.08 MHz ^{13}C NMR spectra of the natural *cis* and *trans*-1,4-polyisoprenes as presented in Duch and Grant, (1970) and (C); The DEPTq 135 ^{13}C NMR spectrum (400 MHz) of HM-1 in CDCl_3 .

3.3 Terpenoids

3.3.1 Friedelane-type triterpenes

The following isolated triterpenes, with the exception of HM-6, incorporate similar structural features represented by the fully saturated pentacyclic six-membered rings skeleton with eight methyl groups usually attached at positions C-4, C-5, C-9, C-13, C-14, C-17 and at C-20 where geminal methyls are located. These compounds have oxygenated functionalities on C-1 and/ or C-3 with a ketone group(s). In some of these compounds, the C-28 methyl group has undergone partial oxidation to ($-\text{CH}_2\text{OH}$), as seen in HM-2 and HM-5. The ^1H NMR spectrum of the compounds containing the 1,3-diketone moiety shows common signals of two deshielded methylene doublets at δ_{H} between 3.23-3.51 ppm, as well as of a methine quartet at δ_{H} in the range between 2.56-2.59 due to H-4 which is coupled with Me-23.

3.3.1.1 Characterisation of HM-2 as canophyllol

HM-2 was isolated from the n-hexane extract of the stem bark as white crystals. On TLC, it appeared as a purple spot after spraying with *p*-anisaldehyde-sulphuric acid reagent followed by heating. Its R_f was 0.6 on SiGel when eluted with the mobile phase 50% hexane in EtOAc.

The positive mode HRESI-MS spectrum showed a quasi-molecular ion $[M+H]^+$ at m/z 443.3886, suggesting a molecular formula of $C_{30}H_{50}O_2$ (DBE=6).

The optical rotation $[\alpha]_D^{20}$ was -21.2° ($c=0.25$, $CHCl_3$) [lit. -28.2 ($c=0.46$, $CHCl_3$) (Nozaki *et al.*, 1986)].

The 1H NMR spectrum (400 MHz, $CDCl_3$, Figure 3.11, Table 3.2) was typical of a pentacyclic triterpene as it displayed signals due to six tertiary methyl singlets at δ_H 0.72, 0.86, 0.91, 0.97, 0.99 and 1.13 as well as one secondary methyl doublet at δ_H 0.87 (3H, *d*, $J=6.9$ Hz). The absence of unsaturated protons in the spectrum indicated that the compound must be fully saturated. The spectrum also showed evidence for the existence of a primary hydroxy group by the presence of an AB quartet signal at δ_H 3.63 (2H, *ABq*). With the aid of an HSQC experiment, two sets of methylene protons and two methines were easily identified with signals at δ_H 2.39 (1H, *ddd*, $J=1.9, 5.1, 13.8$ Hz)/ 2.30 (1H, *ddd*, $J=1.1, 7.3, 13.2$ Hz), 1.96 (1H-*m*)/ 1.68 (1H, *dd*, $J=5.1, 13.0$ Hz), a quartet at δ_H 2.24 (1H, *q*, $J\approx 6.9$ Hz) and a doublet at δ_H 1.55 (1H, *d*, $J=2.7$ Hz), respectively.

From the COSY spectrum (Figure 3.15), the two methylene protons at δ_H 1.96/ 1.68, which were assigned on the carbon at δ_C 22.2 with the aid of the HSQC experiment, showed mutual vicinal couplings to both methylene protons at δ_H 2.39/ 2.30 which were assigned on the carbon at δ_C 41.5 as well as to the methine proton at δ_H 1.55 that was assigned on the carbon at δ_C 59.5. This led to a conclusion that all the previous protons were in the same spin system with the methylene carbon at δ_C 22.2 allocated in between the others. Moreover, the methyl doublet (Me-23) at δ_H 0.87 showed a vicinal coupling to the methine quartet at δ_H 2.24.

The DEPTq135 ^{13}C NMR spectrum (100 MHz, Figure 3.12) clearly revealed the presence of 30 carbon signals corresponding to this compound including seven methyls where the one at δ_C 6.8 attributed to the methyl doublet (Me-23) is characteristic methyl of a friedelane-type triterpene, twelve methylenes with the

signal at δ_C 68.0 which supported the presence of the group (-CH₂OH), four methines, six quaternaries and one saturated ketone at δ_C 213.1.

The position of the saturated ketone group was confirmed by following the correlations from the adjacent protons in the HMBC spectrum (Figure 3.14; A). The methyl doublet (Me-23) at δ_H 0.87 showed ³J correlations to the carbonyl carbon at δ_C 213.1 and to a quaternary carbon at δ_C 42.1 along with ²J correlation to the methine carbon at δ_C 58.2. Additionally, the methylene protons at δ_H 2.39/2.30 and 1.96 along with the methine quartet at δ_H 2.24 showed correlations to the same carbonyl carbon. On the other hand, the previous methylene protons at δ_H 2.39/2.30 displayed ²J and ³J correlations to the methylene carbon at δ_C 22.2 and the methine at δ_C 59.5, respectively, while the methine quartet displayed ²J correlations to the methyl doublet (Me-23) and the quaternary carbon at δ_C 42.1 as well as ³J correlations to the methyl singlet (Me-24) at δ_C 14.7 and the methine at δ_C 59.5, respectively. These data together with the previous COSY observations confirmed the position of the ketone group as C-3 and established the arrangement of the carbons at δ_C 22.2, 41.5, 58.2, 42.1 and 59.5 in the ring A of the pentacyclic compound as (C-1), (C-2), (C-4), (C-5) and (C-10) respectively. Following the correlations from the rest of the methyl groups to their neighbours in the HMBC spectrum as seen in Figure 3.14; (B, C) enabled determining the whole structure of this triterpene. Particularly, the position of the OH group on C-28 was confirmed by detecting the correlations from the methylene protons at δ_H 3.63 to their neighbouring carbons. There were ²J correlation to the quaternary carbon at δ_C 35.1 (C-17) and ³J correlations to the methine carbon at δ_C 39.4 (C-18) and to the two methylenes at δ_C 31.2 (C-22) & 29.1 (C-16) (see Figure 3.14; D). There was some uncertainty in assigning the two methylene carbons at δ_C 31.2 and 31.4 as their chemical shifts were very close to each other; however the methyl singlet (Me-26) showed a definite correlation to the one at δ_C 31.4, hence, it was sited as C-15, resulting in assigning the other one at δ_C 31.2 as C-22.

From the NOESY spectrum (Figure 3.16), the methylene protons 2H-28 (δ_H 3.63) showed strong NOE correlations to the methine proton H-18 (δ_H 1.30) and to the methyl singlet Me-26 (δ_H 0.91) as well as a weak correlation to the methyl singlet Me-29 (δ_H 0.97). The Me-26 showed NOE correlation to the methyl singlet Me-25

(δ_{H} 0.86) which in turn correlated to the Me-24 (δ_{H} 0.72) that gave correlation to the methyl doublet Me-23 (δ_{H} 0.87). These serial NOE correlations confirmed that all the previous methyl groups were placed on the same side (β) of the molecule as well as the primary hydroxy group. On the other hand, the methine proton H-4 (δ_{H} 2.24), which thereafter placed on the α side of the molecule, showed NOE correlation to the methine H-10 (δ_{H} 1.55) which in turn correlated to the methine H-8 (δ_{H} 1.41). The methyl singlet Me-27 (δ_{H} 1.13) also displayed correlation to the methine H-8. This concluded that Me-27/ H-8/ H-10 and H-4 were all located on the α side of the molecule.

On the basis of the above data and in comparison with the literature, HM-2 was identified as 28-hydroxy-3-friedelanone or canophyllol. The NMR data obtained were in good agreement with previous reports with the exception in the assignment of the carbons C-21 (δ_{C} 31.4) and C-22 (δ_{C} 33.2) (Ali *et al.*, 1999; Patra and Chaudhuri, 1987 as cited by Mahato and Kundu, 1994). From the HMBC spectrum, it was found that the methylene protons at δ_{H} 3.63 do not have any correlation with any carbon signal at δ_{C} 33.2 while it has correlation with carbon signal at δ_{C} 31.2 as discussed earlier, hence the carbon on position-22 should indisputably be at δ_{C} 31.2.

This compound was previously reported from the bark of *M. laevis* (Nakagawa *et al.*, 2004) and from other plants of the same family (Celastraceae) such as *M. diversifolia* and *Celastrus hindsii* (Nozaki *et al.*, 1986; Thuy *et al.*, 2007). It was also isolated from plants of other families such as *Calophyllum inophyllum* and *C. flavoramulum* (Calophyllaceae), *C. incrasptum* (Guttiferae) and *Pouzolzia indica* (Urticaceae) (Li *et al.*, 2010; Ferchichi *et al.*, 2012; Abbas *et al.*, 2007; Sangsuwon *et al.*, 2013).

The anti-biotic activity of canophyllol was assessed on fourteen bacterial strains and it showed no effects (Reyes-Chilpa *et al.*, 2004). However, an earlier study by Shaiq Ali *et al.* (1999) showed that it exhibited activity against some Gram positive and negative bacterial strains, while it was inactive against fungal strains. Mitaine-Offer *et al.* (2002) reported that this compound showed potent human leucocyte elastase (HLE) inhibitory activity which was linked to its anti-inflammatory properties. HLE has the ability to cleave the peptide bonds in proteins such as elastin found in the connective tissues. Ngouamegne *et al.* (2008) reported canophyllol as an

active anti-malarial compound with an IC_{50} value of 15 μM . A preliminary evaluation of the cytotoxicity and the anti-trypanosomal activity of HM-2 was performed in this work and the results were compared with those in the literature (see sections 4.1.2.1 and 4.2.2 for more details).

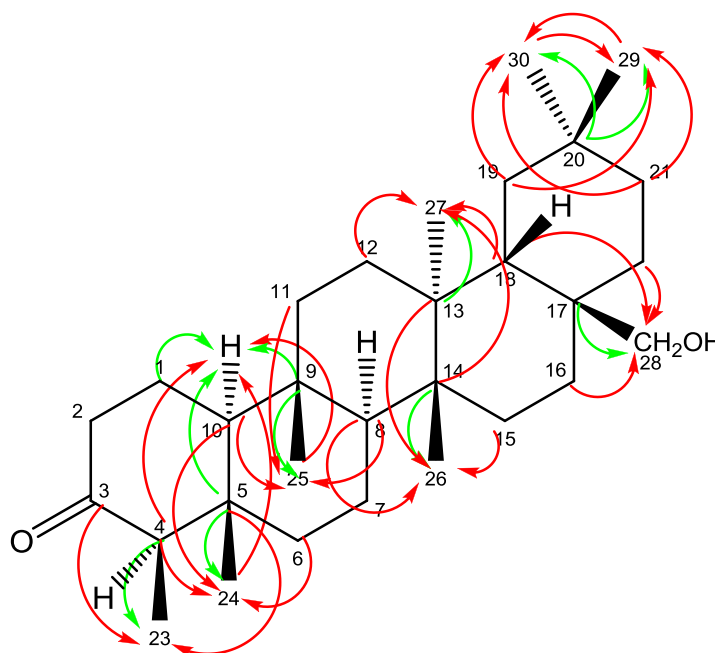


Figure 3.9: Full structure of HM-2 with HMBC correlations
 (\rightarrow) 3J (\rightarrow) 2J ^{13}C to 1H connectivity

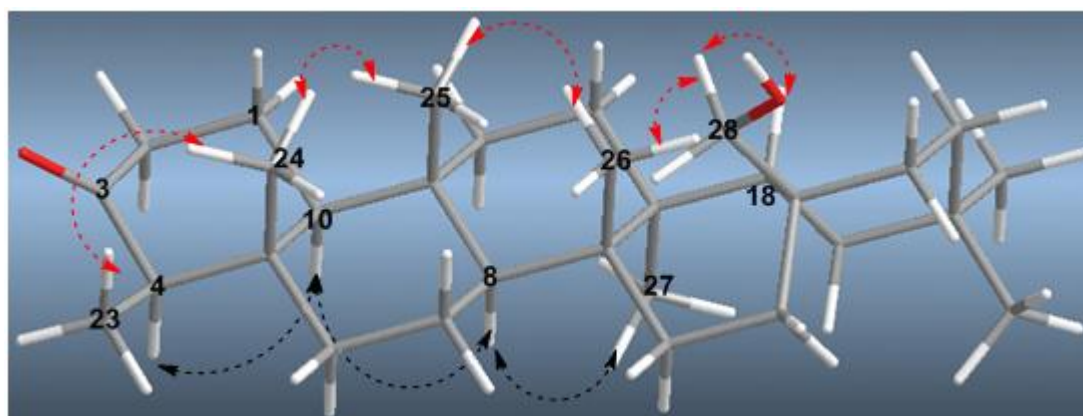


Figure 3.10: 3D structure of HM-2 with important NOESY correlations
 ($\leftarrow \cdot \rightarrow$) β ($\leftarrow \cdot \rightarrow$) α

Table 3.2: ^1H (400 MHz) and ^{13}C (100 MHz) NMR data of HM-2 in CDCl_3

Position	HM-2	
	δ_{H}	δ_{C}
1	1.96 (1H, <i>m</i>)/ 1.68 (1H, <i>dd</i> , $J= 5.1, 13.0$ Hz)	22.2
2	2.39 (1H, <i>ddd</i> , $J= 2.0, 5.1, 13.8$ Hz)/ 2.30 (1H, <i>ddd</i> , $J= 1.1, 7.3, 13.2$ Hz)	41.5
3	-	213.1
4	2.24 (1H, <i>q</i> , $J\approx 6.9$ Hz)	58.2
5	-	42.1
6	1.75 (1H, <i>m</i>)/ 1.29 (1H, <i>m</i>)	41.2
7	1.49 (1H, <i>m</i>)/ 1.39 (1H, <i>m</i>)	18.2
8	1.41 (1H, <i>m</i>)	52.5
9	-	37.4
10	1.55 (1H, <i>d</i> , $J= 2.7$ Hz)	59.5
11	1.31(1H, <i>m</i>)/ 1.47 (1H, <i>m</i>)	35.4
12	1.36 (2H) [1.44-1.25 <i>m</i>]	30.0
13	-	39.3
14	-	38.1
15	1.33 (1H, <i>m</i>)/ 1.46 (1H, <i>m</i>)	31.4
16	1.86 (1H, <i>m</i>)/ 1.31 (1H, <i>m</i>)	29.1
17	-	35.1
18	1.30 (1H, <i>m</i>)	39.4
19	1.46 (1H, <i>m</i>)/ 1.26 (1H, <i>m</i>)	34.5
20	-	28.1
21	1.33 (2H) [1.40-1.23 <i>m</i>]	33.3
22	1.40 (2H, <i>m</i>) complex	31.2
23	0.87 (3H, <i>d</i> , $J= 6.9$ Hz)	6.8
24	0.72 (3H, <i>s</i>)	14.7
25	0.86 (3H, <i>s</i>)	18.0
26	0.91 (3H, <i>s</i>)	19.0
27	1.13 (3H, <i>s</i>)	19.2
28	3.63 (2H, <i>ABq</i>)	68.0
29	0.97 (3H, <i>s</i>)	32.8
30	0.99 (3H, <i>s</i>)	34.2

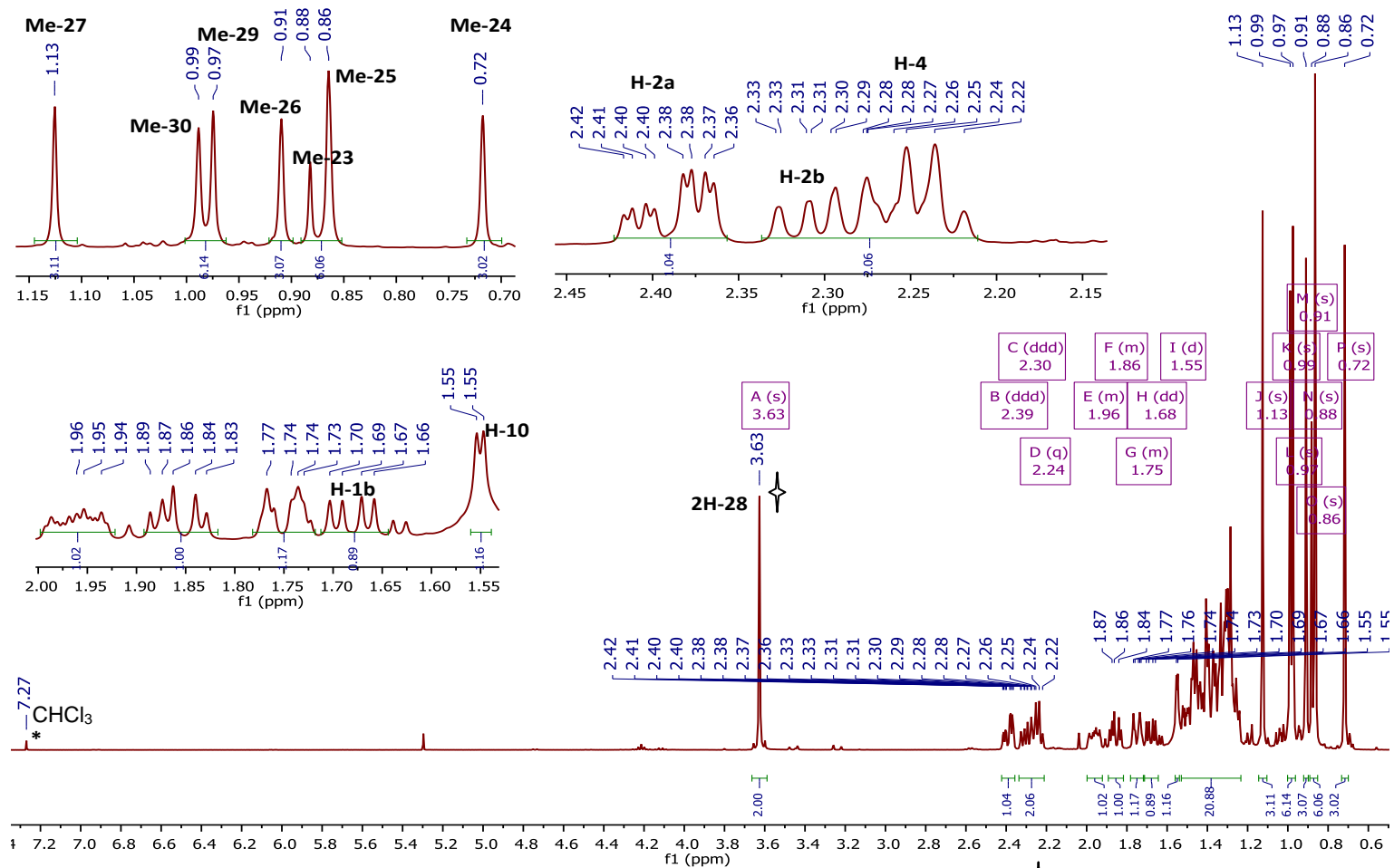


Figure 3.11: Full ^1H NMR spectrum with selected expansions (400 MHz) of HM-2 in CDCl_3 ; ∇ : Really an (ABq) rather than (s)

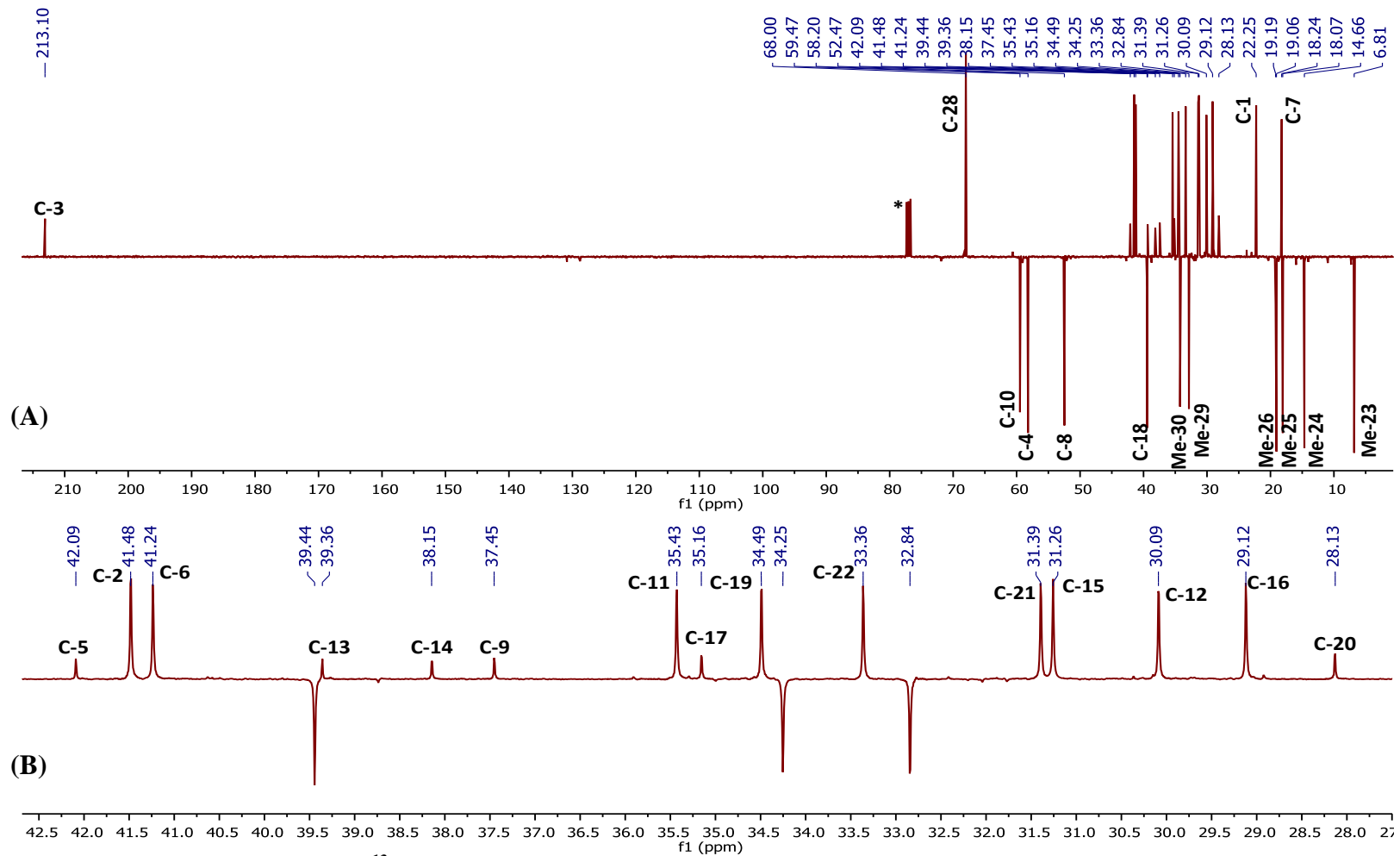


Figure 3.12: (A): Full DEPTq ^{13}C NMR spectrum (100 MHz) of HM-2 in CDCl_3 (*); (B): Selected expansion in aliphatic region

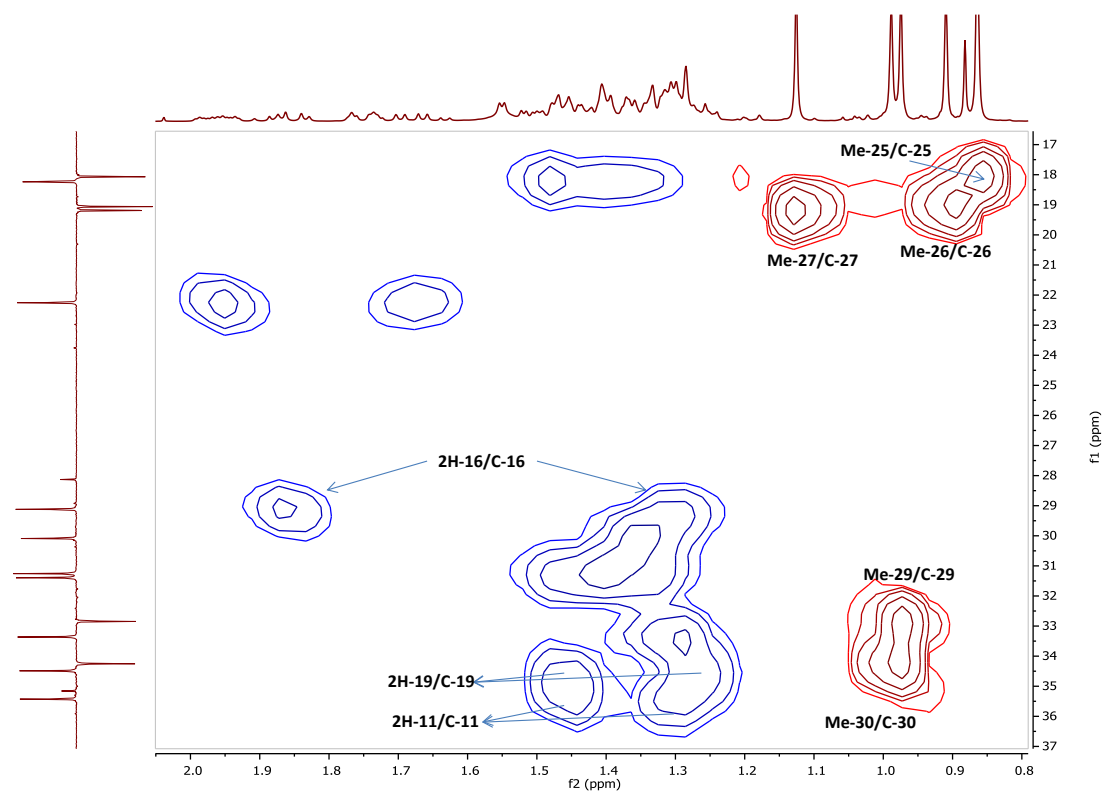
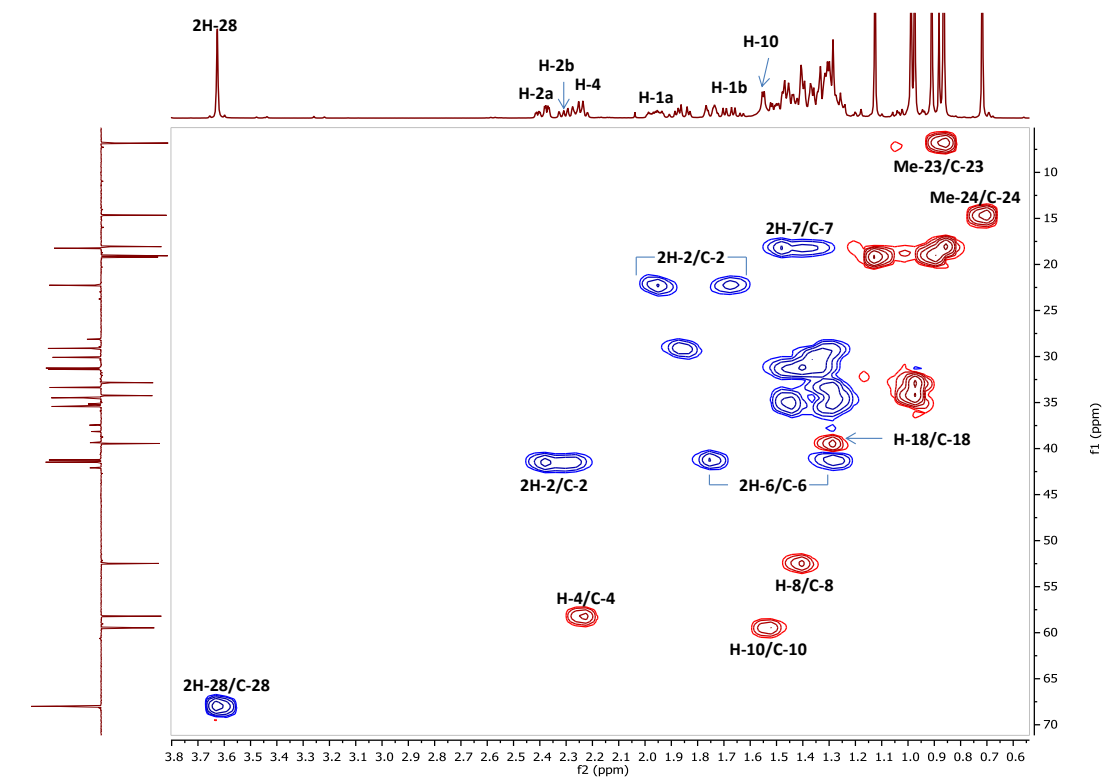
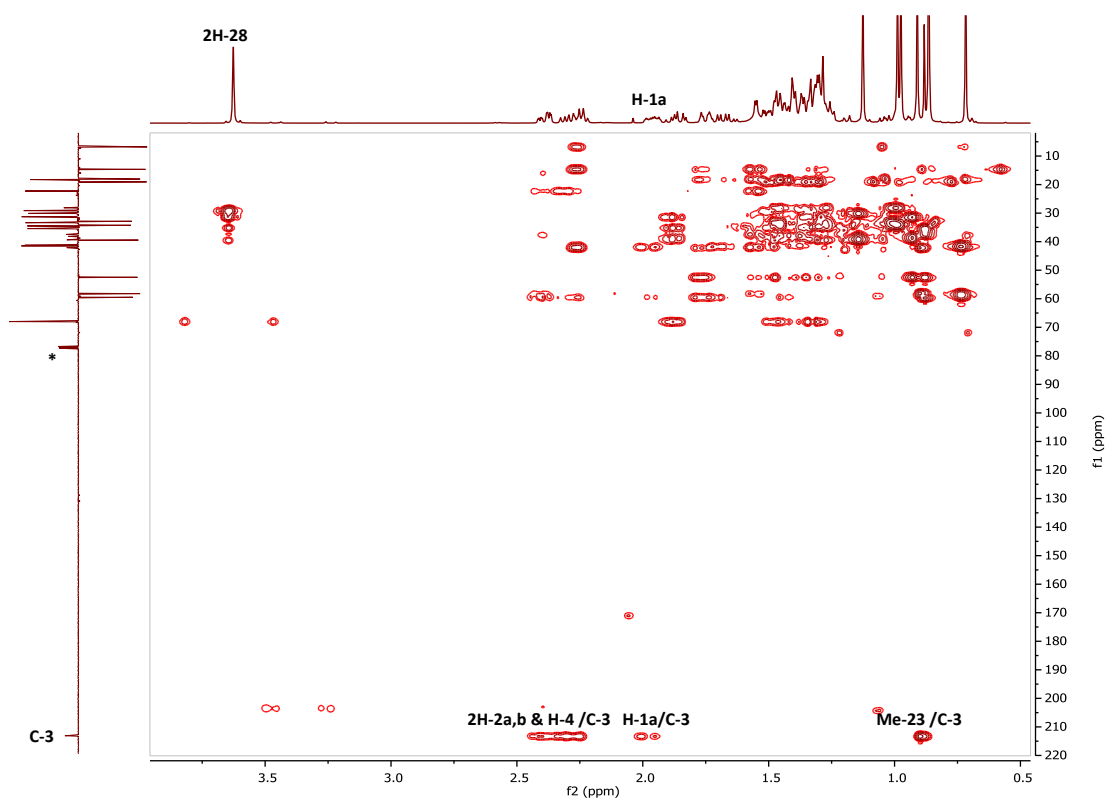
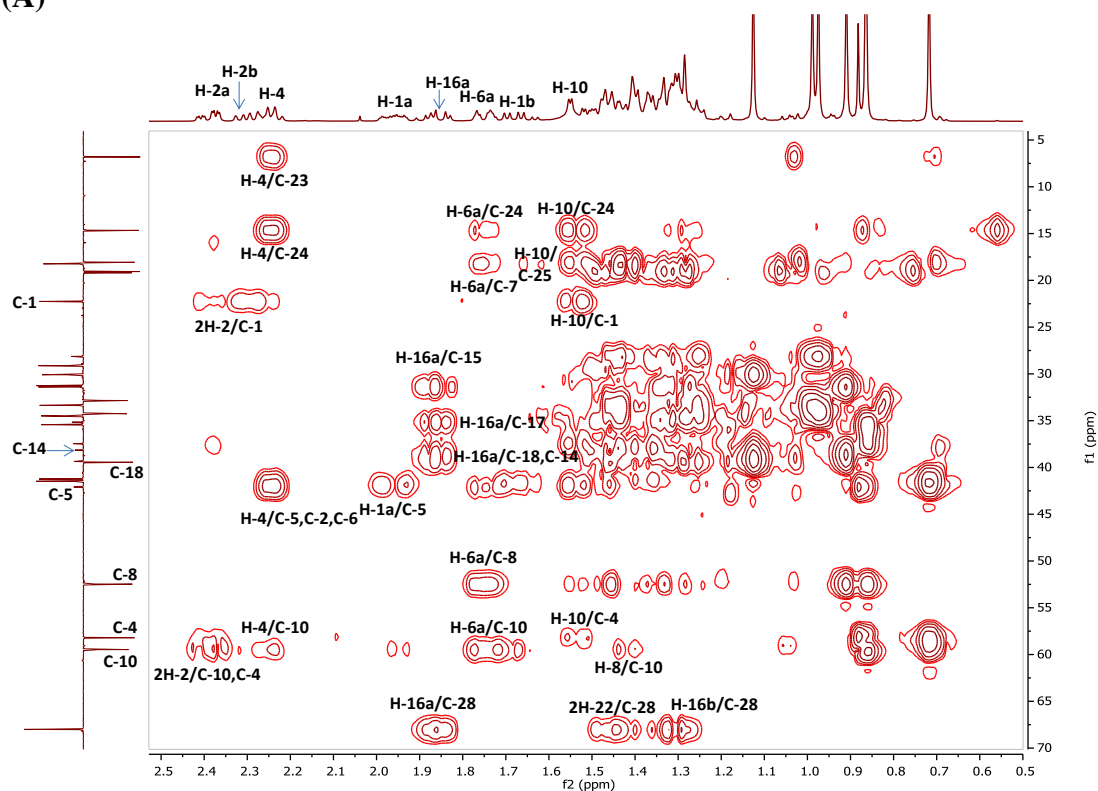


Figure 3.13: HSQC spectrum (400 MHz) of HM-2 in CDCl₃
A: Full HSQC; B: Selected HSQC expansion

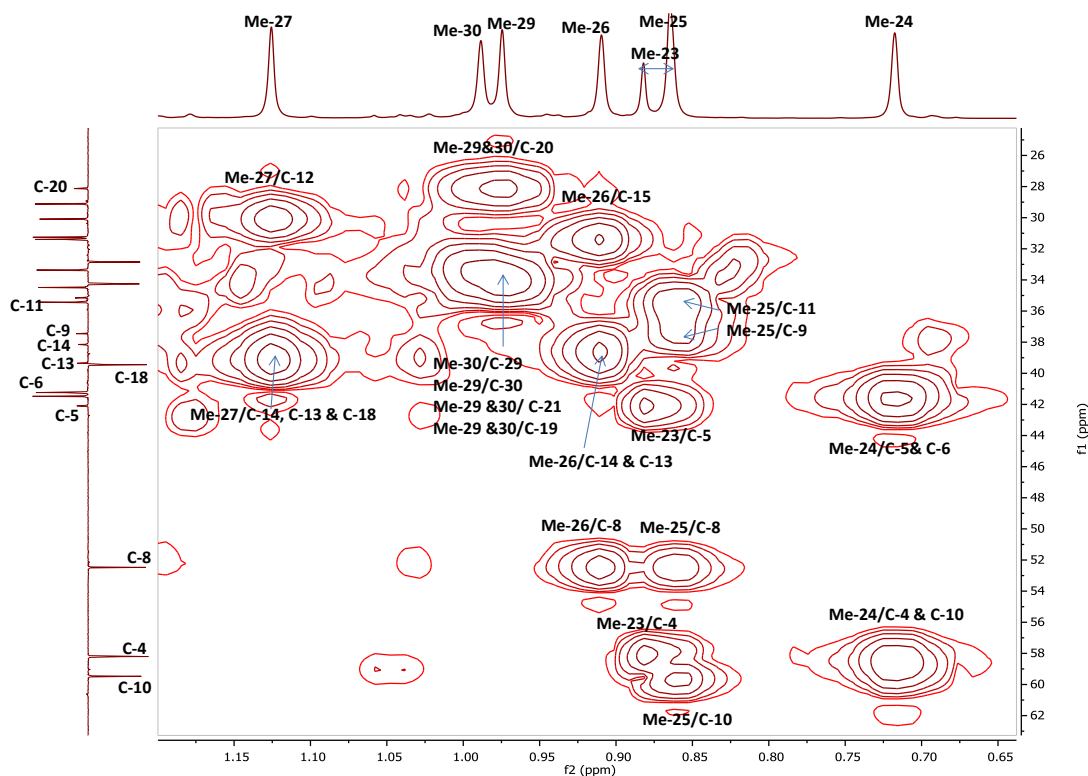


(A)

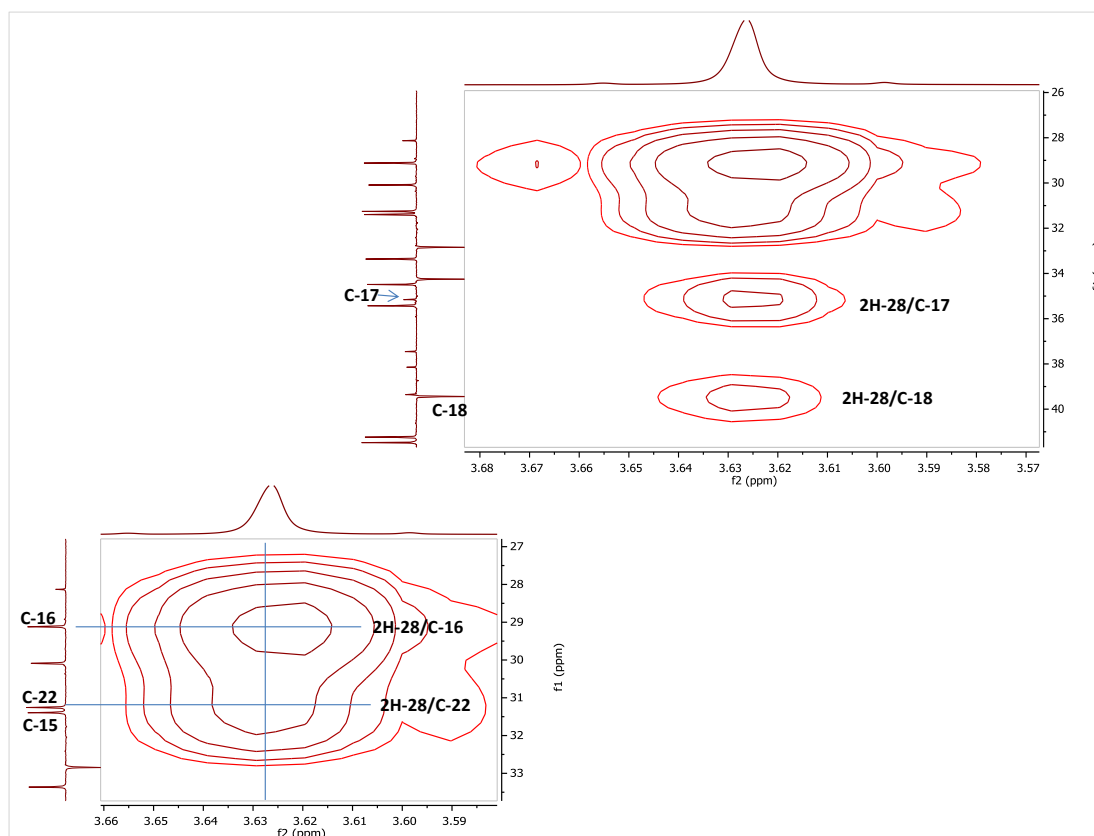


(B)

Figure 3.14: HMBC spectrum (400 MHz) of HM-2 in CDCl₃ (*)
A: Full HMBC; B: Selected HMBC expansion for the aliphatic region



(C)



(D)

Figure 3.14 (Cont.): (C): Selected HMBC expansion for methyl groups;
(D): Selected HMBC expansions for the (-CH₂OH) group

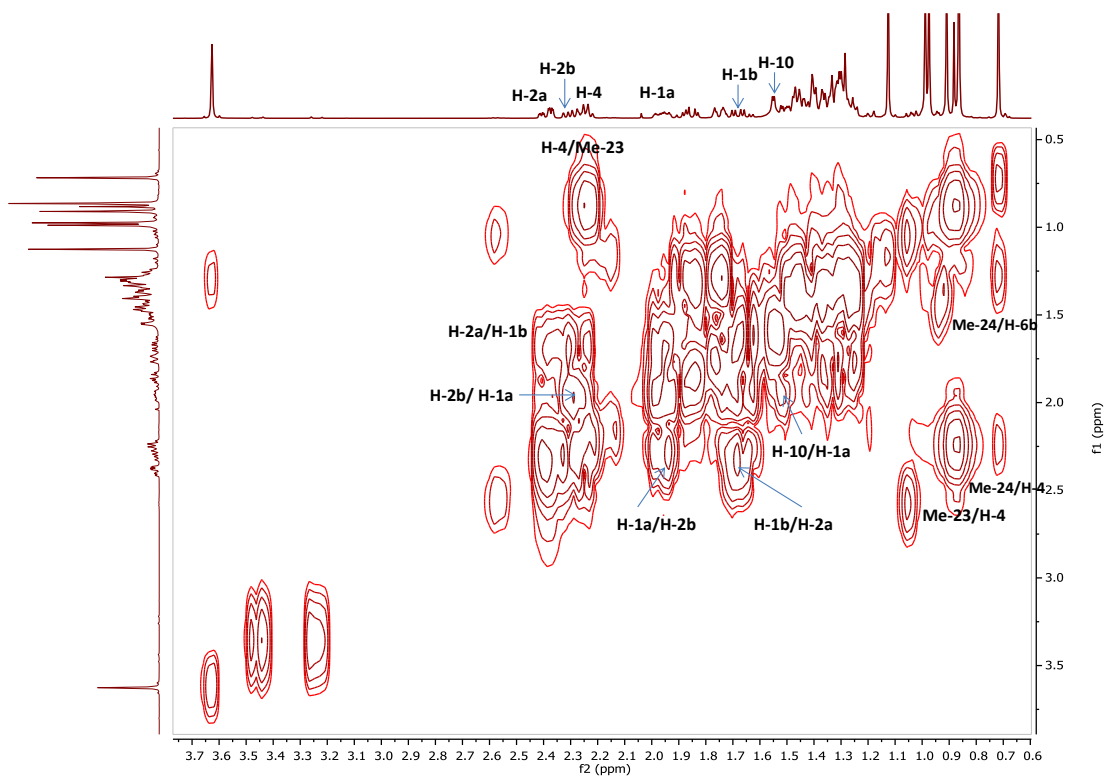


Figure 3.15: Full ^1H - ^1H COSY spectrum (400 MHz) of HM-2 in CDCl_3

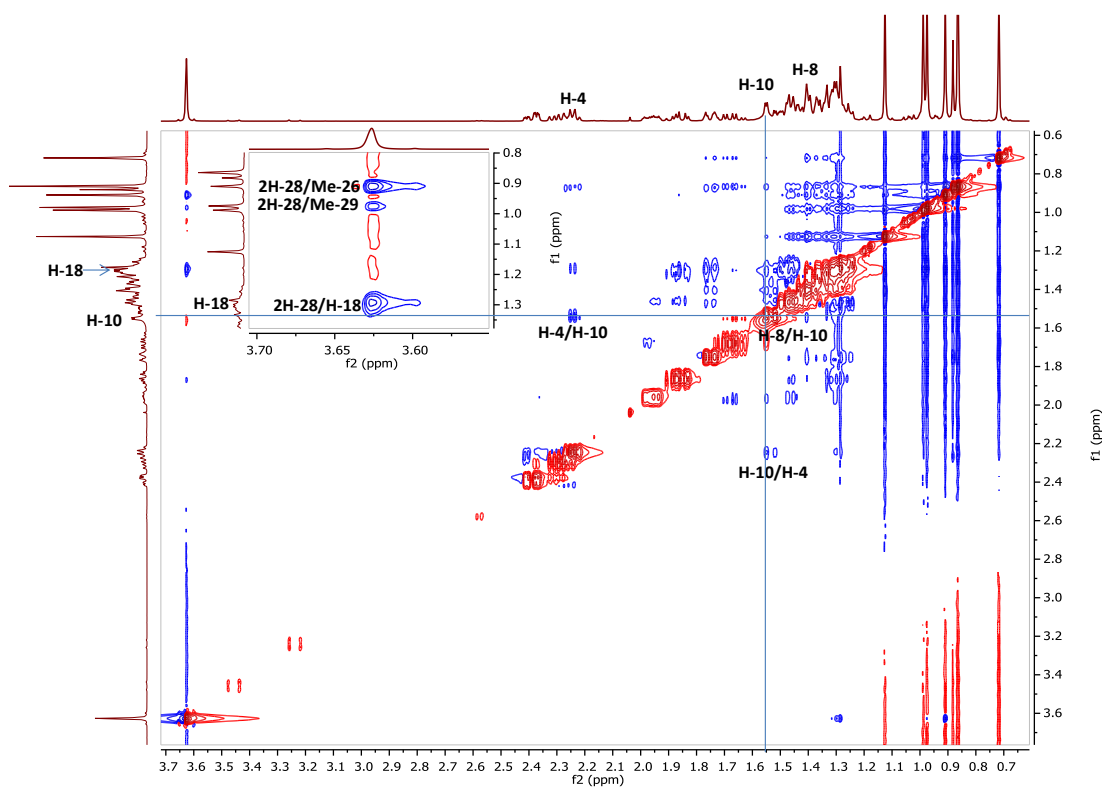


Figure 3.16: Full NOESY spectrum (400 MHz) of HM-2 in CDCl_3 with selected expansion of the $(-\text{CH}_2\text{OH})$ group

3.3.1.2 Characterisation of HM-3 as friedelan-1,3-dione

HM-3 was isolated from the n-hexane extract of the stem bark as colourless needles. On TLC, it appeared as a purple spot after spraying with *p*-anisaldehyde-sulphuric acid reagent followed by heating. Its R_f was 0.7 on SiGel when eluted with the mobile phase 50% hexane in EtOAc.

The MM-ES+APCI positive scan spectrum showed a quasi-molecular ion $[M+H]^+$ at m/z 441.4 which complies with a proposed molecular formula of $C_{30}H_{48}O_2$ (DBE=7).

The optical rotation $[\alpha]_D^{20}$ was $+2.67^\circ$ ($c=0.15$, $CHCl_3$) [lit. $+2.2$ ($c=0.14$, $CHCl_3$) (Klass *et al.*, 1992), $+2.1$ ($c=0.930$, $CHCl_3$) (Tewari *et al.*, 1974)].

The 1H NMR spectrum (400 MHz, $CDCl_3$, Figure 3.19, Table 3.3) displayed signals due to seven methyl singlets at δ_H 0.69, 0.94, 1.00, 1.02, 1.03, 1.18 and 1.20 ppm, as well as one methyl doublet at δ_H 1.05 (3H, *d*, $J=6.6$ Hz) suggesting the presence of a friedelane skeleton of a triterpene compound. The spectrum also showed a set of two methylene doublets of 1,3-diketone at δ_H 3.46/ 3.23 (2H, *d*, $J=15.9$, H-2a/b), a methine quartet at δ_H 2.58 (1H, *q*, $J=6.6$ Hz) and a methine singlet at δ_H 2.38 which were assigned later with the aid of HSQC experiment as H-4 and H-10, respectively.

The DEPTq135 ^{13}C NMR spectrum (100 MHz, Figure 3.20) clearly revealed the presence of 30 carbon signals corresponding to this compound including eight methyls where the one at δ_C 7.3 attributed to Me-23 is the characteristic methyl of the friedelane-type triterpene, ten methylenes, four methines, six quaternaries and two keto-carbonyl carbons at δ_C 202.7 (C-1) and 204.1 (C-3).

Following the 2J and 3J correlations coming from all the methyl groups and the characteristic protons to their neighbours in the HMBC spectrum (Figure 3.22) enabled the determination of the whole structure of the compound. The two methylene doublets at δ_H 3.23/3.46 showed 2J correlations to both carbonyl carbons while the Me-23 showed 3J correlations to one of them at δ_C 204.1 and to a quaternary carbon at δ_C 37.8 (C-5) as well as 2J correlation to a methine carbon at δ_C 59.0 (C-4). Moreover, the methylene H-2b at δ_H 3.23 had 3J correlations to both methines at δ_C 59.0 (C-4) and 71.8 (C-10). It was noticed that the chemical shifts of the latter methine (both δ_H , δ_C) were shifted downfield comparing to the one seen in the related compound HM-2, which was mentioned above in section 3.3.1.1. This can

be due to its position relative to the two keto-carbonyls as adjacent to the carbonyl group (C-1) and anisotropic to the other (C-3) as well as to its site on the junction between the A/B rings. The same case was noticed for the chemical shift of the H-11a comparing to that in HM-2 due to the effect of the ketone (C-1). Therefore, the configuration of the ring A as six-membered ring with two keto-carbonyls at position-1 and 3 was confirmed. Furthermore, the correlations from the methine quartet (H-4) to the carbons at δ_C 7.3 (Me-23), 37.8 (C-5), 71.8 (C-10), 204.1 (C-3) and 15.9 (Me-24) indicated as well the attachment of Me-24 to C-5 which is a quaternary carbon at the junction between the rings A and B. The methyl singlet at δ_H 1.20 gave correlations to all of the following carbons; a quaternary at δ_C 37.2 (C-9), two methines at δ_C 71.8 (C-10) & 52.1 (C-8) and a methylene at δ_C 34.5 (C-11) confirming its position in ring B where C-9 is the attachment site. In addition, the methyl singlet at δ_H 1.03 (Me-26) displayed correlations to the methylene carbon at δ_C 32.4 (C-15), the two quaternaries at δ_C 38.2 (C-14) 39.5 (C-13) and to the methine at δ_C 52.1 (C-8). On the other hand, the methyl singlet at δ_H 1.02 (Me-27) had mutual correlations with the latter two quaternaries (C-13&14), suggesting its position in alignment with (Me-26) on the join between the two six-membered rings C and D. It also showed 3J correlations to a methylene carbon at δ_C 30.1 (C-12) and to a methine at δ_C 42.7 (C-18) where in turn the methyl singlet at δ_H 1.18 (Me-28) had correlations to it as well as to two methylenes at δ_C 35.9 (C-16) & 39.3 (C-22) and to its attachment site the quaternary (C-17) at δ_C 29.9.

Finally, the two methyl singlets at δ_H 0.94 (Me-30) and 1.00 (Me-29) were identified as geminal methyls as they showed 2J correlations to the same quaternary carbon at δ_C 28.1 (C-20) along with 3J correlations to each other carbons. They also both showed 3J correlations to the methylene carbons at δ_H 35.3 (C-19) and 32.7 (C-21).

The chemical shifts of all hydrogen-bearing carbons were assigned from the HSQC spectrum (Figure 3.21) combined with COSY spectrum (Figure 3.23) which was not very helpful to confirm each spin system as most of the cross peaks were overlapped along the diagonal. However, a vicinal coupling between the methine quartet at δ_H of 2.58 and the methyl doublet at δ_H of 1.08 was very clear. The relative stereochemistry was determined from NOESY spectrum (Figure 3.24; A&B). Figure

3.18 shows the 3D structure of HM-3 with all the important NOE correlations extracted from NOESY spectrum.

On the basis of the above data and in comparison with the literature, HM-3 was identified as friedelan-1,3-dione (Figure 3.17). The NMR data obtained were in agreement with previous reports (Jangruang *et al.*, 2009; Klass *et al.*, 1992). This compound was previously reported from other plants of the same family (Celastraceae) such as *Peritassa compta* (Klass *et al.*, 1992), *Salacia verrucosa* (Somwong *et al.*, 2011) and *S. prenoides* (Tewari *et al.*, 1974). However, this is the first report of its isolation from *M. laevis*. In the literature, friedelan-1,3-dione was mainly tested for its cytotoxicity against a number of cell lines. In this study, its cytotoxicity was also evaluated along with its anti-trypanosomal activity (for further details see sections 4.1.2.1 and 4.2.2).

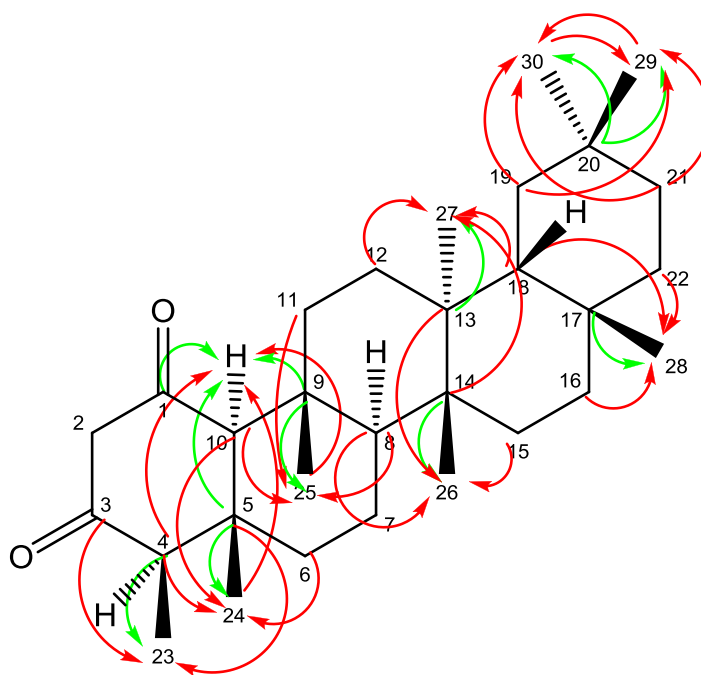


Figure 3.17: Full structure of HM-3 with key HMBC correlations
 (\rightarrow) 3J (\rightarrow) 2J ^{13}C to ^1H connectivity

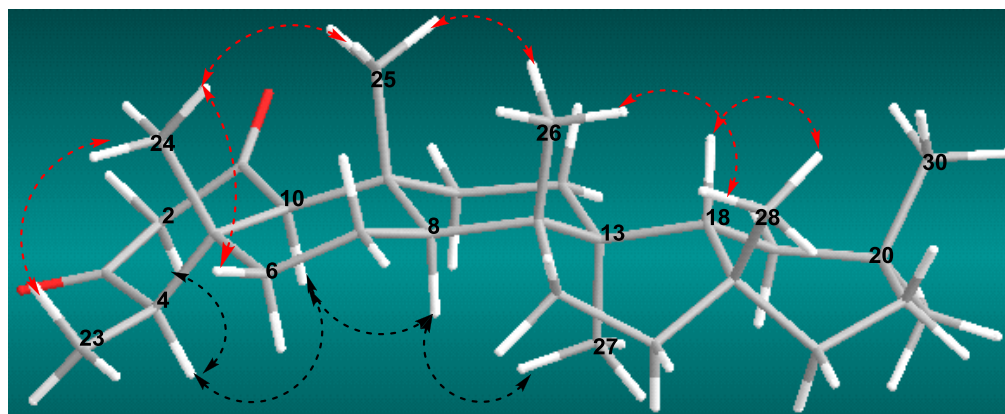


Figure 3.18: Energy minimised 3D structure of HM-3 using ChemDraw Ultra-11.0
 showing the key NOE correlations

Table 3.3: ^1H (400 MHz) and ^{13}C (100 MHz) NMR data of HM-3 in CDCl_3

Position	HM-3	
	δ_{H}	δ_{C}
1	-	202.7
2	3.23 (1H, <i>d</i> , $J= 15.9$ Hz)/ 3.46 (1H, <i>d</i> , $J= 15.9$ Hz)	60.6
3	-	204.1
4	2.58 (1H, <i>q</i> , $J= 6.6$ Hz)	59.0
5	-	37.8
6	1.40 (1H, <i>m</i>) / 1.89 (1H, <i>m</i>)	40.6
7	1.43 (1H, <i>m</i>) / 1.53 (1H, <i>m</i>)	18.04
8	1.25 (1H, <i>m</i>)	52.1
9	-	37.2
10	2.38 (1H, <i>s</i>)	71.8
11	2.15 (1H, <i>dt</i> , $J=13.5, 3.4$ Hz) / 1.15 (1H, <i>m</i>)	34.5
12	1.29 (1H, <i>m</i>) / 1.39 (1H, <i>m</i>)	30.1
13	-	39.5
14	-	38.2
15	1.27 (1H, <i>m</i>) / 1.52 (1H, <i>m</i>)	32.4
16	1.55 (1H, <i>m</i>) / 1.35 (1H, <i>m</i>)	35.9
17	-	29.9
18	1.58 (1H, <i>m</i>)	42.7
19	1.40 (1H, <i>m</i>) / 1.22 (1H, <i>m</i>)	35.3
20	-	28.1
21	1.28 (1H, <i>m</i>) / 1.46 (1H, <i>m</i>)	32.7
22	1.49 (1H, <i>m</i>) / 0.93(1H, <i>m</i>)	39.3
23	1.05 (3H, <i>d</i> , $J= 6.6$ Hz)	7.3
24	0.69 (3H, <i>s</i>)	15.9
25	1.20 (3H, <i>s</i>)	18.0
26	1.03 (3H, <i>s</i>)	20.3
27	1.02 (3H, <i>s</i>)	18.7
28	1.18 (3H, <i>s</i>)	32.0
29	1.00 (3H, <i>s</i>)	31.8
30	0.94 (3H, <i>s</i>)	35.0

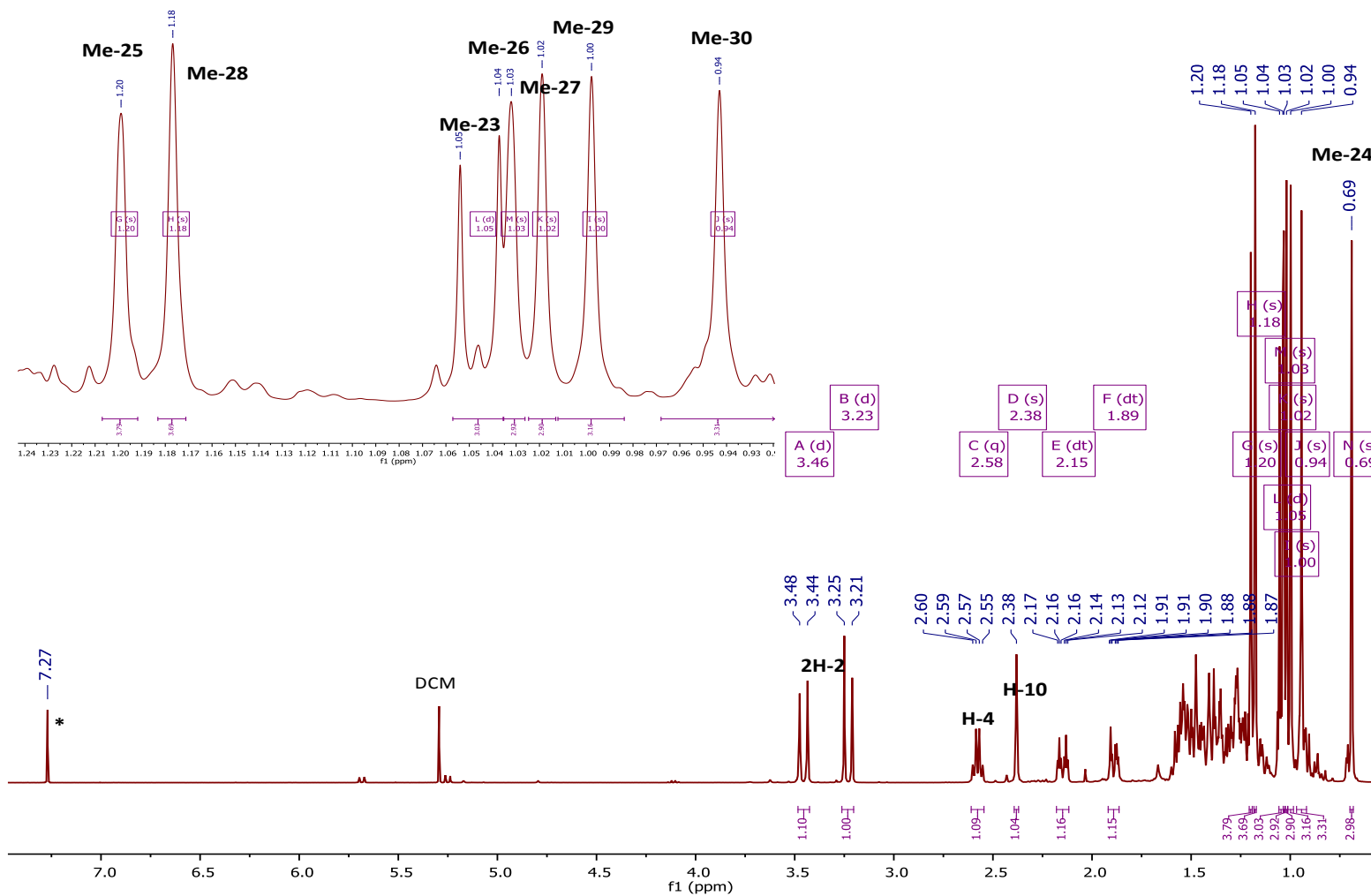


Figure 3.19: Full ^1H NMR spectrum with selected expansion (400 MHz) of HM-3 in CDCl_3 ; (*) CHCl_3 residue (DCM: dichloromethane as solvent impurity)

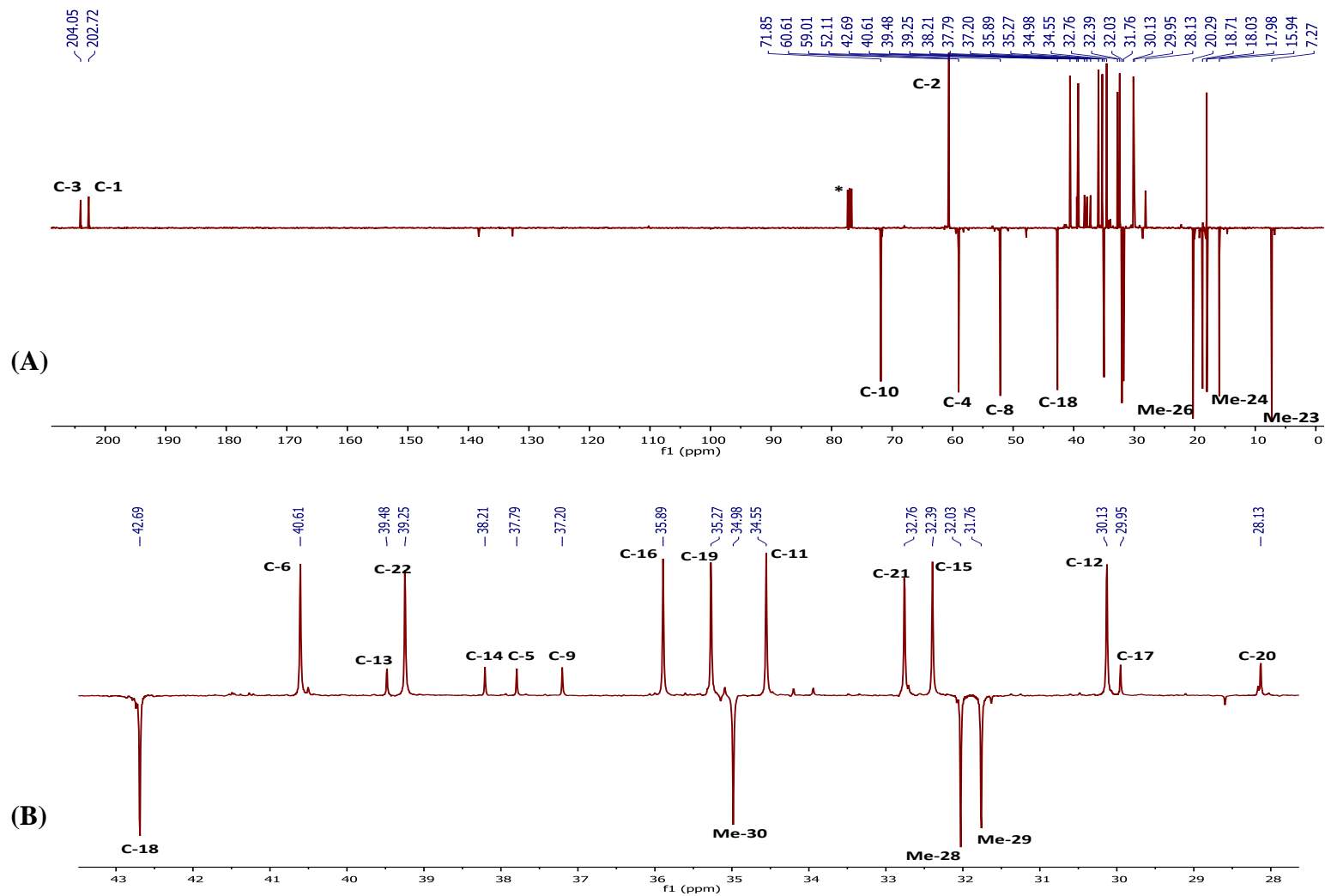


Figure 3.20: (A): Full DEPTq $^{135} \text{ }^{13}\text{C}$ NMR spectrum (100 MHz) of HM-3 in CDCl_3 (*); (B): Selected expansion in aliphatic region

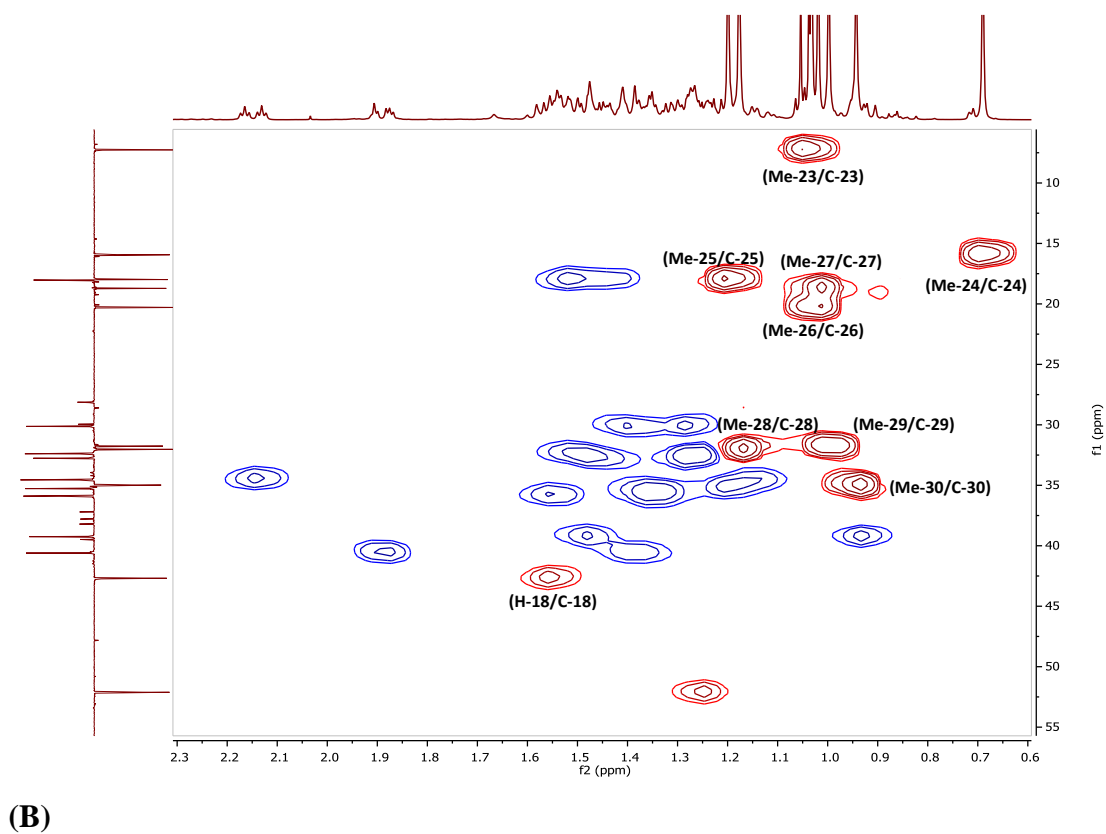
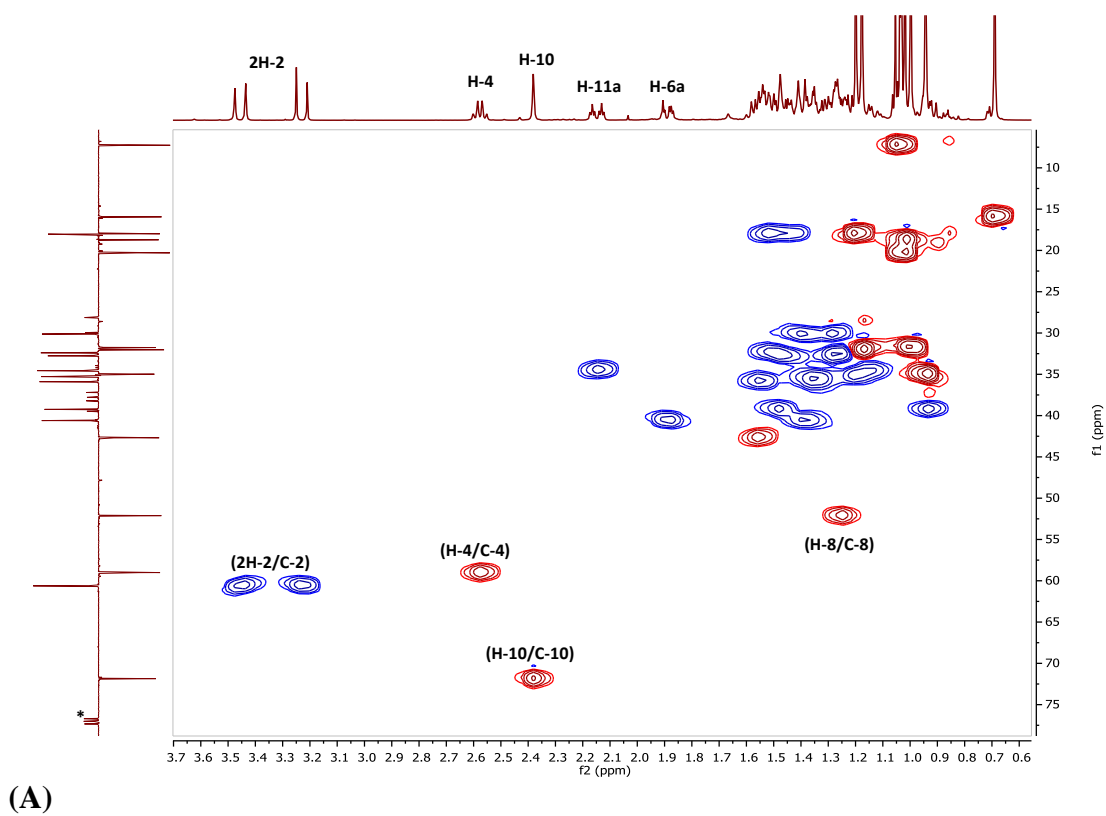
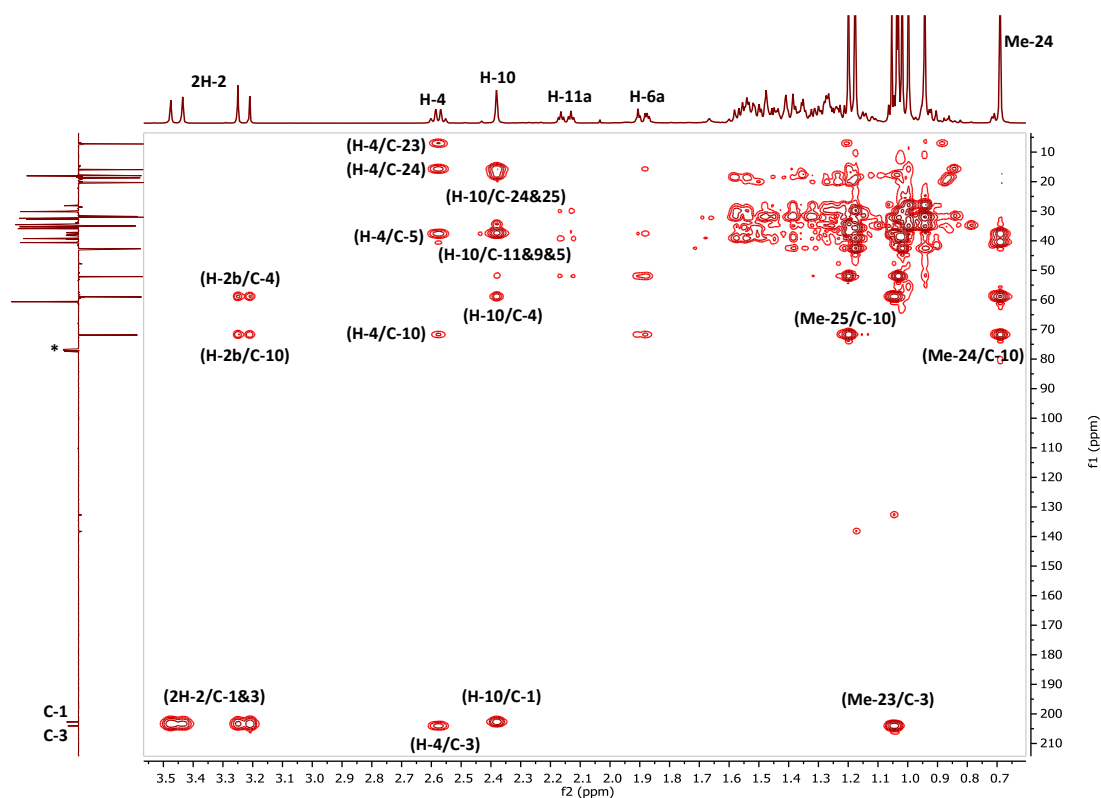
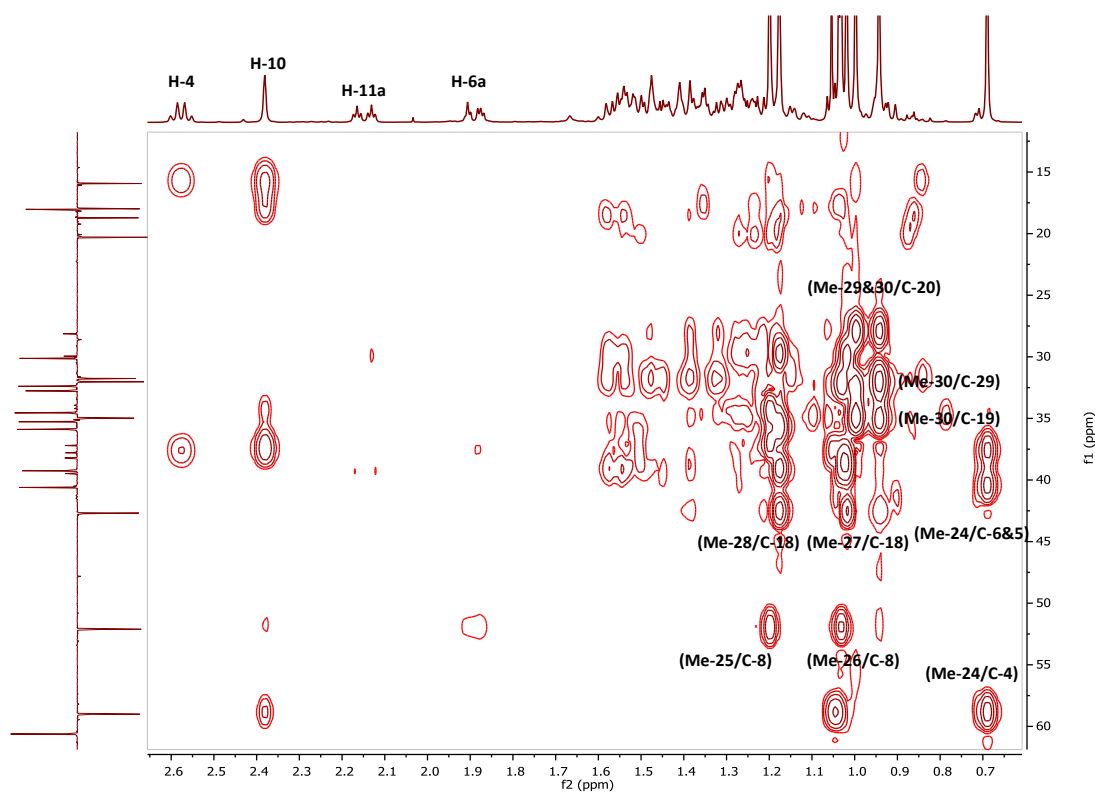


Figure 3.21: HSQC spectrum (400 MHz) of HM-3 in CDCl₃ (*)
A: Full HSQC; B: Selected HSQC expansion



(A)



(B)

Figure 3.22: HMBC spectrum (400 MHz) of HM-3 in CDCl₃ (*)
A: Full HMBC; B: First selected HMBC expansion

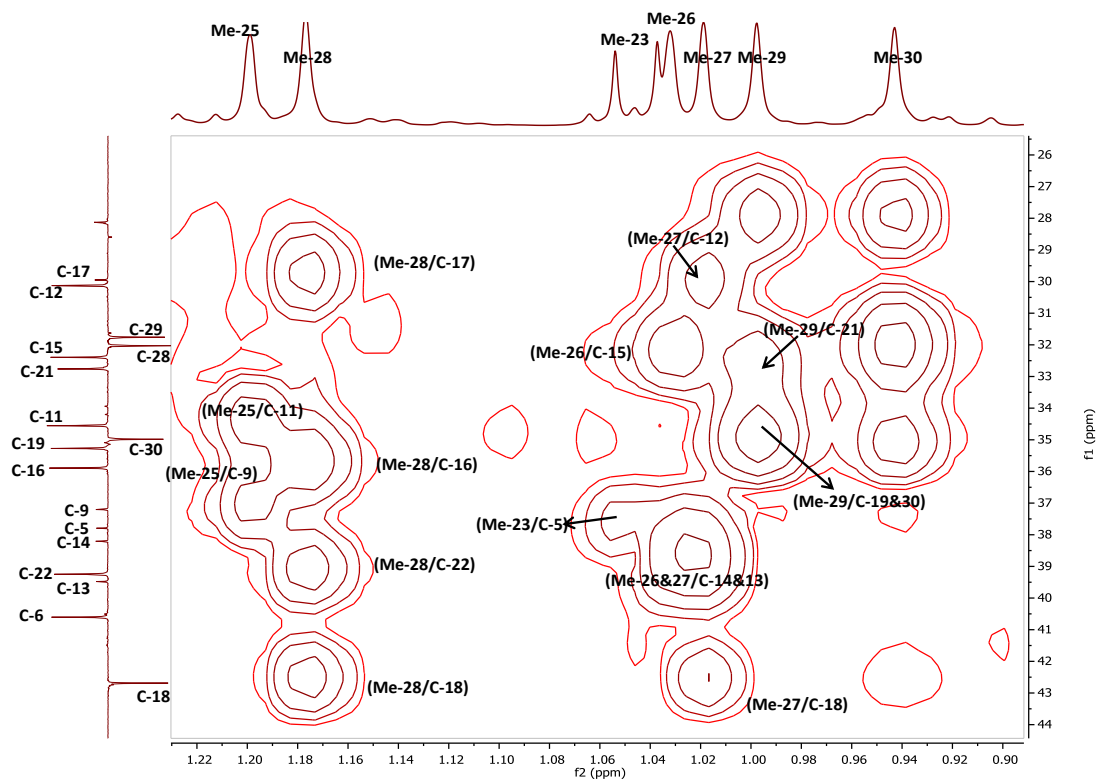


Figure 3.22 (Cont.): (C): Second selected HMBC expansion for methyl groups

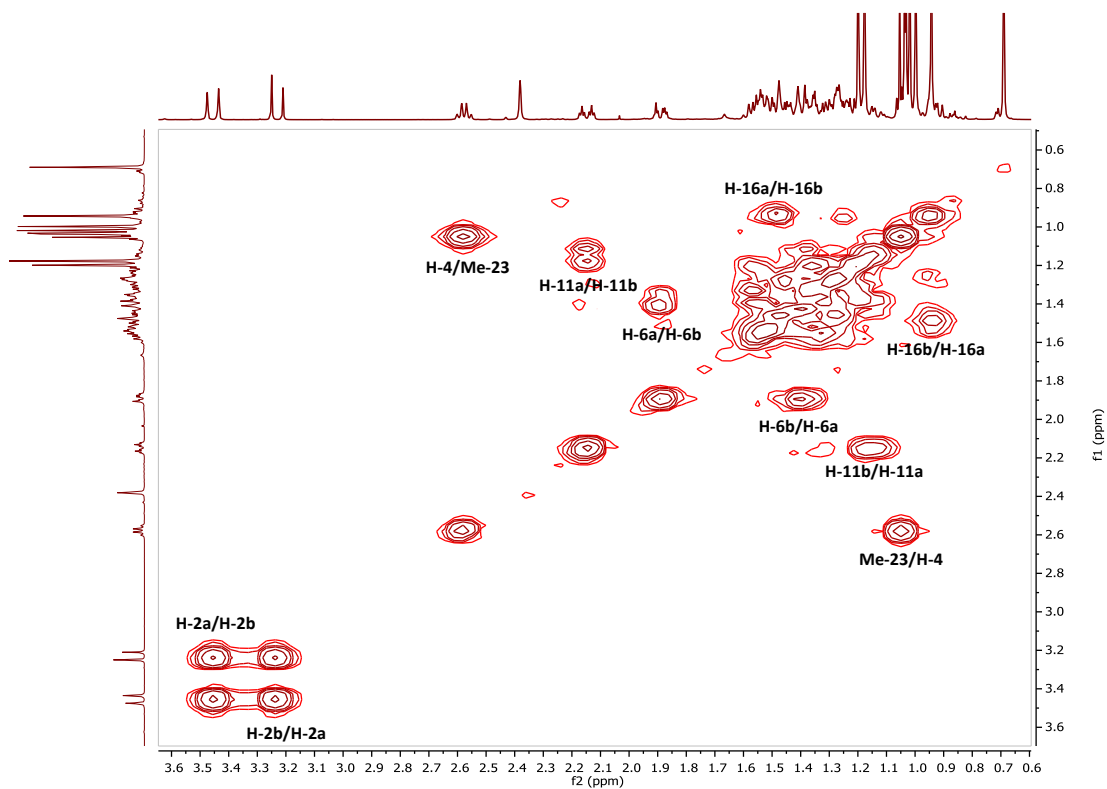
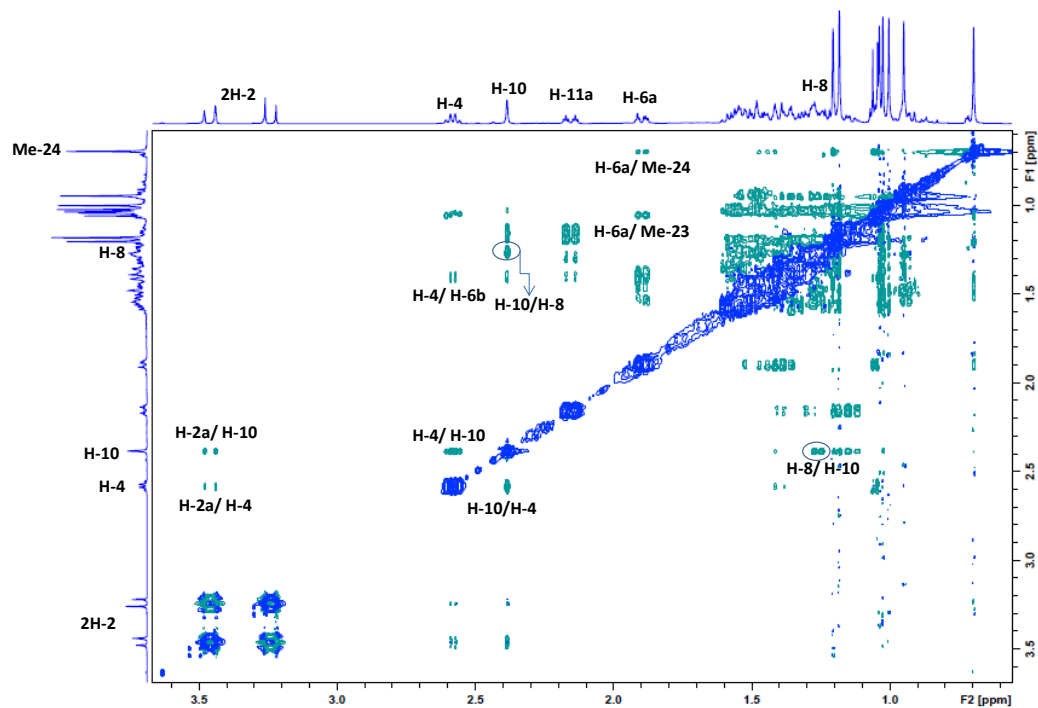
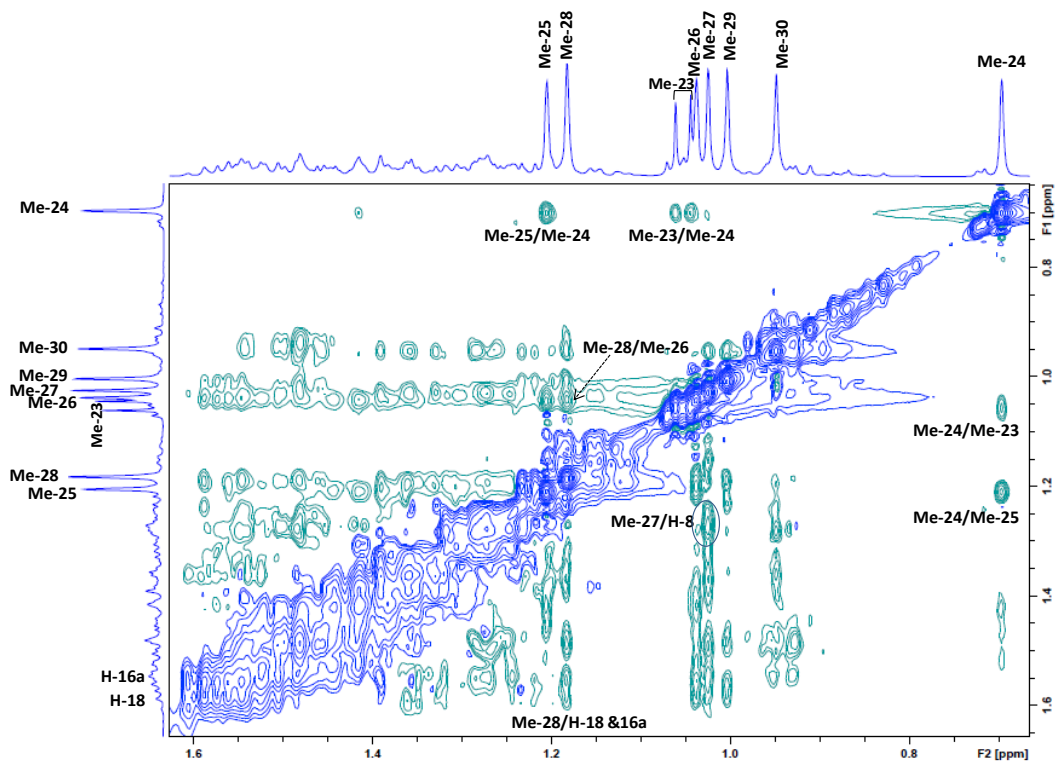


Figure 3.23: ^1H - ^1H COSY spectrum (400 MHz) of HM-3 in CDCl_3



(A)



(B)

Figure 3.24: (A): Full NOESY spectrum (400 MHz) of HM-3 in CDCl_3 using Bruker TopSpin 3.2 software; (B): Selected NOESY expansion of the methyls region

3.3.1.3 Characterisation of HM-4 as the novel triterpene (15(β)-acetoxyfriedelan-1,3-dione)

HM-4 was isolated from the n-hexane extracts of the root and stem barks as an amorphous white solid. On TLC, it appeared as a purple spot after spraying with *p*-anisaldehyde-sulphuric acid reagent followed by heating. Its R_f was 0.56 on SiGel when eluted with the mobile phase 50% hexane in EtOAc.

The MM-ES+APCI positive scan spectrum showed a quasi-molecular ion $[M+H]^+$ at m/z 499.4, which complies with a proposed molecular formula of $C_{32}H_{50}O_4$ (DBE=8).

The optical rotation $[\alpha]_D^{20}$ was -42.4° ($c=0.25$, $CHCl_3$).

The IR spectrum exhibited absorption bands at (1709 and 1725 cm^{-1}) indicated the presence of carbonyl groups and an ester group, (2870, 2932 cm^{-1}) for (C-H) stretch (Williams and Fleming, 2008).

The 1H NMR spectrum (400 MHz, $CDCl_3$, Figure 3.27, Table 3.4) showed similar features to those in the spectrum obtained for the previous compound HM-3 suggesting this compound to be a derivative friedelane triterpene. The spectrum displayed seven methyl singlets at δ_H 0.68, 0.95, 1.01, 1.03, 1.18, 1.22 and 1.25 ppm attributed to Me-24, Me-30, Me-27, Me-29, Me-26, Me-25 and Me-28, respectively, in addition to one methyl doublet at δ_H 1.04 (3H, *d*, $J=6.6$ Hz, Me-23). The methine quartet at δ_H 2.56 (1H, *q*, $J=6.6$ Hz, H-4) and the methine singlet at δ_H 2.37 as well as the two methylene doublets of 1,3-diketone at δ_H 3.46/3.25 (2H, *d*, $J=15.8$ Hz, H-2a/b) were all also observed. The spectrum displayed new features represented by the existence of a methyl singlet at a downfield shift δ_H 2.04 ppm indicating it to be part of an acetyl group and an oxymethine doublet at δ_H 4.75 (1H, *d*, $J=7.9$ Hz, H-15).

From the DEPTq135 ^{13}C NMR spectrum (100 MHz, Figure 3.28), 32 carbon signals, corresponded to this compound, were picked up with the aid of HSQC experiment. These carbons included nine methyls, where the one at an upfield shift δ_C 7.2 ppm attributed to Me-23 is the characteristic methyl of the friedalene-type triterpene, nine methylenes, four methines, one oxymethine at δ_C 77.6 ppm, six quaternary carbons (C-5, 9, 13, 14, 17, 20) and three carbonyl carbons comprising of two keto-carbonyl carbons at δ_C 202.6 (C-1) and 203.8 (C-3) and one at δ_C 170.8 ppm supporting the presence of an ester carbonyl.

From the HMBC spectrum (Figure 3.30: A&B), the construction of the ring A of the penta-cyclic skeleton with two keto-carbonyls at positions 1 and 3 was confirmed by following the typical correlations seen in the previous compound HM-3. The two methyl singlets at δ_{H} 0.95 (Me-30) and 1.03 (Me-29) were identified as geminal methyls as they showed 2J correlations to the same quaternary carbon at δ_{C} 28.1 (C-20) along with 3J correlations to each other carbons. They both also showed 3J correlations to the methylene carbons at δ_{H} 35.5 (C-19) and 31.9 (C-21).

The only correlation from the methyl singlet at δ_{H} 2.04 (Me-32) to the carbonyl carbon at δ_{C} 170.8 established the presence of an acetyl group. The 3J correlations observed from the oxymethine doublet at δ_{H} 4.75 to the carbons at δ_{C} 15.2 (Me-26), 29.8 (C-17), 42.8 (C-13) 52.3 (C-8) and 170.8 (C-31) along with the 2J correlation to the methylene carbon at δ_{C} 45.0 (C-16) implied that the acetyl group should be attached to the carbon at δ_{C} 77.6 (C-15) (see Figure 3.30: C). This position was further supported by the COSY experiment (Figure 3.31), which revealed a vicinal coupling between the oxymethine proton at δ_{H} 4.75 and the methine proton at δ_{H} 2.16 which was assigned on the carbon at δ_{C} 45.0 (C-16). It was also observed that the methine quartet at δ_{H} 2.56 (C-4) exhibited a vicinal coupling with the methyl doublet at δ_{H} 1.04 (Me-23) and a long range coupling with the methylene proton at δ_{H} 3.46 (H-2a). The methine proton at δ_{H} 2.37 (H-10) also had a long range coupling with the methylene protons (2H-2a/b).

The relative stereochemistry of the acetate group was established from the NOESY spectrum (Figure 3.32: A&B). The methine doublet H-15 (δ_{H} 4.75) showed NOE correlations to the methyl singlet Me-27 (δ_{H} 1.01) and to the methine H-8 (δ_{H} 1.40) as well as to the methylene protons H-7b (δ_{H} 1.21) and H-16a (δ_{H} 2.16). The methine proton H-8 correlated to H-10 (δ_{H} 2.37) which in turn showed correlation to H-4 (δ_{H} 2.56). These observations led to the conclusion that H-15 is axial and should be placed on the α side of the molecule implying that the acetate group should be therefore on the β side and in an equatorial orientation.

By the analysis of the 2D NMR data obtained from COSY, HSQC, HMBC and NOESY experiments, the HM-4 signal assignment was completed. The spectral data were in agreement with those of a related friedelane triterpene, friedelan-1,3-dione (HM-3), except for the signals due to the acetyl group. Therefore, HM-4, for which

the trivial name 15(β)-acetoxyfriedelan-1,3-dione (Figure 3.25) is proposed, was determined as a novel friedelane triterpene derivative. This compound has been isolated before from the same sample of the root bark of this plant in preliminary work carried out by an MPharm student (Tait, 2011). However, this is the first report of its isolation from the stem bark of this plant as well, and the first report which explained its relative stereochemistry. HM-4 showed no cytotoxicity effects when tested against the normal fibroblasts cell line Hs27 (section 4.1.2.1).

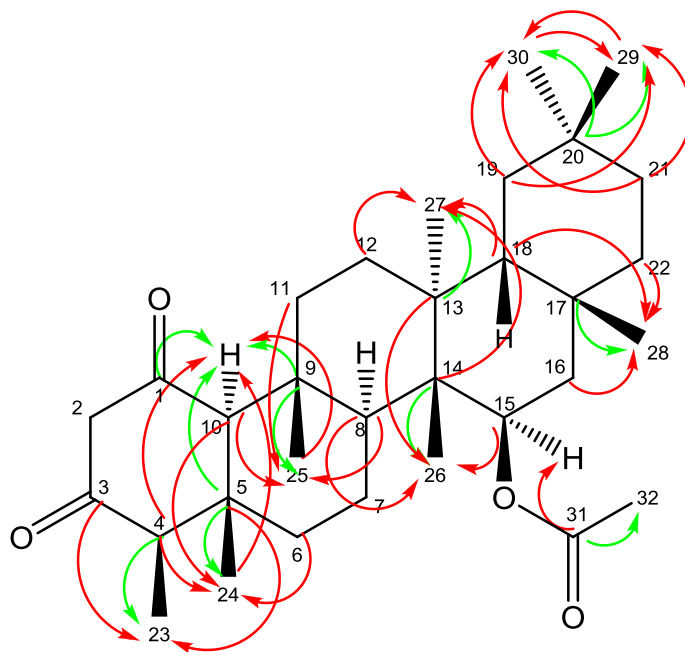


Figure 3.25: Structure of HM-4 with HMBC correlations (\rightarrow) 3J (\rightarrow) 2J

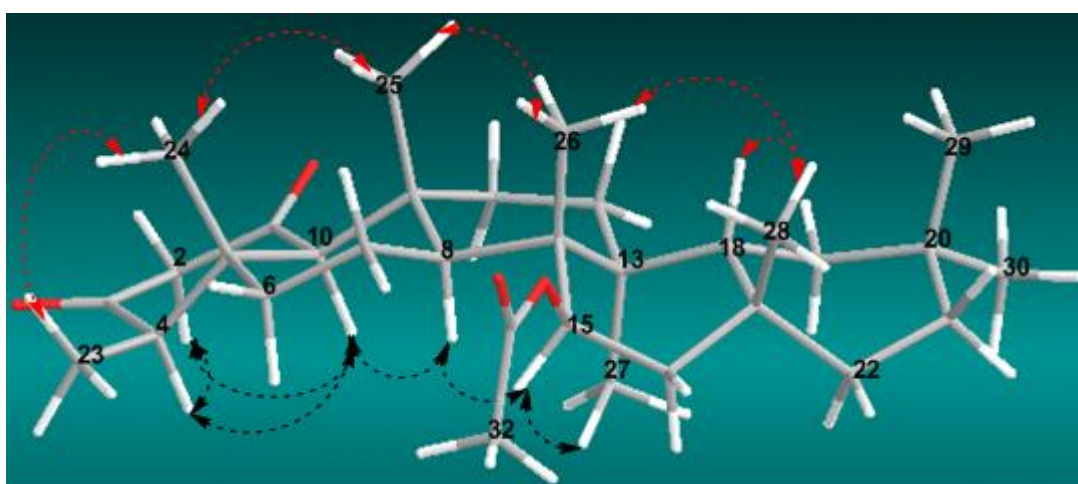


Figure 3.26: Energy minimised 3D structure of HM-4 with important NOE correlations (\leftrightarrow) β (\leftrightarrow) α

Table 3.4: ^1H (400 MHz) and ^{13}C (100 MHz) NMR data of HM-4 in CDCl_3

Position	HM-4	
	δ_{H}	δ_{C}
1	-	202.6
2	3.46 (1H, <i>d</i> , $J=15.8$ Hz)/ 3.25 (1H, <i>d</i> , $J=15.8$ Hz)	60.7
3	-	203.8
4	2.56 (1H, <i>q</i> , $J=6.6$ Hz)	59.0
5	-	37.5*
6	1.41 (1H, <i>m</i>)/ 1.87 (1H, <i>dt</i> , $J=13.3, 3.1$ Hz)	40.5
7	1.21 (1H, <i>m</i>)/ 1.53 (1H, <i>m</i>)	19.0
8	1.40 (1H, <i>m</i>)	52.3
9	-	37.6*
10	2.37 (1H, <i>s</i>)	71.7
11	1.12 (1H, <i>m</i>)/ 2.20 (1H, <i>m</i>)	34.5
12	1.32 (1H, <i>m</i>)/ 1.57 (1H, <i>m</i>)	30.5
13	-	42.8
14	-	40.2
15	4.75 (1H, <i>d</i> , $J=7.9$ Hz)	77.6
16	1.21 (1H, <i>m</i>)/ 2.16 (1H, <i>m</i>)	45.0
17	-	29.8
18	1.65 (1H, <i>dd</i> , $J=5.4, 12.6$ Hz)	41.5
19	1.17 (1H, <i>m</i>)/ 1.30 (1H, <i>m</i>)	35.5
20	-	28.1
21	1.31 (1H, <i>m</i>)/ 1.44 (1H, <i>m</i>)	31.9
22	0.95 (1H, <i>m</i>)/ 1.37 (1H, <i>m</i>)	38.7
23	1.04 (3H, <i>d</i> , $J=6.6$ Hz)	7.2
24	0.68 (3H, <i>s</i>)	15.7
25	1.22 (3H, <i>s</i>)	18.0
26	1.18 (3H, <i>s</i>)	15.2
27	1.01 (3H, <i>s</i>)	18.9
28	1.25 (3H, <i>s</i>)	32.2
29	1.03 (3H, <i>s</i>)	30.9
30	0.95 (3H, <i>s</i>)	35.6
31	-	170.8
32	2.04 (3H, <i>s</i>)	21.9

* These carbons are exchangeable.

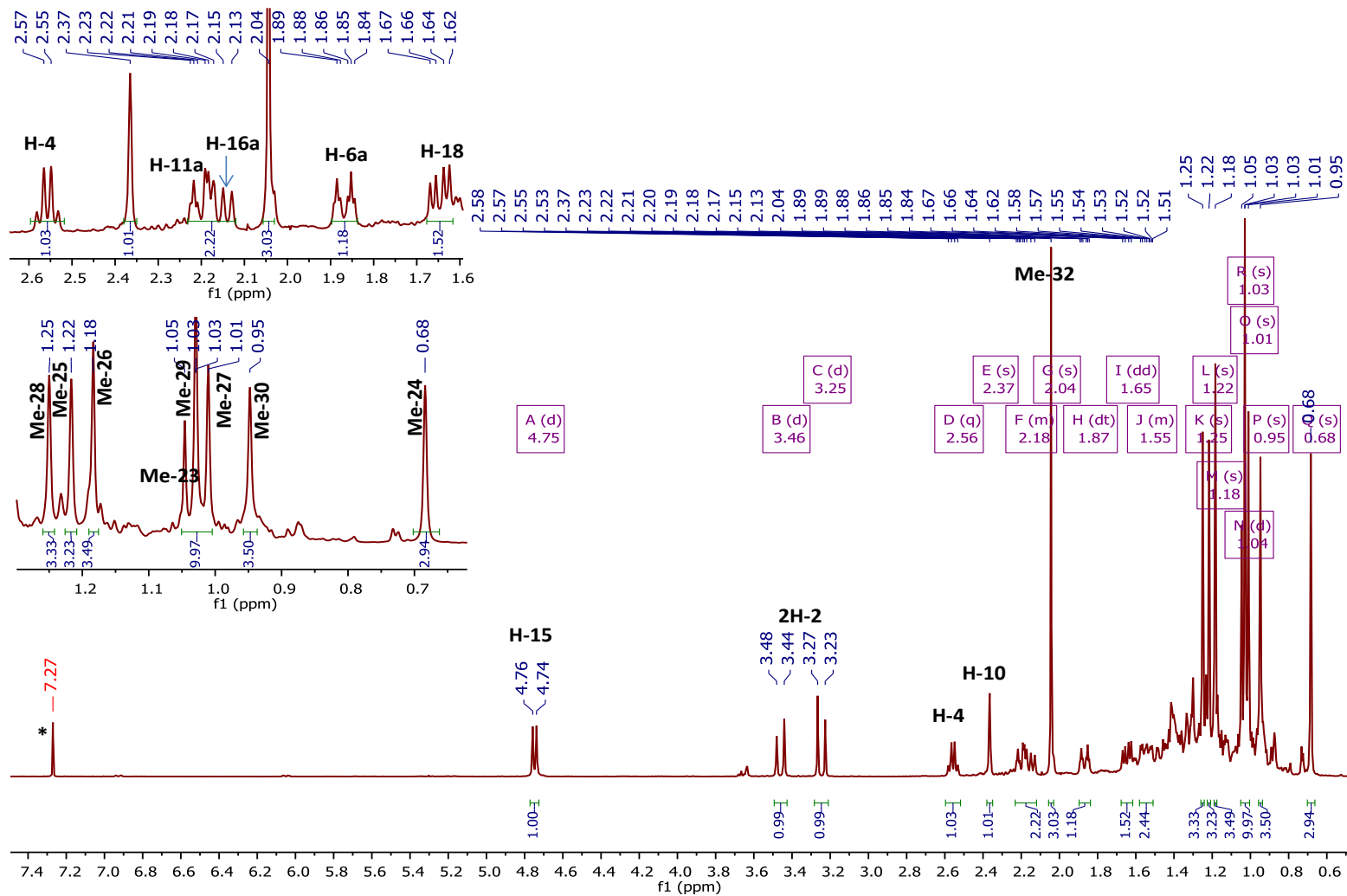


Figure 3.27: Full ¹H NMR spectrum with selected expansions (400 MHz) of HM-4 in CDCl₃; (*) CHCl₃ residue

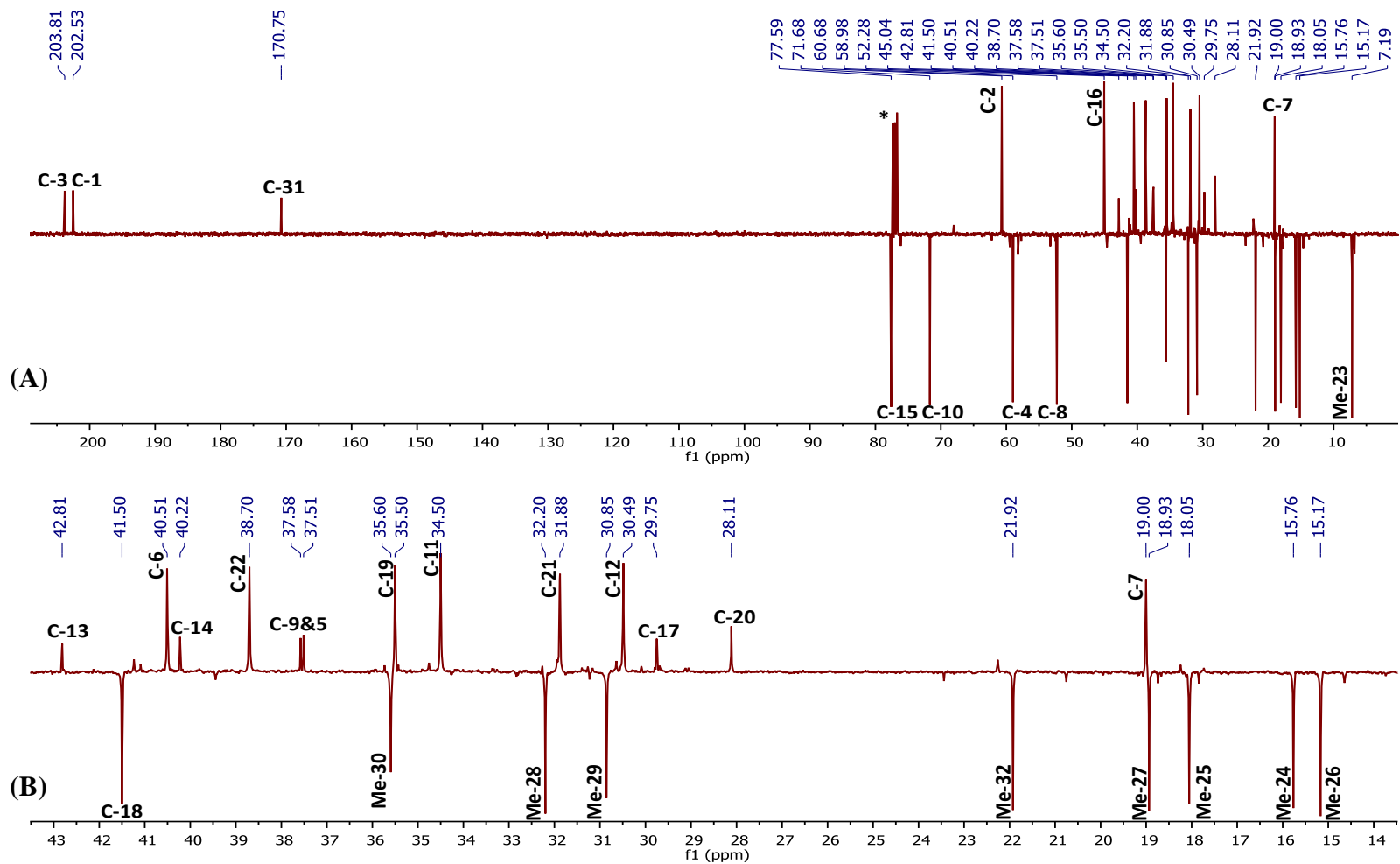
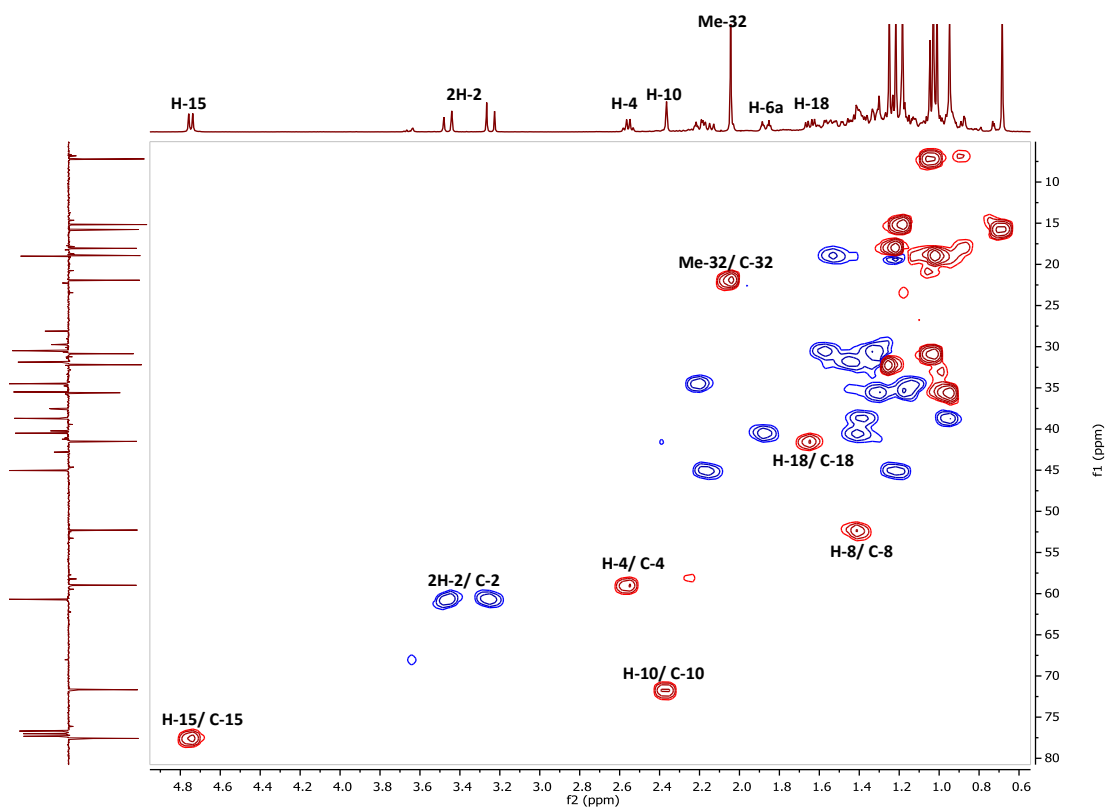
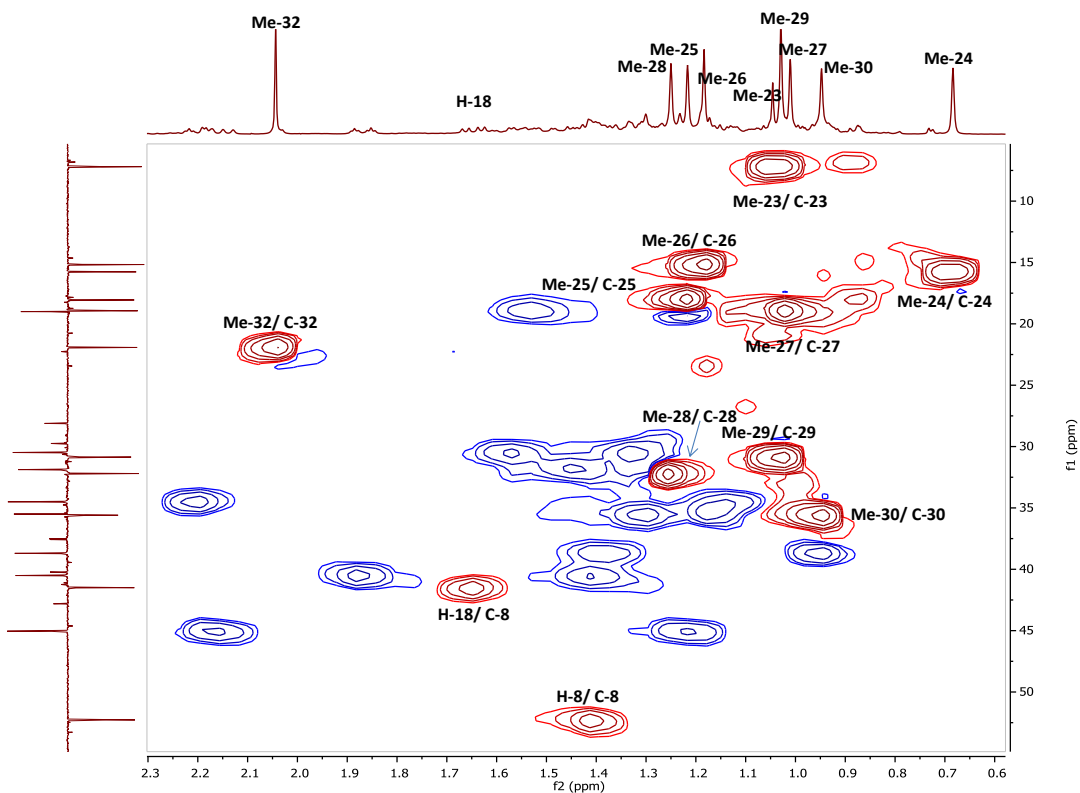


Figure 3.28: (A): Full DEPTq ^{13}C NMR spectrum (100 MHz) of HM-4 in CDCl_3 (*); (B): Selected expansion in aliphatic region

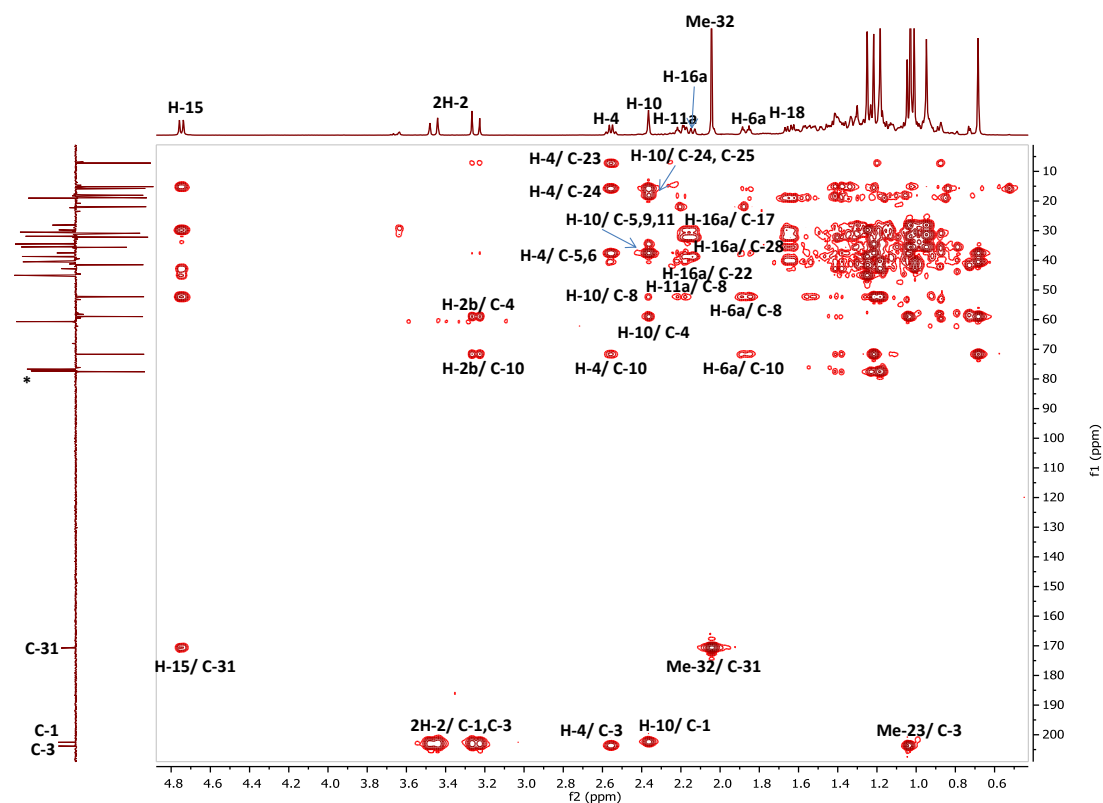


(A)

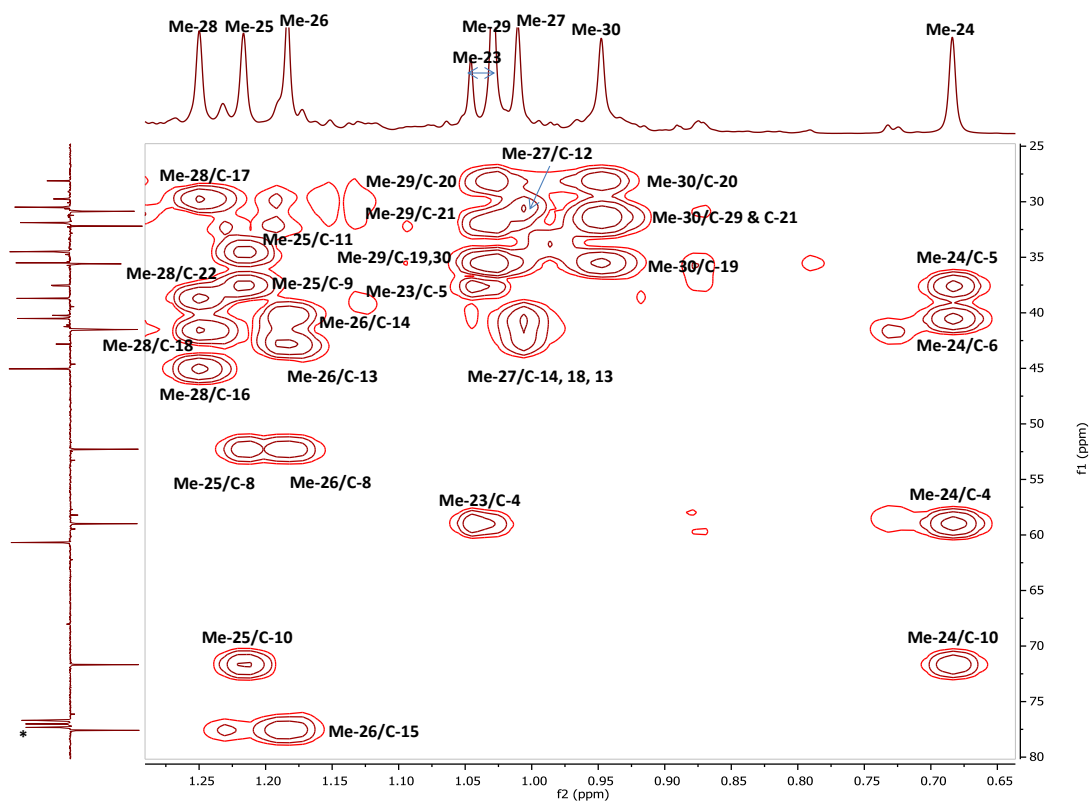


(B)

Figure 3.29: HSQC spectrum (400 MHz) of HM-4 in CDCl_3
 A: Full HSQC; B: Selected HSQC expansion



(A)



(B)

Figure 3.30: HMBC spectrum (400 MHz) of HM-4 in CDCl_3 (*)
 A: Full HMBC; B: Selected expansion for the methyl group

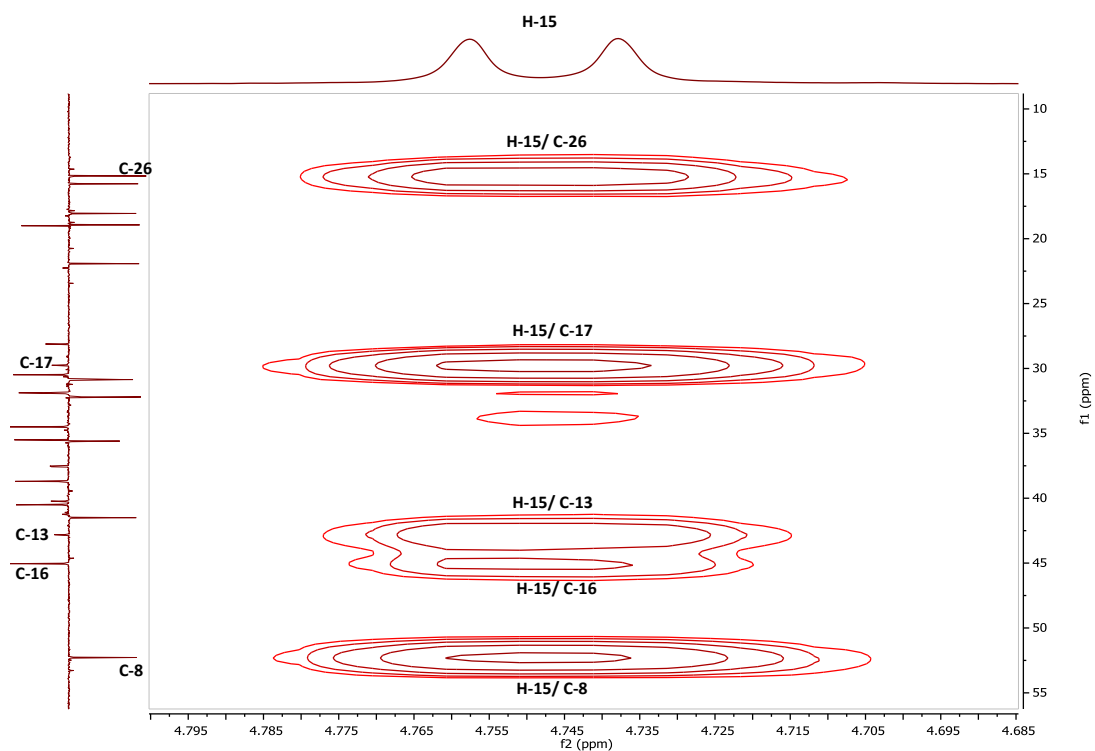


Figure 3.30 (Cont.): (C): Selected HMBC expansion for the oxymethine correlations

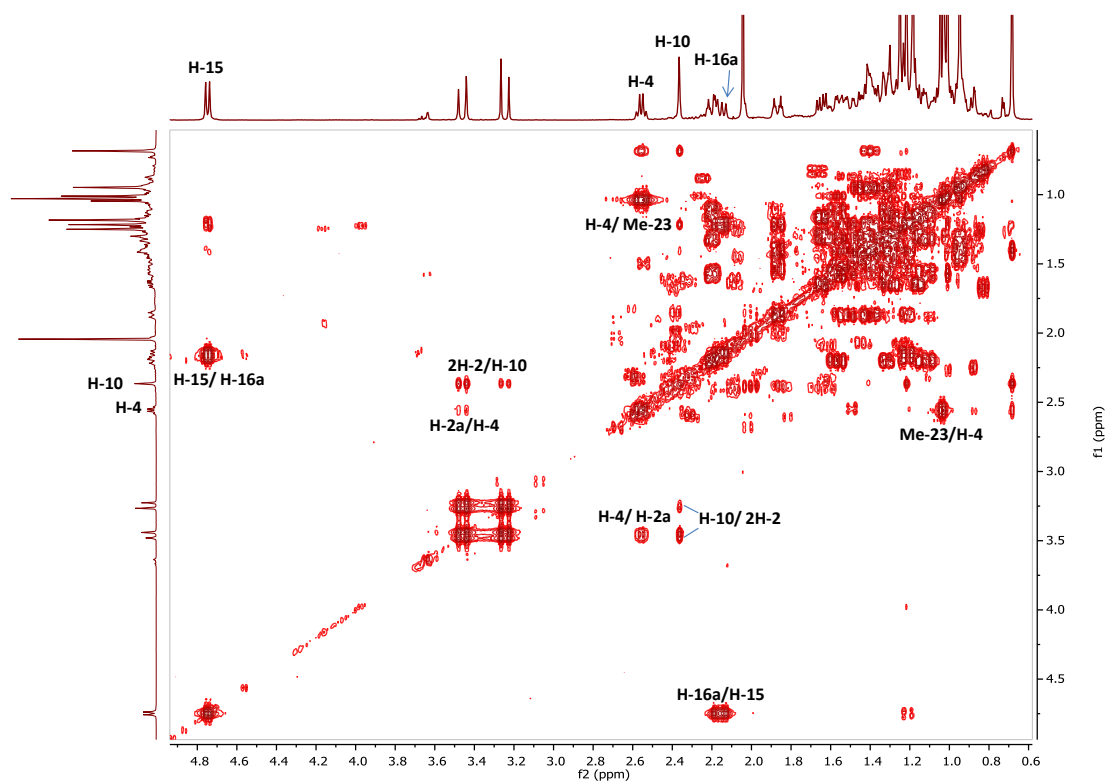
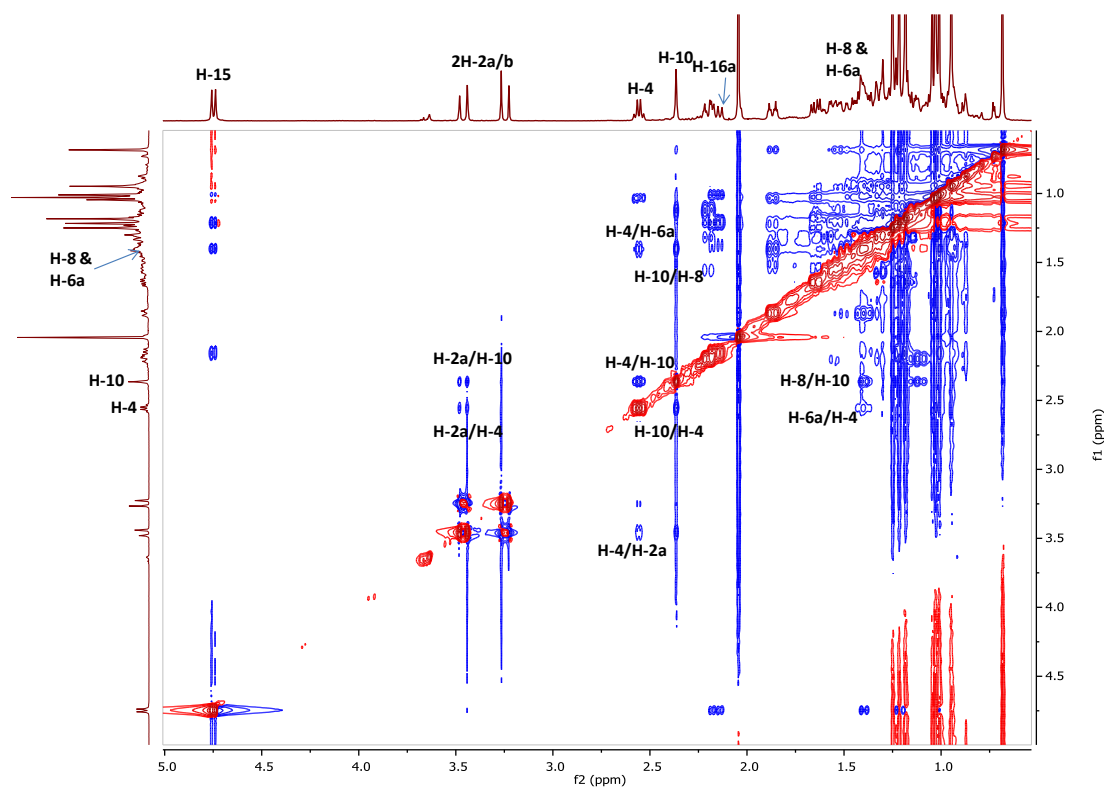
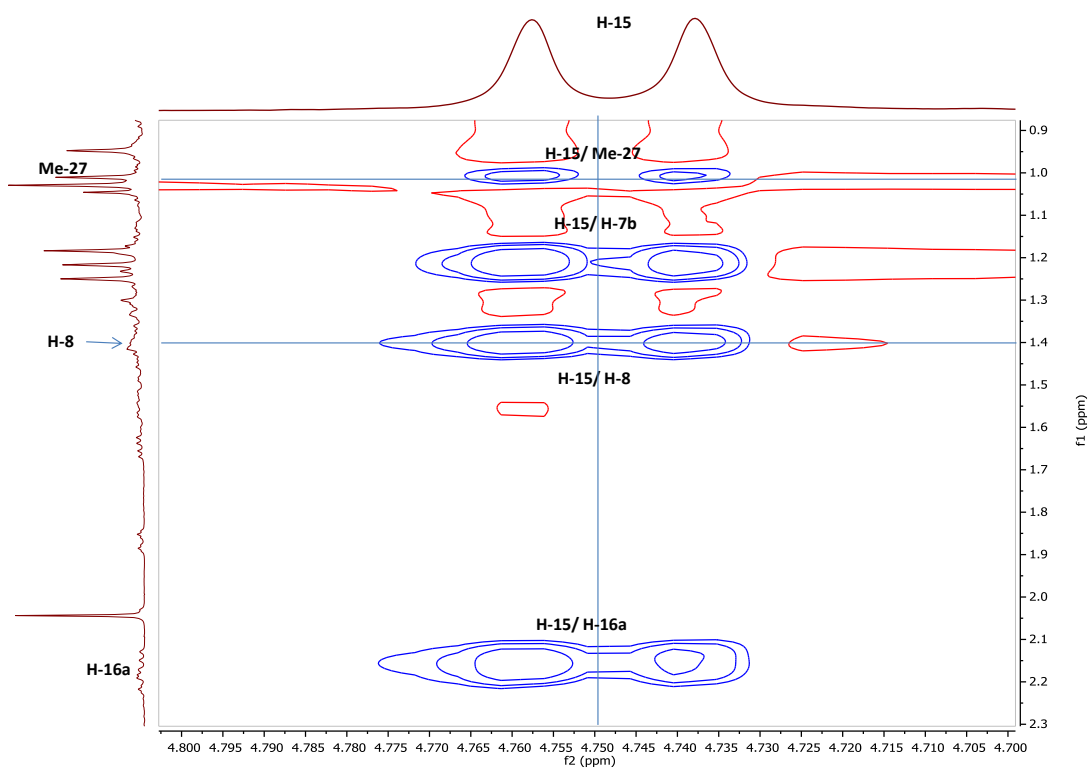


Figure 3.31: Full ^1H - ^1H COSY spectrum (400 MHz) of HM-4 in CDCl_3



(A)



(B)

Figure 3.32: (A): Full NOESY spectrum (400 MHz) of HM-4 in CDCl_3 ; (B): Selected NOESY expansion of the oxymethine proton

3.3.1.4 Characterisation of HM-5 as a 28-Hydroxyfriedelan-1,3-dione

HM-5 was isolated from the n-hexane extract of the stem bark as an amorphous white solid. On TLC, it appeared as a purple spot after spraying with *p*-anisaldehyde-sulphuric acid reagent followed by heating. Its R_f was 0.55 on SiGel when eluted with the mobile phase 50% hexane in EtOAc.

The positive mode HRESI-MS spectrum showed a quasi-molecular ion $[M+H]^+$ at m/z 457.3676, suggesting a molecular formula of $C_{30}H_{48}O_3$ (DBE=7).

The 1H NMR spectrum (400 MHz, $CDCl_3$, Figure 3.35, Table 3.5) revealed similar features to those in the spectrum obtained for the HM-3 suggesting this compound to be another triterpene of the friedelane-type. However, there were six tertiary methyl singlets instead of seven at δ_H 0.69, 0.94, 0.97, 0.98, 1.10 and 1.20, as well as one secondary methyl doublet at δ_H 1.05 (3H, *d*, $J=6.6$ Hz, Me-23). In addition to the presence of the two methylene doublets of 1,3-diketone at δ_H 3.46/3.25 (2H, *d*, $J=15.9$, H-2a/b), the spectrum also showed evident for the existence of a primary hydroxyl group by the presence of an AB quartet signal at δ_H 3.63 (2H, ABq).

The DEPTq135 ^{13}C NMR spectrum (100 MHz, Figure 3.36) showed small signals belong to some impurities from other triterpene derivatives along with the major signals of the compound of interest. 26 signals were simply assigned to be corresponded to this compound, while four other signals were determined with the aid of the HMBC and HSQC experiments to give a total of 30 carbons. These carbons included seven methyls, where the one at δ_C 7.3 attributed to Me-23 is the characteristic methyl of the friedelane-type triterpene, eleven methylenes together with the signal at δ_C 67.9 which supported the presence of the group (-CH₂OH), four methines, six quaternaries and two keto-carbonyl carbons at δ_C 202.8 (C-1) and 204.1 (C-3).

The HMBC spectrum (Figure 3.38: A & B) demonstrated the typical correlations for the protons of the rings A, B, C, D and E to those observed for the known compound HM-3. However, the 3J and 2J correlations that usually come from a methyl singlet at position-28 to two methylene carbons (C-16 & 22), a methine (C-18) and a quaternary (C-17), respectively, were here coming from the ABq signal at δ_H 3.63. This established the position of the group OH on (C-28) (Figure 3.38; C).

The relative stereochemistry of the primary hydroxyl group was confirmed by the analysis of the NOESY spectrum (Figure 3.40). The 2H-28 showed NOE correlations to the methine H-18 (δ_{H} 1.30) and the methyl singlet Me-26 (δ_{H} 0.94) (Figure 3.41; A). The Me-26 showed correlations to H-18 and Me-25 (δ_{H} 1.20) which in turn had correlations to Me-24 (δ_{H} 0.69). The latter methyl (Me-24) had correlation to the methyl doublet Me-23 (δ_{H} 1.05), which also in turn showed correlation to H-6a (δ_{H} 1.90) (Figure 3.41; B). These sequential NOE correlations led to the conclusion that H-18/ Me-26/ Me-25/ Me-23/ H-6a and the $-\text{CH}_2\text{OH}$ group were all placed on the same side (β) of the molecule. On the other hand, it was found that H-10 (δ_{H} 2.39)/ H-4 (δ_{H} 2.59)/ H-11b (δ_{H} 1.17)/ H-2a (δ_{H} 3.46)/ H-8 (δ_{H} 1.29) and Me-27 (δ_{H} 1.10) were all placed on the α side of the molecule by observing the NOE correlations in the NOESY spectrum.

The chemical shifts of all hydrogen-bearing carbons were assigned from the HSQC spectrum (Figure 3.37) combined with COSY spectrum (Figure 3.39) which was not informative enough as most of the cross peaks were clustered along the diagonal in the aliphatic region.

On the basis of the above data and in comparison with the literature, HM-5 was identified as 28-hydroxyfriedelan-1,3-dione (Figure 3.33). This is the first report of its isolation from *M. laevis*, yet, it was only reported previously from the stem bark exudates of *M. macrocarpa*, which is also referred to as Chuchuguasa (Chávez *et al.*, 1998). Nevertheless, some of the NMR data obtained in this work were not in full agreement with the literature.

Table 3.6 demonstrates the HMBC correlations, which eliminate the confusion in the chemical shifts and the positions of the "conflicting" carbons with the literature. The two carbons at δ_{C} 37.2 and 37.8 were set on positions-5&9, respectively in the report, while depending on the NMR data obtained in this work they should be in reverse order as both of Me-23 & 24 have either 2J or 3J correlations to δ_{C} 37.8 as well as Me-25 and H-11a have 2J correlations to δ_{C} 37.2 which confirmed their sites on C-5 and C-9, respectively. On the other hand, the two methyls Me-26 & 27 have mutual correlations to a quaternary carbon at δ_{C} 38.0 (C-14) instead of δ_{C} 39.0 assigned as C-14 by Chávez *et al.* (1998) which does not exist at all as a chemical shift for any of the carbons corresponding to this compound in the NMR data

obtained in the present work. Furthermore, the primary hydroxyl group at position-28 showed 3J correlations to two methylenes at δ_C 31.2 and 29.0 which could be assigned as C-22 and C-16 or *vice versa* (but not δ_C 34.3 and 29.0 as reported by Chávez *et al.* (1998). However, the methylene proton at δ_H 1.87 attached to the carbon at δ_C 29.0 displayed 3J correlations to the methine at δ_C 39.3 (C-18), the quaternary at δ_C 38.0 (C-14) and to (C-28), as well as 2J correlations to the quaternary at δ_C 35.1 (C-17) and the methylene at δ_C 31.3 (C-15), confirming its carbon to be on the site 16 in ring D rather than 22. In the COSY spectrum, it was observed that H-16a (δ_H 1.87) had correlation to another methylene proton at δ_H 1.31 (H-15a) which supported its position even further. Finally, from the HMBC spectrum, the two geminal methyls Me-29 & 30 showed mutual 3J correlations to two methylenes which were certainly at δ_C 34.4 and 33.3 (but not at δ_C 34.4 and 31.3 as reported by Chávez *et al.* (1998). These two carbons were interchangeable (C-19/C-21) due to the fact that the chemical shifts of all the methylene protons in the ring E were in the range between 1.27-1.45 causing uncertainty in confirming their neighbours by COSY experiment hence their exact positions in the ring.

In the report, it was declared that their NMR data were collected on a Bruker instrument at 400MHz in $CDCl_3$, which suggested that the only justification for these discrepancies could be due to the presence of an impurity in the sample used in this work. This impurity (similar compound) was accounted for 15% as it is shown in Figure 3.35.

28-hydroxyfriedelan-1,3-dione showed weak inhibitory activity against aldose reductase (AR) with an IC_{50} of 12 mg/ml, and it was also found to be inactive against a number of tumour cell lines (Chávez *et al.*, 1998). The cytotoxicity of HM-5 was also evaluated in this work (see section 4.1.2.1 for further details).

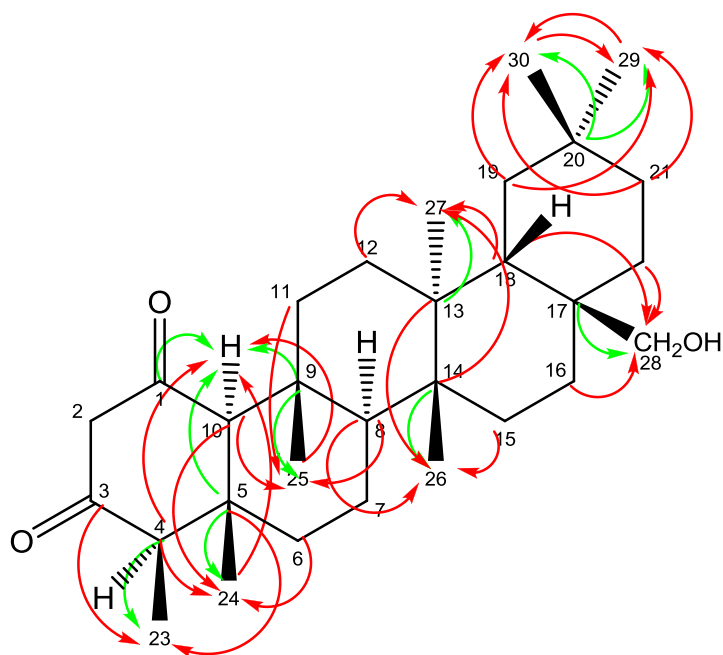


Figure 3.33: Full structure of HM-5 with key HMBC correlations
 (\rightarrow) 3J (\rightarrow) 2J ^{13}C to ^1H connectivity

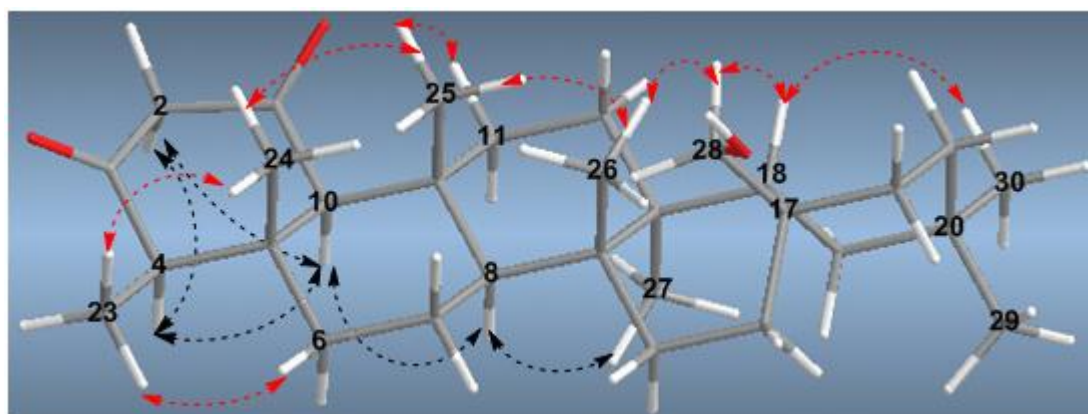


Figure 3.34: 3D structure of HM-5 with important NOESY correlations
 ($\leftarrow \rightarrow$) β ($\leftarrow \rightarrow$) α

Table 3.5: Comparison of the HSQC data [¹H (400 MHz) and ¹³C (100 MHz)] in CDCl₃ of HM-5 and a similarly 28-hydroxyfriedelane-1.3-dione (Chávez *et al.*, 1998)

Position	HM-5		28-Hydroxyfriedelane-1.3-dione	
	δ_{H}	δ_{C}	δ_{H}	δ_{C}
1	-	202.8	-	202.73
2	3.46 (1H, <i>d</i> , <i>J</i> = 15.9 Hz)/ 3.25 (1H, <i>d</i> , <i>J</i> = 15.9 Hz)	60.6	3.46 (<i>d</i> , <i>J</i> = 16 Hz)/ 3.25 (<i>d</i> , <i>J</i> = 16 Hz)	60.60
3	-	204.1	-	204.06
4	2.59 (1H, <i>q</i> , <i>J</i> = 6.6 Hz)	59.0	2.58 (<i>q</i> , <i>J</i> = 6.7 Hz)	59.05
5	-	37.8	-	37.23
6	1.90 (1H, <i>m</i>) / 1.41 (1H, <i>m</i>)	40.5	1.84-1.91 <i>m</i>	40.57
7	1.42 (1H, <i>m</i>) / 1.52 (1H, <i>m</i>)	18.0	1.50 <i>m</i>	18.04
8	1.29 (1H, <i>m</i>)	51.46	1.20 <i>m</i>	51.51
9	-	37.2	-	37.79
10	2.39 (1H, <i>s</i>)	71.8	2.39 <i>s</i>	71.88
11	2.16 (1H, <i>dt</i> , 13.5, 3.6 Hz)/ 1.17 (1H, <i>m</i>)	34.3	2.15 (<i>t</i> , <i>J</i> =3.4 Hz)/ 2.17(<i>t</i>, <i>J</i>=3.4 Hz)	33.36
12	1.35 (2H) [1.52-1.28 <i>m</i>]	29.7	1.50-1.30 <i>m</i>	29.71
13	-	39.1	-	39.16
14	-	38.0	-	39.08
15	1.47 (1H, <i>m</i>) / 1.31 (1H, <i>m</i>)	31.3	1.50-1.30 <i>m</i>	31.24
16	1.87 (1H, <i>m</i>) / 1.28 (1H, <i>m</i>)	29.0	1.84-1.91 <i>m</i>	29.02
17	-	35.1	-	35.13
18	1.30 (1H, <i>m</i>)	39.3	1.40 <i>m</i>	39.32
19	1.44 (1H, <i>m</i>) / 1.27 (1H, <i>m</i>)	34.4*	1.30 <i>m</i>	34.45
20	-	28.1	-	28.12
21	1.31 (2H) [1.42-1.25 <i>m</i>]	33.3*	1.50-1.30 <i>m</i>	31.39
22	1.41 (2H) [1.44-1.35 <i>m</i>]	31.2	1.40 <i>m</i>	34.35
23	1.05 (3H, <i>d</i> , <i>J</i> = 6.6 Hz)	7.29	1.06 (<i>d</i> , <i>J</i> = 6.7 Hz)	7.27
24	0.69 (3H, <i>s</i>)	15.96	0.69 <i>s</i>	15.95
25	1.20 (3H, <i>s</i>)	18.10	1.26 <i>s</i>	18.10
26	0.94 (3H, <i>s</i>)	19.08	0.94 <i>s</i>	19.08
27	1.10 (3H, <i>s</i>)	19.26	1.10 <i>s</i>	19.24
28	3.63 (2H, <i>ABq</i>)	67.94	3.68 <i>br. s</i>	67.98
29	0.98 (3H, <i>s</i>)	34.20	1.00 <i>s</i>	34.20
30	0.977 (3H, <i>s</i>)	32.85	0.98 <i>s</i>	32.82

† The highlighted rows indicate the differences in chemical shifts of both carbons and protons.

* These two carbons are interchangeable.

Table 3.6: Some selected HMBC correlations for HM-5 in CDCl₃

Position	HSQC		Selected HMBC correlations	
	¹ H _δ	¹³ C _δ	² J	³ J
23	1.05	7.3	C-4 (59.0)	C-3 (204.1), C-5 (37.8)
24	0.69	15.9	C-5 (37.8)	C-10 (71.8), C-4 (59.0), C-6 (40.5)
25	1.20	18.1	C-9 (37.2)	C-10 (71.8), C-8 (51.4), C-11 (34.3)
10	2.39	71.8	C-5, C-9	-
11a	2.16	34.3	C-9 (37.2)	-
26	0.94	19.0	C-14 (38.0)	C-8 (51.4), C-13 (39.1), C-15 (31.3)
27	1.10	19.2	C-13 (39.1)	C-12 (29.7), C-14 (38.0) , C-18 (39.3)
28	3.63	67.9	C-17 (35.1)	C-16 (29.0), C-22 (31.2) , C-18 (39.3)
29	0.98	34.2	C-20 (28.1)	C-21 (33.3) , C-19 (34.4), C-30 (32.8)
30	0.97	32.8	C-20 (28.1)	C-21 (33.3) , C-19 (34.4), C-29 (34.2)

*Each colour of the highlighted rows demonstrates the correlations to specific carbons.

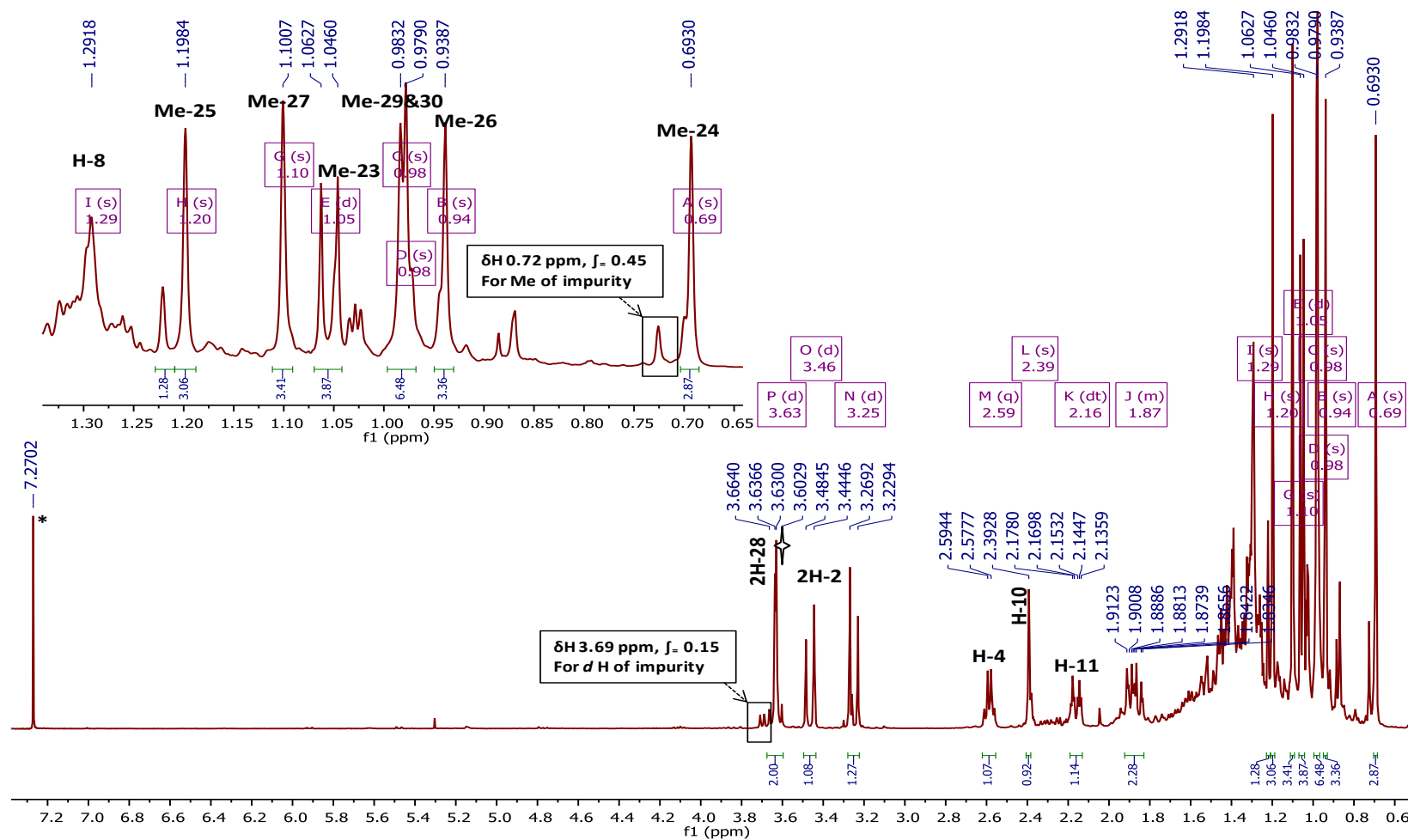


Figure 3.35: Full ¹H NMR spectrum with selected expansion (400 MHz) of HM-5 in CDCl₃; (*) CHCl₃ residue, † really an (ABq) rather than (d)

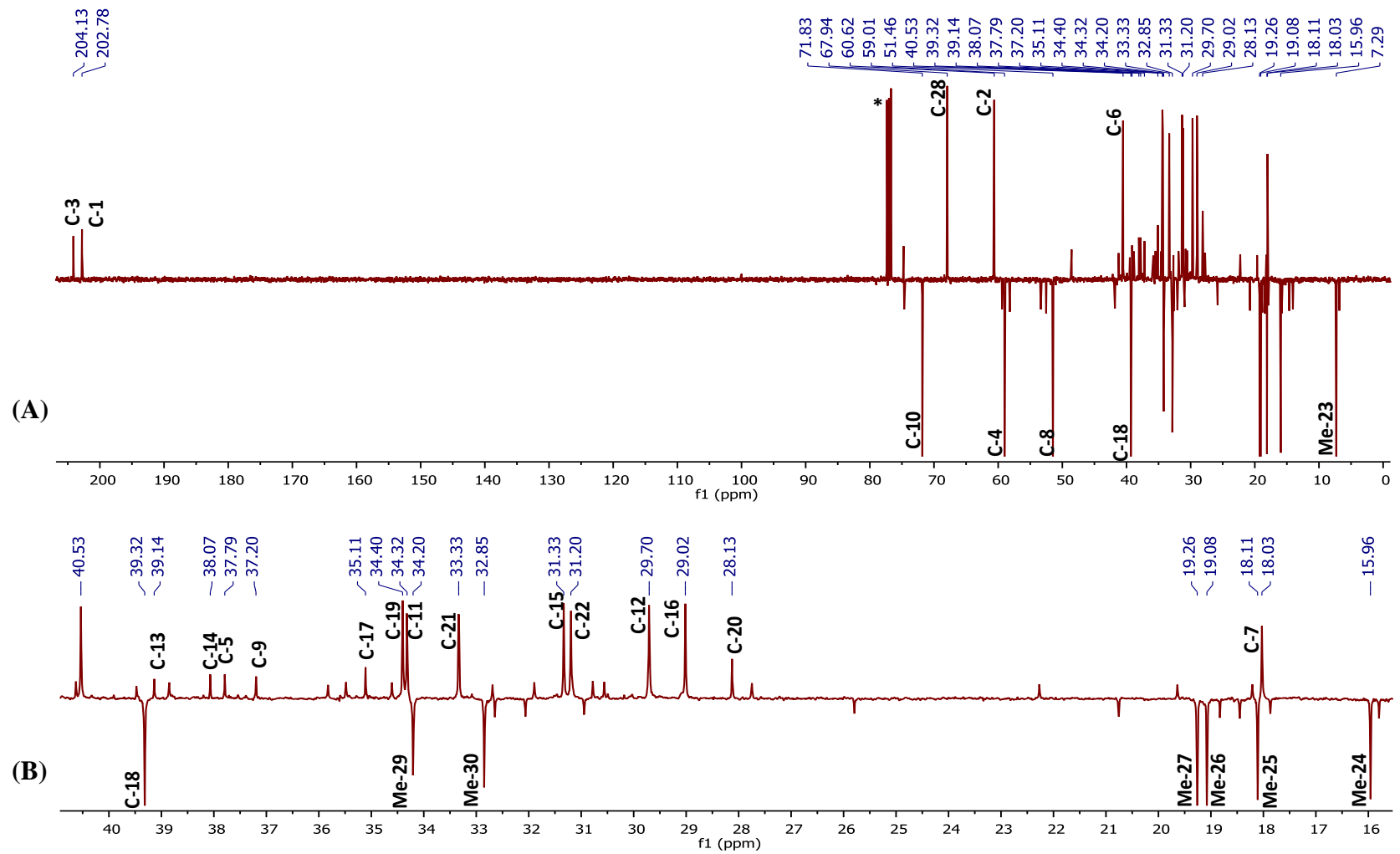
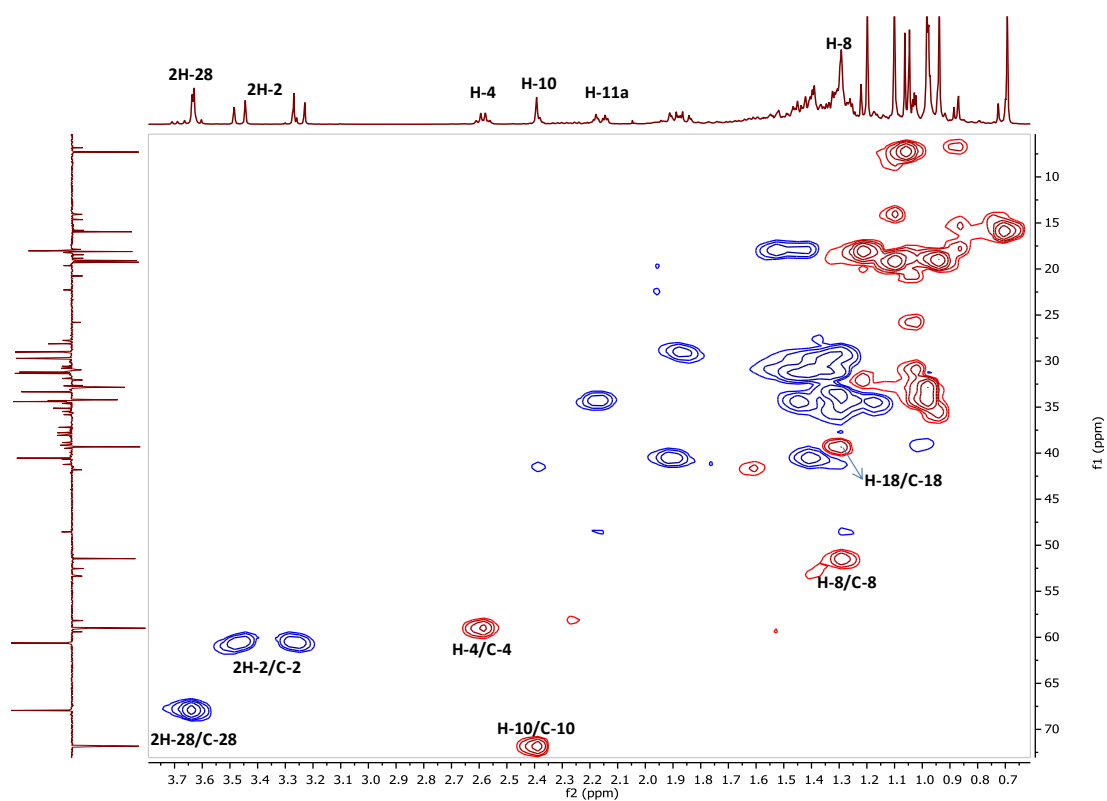
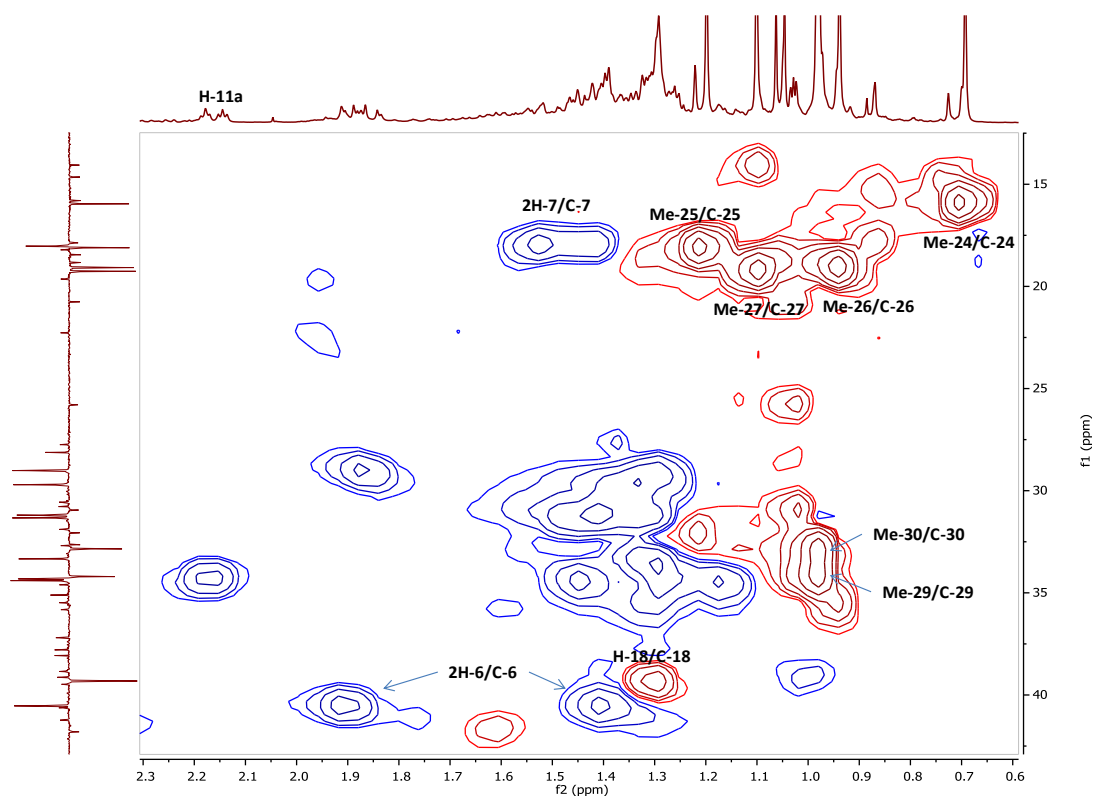


Figure 3.36: (A): Full DEPTq ^{13}C NMR spectrum (100 MHz) of HM-5 in CDCl_3 (*); (B): Selected expansion in aliphatic region

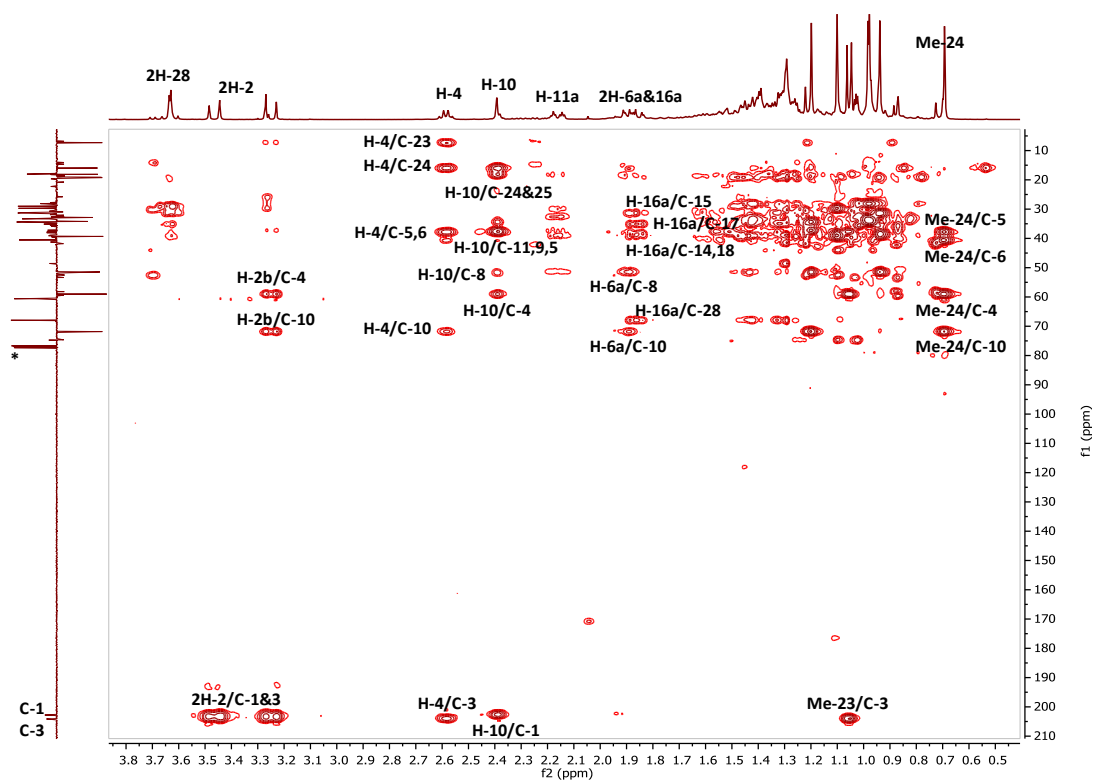


(A)

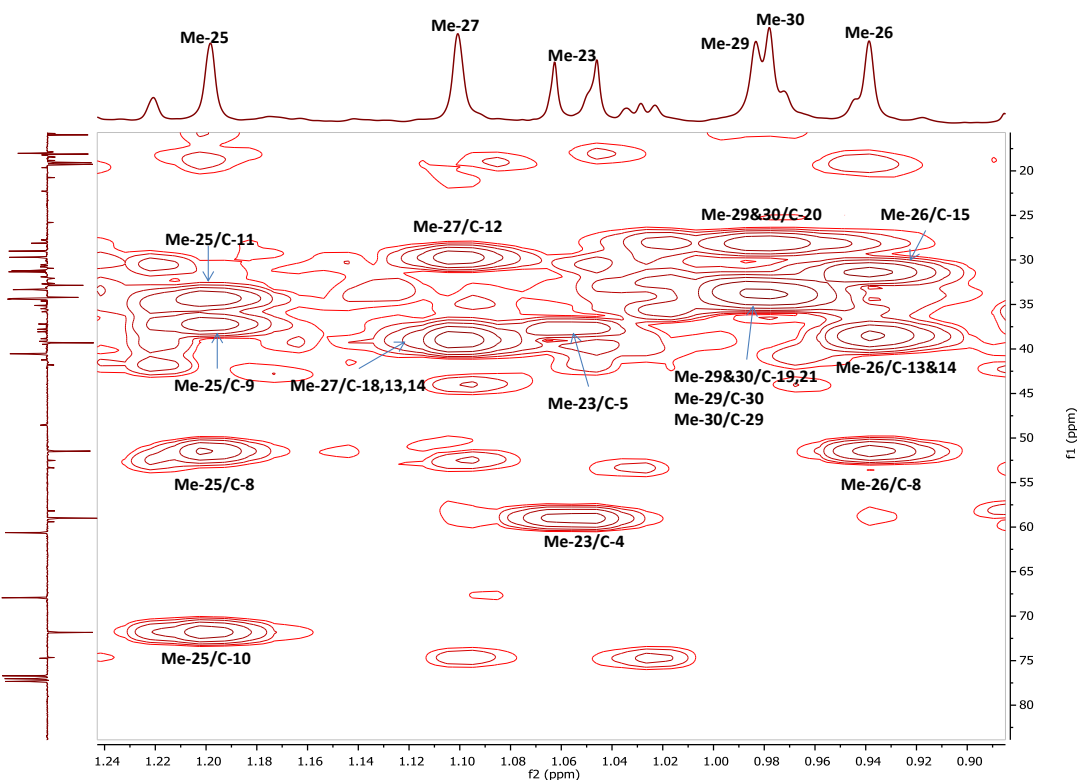


(B)

Figure 3.37: HSQC spectrum (400 MHz) of HM-5 in CDCl_3
 A: Full HSQC; B: Selected HSQC expansion



(A)



(B)

Figure 3.38: HMBC spectrum (400 MHz) of HM-5 in CDCl₃ (*)
(A): Full HMBC; (B): Selected HMBC expansion for the methyl groups

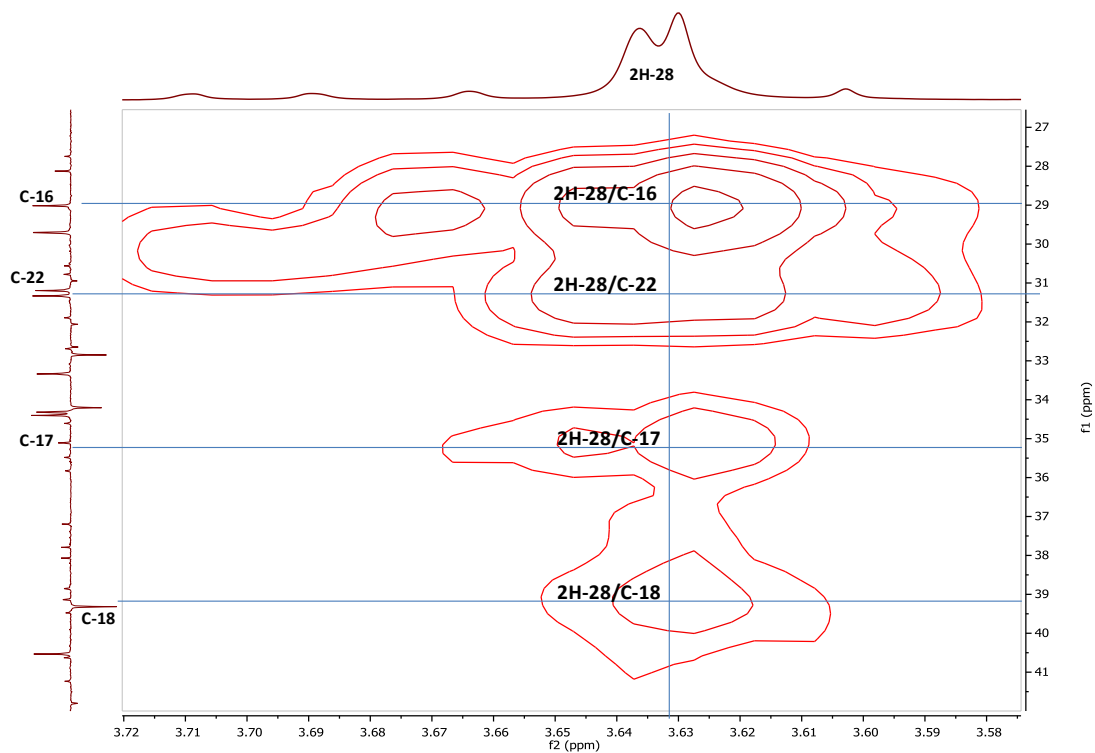


Figure 3.38 (cont.): (C): Selected HMBC expansion for the (-CH₂OH) group

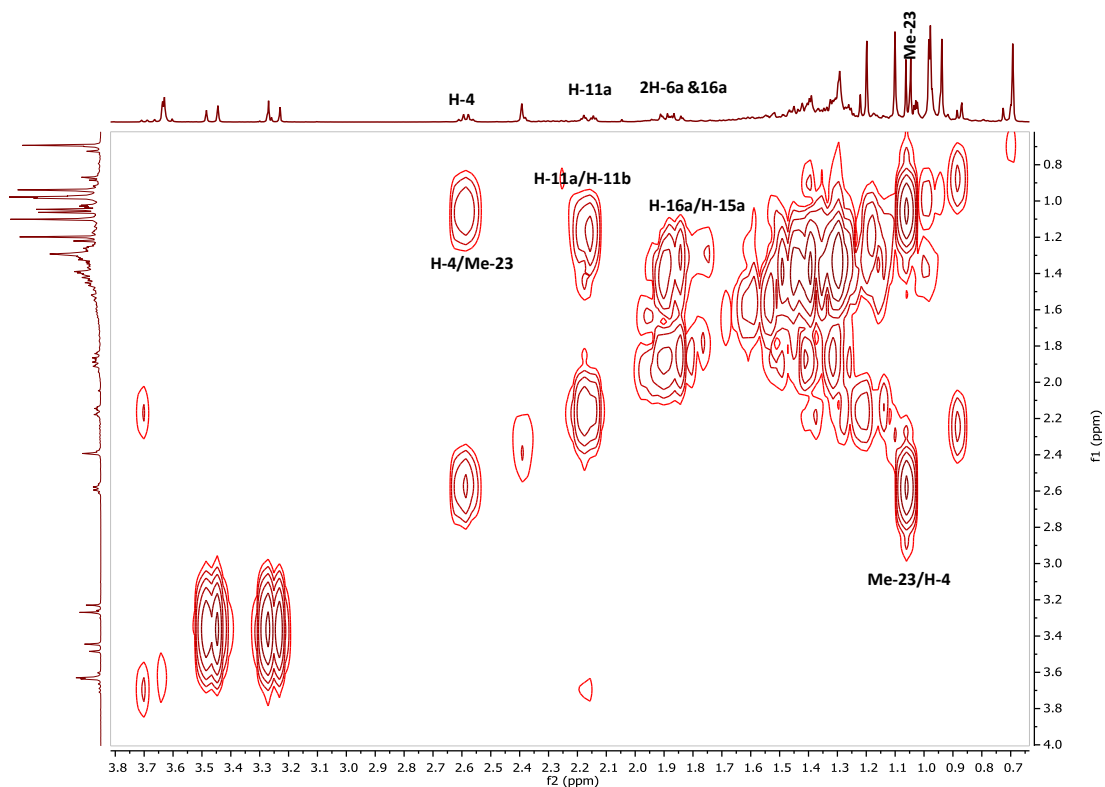


Figure 3.39: ¹H-¹H COSY spectrum (400 MHz) of HM-5 in CDCl₃

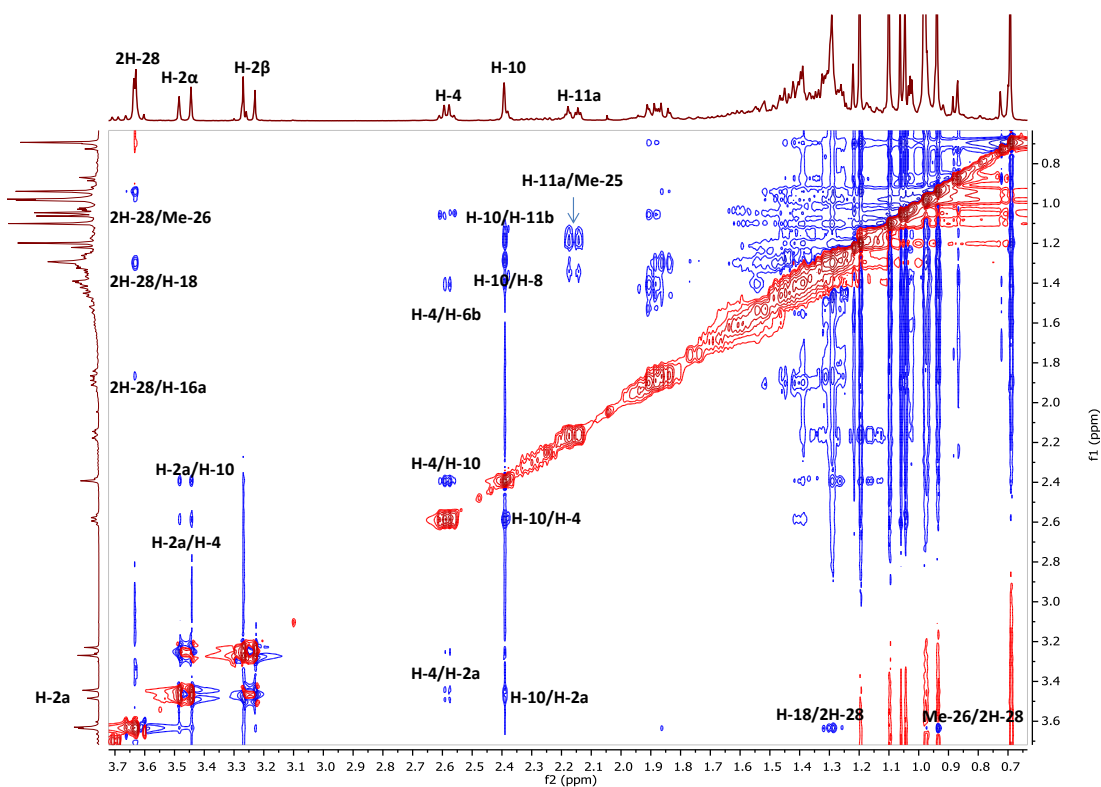


Figure 3.40: (A) Full NOESY spectrum (400 MHz) of HM-5 in CDCl_3

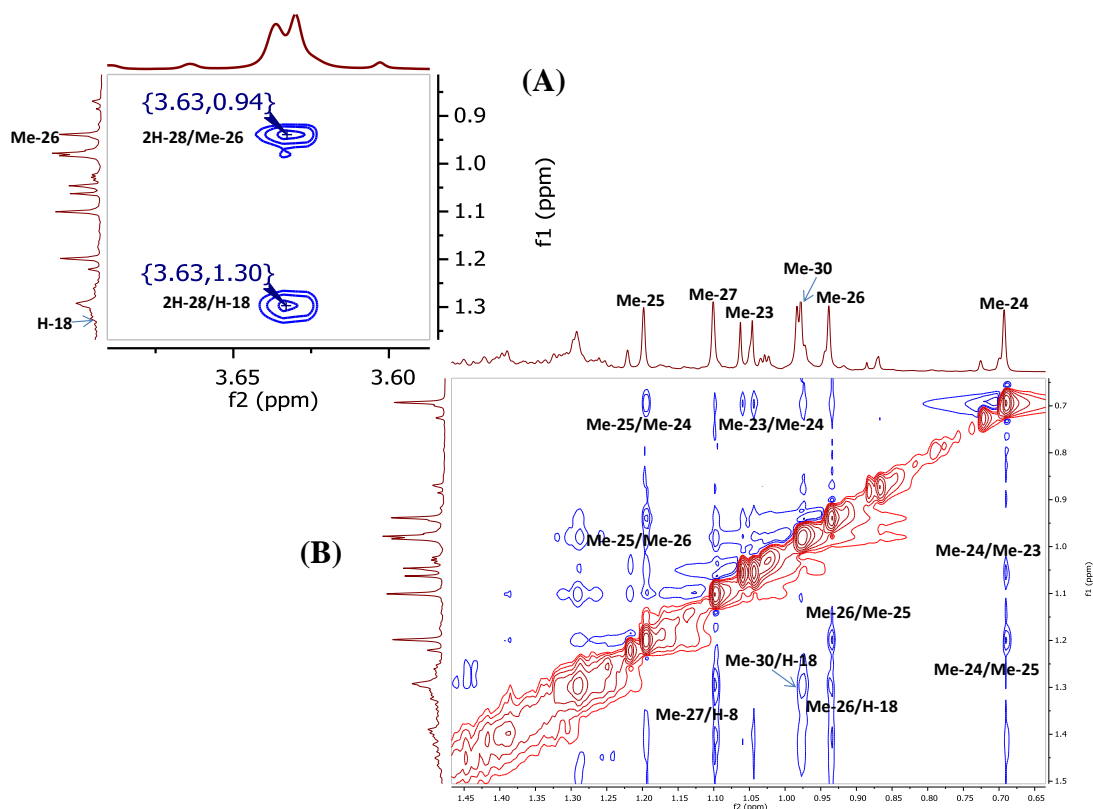


Figure 3.41: (A): Selected NOESY expansion of the $(-\text{CH}_2\text{OH})$ group;
(B): Selected NOESY expansion for the methyl groups

3.3.1.5 Characterisation of HM-6 as the novel corredorane-type triterpene 1,3-dioxocorredor-14,26-ene

HM-6 was isolated from the n-hexane extract of the stem bark as white crystals. On TLC, the compound appeared as a pink spot after spraying with *p*-anisaldehyde-sulphuric acid reagent followed by heating. Its R_f was 0.68 on SiGel when eluted with the mobile phase 50% hexane in EtOAc.

The positive mode HRESI-MS spectrum showed a quasi-molecular ion $[M+H]^+$ at m/z 439.3570, suggesting a molecular formula of $C_{30}H_{46}O_2$ (DBE=8).

The optical rotation $[\alpha]_D^{20}$ was -27° ($c=0.1$, $CHCl_3$).

The IR spectrum indicated the presence of two carbonyl groups (1719 , 1700 cm^{-1}) and (C-H) (2937 cm^{-1}) (Williams and Fleming, 2008).

This compound was isolated after a series of chromatographic techniques ending with use of the Reveleris[®] flash chromatography system. The 1H NMR of the targeted sample, obtained from PTLC, showed the presence of a mixture that contained two very similar compounds as majors, one of them was friedelan-1,3-dione (HM-3), which was isolated earlier in this work (see section 3.3.1.2). The other major compound resulting from the separation process was analysed by NMR to elucidate its structure.

The 1H NMR spectrum (400 MHz, $CDCl_3$, Figure 3.48, Table 3.7) revealed similar features to those in the spectrum obtained for HM-3. However, the presence of exomethylene protons at δ_H 4.82 (1H, *brs*) and 5.19 (1H, *brs*), comparable to those usually seen in lupane-type triterpenes yet with downfield shift, as well as a set of six methyl singlets instead of seven at δ_H of 0.74, 0.85, 0.93, 1.14, 1.16 and 1.24 ppm suggested some abnormalities in the usual friedelane or lupane skeletons of triterpene-type compounds. The spectrum also featured one methyl doublet at δ_H 1.08 (3H, *d*, $J=6.6$ Hz) which showed vicinal coupling with a methine quartet at δ_H 2.57 (1H, *q*, $J=6.6$ Hz) in COSY spectrum (Figure 3.54). A set of two doublets (AB quartet) of deshielded methylene protons of a 1,3-diketone at δ_H 3.29/3.51 (2H, *d*, $J=15.5$ Hz) and another two methines at δ_H 2.49 (1H, *s*) and δ_H 2.31 (1H, *br.d*, $J=10.2$ Hz) were also observed.

The DEPTq135 ^{13}C NMR spectrum was unexpectedly ambiguous as some signals appeared broad while others were apparently missing when trying to assign them

with the aid of the HSQC spectrum. Thus, all the NMR experiments were repeated but by increasing the probe temperature (normally 25°C) to 40°C in an attempt to generate better spectra. There was a noticeable, yet not really definitive, improvement in the quality of the carbon spectrum in comparison to that at lower temperature especially in the upfield region (Figure 3.49) while all the other experiments were barely enhanced. A total of 30 carbons were found to belong to the compound. 27 carbon signals were precisely assigned from the carbon spectrum (Figure 3.50) while the other three carbons were extracted from the HSQC and HMBC spectra as the chemical shifts of the quaternaries and the methylenes were very closely bunched. These carbons were composed of seven methyls including the one which is characteristic of the friedalene-type triterpene at δ_C 7.4 (Me-23), nine aliphatic methylenes, two olefinic carbons at δ_C 110.3 (methylene) and 153.5 (quaternary), five methines, five aliphatic quaternaries and two keto-carbonyl carbons at δ_C 202.6 (C-1) and 203.8 (C-3).

The HMBC spectrum (Figure 3.52; A) demonstrated some similar correlations for the protons of the rings A, B and E to those observed for the known compound HM-3. Thus it was initially confirmed that this compound has a poly-cyclic skeleton with similar structure in these rings to the latter where ring A has two keto-carbonyls at positions 1 and 3 (Figure 3.42; part A) and ring E has two geminal methyls at δ_H 0.93 (Me-29) and 0.85 (Me-30) at position 20 and another one at position 17 (Figure 3.42; part B). On the other hand, and rather unusually for a friedalene triterpene, it was found that there were exomethylene protons at δ_H 4.82 (1H, *brs*) and 5.19 (1H, *brs*) which had 3J correlations to two methine carbons where one of them was assigned at δ_C 53.6 and allocated to position-8 in the cycle B (see part A; Figure 3.42) and the other one at δ_C 57.5. In reverse, the methine proton at δ_H 2.31 corresponding to the latter carbon displayed 3J and 2J correlations to the olefinic carbon at δ_C 110.3 bearing the exomethylene protons and to the olefinic quaternary carbon at δ_C 153.5, respectively, while the other methine proton at position-8 displayed 2J correlations to the same olefinic quaternary carbon. This confirmed that cycle B should have an extended structure as shown in Figure 3.42; (part A).

The HMBC correlations between the two identified parts were obscure and difficult to interpret, although a methyl at δ_H 1.14 was found to get 3J correlation

with the methine carbon at δ_C 57.5 allocated in part A. Thus, good quality crystals obtained from $CDCl_3$ were sent for X-Ray crystallography in an attempt to determine the crystal structure as explained in section 2.2.3.3. The molecular diagram shown in Figure 3.43 was generated after processing the collected data.

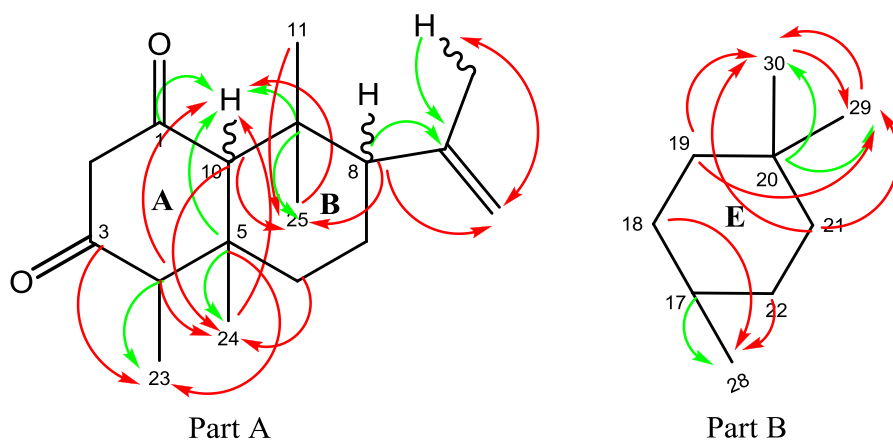


Figure 3.42: Part structures of HM-6 with key HMBC correlations
 (\rightarrow) 3J (\rightarrow) 2J

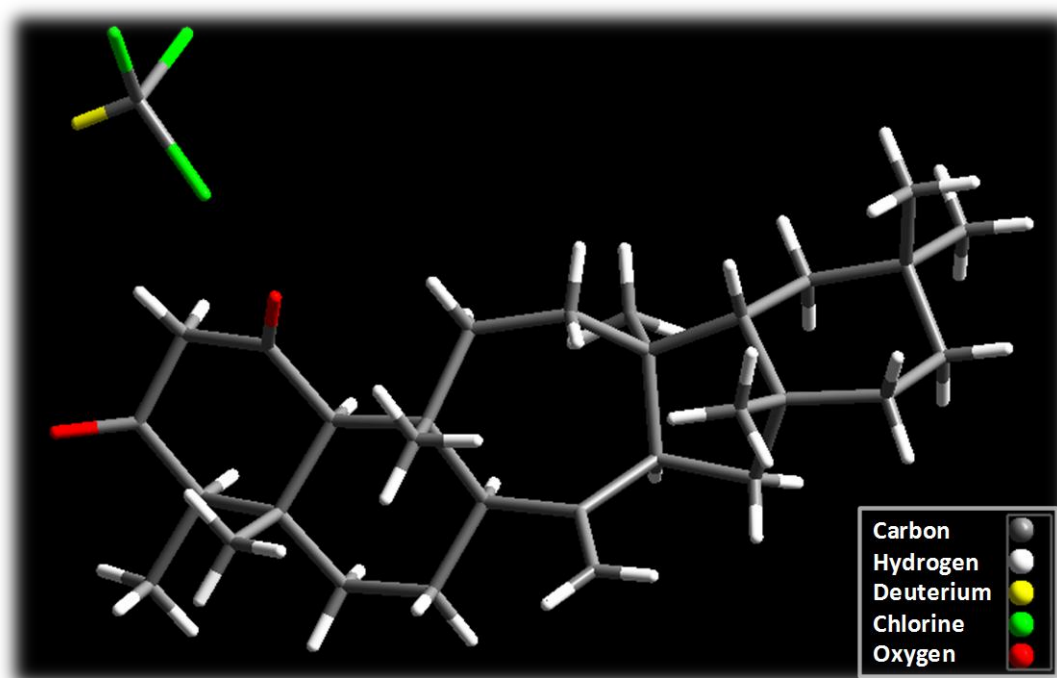


Figure 3.43: Solvated (in $CDCl_3$) "sticks" format taken from crystal structure of HM-6

The X-Ray crystallographic analysis defined by the Oak Ridge Thermal Ellipsoid Plot (ORTEP) (Figure 3.44) gave the structure unequivocally. The indistinctness, particularly, in the carbon spectrum (DEPTq135 NMR experiment) (Figure 3.49,

Figure 3.50), where some of the signals were unexpectedly broad or short, could be due to the flexibility of the seven-membered ring C in "solution state".

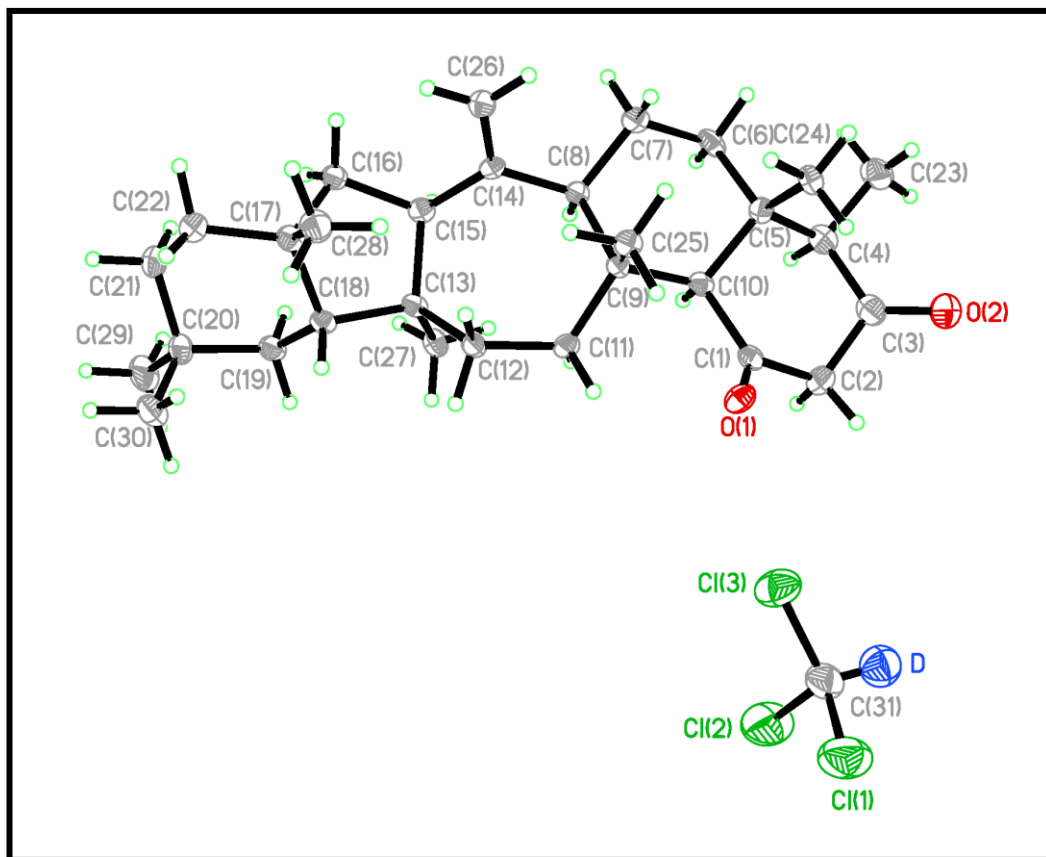


Figure 3.44: The Oak Ridge Thermal Ellipsoid Plot (ORTEP) of the crystal structure of HM-6 with atoms labelling

Therefore, with the aid of the resultant crystal structure, the complete assignment of the compound HM-6 was verifiable and the middle rings C and D were confirmed from the HMBC spectrum. The methyl singlet at δ_{H} 1.14 (Me-27) displayed 3J correlations to a methylene carbon and two methines at δ_{C} 37.8 (C-12), 55.3 (C-18) and 57.5 (C-15), respectively, as well as a 2J correlation to a quaternary carbon at δ_{C} 48.3 (C-13) (Figure 3.45). Moreover, the methine proton (H-15) (*br.d.*, $J = 10.2$ Hz) showed 3J correlation to the Me-27 and 2J correlations to its neighbouring carbons at δ_{C} 48.3 (C-13) and 40.4 (C-16). From the COSY spectrum, it was also found that this proton (H-15) showed a 4J or an allylic coupling with the exomethylene protons at δ_{H} 4.82/5.19 and a vicinal coupling with the adjacent proton at δ_{H} 1.98 (H-16a).

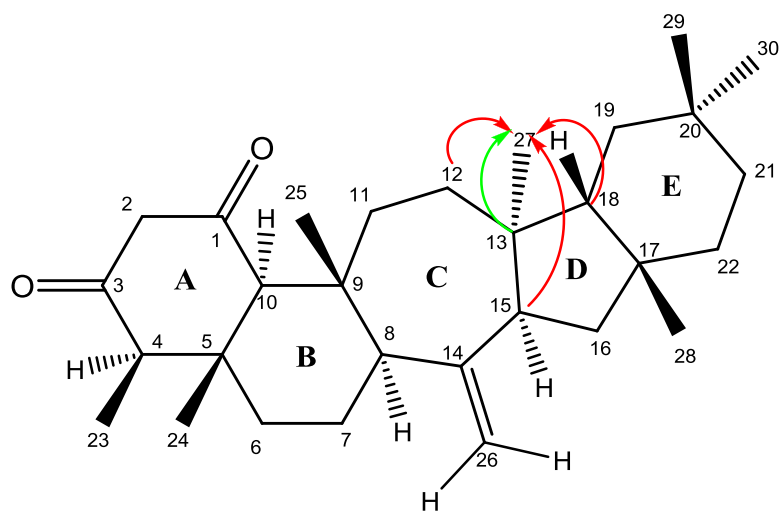


Figure 3.45: Full structure of HM-6 showing the non-systematic numbering and the key HMBC correlations of Me-27
 (→) 3J (→) 2J

By comparing these correlations to those seen in the compound HM-3, the only difference was that the Me-27 in the latter had mutual correlation with the Me-26 to a quaternary carbon at position-14 instead of a methine as they were both aligned on the junction between the six-membered rings C and D. This can be explained by the fact that structural reorganizational shifts have happened within the molecule leading to the formation of seven-membered ring and five-membered ring C and D, respectively, instead of two six-membered rings. The methyl singlet Me-26 [as in HM-3], linked at position-14 on the ring C & D junction, has been converted to an exomethylene group and migrated one bond away from the join into the expanded (heptagonal) ring C (see Figure 3.46 for transformation of HM-3 type into HM-6).

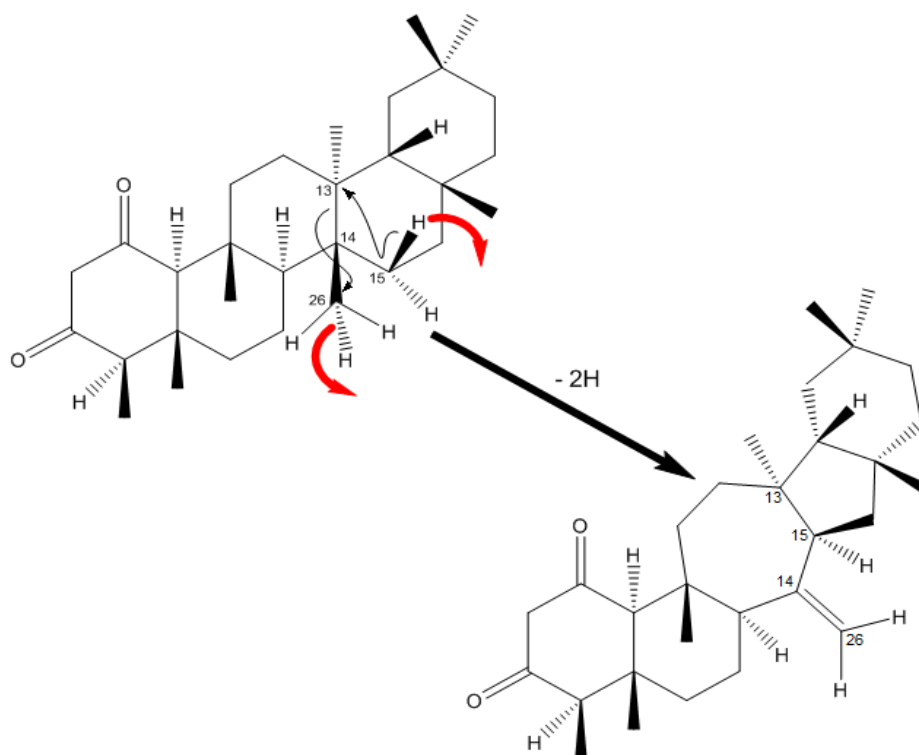


Figure 3.46: Putative bioconversion of HM-3 into HM-6

Concerted actions occur: when the bond between carbons 13/14 breaks, a new bond between carbons 13/15 forms with the loss of (1H-15) leading to expansion of ring C and contraction of ring D. Simultaneously, a double bond forms between carbons 14/26 with the loss of another proton (1H-26).

The NOESY spectrum (Figure 3.53) showed that the two methine protons H-10 (δ_{H} 2.49) and H-4 (δ_{H} 2.57) had mutual correlations to each other and to one of the methylene protons H-2a (δ_{H} 3.51). Furthermore, the proton H-10 correlated to H-8 (δ_{H} 1.82) which in turn correlated to H-15 (δ_{H} 2.31) and the proton H-4 correlated to H-6b (δ_{H} 1.38). The spectrum also showed NOE effect between H-15 and the methyl Me-27. This led to the conclusion that H-10/ H-4/ H-2a/ H-6b/ H-8/ H-15 and Me-27 were all placed on the α side of the molecule. On the other hand, the Me-23 (δ_{H} 1.08) which should therefore be on the β side correlated to H-6a (δ_{H} 1.88) and to Me-24 (δ_{H} 0.74) which also in turn correlated to Me-25 (δ_{H} 1.24). Thus Me-23/ Me-24 and Me-25 were all on the β side.

The selected expansion of NOESY spectrum for the olefinic region (Figure 3.53; B) displayed very clearly the NOE effects of both exomethylene protons. The H-26a (δ_{H} 5.19) correlated to the methylene proton H-16b (δ_{H} 1.79) and to Me-28 (δ_{H} 1.16), which in turn correlated to the methine proton H-18 (δ_{H} 1.36) and to Me-29 (δ_{H}

0.93). On the other hand, the second exomethylene proton H-26b (δ_{H} 4.82) showed correlations to the methylene proton H-7a (δ_{H} 1.83) as well as to Me-25 (δ_{H} 1.24). This confirmed that all of the Me-28/ Me-29 and H-18 were also placed on the β side of the molecule. Elucidation of the relative stereochemistry of this compound depending on the NOESY correlations and the X-ray data can be seen in Figure 3.47.

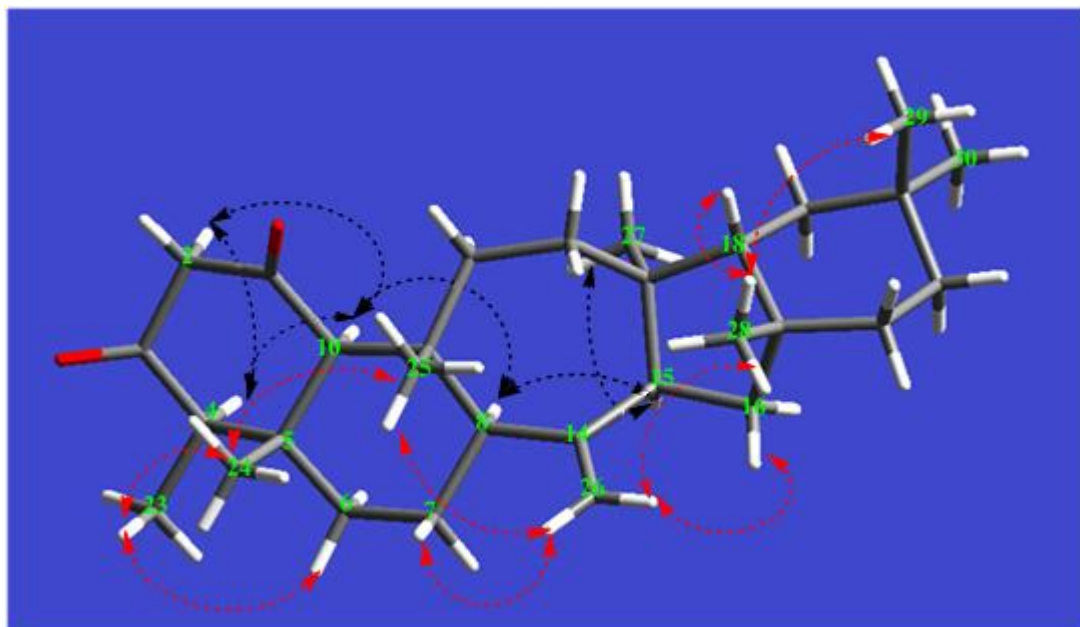


Figure 3.47: 3D structure of HM-6 with important NOESY correlations
 (↔) β (↔) α

The cross peaks in the COSY spectrum, resulting from the geminal or vicinal couplings between protons, were clustered in the upfield region due to the convergence of the chemical shifts of the methylene and methine protons which made it difficult to confirm each spin system. However, based on the information obtained by the analysis of the other 1D/2D NMR spectra and with the aid of the X-ray crystallography data as well as comparing with the spectral data of the related friedelane triterpene (friedelan-1,3-dione), HM-6 was identified as (4R,4aR,6aR,7aS,8aR,12aR,12bS,14aR,14bS)-4,4a,8a,11,11,12b,14a-heptamethyl-7-methyleneoctadecahydrobenzo[a]naphtho[2,1-f]azulene-1,3(2H,14bH)-dione. This compound, for which corredorane is proposed as a trivial name for the skeleton and 1,3-dioxocorredor-14,26-ene for the compound, was determined as a novel triterpene. HM-6 showed no cytotoxic effects when tested against the melanoma cell line A375 and the normal fibroblast cell line Hs27 even at the highest concentration 100 $\mu\text{g/ml}$ (see section 4.1.2.1 for further details).

Table 3.7: ^1H (400 MHz) and ^{13}C (100 MHz) NMR data of HM-6 in CDCl_3

Position	HM-6	
	δ_{H}	δ_{C}
1	-	202.6
2	3.51 (1H, <i>d</i> , $J= 15.5$ Hz)/ 3.29 (1H, <i>d</i> , $J= 15.5$ Hz)	61.3
3	-	203.8
4	2.57 (1H, <i>q</i> , $J= 6.6$ Hz)	59.2
5	-	37.7
6	1.88 (1H, <i>m</i>)/ 1.38 (1H, <i>m</i>)	39.6
7	1.83 (1H, <i>m</i>)/ 1.40 (1H, <i>m</i>)	26.2
8	1.82 (1H, <i>m</i>)	53.6
9	-	38.6
10	2.49 (1H, <i>s</i>)	70.2
11	2.04 (1H, <i>m</i>)/ 1.41 (1H, <i>m</i>)	38.1
12	1.44 (1H, <i>m</i>)/ 1.23 (1H, <i>m</i>)	37.8
13	-	48.3
14	-	153.5
15	2.31 (1H, <i>br.d</i> , $J= 10.2$ Hz)	57.5
16	1.98 (1H, <i>m</i>)/ 1.79 (1H, <i>m</i>)	40.4
17	-	40.9
18	1.36 (1H, <i>m</i>)	55.3
19	1.17 (2H) [1.21-1.11 <i>m</i>]	38.9*
20	-	30.0
21	1.18 (2H) [1.25-1.14 <i>m</i>]	34.6*
22	1.37 (2H) [1.43-1.33 <i>m</i>]	35.0
23	1.08 (3H, <i>d</i> , $J= 6.6$ Hz)	7.4
24	0.74 (3H, <i>s</i>)	15.2
25	1.24 (3H, <i>s</i>)	15.18
26	5.19 (1H, <i>br.s</i>)/ 4.82 (1H, <i>br.s</i>)	110.3
27	1.14 (3H, <i>s</i>)	26.8
28	1.16 (3H, <i>s</i>)	31.4
29	0.93 (3H, <i>s</i>)	32.6
30	0.85 (3H, <i>s</i>)	26.6

* Interchangable carbons

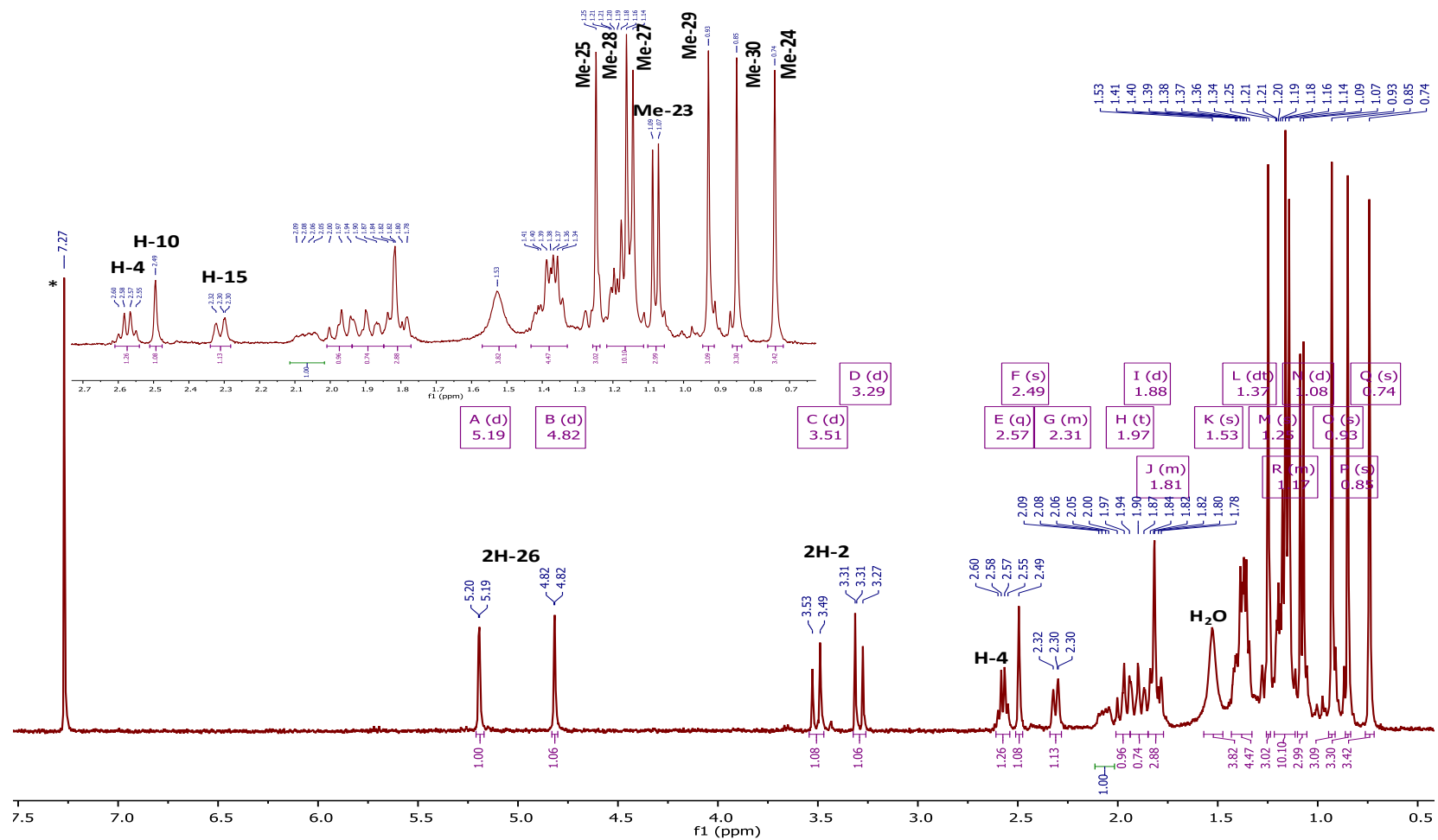


Figure 3.48: Full ^1H NMR spectrum with selected expansion (400 MHz) of HM-6 in CDCl_3 ; (*) CHCl_3 residue

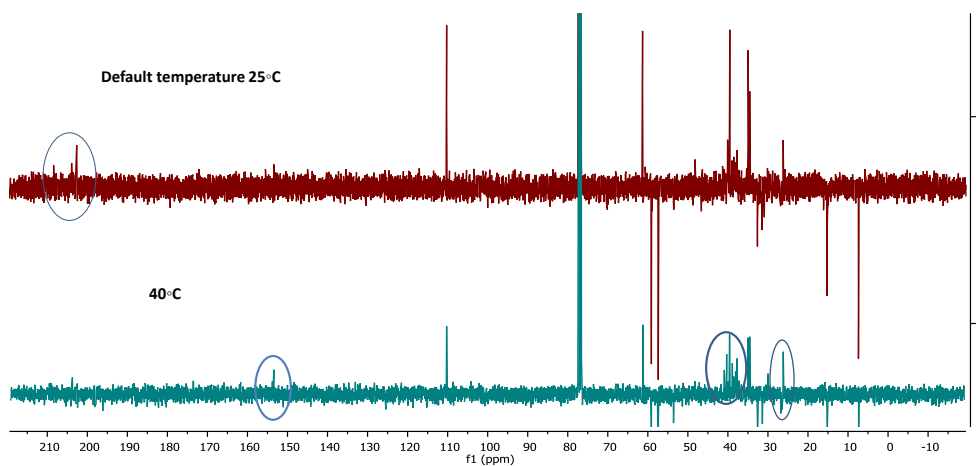


Figure 3.49: Stacked DEPTq ^{13}C spectrum (100MHz) showing the differences at two temperature settings

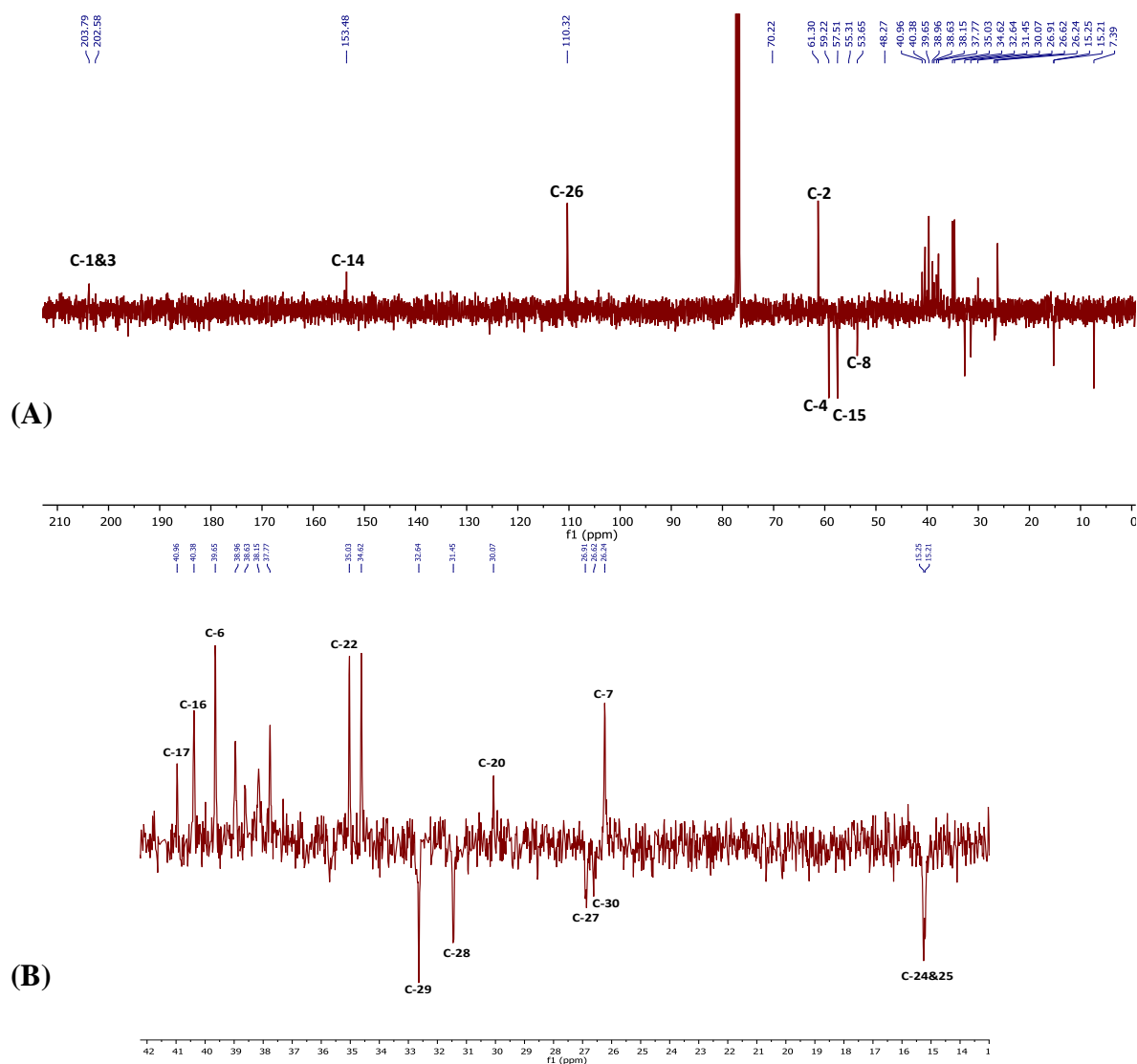
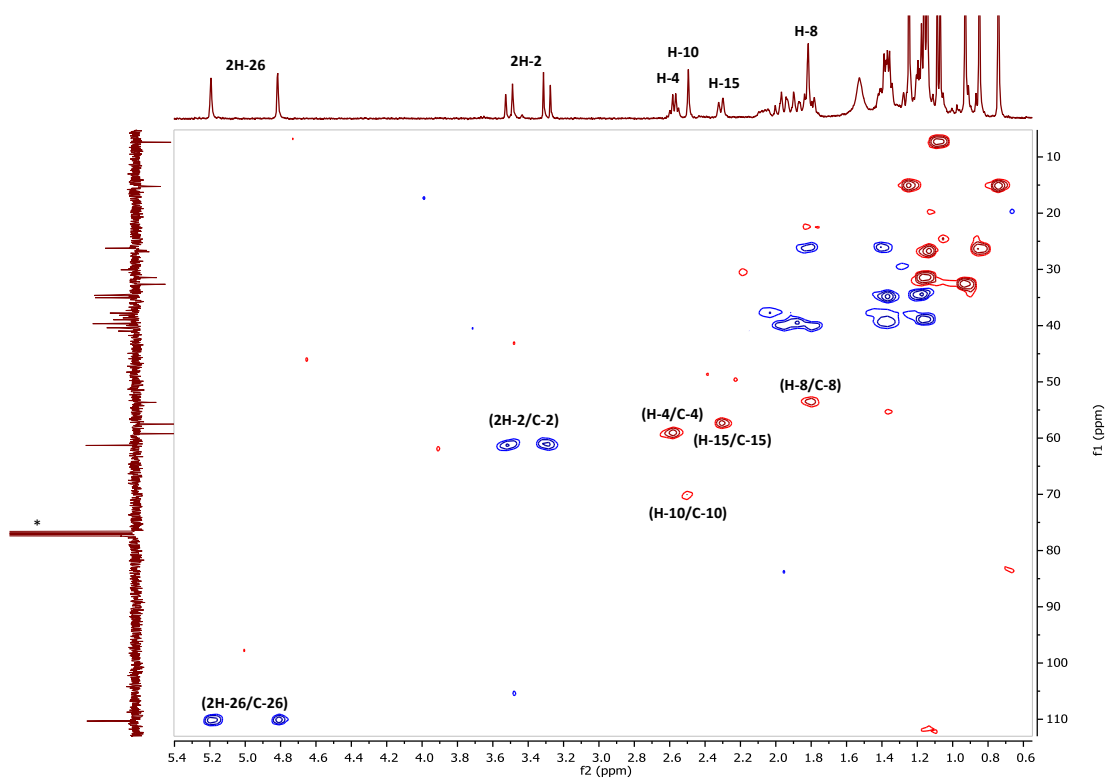
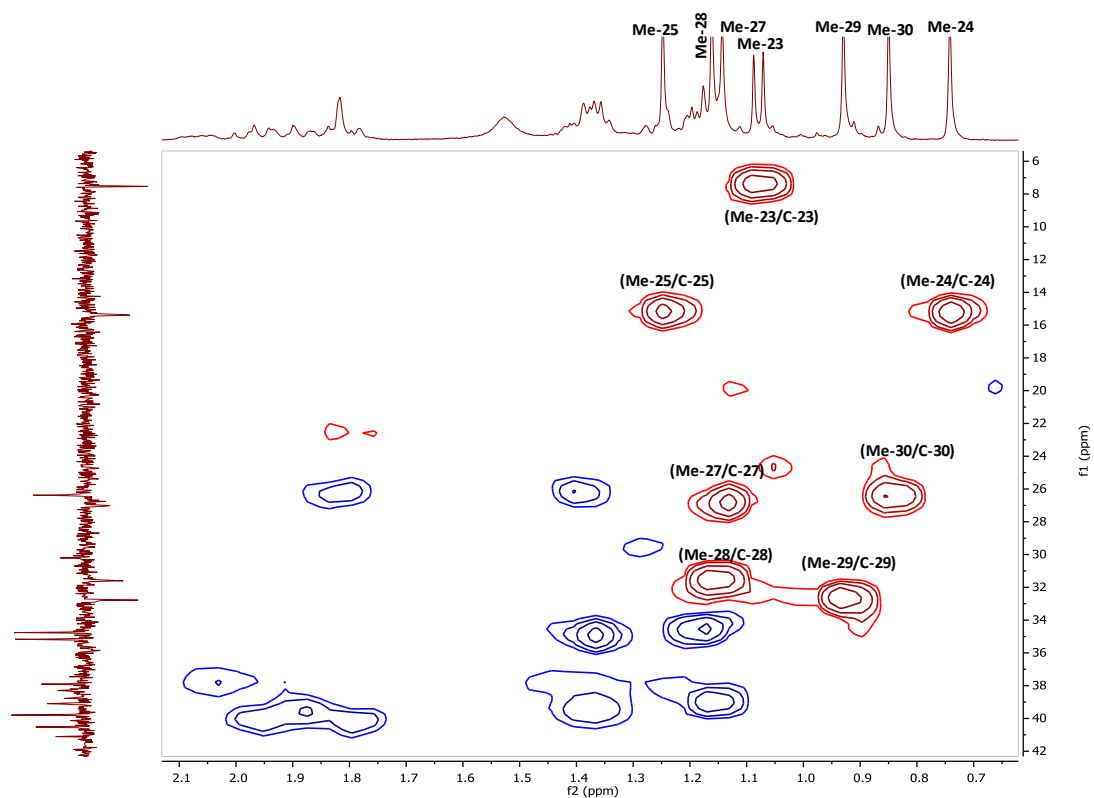


Figure 3.50: (A) DEPTq ^{13}C NMR spectrum (100 MHz) of HM-6 in CDCl_3 (*)
(B) Selected expansion in aliphatic region

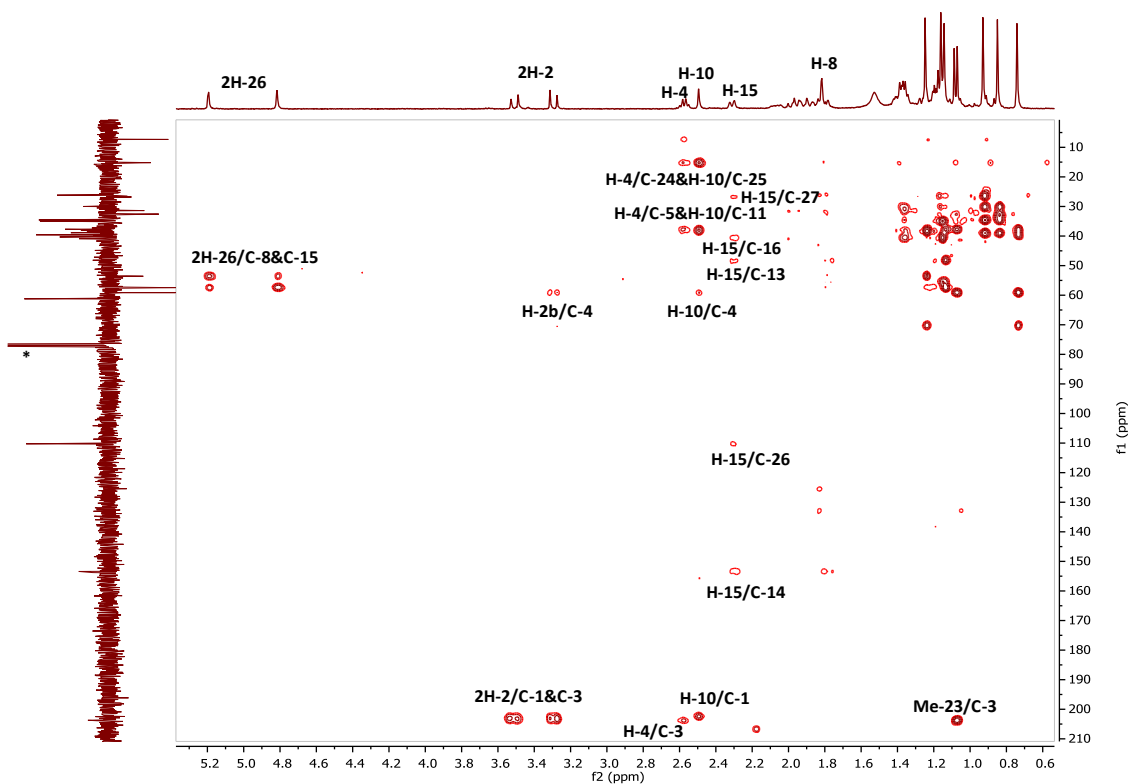


(A)

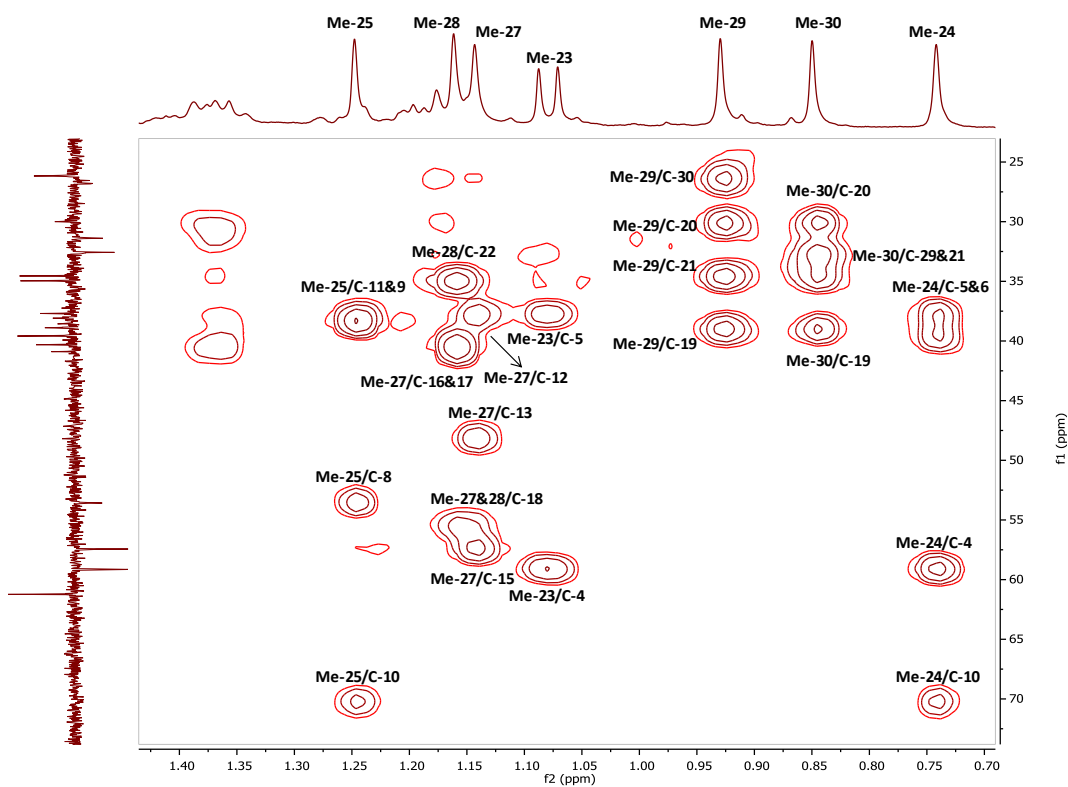


(B)

Figure 3.51: HSQC spectrum (400 MHz) of HM-6 in CDCl_3 (*)
 A: Full HSQC; B: Selected HSQC expansion

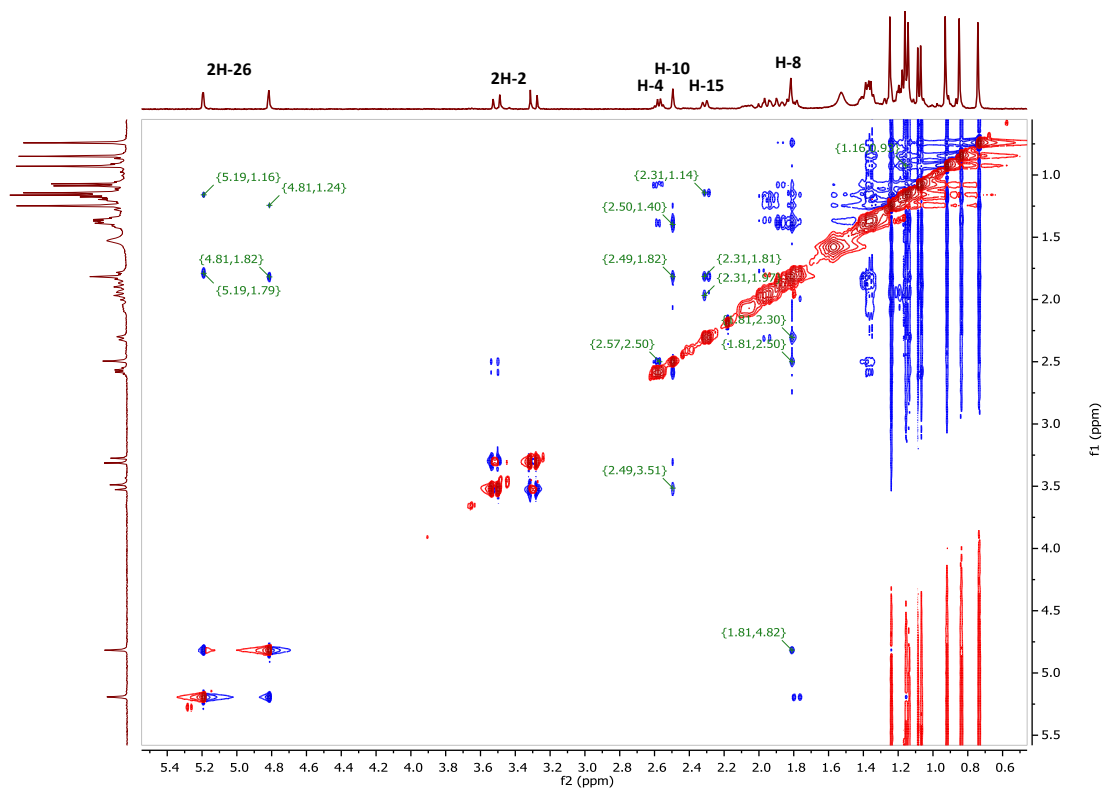


(A)

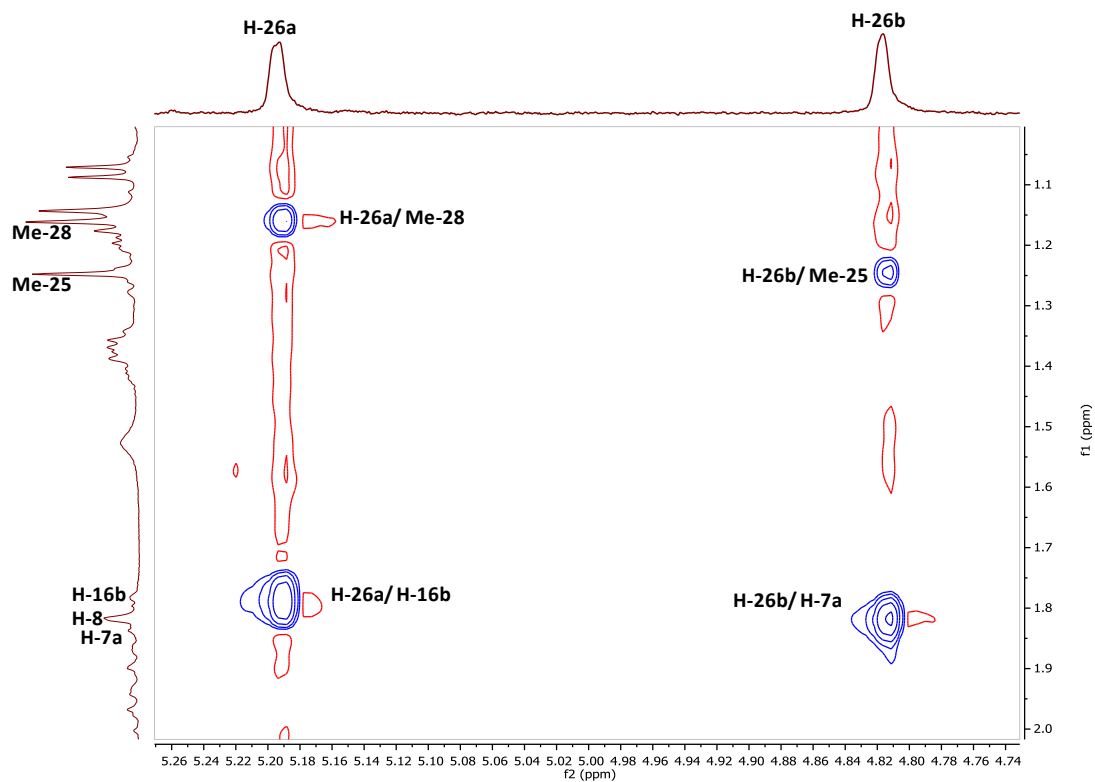


(B)

Figure 3.52: HMBC spectrum (400 MHz) of HM-6 in CDCl_3 (*)
 (A) Full HMBC; (B) Selected expansion for methyl groups



(A)



(B)

Figure 3.53: (A) Full NOESY spectrum (400 MHz) of HM-6 in CDCl_3
 (B) Selected expansion in olefinic region

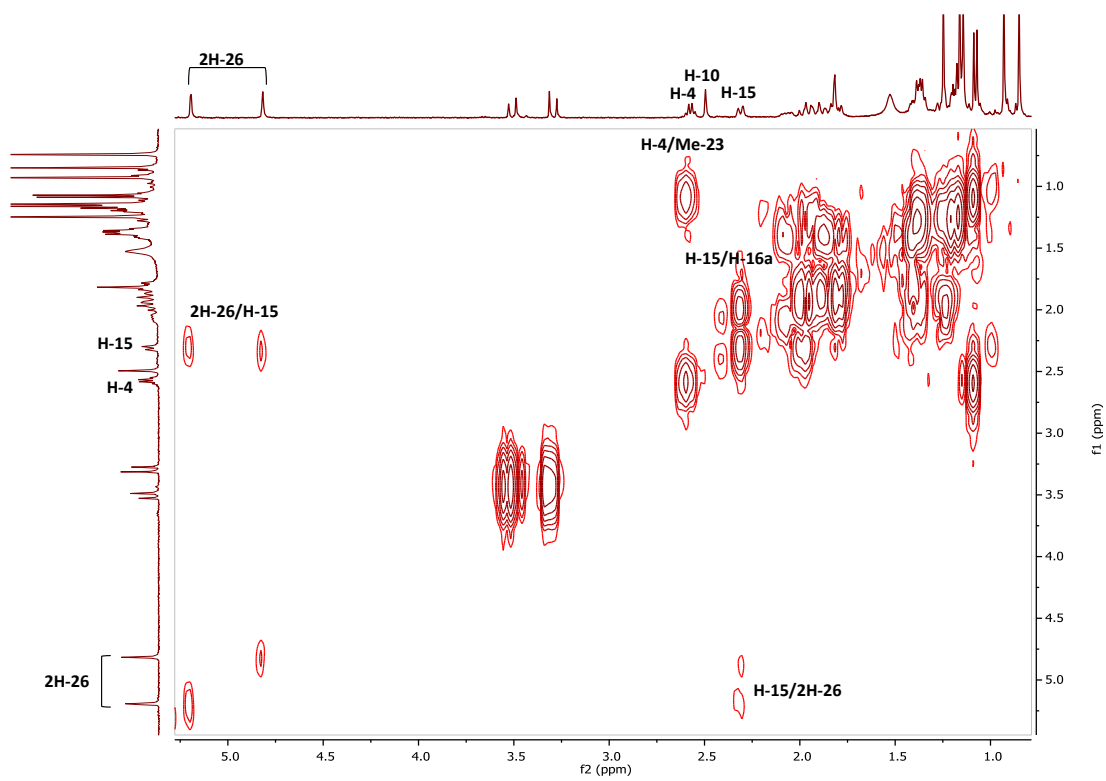


Figure 3.54: Full ^1H - ^1H COSY spectrum (400 MHz) of HM-6 in CDCl_3

3.3.2 Quinonemethide-type triterpenes (*celastroloids*)

All of the following isolated triterpenes incorporate similar structural features represented by the pentacyclic six-membered rings skeleton which invariably has oxygenated functionalities at C-2 (a ketone) and C-3 (a hydroxyl group). The characteristic feature of this type of the triterpenes comprises of the conjugated double bond system (i.e. chromophore) extended over A and B rings which causes quenching under short UV light (λ 254 nm) and imports the red-orange colour of these compounds. In the ^1H NMR spectrum, it manifests by the distinctive pattern of three olefinic-type protons (H-1, H-6 and H-7) in the aromatic region between δ_{H} 6.16 and 7.18 ppm. Due to this fact, all these compounds lack the methyl singlet at position-5 (Me-24), hence, they are classified as 24-nor-D: A-friedo-oleanane (Gunatilaka, 1996). The two singlet methyls Me-26 and Me-27 are usually aligned on the junction between rings C/D at positions-14 and -13, respectively, as seen in the compounds HM-10, HM-11 and HM-12. However, in the other compounds HM-7, HM-8 and HM-9, the conjugation is extended into the ring D with an extra double bond located between Δ 14, 15 resulting in the migration of Me-26 to the position-15. These compounds have common oxidation sites on 21, 22 and 29. The methyl at position-29 has undergone a complete oxidation to form (-COOH) as HM-11 and HM-12 which followed by methylation to form (-COOMe) as seen in the rest of the isolated quinonemethides.

3.3.2.1 Characterisation of HM-7 as *netzahualcoyondiol*

HM-7 was isolated from the n-hexane and EtOAc extracts of the root bark by PTLC as an amorphous red/brown solid. On TLC, the compound appeared as a dark spot under UV light (λ 254 nm) indicating the presence of conjugated double bonds. After treatment with *p*-anisaldehyde-sulphuric acid reagent and heating it turned to a dark pink spot with R_f value 0.16 on SiGel when eluted with the mobile phase 50% hexane in EtOAc.

The positive mode HRESI-MS spectrum showed a quasi-molecular ion $[\text{M}+\text{H}]^+$ at m/z 495.2751, suggesting a molecular formula of $\text{C}_{30}\text{H}_{38}\text{O}_6$ (DBE=12).

The ^1H NMR spectrum (400 MHz, CDCl_3 , Figure 3.56, Table 3.8) displayed six methyl singlets at δ_{H} 0.87, 1.30, 1.38, 1.42, 1.73 and a deshielded one at δ_{H} 2.27 ppm

indicating the presence of a triterpene compound which was also supported by the molecular formula. The unsaturated region of the spectrum showed a very distinctive pattern characterized by three vinyl protons as a doublet at δ_{H} 6.16 (1H, *d*, $J = 6.8$ Hz), a narrow doublet at δ_{H} 6.58 (1H, *d*, $J = 1.4$ Hz) and a doublet of doublet at δ_{H} 7.17 (1H, *dd*, $J = 6.8, 1.4$ Hz) corresponded to the protons H-7, H-1 and H-6, respectively, which are attributable to a quinonemethide moiety as described in section 3.3.2. The deshielded singlet at δ_{H} 2.27 (Me-23) characteristic of a methyl group attached to a sp^2 carbon also emphasized the presence of a quinonemethide system. Furthermore, the spectrum showed two doublets at δ_{H} 4.16 (1H, *d*, $J = 3.3$ Hz) and at δ_{H} 3.54 (1H, *d*, $J = 3.3$ Hz) indicating the presence of two oxymethine protons in addition to a carboxymethyl group at δ_{H} 3.72 attributed to (3H-31).

The DEPTq135 ^{13}C NMR spectrum (100 MHz, Figure 3.57) revealed the presence of 30 carbons including six methyls, four methylenes, four methines, two oxymethines at δ_{C} 69.3 and 79.5, one methoxyl carbon at δ_{C} 52.3 and thirteen quaternary carbons including the most significant signals as oxygen-bearing one at δ_{C} 146.3 (C-3) and two carbonyl carbons at δ_{C} 179.1 and 178.1 attributed to (C-29) and (C-2), respectively.

The chemical shifts of all hydrogen-bearing carbons were assigned from the HSQC spectrum (Figure 3.58) combined with the COSY spectrum (Figure 3.60) which revealed the vicinal coupling between H-6 and H-7 and the long range coupling between H-1 and H-6, as well as a vicinal coupling between the two oxymethine protons at δ_{H} 4.16 and 3.54, implying their positions as neighbours in the same spin system, H-21 & 22, respectively.

More rigorous analysis was achieved by the 2D HMBC spectrum (Figure 3.59). The methyl singlet at δ_{H} 1.42 showed 3J correlations to the oxymethine carbon at δ_{C} 69.3 as well as to the carbonyl carbon at δ_{C} 179.1 (C-29). In return, the same oxymethine proton at δ_{H} 4.16 showed 3J correlations to the latter methyl at δ_{C} 17.2 and to the same carbonyl. This confirmed the presence of a hydroxyl group located at position-21 and that the methyl singlet should be assigned as Me-30. On the other hand, the methyl singlet at δ_{H} 1.38 (Me-28) showed correlations to the other oxymethine carbon at δ_{C} 79.5 as well as to the carbons at δ_{C} 38.9 (C-17), 37.9 (C-16) and 38.8 (C-18) while the corresponding oxymethine proton at δ_{H} 3.54 had

correlations to the same carbons assigned as (C-17) and (C-18). Along with the observations in COSY experiment, the above data established the presence of another hydroxyl group attached at position-22 in the ring E of the pentacyclic skeleton. The ester group was confirmed by the 3J correlation of the singlet at δ_H 3.73 (3H) attributed to the methoxyl portion of an ester group to the carbonyl carbon at δ_C 179.1 (C-29).

The full interpretation of the HMBC and HSQC spectra allowed the complete unambiguous signal assignment and the structural determination of this quinonemethide triterpene, which was identified as netzahualcoyondiol (Figure 3.55). The spectral data obtained were in good agreement with a previous report (Jeller *et al.*, 2004). This is the first report of the isolation of netzahualcoyondiol from *M. laevis*, however, it has been previously isolated from other plants belonging to the Celastraceae family such as *Orthosphenia mexicana*, (Gonzalez *et al.*, 1988), *Rzedowskia tolantonguensis* (Gonzalez *et al.*, 1987) and *M. horrida* (Moujir *et al.*, 1990). In the latter study, this compound showed an inhibitory activity against the Gram positive bacterium *Staphylococcus aureus* with MIC in the range of 20 to 25 $\mu\text{g/ml}$, while it was not active against Gram negative bacterial strains. Jeller *et al.*, (2004) study found that netzahualcoyondiol has an antioxidant activity, which was evaluated by its free radical scavenging ability on the free radical 2,2-diphenyl-picryl hydrazyl (DPPH). It caused 45% inhibition at 60 μM compared to the standard rutin (66% inhibition at the same concentration). The cytotoxicity and the anti-trypanosomal activity of HM-7 were also evaluated in this work (for further details see sections 4.1.1.1 and 4.2.2).

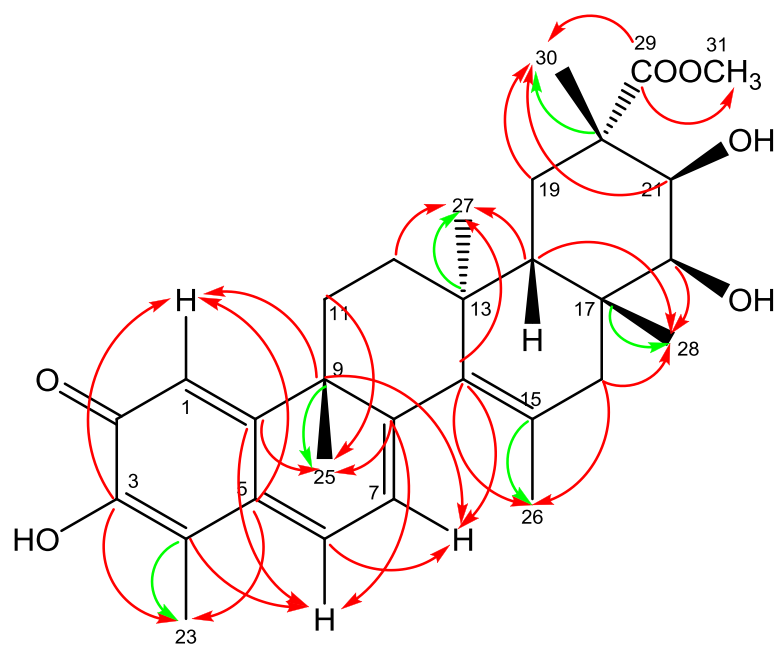


Figure 3.55: Structure of HM-7 with the HMBC correlations
 (→) 3J (→) 2J ^{13}C to ^1H connectivity

Table 3.8: ^1H (400 MHz) and ^{13}C (100 MHz) NMR data of HM-7 in CDCl_3

Position	HM-7	
	δ_{H}	δ_{C}
1	6.58 (1H, <i>d</i> , $J= 1.4$)	120.1
2	-	178.1
3	-	146.3
4	-	116.7
5	-	127.8
6	7.17 (1H, <i>dd</i> , $J= 6.8, 1.4$ Hz)	134.5
7	6.16 (1H, <i>d</i> , $J= 6.8$ Hz)	121.5
8	-	159.0
9	-	44.5
10	-	159.9
11	1.98 (2H) [2.05-1.88 <i>m</i>]	37.5
12	1.36 (1H, <i>m</i>)/ 2.56 (1H, <i>dt</i> , $J= 13.2, 5.6$ Hz)	34.8
13	-	42.5
14	-	136.1
15	-	126.7
16	1.47 (1H, <i>d</i> , $J= 16.6$ Hz) 2.44 (1H, <i>br. d</i> , $J= 16.6$ Hz)	37.9
17	-	38.9
18	1.86 (1H, <i>dd</i> , $J=13.2, 2.9$ Hz)	38.8
19	1.55 (1H, <i>d</i> , $J= 13.5$)/ 1.94 (1H, <i>m</i>)	33.9
20	-	47.4
21	4.16 (1H, <i>d</i> , $J= 3.3$ Hz)	69.3
22	3.54 (1H, <i>d</i> , $J= 3.3$ Hz)	79.5
23	2.27 (3H, <i>s</i>)	10.4
24	-	-
25	1.30 (3H, <i>s</i>)	29.5
26	1.73 (3H, <i>s</i>)	21.8
27	0.87 (3H, <i>s</i>)	24.6
28	1.38 (3H, <i>s</i>)	27.1
29	-	179.1
30	1.42 (3H, <i>s</i>)	17.2
31	3.73 (3H, <i>s</i>)	52.3

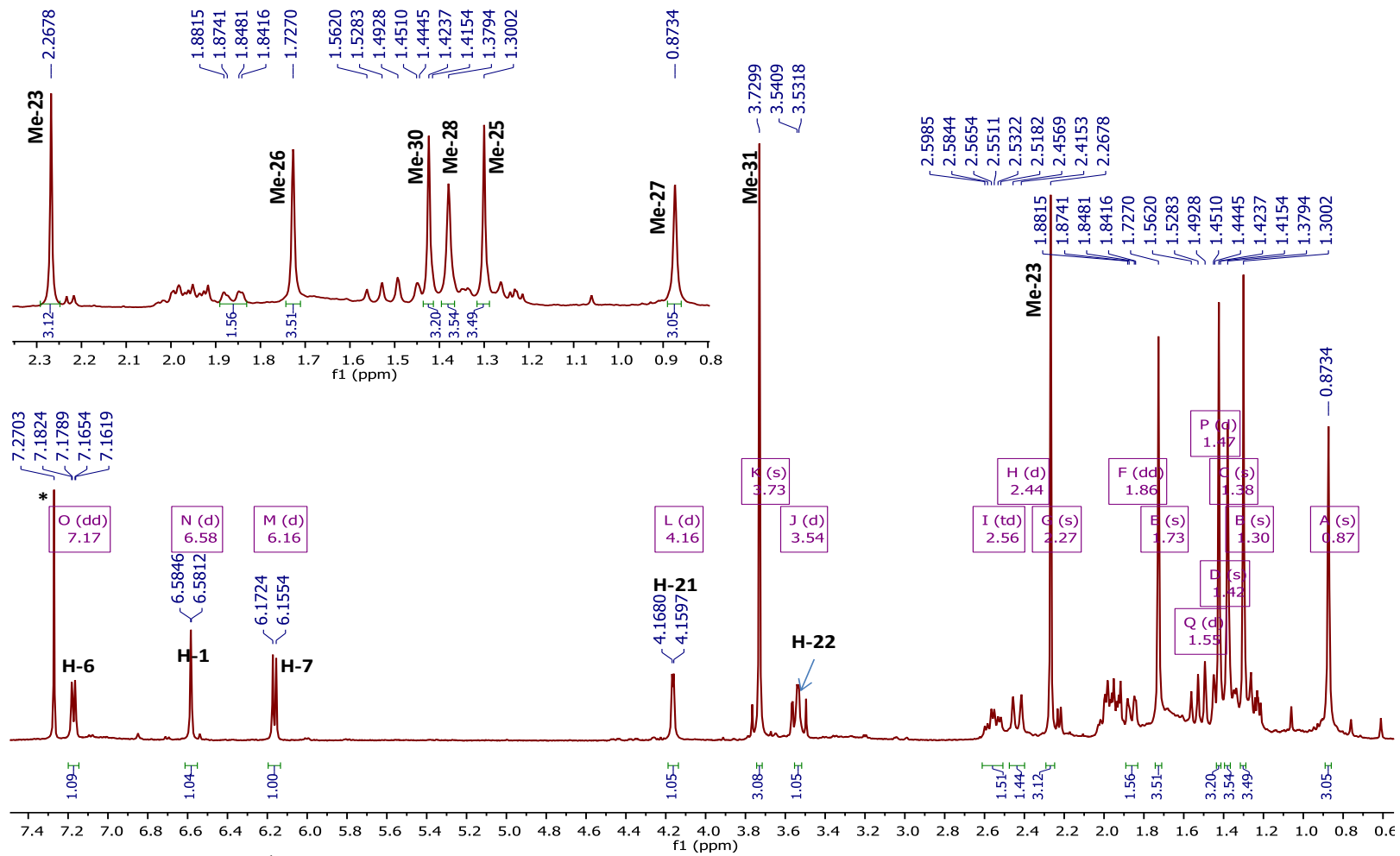


Figure 3.56: ^1H NMR spectrum with selected expansions (400 MHz) of HM-7 in CDCl_3 ; (*) CHCl_3 residue

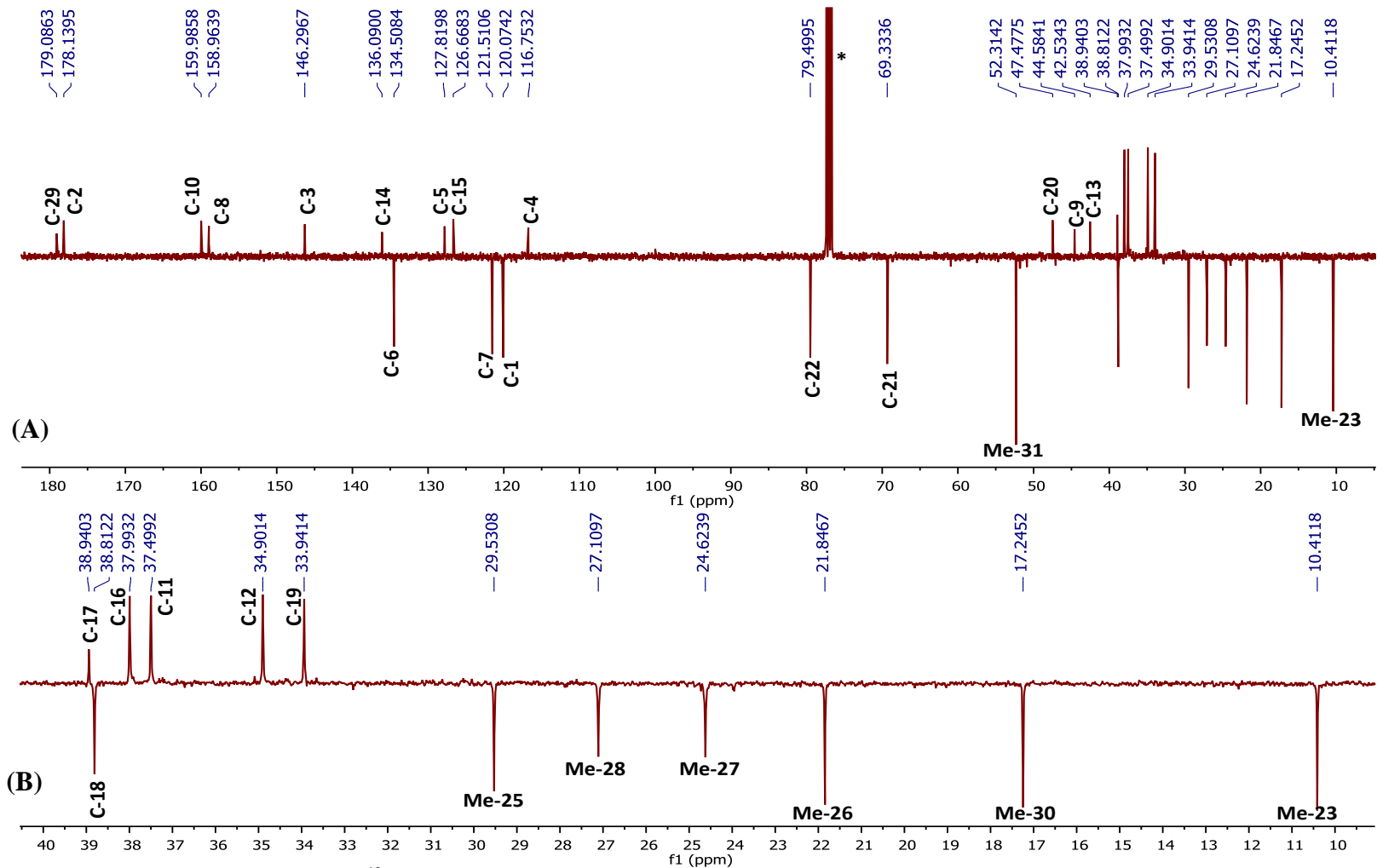
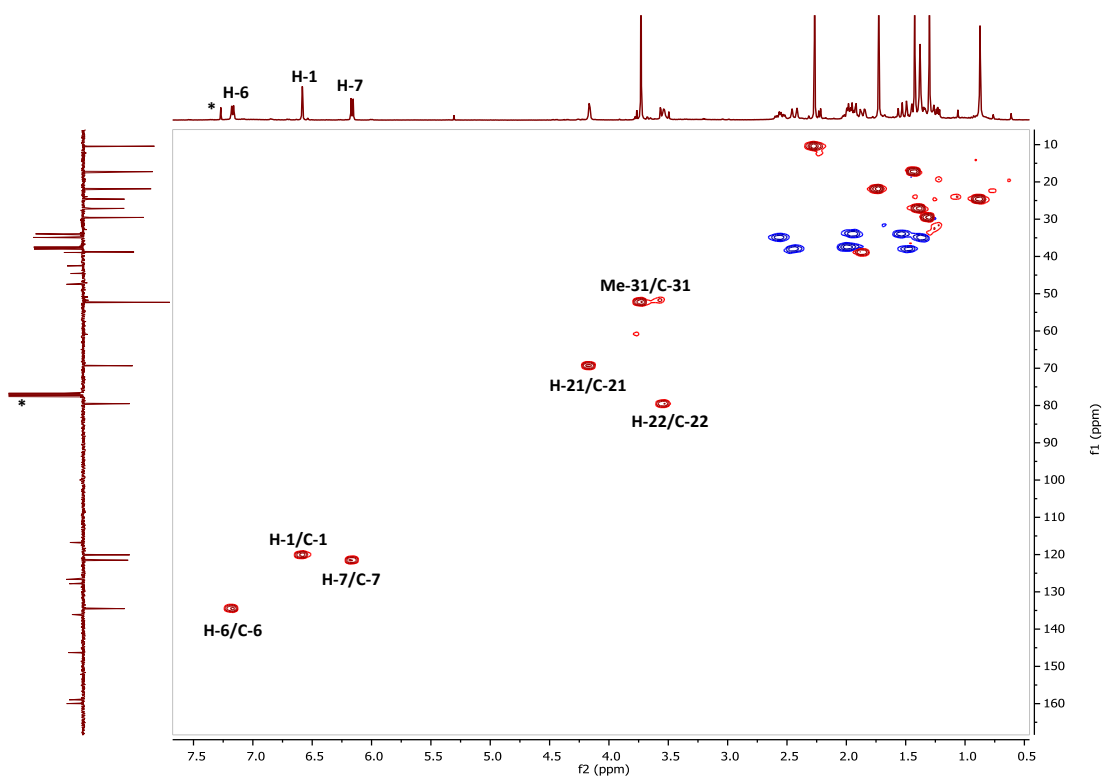
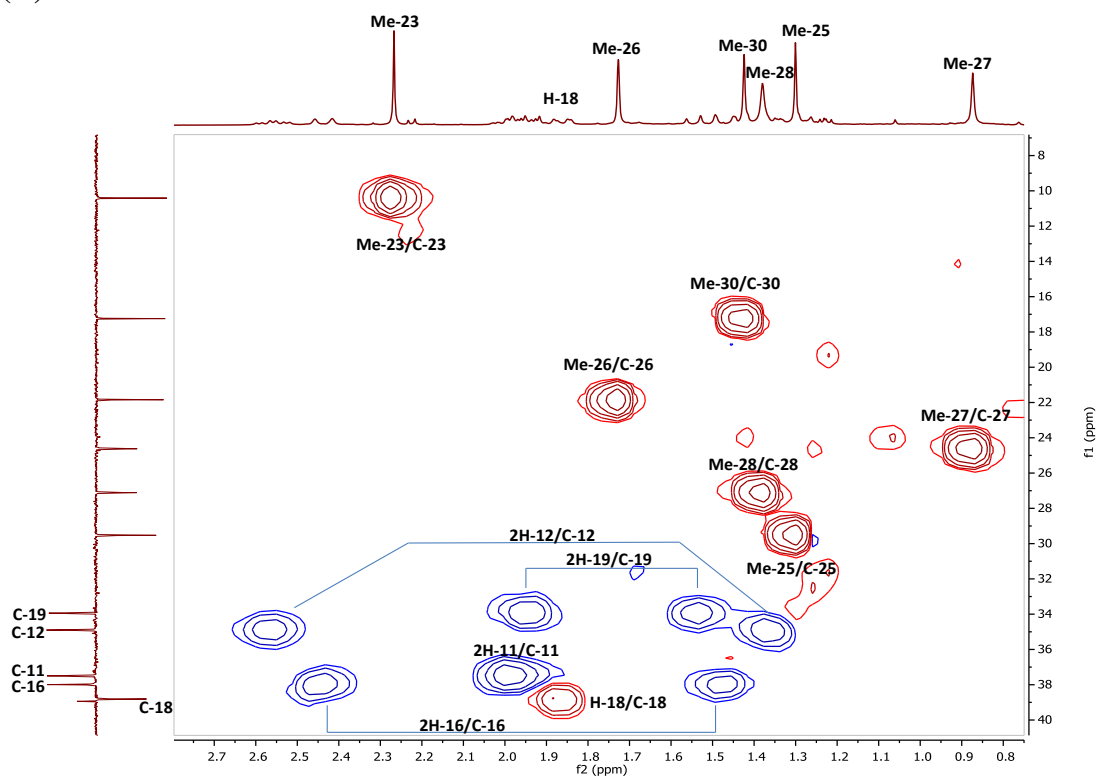


Figure 3.57: (A): Full DEPTq $^{135} \text{C}$ NMR spectrum (100 MHz) of HM-7 in CDCl_3 (*); (B): Selected expansion in aliphatic region

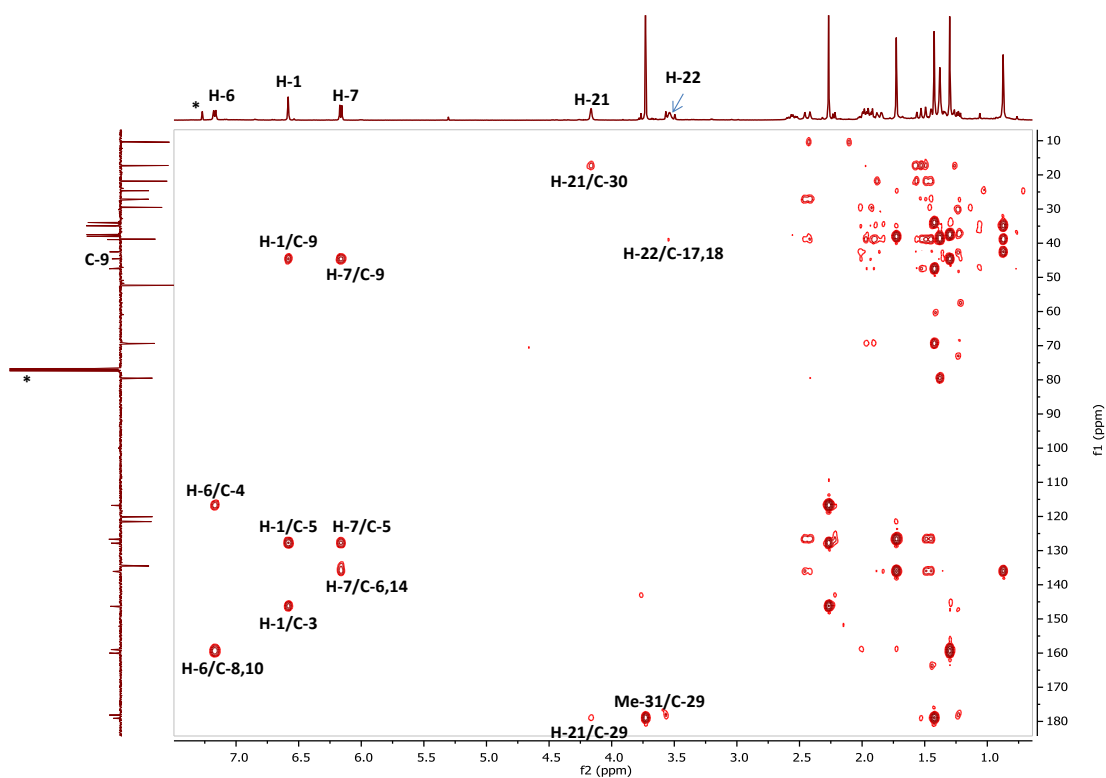


(A)

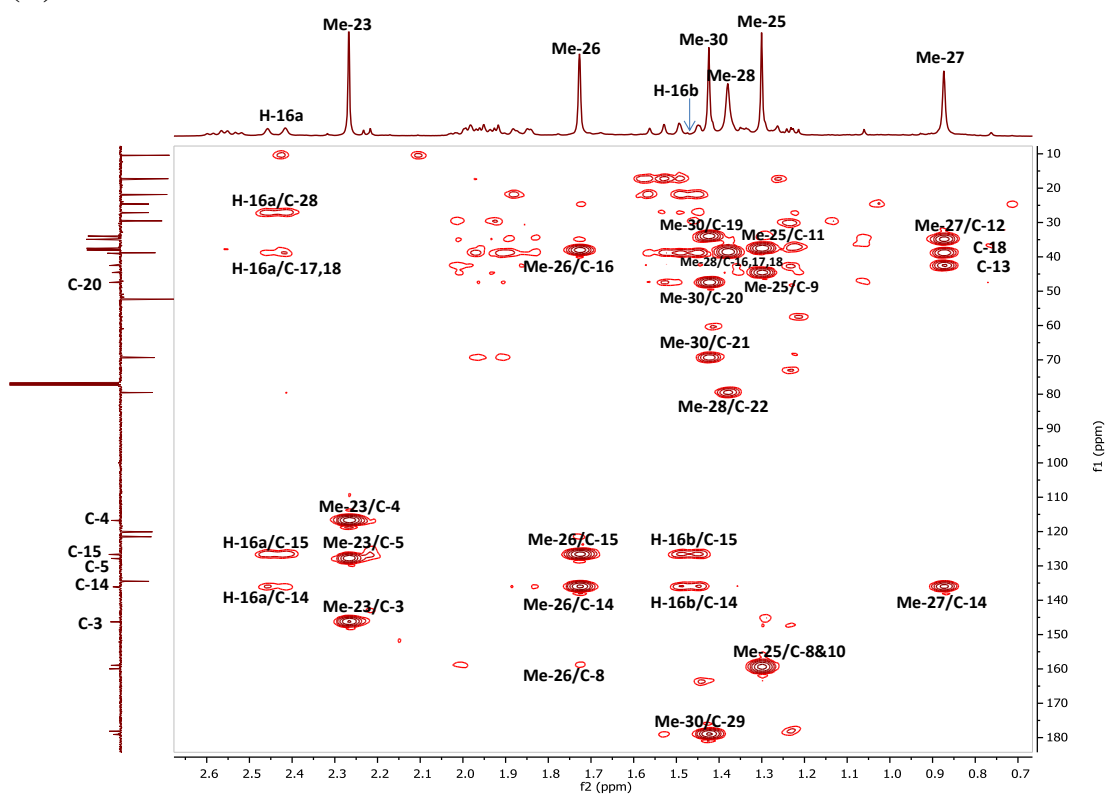


(B)

Figure 3.58: HSQC spectrum (400 MHz) of HM-7 in CDCl_3 (*)
 (A): Full HSQC; (B): Selected HSQC expansion for the aliphatic region of (F_2+F_1)



(A)



(B)

Figure 3.59: HMBC spectrum (400 MHz) of HM-7 in CDCl_3 (*)
A: Full HMBC; B: Selected HMBC expansion for the aliphatic region of F_2

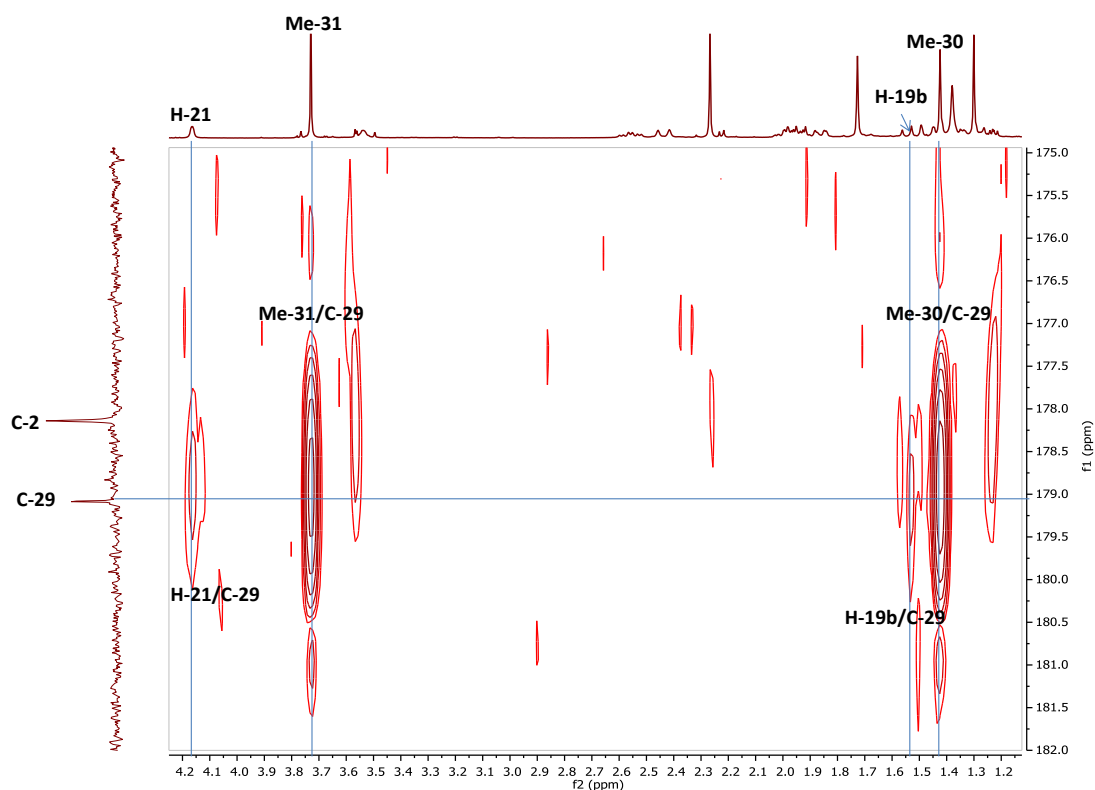


Figure 3.59 (Cont.): (C): Selected HMBC expansion showing the ketones correlations

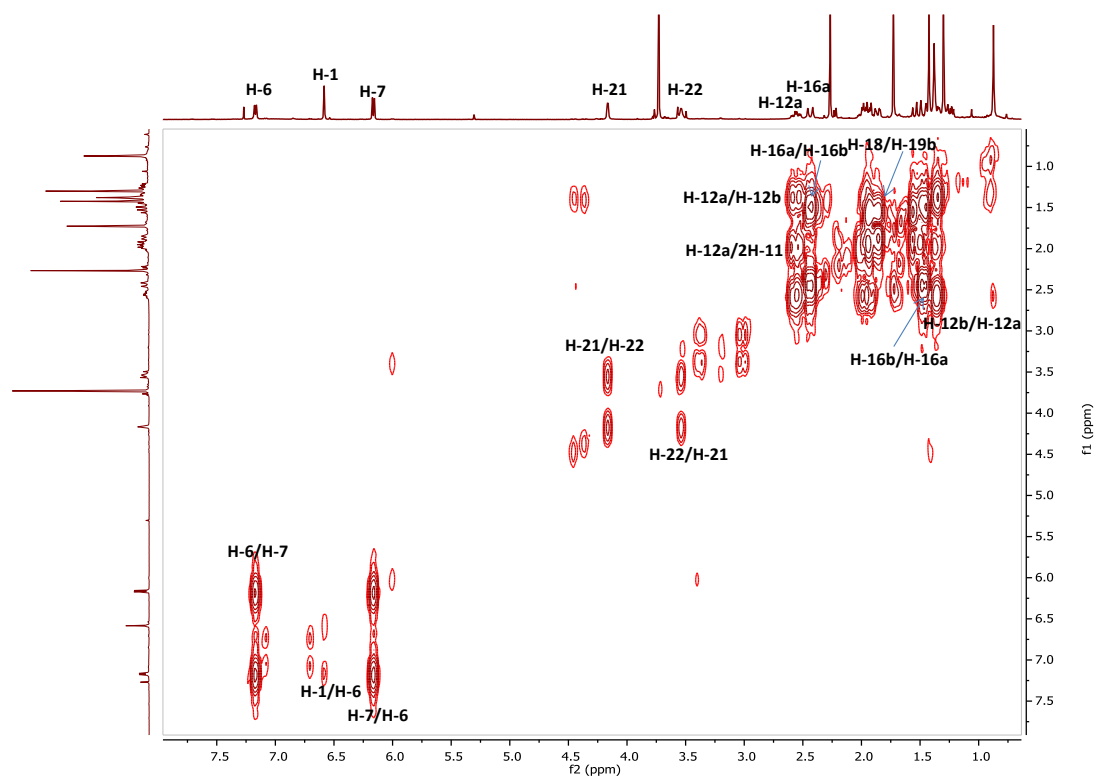


Figure 3.60: Full ¹H-¹H COSY spectrum (400 MHz) of HM-7 in CDCl₃

3.3.2.2 Characterisation of HM-8 as netzahualcoyone

HM-8 was isolated from the n-hexane extract of the root bark by semi-preparative HPLC as an amorphous red solid. On TLC, the compound appeared as a dark spot under UV light (λ 254) and after treatment with *p*-anisaldehyde-sulphuric acid reagent and heating it turned to a dark pink spot with R_f value 0.33 on SiGel when eluted with the mobile phase 50% hexane in EtOAc.

The positive mode HRESI-MS spectrum showed a quasi-molecular ion $[M+H]^+$ at m/z 493.2589, suggesting a molecular formula of $C_{30}H_{36}O_6$ (DBE=13).

The molecular formula and the pattern of the 1H NMR spectrum (400 MHz, $CDCl_3$, Figure 3.63, Table 3.9 on p.149) suggested another quinonemethide-type triterpene with very close similarity to HM-7. The spectrum displayed six methyl singlets at δ_H 0.93, 1.02, 1.30, 1.45, 1.79 and 2.27 attributed to Me-27, Me-30, Me-25, Me-28, Me-26 and Me-23, respectively, a carboxymethyl group at δ_H 3.79 attributed to (3H-31), the three characteristic olefinic protons at δ_H 6.21 (1H, *d*, $J = 6.9$ Hz, H-7), 6.57 (1H, *d*, $J = 1.4$ Hz, H-1) and at δ_H 7.17 (1H, *dd*, $J = 6.9, 1.4$ Hz, H-6). A deshielded doublet signal at δ_H 5.00 (1H, *d*, $J = 4.3$ Hz) was attributed to an oxymethine proton assigned at the position-21 of the pentacyclic skeleton as the Me-30 showed in the HMBC spectrum (Figure 3.66; B) 3J correlations to the carbons at δ_C 74.4 (C-21), 34.2 (C-19) and 175.3 (C-29), and, additionally, the methylene protons at δ_H 2.18ax (*t*, $J = 13.7$ Hz)/1.92eq (*m*) associated to C-19 at δ_C 34.2 exhibited 3J correlations to the oxymethine carbon at δ_C 74.4 (C-21). Moreover, a doublet at δ_H 3.70 with a coupling constant ($J = 4.3$ Hz) equal to that of H-21 was assigned with the aid of the HSQC spectrum (Figure 3.65) as a geminal secondary hydroxyl group to the H-21 which showed correlations to the quaternary carbon at δ_C 50.4 (C-20) and to its oxymethine carbon at δ_C 74.4 (C-21). This was also supported by the cross peak between H-21 and OH-21 appeared in the COSY spectrum (Figure 3.67). Finally, the broad singlet at δ_H 7.06 was assigned as a tertiary hydroxyl group at position-3 as it showed correlation to the olefinic carbon at δ_C 116.7 (C-4), while the singlet signal at δ_H 1.60 ppm was an indication for water traces.

The data obtained from the DEPTq135 ^{13}C NMR spectrum (100 MHz, Figure 3.64) resembled those of HM-7, but with a few differences manifesting clearly in the data for the carbons making up the ring E. The spectrum revealed the presence of 30

carbons including six methyls, four methylenes, four methines, one oxymethine at δ_C 74.4, eleven quaternary carbons including an oxygen-bearing one C-3 at δ_C 146.3, one methoxyl carbon at δ_C 52.7 and three carbonyl carbon signals at δ_C 175.3, 178.2 and 213.9 attributed to C-29, C-2 and C-22, respectively.

The chemical shifts of all hydrogen-bearing carbons were assigned from the HSQC spectrum combined with COSY spectrum which showed a long range coupling between H-1/ H-6 and vicinal coupling between H-6/ H-7 and between 2H-12/ 2H-11 confirming their positions in each spin system.

The correlations observed in the HMBC spectrum (Figure 3.66; A) were all similar to those in the compound HM-7, confirming the presence of a quinonemethide-type compound, which has almost an identical structure with the only difference in the presence of a saturated ketone function instead of an alcoholic group at position-22 in the ring E. The downfield shift of the H-21 by 0.84 ppm comparing to that in the HM-7 (δ_H 4.16) suggested the presence of an adjacent electron withdrawing group (a ketone group) which was confirmed by the 3J and 2J correlations coming from the secondary hydroxyl group and the oxymethine proton at the position-21 to the carbonyl carbon at δ_C 213.9, respectively, in addition to the 3J correlation from the methyl singlet Me-28 and the methylene proton at δ_H 2.80 (*br.d*, $J= 16.2$ Hz, H-16a) to the same carbonyl carbon. In Figure 3.66; (A), some correlations were "folded" due to the carbonyl carbon at δ_C 213.9 being left outside the acquisition window, therefore, the software folded them back into the 2D map at the other end of the F_1 domain.

The relative stereochemistry of the (OH-21) was justified by reference to the X-ray crystallographic data in literature (González *et al.*, 1983) along with the NOE correlations observed in the NOESY spectrum obtained here (Figure 3.68). The X-ray data confirmed that the configuration of the penta-cyclic skeleton was as the following; rings A and B are planar, while ring C and E are chairs and ring D is an envelope. From the NOESY spectrum, the methine proton H-18 (δ_H 1.82) showed correlations to the methyl Me-28 (δ_H 1.45) confirming the *cis* configuration of the D/E ring junction as well as to the methyl Me-30 (δ_H 1.02) which is placed on the β side and in axial orientation with regard to the ring E_{chair} . On the other hand, the oxymethine proton H-21(δ_H 5.00) showed correlation to the methylene triplet H-19a

(δ_{H} 2.18) which has a transoid configuration with the methine proton H-18 with coupling constant ($J=13.7$ Hz), indicating their position on the α side of the molecule in an axial orientation. This concluded that the secondary hydroxyl group (OH-21) should be placed on the β side in an equatorial orientation (Figure 3.62).

On the basis of these results and by comparison with previous published data, HM-8 was identified as netzahualcoyone (Figure 3.61). The assignment of ^{13}C NMR signals matched to a large extent with the previous report (Jeller *et al.*, 2004) except for the two carbons at the positions-8 and 10 which were assigned in reverse order. However, the long range correlation 4J from the methyl singlet Me-26 to the carbon signal at δ_{C} 157.1 confirmed this to be C-8, while the 2J correlation from the methine proton H-1 to the carbon signal at δ_{C} 159.4 confirmed the latter to be C-10 as clarified in the HMBC spectrum. This compound has been previously isolated from other plants belonging to the Celastraceae family such as *Orthosphenia mexicana* (González *et al.*, 1983) and *R. tolantonguensis* (González *et al.*, 1989), but, this is the first report of its isolation from *M. laevis*. Netzahualcoyone, isolated from the roots of the *Schaefferia cuneifolia* Stanley (Celastraceae) by Moujir *et al.* (1990), showed a strong activity against a series of Gram positive bacteria including *S. aureus* and *Bacillus subtilis* with MIC values in the range of 1.50-1.62 and 0.625-1.25 $\mu\text{g/ml}$, respectively, while it was not active against the tested Gram negative bacterial strains such as *E. coli* and *Salmonella* sp. with MIC > 200 $\mu\text{g/ml}$. It was found that the quinonemethide skeleton is a structural requirement for this activity and the type of functional groups present in ring E affects its potency. With a ketone group at C-22 and a hydroxyl group at C-21, the anti-microbial activity against *S. aureus* for netzahualcoyone was thirteen to fifteen times more than netzahualcoyondiol with two hydroxyl groups at positions-21 and 22. Studying the mechanism of action of this compound showed that it inhibited the respiration of intact cells of the Gram positive bacteria, *B. subtilis*, but not the Gram negative ones, *Escherichia coli*. This was linked by experiments to the presence of a permeability barrier, the outer membrane of the latter bacteria (Moujir *et al.*, 1991). The free radical scavenging activity of this compound was also reported by Jeller *et al.* (2004) study. In this work, the cytotoxicity and the anti-trypanosomal activity of HM-8 were also evaluated (for further details see sections 4.1.1.1 and 4.2.2).

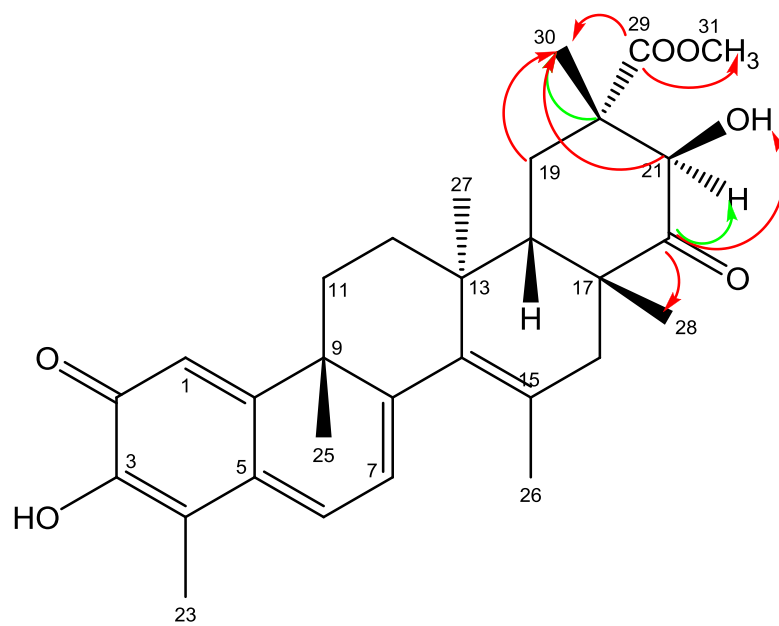


Figure 3.61: Structure of HM-8 with the key HMBC correlations (\rightarrow) 3J (\rightarrow) 2J ^{13}C to ^1H connectivity

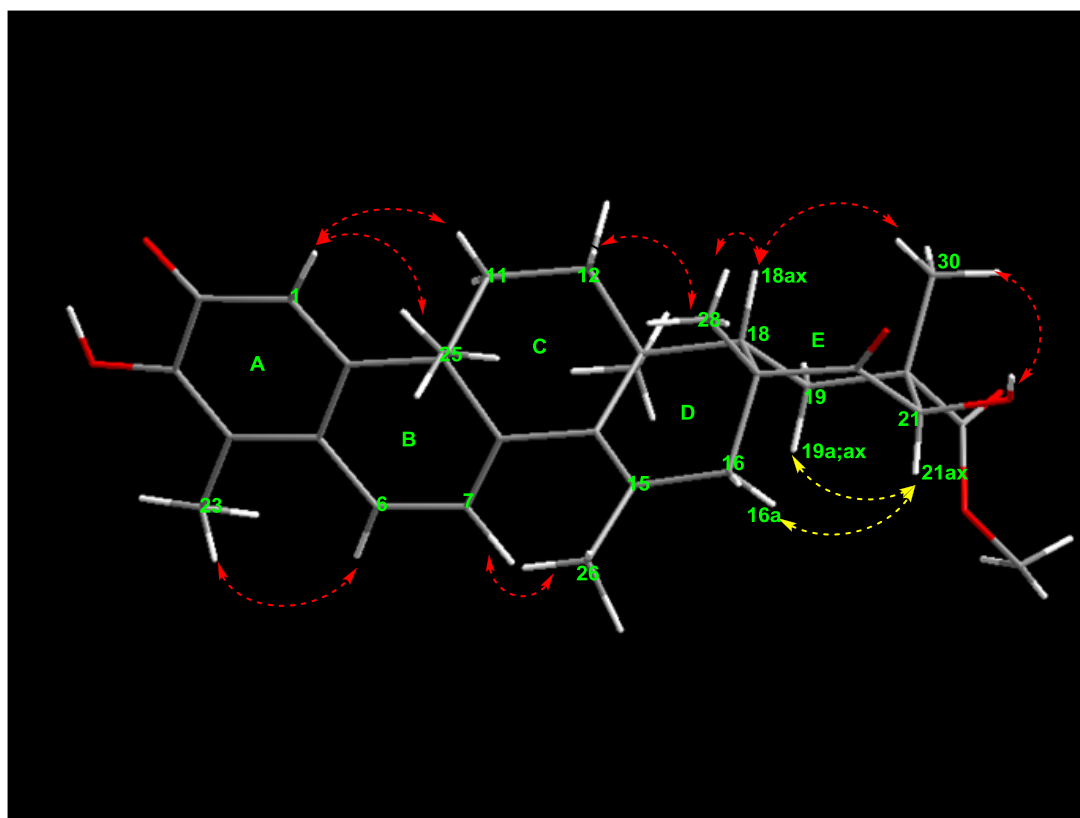
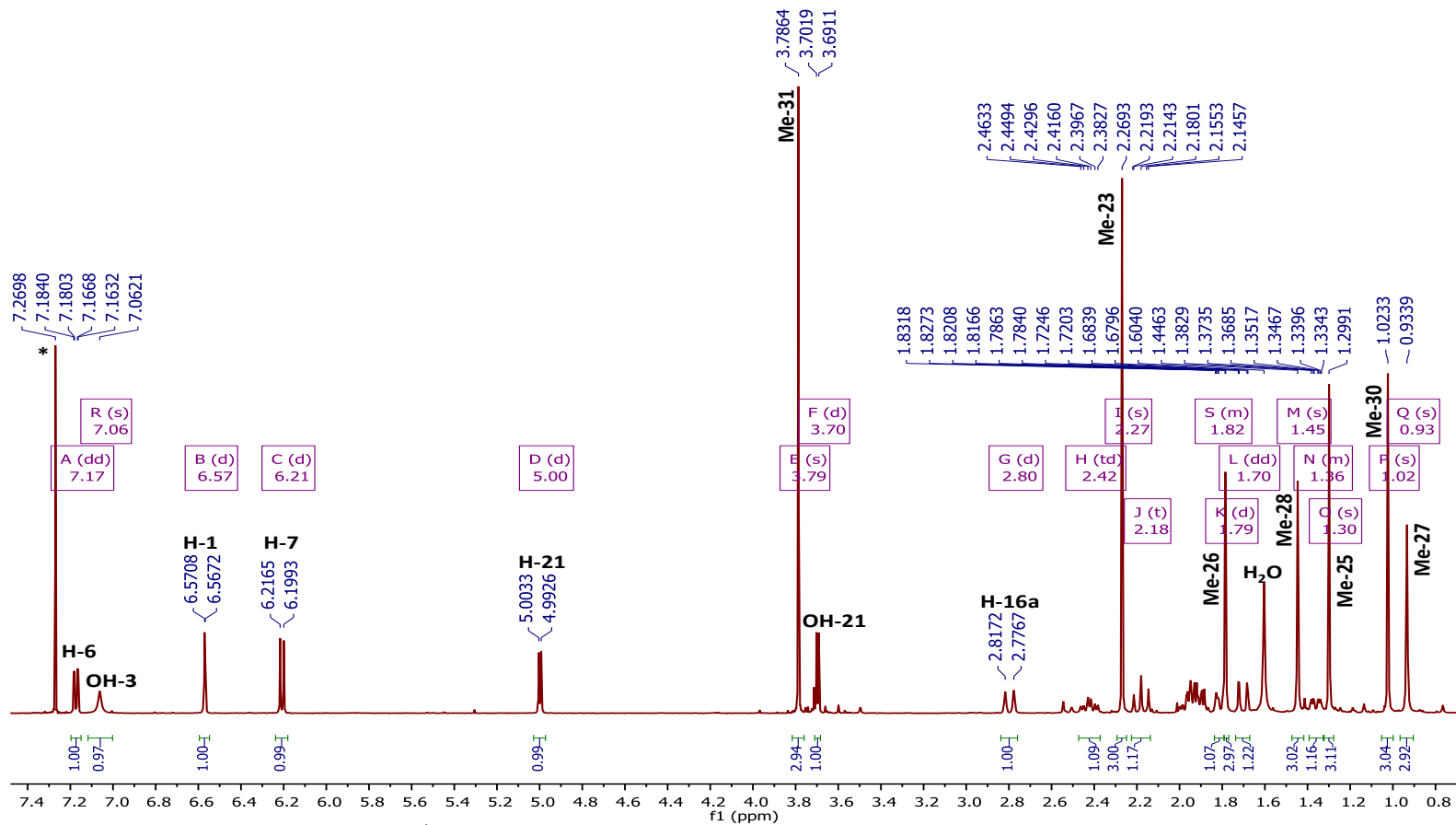


Figure 3.62: X-Ray model of Netzahualcoyone (González *et al.*, 1983) with selected NOESY correlations β (\leftrightarrow), α (\leftrightarrow) observed in this study on HM-8



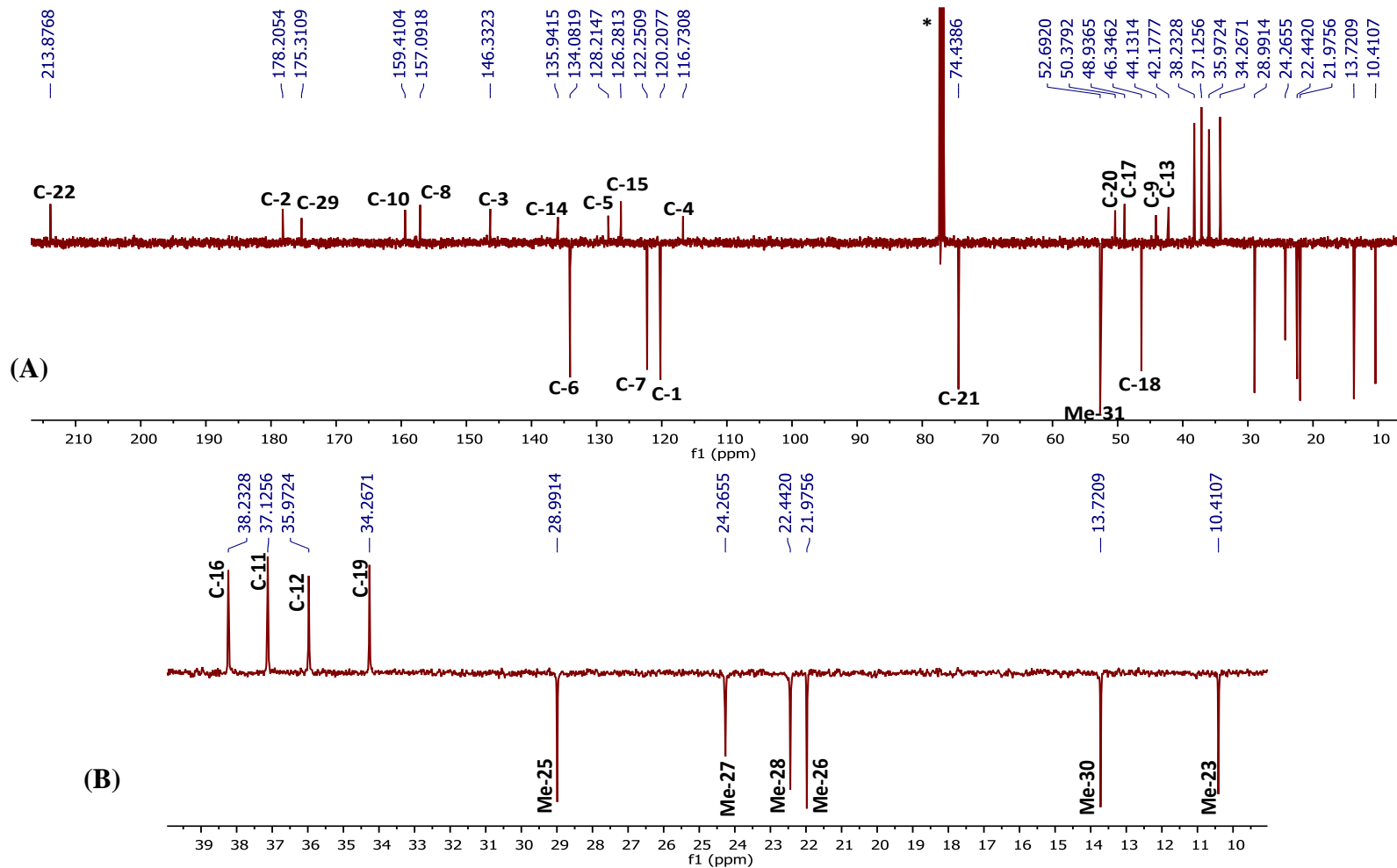
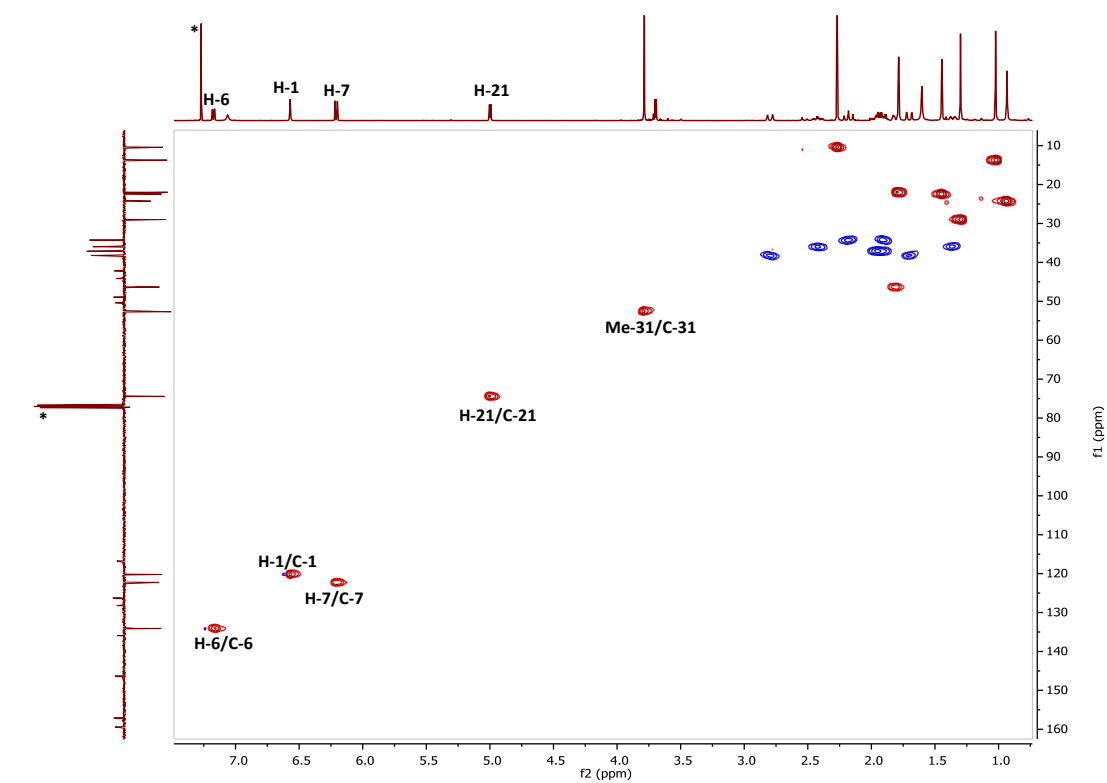
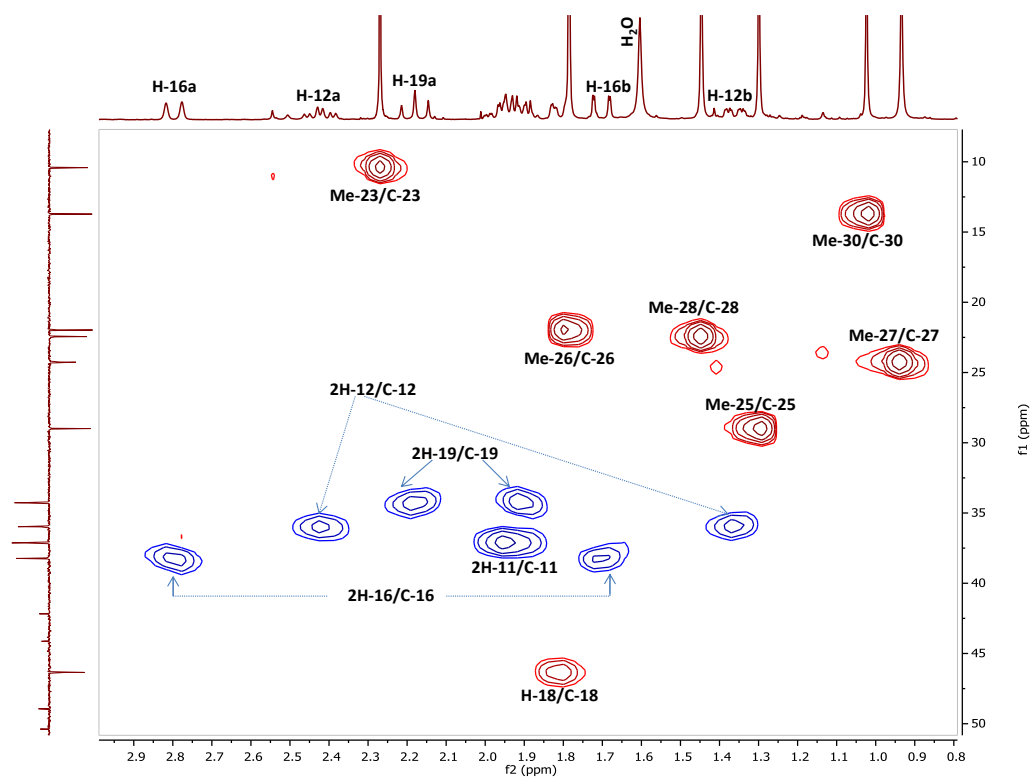


Figure 3.64: Full DEPTq ^{13}C NMR spectrum (100 MHz) of HM-8 in CDCl_3 (*); (B): Selected expansion in aliphatic region

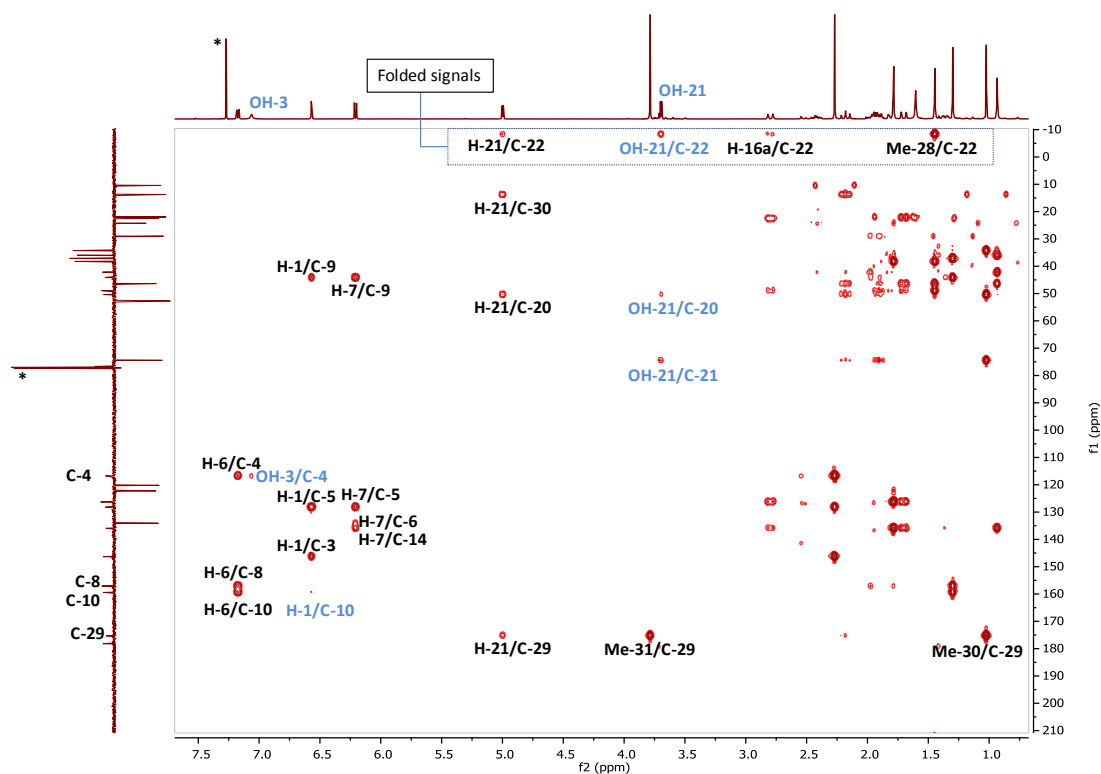


(A)

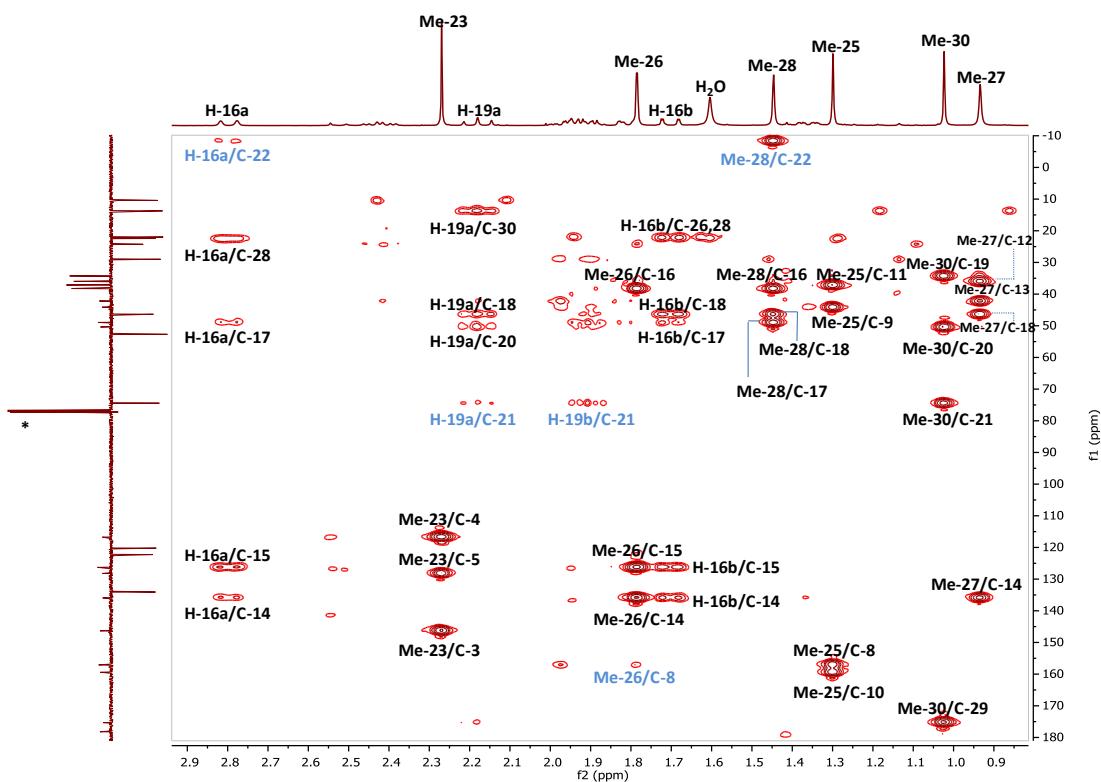


(B)

Figure 3.65: HSQC spectrum (400 MHz) of HM-8 in CDCl_3 (*)
 A: Full HSQC; B: Selected HSQC expansion



(A)



(B)

Figure 3.66: HMBC spectrum (400 MHz) of HM-8 in CDCl_3 (*)
(A): Full HMBC; (B): Selected HMBC expansion for the aliphatic region of F_2

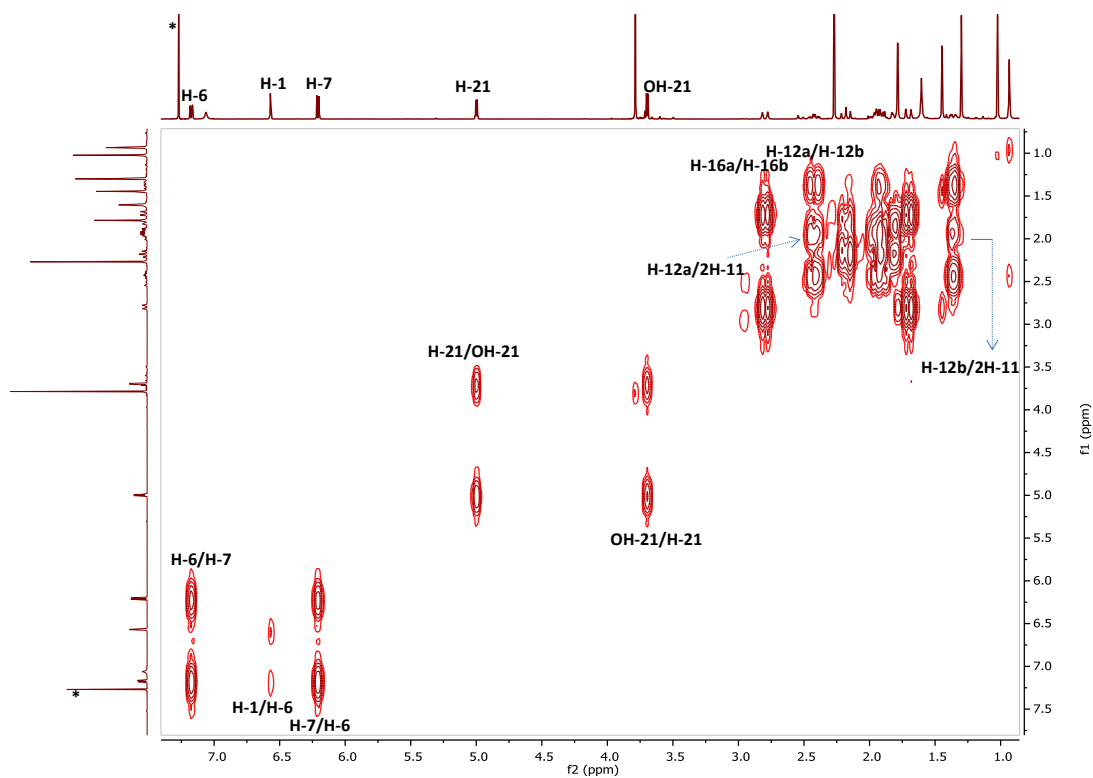


Figure 3.67: Full ^1H - ^1H COSY spectrum (400 MHz) of HM-8 in CDCl_3

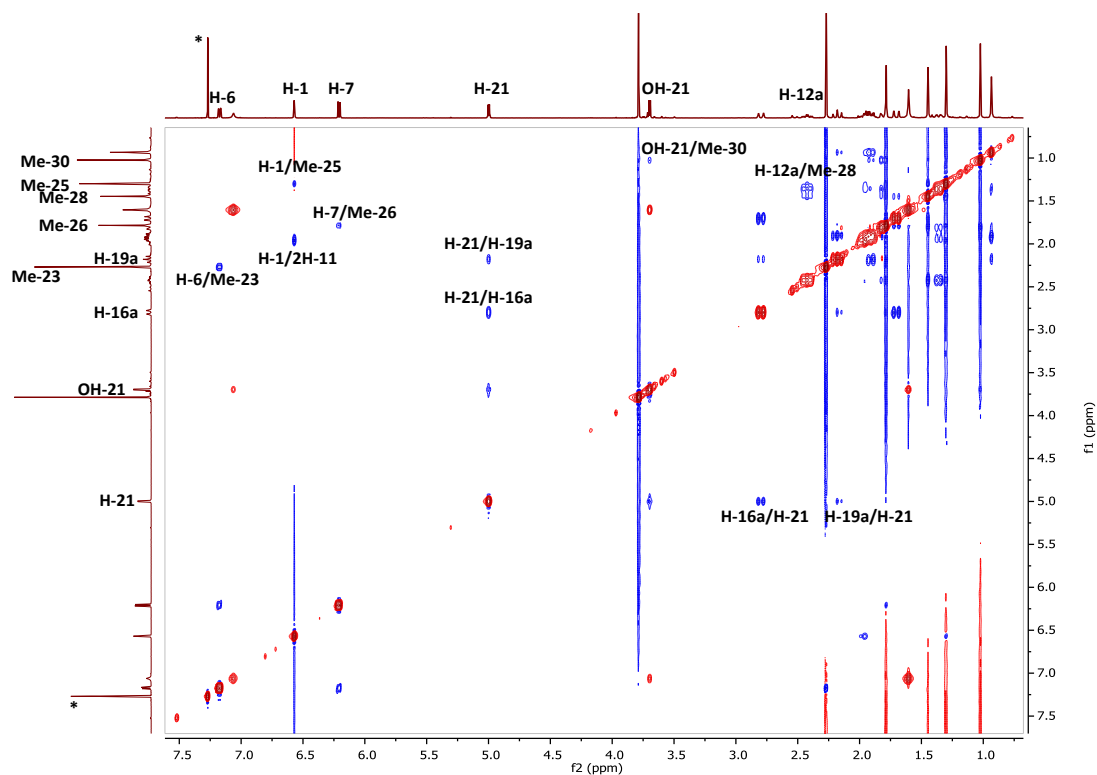


Figure 3.68: Full NOESY spectrum (400 MHz) of HM-8 in CDCl_3

3.3.2.3 Characterisation of HM-9 as the new celastroid, 22(α)-hydroxynetzahualcoyene

A semi-preparative HPLC method was used to separate the compound HM-9 from another structural analogue HM-8 in a VLC fraction from the n-hexane extract of the root bark of *M. laevis*. The amorphous red solid appeared on TLC as a dark spot under UV light (λ 254 nm) which turned to a bluish-purple spot after treatment with *p*-anisaldehyde-sulphuric acid reagent and heating. Its R_f was 0.29 on SiGel when eluted with the mobile phase 50% hexane in EtOAc.

The positive mode HRESI-MS spectrum showed a quasi-molecular ion $[M+H]^+$ at m/z 479.2797, suggesting a molecular formula of $C_{30}H_{38}O_5$ (DBE=12).

The optical rotation $[\alpha]_D^{20}$ was $+639.85^\circ$ ($c=0.052$, $CHCl_3$).

The IR spectrum exhibited absorption bands at 3352 cm^{-1} that indicated the presence of a hydroxyl group, (2921 cm^{-1}) for (C-H) stretch and (1723 , 1641 cm^{-1}) for an ester C=O and conjugated C=O (Williams and Fleming, 2008).

The 1H NMR spectrum (400 MHz, $CDCl_3$, Figure 3.72, Table 3.9) suggested this compound to be another quinonemethide derivative related to the compounds HM-7 and HM-8, even though the colour on TLC after spraying with *p*-anisaldehyde/ H_2SO_4 and heating was different. By comparing this spectrum with that of HM-7, the only difference was the absence of the narrow doublet signal for a proton geminal to a secondary alcohol group at δ_H 4.16. Thus, the spectrum displayed five methyl signals at δ_H 0.86, 1.30, 1.43, 1.74 and 2.27 attributed to six groups; Me-27, Me-25 & 28, Me-30, Me-26 and Me-23, respectively, where the signal at δ_H 1.30 integrated for 6 protons. The characteristic protons of the quinonemethide moiety appeared at δ_H 6.19 (1H, *d*, $J = 6.8$ Hz, H-7), 6.59 (1H, *d*, $J = 1.4$ Hz, H-1) and 7.18 (1H, *dd*, $J = 6.8$, 1.4 Hz, H-6). The spectrum also showed the carboxymethyl group at δ_H 3.69 attributed to (3H-31), a multiplet at δ_H 3.58 and a broad singlet at δ_H 7.07 which were assigned with the aid of the HSQC and COSY spectra for an oxymethine proton at position-22 of the pentacyclic skeleton and for a tertiary alcohol group at position-3, respectively.

The DEPTq135 ^{13}C NMR spectrum (100 MHz, Figure 3.73) displayed 28 carbon signals including five methyls, five methylenes, four methines, one oxymethine at δ_C 77.1, ten quaternary carbons including oxygen-bearing one C-3 at δ_C 146.3, one

methoxyl carbon at δ_C 52.0 and two carbonyl carbon signals at δ_C 179.2 and 178.1 attributed to C-29 and C-2, respectively. However, with the aid of the HSQC spectrum (Figure 3.74), the signal at δ_C 24.0 was assigned for the two methyl groups Me-27 and Me-30, while the HMBC spectrum (Figure 3.75) revealed that the signal at δ_C 127.7 should be assigned for the two quaternaries (C-5) & (C-15) as the two methyls Me-23 and Me-26 as well as the methylene protons (2H-16) have correlations to this carbon signal. These observations brought the total number of carbon signals to sum up to 30.

These data with the molecular formula indicated this compound to be a deoxy derivative of compound HM-8. Therefore, a primary structure was proposed to be similar to netzahualcoyonol (Figure 3.69), a compound isolated from *O. mexicana* (Celastraceae) (Gonzalez *et al.*, 1988) and from *Cheiloclinium cognatum* (Hippocrateaceae) (Jeller *et al.*, 2004). In comparison with the published data on this compound, a number of discrepancies were found in the assignment of the ^{13}C data. Moreover, the position of the secondary hydroxyl group was assigned at C-21. The analysis of 2D NMR spectra mostly based on HSQC and HMBC experiments allowed precise assignment of the carbon signals. The 3J correlations observed in the HMBC spectrum (Figure 3.75; B) from the singlet at δ_H 1.30 (Me-28) to the oxymethine carbon at δ_C 77.1, the signals at δ_C 38.47 (C-16) and 39.8 (C-18), in addition to the 2J correlation to the quaternary carbon at δ_C of 38.5 (C-17), confirmed the attachment of the hydroxyl group at C-22 rather than C-21. This was further verified by the 3J correlation of the methylene proton at δ_H 2.41 (H-16) to the same oxymethine carbon. On the other hand, the 3J correlations observed from the singlet at δ_H 1.43 (Me-30) to the two methylene carbons at δ_C of 33.7 (C-19) and 35.5 (C-21) as well as to the carbonyl carbon at δ_C 179.2 (C-29) along with the 2J correlation to the quaternary carbon at δ_C 41.9 (C-20), supported the previous suggestion that the only possibility for the hydroxyl group position is to be at C-22.

The COSY spectrum (Figure 3.76) showed the vicinal coupling between the methylene protons (2H-21) and the oxymethine proton (H-22) as well as between H-6/ H-7 and 2H-12/ 2H-11 confirming their positions in each spin system in addition to the long range coupling between H-1/ H-6.

The relative stereochemistry of the OH-22 was determined from the NOE correlations observed in NOESY spectrum (Figure 3.77). The oxymethine proton H-22 (δ_{H} 3.58) showed NOE correlations to the methyl at (δ_{H} 1.30) (Me-28) and to the methylene proton at δ_{H} 1.47 (H-16b). In turn, Me-28 showed correlation to the methine proton H-18 at (δ_{H} 1.81) indicating the *cis* configuration of the D/E ring junction as seen in the previous compound HM-8. These observations concluded that the OH-22 should be therefore placed on the α side of the molecule. All the observed NOE correlations are presented on the energy minimised 3D structure of HM-9 generated by ChemDraw Ultra 11.0 software in Figure 3.71.

The above combined data justified that HM-9 (Figure 3.70) is not netzahualcoyonol but another structural analogue, which has not been reported so far and has been given the trivial name 22(α)-hydroxynetzahualcoyene. The cytotoxicity and the anti-trypansomal activity of HM-9 were also evaluated in this work. It showed high toxicity on both tested cell lines as well as high activity against *T. b. brucei* at the initial tested concentrations 20 and 5 μM . For further details see sections 4.1.1.1 and 4.2.2.

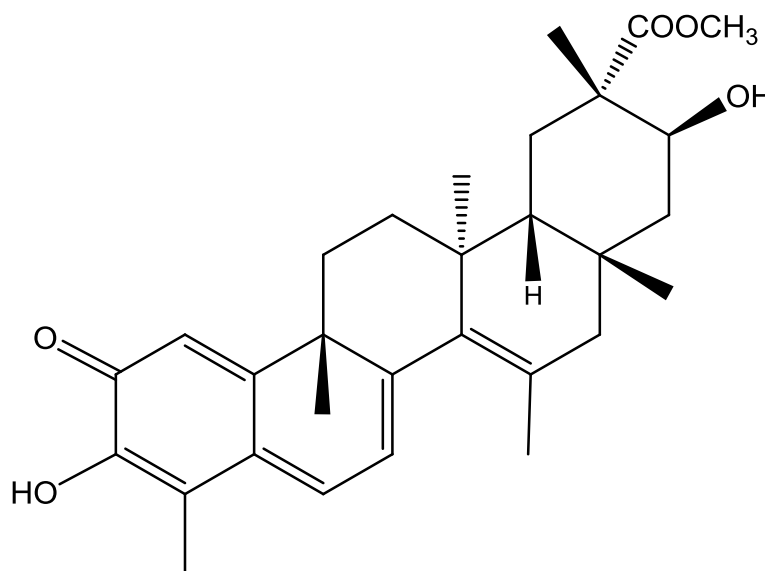


Figure 3.69: Structure of netzahualcoyonol as reported by Jeller *et al.*, (2004)

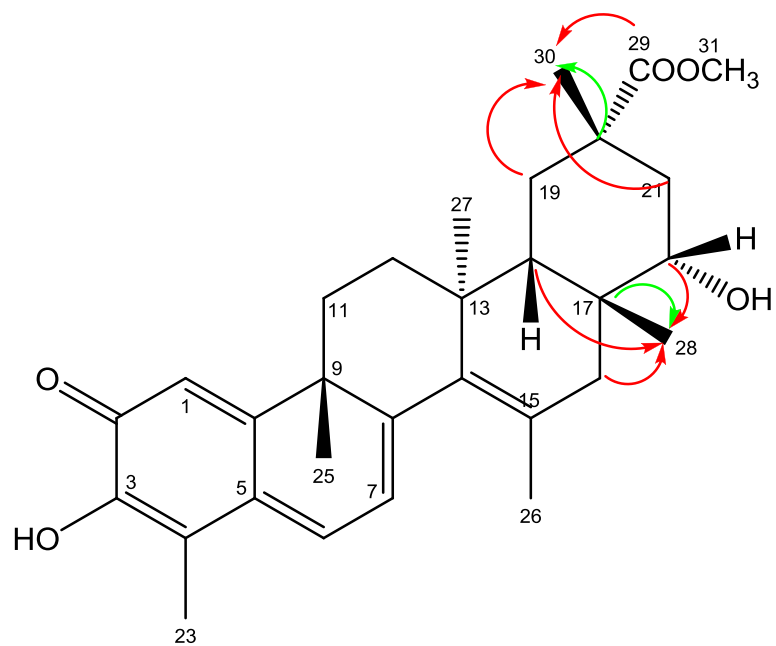


Figure 3.70: Structure of HM-9 with the key HMBC correlations
 (→) 3J (→) 2J ^{13}C to ^1H connectivity

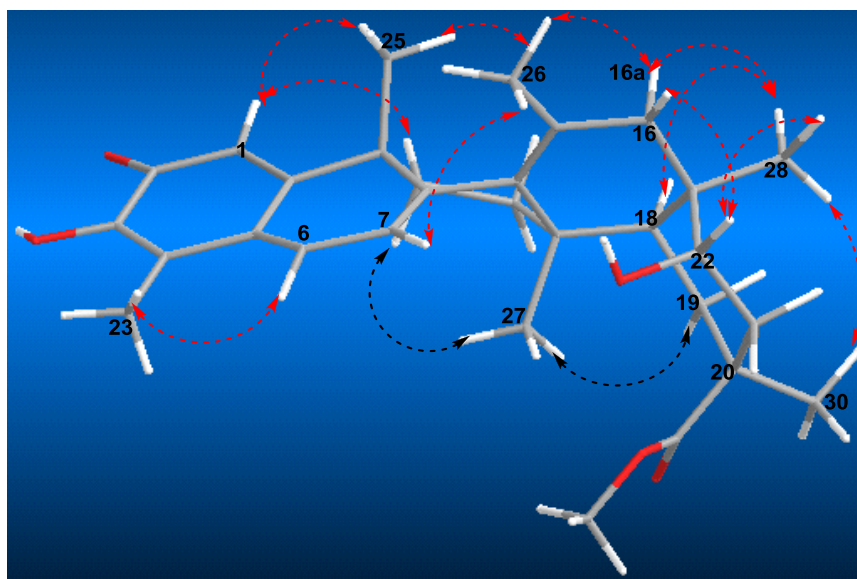
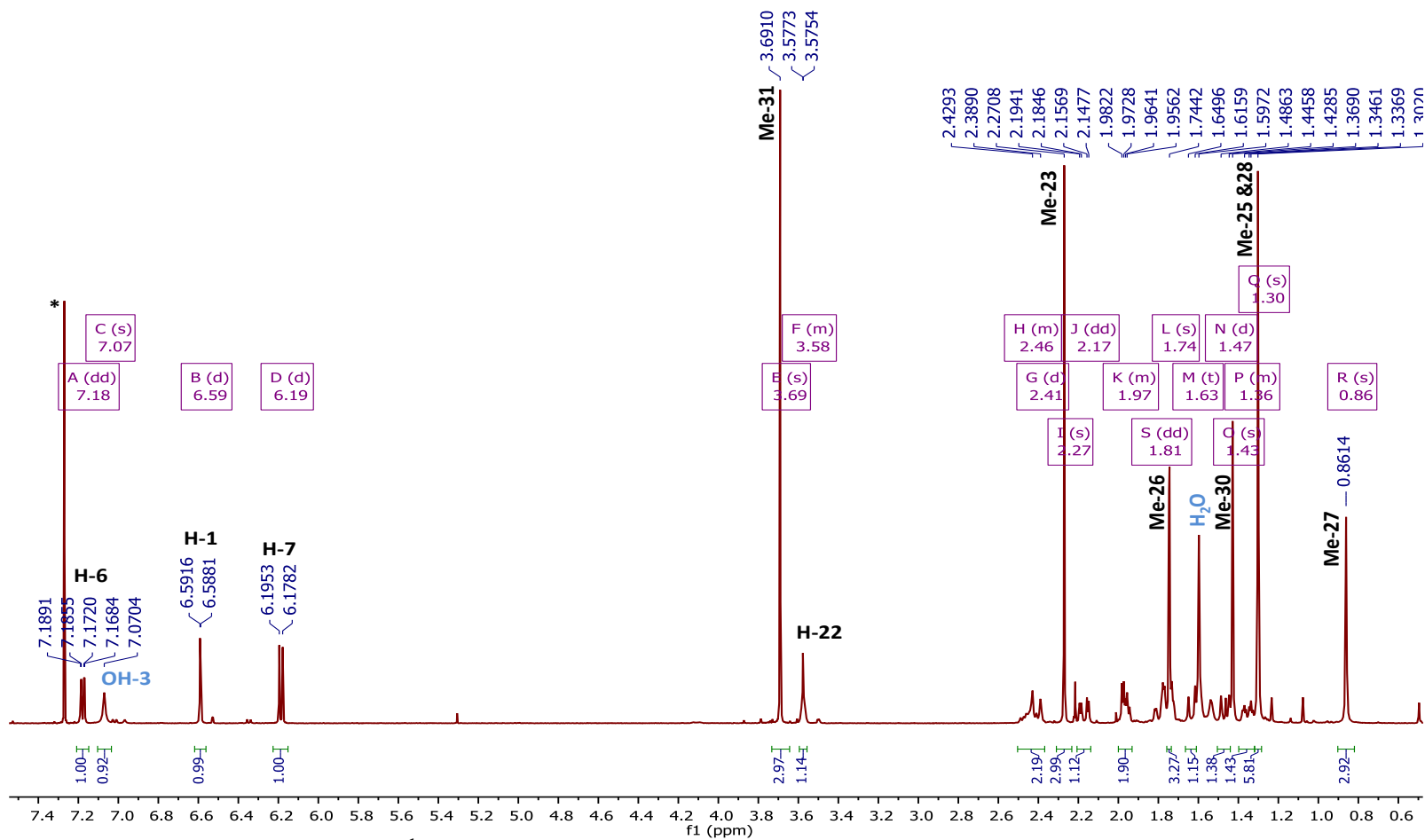


Figure 3.71: Energy minimised 3D structure of HM-9 by ChemDraw Ultra 11.0
 software with the key NOE correlations

Table 3.9: ^1H (400 MHz) and ^{13}C (100 MHz) NMR data of HM-8 and HM-9 in CDCl_3

Position	HM-8		HM-9	
	δ_{H}	δ_{C}	δ_{H}	δ_{C}
1	6.57 (1H, <i>d</i> , $J=1.4$ Hz)	120.2	6.59 (1H, <i>d</i> , $J=1.4$ Hz)	120.0
2	-	178.2	-	178.1
3	7.06 (OH, <i>br.s</i>)	146.3	7.07 (OH, <i>br.s</i>)	146.3
4	-	116.7	-	116.8
5	-	128.2	-	127.7
6	7.17(1H, <i>dd</i> , $J=6.9,1.4$ Hz)	134.1	7.18(1H, <i>dd</i> , $J=6.8,1.4$ Hz)	134.6
7	6.21 (1H, <i>d</i> , $J=6.9$ Hz)	122.2	6.19 (1H, <i>d</i> , $J=6.8$ Hz)	121.6
8	-	157.1	-	159.3
9	-	44.1	-	44.6
10	-	159.4	-	160.0
11	1.96 (2H) [2.02-1.85 <i>m</i>]	37.1	1.97 (2H) [2.02-1.92 <i>m</i>]	37.5
12	2.42 _{ax} (1H, <i>dt</i> , $J=13.4, 5.6$ Hz) 1.36 _{eq} (1H, <i>ddd</i> , $J=13.4, \dagger$ Hz)	35.9	2.44(1H, <i>m</i>)/ 1.36 (1H, <i>m</i>)	35.2
13	-	42.2	-	42.9
14	-	135.9	-	136.4
15	-	126.3	-	127.7
16	2.80 _{ax} (1H, <i>br.d</i> , $J=16.2$ Hz) 1.70 _{eq} (1H, <i>dd</i> , $J=16.2, 1.7$ Hz)	38.2	2.41(1H, <i>br.d</i> , $J=16.2$ Hz) 1.47(1H, <i>br.d</i> , $J=16.2$ Hz)	38.48
17	-	48.9	-	38.56
18	1.82 (1H, $J=13.7, \dagger$ Hz, <i>m</i>)	46.3	1.81(1H, $J=13.5, \dagger$ Hz, <i>m</i>)	39.8
19	2.18 (1H, <i>t</i> , $J=13.7$ Hz) 1.92 (1H, <i>m</i>)	34.2	1.63 (1H, <i>t</i> , $J=13.5$ Hz) 1.75 (1H, <i>m</i>)	33.7
20	-	50.4	-	41.9
21	5.00 (1H, <i>d</i> , $J=4.3$ Hz) 3.70 (OH, <i>d</i> , $J=4.3$ Hz)	74.4	2.17(1H, <i>dd</i> , $J=3.7,14.8$ Hz) 1.76 (1H, <i>m</i>)	35.5
22	-	213.9	3.58 (1H, <i>m</i>)	77.1
23	2.27 (3H, <i>s</i>)	10.4	2.27 (3H, <i>s</i>)	10.4
24	-	-	-	-
25	1.30 (3H, <i>s</i>)	29.0	1.30 (3H, <i>s</i>)	29.7
26	1.79 (3H, <i>s</i>)	22.0	1.74 (3H, <i>s</i>)	22.0
27	0.93 (3H, <i>s</i>)	24.2	0.86 (3H, <i>s</i>)	24.0
28	1.45 (3H, <i>s</i>)	22.4	1.30 (3H, <i>s</i>)	26.3
29	-	175.3	-	179.2
30	1.02 (3H, <i>s</i>)	13.7	1.43 (3H, <i>s</i>)	24.0
31	3.79 (3H, <i>s</i>)	52.7	3.69 (3H, <i>s</i>)	52.0

(†) None determined coupling constants due to ambiguity or overlapping.



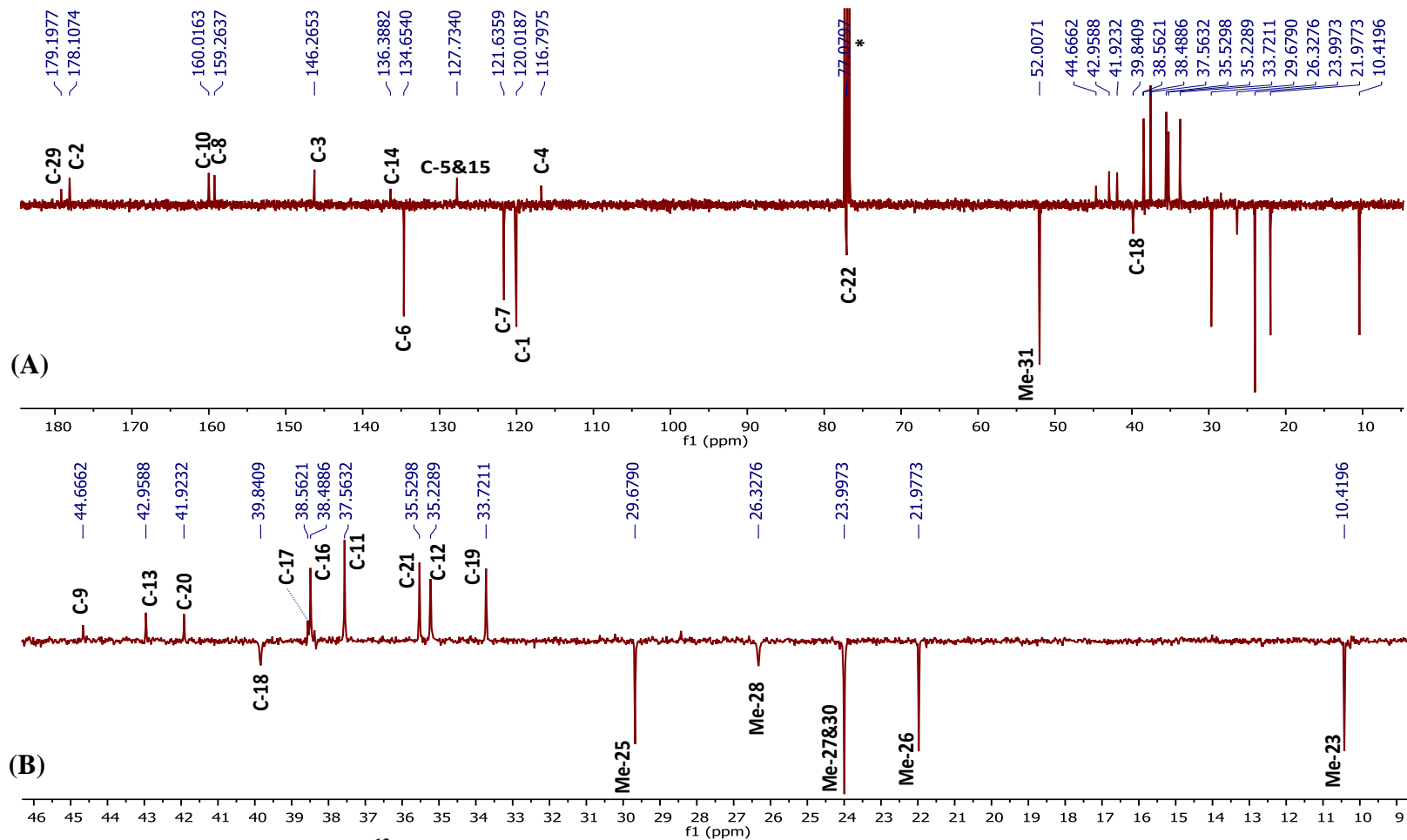
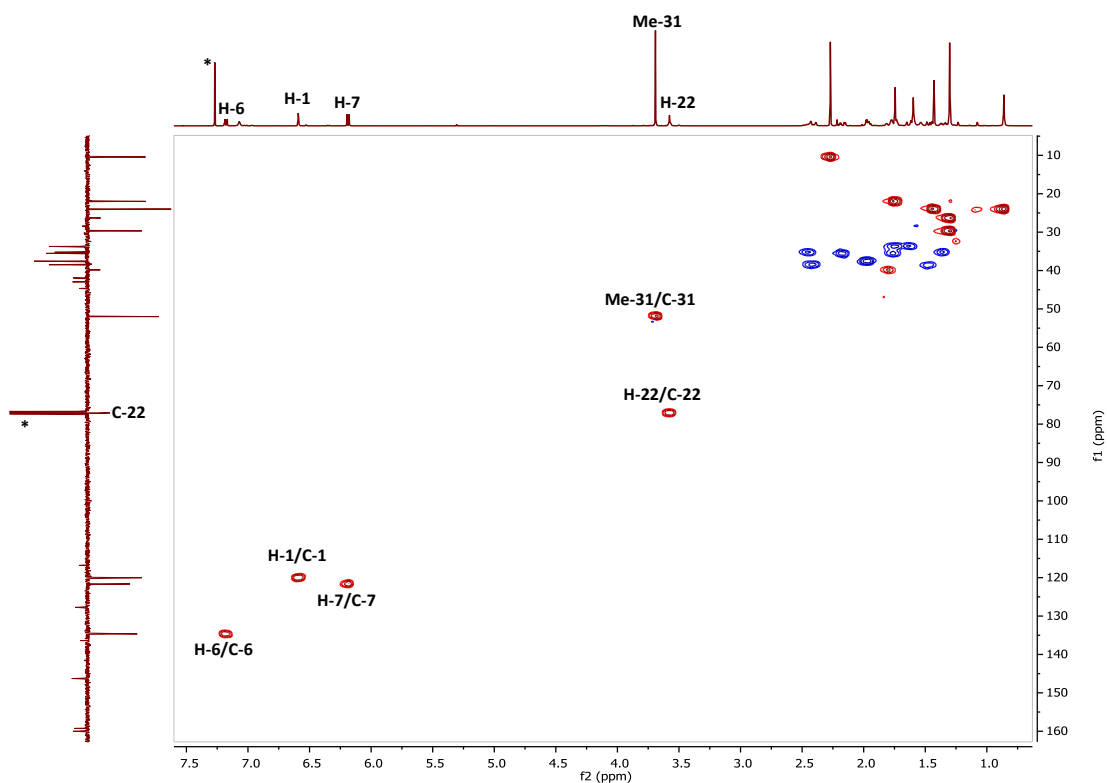
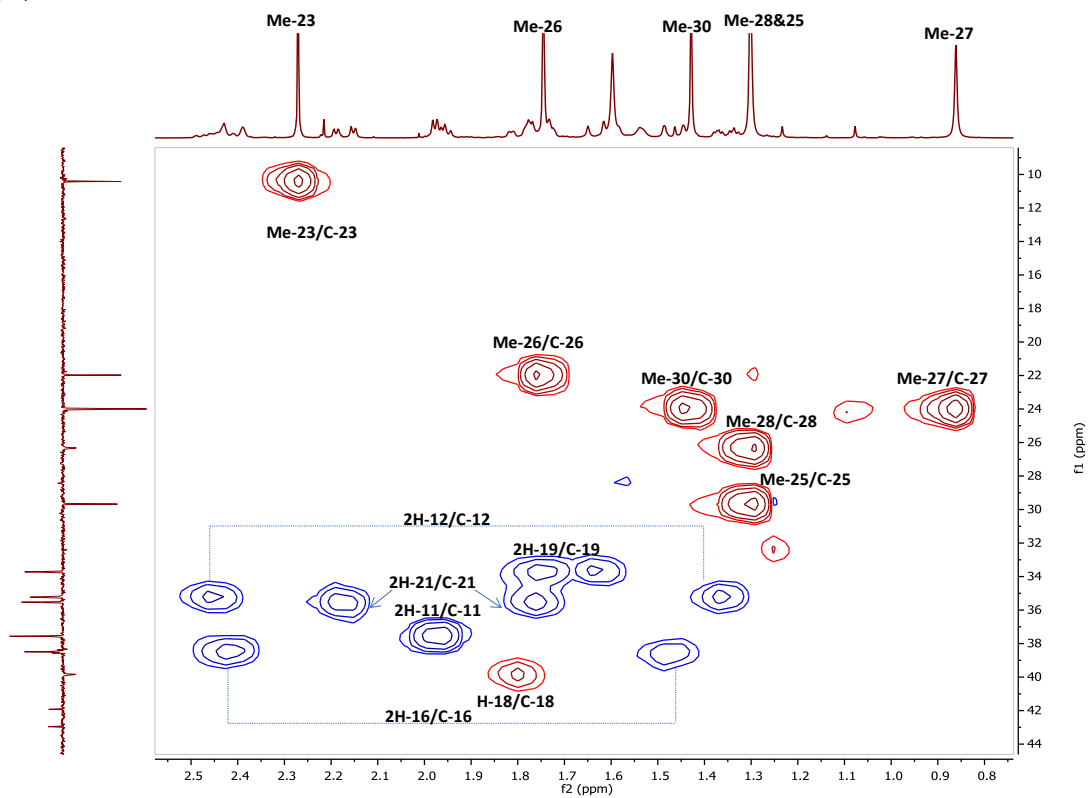


Figure 3.73: (A): Full DEPTq ^{13}C NMR spectrum (100 MHz) of HM-9 in CDCl_3 (*); (B): Selected expansion in aliphatic region

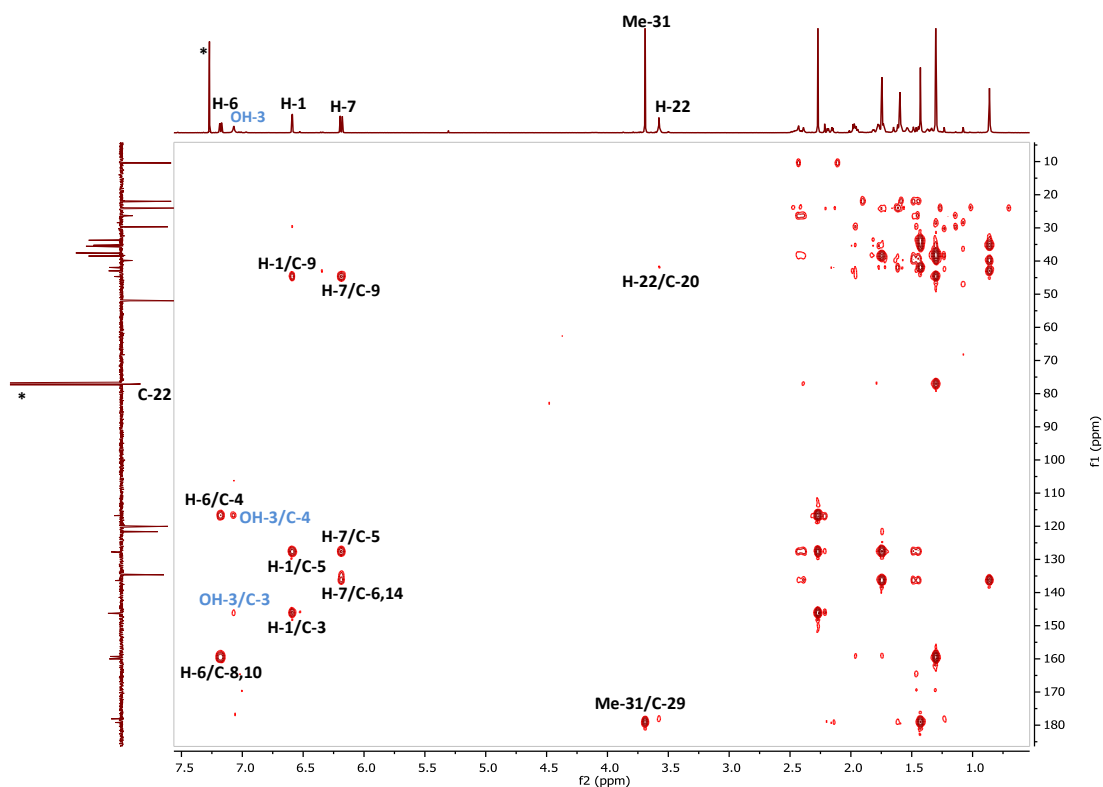


(A)

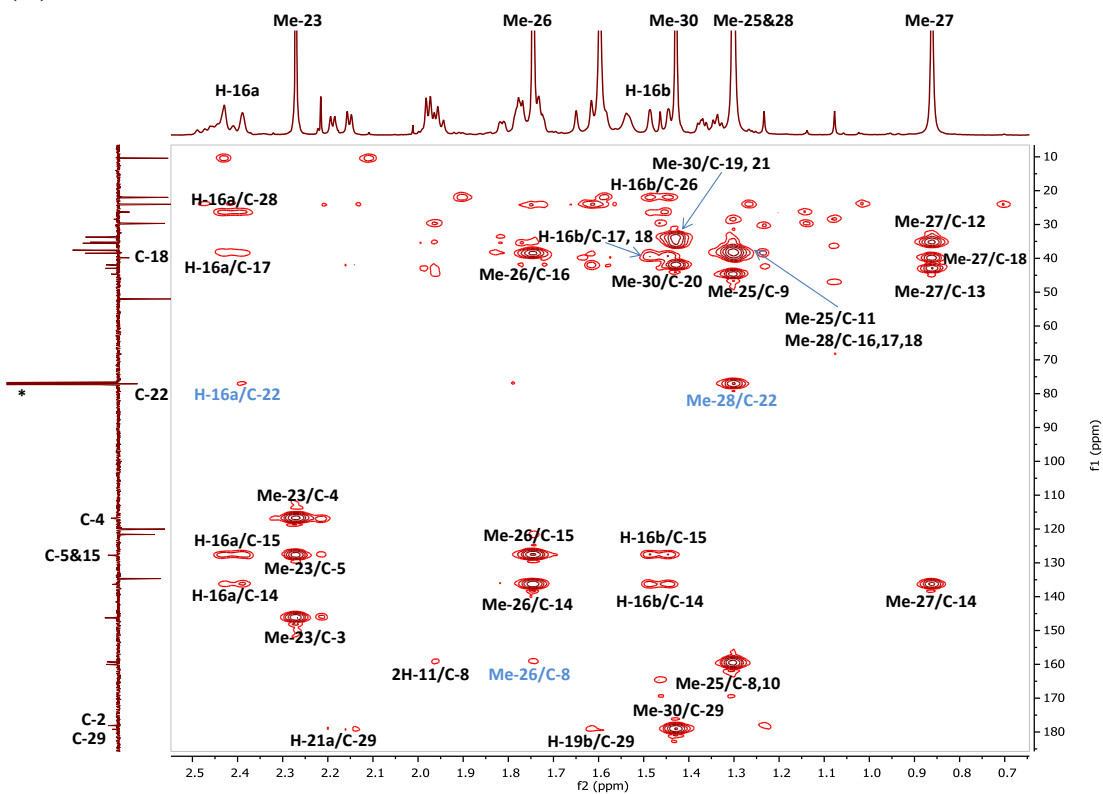


(B)

Figure 3.74: HSQC spectrum (400 MHz) of HM-9 in CDCl_3 (*)
 A: Full HSQC; B: Selected HSQC expansion



(A)



(B)

Figure 3.75: HMBC spectrum (400 MHz) of HM-9 in CDCl_3 (*)
 A: Full HMBC; B: Selected HMBC expansion for the aliphatic region of F_2 (^1H domain)

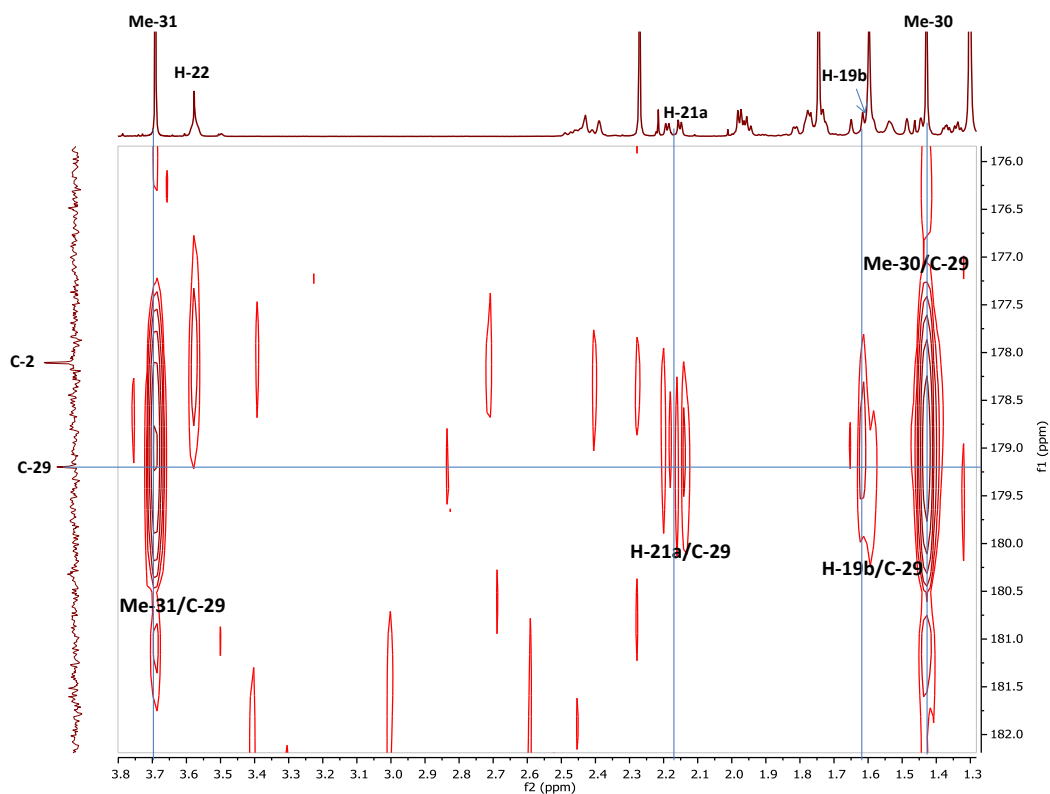


Figure 3.75 (Cont.): (C): Selected HMBC expansion showing the ketones correlations

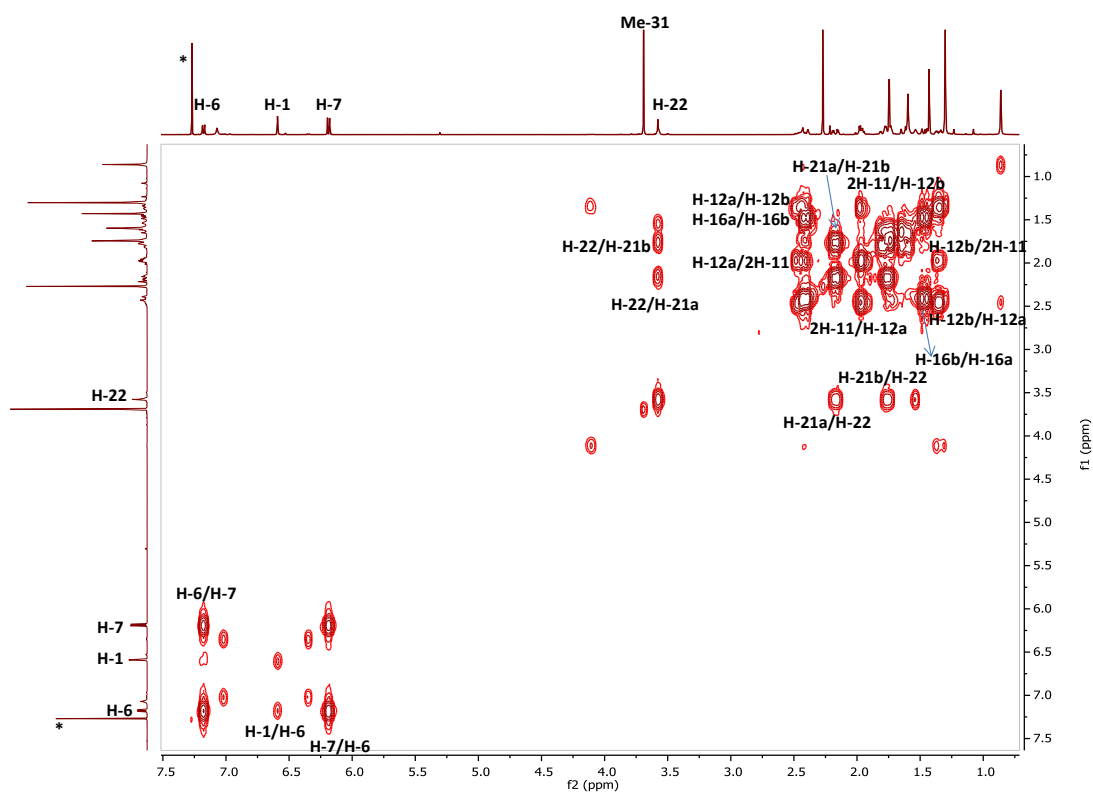
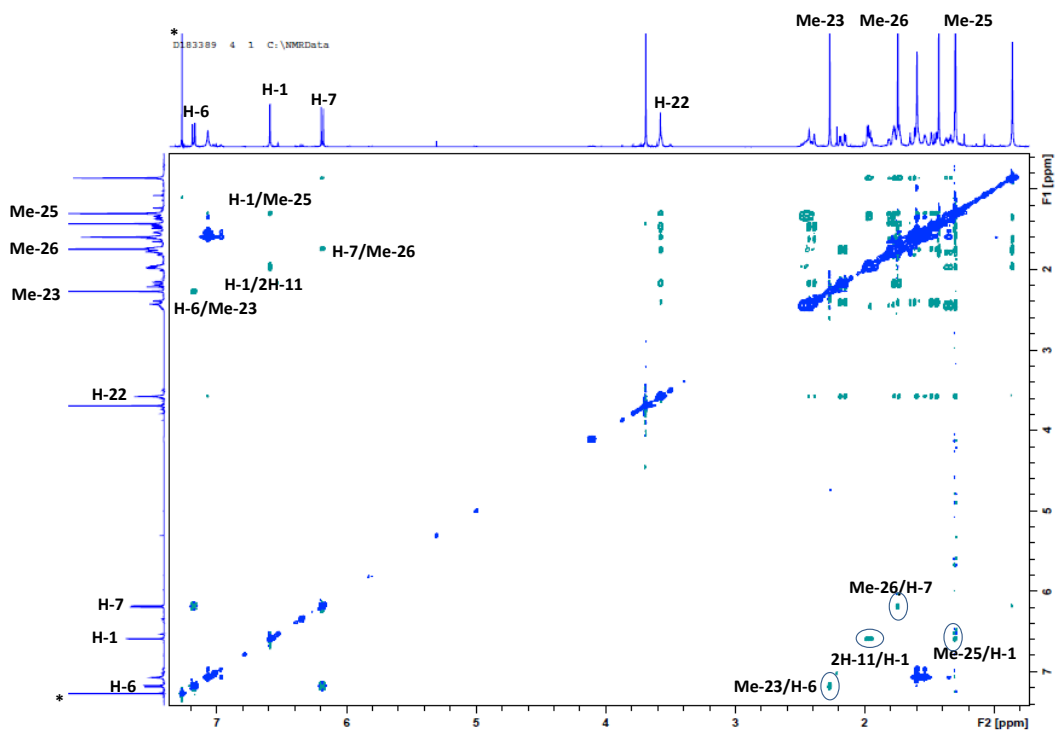
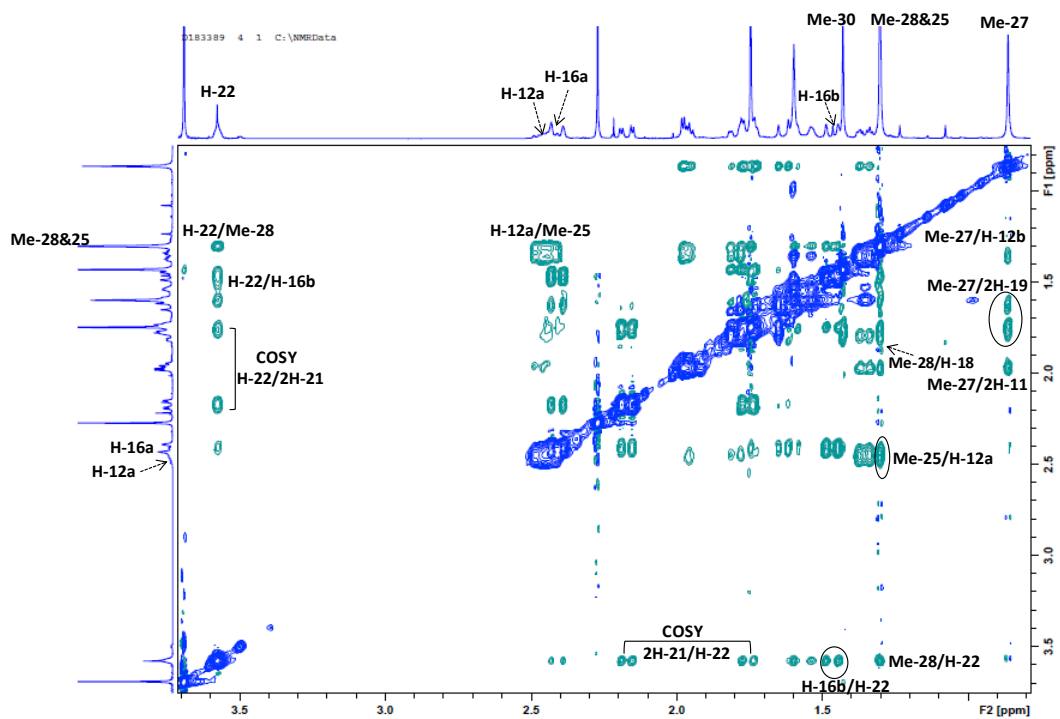


Figure 3.76: Full ^1H - ^1H COSY spectrum (400 MHz) of HM-9 in CDCl_3



(A)



(B)

Figure 3.77: (A): Full NOESY spectrum (400 MHz) of HM-9 in CDCl_3 using TopSpin 3.2 software; (B): Selected expansion

3.3.2.4 Characterisation of HM-10 as pristimerin

HM-10 was isolated from the n-hexane extract of the root bark by PTLC as an amorphous orange/red solid. On TLC, the compound appeared as a dark spot under UV light (λ 254). After treatment with *p*-anisaldehyde-sulphuric acid reagent and heating it turned to a dark pink spot. Its R_f was 0.61 on SiGel when eluted with the mobile phase 50% hexane in EtOAc.

The MM-ES+APCI positive scan spectrum of HM-10 showed a quasi-molecular ion $[M+H]^+$ at m/z 465.3 corresponding to the molecular formula $C_{30}H_{40}O_4$ (DBE=11).

The 1H NMR spectrum (400 MHz, $CDCl_3$, Figure 3.80, Table 3.10), was fairly similar to that of HM-7 except in the absence of the signals of the two oxymethine protons at positions-21 and 22. Thus, six methyl singlets at δ_H 0.54, 1.10, 1.18, 1.27, 1.46 and 2.21 attributed to Me-27, Me-28, Me-30, Me-26, Me-25 and Me-23, respectively, a carboxymethyl group at δ_H 3.56 attributed to (3H-31) were observed, in addition to the characteristic protons of the quinonemethide moiety as a doublet at δ_H 6.35 (1H, *d*, $J = 7.1$ Hz, H-7), a narrow doublet at δ_H 6.54 (1H, *d*, $J = 1.4$ Hz, H-1) and a doublet of doublet at δ_H 7.02 (1H, *dd*, $J = 7.1, 1.4$ Hz, H-6). The assignments of the olefinic protons were also confirmed from the COSY spectrum (Figure 3.84) where mutual correlations between H-6 and H-7 were observed as well as the long range coupling between H-1 and H-6.

The DEPTq135 ^{13}C NMR spectrum (100 MHz, Figure 3.81) revealed the presence of 30 carbons and was closely similar in the data obtained for the carbons of rings A and B for HM-7 verifying the quinonemethide skeleton with the conjugated C=C in these rings. However, there were some differences in the data of the rest of the carbons comprising the other three rings. The spectrum lacked the signals due to the olefinic quaternaries at positions-14 & 15 as well as those corresponding to the two carbons bearing oxygen at positions-21 & 22 whereas it showed the presence of an extra three methylenes to reach the total of seven instead of four comparing to HM-7, which suggested a full saturation in the rings C, D and E.

The HMBC spectrum (Figure 3.83) showed all the typical correlations as in HM-7 with the exception of those for the methyl group (Me-26). This methyl was attached to the carbon at position-15 in the compound HM-7 while it has now been shifted to the position-14. This was established from the fact that this methyl showed four clear

HMBC correlations instead of three due to its position at the junction between the rings C and D. These correlations were from this singlet methyl at δ_H 1.27 (Me-26) to the methylene carbon at δ_C 28.6 (C-15) and to the two quaternaries at δ_C 39.4 (C-13) and 45.1 (C-14), which were aligned on the junction C/D, and to the olefinic quaternary at δ_C 170.0 (C-8). The methyl singlet (Me-30) at δ_H 1.18 showed 3J correlations to two methylene carbons at δ_C 30.9 (C-19) & 29.9 (C-21) and to the carbonyl carbon at δ_C 178.7 (C-29) (Figure 3.83; C) along with the 2J correlation to the quaternary carbon at δ_C 40.4 (C-20) which emphasized the absence of any functional groups at position-21. This was also the same fact for position-22 as the methyl singlet (Me-28) at δ_H 1.10 showed 3J correlations to the two methylene carbons at δ_C 34.8 (C-22) & 36.4 (C-16) and to the methine carbon at δ_C 44.3 (C-18). The chemical shifts of all hydrogen-bearing carbons were assigned from the HSQC spectrum (Figure 3.82) combined with COSY spectrum to confirm each spin system. The complete analysis of the 2D NMR spectra and by comparing with previous reports, HM-10 was identified as pristimerin (Figure 3.79).

Biosynthetically, the compound HM-7 may be obtained by dehydrogenation and rearrangement of the corresponding quinonemethide (Figure 3.78) (Fernando *et al.*, 1988) as cited by González *et al.* (1989).

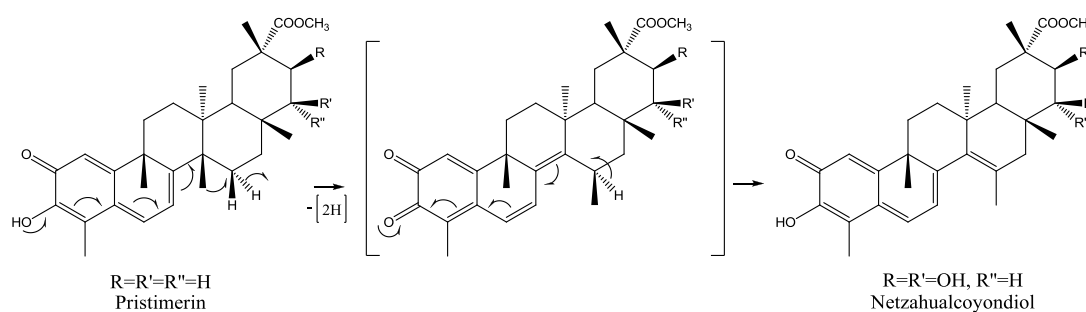


Figure 3.78: Possible biosynthetic scheme for the conversion of pristimerin to netzahualcoyondiol as shown in González *et al.*, (1989)

The spectral data were in very good agreement with the literature (Dos Santos *et al.*, 2013). Pristimerin has been isolated before from the bark of *M. chuchuhuasca* (Morita *et al.*, 2008), however, due to the confusion about the actual plants which are referred to in their locality as "Chuchuguasa", this could be the first report of the isolation of this compound from the root bark of *M. laevis*. It has also been isolated

from other plants of the same genus such as *M. ilicifolia*, *M. senegalensis* as well as from other plants of Celastraceae family such as *Celastrus aculeatus*, *R. tolantonguensis* (Harada *et al.*, 1962; Khalid *et al.*, 2007; Xie *et al.*, 2012).

This compound neither showed significant antimicrobial nor antifungal activities when tested against a series of Gram positive and negative bacterial strains along with a number of fungi and yeasts (Aguilar-Gonzalez *et al.*, 2005). These results were in accordance with an earlier report, (Moujir *et al.*, 1990), where pristimerin was found to be inactive against *S. aureus* with MIC value > 100 µg/ml. The free radical scavenging activity of this compound was reported by Carvalho *et al.* (2005) and Jeller *et al.* (2004) and found that it was less effective (20% inhibition at 50 µM) than other quinonemethide triterpenes with more extended conjugation through ring D, such as netzahualcoyondiol (HM-7) and netzahualcoyone (HM-8), as mentioned earlier in section 3.3.2.2. Pristimerin also exhibited promising *in vitro* anti-parasitic activity against the chloroquine-resistant strain (Dd2) of *Plasmodium falciparum* and the promastigotes of *L. major* with IC₅₀ values of 0.5 and 6.8 µg/ml, respectively (Khalid *et al.*, 2007). The anti-cancer activity of pristimerin was evaluated in several studies and its ability to induce apoptosis was reported on different cancer cell lines, (see sections 4.1.1.1 and 4.2.2 for further details on the cytotoxicity of HM-10 as assessed in this work and in the literature along with its anti-trypanosomal activity).

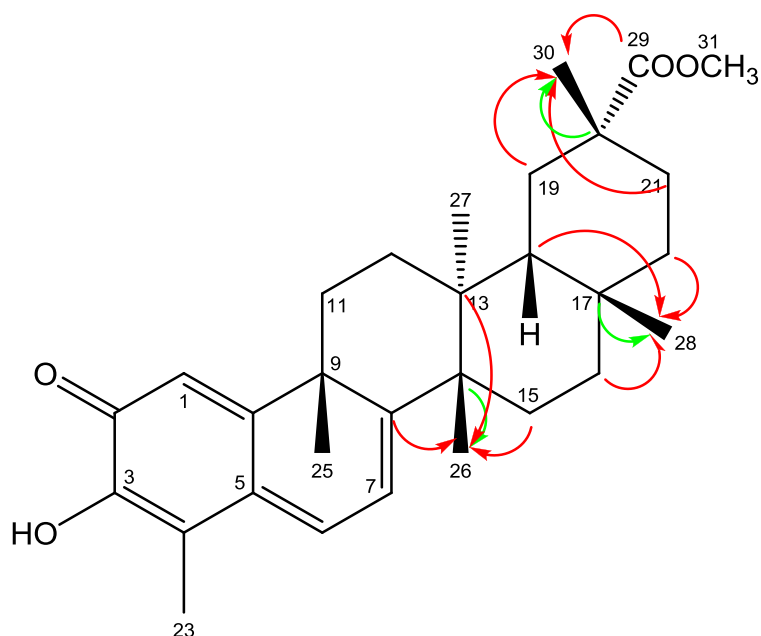


Figure 3.79: Structure of HM-10 with the key HMBC correlations
 (→) ³J (→) ²J ¹³C to ¹H connectivity

Table 3.10: ^1H (400 MHz) and ^{13}C (100 MHz) NMR data of HM-10 in CDCl_3

Position	HM-10	
	δ_{H}	δ_{C}
1	6.54 (1H, <i>d</i> , $J= 1.4$ Hz)	119.6
2	-	178.3
3	-	146.0
4	-	117.1
5	-	127.4
6	7.02 (1H, <i>dd</i> , $J= 7.1, 1.4$ Hz)	134.0
7	6.35 (1H, <i>d</i> , $J= 7.1$ Hz)	118.1
8	-	170.0
9	-	42.9
10	-	164.7
11	2.15 (1H, <i>m</i>)/ 1.86 (1H, <i>m</i>)	33.6
12	1.79 (1H, <i>m</i>)/ 1.70 (1H, <i>m</i>)	29.6
13	-	39.4
14	-	45.0
15	1.66 (1H, <i>m</i>)/ 1.57(1H, <i>m</i>)	28.6
16	1.88 (1H, <i>m</i>)/ 1.50 (1H, <i>m</i>)	36.4
17	-	30.5
18	1.59 (1H, <i>m</i>)	44.3
19	2.43(1H, <i>br.d</i> , $J= 15.8$ Hz)/ 1.69 (1H, <i>m</i>)	30.9
20	-	40.4
21	2.20 (1H, <i>m</i>)/ 1.38 (1H, <i>m</i>)	29.9
22	2.05 (1H, <i>m</i>)/ 0.98 (1H, <i>m</i>)	34.8
23	2.21 (3H, <i>s</i>)	10.2
24	-	-
25	1.46 (3H, <i>s</i>)	38.3
26	1.27 (3H, <i>s</i>)	21.6
27	0.54 (3H, <i>s</i>)	18.3
28	1.10 (3H, <i>s</i>)	31.6
29	-	178.7
30	1.18 (3H, <i>s</i>)	32.7
31	3.56 (3H, <i>s</i>)	51.5

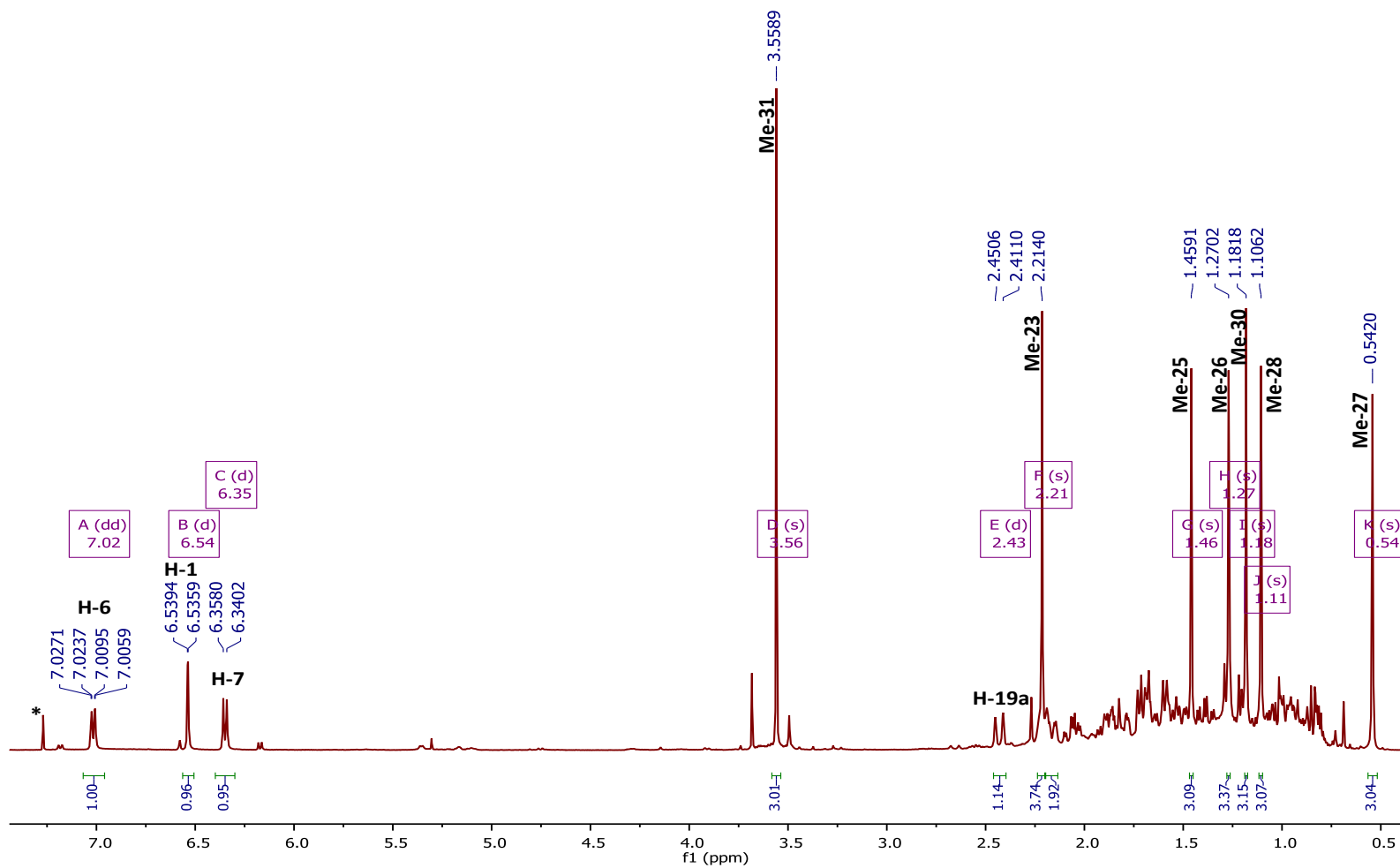


Figure 3.80: ^1H NMR spectrum (400 MHz) of HM-10 in CDCl_3 ; (*) CHCl_3 residue

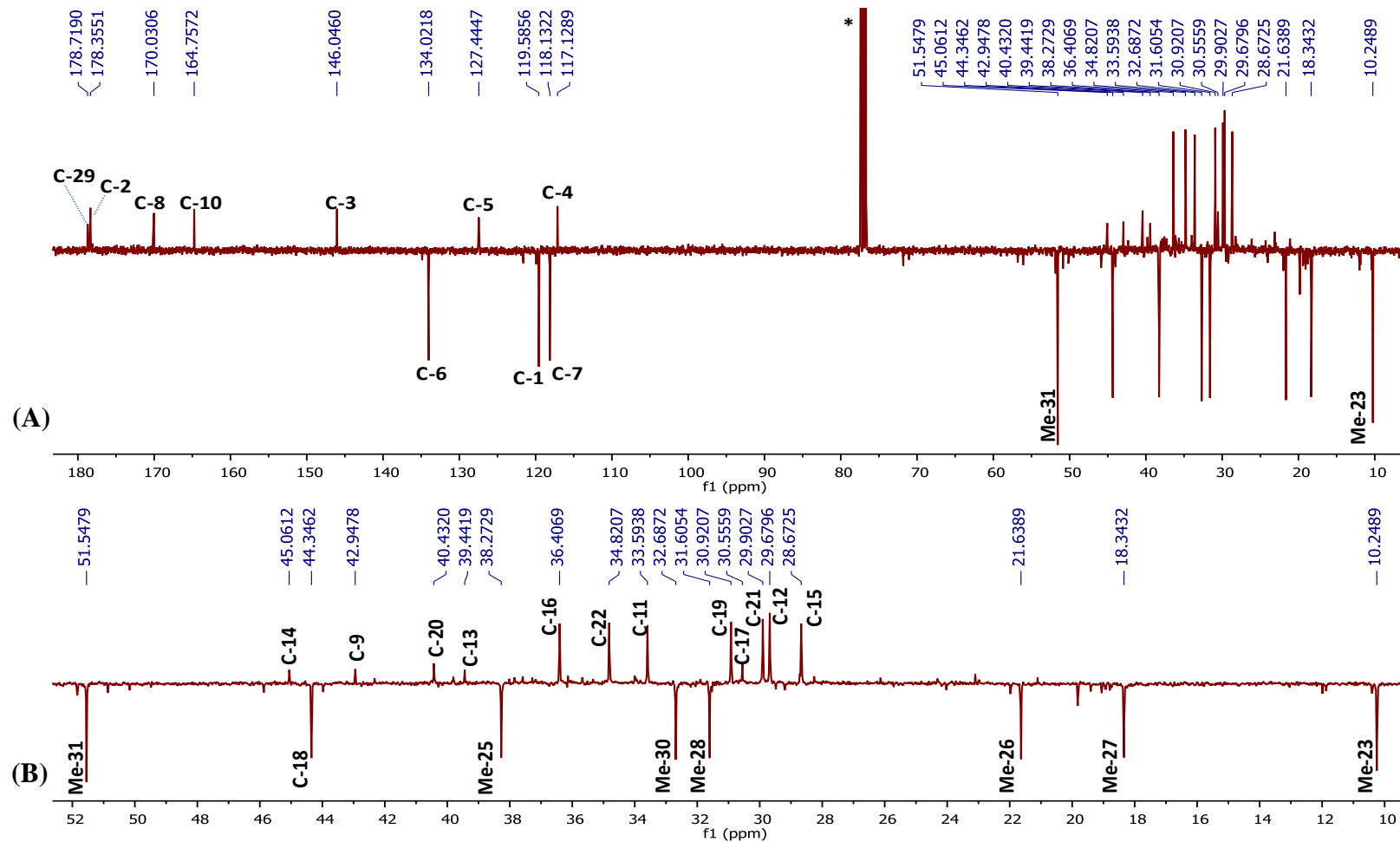
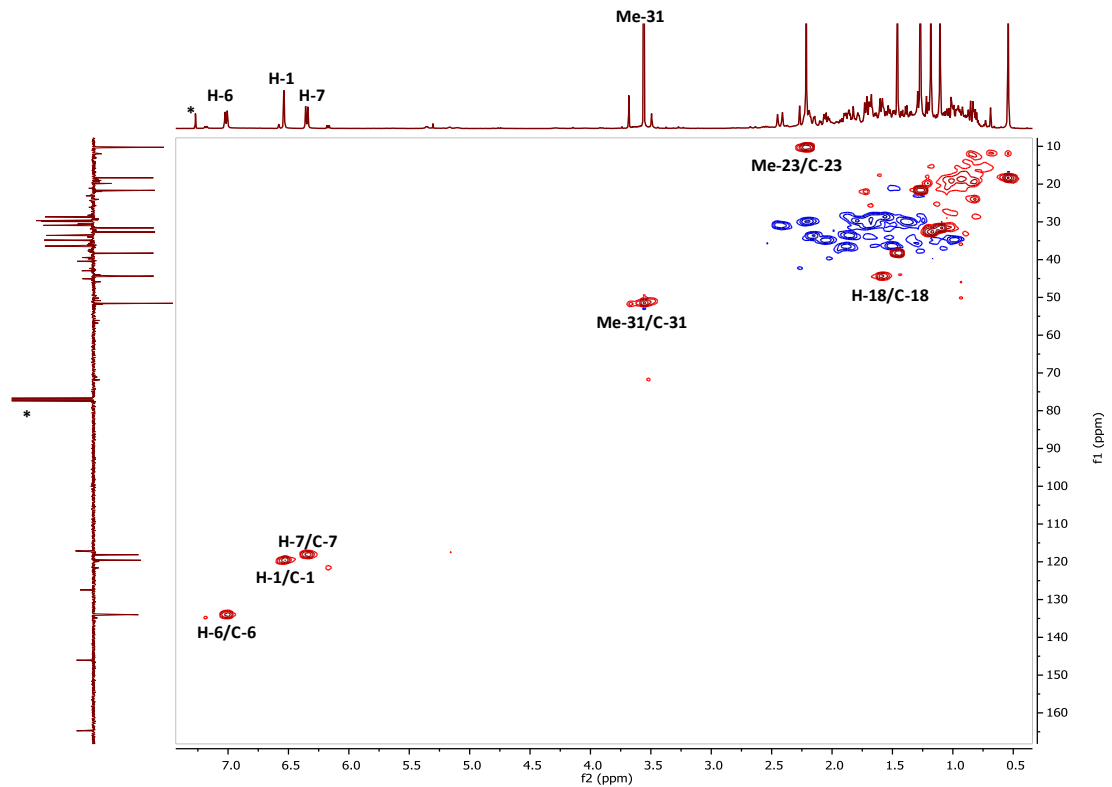
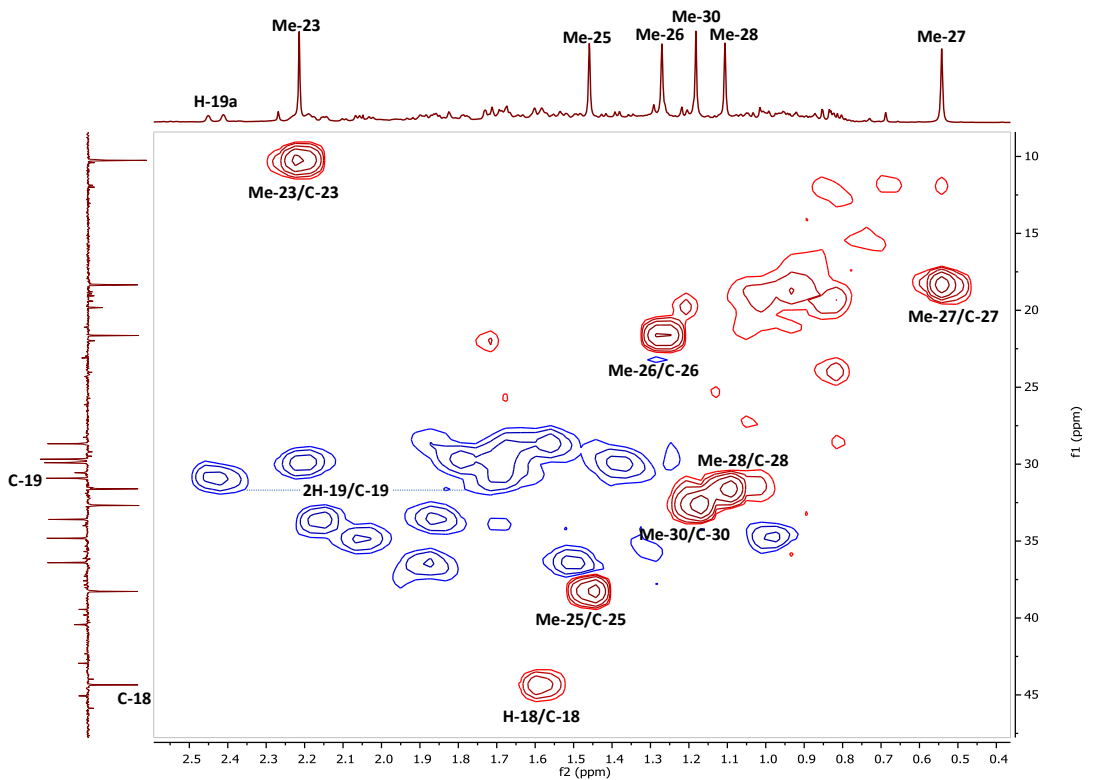


Figure 3.81: (A): Full DEPTq ^{13}C NMR spectrum (100 MHz) of HM-10 in CDCl_3 (*); (B): Selected expansion in aliphatic region

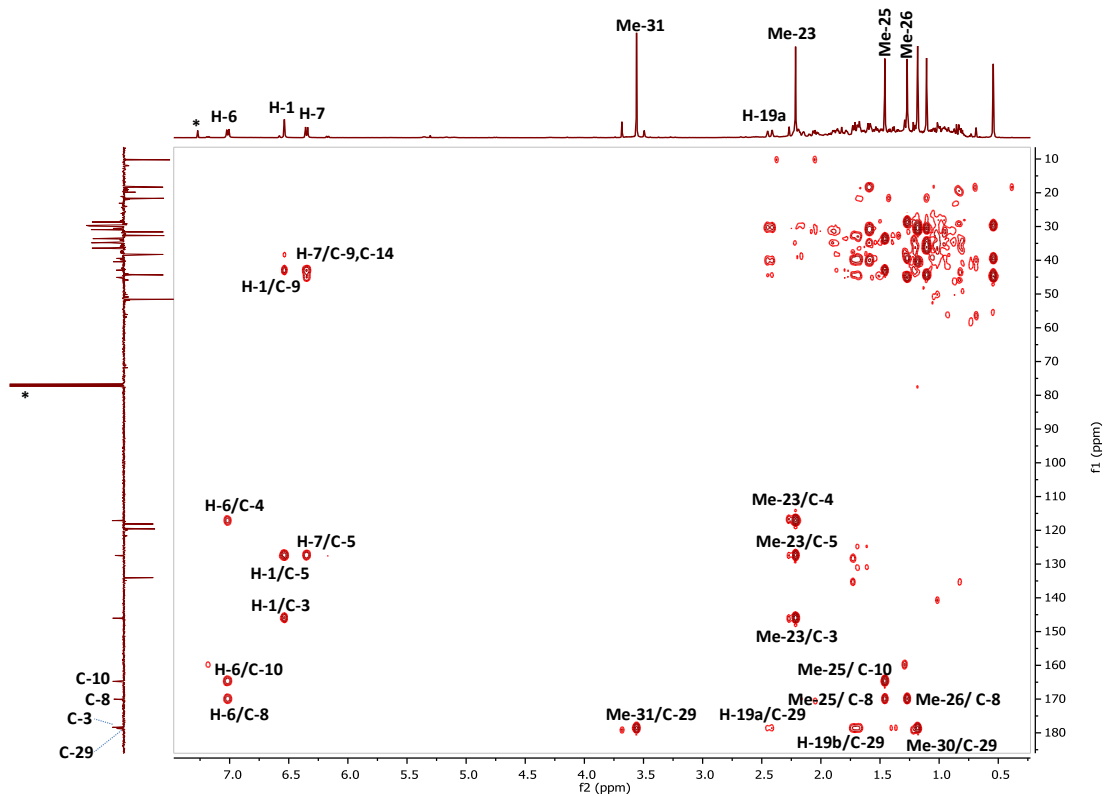


(A)

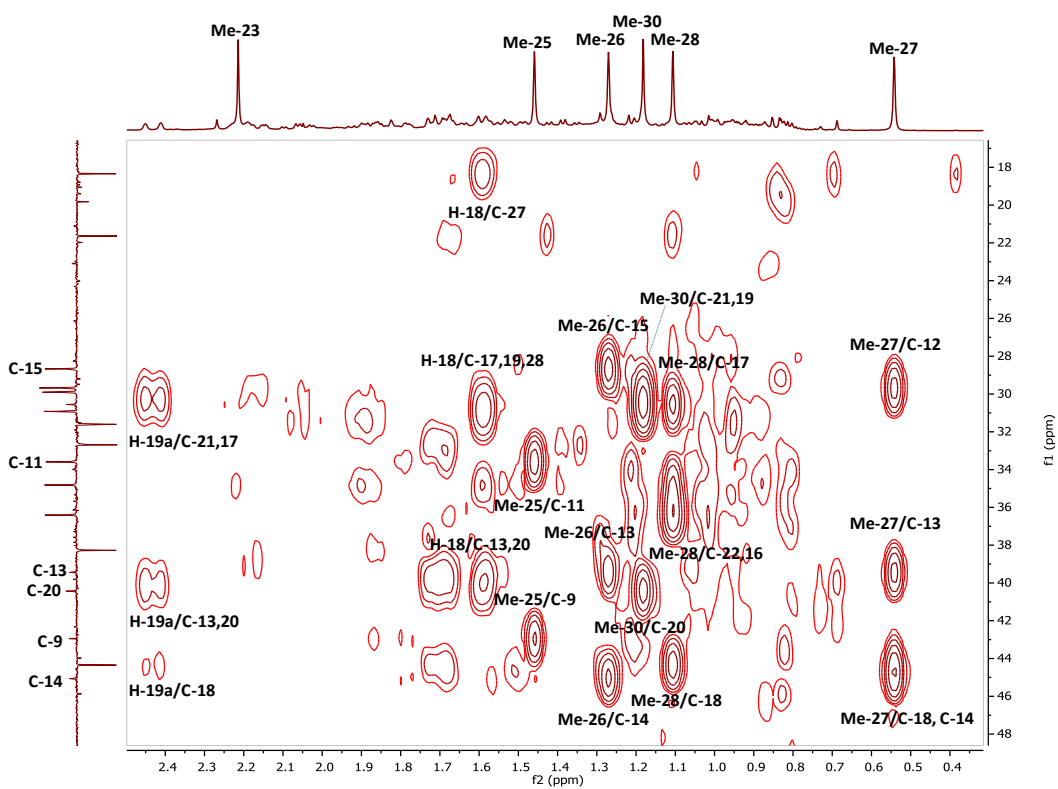


(B)

Figure 3.82: HSQC spectrum (400 MHz) of HM-10 in CDCl_3 (*)
 A: Full HSQC; B: Selected HSQC expansion



(A)



(B)

Figure 3.83: HMBC spectrum (400 MHz) of HM-10 in CDCl_3 (*)
A: Full HMBC; B: Selected HMBC expansion for the aliphatic region

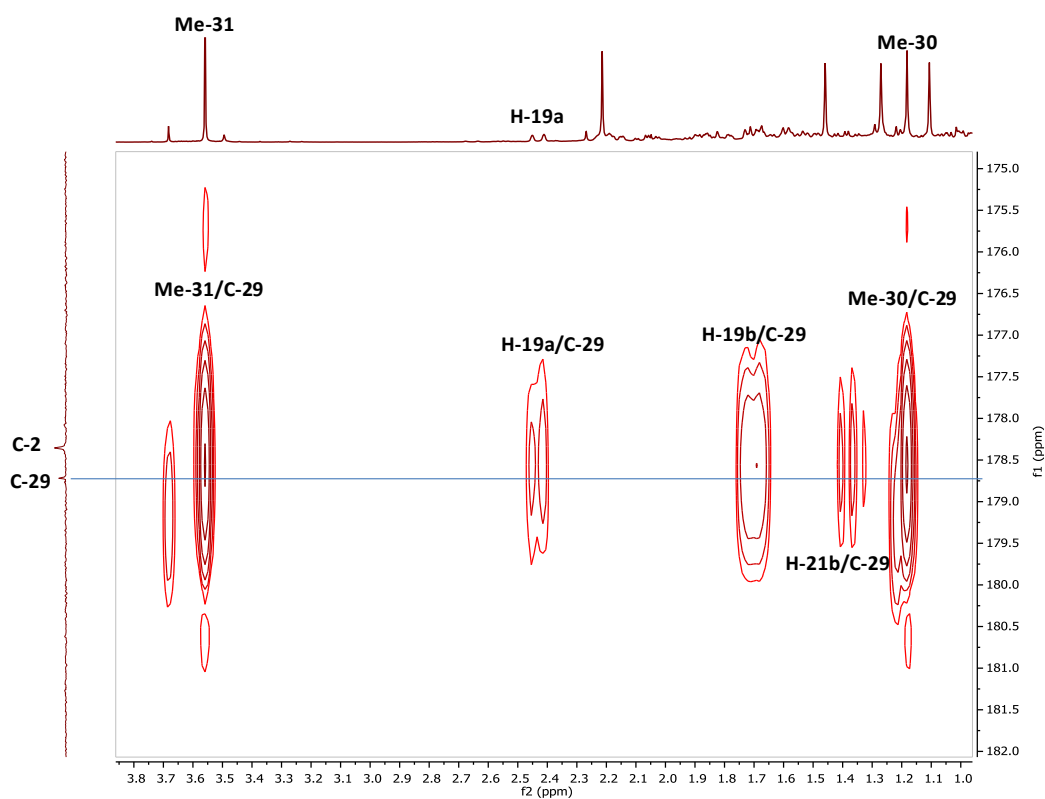


Figure 3.83 (Cont.): (C); Selected HMBC expansion showing the ketones correlations

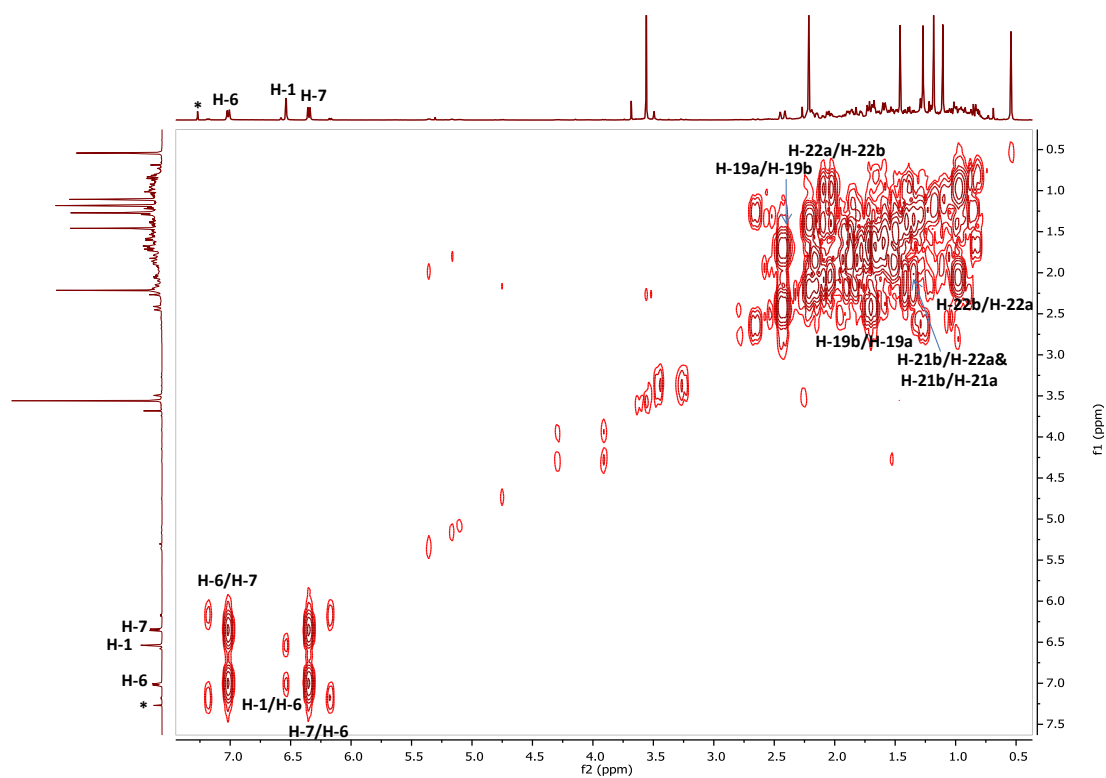


Figure 3.84: Full ¹H-¹H COSY spectrum (400 MHz) of HM-10 in CDCl₃

3.3.2.5 Characterisation of HM-11 as celastrol

HM-11 was isolated from the n-hexane extract of the stem bark by PTLC as an amorphous red solid. On TLC, the compound appeared as a dark spot under UV light (λ 254). After treatment with *p*-anisaldehyde-sulphuric acid reagent followed by heating, it turned to a dark red (brownish) spot. Its R_f was 0.4 on SiGel when eluted with the mobile phase 50% hexane in EtOAc.

The positive mode HRESI-MS spectrum showed a quasi-molecular ion $[M+H]^+$ at m/z 451.2843, suggesting a molecular formula of $C_{29}H_{38}O_4$ (DBE=11).

The pattern of the 1H NMR spectrum (400 MHz, $CDCl_3$, Figure 3.86, Table 3.11 on p.176) was typical of a quinonemethide type triterpene suggesting another compound from the same group. The spectrum displayed six methyl singlets at δ_H 0.59, 1.09, 1.25, 1.26, 1.42 and 2.20 attributed to Me-27, Me-28, Me-26, Me-30, Me-25 and Me-23, respectively. The quinonemethide moiety was characterised by a doublet at δ_H 6.32 (1H, *d*, $J = 7.2$ Hz, H-7), a singlet at δ_H 6.50 (1H, *s*, H-1) and another doublet at δ_H 7.05 (1H, *d*, $J = 7.2$ Hz, H-6). The assignments of the vinyl protons were also confirmed from the COSY spectrum (Figure 3.90) where mutual correlations between H-6 and H-7 were observed as well as the long range coupling between H-1 and H-6, however in the 1H NMR spectrum these signals were not clearly resolved to show the usual multiplicity of proton H-1 and H-6 as doublet and doublet of doublet, respectively. The 1H NMR spectrum was fairly similar to that of HM-10, yet it lacked the existence of the signal attributed to the carboxymethyl group.

The DEPTq135 ^{13}C NMR spectrum (100 MHz, Figure 3.87) revealed the presence of 29 carbons including six methyls, seven methylenes, four methines, ten quaternaries including oxygen-bearing carbon (C-3) at δ_C 146.9 and finally two carbonyl carbons at δ_C 178.3 and 182.8 attributed to a ketone (C-2) and a carboxyl carbon (C-29), respectively. The carbon signal at δ_C 29.7 was found to correlate to the proton signal at δ_H 1.26, in the HSQC spectrum (Figure 3.88), which was formerly assigned for the methyl group (Me-30). This was due to the presence of some fat in the sample where its signal overlapped with those for the methyls (Me-30 and 26) since their integration was far more than 6. The chemical shifts of all

hydrogen-bearing carbons were assigned from the HSQC spectrum combined with COSY spectrum to confirm each spin system.

The comparison between the generated data from the 2D NMR experiments and those of the previously isolated quinonemethide triterpene HM-10, in particular, suggested this compound to be quite similar in its structure. The HMBC spectrum (Figure 3.89) showed typical correlations to those in the one for the HM-10. However, the 3J correlation from the methyl singlet at δ_{H} 1.26 (Me-30) to the most downfield carbonyl carbon signal at δ_{C} 182.8 (C-29) established the presence of a carboxylic function rather than an ester. This was further supported by the molecular formula of this compound as well as by the absence of the characteristic signal of a carboxymethyl group in the ^1H NMR spectrum.

On the basis of these results and by comparison with previously published data, HM-11 was identified as celastrol (Figure 3.85) meaning that HM-10 (pristimerin) is the methyl ester of celastrol. The spectral data obtained were in agreement with previous reports (Ngassapa *et al.*, 1994) and (Jo *et al.*, 2006, where the data were collected in CD_3OD , 500 MHz). With the exception of *M. chuchuhuasca*, which has been reported to contain this compound by Morita *et al.*, (2008), this could be the first report of its isolation from *M. laevis*. It has also been previously isolated from other plants of the Celastraceae family and has been shown to possess various bioactivities.

Isolated from the stem bark of *Tripterygium wilfordii* (Celastraceae) by Takaishi *et al.* (1997), it showed strong inhibitory activity for the secretion of IL-1 α and IL-1 β from human peripheral mononuclear cells compared to prednisolone which provides in part some scientific basis for the ethnomedicinal use of *M. laevis* in Muinane, Uitoto and other Amazonian communities for the treatment of arthritis, rheumatism and back pain. It also exhibited a potent antitumor-promoting activity by inhibiting the Epstein-Barr virus early antigen activation as reported in the same study. Another study by Allison *et al.* (2001) confirmed the anti-inflammatory activity of celastrol along with its activity as antioxidant agent, which proposed it as a possible treatment for Alzheimer's disease. Owing to these properties, it was also suggested as a potential therapy for the treatment of human amyotrophic lateral sclerosis (ALS) (Kiaei *et al.*, 2005) and allergic asthma (Kim *et al.*, 2009). In Luo *et al.* (2005) study,

celastrol from the roots of *Celastrus hypoleucus* showed significant *in vitro* and *in vivo* antifungal activity against diverse plant pathogenic fungi. A study by Moujir *et al.* (1990) reported the potent anti-microbial activity of celastrol against *S. aureus*, with MIC value in the range of 0.5-1 $\mu\text{g/ml}$ but not against Gram negative strains. The presence of the quinonemethide skeleton was a necessity for the activity, while the presence of a carboxyl function at C-20 in ring E was the key factor for its potency comparing to other quinonemethide triterpenes such as pristimerin (HM-10) where this activity was lost due to the methylation of this group as mentioned in section 3.3.2.4. The anti-cancer activity of celastrol attracted lots of attention as it possessed high potency against several tumour cell lines. Further details regarding this aspect and those evaluated in this work are found in sections 4.1.2.1 and 4.2.2.

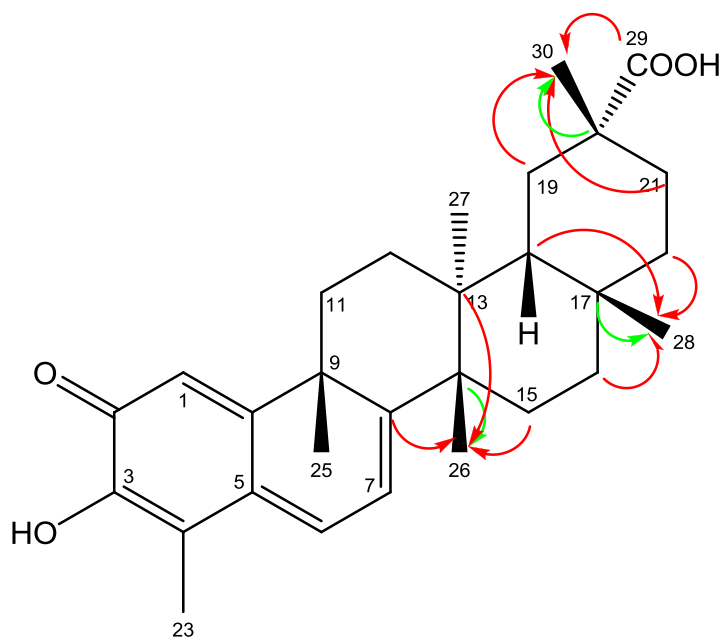


Figure 3.85: Structure of HM-11 with the key HMBC correlations
 (\rightarrow) 3J (\rightarrow) 2J ^{13}C to ^1H connectivity

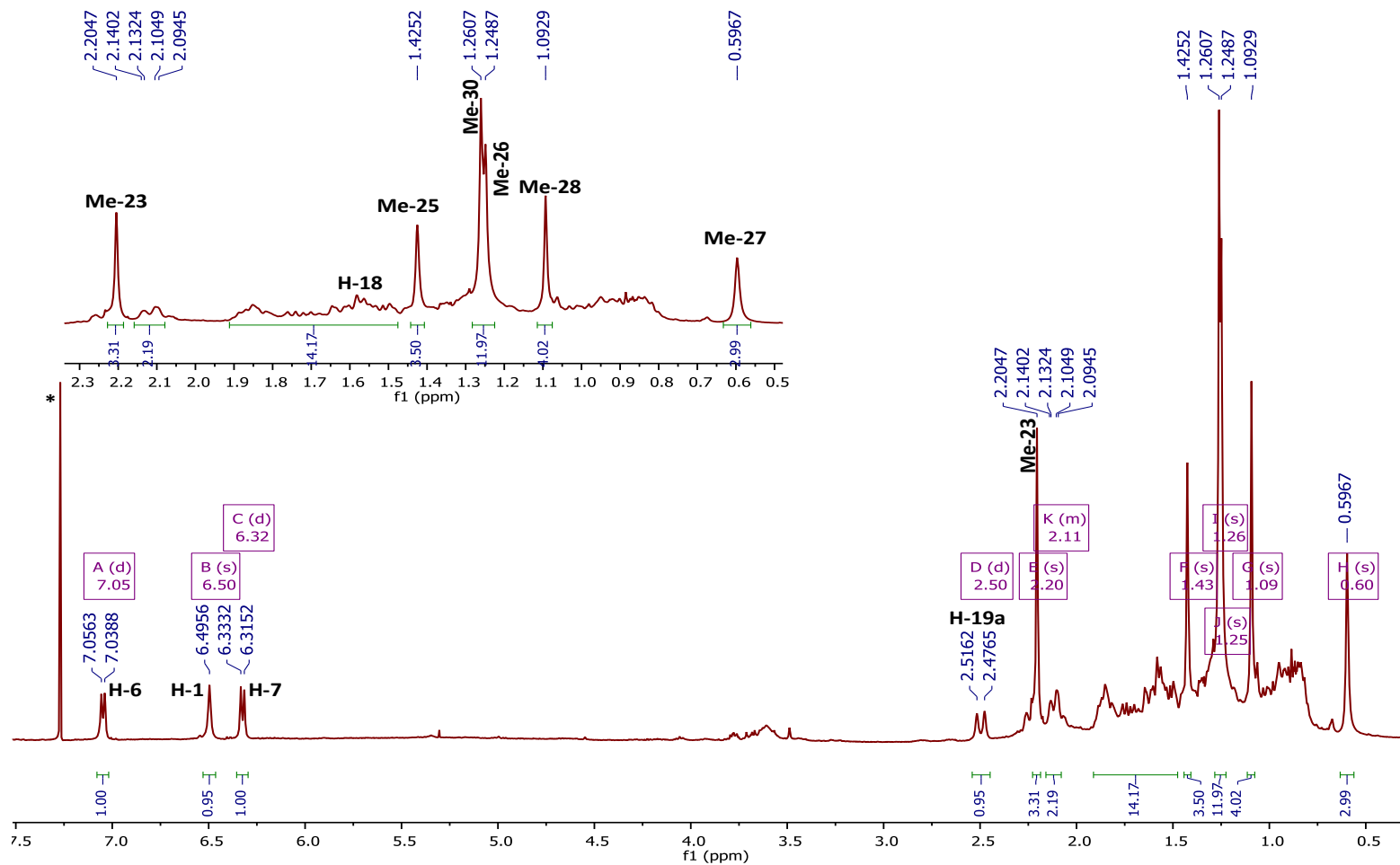


Figure 3.86: ¹H NMR spectrum (400 MHz) of HM-11 in CDCl₃ with selected expansion of the methyls; (*) CHCl₃ residue

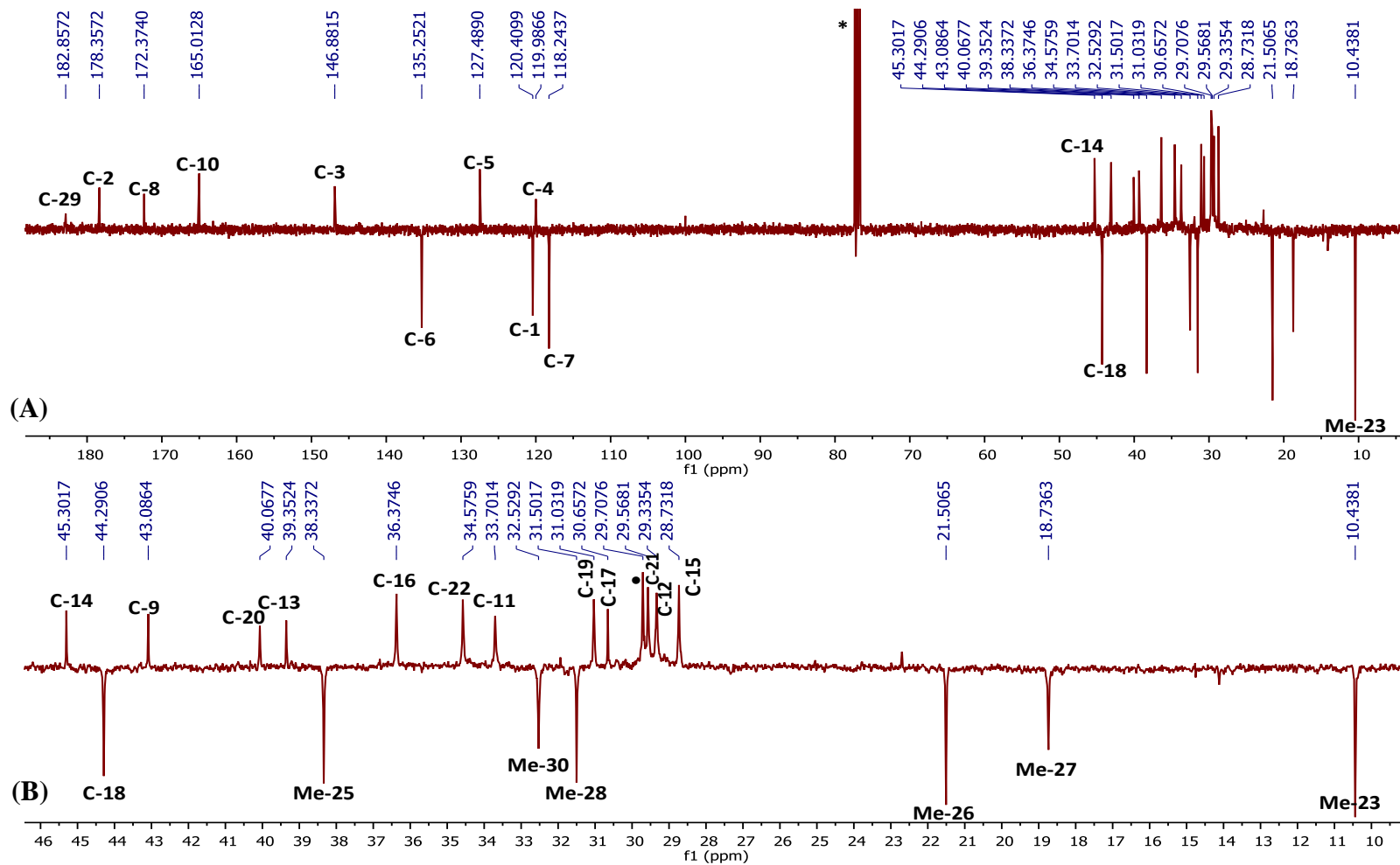
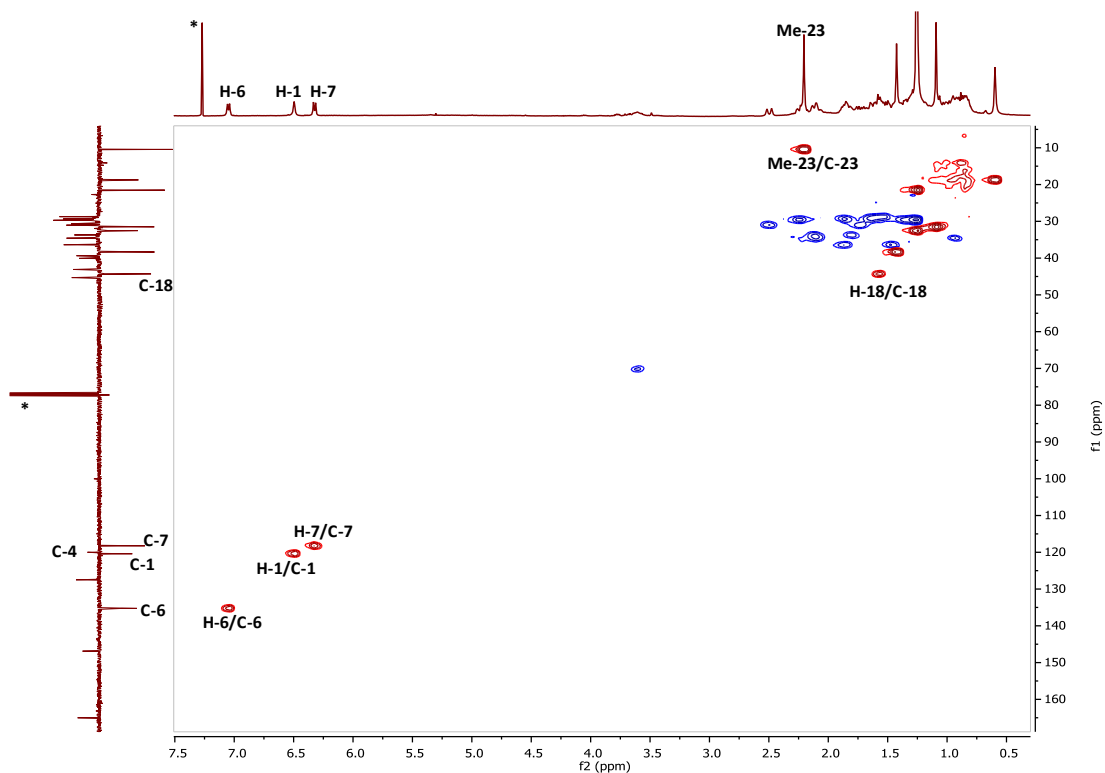
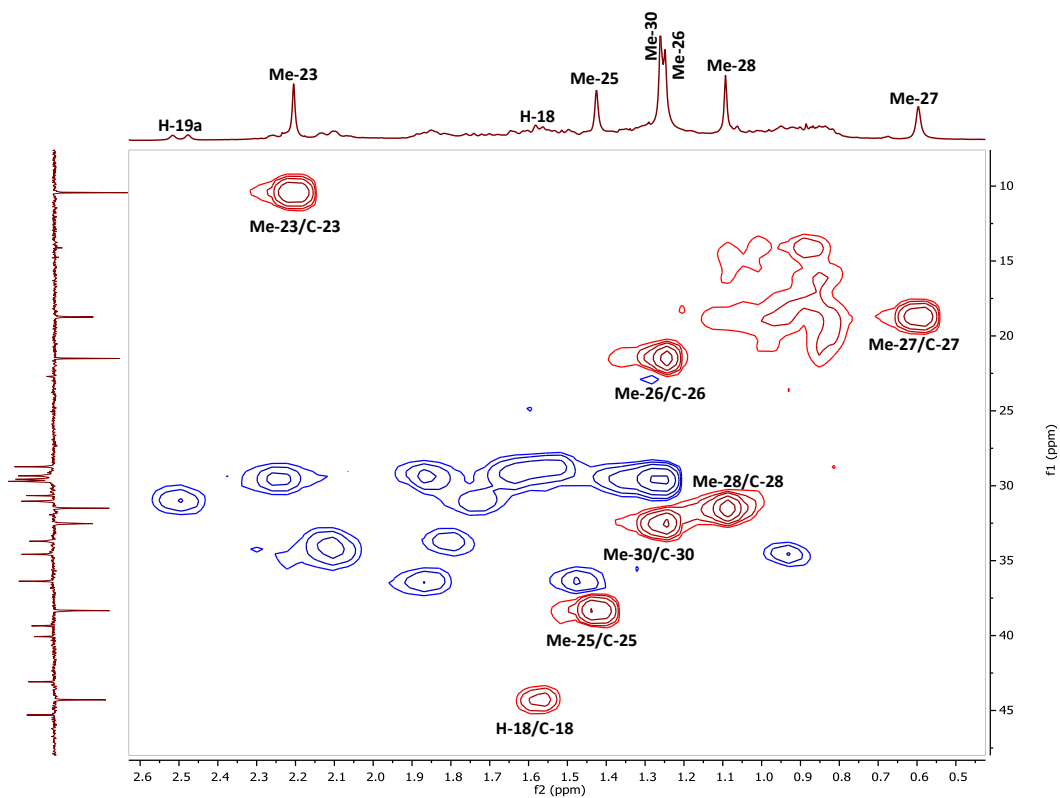


Figure 3.87: (A): Full DEPTq ^{13}C NMR spectrum (100 MHz) of HM-11 in CDCl_3 (*); (B): Selected expansion in aliphatic region

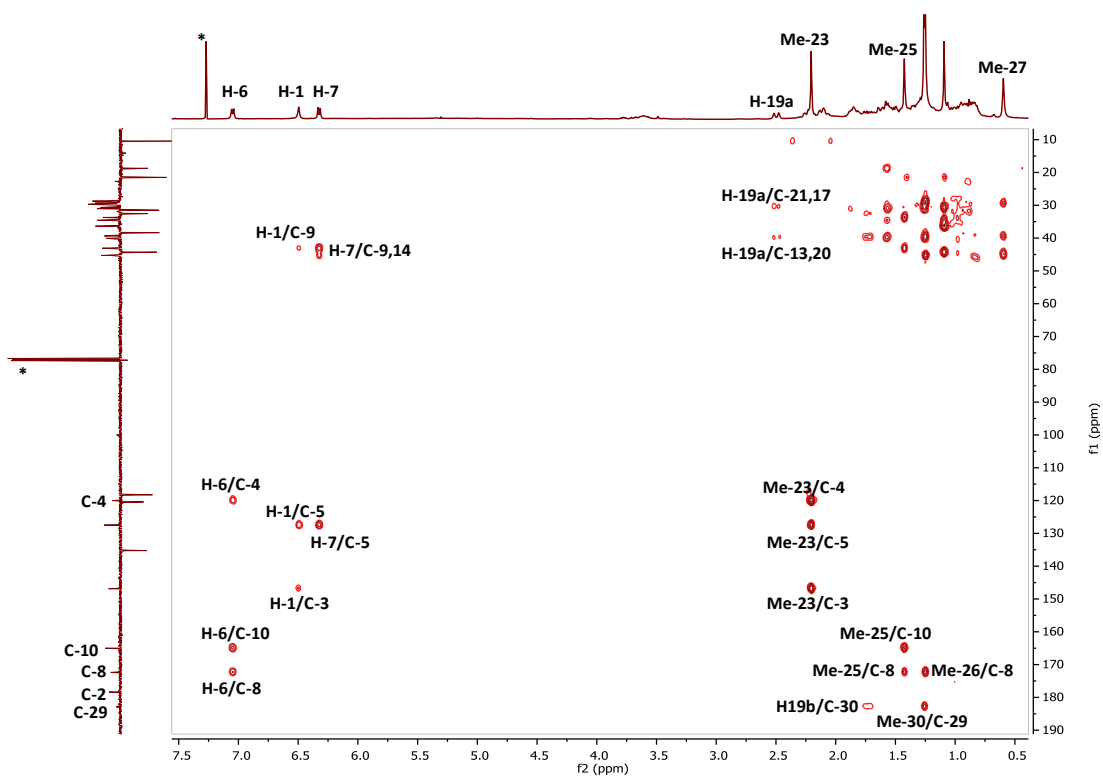


(A)

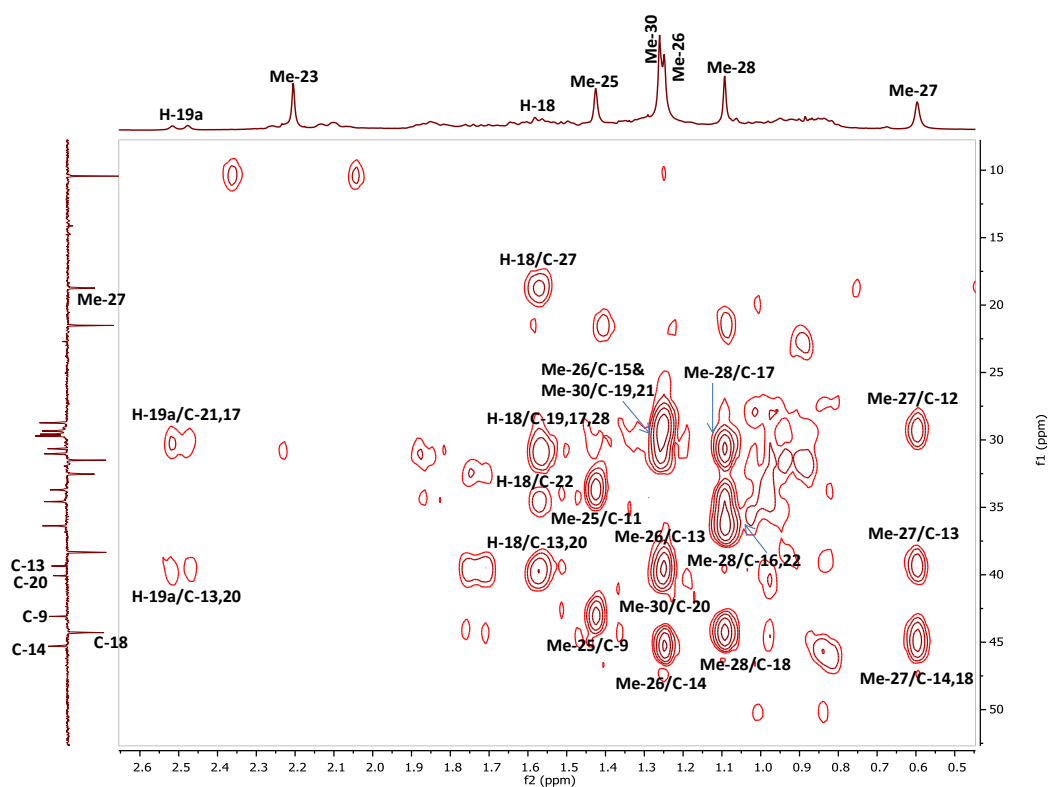


(B)

Figure 3.88: HSQC spectrum (400 MHz) of HM-11 in CDCl_3 (*)
 A: Full HSQC; B: Selected HSQC expansion



(A)



(B)

Figure 3.89: HMBC spectrum (400 MHz) of HM-11 in CDCl₃ (*)
A: Full HMBC; B: Selected HMBC expansion for the aliphatic region

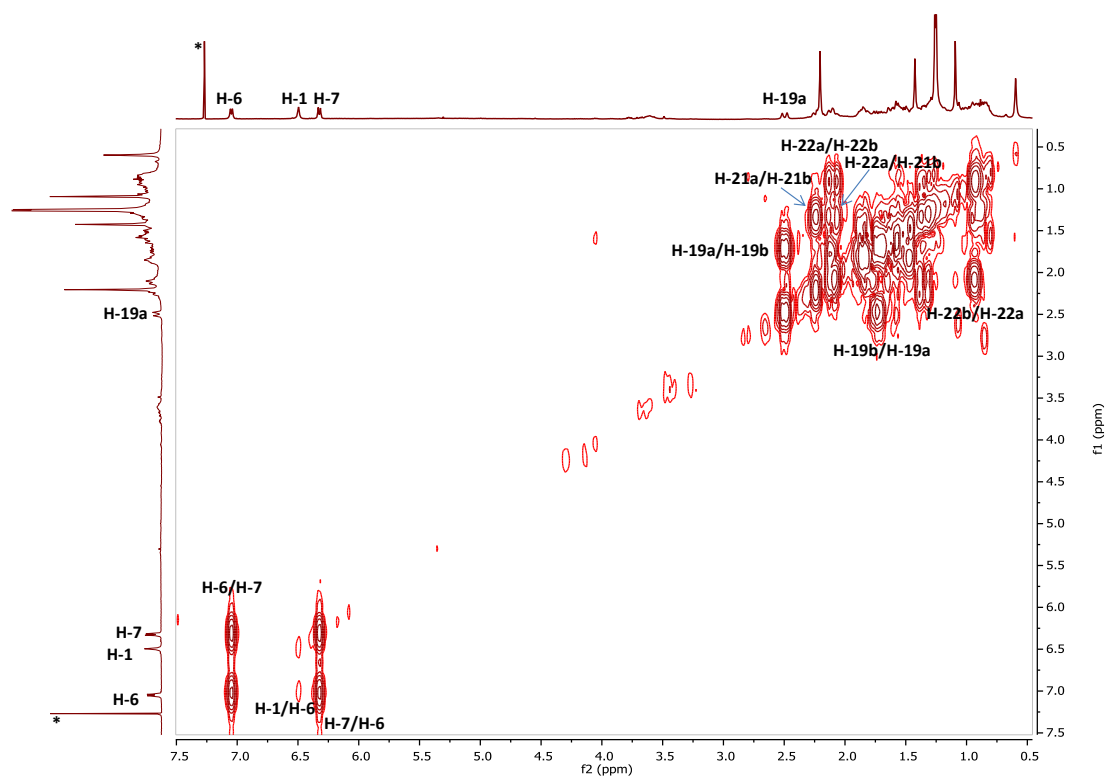


Figure 3.90: Full ¹H-¹H COSY spectrum (400 MHz) of HM-11 in CDCl₃

3.3.2.6 Characterisation of HM-12 as the new celastroid, 22(β)-hydroxycelastrol

HM-12 was isolated from the EtOAc extract of the root bark by using Sephadex LH-20 as a reddish orange amorphous solid. On TLC, the compound appeared as a dark spot under UV light (λ 254 nm) which turned to purple after spraying with anisaldehyde-sulphuric acid reagent and heating. Its R_f was 0.12 on SiGel when eluted with the mobile phase 50% hexane in EtOAc.

The negative mode HRESI-MS spectrum showed a quasi-molecular ion $[M-H]^+$ at m/z 465.2630, suggesting a molecular formula of $C_{29}H_{38}O_5$ (DBE=11).

The optical rotation $[\alpha]_D^{20}$ was $+98^\circ$ ($c=0.15$, $CHCl_3$).

The IR spectrum exhibited absorption bands at 3387 cm^{-1} indicating the presence of a hydroxyl group, 2938 , 2871 cm^{-1} for (C-H) stretch and 1708 cm^{-1} for a carboxylic acid C=O stretch (Williams and Fleming, 2008).

The 1H NMR spectrum (400 MHz, $CDCl_3$, Figure 3.92, Table 3.11) was typical of that of the quinonemethide type triterpenes. It displayed six methyl singlets at δ_H 0.42, 1.04, 1.23, 1.31, 1.41 and 2.25 attributed to Me-27, Me-28, Me-26, Me-30, Me-25 and Me-23, respectively. The quinonemethide moiety was characterised by a doublet at δ_H 6.16 (1H, d , $J = 7.1$ Hz, H-7), a narrow doublet at δ_H 6.51 (1H, d , $J = 1.4$ Hz, H-1) and a doublet of doublet at δ_H 7.03 (1H, dd , $J = 7.1, 1.4$ Hz, H-6). The assignments of the olefinic protons were also confirmed from the COSY spectrum (Figure 3.97; A) as the mutual correlations between H-6 and H-7 as well as the long range coupling between H-1 and H-6 were all observed. Furthermore, the 1H NMR spectrum revealed the presence of a doublet of doublet signal at δ_H 4.07 (1H, dd , $J = 11.6, 4.9$ Hz) indicated the presence of an oxymethine proton.

The DEPTq135 ^{13}C NMR spectrum (100 MHz, Figure 3.93) revealed the presence of 29 carbons including six methyls, six methylenes, four methines, one oxymethine at δ_C 67.4, ten quaternaries including oxygen-bearing carbon (C-3) at δ_C 146.8 and two carbonyl carbon signals at δ_C 178.1 and 183.3 attributed to C-2 and C-29, respectively. The chemical shifts of all hydrogen-bearing carbons were assigned from the HSQC spectrum (Figure 3.94).

By comparing the generated data from the 2D NMR experiments with those of the isolated quinonemethide derivatives in this work, this compound was found to be

very similar in structure to the HM-11 (celastrol), in particular. The HMBC spectrum (Figure 3.95) demonstrated the typical correlations for the protons of the rings A, B, C, D and E to those observed for the known compound HM-11. However, the methyl singlet at δ_{H} 1.04 (Me-28) showed 3J correlation to an oxymethine carbon at δ_{C} 67.4 instead of a methylene carbon along with its correlations to the carbon signals at δ_{C} 28.4 (C-16), 46.5 (C-18) and 36.6 (C-17). These observations established the attachment of a hydroxyl group at the position-22. This was further supported by detecting the 3J correlations from the methyl singlet at δ_{H} 1.31 (Me-30) to the two methylene carbons at δ_{C} 30.0 (C-19) and 37.5 (C-21) and to the carbonyl carbon at δ_{C} 183.3 (C-29) in addition to the 2J correlation to the quaternary carbon at δ_{C} 42.2 (C-20), which negates the possibility of the attachment of the hydroxyl group at any position other than the 22.

The molecular formula as well as the absence of the characteristic signal of a carboxymethyl group in the ^1H NMR spectrum indicated that the carbonyl carbon at δ_{C} 183.3 assigned for (C-29) belongs to a carboxylic acid function and not to an ester group.

The relative stereochemistry of the H-22 was deduced by the large coupling constant value (δ_{H} 4.07, *dd*, $J = 4.9, 11.6$ Hz), which corroborated its axial orientation and consequently the equatorial orientation of the hydroxyl group. In the NOESY spectrum (Figure 3.96; A), this oxymethine proton H-22 (δ_{H} 4.07) showed correlation to the methyl singlet Me-27 (δ_{H} 0.42) and thus it was placed on the α side of the molecule while the OH-22 should be on the β side. The methyl singlets Me-26, Me-28 and Me-30 showed NOE correlations to the methine proton H-18 (δ_{H} 1.74) (Figure 3.96; B) which confirmed their positions on the β side of the molecule while implying that the carboxylic group should be located on the α side.

The complete assignment of HM-12 has been accomplished by the analysis of the obtained 2D NMR experiments and by comparing with the previously published data on the related derivatives such as celastrol (HM-11) and 22 β -hydroxypristimerin which was isolated from *Cheiloclinium cognatum* (Hippocrateaceae) (Jeller *et al.*, 2004). Thus, HM-12 was identified as 3, 22 β -dihydroxy-24-nor-2-oxo-1(10),3,5,7-friedelatetraen-29-oic acid (Figure 3.91). This compound, for which the trivial name 22(β)-hydroxycelastrol is proposed, was established to be a celastroid that has

never been reported before. The cytotoxicity and the anti-trypanosomal activity of HM-12 were evaluated in this work. It showed high toxicity on both tested cell lines as well as high activity against *T. b. brucei* at the initial tested concentrations 20 and 5 μM . For further details see sections 4.1.1.2 and 4.2.2.

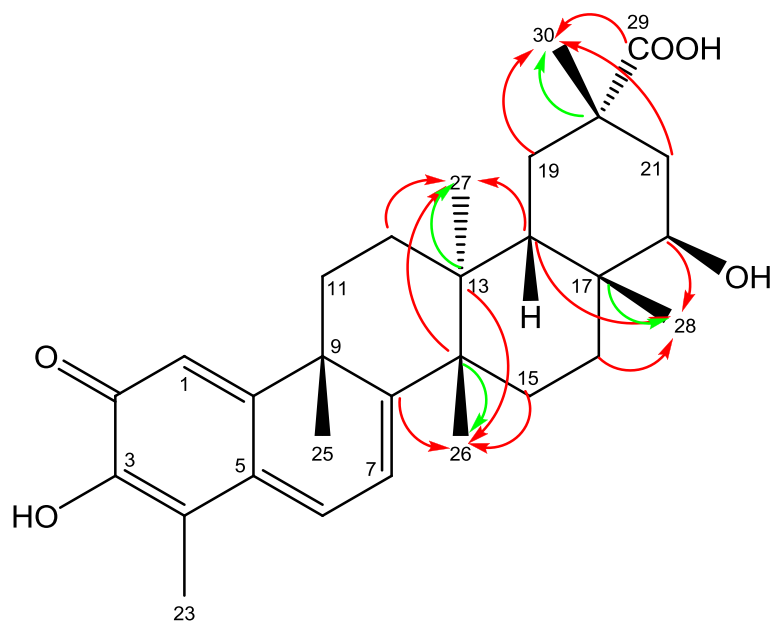


Figure 3.91: Structure of HM-12 with the key HMBC correlations
(\rightarrow) 3J (\rightarrow) 2J ^{13}C to ^1H connectivity

Table 3.11: ^1H (400 MHz) and ^{13}C (100 MHz) NMR data of HM-11 and HM-12 in CDCl_3

Position	HM-11		HM-12	
	δ_{H}	δ_{C}	δ_{H}	δ_{C}
1	6.50 (1H, <i>br.s</i>)	120.4	6.51 (1H, <i>d</i> , $J= 1.4$ Hz)	120.1
2	-	178.3	-	178.1
3	-	146.9	-	146.8
4	-	120.0	-	119.8
5	-	127.5	-	127.4
6	7.05 (1H, <i>d</i> , $J= 7.2$ Hz)	135.2	7.03 (1H, <i>dd</i> , $J= 7.1, 1.4$ Hz)	135.3
7	6.32 (1H, <i>d</i> , $J= 7.2$ Hz)	118.2	6.16 (1H, <i>d</i> , $J= 7.1$ Hz)	118.1
8	-	172.4	-	172.9
9	-	43.1	-	43.0
10	-	165.0	-	165.4
11	2.12 (1H, <i>m</i>)/ 1.80 (1H, <i>m</i>)	33.7	2.08 (1H, <i>m</i>)/ 1.77 (1H, <i>m</i>)	33.6
12	1.86 (1H, <i>m</i>)/ 1.64 (1H, <i>m</i>)	29.3	1.85 (1H, <i>m</i>)/ 1.62 (1H, <i>m</i>)	28.7
13	-	39.3	-	38.8
14	-	45.3	-	44.9
15	1.54 (2H) [1.70-1.48 <i>m</i>]	28.7	2.15 (1H, <i>m</i>)/ 1.40 (1H, <i>m</i>)	28.5*
16	1.87 (1H, <i>m</i>)/ 1.47 (1H, <i>m</i>)	36.4	1.44 (1H, <i>m</i>)/ 1.25 (1H, <i>m</i>)	28.4*
17	-	30.6	-	36.7
18	1.57 (1H, <i>m</i>)	44.3	1.74 (1H, <i>s</i>)	46.6
19	2.50 (1H, <i>br.d</i> , $J=15.9$ Hz)/ 1.73 (1H, <i>m</i>)	31.0	2.49 (1H, <i>br.d</i> , $J= 14.5$ Hz)/ 1.72 (1H, <i>m</i>)	30.0
20	-	40.0	-	42.3
21	2.24 (1H, <i>m</i>)/ 1.36 (1H, <i>m</i>)	29.5	2.49 (1H, <i>br.d</i> , $J= 14.5$ Hz)/ 1.33 (1H, <i>m</i>)	37.5
22	2.10 (1H, <i>m</i>)/ 0.94 (1H, <i>m</i>)	34.6	4.07(1H, <i>dd</i> , $J= 4.9, 11.6$ Hz)	67.5
23	2.20 (3H, <i>s</i>)	10.4	2.25 (3H, <i>s</i>)	10.4
24	-	-	-	-
25	1.42 (3H, <i>s</i>)	38.3	1.41 (3H, <i>s</i>)	38.6
26	1.25 (3H, <i>s</i>)	21.5	1.23 (3H, <i>s</i>)	21.4
27	0.59 (3H, <i>s</i>) [†]	18.7	0.42 (3H, <i>s</i>)	20.4
28	1.09 (3H, <i>s</i>)	31.5	1.04 (3H, <i>s</i>)	24.2
29	-	182.8	-	183.3
30	1.26 (3H, <i>s</i>) [†]	32.5	1.31 (3H, <i>s</i>)	32.4

[†] These values were exchanged in literature in CD_3OD (Jo *et al.*, 2006)

* These carbons and protons might be exchangeable

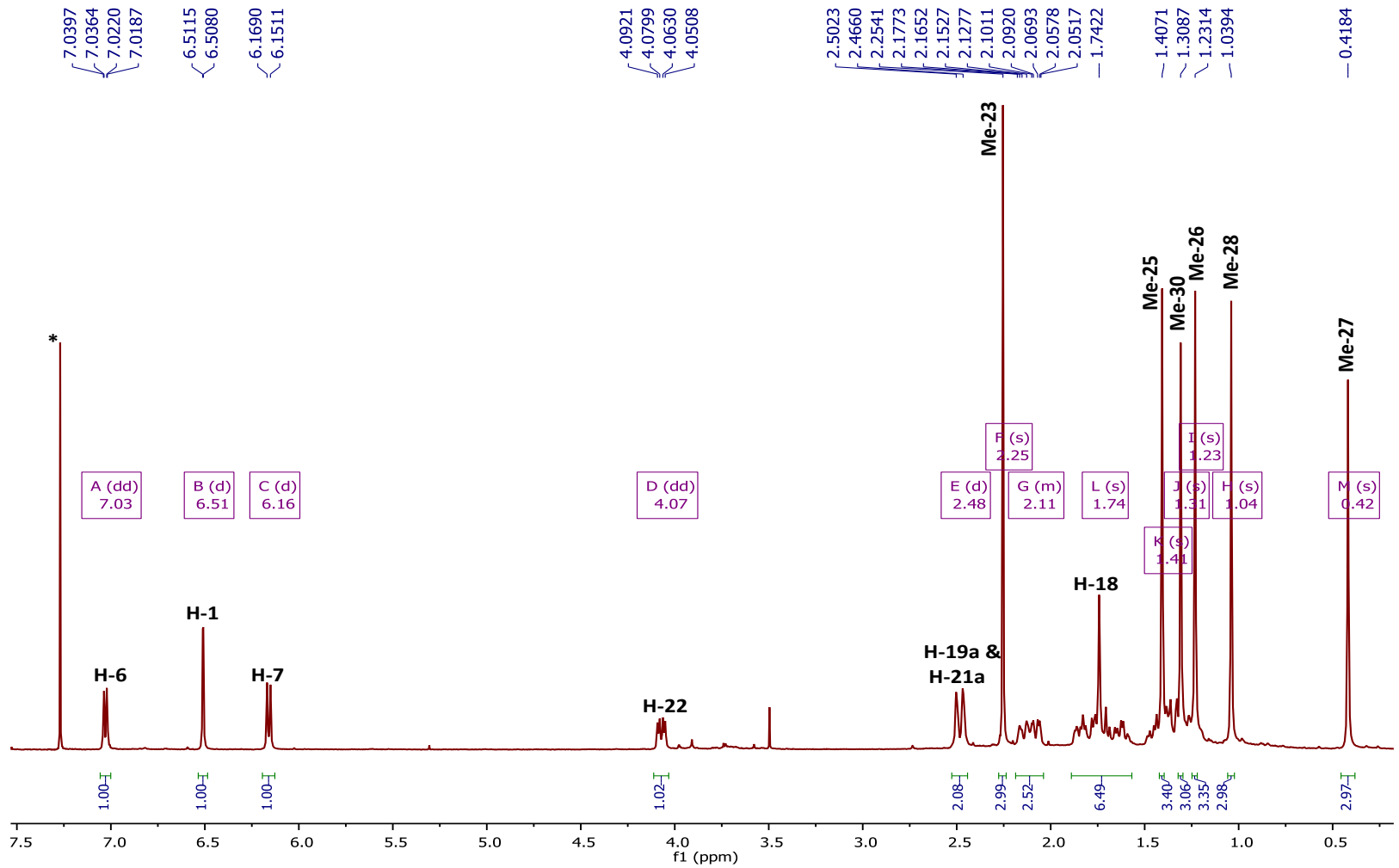


Figure 3.92: ^1H NMR spectrum (400 MHz) of HM-12 in CDCl_3 ; (*) CHCl_3 residue

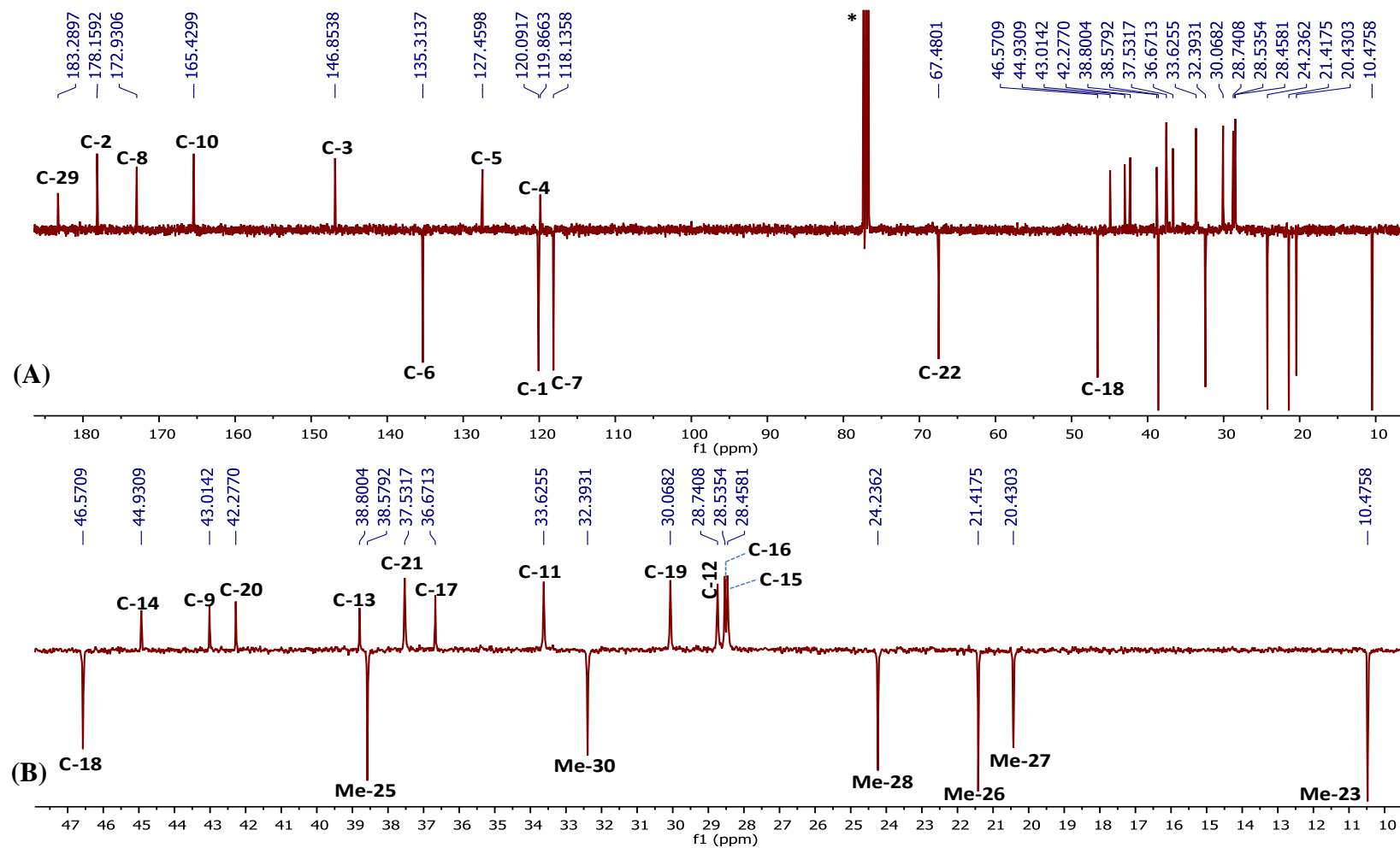


Figure 3.93: (A): Full DEPTq ^{13}C NMR spectrum (100 MHz) of HM-12 in CDCl_3 (*); (B): Selected expansion in aliphatic region

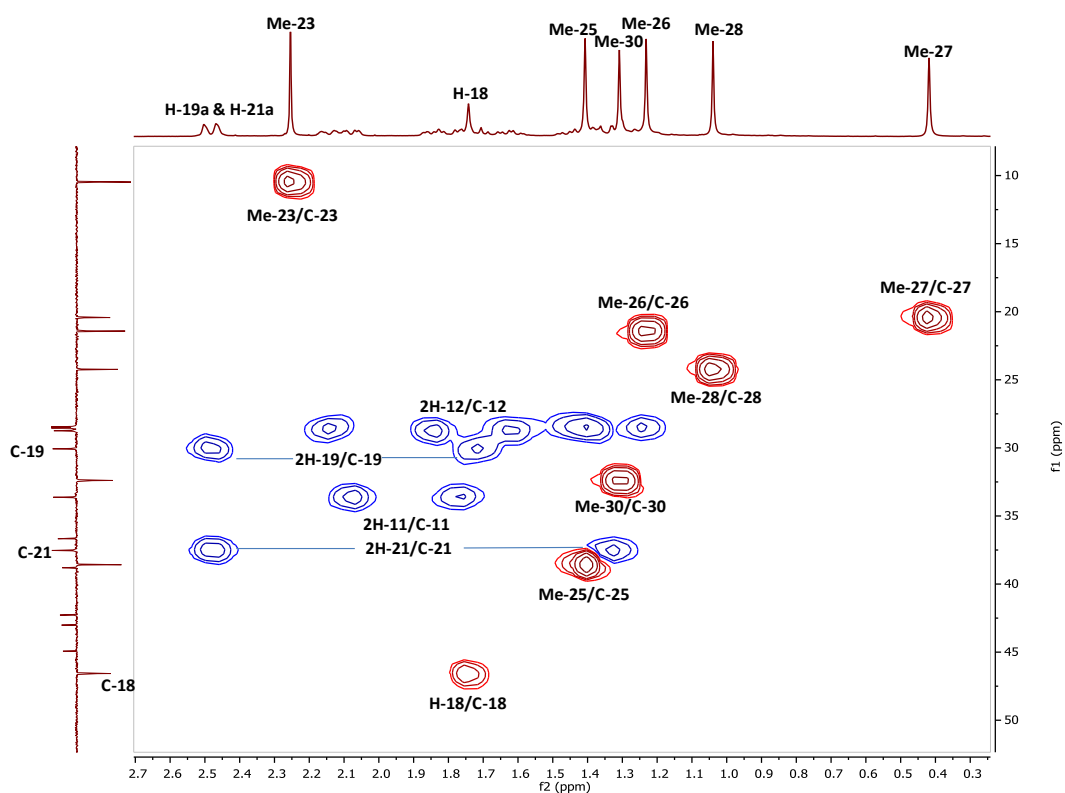
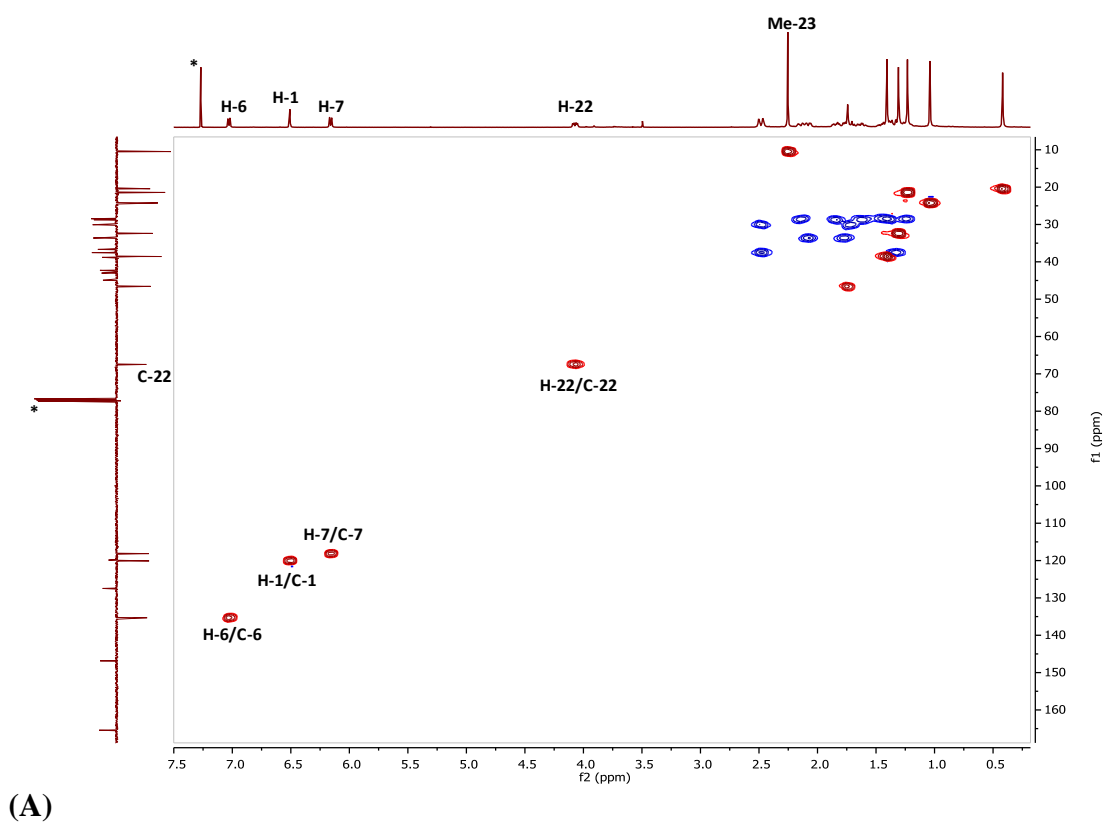
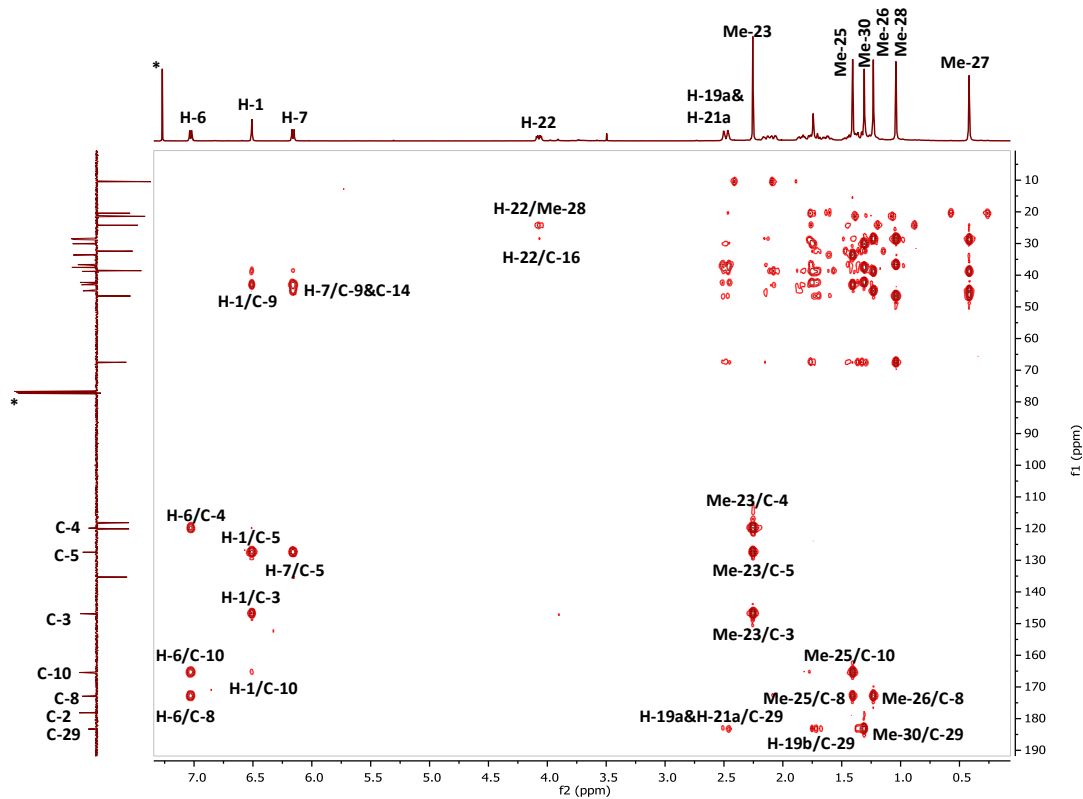
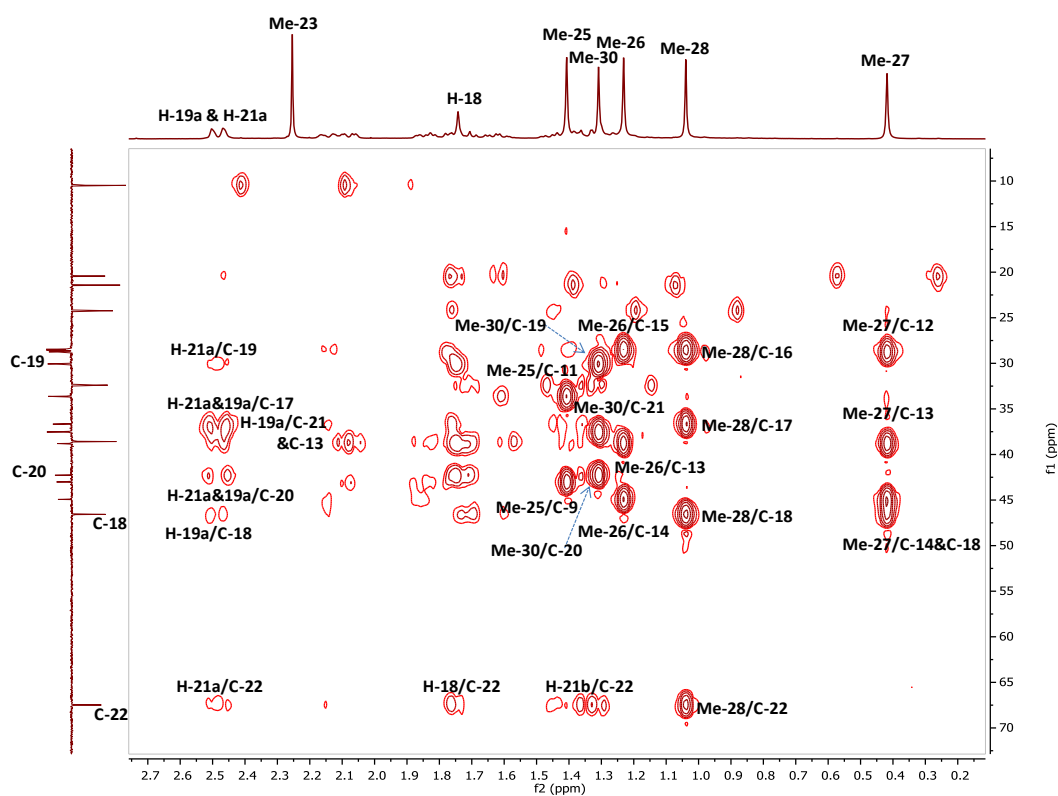


Figure 3.94: HSQC spectrum (400 MHz) of HM-12 in CDCl₃ (*)
 A: Full HSQC; B: Selected HSQC expansion

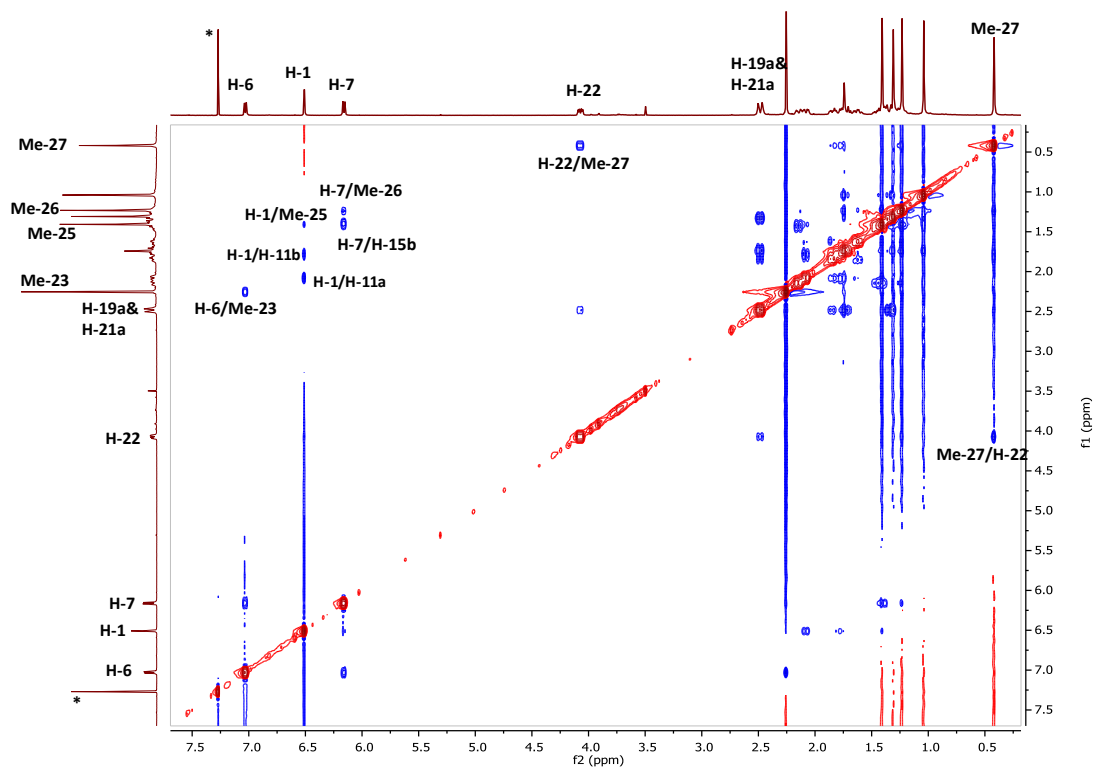


(A)

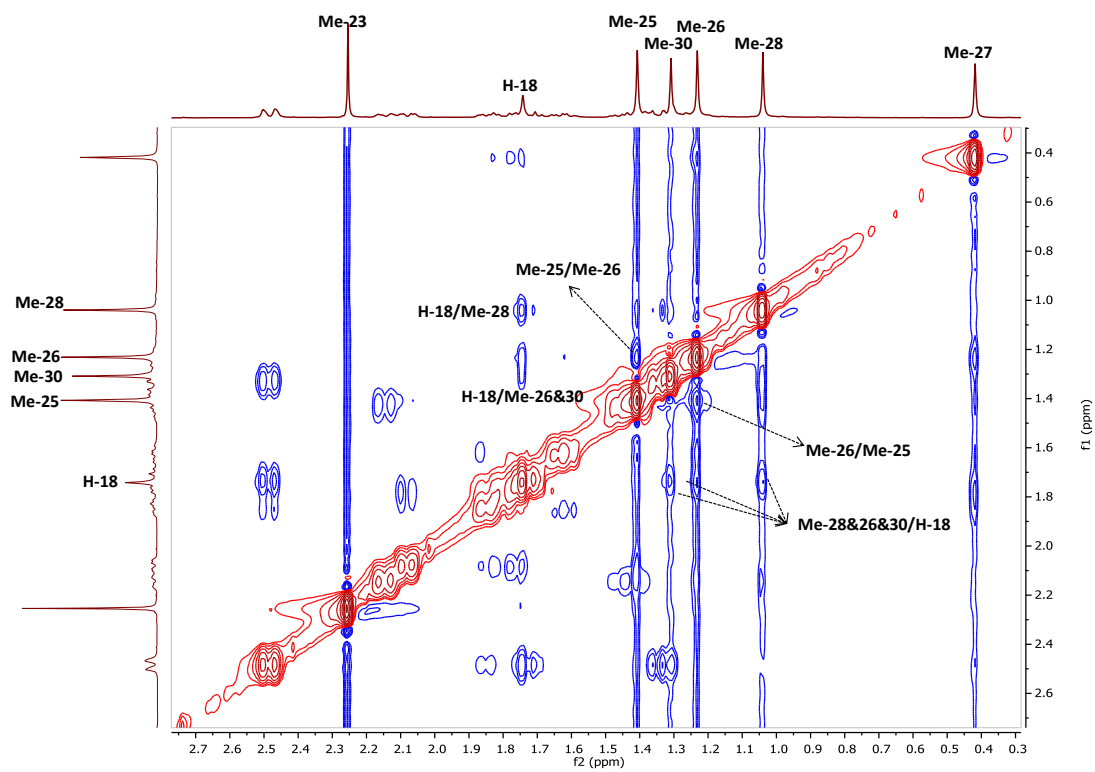


(B)

Figure 3.95: HMBC spectrum (400 MHz) of HM-12 in CDCl₃ (*)
A: Full HMBC; B: Selected HMBC expansion of the aliphatic region

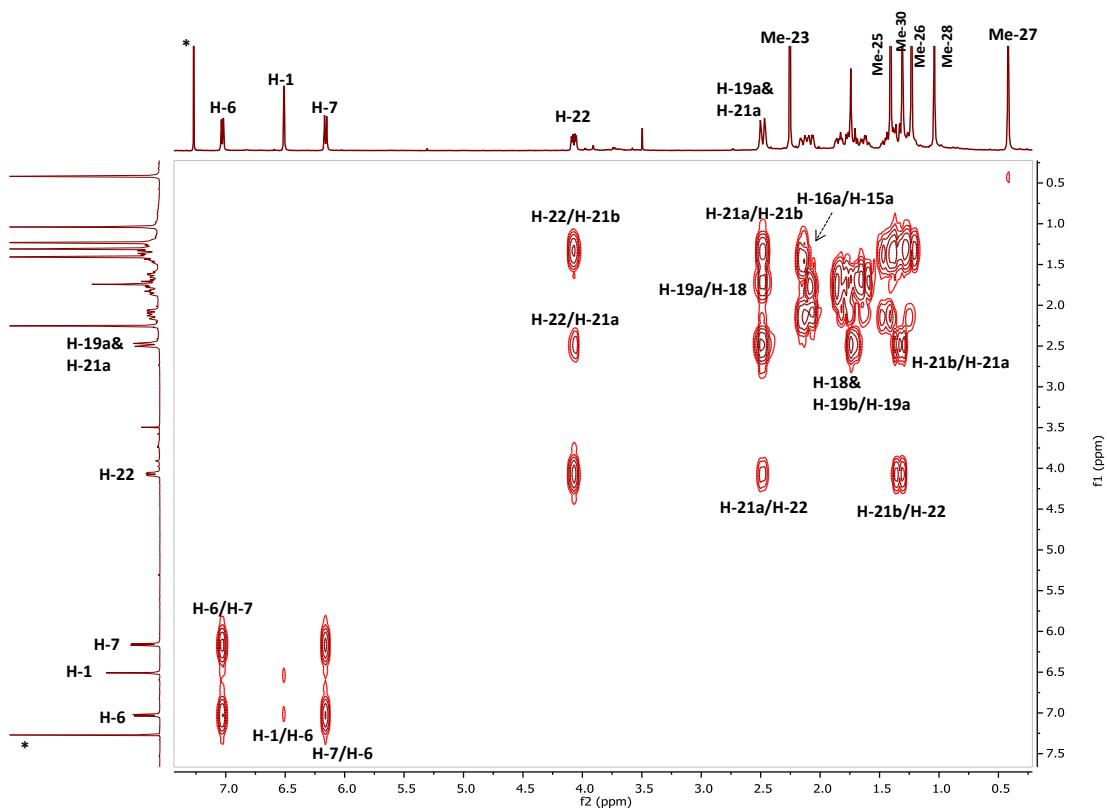


(A)

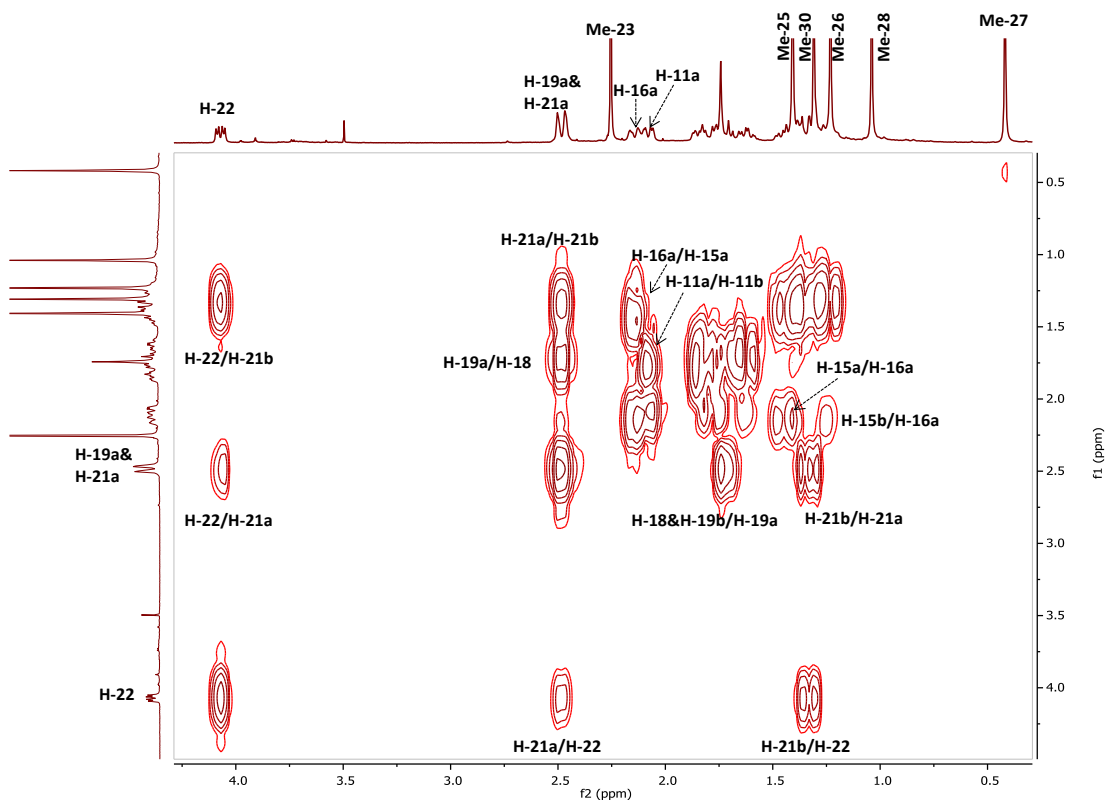


(B)

**Figure 3.96: NOESY spectrum (400 MHz) of HM-8 in CDCl_3
 (A): Full NOESY spectrum; (B): Selected NOESY expansion**



(A)



(B)

Figure 3.97: (A): Full ^1H - ^1H COSY spectrum (400 MHz) of HM-12 in CDCl_3 ;
(B): Selected expansion

3.3.3 *Norfriedelane-type triterpenes and aromatic triterpenes*

The following isolated triterpenes were arranged under this classification due to either the lack of methyl group such as Me-29 or Me-25 and/ or the presence of a fully aromatic ring A.

3.3.3.1 *Characterisation of HM-13 as salaquinone A*

HM-13 was isolated from the n-hexane extract of the stem bark by PTLC as an amorphous red powder. On TLC, the compound appeared as a dark spot under UV light (λ 254 nm). After treatment with *p*-anisaldehyde-sulphuric acid reagent followed by heating, it turned to a brownish spot. Its R_f was 0.17 on SiGel when eluted with the mobile phase 50% hexane in EtOAc.

The positive mode HRESI-MS spectrum showed a quasi-molecular ion $[M+H]^+$ at m/z 451.2479, suggesting a molecular formula of $C_{28}H_{34}O_5$ (DBE=12).

The pattern of the 1H NMR spectrum (400 MHz, $CDCl_3$, Figure 3.100, Table 3.12) indicated the presence of a triterpene compound. It displayed signals at δ_H 1.06, 1.06, 1.50, 1.72 and 2.22 which were assigned with the aid of the HSQC spectrum (Figure 3.102) for five methyl singlets Me-27, Me-28, Me-25, Me-26 and Me-23, respectively, in addition to one methyl doublet at δ_H 1.16 (3H, *d*, $J=6.6$ Hz) attributed to Me-30. The COSY spectrum (Figure 3.104) showed a vicinal coupling between a methine proton at δ_H 2.68 (1H, *m*) and Me-30 confirming the latter multiplicity. The 1H NMR spectrum also showed the presence of two methylene protons at δ_H 2.97 (1H, *d*, $J=15.8$ Hz) and 2.76 (1H, *d*, $J=15.8$ Hz), an oxymethine proton at δ_H 4.43 (1H, *s*), as well as three olefinic protons at δ_H 6.50 (1H, *d*, $J=1.3$ Hz), 6.98 (1H, *d*, $J=7.2$ Hz) and 7.03 (1H, *dd*, $J=7.2, 1.3$ Hz). These olefinic protons were similar to those which are characteristic to the quinonemethide moiety, but with difference in their sequential order than usual. By the aid of the HMBC experiment (Figure 3.103: A), the assignments of these protons were still as H-1, H-7 and H-6, respectively. The COSY spectrum was not informative enough here to show the coupling between these protons since the methine proton H-7 was quite deshielded comparing to that in the other quinonemethides isolated in this work, and its chemical shift was relatively close to the proton H-6 leading to an overlapping in their cross peaks.

The ^1H NMR spectrum showed a small amount of impurities which were difficult to eliminate due to the very low yield. The signal at δ_{H} 1.26 which correlated to the methylene carbon at δ_{C} 29.7 attributed to the presence of some fats in the sample.

The small quantity of the sample affected the signal intensity in the DEPTq135 ^{13}C NMR spectrum (100 MHz, Figure 3.101) causing some ambiguity especially in the aromatic and the carbonyl regions. However, these signals were precisely extracted from the HSQC spectrum. A total of 28 carbons were assigned including six methyls, four methylenes, five methines, one oxymethine at δ_{C} 78.2, nine quaternaries including oxygen-bearing carbon (C-3) at δ_{C} 146.2 and three carbonyl groups at δ_{C} 178.3, 209.7 and 212.3 attributed to C-2, C-15 and C-21, respectively.

More rigorous analysis was achieved by the 2D HMBC spectrum (Figure 3.103; B & C). The partial structure with rings A and B was determined by following the long-range correlations from the vinyl protons H-1, H-6 and H-7 to their adjacent carbons which were typical to those of the other isolated quinonemethides. The two singlet methyls Me-26 (δ_{H} 1.72) and Me-27 (δ_{H} 1.06) were aligned on the junction C/D due to their correlations to the two quaternary carbons at δ_{C} 43.9 (C-13) and 58.1 (C-14). Additionally, the methyl singlet Me-26 showed 3J correlations to the carbonyl carbon at δ_{C} 209.7 and to the olefinic quaternary at δ_{C} 157.3 (C-8). On the other hand, the two methylene protons, assigned at position-16, had 2J correlations to the same carbonyl carbon at δ_{C} 209.7 as well as to the quaternary at δ_{C} 47.8 (C-17). This established the site of the latter carbonyl on position-15, hence, justified the downfield shift of the methine proton H-7. The methyl singlet Me-28 (δ_{H} 1.06) showed 3J correlations to the oxymethine carbon at δ_{C} 78.2, the methylene at δ_{C} 47.9 (C-16) and to the methine at δ_{C} 44.0 (C-18). The two methylene protons (2H-16) also showed 3J correlation to the same oxymethine carbon which confirmed the existence of a hydroxyl group at the position-22 in the ring E. Finally, the methyl doublet Me-30 (δ_{H} 1.16) exhibited 3J correlations to the methylene carbon at δ_{C} 30.3 and to the carbonyl at δ_{C} 212.3 along with the 2J correlation to the methine at δ_{C} 39.9 (C-20). This suggested that the latter carbonyl could be sited on either position-19 or 21. However, the methine proton H-22 (δ_{H} 4.43) did not couple with any other proton and appeared as singlet, while the methine proton H-18 (δ_{H} 2.25) appeared as multiplet and showed vicinal coupling with the methylene protons at δ_{H} 1.84/ 2.33 in

COSY spectrum, therefore, the carbonyl carbon (δ_C 212.3) should definitely be located on position-21 and the methylene carbon (δ_C 39.9) on position-19.

The relative stereochemistry of the compound HM-13 was established from the NOESY spectrum (Figure 3.105). The NOE correlations, which were observed between the proton pairs [H-22/ Me-27, H-16a (δ_H 2.97), H-20, H-19ax (δ_H 2.33)] led to the conclusion that the oxymethine proton H-22 should be axial and positioned on the α side of the molecule, implying that the hydroxyl group should be located on the β side of the molecule and in equatorial orientation. On the other hand, the NOE correlations between the proton pairs [H-16b (δ_H 2.76)/ Me-26, Me-28]; [H-18/Me-28] and [Me-26/ Me-25] established that Me-25, Me-26, Me-28, Me-30 and the methine proton H-18 were on the β side of the molecule. It was also found that the methine proton H-6 correlated to the methyl singlet Me-23 and the methine proton H-1 correlated to the methylene protons 2H-11. The energy minimized 3D structure of HM-13 (Figure 3.99) proposed that the two rings A and B are planar, similar to HM-8, consequently, H-1, H-6, H-7 and Me-23 were extended from these rings on the same level.

Based on the above information, HM-13 was identified as a 24, 29-dinorfriedelane-type triterpene named salaquinone A (Figure 3.98). This compound has only been previously isolated from *S. chinensis* (Hippocrateaceae) and the spectral data obtained in this work were in agreement with those reported by Morikawa *et al.*, (2003). Therefore, this is the first report of its isolation from *M. laevis* (Celastraceae) so far.

There are no previous studies about the biological activities of this compound. However, its cytotoxicity and anti-trypanosomal activity were evaluated in this work. HM-13 possessed a potent cytotoxic activity against the melanoma cell line A375 and the normal cell line Hs27, as well as a high potency against *T. b. brucei* blood stream form (further details are found in sections 4.1.2.1 and 4.2.2)

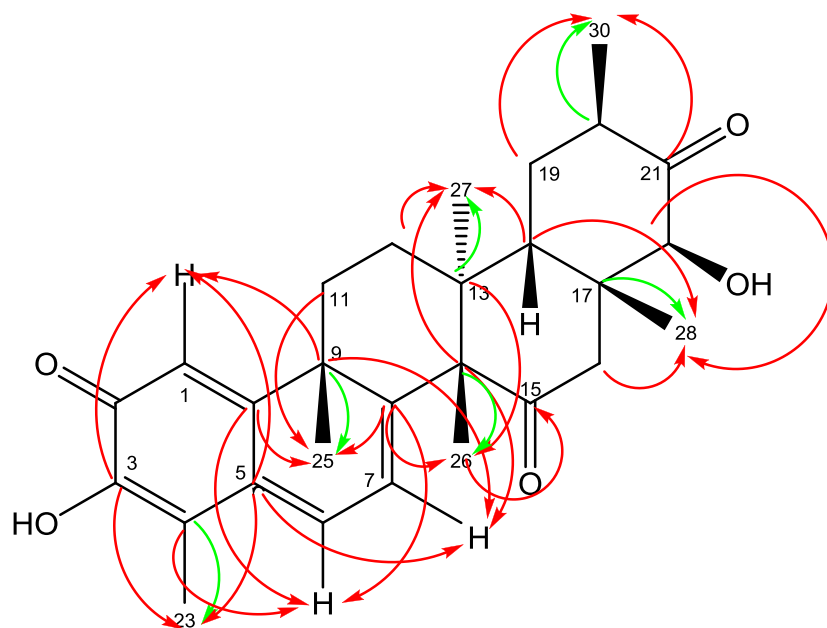


Figure 3.98: Structure of HM-13 with the HMBC correlations
 (→) 3J (→) 2J ^{13}C to ^1H connectivity

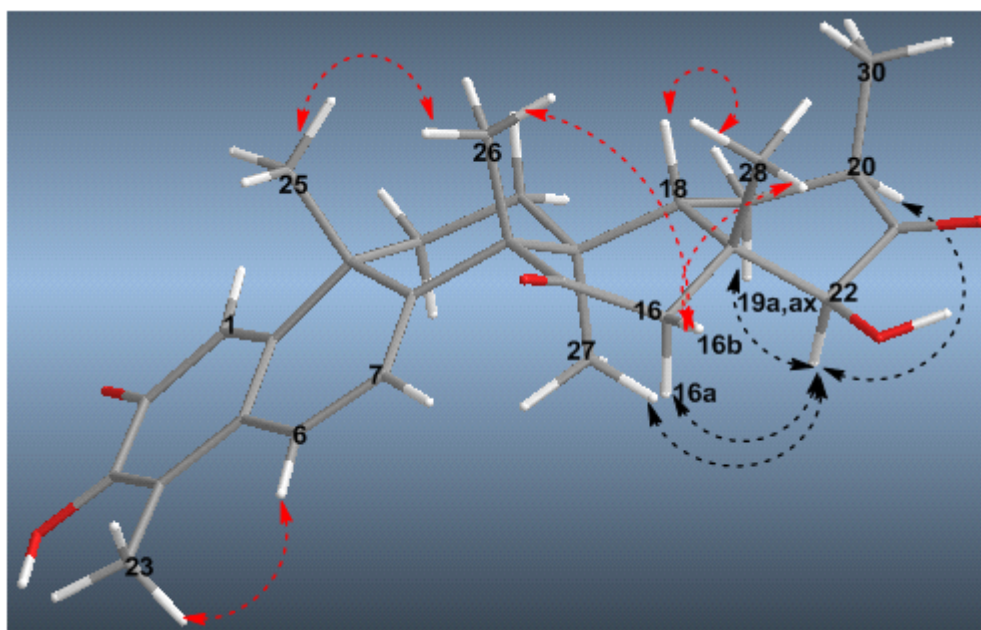


Figure 3.99: Energy minimised 3D structure of HM-13 showing NOESY correlations
 (↔) β (↔) α

Table 3.12: ^1H (400 MHz) and ^{13}C (100 MHz) NMR data of HM-13 in CDCl_3

Position	HM-13	
	δ_{H}	δ_{C}
1	6.50 (1H, <i>d</i> , $J=1.3$ Hz)	119.5
2	-	178.3
3	-	146.2
4	-	117.7
5	-	128.2
6	7.03 (1H, <i>dd</i> , $J=1.3, 7.2$ Hz)	133.1
7	6.98 (1H, <i>d</i> , $J=7.2$ Hz)	124.5
8	-	157.3
9	-	42.6
10	-	163.3
11	2.14 (1H, <i>m</i>)/ 1.97 (1H, <i>m</i>)	31.8
12	1.96 (2H) [2.04-1.91 <i>m</i>]	29.0
13	-	43.9
14	-	58.1
15	-	209.7
16	2.97 (1H, <i>d</i> , $J=15.8$ Hz)/ 2.76 (1H, <i>d</i> , $J=15.8$ Hz)	47.9
17	-	47.8
18	2.25 (1H, <i>m</i>)	44.0
19	2.33 (1H, <i>m</i>)/ 1.84 (1H, <i>m</i>)	30.3
20	2.68 (1H, <i>m</i>)	39.9
21	-	212.3
22	4.43 (1H, <i>br.s</i>)	78.2
23	2.22 (3H, <i>s</i>)	10.3
24	-	-
25	1.50 (3H, <i>s</i>)	39.4
26	1.72 (3H, <i>s</i>)	24.4*
27	1.06 (3H, <i>s</i>)	21.5*
28	1.06 (3H, <i>s</i>)	24.8
29	-	-
30	1.16 (3H, <i>d</i> , $J= 6.6$ Hz)	15.0

* These carbons were assigned in reverse order in literature (Morikawa *et al.*, 2003)

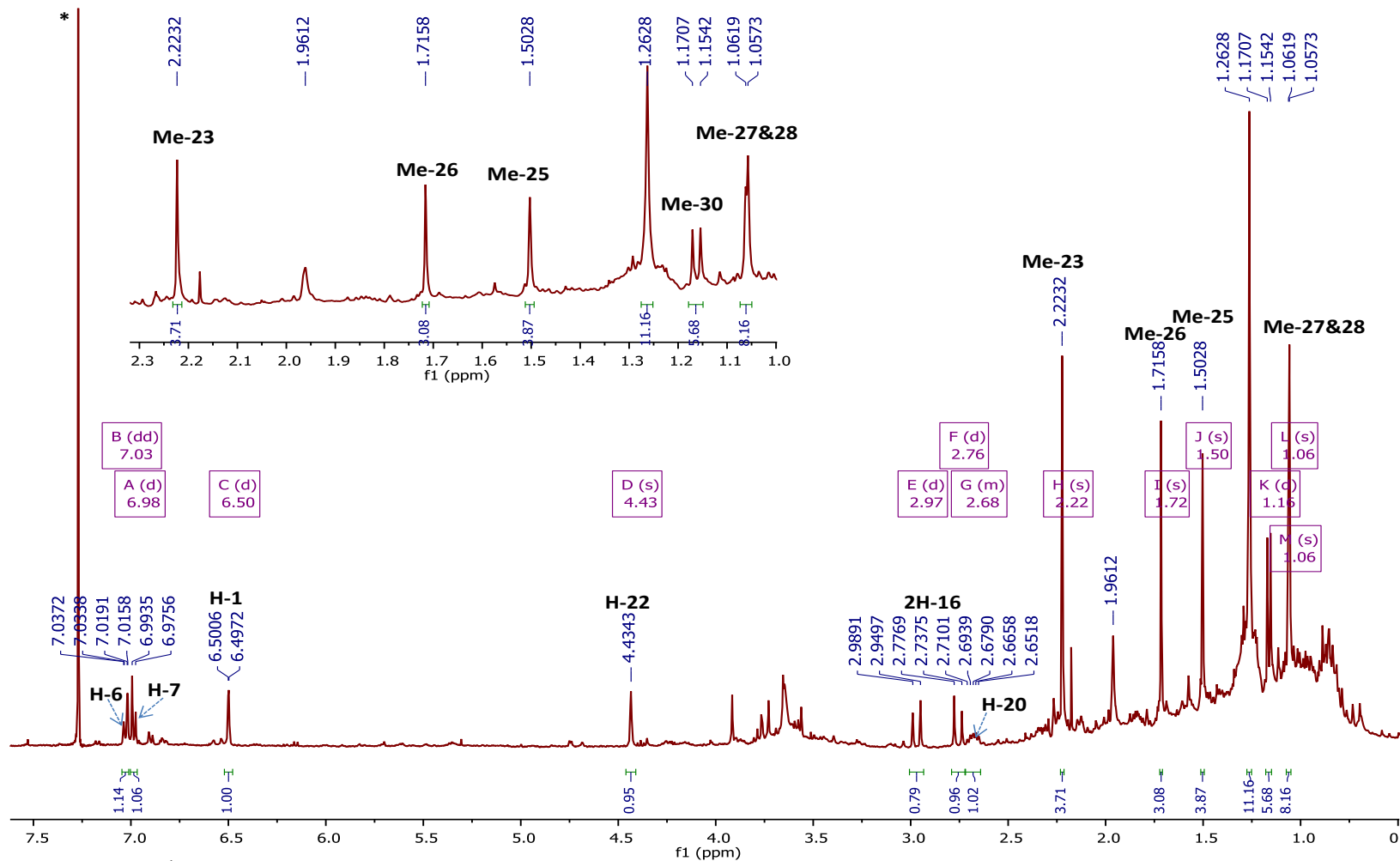


Figure 3.100: ¹H NMR spectrum (400 MHz) of HM-13 in CDCl₃ with selected expansion of the methyl region; (*) CHCl₃ residue

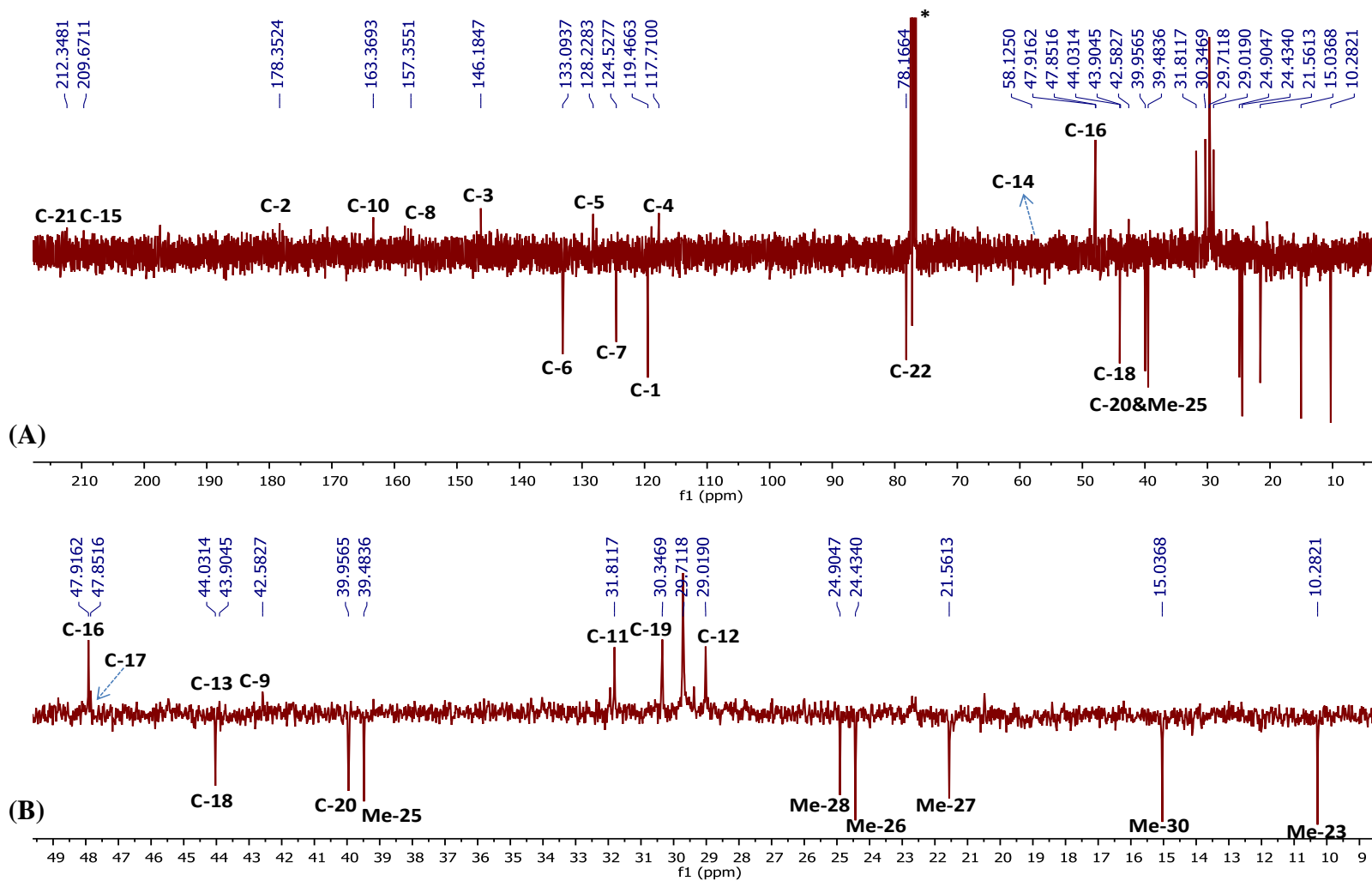
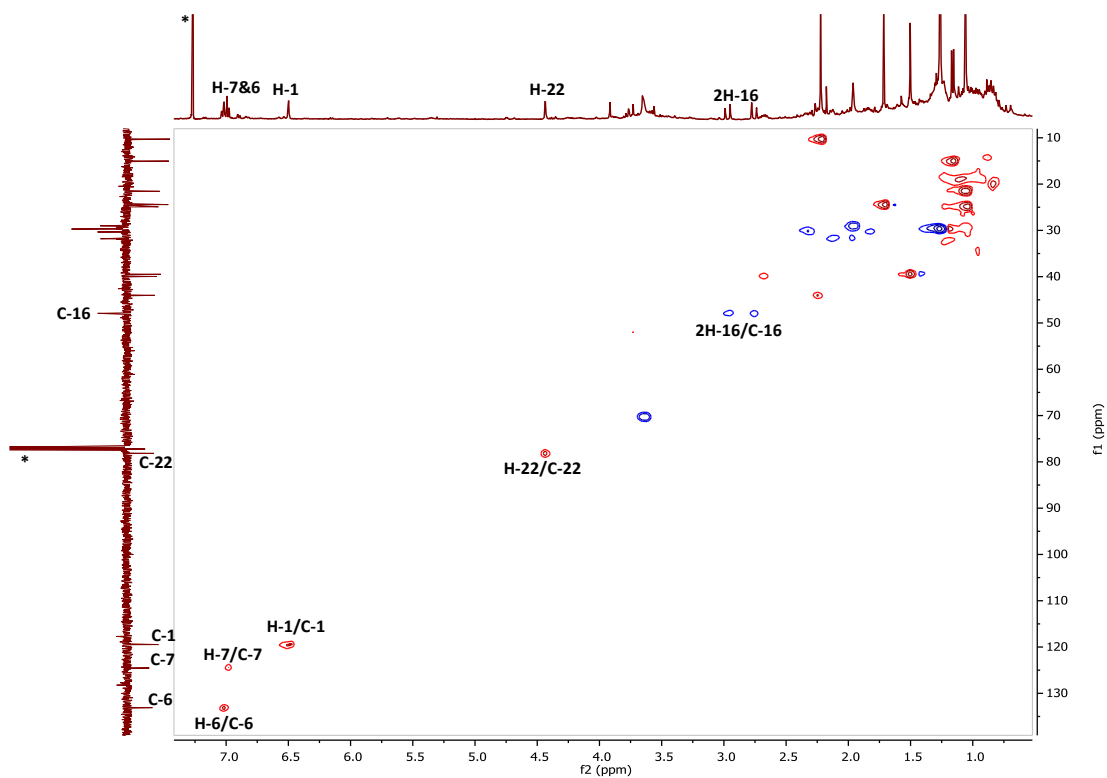
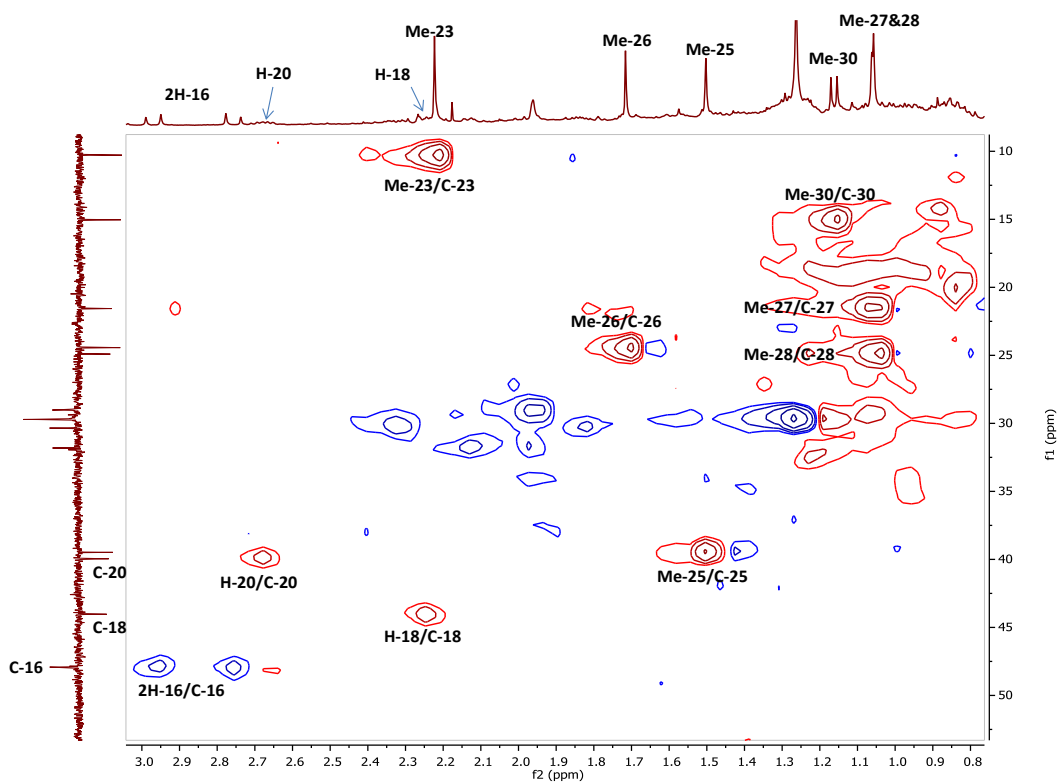


Figure 3.101: (A): Full DEPTq 135 ^{13}C NMR spectrum (100 MHz) of HM-13 in CDCl_3 (*); (B): Selected expansion in aliphatic region

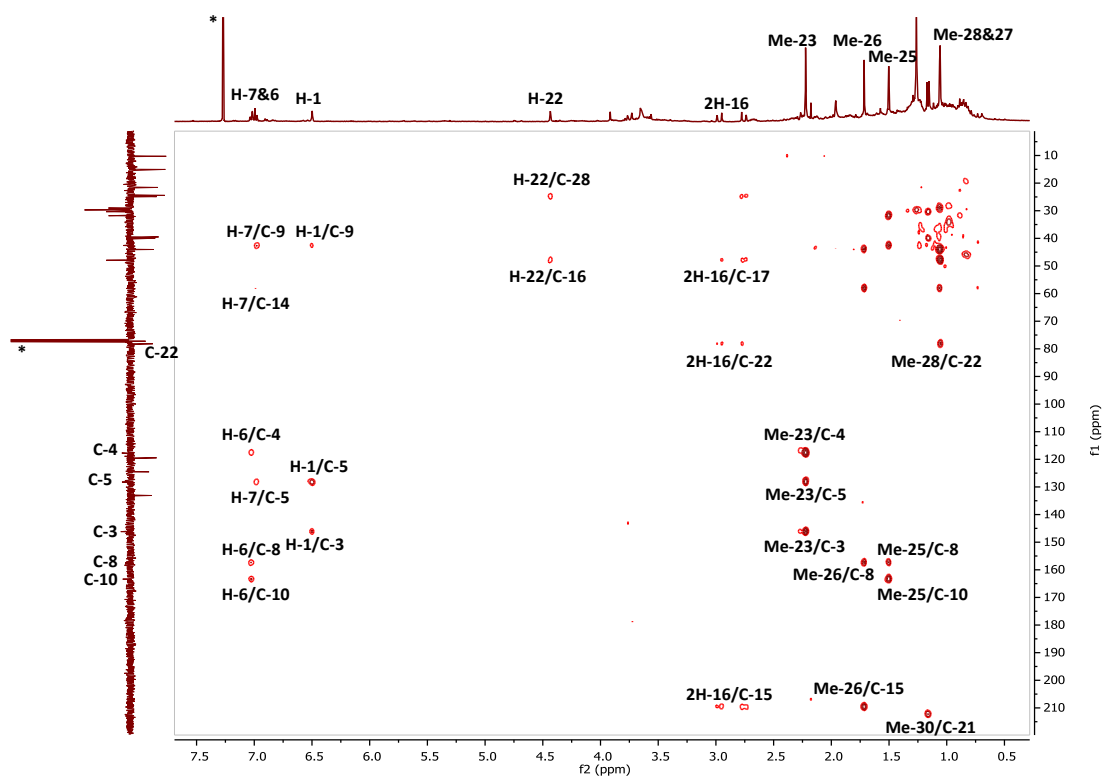


(A)

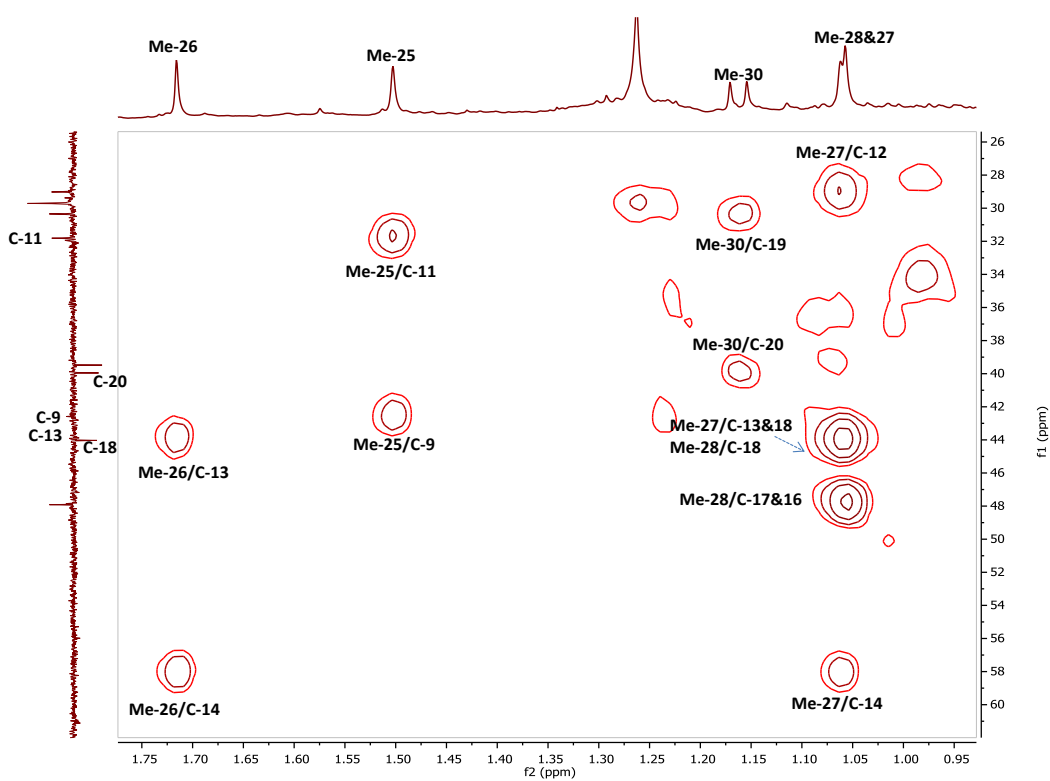


(B)

Figure 3.102: HSQC spectrum (400 MHz) of HM-13 in CDCl_3 (*)
 A: Full HSQC; B: Selected HSQC expansion



(A)



(B)

Figure 3.103: HMBC spectrum (400 MHz) of HM-13 in CDCl₃ (*)
A: Full HMBC; B: Selected HMBC expansion of the aliphatic region of F₂ domain

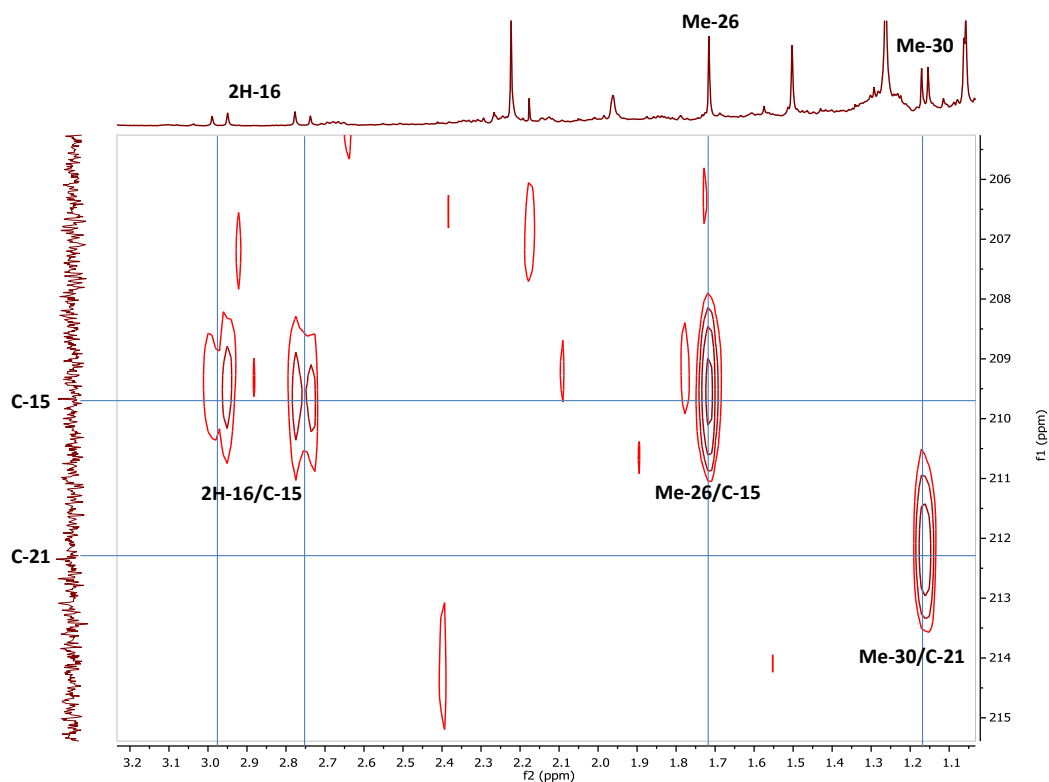


Figure 3.103 (Cont.): (C); Selected HMBC expansion showing the ketones correlations

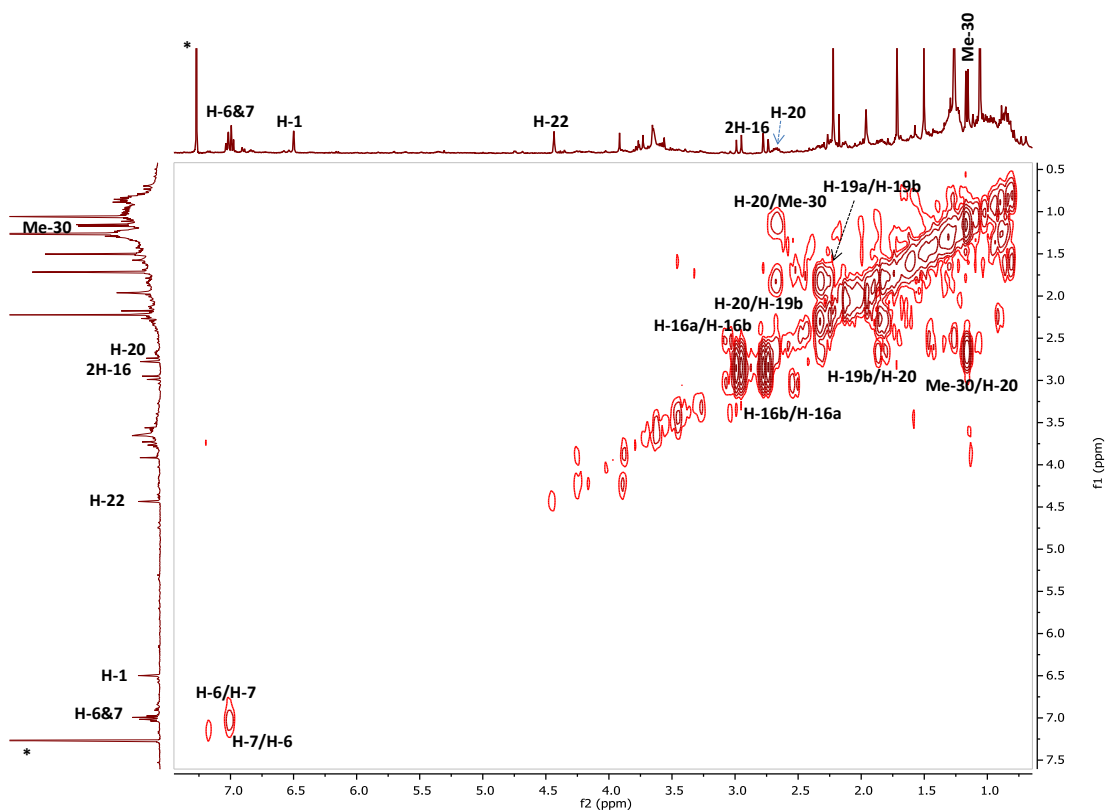
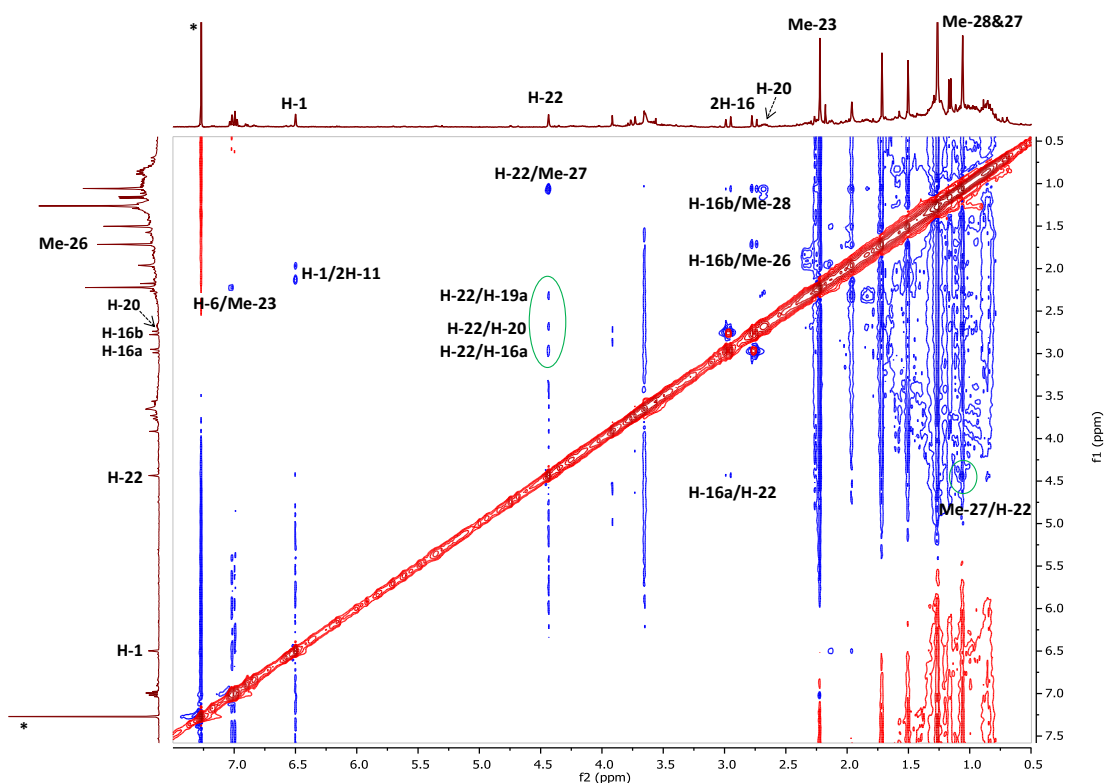
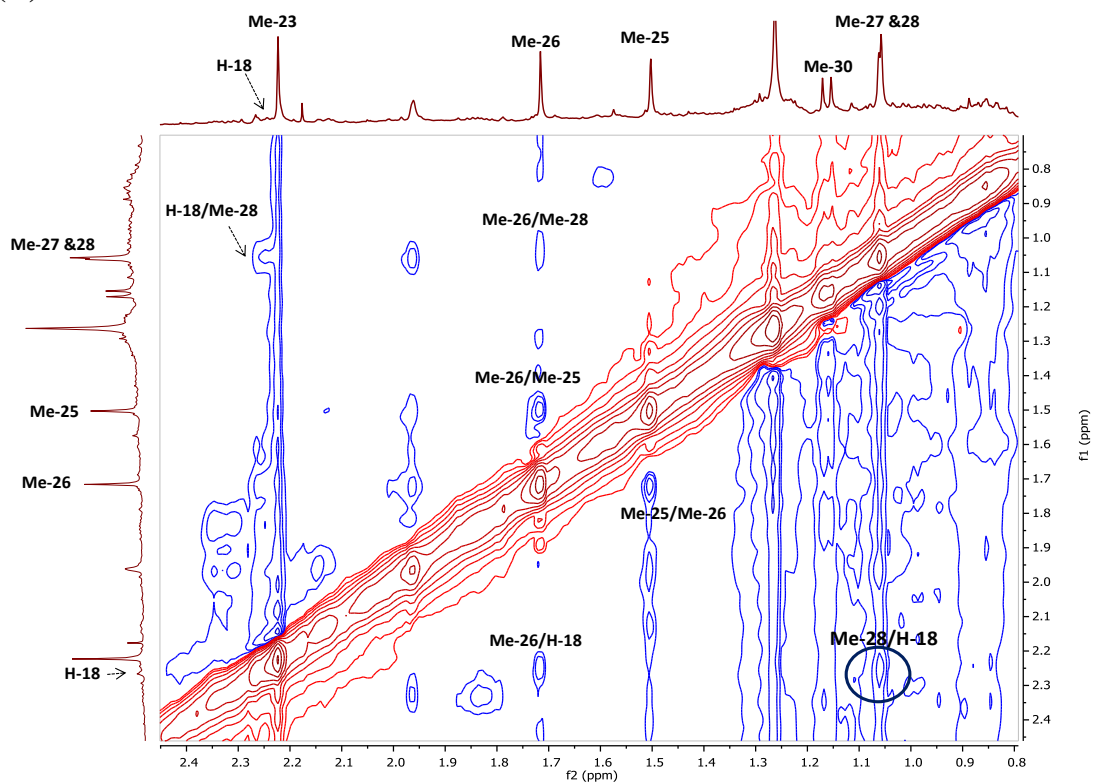


Figure 3.104: Full ¹H-¹H COSY spectrum (400 MHz) of HM-13 in CDCl₃



(A)



(B)

**Figure 3.105: NOESY spectrum (400 MHz) of HM-13 in CDCl_3
 (A): Full NOESY spectrum; (B): Selected NOESY expansion**

3.3.3.2 Characterisation of HM-14 as regeol A

HM-14 was isolated from the EtOAc extract of the stem bark by PTLC as an amorphous orange powder. On TLC, the compound appeared as a dark spot under UV light (λ 254 nm) and turned to purple after spraying with *p*-anisaldehyde-sulphuric acid reagent followed by heating. Its R_f was 0.44 on SiGel when eluted with the mobile phase 50% hexane in EtOAc.

The positive mode HRESI-MS spectrum showed a quasi-molecular ion $[M+H]^+$ at m/z 441.3006, suggesting a molecular formula of $C_{28}H_{40}O_4$ (DBE=9).

HM-14 was accompanied by a phenolic compound in a Sephadex-LH20 resulted fraction. The structure elucidation using 1D and 2D NMR experiments was carried out on the mixture of the two compounds which was afterwards subjected to PTLC to separate them (see Appendix III; D). A 1H NMR experiment was followed to detect the sub-fractions and to confirm the separation. The very small yield of the purified compound did not allow getting good quality NMR experiments, therefore, the spectra displayed in this work were the ones for the mixture since there was no overlapping in the signals attributed to the two compounds.

The 1H NMR spectrum (400 MHz, $CDCl_3$, Figure 3.107; A & B, Table 3.13) revealed the presence of five singlet methyls at δ_H 0.86, 1.02, 1.23, 1.26 and 2.11, in addition to one methyl doublet at δ_H 1.07 (3H, *d*, $J=6.3$ Hz). The COSY spectrum (Figure 3.112) showed a vicinal coupling between a methine proton at δ_H 2.75 (1H, *q*, $J=6.3$ Hz) and the latter methyl doublet confirming their multiplicity. These methyls were assigned with the aid of the HSQC and HMBC experiments as Me-28, Me-26, Me-25, Me-27, Me-23 and Me-30, respectively. The 1H NMR spectrum also showed the presence of an oxymethine proton at δ_H 4.59 (1H, *s*) and another aromatic methine proton at δ_H 6.67 (1H, *s*). The signal at δ_H 3.70, which has no carbon, was assigned to a hydroxyl group attached to the carbon at δ_C 77.5 corresponded to the oxymethine proton, in view of the fact that it showed a vicinal coupling to the latter proton in COSY spectrum.

The ^{13}C NMR spectrum (100 MHz, Figure 3.108 and Figure 3.109; A & B) revealed the presence of 28 carbons attributed to HM-14 apart from the signals of the phenolic compound and those for the solvent residue $[(CH_3)_2CO]$ at δ_C 207.2 and 30.9. These carbons were identified with the aid of the DEPT 135 experiment as six

methyls, seven methylenes, four methines including aromatic one at δ_C 108.2, one oxymethine at δ_C 77.5, nine quaternaries including five aromatic carbons at δ_C 122.2, 126.3, 139.8, 141.2 and 143.8, and finally, one carbonyl signal at δ_C 214.2.

The chemical shifts of all hydrogen-bearing carbons were unambiguously assigned from the HSQC spectrum (Figure 3.110).

Due to the carbon number (28) and the presence of six methyls, HM-14 was assumed to be another norfriedelane-type triterpene with close similarity to salaquinone A (HM-13). However, the existence of one aromatic methine proton instead of the three characteristic olefinic protons of the quinonemethide moiety in rings A & B, and with DBE of 9 suggested this compound to have less conjugation, hence, to be more saturated. On the other hand, HM-13 had an extra oxygen function positioned in ring D, which affected the chemical shifts of the adjacent protons and carbons when comparing its data with those of this compound. Therefore, by searching in literature for the same type of triterpenes isolated from *M. laevis* which had similar sub-structure, tingenine B or 22(β)-hydroxytingenone (**66**) (Figure 1.4, p.21), was found to have the same system in rings C, D and E with a ketone and a hydroxyl group at positions-21 and 22, respectively. This was further confirmed by the 2D NMR experiments.

From the HMBC spectrum (Figure 3.111), the methyl singlet at δ_H 0.86 (Me-28) showed 3J correlations to the oxymethine carbon at δ_C 77.5, the methylene carbon at δ_C 29.6 (C-16), and to the methine carbon at δ_C 45.4 (C-18). Moreover, the methine proton at δ_H 1.83 assigned as H-18 also showed 3J correlation to the same oxymethine carbon. This established the attachment of the hydroxyl group at position-22. The 3J correlations from the methyl doublet at δ_H 1.07 (Me-30) and the methylene proton at δ_H 2.26 (H-19a) along with the 2J correlation from the methine quartet at δ_H 2.75 (H-20) to the carbonyl carbon at δ_C 214.2 [folded in the HMBC spectrum] confirmed the position of the ketone function on C-21 as clarified in Figure 3.111; (B). In COSY spectrum, a mutual correlations between the methylene protons (2H-19) and the methine proton (H-20) were observed as well as between (H-16a) and (2H-15) indicating their positions as neighbours in each spin system.

The constitution of rings A and B was determined by following the long range 1H - ^{13}C correlations. The aromatic methine proton at δ_H 6.67 (H-1) showed 3J

correlations to the carbons at δ_C 36.7 (C-9), 126.3 (C-5) and 139.8 (C-3), along with the 2J correlation to the carbon at δ_C 141.2 (C-2). The methyl singlet at δ_H 2.11 (Me-23) showed 3J correlations to the carbons at δ_C 126.3 (C-5) and 139.8 (C-3) as well as 2J correlation to the carbon at δ_C 122.2 (C-4). Furthermore, the methyl singlet at δ_H 1.23 (Me-25) showed 3J couplings to the carbons at δ_C 34.2 (C-11), 43.4 (C-8) and 143.8 (C-10) along with the 2J coupling to the quaternary carbon at δ_C 36.7 (C-9). In COSY spectrum, the methylene proton at δ_H 2.78 (1H, *m*, H-6a), which had long range 1H - ^{13}C correlations to the carbons at δ_C 126.3 (C-5) and 43.4 (C-8), showed a vicinal coupling to the methylene proton at δ_H 1.74 (H-7b). These observations indicated that the ring A is fully aromatic with two oxygen functions attached at C-2 and C-3 due to the fact that their chemical shifts were shifted downfield comparing to the optimal values of the ones in the benzene ring. The molecular formula of this compound (C₂₈H₄₀O₄) confirmed that these two oxygen functions should be hydroxyl groups.

The relative stereochemistry of the hydroxyl group (OH-22) was determined by observing the NOE correlations of the oxymethine proton (H-22) in the NOESY spectrum (Figure 3.113; A & B). H-22 showed mutual correlations with the methyl singlet Me-27 (δ_H 1.26), the methine proton H-20 (δ_H 2.75) and the methylene proton H-16a (δ_H 2.15). In turn, Me-27 showed mutual correlations with H-20 and H-8 (δ_H 1.82). These observations concluded that H-22, H-20, H-16a, H-8, and Me-27 should all be placed on the α side of the molecule, hence, Me-30 and OH-22 should be placed on the β side. On the other hand, the methyl singlet Me-28 (δ_H 0.86) showed NOE correlations with H-16b (δ_H 1.53) and H-18 (δ_H 1.83), which in turn correlated with the methyl singlet Me-26 (δ_H 1.02), therefore, they were all located on the β side of the molecule. The methyl singlet Me-23 (δ_H 2.11), emerging from the planar ring A, showed NOE effect to the methylene protons 2H-6 (δ_H 2.78/ 2.62), while the aromatic methine H-1 (δ_H 6.67) correlated with the methylene protons 2H-11 (δ_H 1.92-2.05 *m*). All the important NOE correlations are shown on the energy minimized 3D structure of HM-14 (Figure 3.114).

On the basis of these results and by comparison with previously published spectral data which were analogous to a large extent, HM-14 was identified as 2,3,22 β -trihydroxy-21-oxo-24,29-nor-D:A-friedooleana-1,3,5(10)-triene or regeol A

(Figure 3.106) (Takaishi *et al.*, 1997). This is the first report of the isolation of this compound from *M. laevis*. However, it was previously isolated from other plants of Celastraceae family such as *T. wilfordii* (stem bark) by Takaishi *et al.* (1997), where it showed moderate inhibition for the secretion of IL-1 α and IL-1 β from the human peripheral mononuclear cells. It was also isolated from other plants of the related family, Hippocrateaceae, such as *S. amplifolia* (roots) by Wang *et al.* (2011), and *S. chinensis* (stem) by Morikawa *et al.* (2003) where it exhibited an inhibitory effect on the rat lens aldose reductase with an IC₅₀ value of 30 μ M, as well as by Kishi *et al.* (2003) who reported the DPPH radical scavenging activity of regeol A (i.e. antioxidant activity) with SC₅₀ of 10 μ M. The present study reports its potent anti-tryanosomal activity at the preliminary tested concentration 20 μ M (for further details see section 4.2.2).

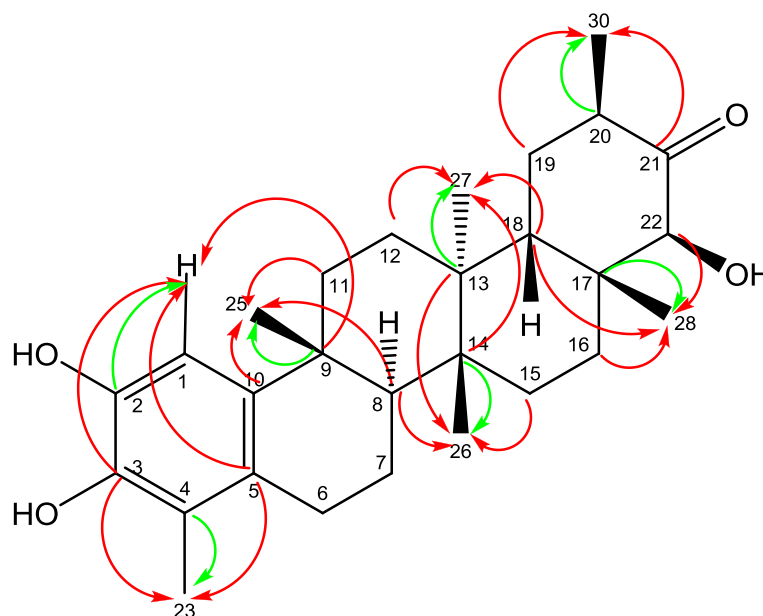


Figure 3.106: Structure of HM-14 with the HMBC correlations
 (\rightarrow) 3J (\rightarrow) 2J ^{13}C to 1H connectivity

Table 3.13: ^1H (400 MHz) and ^{13}C (100 MHz) NMR data of HM-14 in CDCl_3

Position	HM-14	
	δ_{H}	δ_{C}
1	6.67 (1H, <i>s</i>)	108.2
2	-	141.2
3	-	139.8
4	-	122.2
5	-	126.3
6	2.78 (1H, <i>m</i>)/ 2.62 (1H, <i>m</i>)	28.0
7	1.88 (1H, <i>m</i>)/ 1.74 (1H, <i>m</i>)	18.3
8	1.82 (1H, <i>m</i>)	43.4
9	-	36.7
10	-	143.8
11	(2H) [1.92-2.05 <i>m</i>]	34.2
12	1.69 (1H, <i>m</i>)/ 1.58 (1H, <i>m</i>)	30.1
13	-	40.0
14	-	39.3
15	(2H) [1.42-1.56 <i>m</i>]	28.0
16	2.15 (1H, <i>m</i>)/ 1.53 (1H, <i>m</i>)	29.6
17	-	44.9
18	1.83 (1H, <i>m</i>)	45.4
19	2.26 (1H, <i>m</i>)/ 1.72 (1H, <i>m</i>)	31.7
20	2.75 (1H, <i>q</i> , $J=6.3$ Hz)	41.3
21	-	214.2
22	4.59 (1H, <i>s</i>)	77.5
23	2.11 (3H, <i>s</i>)	11.4
24	-	-
25	1.23 (3H, <i>s</i>)	28.2
26	1.02 (3H, <i>s</i>)	15.3
27	1.26 (3H, <i>s</i>)	19.2
28	0.86 (3H, <i>s</i>)	25.2
29	-	-
30	1.07 (3H, <i>d</i> , $J=6.3$ Hz)	14.8

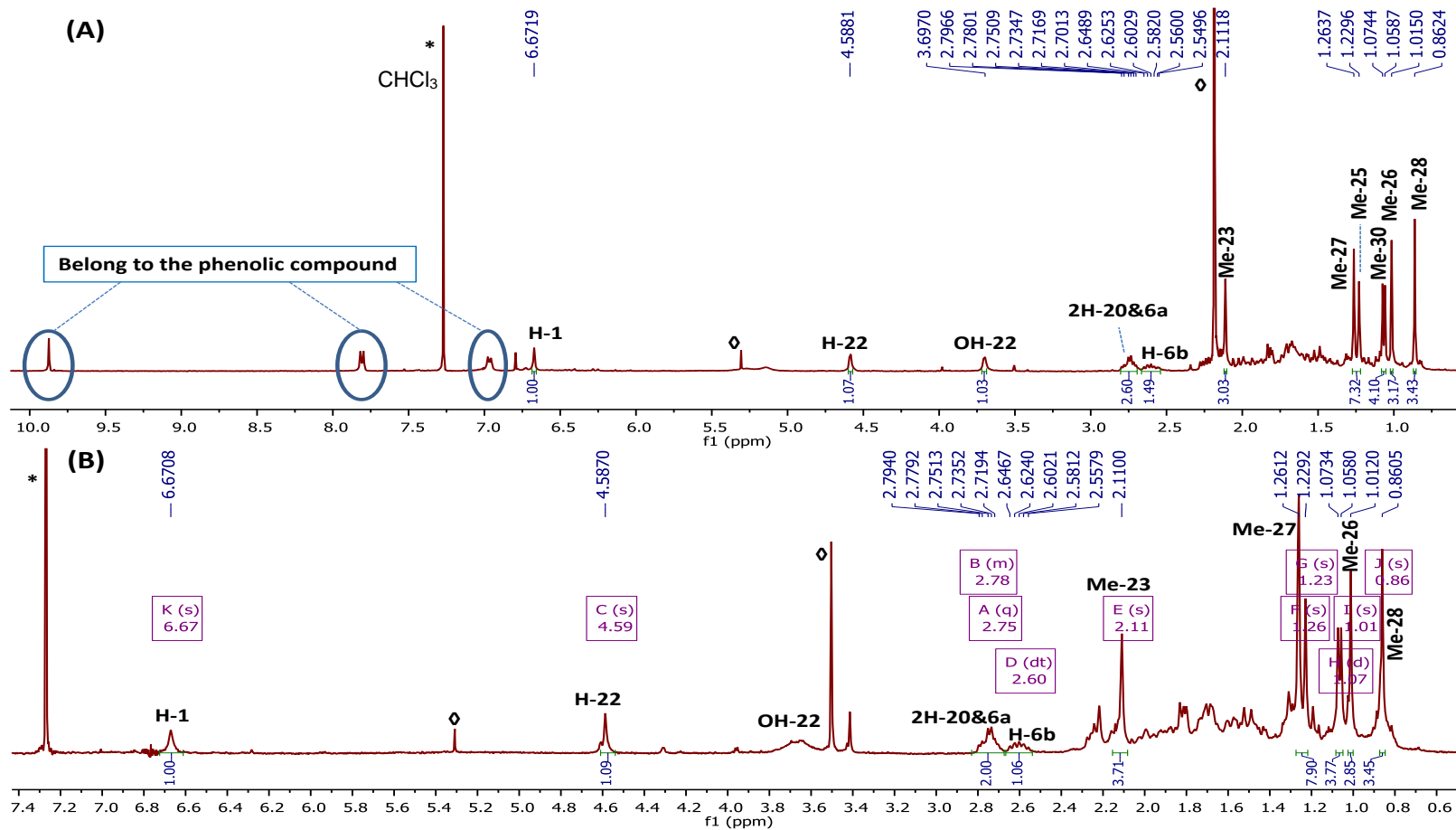


Figure 3.107: (A); ¹H NMR spectrum (400 MHz) of HM-14 in CDCl₃ in mixture, (◇) Solvent impurity [(CH₃)₂CO & DCM]
 (B); ¹H NMR spectrum (400 MHz) of HM-14 in CHCl₃ (*) after separation, (◇) Solvent impurity [MeOH & DCM]

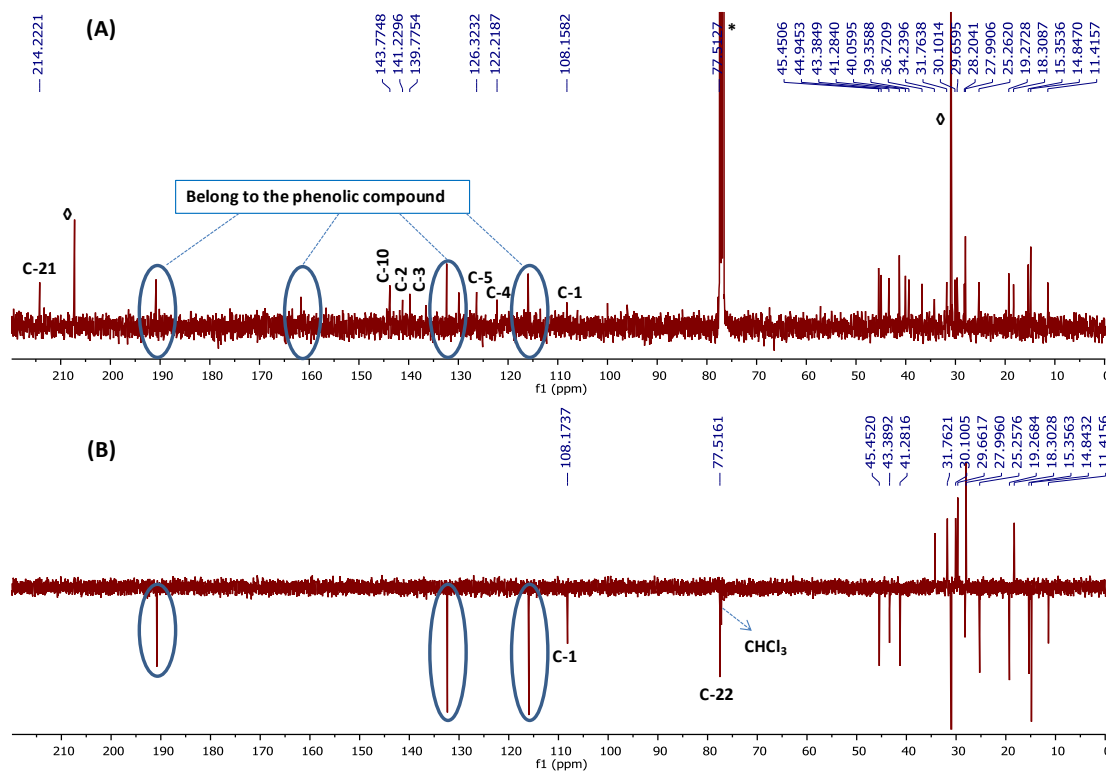


Figure 3.108: Full ^{13}C NMR (A) and DEPT 135 (B) spectra (100 MHz) of HM-14 in CDCl_3 (*), (\diamond) Solvent impurity [$(\text{CH}_3)_2\text{CO}$]

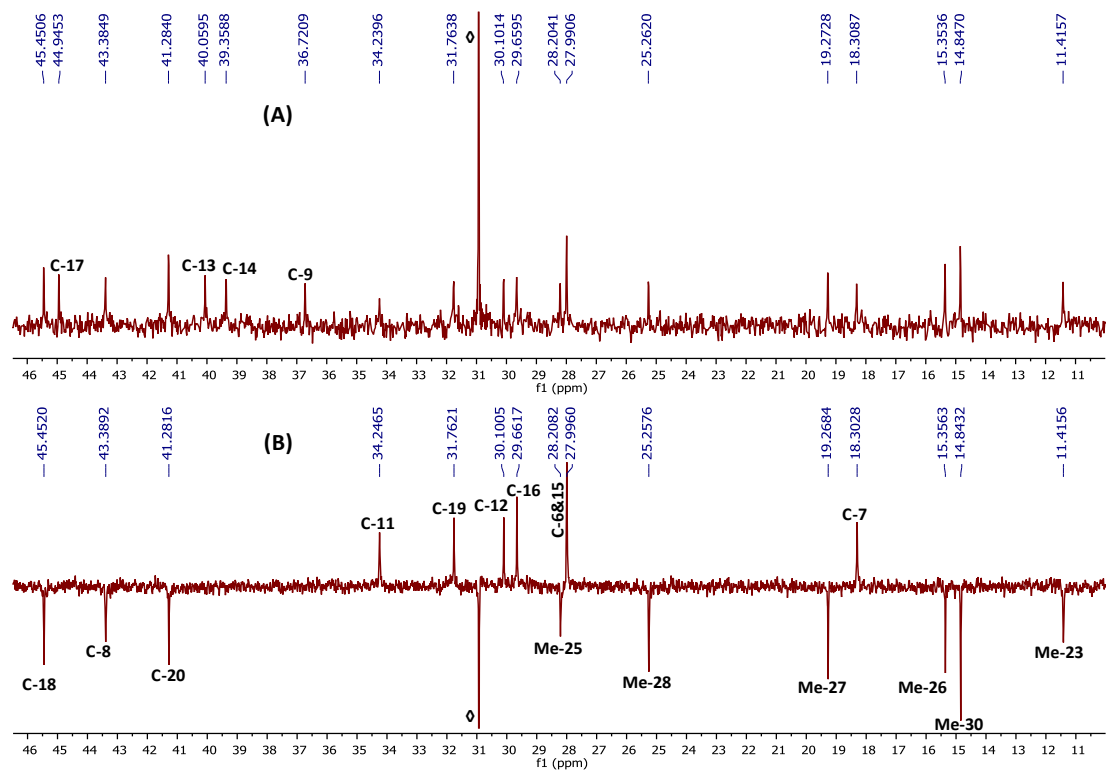
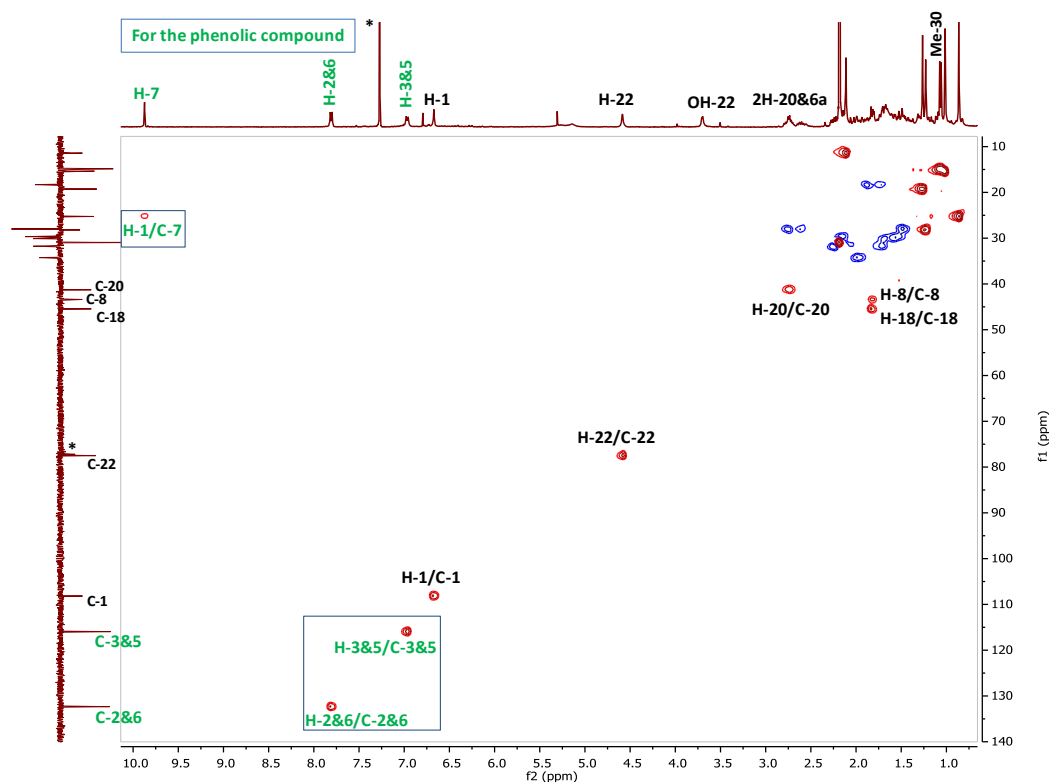
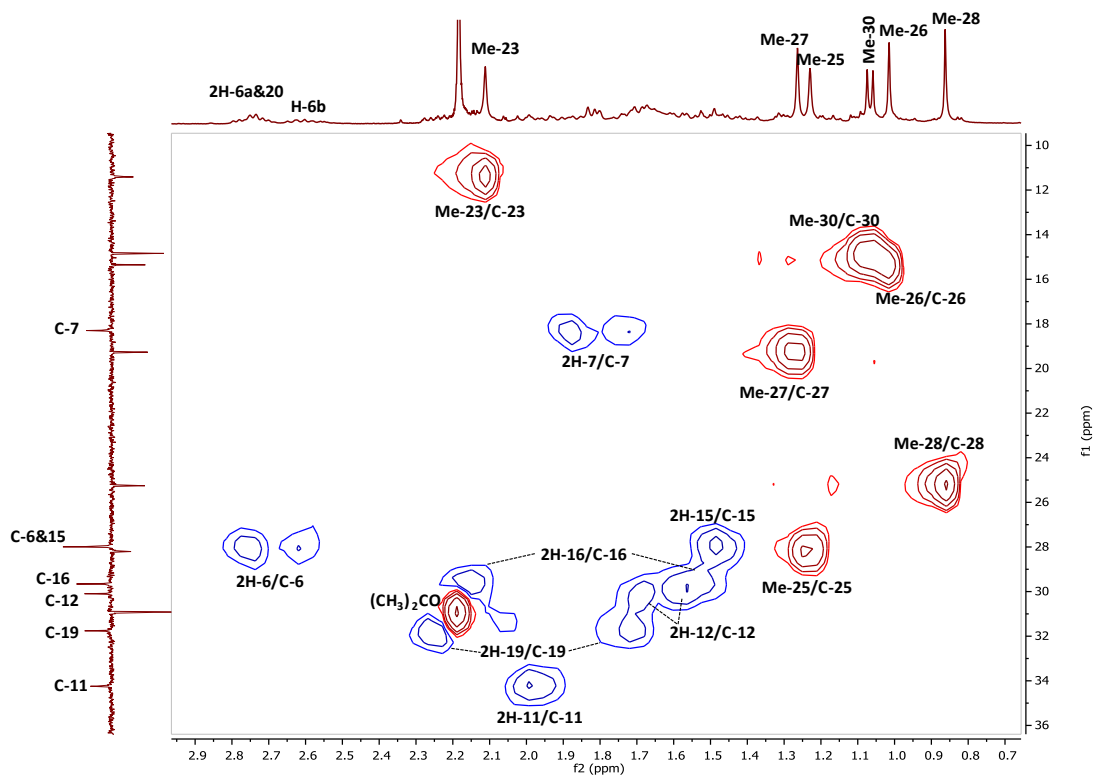


Figure 3.109: Selected expansion in the aliphatic region of ^{13}C NMR (A) and DEPT 135 (B) spectra (100 MHz) of HM-14 in CDCl_3 (*)

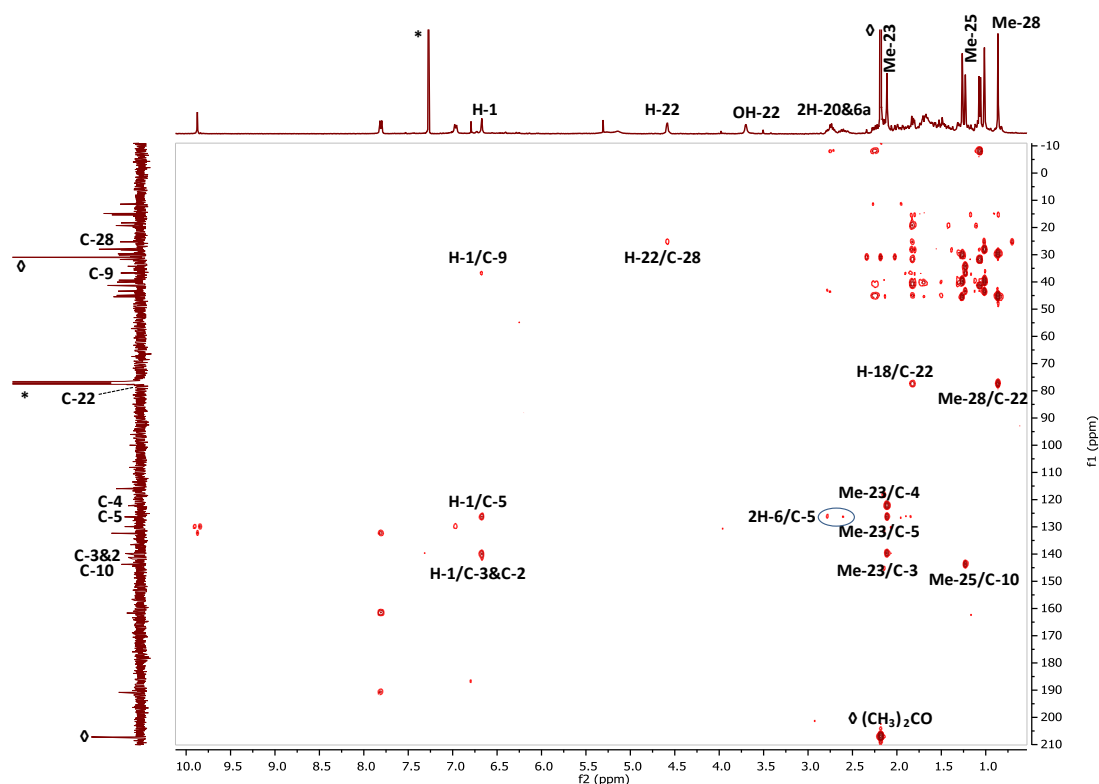


(A): Full HSQC spectrum

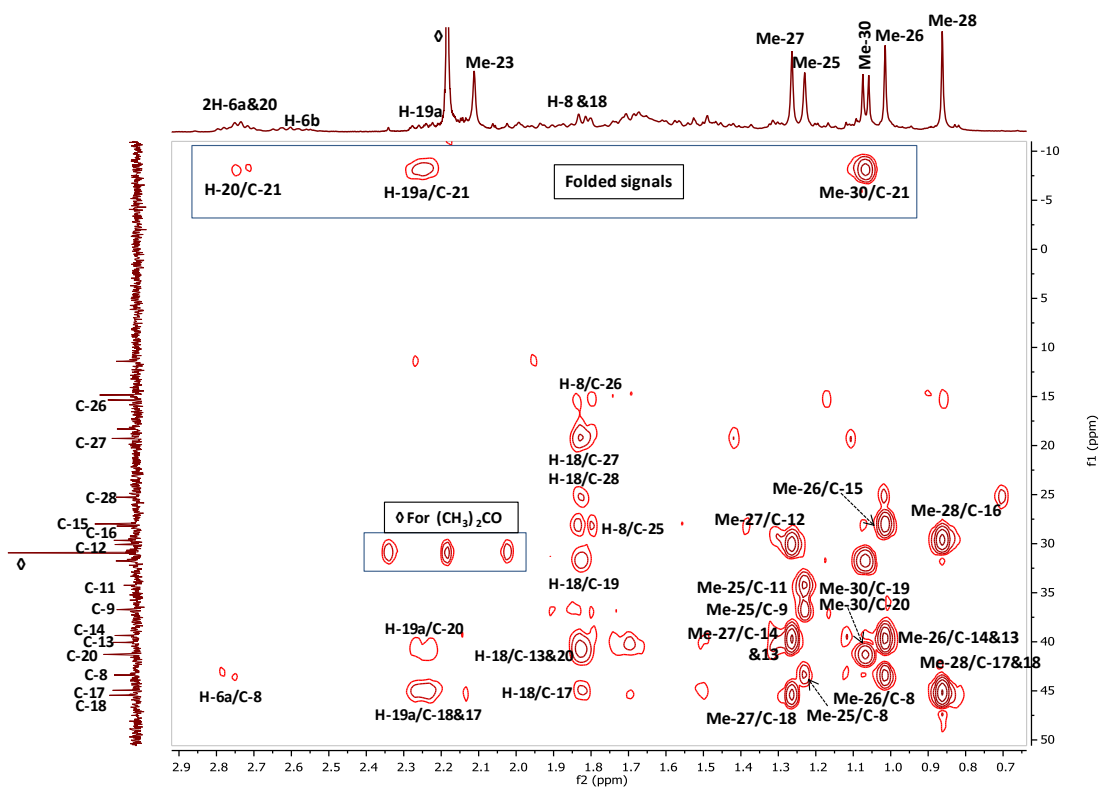


(B): Selected HSQC expansion

Figure 3.110: HSQC spectrum (400 MHz) of HM-14 in CDCl₃ (*)



(A): Full HMBC spectrum (400 MHz) with ^{13}C NMR spectrum as F_1 projection



(B): Selected HMBC expansion for the aliphatic region of F_2 domain

Figure 3.111: HMBC spectrum (400 MHz) of HM-14 in CDCl_3

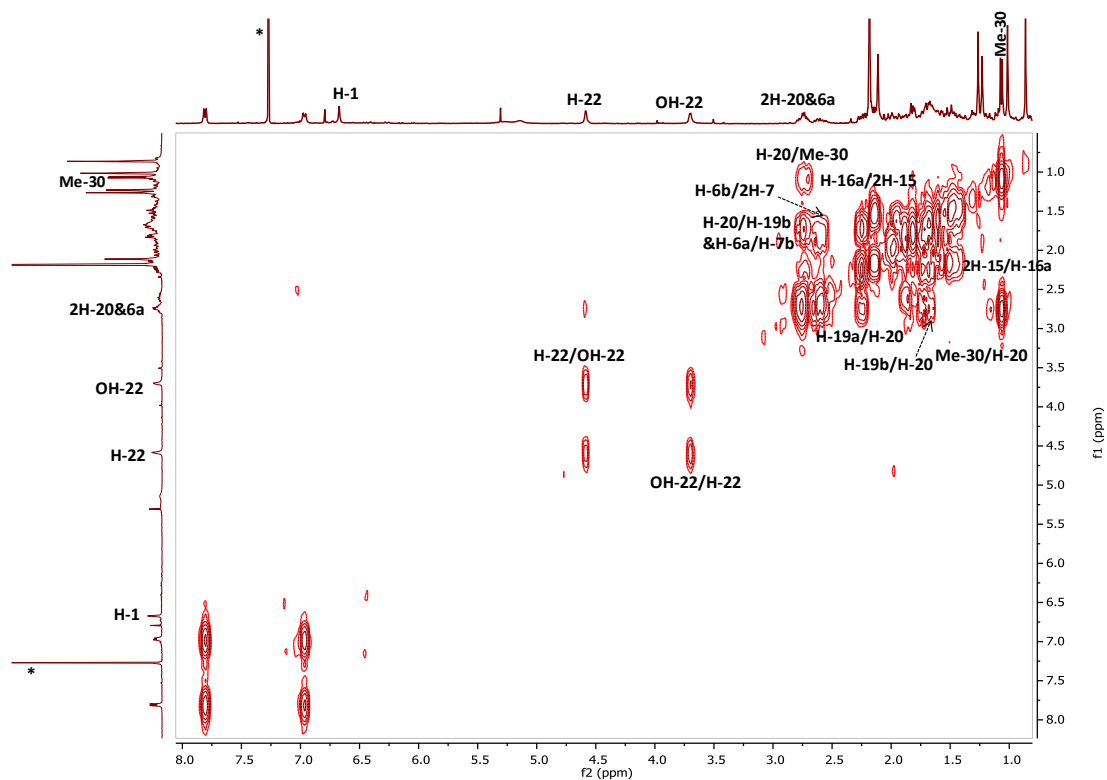


Figure 3.112: Full ^1H - ^1H COSY spectrum (400 MHz) of HM-14 in CDCl_3

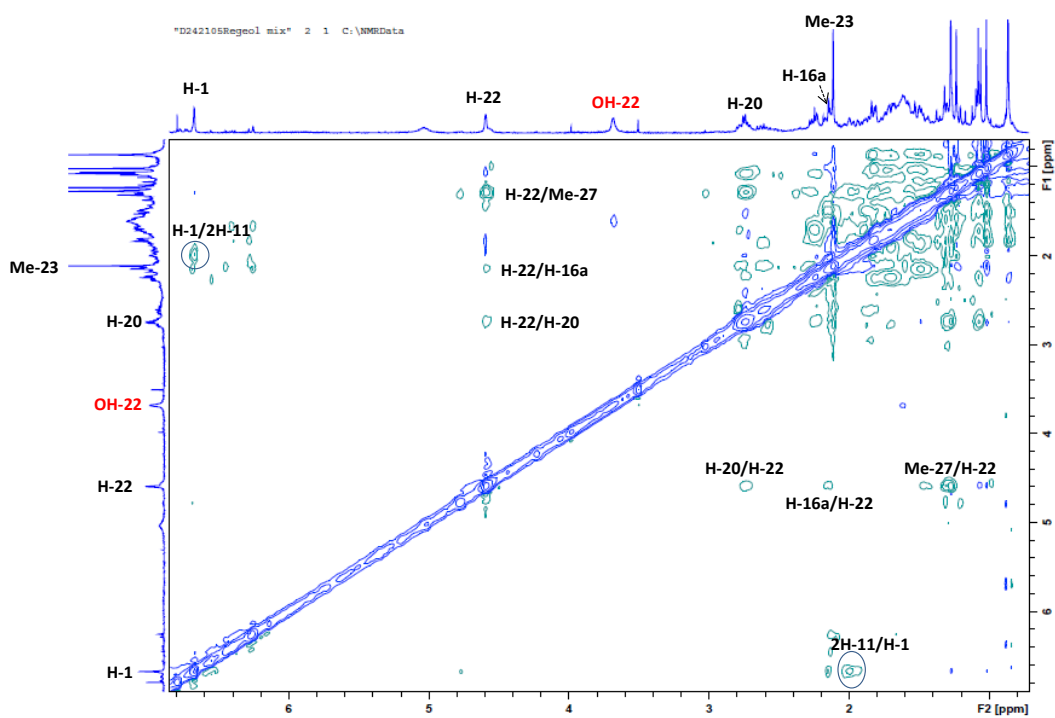


Figure 3.113: (A); Full NOESY spectrum (400 MHz) of HM-14 in CDCl_3 using TopSpin 3.2 software

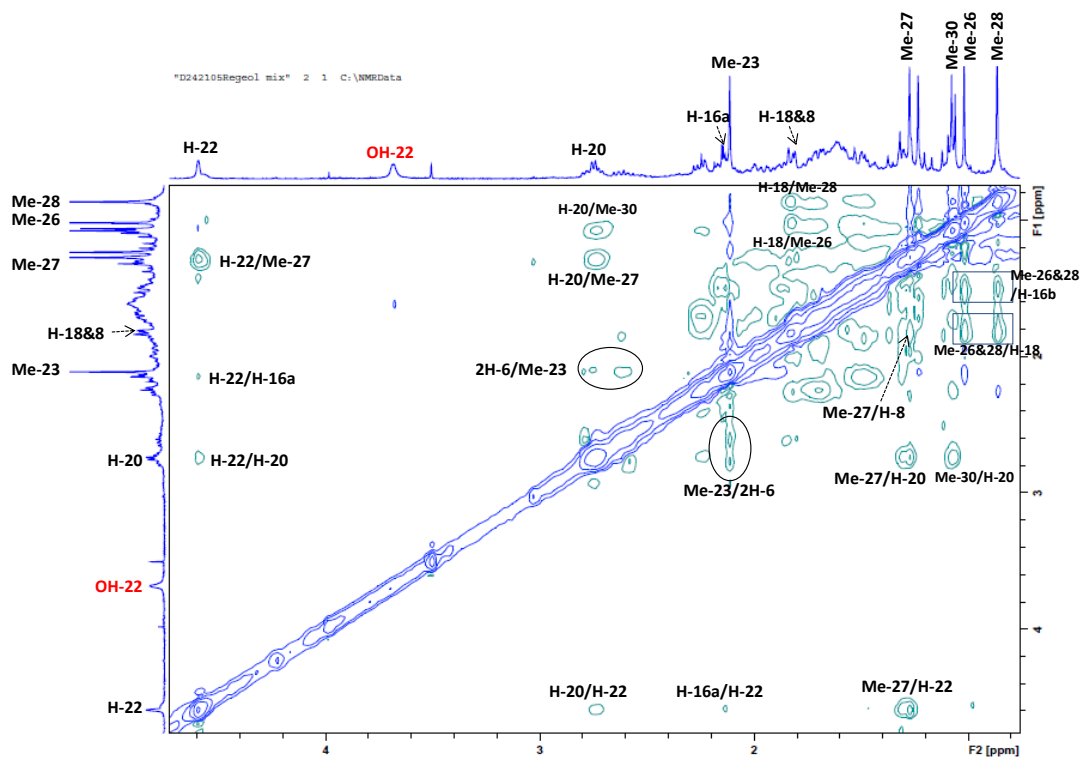


Figure 3.113 (Cont.): (B): Selected expansion of NOESY spectrum for the olefinic and aliphatic regions

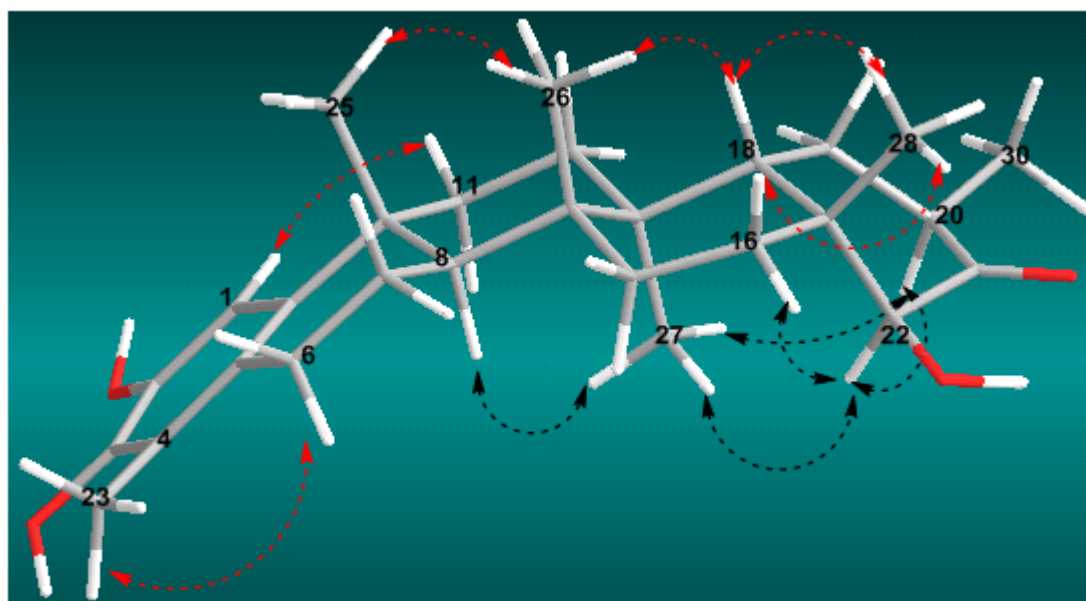


Figure 3.114: Energy minimised 3D structure of HM-14 showing NOESY correlations
 (↔) β (↔) α

3.3.3.3 Characterisation of HM-15 as the new aromatic triterpene, methyl 2,3,22 α -trihydroxy-24,25-dinorfriedelan-1,3,5(10),6,8,14-hexaen-29-oate

HM-15 was isolated from the EtOAc extract of the root bark by PTLC as a brown solid. On TLC, the compound appeared as a dark spot under UV light (λ 254 nm) and turned to purple after spraying with *p*-anisaldehyde-sulphuric acid reagent followed by heating. Its R_f was 0.27 on SiGel when eluted with the mobile phase 50% hexane in EtOAc.

The negative mode HRESI-MS spectrum showed a quasi-molecular ion $[M-H]^-$ at m/z 463.2491, suggesting a molecular formula of $C_{29}H_{36}O_5$ (DBE=12).

The optical rotation $[\alpha]_D^{20}$ was $+23^\circ$ ($c=0.1$, $CHCl_3$).

The IR spectrum exhibited absorption bands at 3395 cm^{-1} indicated the presence of hydroxyl groups, 2919 cm^{-1} for (=C-H) stretch, 1724 cm^{-1} for an ester C=O, and $1585, 1433\text{ cm}^{-1}$ for C-C stretch (in aromatic ring) (Williams and Fleming, 2008).

The $^1\text{H-NMR}$ spectrum (400 MHz, $(\text{CD}_3)_2\text{CO}$, Figure 3.116, Table 3.14) indicated the presence of a triterpene type compound. It displayed five methyl singlets at δ_H 0.77, 1.15, 1.41, 1.90 and 2.51, which were assigned with the aid of the HSQC and HMBC experiments for Me-27, Me-28, Me-30, Me-26 and Me-23, respectively. A carboxymethyl group at δ_H 3.65 attributed to (3H-31) was also shown. The three usual characteristic protons of the quinonemethide moiety were shifted downfield as they appeared at δ_H 7.20 (1H, *d*, $J = 8.6$ Hz, H-7), 7.31 (1H, *br.s*, H-1) and 7.61 (1H, *d*, $J = 8.6$ Hz, H-6). The HSQC spectrum (Figure 3.118) revealed the presence of a proton signal at δ_H 3.62, which was not clear in the $^1\text{HNMR}$ spectrum, attached to an oxymethine carbon at δ_C 75.8.

The molecular formula of this compound confirmed that it comprised of 29 carbons. However, from the DEPTq135 ^{13}C NMR spectrum (100 MHz, Figure 3.117), only 27 carbon signals were assigned for this compound counting for five methyls, five methylenes, four methines, one oxymethine at δ_C 75.8, ten quaternary carbons including two oxygen-bearing carbons at δ_C 146.4 and 144.1, one methoxyl carbon at δ_C 52.0 and one carbonyl carbon signal at δ_C 179.5 attributed to C-29. The rest of the two carbons, which appeared to be olefinic quaternaries at δ_C 133.4 and 126.1, were extracted by following the $^1\text{H-}^{13}\text{C}$ long range correlations in the HMBC spectrum.

The three aromatic protons have an arrangement pattern in the ^1H NMR spectrum "typical" of that, yet much more deshielded, of the quinonemethide compounds. This was further confirmed from COSY spectrum (Figure 3.120) as the mutual correlations between H-6 and H-7 was observed. However, these protons showed the following 3J correlations in the HMBC spectrum (Figure 3.119; B); the deshielded proton at δ_{H} 7.31 (H-1) correlated to the aromatic quaternary carbons at δ_{C} 128.5 (C-5) and 144.1 (C-3), and the methine proton at δ_{H} 7.61 (H-6) correlated to the aromatic quaternaries at δ_{C} 116.9 (C-4), 127.6 (C-10) and 133.2 (C-8), while the methine proton (H-7) at δ_{H} 7.20 correlated to those at δ_{C} 128.5 (C-5), 133.4 (C-9) and the olefinic quaternary at δ_{C} 137.0. These observations suggested that these protons were positioned on fully aromatic six-membered rings A and B. This sub-structure justified the absence of the sixth methyl signal (Me-25) which is usually observed in attachment with the aliphatic carbon (C-9) of a quinonemethide fragment (see earlier celasroloids 3.3.2).

Furthermore, as seen in the HMBC spectrum (Figure 3.119; A&C) both methyls at δ_{H} 1.90 (Me-26) and 0.77 (Me-27) have 3J correlations to the olefinic quaternary at δ_{C} 137.0. The former methyl correlated to another olefinic quaternary at δ_{C} 126.1 and to a methylene carbon at δ_{C} 40.7 (C-16), while the latter methyl correlated to a methylene carbon at δ_{C} 38.9 (C-12), a methine at δ_{C} 41.7 (C-18) and to an aliphatic quaternary at δ_{C} 39.55 (C-13). This concluded that the methyl Me-26 was attached at position-15 in ring D and not aligned on the junction C/D with Me-27, in addition that the conjugated system in rings A and B was extended by the double bond at Δ 14, 15. Moreover, the 3J and 2J correlations observed from the singlet methyl at δ_{H} 1.15 (Me-28) to the oxymethine carbon at δ_{C} 75.8, the methylene at δ_{C} 40.7 (C-16), the methine at δ_{C} 41.7 (C-18) and to the quaternary at δ_{C} 39.53 (C-17), respectively, suggested the attachment of a secondary hydroxyl group at C-22. The 3J correlations from the methylene protons (2H-16a/b) at δ_{H} 2.49/ 1.65 to the oxymethine carbon at δ_{C} 75.8 gave additional evidence for the aforementioned attachment. In COSY spectrum, the mutual vicinal couplings between H-22/H-21a and H-22/ H-21b were observed. The presence of an ester group was confirmed by the 3J correlations from the singlet at δ_{H} 3.65 (3H-31) as well as from the methyl singlet at δ_{H} 1.41 (Me-30) to the carbonyl carbon at δ_{C} 179.5 (C-29).

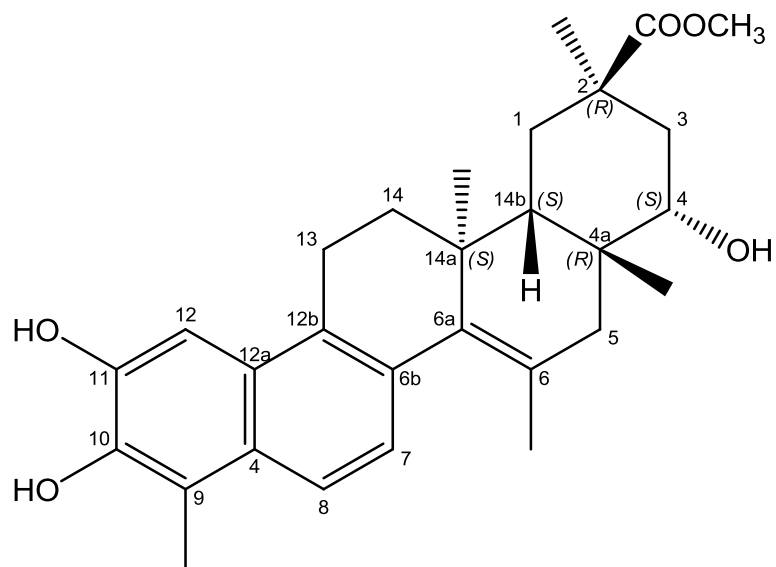
Depending on the molecular formula and the fact of the absence of another ketone carbon signal, besides the shielding effect on the methine carbon at δ_C 104.1 (C-1), the attachment of a hydroxyl group at C-2 rather than a ketone and another on at C-3 was confirmed.

The relative stereochemistry of HM-15 was determined by tracking the NOE correlations in the NOESY spectrum (Figure 3.121; A & B) and by applying them on the energy minimised 3D model obtained by ChemDraw Ultra 11.0 software as seen in Figure 3.122; (A & B).

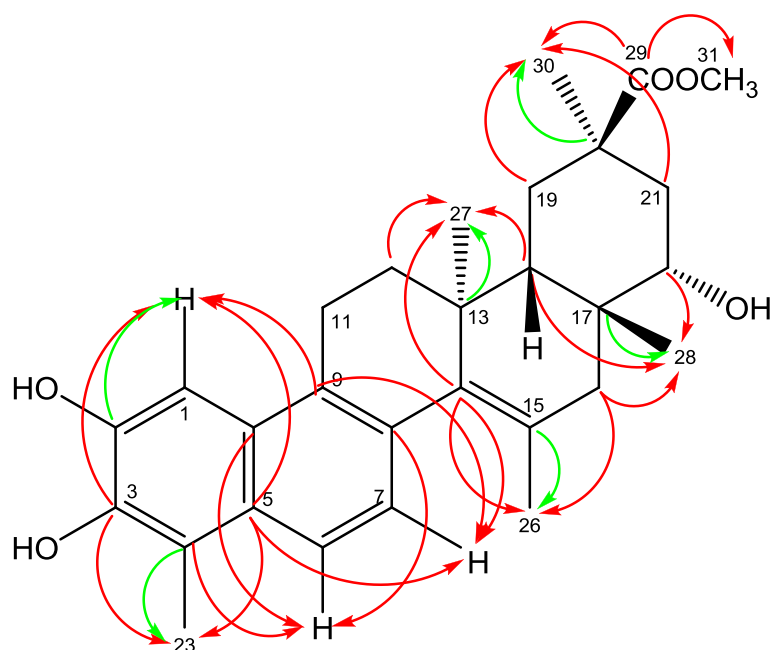
The mutual NOE correlations between H-1/ H-11a_{eq} (δ_H 3.08, *dt*, $J=15.3$, 5.6 Hz), H-6/Me-23 and H-7/Me-26 were typical to those seen in the isolated quinonemethide triterpenes. The oxymethine proton H-22 (δ_H 3.62, *m*) was found to have a small coupling with its adjacent methylene proton H-21a_{eq} (δ_H 2.20, *dd*, $J=3.7$, 14.2 Hz) rather than H-21b_{ax} (δ_H 1.68, *m*), which accounted for its *trans*-diaxial configuration with H-21b. In NOESY spectrum, this oxymethine showed correlations with the methine H-18 (δ_H 1.88) and Me-28 (δ_H 1.15), which in turn showed NOE correlations with the latter proton (H-18), the methylene protons H-12a (δ_H 2.34), H-11b_{ax} (δ_H 2.66, *ddd*, $J=15.3$, 7.7 Hz) and H-16b (δ_H 1.65), which also in turn correlated with Me-26 (δ_H 1.90). These observations led to a conclusion that H-22/ H-18/ Me-28/ H-12a/ H-11b and H-16b should all be positioned on the β side of the molecule, hence, the secondary hydroxyl group (OH-22) should be located on the α side with an equatorial orientation. On the other hand, the Me-27 (δ_H 0.77) showed NOE correlations with the H-16a (δ_H 2.49), the methylene protons H-19a/b (δ_H 1.84/1.67) and H-12b (δ_H 1.39) indicating their locations on the α side of the molecule. Finally, the Me-30 (δ_H 1.41) was placed on the α side of the of ring E due to its NOE correlation with the methylene proton H-21b (δ_H 1.68).

The complete assignment of HM-15 by the analysis of the 2D NMR experiments, and other spectroscopic techniques, established it to be identified as (2R,4S,4aR,14aS,14bS) -methyl 4,10,11-trihydroxy-2,4a,6,9,14a-pentamethyl-1,2,3,4,4a,5,13,14,14a,14b-decahydropicene-2-carboxylate (Figure 3.115: A). This compound, for which the trivial name methyl 2,3,22 α -trihydroxy-24,25-dinorfriedelan-1,3,5(10),6,8,14-hexaen-29-oate (Figure 3.115; B) is proposed, was determined as a new aromatic triterpene. The cytotoxicity of HM-15 was also

evaluated here, and it showed a moderate, yet selective activity against the melanoma cell line A375 (see section 4.1.1.2 for more details).



(A): Structure of HM-15 with the IUPAC numbering system



(B): Structure of HM-15 with the non-systematic numbering and the key HMBC correlations
 (\rightarrow) 3J (\rightarrow) 2J

Figure 3.115: Structure of HM-15 by two numbering systems

Table 3.14: ^1H (400 MHz) and ^{13}C (100 MHz) NMR data of HM-15 in acetone- d_6

Position	HM-15	
	δ_{H}	δ_{C}
1	7.31 (1H, <i>br.s</i>)	104.1
2	-	146.4
3	-	144.1
4	-	116.9
5	-	128.5
6	7.61 (1H, <i>d</i> , $J=8.6$ Hz)	120.1
7	7.20 (1H, <i>d</i> , $J=8.6$ Hz)	126.4
8	-	133.24 ^a
9	-	133.37 ^a
10	-	127.5
11	3.08 (1H, <i>dt</i> , $J=15.3, 5.6$ Hz)/ 2.66 (1H, <i>ddd</i> , $J=15.3, 7.7$ Hz)	23.7
12	2.34 (1H, <i>m</i>)/ 1.39 (1H, <i>m</i>)	38.9
13	-	39.53 ^b
14	-	137.0
15	-	126.1
16	2.49 (1H, <i>d</i> , $J=11.7$ Hz)/ 1.65 (1H, <i>m</i>)	40.7
17	-	39.55 ^b
18	1.88 (1H, <i>m</i>)	41.7
19	1.84 (1H, <i>m</i>)/ 1.67 (1H, <i>m</i>)	33.6
20	-	42.4
21	2.20 (1H, <i>dd</i> , $J=14.2, 3.7$ Hz)/ 1.68 (1H, <i>m</i>)	36.9
22	3.62 (1H, <i>m</i>)	75.8
23	2.51 (3H, <i>s</i>)	11.1
24	-	-
25	-	-
26	1.90 (3H, <i>s</i>)	23.4
27	0.77 (3H, <i>s</i>)	26.6
28	1.15 (3H, <i>s</i>)	25.3
29	-	179.5
30	1.41 (3H, <i>s</i>)	24.9
31	3.65 (3H, <i>s</i>)	52.0

a, b These carbons are exchangeable

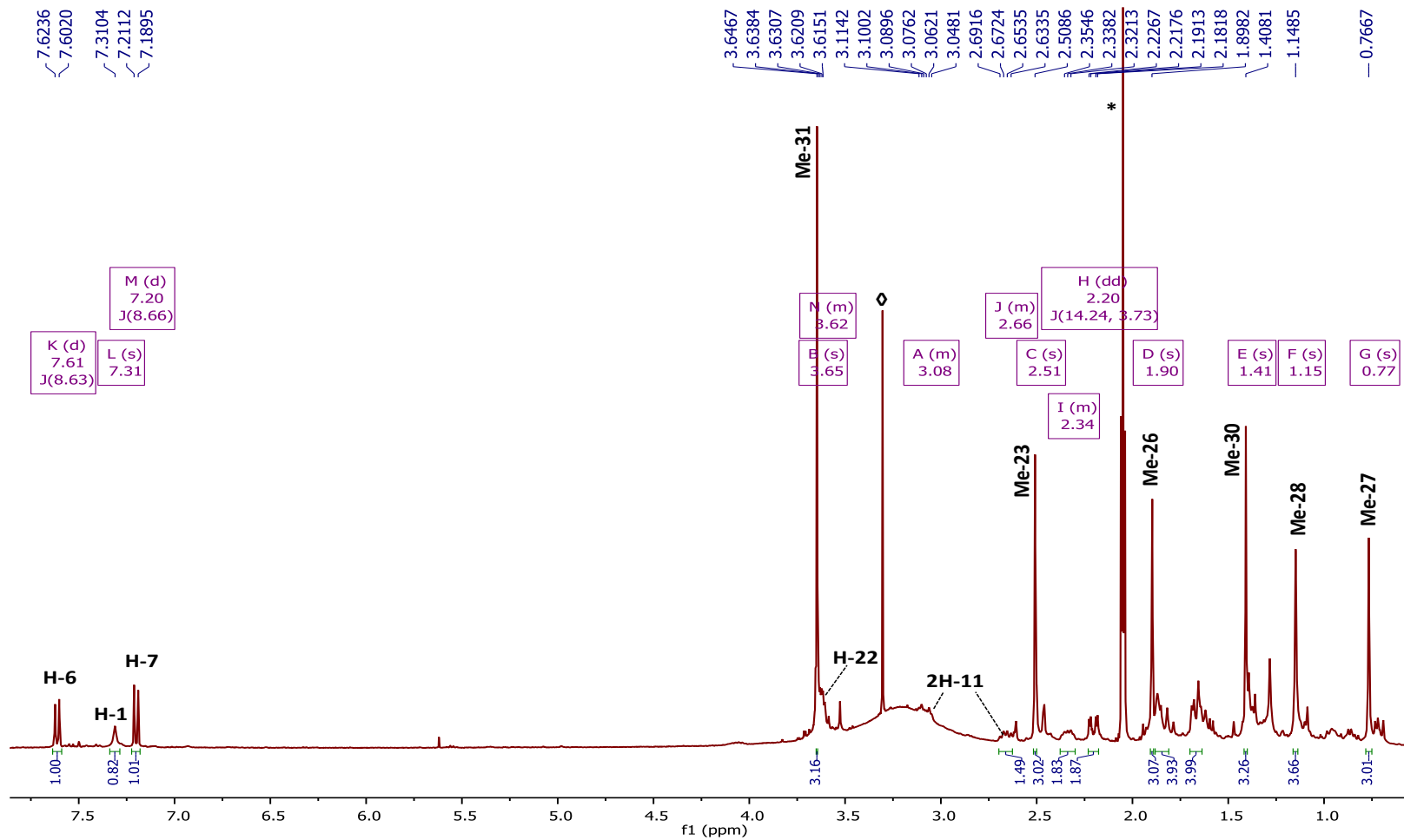


Figure 3.116: ^1H NMR spectrum (400 MHz) of HM-15 in $(\text{CD}_3)_2\text{CO}$; (*) $(\text{CH}_3)_2\text{CO}$ residue, (\diamond) Solvent impurity [MeOH]

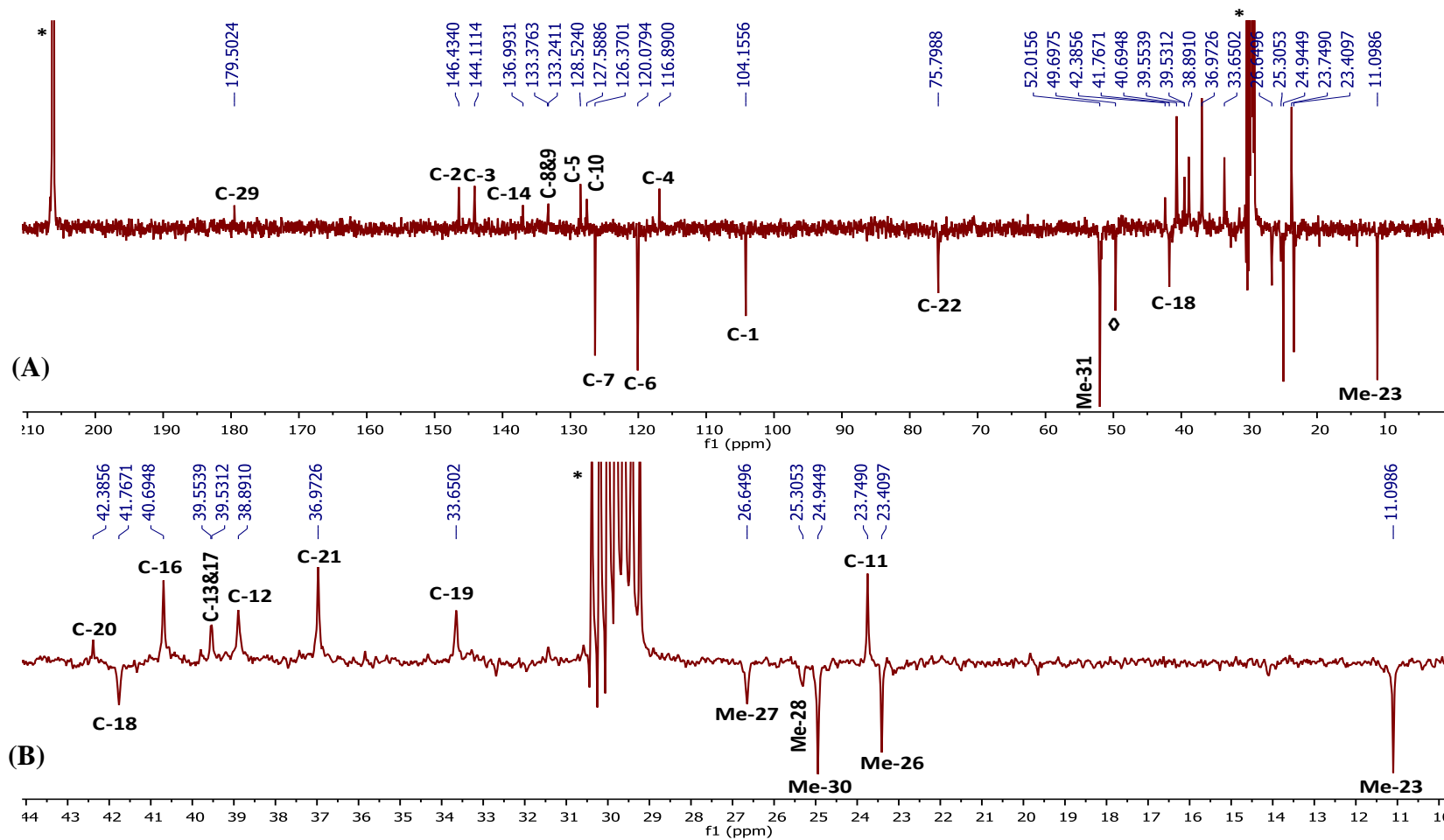
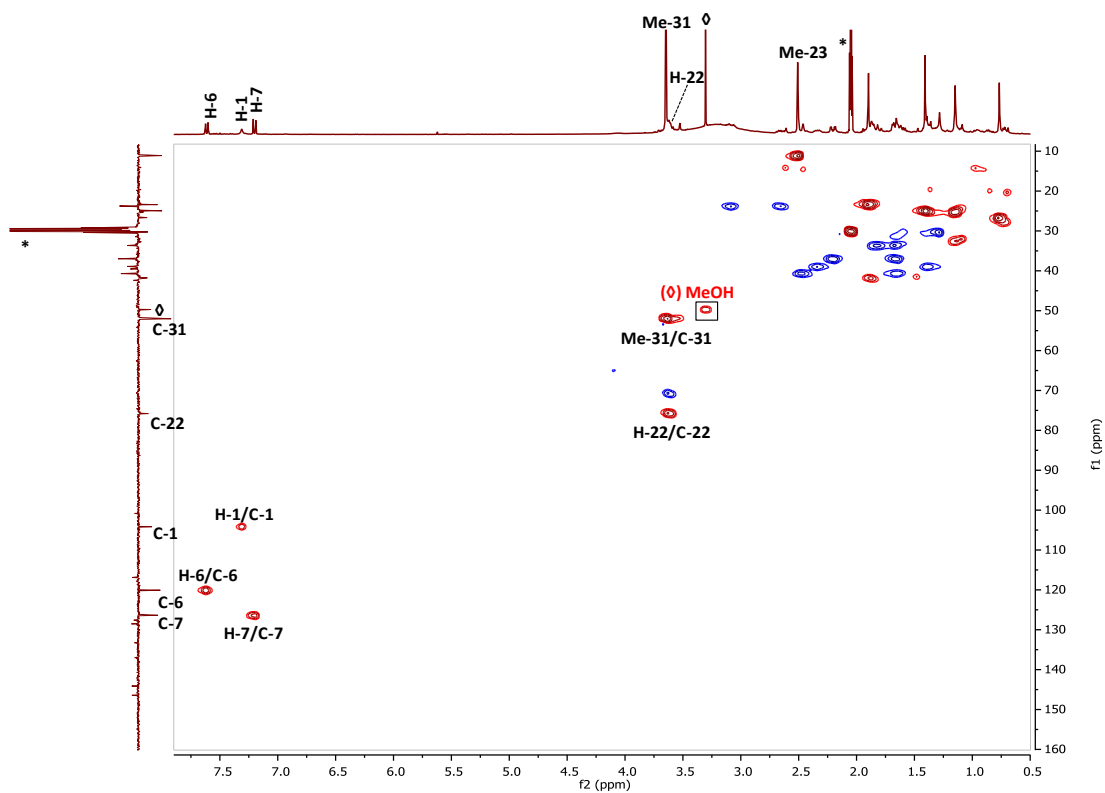
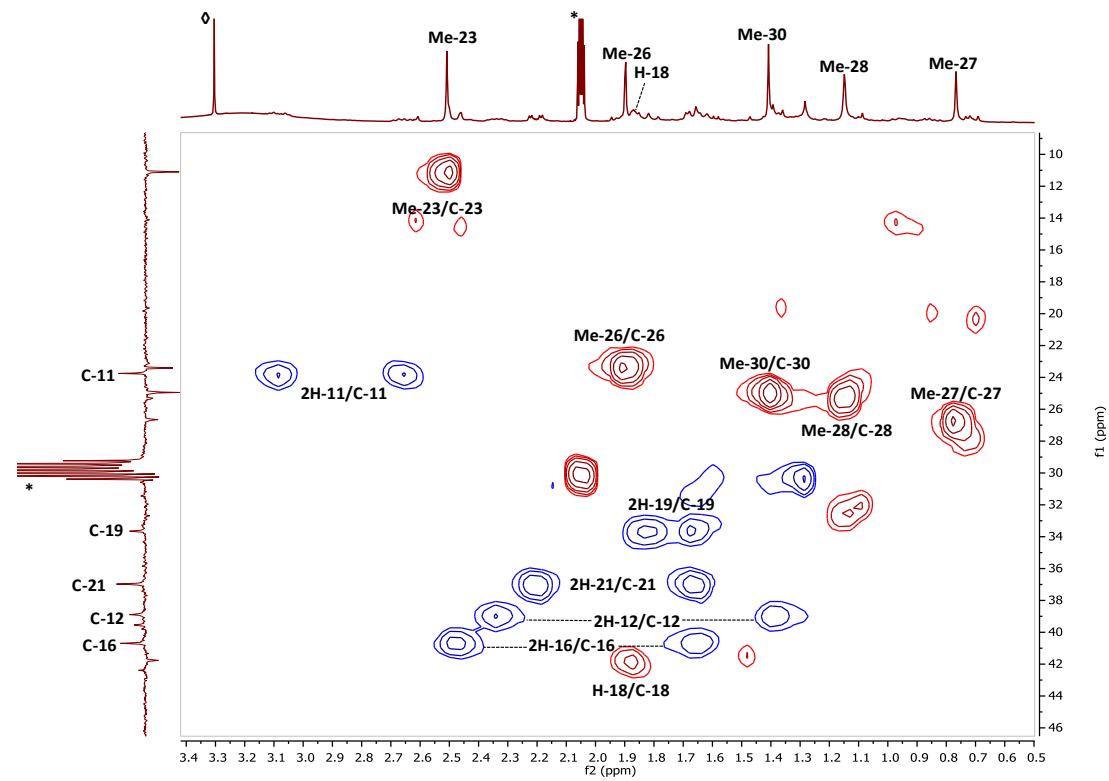


Figure 3.117: (A): Full DEPTq ^{13}C NMR spectrum (100 MHz) of HM-15 in $(\text{CD}_3)_2\text{CO}$ (*); (B): Selected expansion in aliphatic region

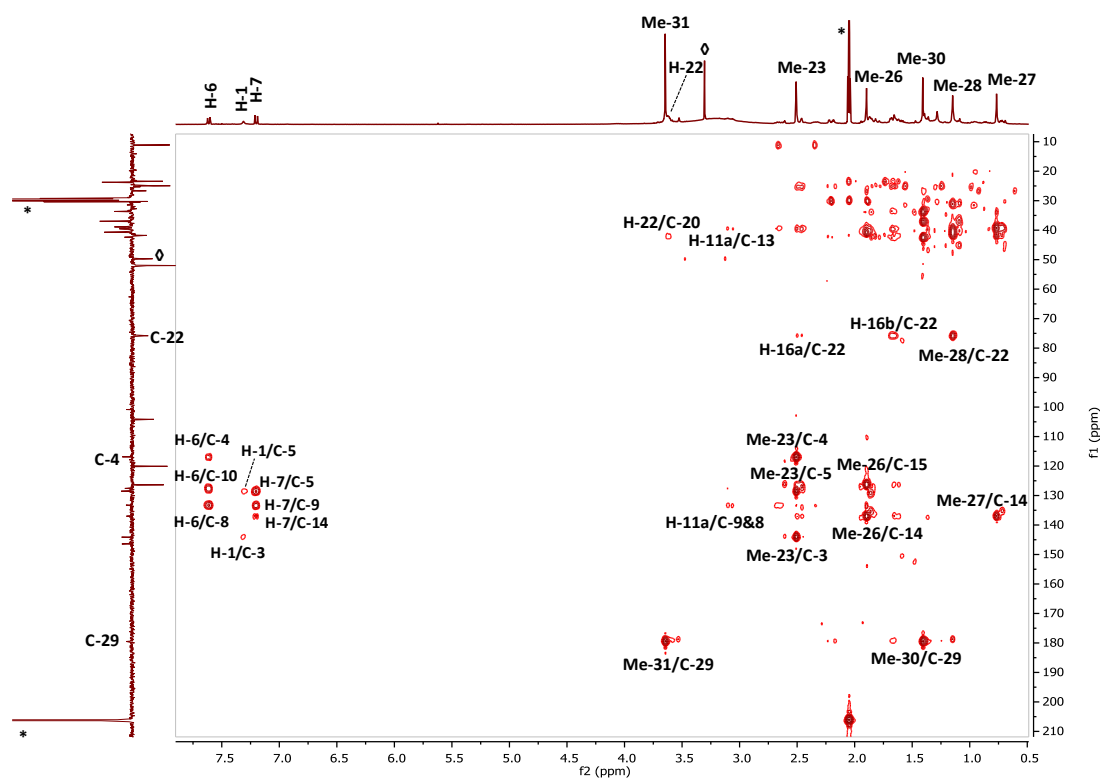


(A)

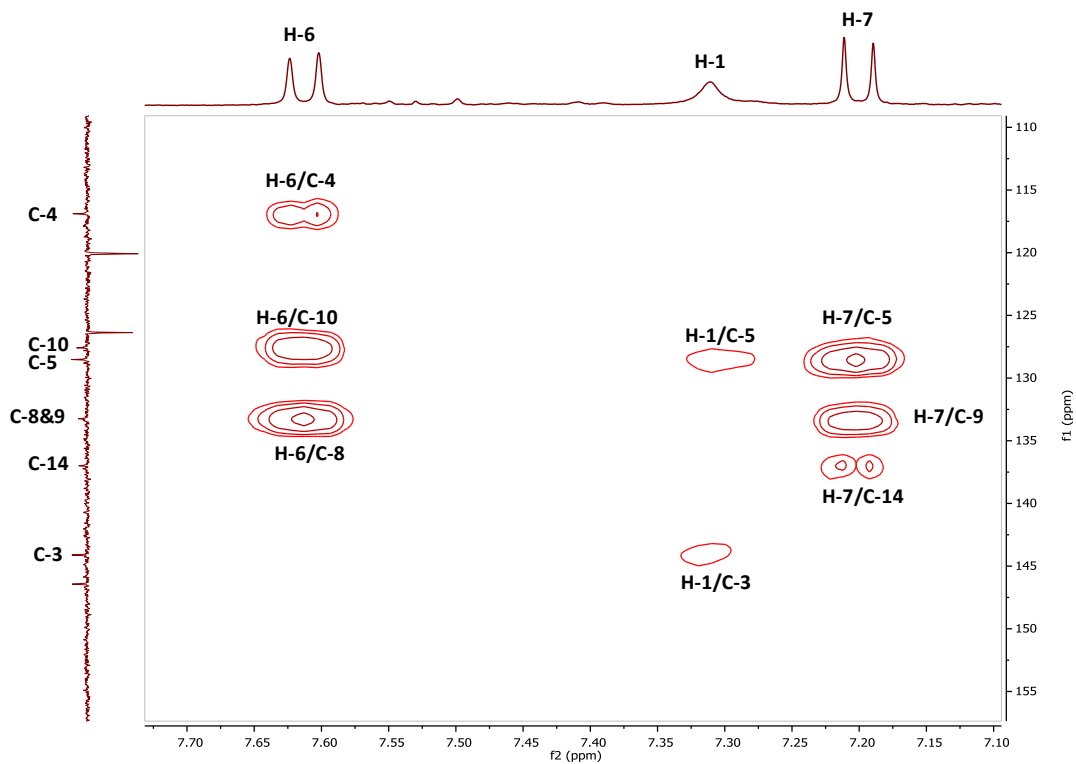


(B)

Figure 3.118: HSQC spectrum (400 MHz) of HM-15 in $(\text{CD}_3)_2\text{CO}$ (*)
 A: Full HSQC; B: Selected HSQC expansion



(A)



(B)

Figure 3.119: HMBC spectrum (400 MHz) of HM-15 in $(\text{CD}_3)_2\text{CO}$ (*)
(A): Full HMBC; (B): Selected HMBC expansion of the aromatic region of F_1 & F_2

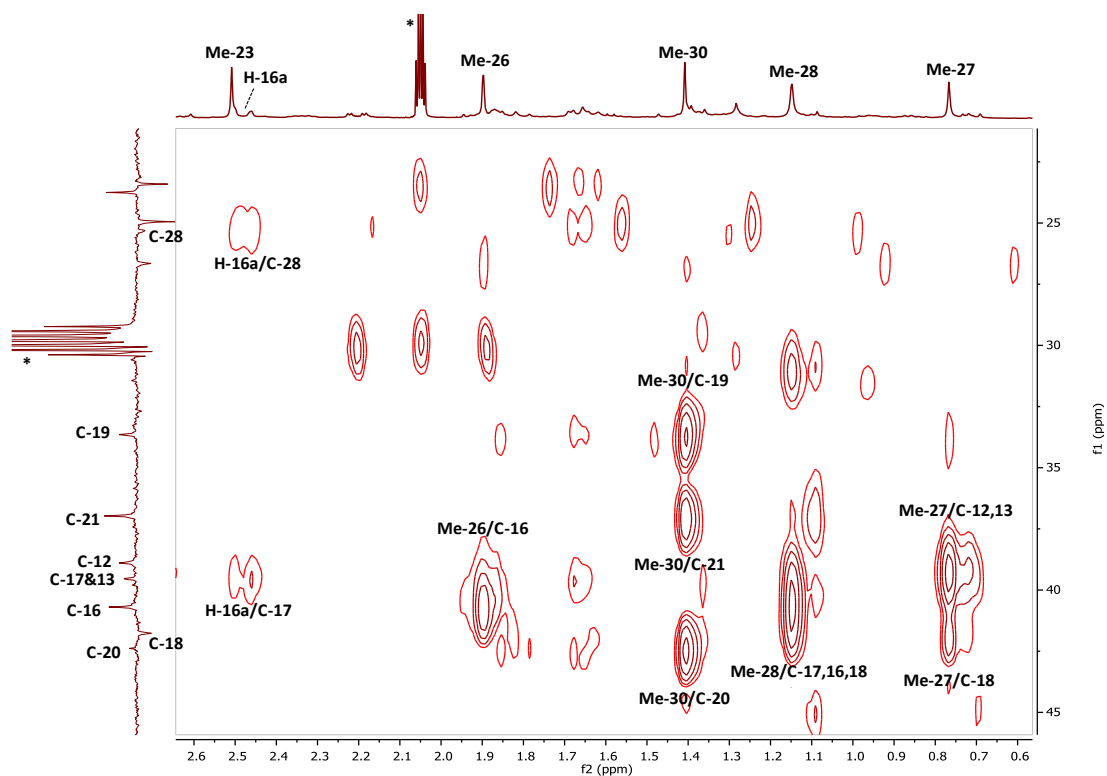


Figure 3.119 (Cont.): (C): Selected HMBC expansion of the methyl groups

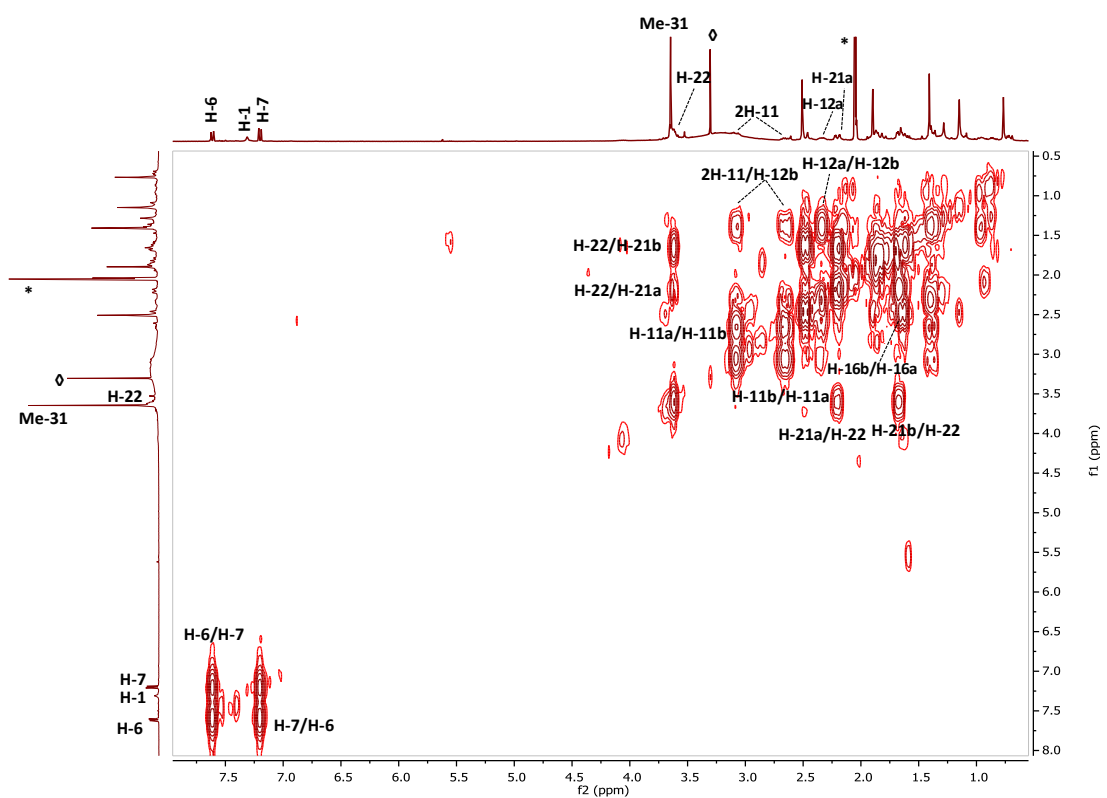
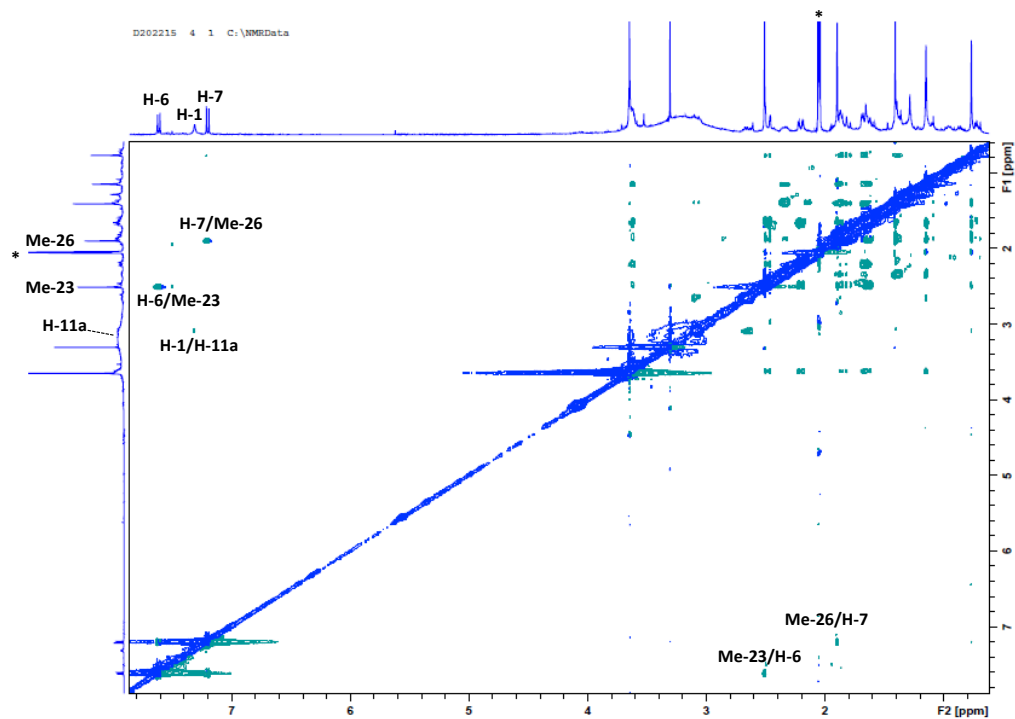
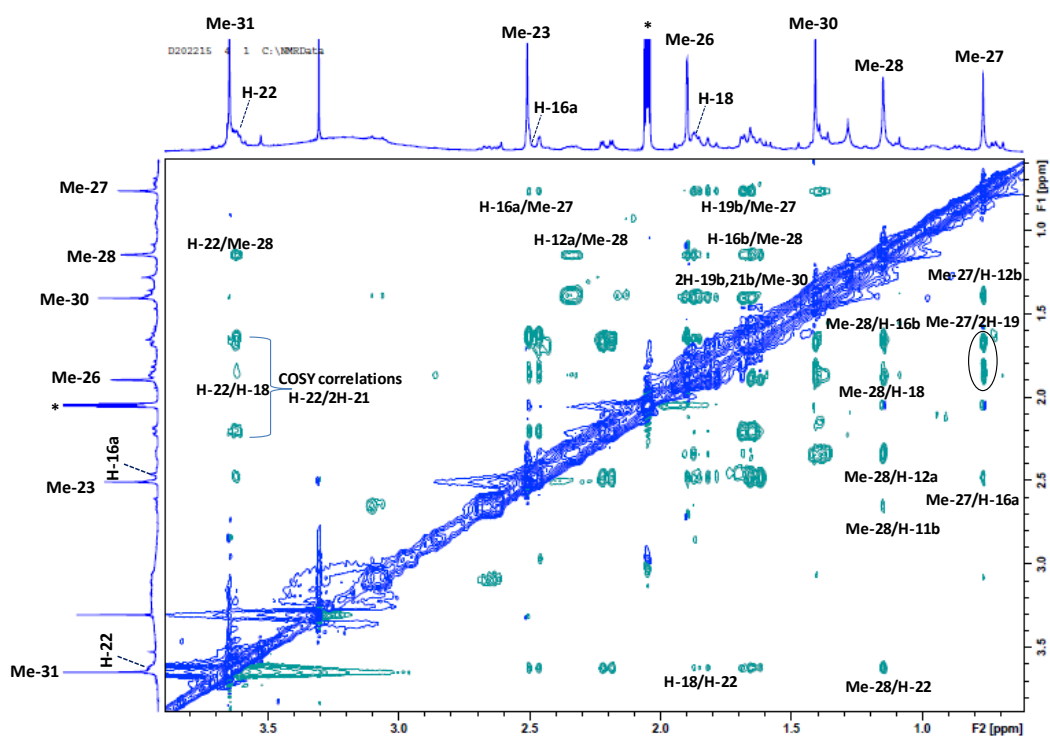


Figure 3.120: Full ^1H - ^1H COSY spectrum (400 MHz) of HM-15 in $(\text{CD}_3)_2\text{CO}$; (\diamond) Solvent impurity [MeOH]

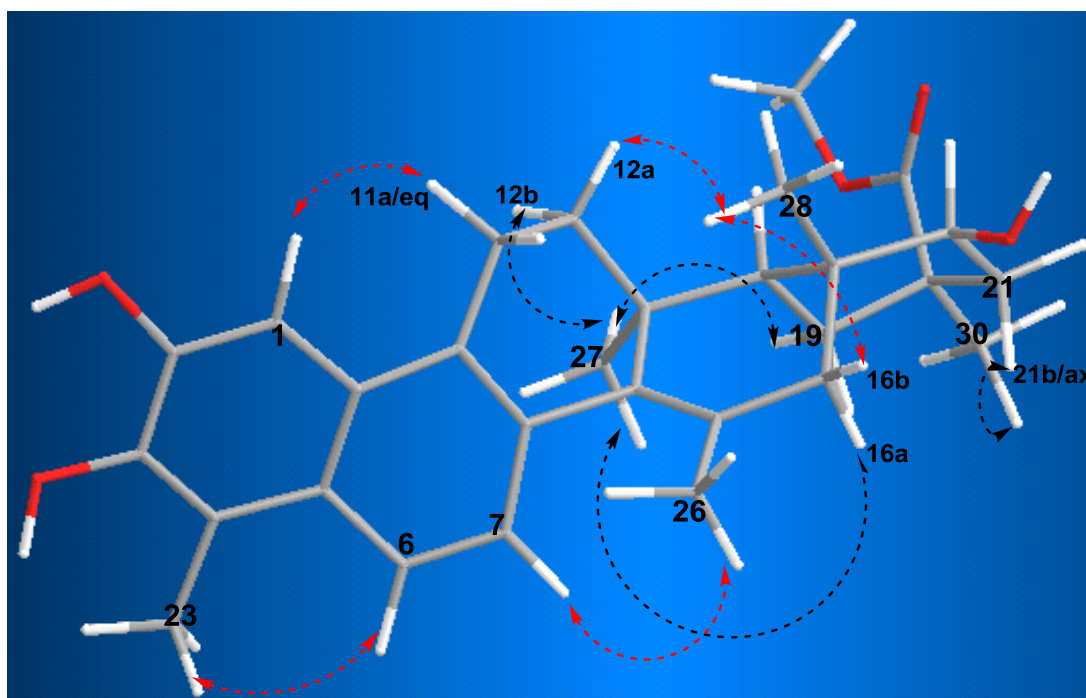


(A)

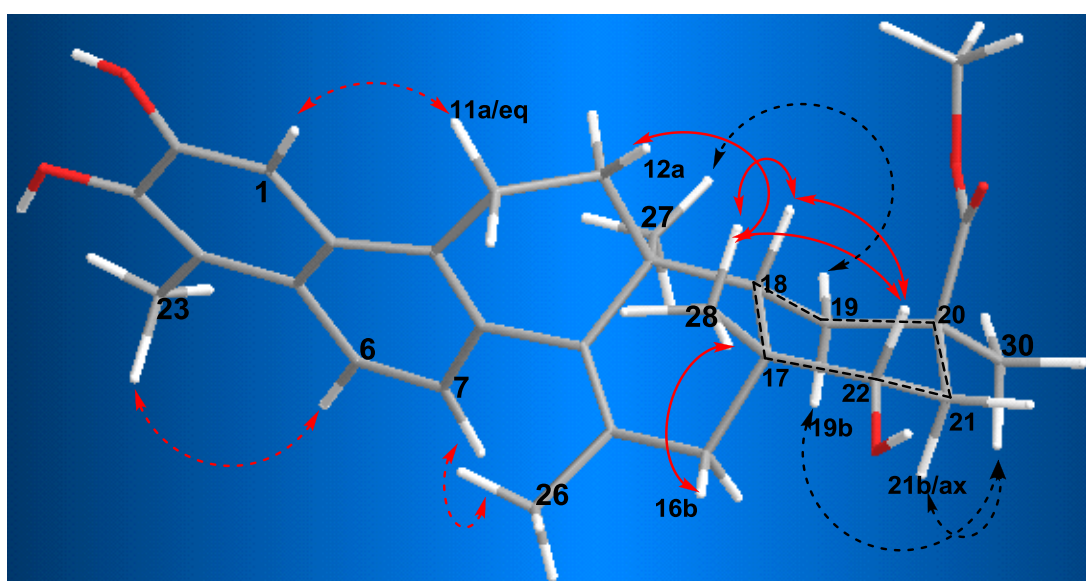


(B)

Figure 3.121: (A): Full NOESY spectrum (400 MHz) of HM-15 in $(\text{CD}_3)_2\text{CO}$ using TopSpin 3.2 software; (B): Selected expansion in the methyl region



(A): This image clarifies the NOEs in rings A-D



(B): This image clarifies the chair configuration of ring E

Figure 3.122: (A & B) show the energy minimised 3D structure of HM-15 from two different sides using ChemDraw Ultra-11.0 software and the important NOESY correlations ($\leftarrow \rightarrow$) β ($\leftarrow \rightarrow$) α

3.3.3.4 Characterisation of HM-16 as the new triterpene, 2,22-dihydroxy-3-methoxy-15,12-dioxo-5,8-oxa-24,30-dinor-5,6-seco-friedelan-1,3,5(10)-trien-6-al (jujuborreal)

HM-16 was isolated from the EtOAc of the stem bark by PTLC as a reddish brown solid. On TLC, the compound appeared as dark spot under UV light (λ 254 nm) and turned to greenish blue after spraying with *p*-anisaldehyde-sulphuric acid reagent followed by heating. Its R_f was 0.17 on SiGel when eluted with the mobile phase 50% hexane in EtOAc.

The positive mode HRESI-MS spectrum showed a quasi-molecular ion $[M+H]^+$ at m/z 499.2690, suggesting a molecular formula of $C_{29}H_{38}O_7$ (DBE=11).

The optical rotation $[\alpha]_D^{20}$ was -22° ($c=0.1$, $CHCl_3$).

The IR spectrum exhibited absorption bands at 3410 cm^{-1} indicated the presence of hydroxyl groups, 2916 cm^{-1} for C-H stretch, 2848 cm^{-1} for $-OCH_3$ stretch, 1701 cm^{-1} for C=O, and 1561 & 1460 cm^{-1} for C-C stretch (in aromatic ring) (Williams and Fleming, 2008).

The 1H NMR spectrum (400 MHz, $CDCl_3$, Figure 3.125, Table 3.15) displayed five methyl singlets at δ_H 1.04, 1.40, 1.45, 1.48 and 2.15, in addition to one methyl doublet at δ_H 1.25 (3H, *d*, $J=7.4$ Hz), which showed a vicinal coupling with a deshielded methine proton at δ_H 2.45 (1H, *m*) in the COSY spectrum (Figure 3.127). A set of two pairs of deshielded methylene protons at δ_H 3.36 (1H, *dd*, $J=14.9, 4.0$ Hz)/ 2.68 (1H, *dd*, $J=14.9, 2.5$ Hz) and at δ_H 3.12 (1H, *d*, $J=19.4$ Hz)/ 2.53 (1H, *d*, $J=19.4$ Hz) were also observed. Moreover, the spectrum revealed the presence of a methoxy group at δ_H 3.79 (3H, *s*), a methine proton at δ_H 2.23 (1H, *m*), an oxymethine proton at δ_H 4.35 (1H, *s*) and an aromatic proton at δ_H 6.52 (1H, narrow *d*, $J=0.70$ Hz). Finally, the signal appeared at δ_H 9.36 (1H, *dd*, $J=4.0, 2.5$ Hz) was found to be correlated with a carbonyl carbon at δ_C 198.6 indicating the existence of an aldehyde function. The latter methine proton showed vicinal couplings with the methylene protons at δ_H 3.36/ 2.68 in the COSY spectrum, suggesting their positions in the same spin system as neighbours.

The spectrum showed some traces of n-hexane and fatty alcohol by the signals at δ_H 0.88 (CH_3 , *t*), 1.26 ($-CH_2$) and 3.65 ($-CH_2-OH$).

The DEPTq ^{13}C NMR spectrum (100 MHz, Figure 3.126) indicated the presence of a 29 carbons comprising of six methyls, five methylenes, two aliphatic methines,

four aliphatic quaternaries, one methoxy carbon at δ_C 61.0, one oxymethine at δ_C 79.5, one oxygen-bearing quaternary carbon at δ_C 95.3, one aromatic methine, five aromatic quaternaries including three oxygen-bearing ones and three carbonyls consisting of two ketones at δ_C 210.5 and 213.9 and one aldehyde at δ_C 198.6. The signals at δ_C (14.1, 22.7 and 31.9) and at δ_C (29.7, 63.12 and 70.5) were excluded as they belonged to the solvent impurity (n-hexane) and to the fatty alcohol, respectively. All hydrogen-bearing carbons were assigned unambiguously by the HSQC experiment (Figure 3.128).

So far, the obtained results along with the molecular formula assumed this compound to be another penta-cyclic triterpene. In the HMBC experiment (Figure 3.129; A), the methine proton at δ_H 6.52 showed 2J and 3J correlations to all of the three oxygen-bearing aromatic quaternary carbons at δ_C 143.9 and 144.9, 147.0, respectively, as well as 3J correlation to the aliphatic quaternary at δ_C 49.1. Moreover, the most deshielded methyl singlet at δ_H 2.15, which is usually assigned as (Me-23), showed 2J correlation to the aromatic quaternary at δ_C 114.5 and 3J correlations to the same quaternaries at δ_C 144.9 and 147.0. On the other hand, the methoxy group at δ_H 3.79 only had one 3J correlation to the quaternary at δ_C 144.9, implying its attachment site on that carbon. These observations indicated that ring A should be fully aromatic with a methoxy group attached at position-3. This was further supported by the NOE correlation between the methoxy group and Me-23 as seen in the NOESY spectrum (Figure 3.130).

In Figure 3.129; (B), the methyl singlet at δ_H 1.45 showed 2J correlation to the aliphatic quaternary at δ_C 49.1 and 3J correlations to the aromatic quaternary at δ_C 133.2, the methylene carbon at δ_C 36.2, and to the oxygen-bearing quaternary at δ_C 95.3. The latter carbon also got 3J correlation from the methyl singlet at δ_H 1.40, which correlated with a ketone at δ_C 210.5 and with two quaternaries at δ_C 54.4 and 41.2, as well. Furthermore, the deshielded methylene protons at δ_H 3.36/2.68 showed 2J correlations to the same quaternary at δ_C 95.3 as well as to the aldehyde carbonyl at δ_C 198.6. Additionally, they showed three-bond NOE interactions with the two previous methyls. This suggested that ring A should be extended as seen in the partial structure in Figure 3.123.

The methyl singlet at δ_{H} 1.48 appeared to be aligned with the methyl at δ_{H} 1.40 due to its correlations to the same two quaternaries at δ_{C} 41.2 (C-13) and 54.4 (C-14). It also showed 3J correlations to the methylene carbon at δ_{C} 28.6 and to the methine carbon at δ_{C} 45.8. The latter methine appeared to get 3J correlation from a singlet methyl at δ_{H} 1.04 which correlated with a methylene carbon at δ_{C} 49.5, a quaternary carbon at δ_{C} 35.7 (the attachment site), and an oxymethine carbon at δ_{C} 79.5. These correlations were typical to those usually seen from the methyl at position-28. The methyl doublet at δ_{H} 1.25 showed 3J correlations to a ketone at δ_{C} 213.9 and to a methylene carbon at δ_{C} 27.2 as well as 2J correlation to its attachment site the methine carbon at δ_{C} 39.6. All the last observations led to a conclusion that the partial structure of this compound should be extended by three six-membered rings C, D and E, typical to those in the previous isolated compounds, where the saturated ring E has a ketone function at position-21 and a secondary hydroxyl group at position-22. This was further supported by following the correlations from the methine proton at δ_{H} 4.35 (H-22) as pointed out in Figure 3.129; (A), in addition to the vicinal couplings observed between H-18/ 2H-19 and between 2H-19/ H-20 in COSY spectrum.

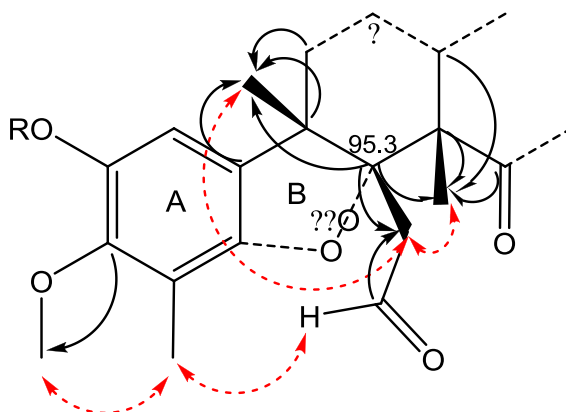


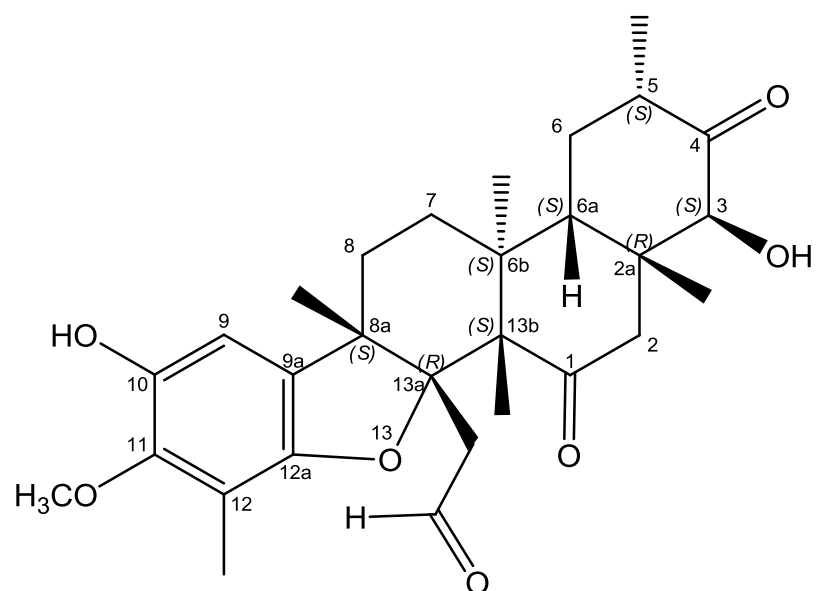
Figure 3.123: Partial structure of HM-16 showing the key HMBC (→) and NOESY (↔) correlations

The generated molecular formula of this compound included seven oxygen atoms which, after assigning each of them, eliminated the possibility of the presence of an endoperoxide bridge between carbons 5-8, hence, confirmed the formation of a dihydrofuran ring with an acetaldehyde side chain attached at position-8 (δ_{C} 95.3)

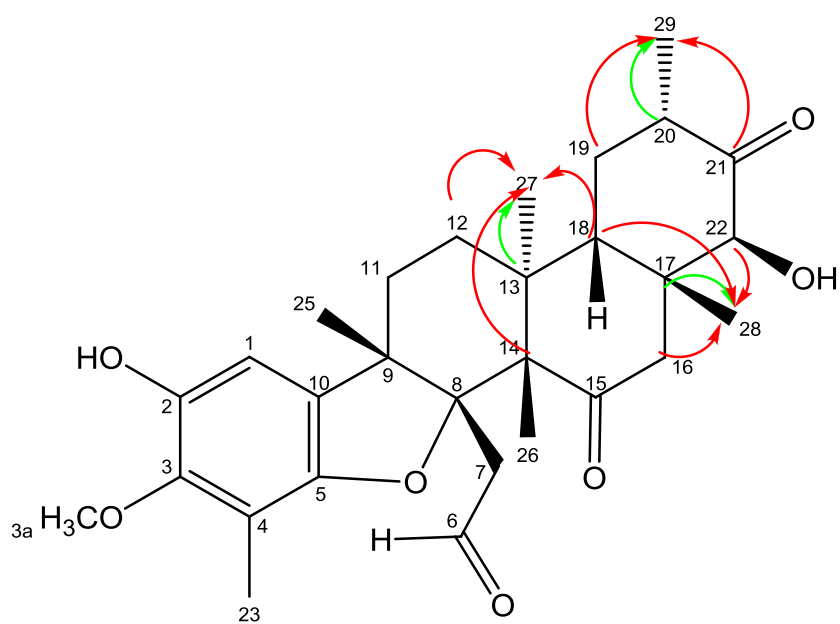
due to ring-B fission. The proton of the aldehyde function H-6 (δ_{H} 9.36) gave an NOE correlation to Me-23 (δ_{H} 2.15).

The relative stereo-chemical configuration of HM-16 was established from the NOESY experiment. The Me-28 (δ_{H} 1.04) showed NOE correlations to the methylene proton H-16b (δ_{H} 2.53), the methine proton H-20 (δ_{H} 2.45) and to the methine proton H-18 (δ_{H} 2.23). The latter proton H-18 correlated with H-20 and with Me-26 (δ_{H} 1.40), which in turn correlated with Me-25 (δ_{H} 1.45). This concluded that Me-25/ Me-26/ Me-28/ H-16b/ H-18 and H-20 were all located on the β side of the molecule while Me-29 (δ_{H} 1.25) was on the α side. On the other hand, Me-27 (δ_{H} 1.48) showed NOE correlations with the methylene protons H-11a (δ_{H} 1.72) and H-16a (δ_{H} 3.12) and with the oxymethine proton H-22 (δ_{H} 4.35), which in turn correlated with H-16a as well. These observations indicated that Me-27/ H-16a and H-22 should be located on the α side of the molecule, hence, implying that the secondary hydroxyl group (OH-22) should be therefore on the β side (see Figure 3.131).

On the basis of the above structural information, HM-16 was identified as 2-((2a*R*,3*S*,5*S*,6a*S*,6b*S*,8a*S*,13a*R*,13b*S*)-3,10-dihydroxy-11-methoxy-2a,5,6b,8a,12,13b-hexamethyl-1,4-dioxo-1,2,2a,3,4,5,6,6a,6b,7,8,8a,13a,13b-tetradecahydrobenzo[*b*]phenanthro[2,1-*d*]furan-13a-yl)acetaldehyde (Figure 3.124: A). This compound, for which the trivial name jujuborreal is proposed (Figure 3.124: B), was found to be a new triterpene. The cytotoxicity of HM-16 was evaluated here, and it showed a moderate, yet, selective activity against the tested melanoma cell line A375 (see section 4.1.2.2 for more details).



(A): Structure of HM-16 with the IUPAC numbering system



(B): Structure of HM-16 with the non-systematic numbering and the key HMBC correlations
 (→) 3J (→) 2J

Figure 3.124: Structure of HM-16 by two numbering systems

Table 3.15: ^1H (400 MHz) and ^{13}C (100 MHz) NMR data of HM-16 in CDCl_3

Position	HM-16	
	δ_{H}	δ_{C}
1	6.52 (1H, <i>d</i> , $J=0.7$ Hz)	105.8
2	-	143.9
3	-	144.9
4	-	114.5
5	-	147.0
6	9.36 (1H, <i>dd</i> , $J=4.0, 2.5$ Hz)	198.6
7	3.36 (1H, <i>dd</i> , $J=14.9, 4.0$ Hz)/ 2.68 (1H, <i>dd</i> , $J=14.9, 2.5$ Hz)	47.9
8	-	95.3
9	-	49.1
10	-	133.2
11	1.72 (1H, <i>m</i>)/ 1.60 (1H, <i>m</i>)	36.2
12	1.58 (1H, <i>m</i>)/ 1.50 (1H, <i>m</i>)	28.6
13	-	41.2
14	-	54.4
15	-	210.5
16	3.12 (1H, <i>d</i> , $J=19.4$ Hz)/ 2.53 (1H, <i>d</i> , $J=19.4$ Hz)	49.5
17	-	35.7
18	2.23 (1H, <i>m</i>)	45.8
19	(2H) [1.96-1.79 <i>m</i>]	27.2
20	2.45 (1H, <i>m</i>)	39.6
21	-	213.9
22	4.35 (1H, <i>s</i>)	79.5
23	2.15 (3H, <i>s</i>)	9.5
24	-	-
25	1.45 (3H, <i>s</i>)	20.9
26	1.40 (3H, <i>s</i>)	18.6
27	1.48 (3H, <i>s</i>)	19.9
28	1.04 (3H, <i>s</i>)	26.4
29	1.25 (3H, <i>d</i> , $J=7.4$ Hz)	16.5
30	-	-
OCH₃-3	3.79 (3H, <i>s</i>)	61.0

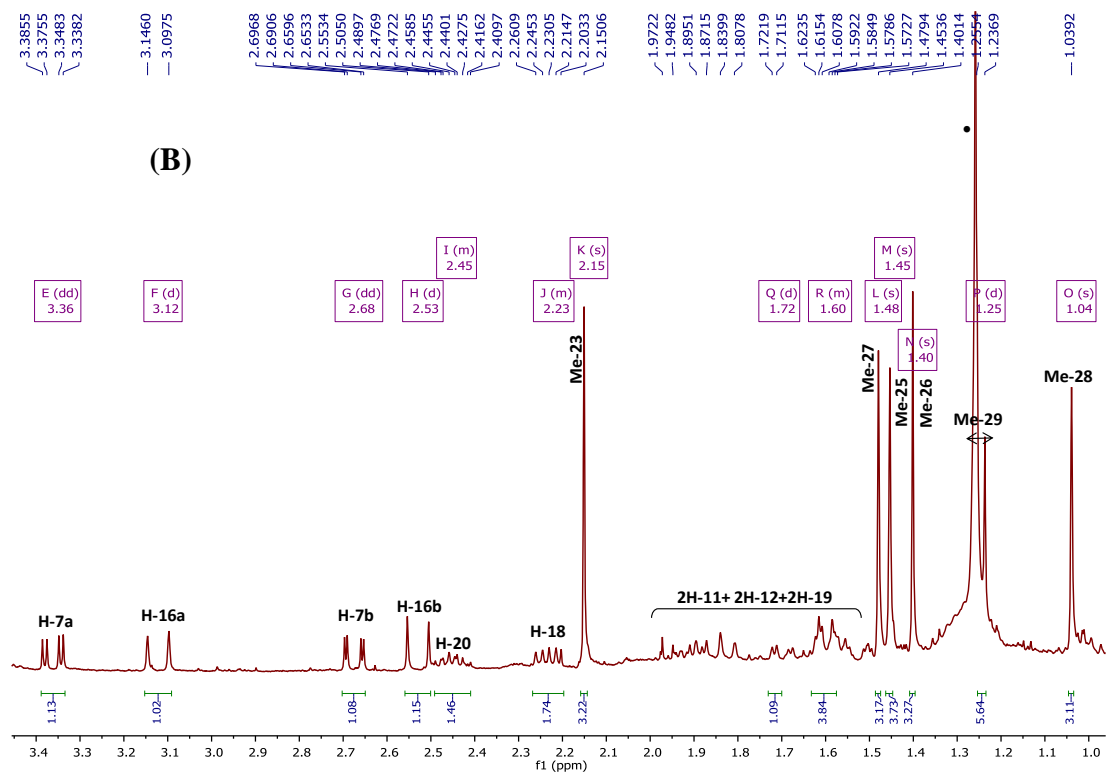
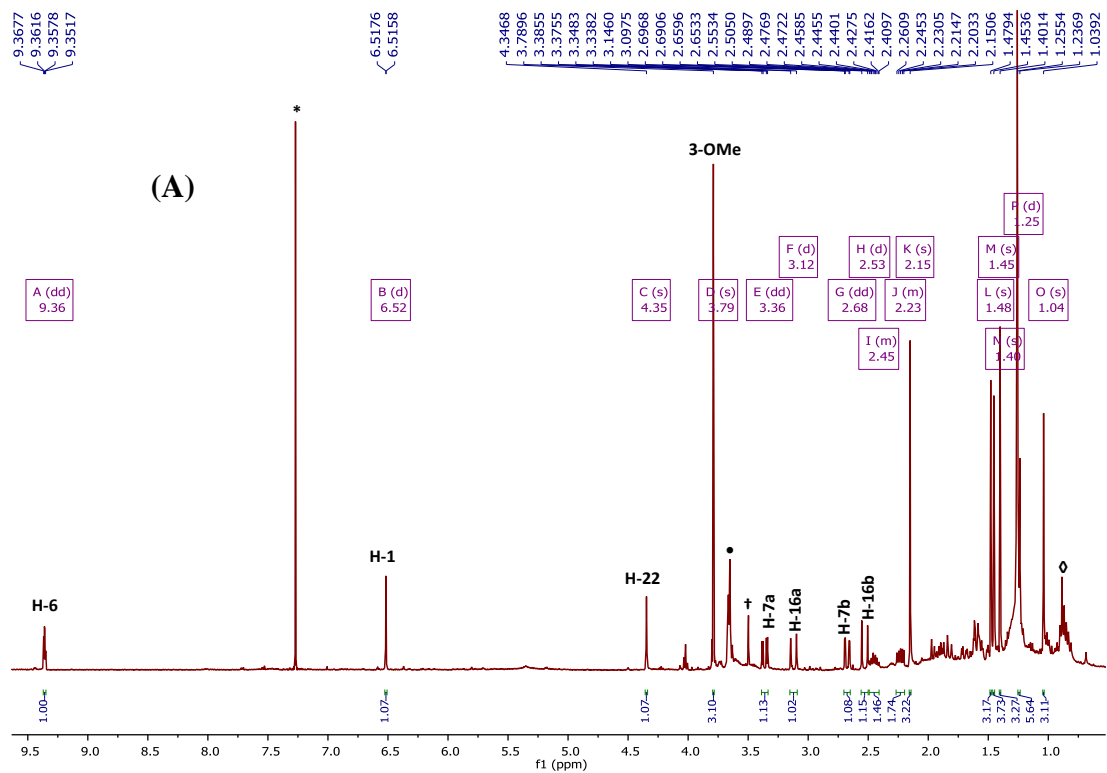


Figure 3.125: (A): Full ^1H NMR spectrum (400 MHz) of HM-16 in CDCl_3 ; (*) CHCl_3 residue; (B): Selected expansion in the aliphatic region. (•), (◊), (+): impurities [Fatty alcohol, n-hexane and MeOH]

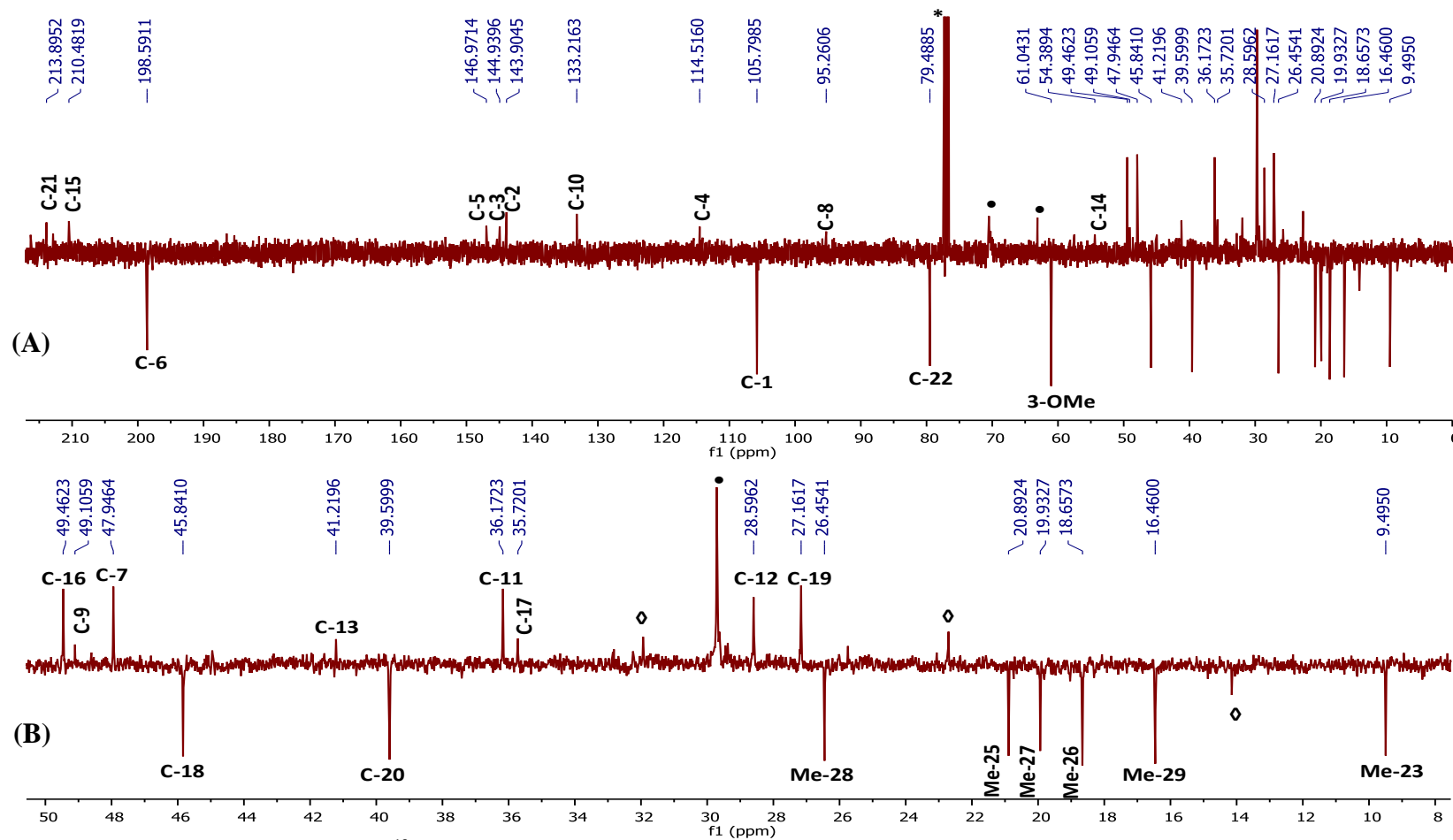
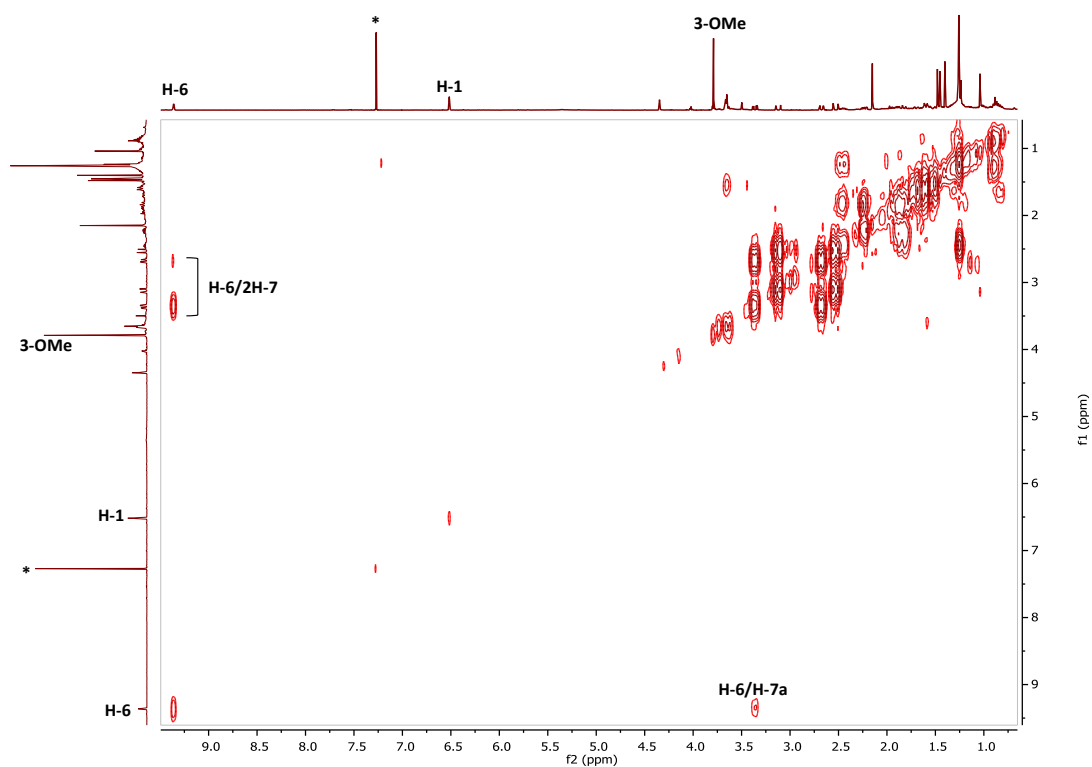
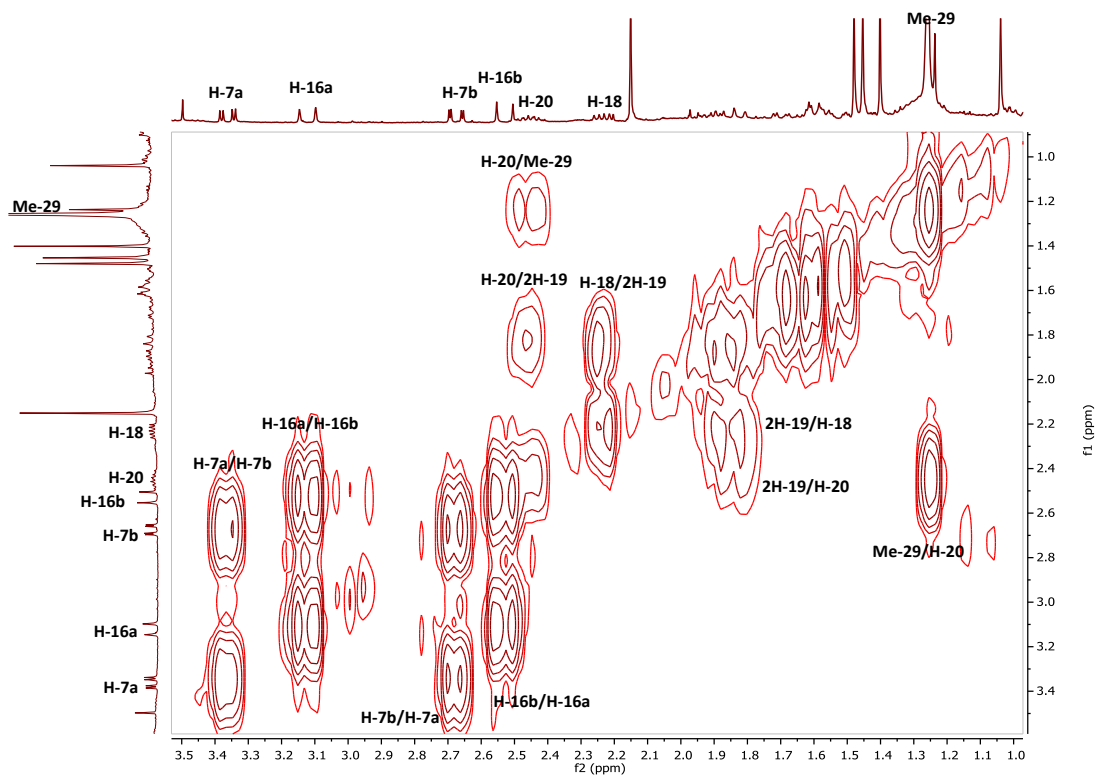


Figure 3.126: (A): Full DEPTq ^{13}C NMR spectrum (100 MHz) of HM-16 in CDCl_3 (*); (B): Selected expansion in aliphatic region (*), (\diamond): impurities [Fatty alcohol and n-hexane]

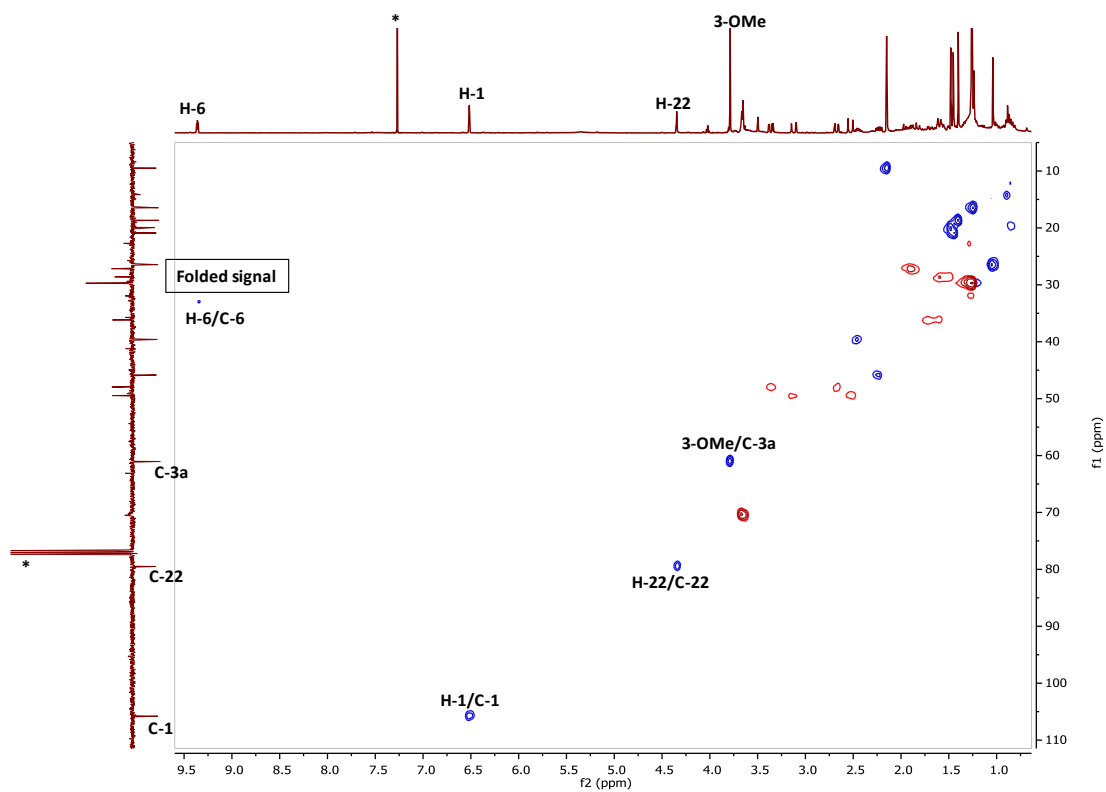


(A)

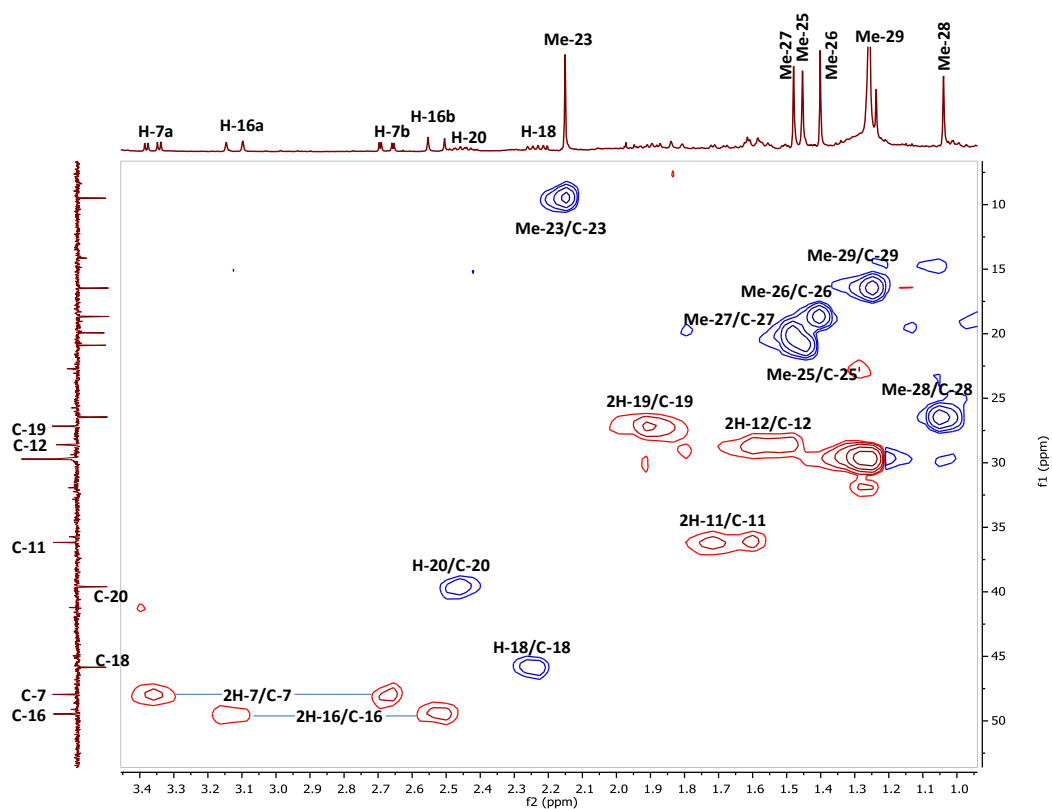


(B)

Figure 3.127: (A): Full ^1H - ^1H COSY spectrum (400 MHz) of HM-16 in CDCl_3 ; (B): Selected expansion in the aliphatic region

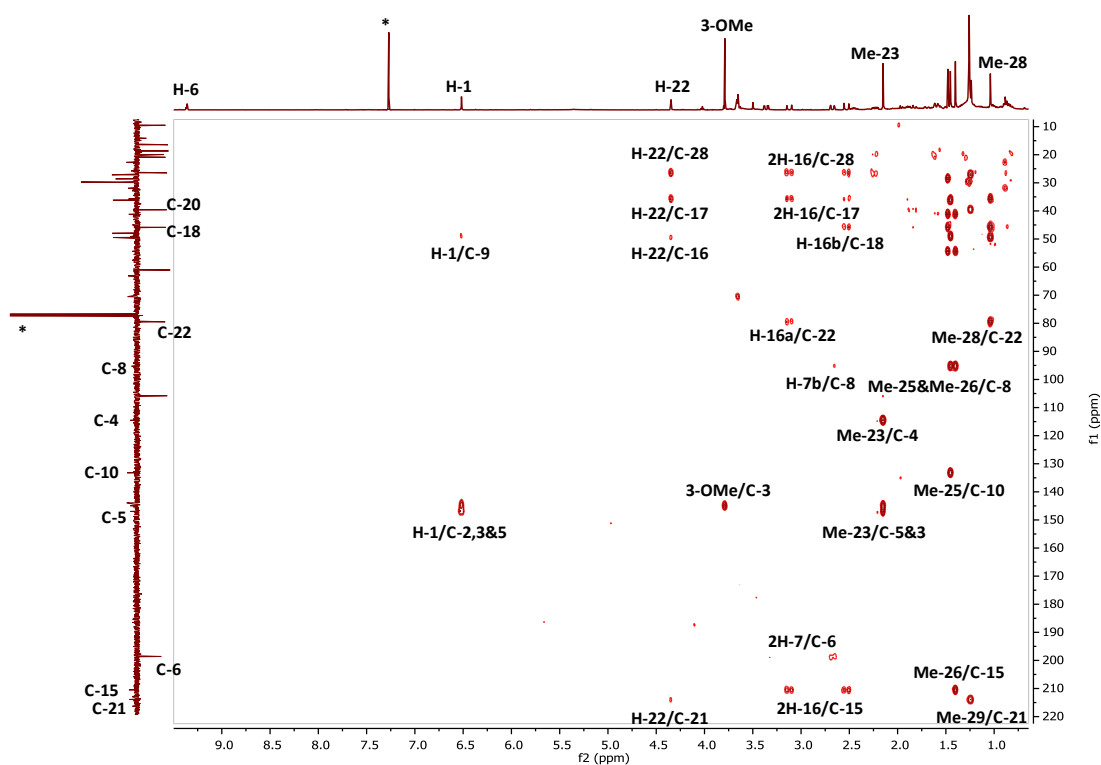


(A)

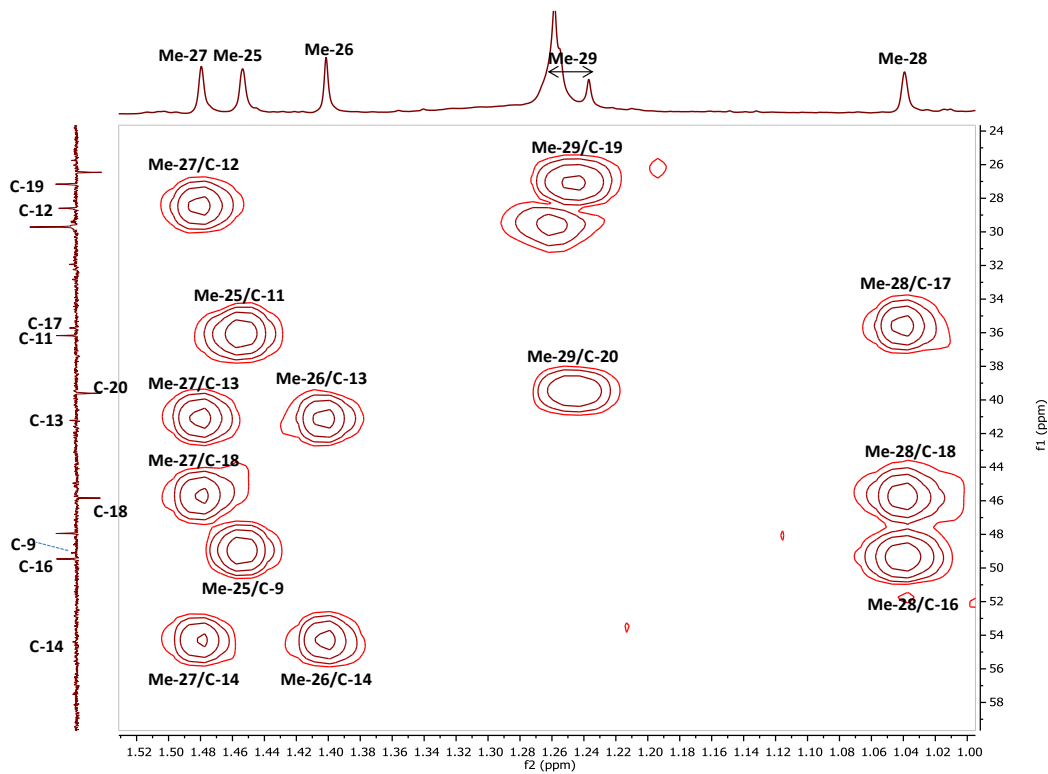


(B)

Figure 3.128: HSQC spectrum (400 MHz) of HM-16 in CDCl_3 (*)
 A: Full HSQC; B: Selected HSQC expansion



(A)



(B)

Figure 3.129: HMBC spectrum (400 MHz) of HM-16 in CDCl_3 (*)
 (A): Full HMBC; (B): Selected HMBC expansion of the methyl groups

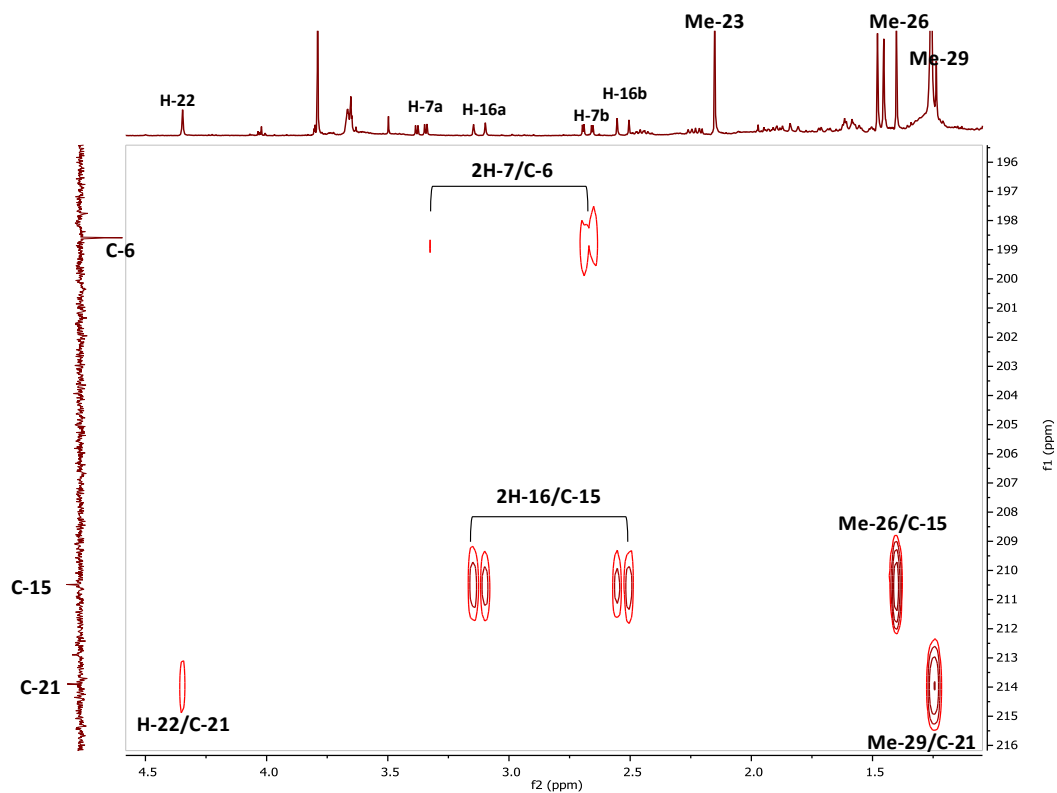


Figure 3.129 (Cont.): (C): Selected HMBC expansion of the carbonyls

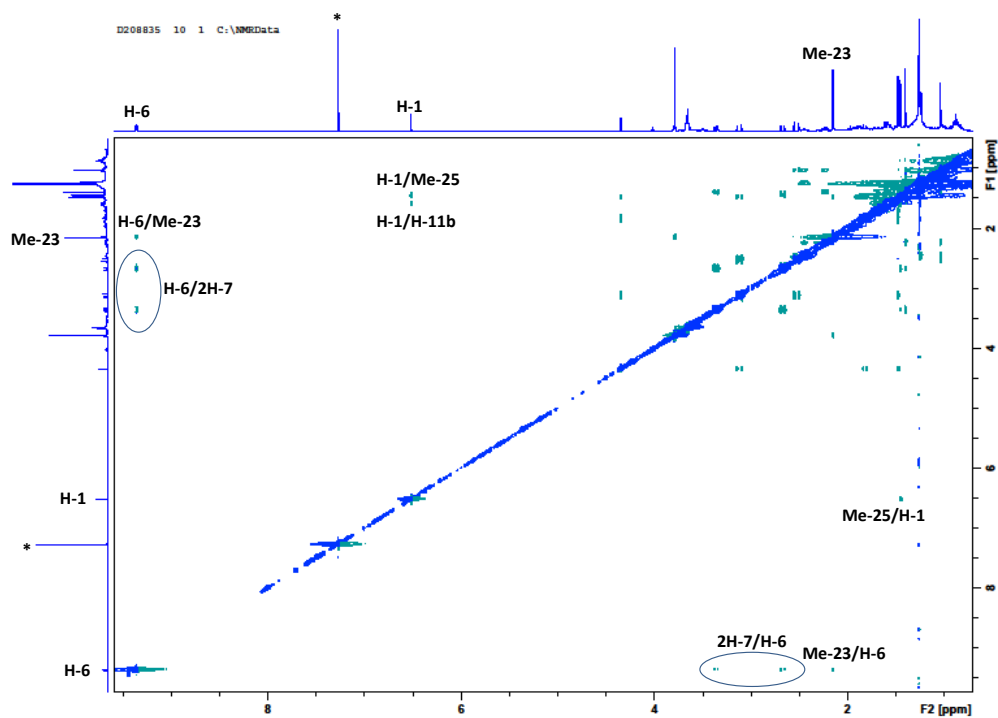


Figure 3.130: (A): Full NOESY spectrum (400 MHz) of HM-16 in CDCl₃ using TopSpin 3.2 software

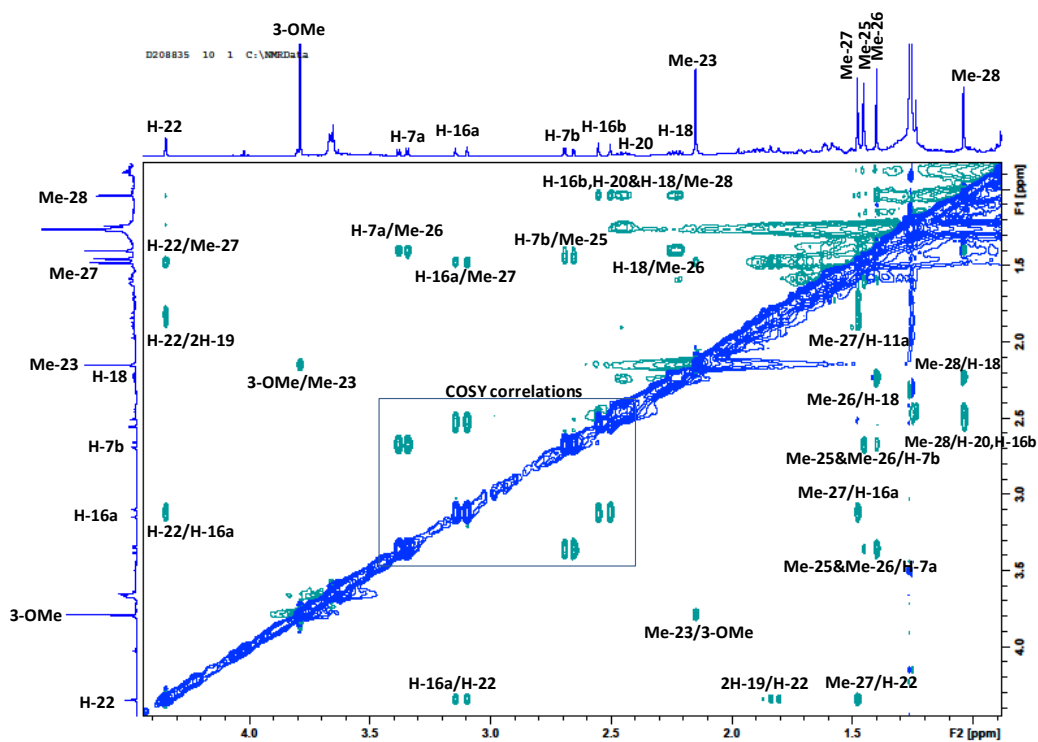


Figure 3.130 (Cont.): (B): Selected expansion of NOESY spectrum in the aliphatic region

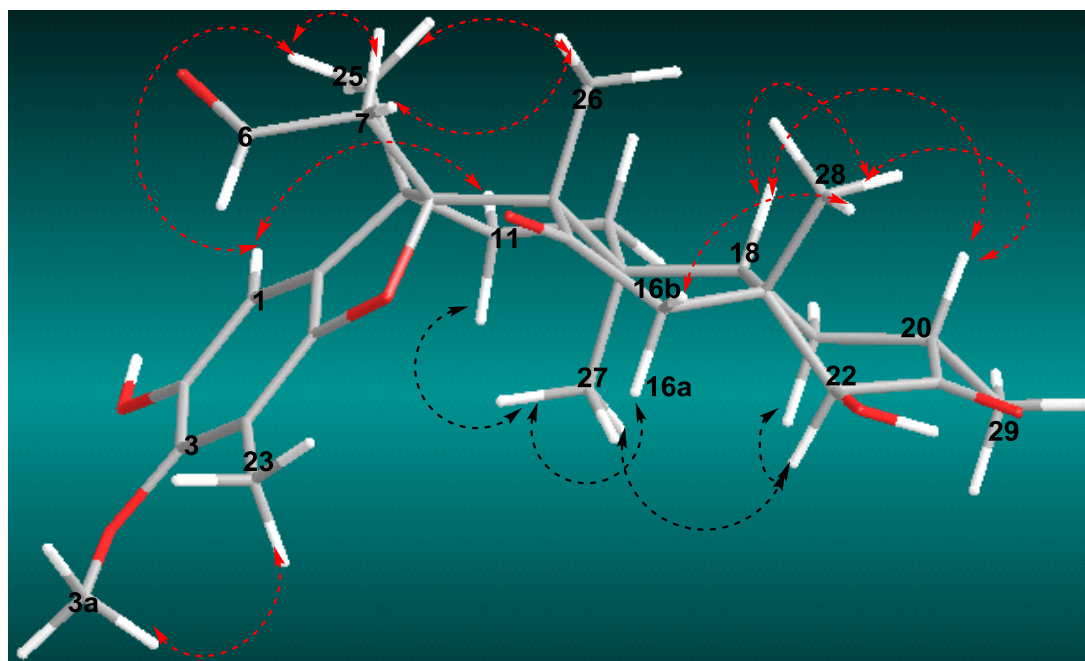


Figure 3.131: Energy minimised 3D structure of HM-16 showing NOESY correlations
 (↔) β (↔) α

3.4 Steroids

3.4.1 Characterisation of HM-17 as β -sitosterol

HM-17 was isolated from the n-hexane extract of the stem bark as white crystals. On TLC, the compound appeared as a pink spot after spraying with *p*-anisaldehyde-sulphuric acid reagent followed by heating. Its R_f was 0.47 on SiGel when eluted with the mobile phase 50% hexane in EtOAc.

The ^1H NMR spectrum (400 MHz, CDCl_3 , Figure 3.133) indicated the presence of a phytosterol skeleton with a set of six methyl groups including two tertiary methyls at δ_{H} 0.69 (Me-18) and 1.02 (Me-19), three secondary methyls at δ_{H} 0.93 (Me-21), 0.85 (Me-26), 0.83 (Me-27) and one primary at δ_{H} 0.86 (Me-29). The spectrum also displayed a doublet signal due to an olefinic proton at 5.36 (1H, *d*, $J=5.3$ Hz) attributed to H-6 and a multiplet signal at 3.52 (1H, *m*) which was assigned to the axial oxymethine proton at C-3 as its cross peak in the HSQC spectrum was relatively stretched (72 Hz). The DEPTq135 ^{13}C NMR spectrum (100 MHz, CDCl_3 , Figure 3.134) displayed distinctive signals represented by the two olefinic carbon signals at δ_{C} 140.8 (C-5) and 121.7 (C-6) as well as a signal for a carbon bearing hydroxyl group at δ_{C} 71.8 ppm (C-3).

Based on the above spectral data which was consistent with the reported literature (Chaturvedula and Prakash, 2012; Pateh *et al.*, 2009), this compound was identified as β -sitosterol (Figure 3.132). The identity was further supported by co-TLC with an authentic sample (Sigma, Germany). This compound was previously reported from the bark of *M. laevis* (Nakagawa *et al.*, 2004; Sousa *et al.*, 1990) and is found in every other plant.

Several experimental studies were published on β -sitosterol and its biological activities for being a natural nutrient with related structure to cholesterol. For example; in Gupta *et al.* (1980) study, it was found to have anti-inflammatory activity similar to hydrocortisone and antipyretic activity similar to acetylsalicylic acid when administered *in vivo* intraperitoneally and orally. Similar findings were established by Nirmal *et al.* (2012). In Graziose *et al.* (2012) study, β -sitosterol was found to be inactive when screened for its activity against *P. falciparum* and *L. tarentolae* with $\text{IC}_{50} > 200$ and > 40 μM , respectively. However, a previous study by

Kirmizibekmez *et al.* (2011) reported β -sitosterol as a potent anti-plasmodial, yet, a weak anti-leishmanial compound with an IC_{50} of 3.6 and 27.8 $\mu\text{g/ml}$, respectively. This phytosterol also possessed potent antimicrobial activity compared with the standard gentamicin (Sen *et al.*, 2012), and a chemopreventive effect in colon cancer by inducing apoptosis and suppressing the expression of β -catenin and proliferating cell nuclear (PCNA) antigens, which are markers of proliferative activity in colon carcinogenesis (Baskar *et al.*, 2010). In this work, HM-17 was found to be inactive against the melanoma cells A375 and normal cells Hs27 within the tested concentration range (see section 4.1.2.1 for further details).

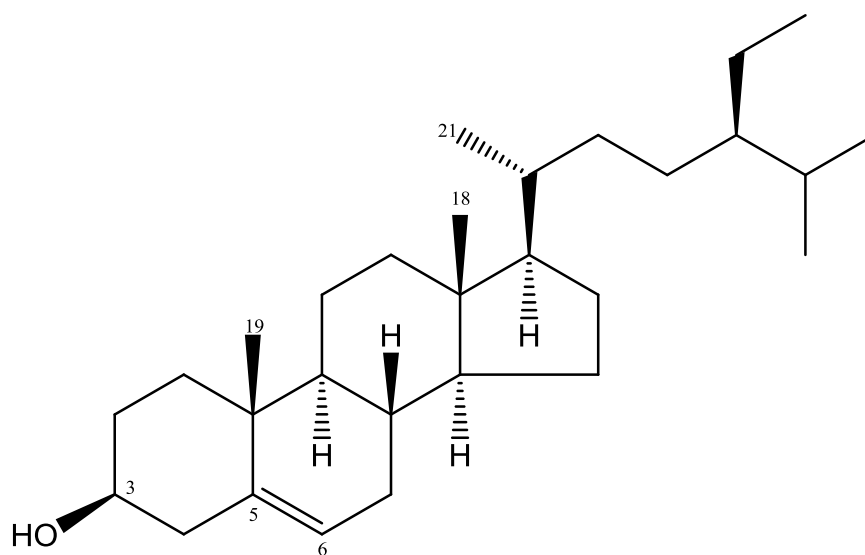


Figure 3.132: Full structure of HM-17 ($C_{29}H_{50}O$)

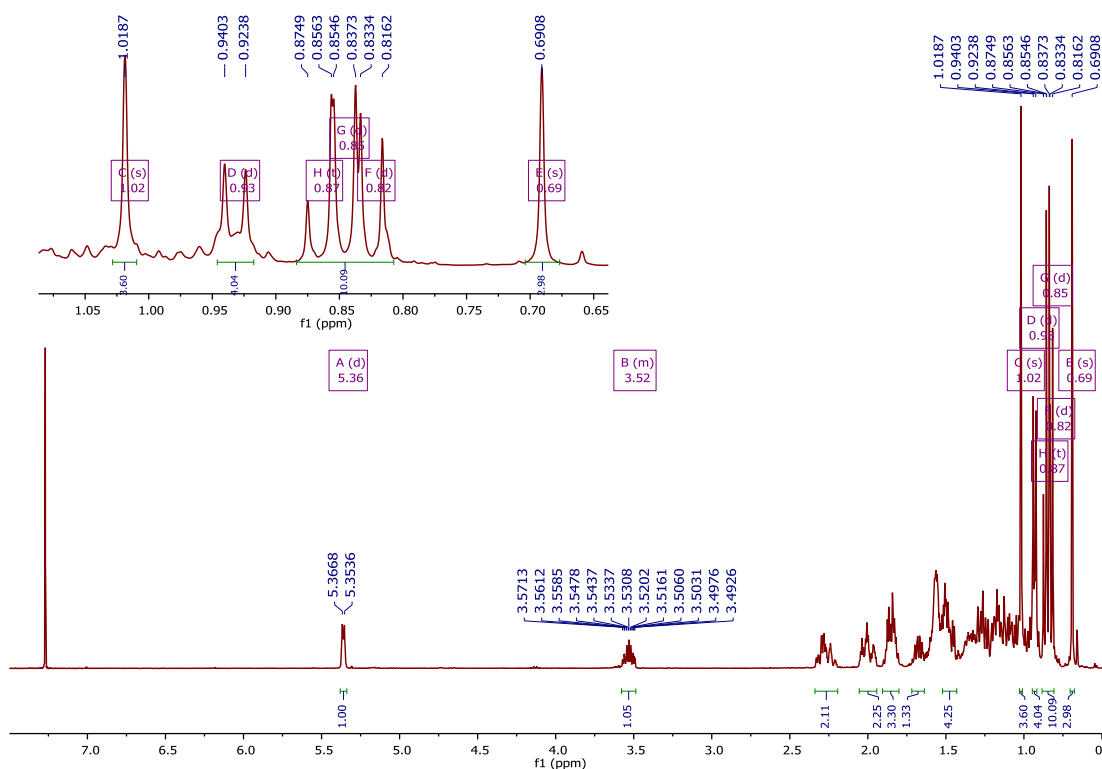


Figure 3.133: Full ^1H NMR spectrum (400 MHz) of HM-17 in CDCl_3 with selected expansion of the methyls

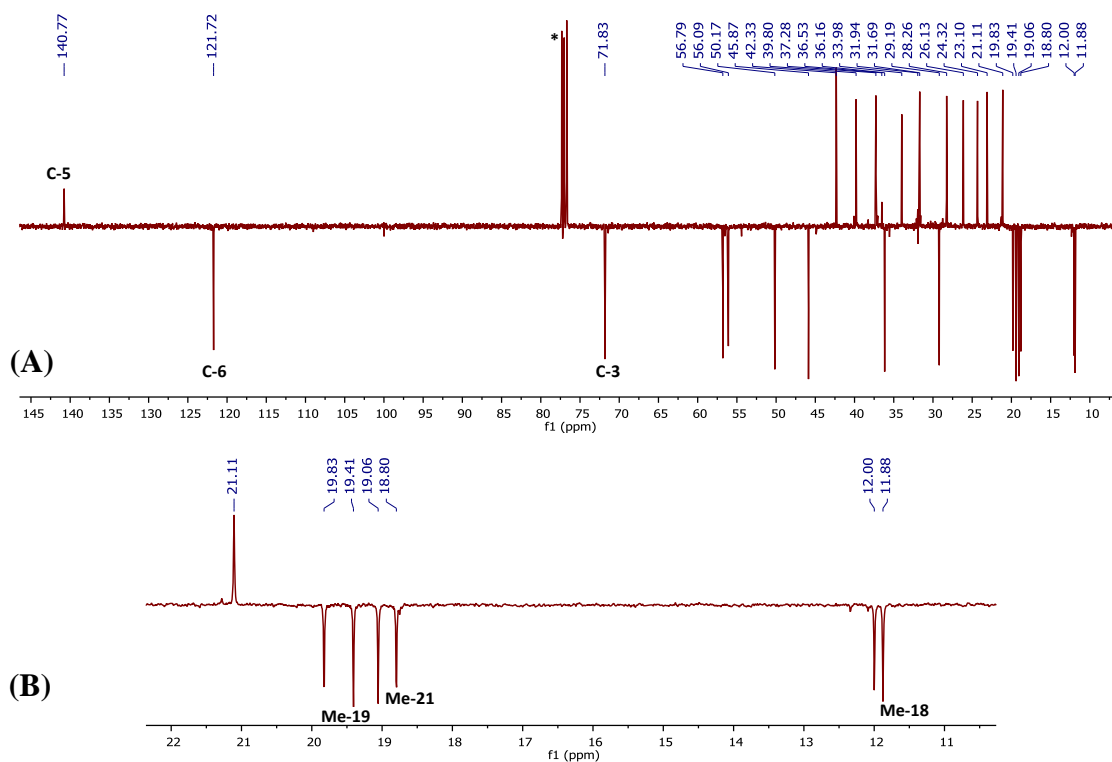


Figure 3.134: (A): Full DEPTq 135 ^{13}C NMR spectrum (100 MHz) of HM-17 in CDCl_3 (*); (B): Selected expansion of the methyl groups

3.4.2 Characterisation of HM-18 as stigmast-4-en-3-one

HM-18 was isolated from the n-hexane extract of the stem bark as a yellowish oily substance. On TLC, the compound showed quenching under short UV (λ 254 nm) and appeared as a pink spot after spraying with *p*-anisaldehyde-sulphuric acid reagent followed by heating. Its R_f was 0.71 on SiGel when eluted with the mobile phase 50% hexane in EtOAc.

The MM-ES+APCI positive scan spectrum showed a quasi-molecular ion $[M+H]^+$ at m/z 413.4, which complies with a proposed molecular formula of $C_{29}H_{48}O$ (DBE=6).

The 1H NMR spectrum (400 MHz, $CDCl_3$, Figure 3.136, Table 3.16) showed an olefinic methine at δ_H 5.73 (1H, *d*, $J=$ 1.6 Hz) and a set of six methyl groups including two tertiary methyls at δ_H 0.72 (Me-18) and 1.19 (Me-19), three secondary methyls at δ_H 0.93 (Me-21), 0.85 (Me-26), 0.82 (Me-27) and one primary at δ_H 0.86 (Me-29). These data suggested the presence of a phytosterol. The spectrum also indicated the presence of a small amount of fatty alcohol with a signal at δ_H 1.26.

The DEPTq135 ^{13}C NMR spectrum (100 MHz, $CDCl_3$, Figure 3.137) displayed 29 signals corresponded to this compound including six methyls, eleven methylenes, seven methines, two quaternaries in addition to the distinctive signals represented by the two olefinic carbon signals at δ_C 171.7 (C-5) and 123.7 (C-4) as well as an α,β unsaturated carbonyl carbon at δ_C 199.6 (C-3) which indicated the presence of a steroid ketone.

In the HMBC experiment (Figure 3.140), the methyl singlet at δ_H 1.19 (Me-19) showed 3J correlations to the methylene carbon at δ_C 35.7 (C-1), the methine carbon at δ_C 53.8 (C-9) and to the quaternary olefinic carbon at δ_C 171.7 (C-5) along with 2J correlation to the quaternary carbon at δ_C 38.6 (C-10). The olefinic methine proton at δ_H 5.73 (H-4) showed 3J correlations to two methylene carbons at δ_C 34.0 (C-2) and δ_C 32.9 (C-6) as well as to the quaternary carbon at δ_C 38.6 (C-10). This data suggested the presence of a double bond between C-4/C-5 on the phytosterol skeleton. The position of the ketone group at C-3 was established from the presence of a 3J correlation between the methylene proton at δ_H 2.03 (H-1a) and the carbon at δ_C 199.6. The chemical shifts of all hydrogen-bearing carbons were assigned from the HSQC spectrum (Figure 3.138) combined with COSY spectrum (Figure 3.139).

On the basis of the 2D NMR data, HM-18 was identified as stigmast-4-en-3-one or β -sitotenone (Figure 3.135) and these data were in agreement with previous reports (Gaspar and das Neves, 1993; Lee *et al.*, 2005). This compound has been isolated previously from many plants as a natural constituent produced by enzymatic reactions (Barla *et al.*, 2006; Fernández *et al.*, 1983; Su *et al.*, 2009), however, it is reported here for the first time from *M. laevis*.

Stigmast-4-en-3-one caused a hypoglycaemic effect when administered intravenously to healthy dogs at a dose of 1.3 mg/ kg body weight (Alexander-Lindo *et al.*, 2004). It also showed a significant vasodepressor effect by measuring the direct blood pressure after 2 mg/kg intravenous dose to adult male Wistar Albino rats (Barla *et al.*, 2006). Habsah *et al.* (2005) reported that this compound presented a strong antitumor-promoting activity in Raji cell line with an inhibition rate of 78.4%. Its potent ability to inhibit nitric oxide (NO), an inflammatory mediator, produced by RAW264.7 macrophage cells with IC₅₀ value of 15.9 μ M could reflect a possible anti-inflammatory activity (Tewtrakul *et al.*, 2010). At a concentration of 5 μ M, stigmast-4-en-3-one exhibited a minor tyrosinase inhibition activity and reduced the melanin content in melanoma cells B16F10, without toxic effect, indicating its potential use in cosmetic skin whitening products (Chu *et al.*, 2015). The cytotoxicity and the anti-trypanosomal activity of HM-18 were also evaluated in the present study (see sections 4.1.2.1 and 4.2.2 for further details).

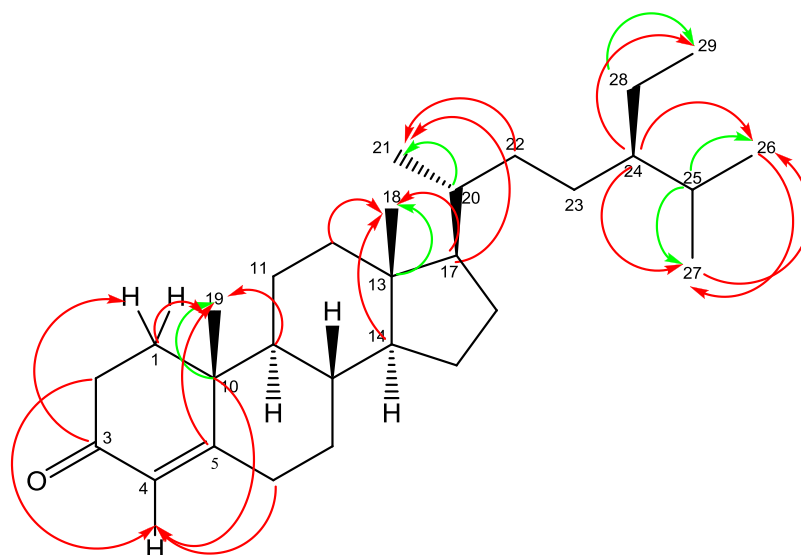


Figure 3.135: Full structure of HM-18 with the key HMBC correlations
 (\rightarrow) 3J (\rightarrow) 2J ^{13}C to 1H connectivity

Table 3.16: ^1H (400 MHz) and ^{13}C (100 MHz) NMR data of HM-18 in CDCl_3

Position	HM-18	
	δ_{H}	δ_{C}
1	2.03 (1H, <i>m</i>)/ 1.70 (1H, <i>m</i>)	35.7
2	2.44 (1H, <i>m</i>)/ 2.36 (1H, <i>m</i>)	34.0
3	-	199.6
4	5.73 (1H, <i>d</i> , $J= 1.6$ Hz)	123.7
5	-	171.7
6	2.40 (1H, <i>m</i>)/ 2.28 (1H, <i>m</i>)	32.9
7	1.85 (1H, <i>m</i>)/ 1.05 (1H, <i>m</i>)	32.0
8	1.52 (1H, <i>m</i>)	35.6
9	0.93 (1H, <i>m</i>)	53.8
10	-	38.6
11	1.52 (1H, <i>m</i>)/ 1.44 (1H, <i>m</i>)	21.0
12	2.04 (1H, <i>m</i>)/ 1.17 (1H, <i>m</i>)	39.6
13	-	42.4
14	1.02 (1H, <i>m</i>)	55.9
15	1.62 (1H, <i>m</i>)/ 1.12 (1H, <i>m</i>)	24.2*
16	1.87 (1H, <i>m</i>)/ 1.29 (1H, <i>m</i>)	28.2*
17	1.12 (1H, <i>m</i>)	56.0
18	0.72 (3H, <i>s</i>)	11.97
19	1.19 (3H, <i>s</i>)	17.4
20	1.38 (1H, <i>m</i>)	36.1
21	0.93 (3H, <i>d</i> , $J= 6.6$ Hz)	18.7
22	1.34 (1H, <i>m</i>)/ 1.03 (1H, <i>m</i>)	33.9
23	1.32 (1H, <i>m</i>)/ 1.17 (1H, <i>m</i>)	26.1
24	0.94 (1H, <i>m</i>)	45.8
25	1.68 (1H, <i>m</i>)	29.2
26	0.85 (3H, <i>d</i> , †)	19.8
27	0.82 (3H, <i>d</i> , †)	19.0
28	1.27 (2H) [1.37-1.19 <i>m</i>]	23.1
29	0.86 (3H, <i>t</i> , †)	11.99

(†) Unassigned coupling constants due to overlapping.

(*) unconfirmed positions.

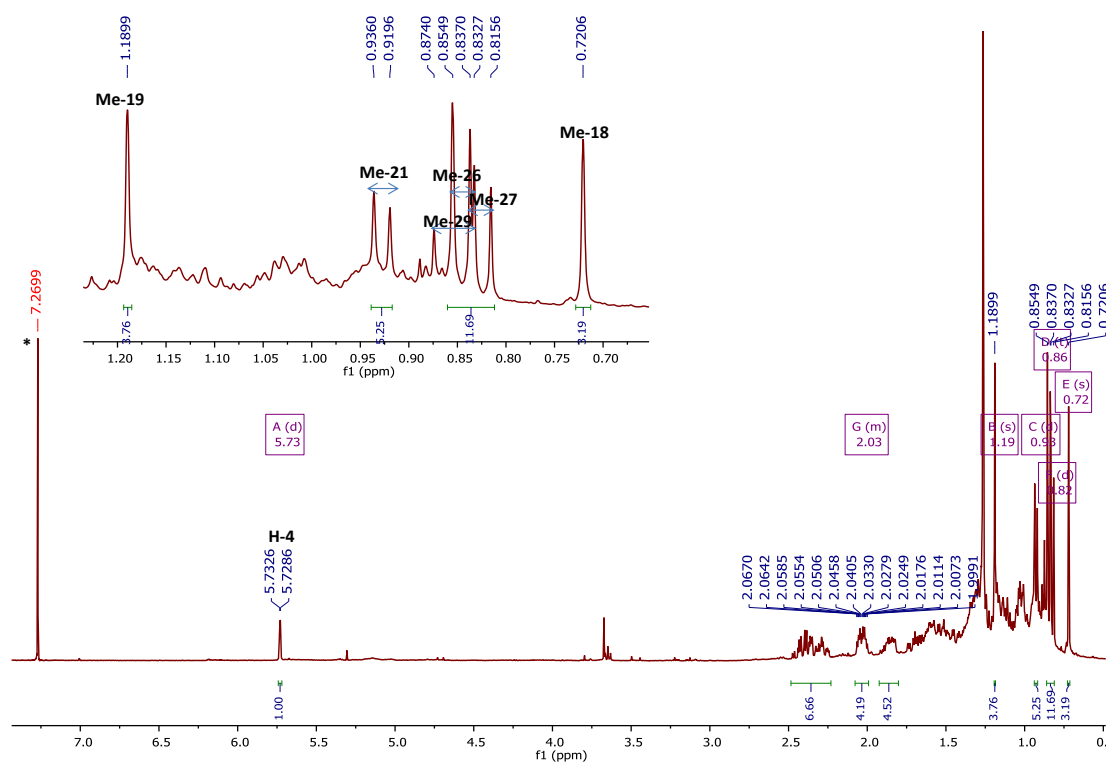


Figure 3.136: Full ^1H NMR spectrum (400 MHz) of HM-18 in CDCl_3 with selected expansion of the methyls; (*) CHCl_3 residue

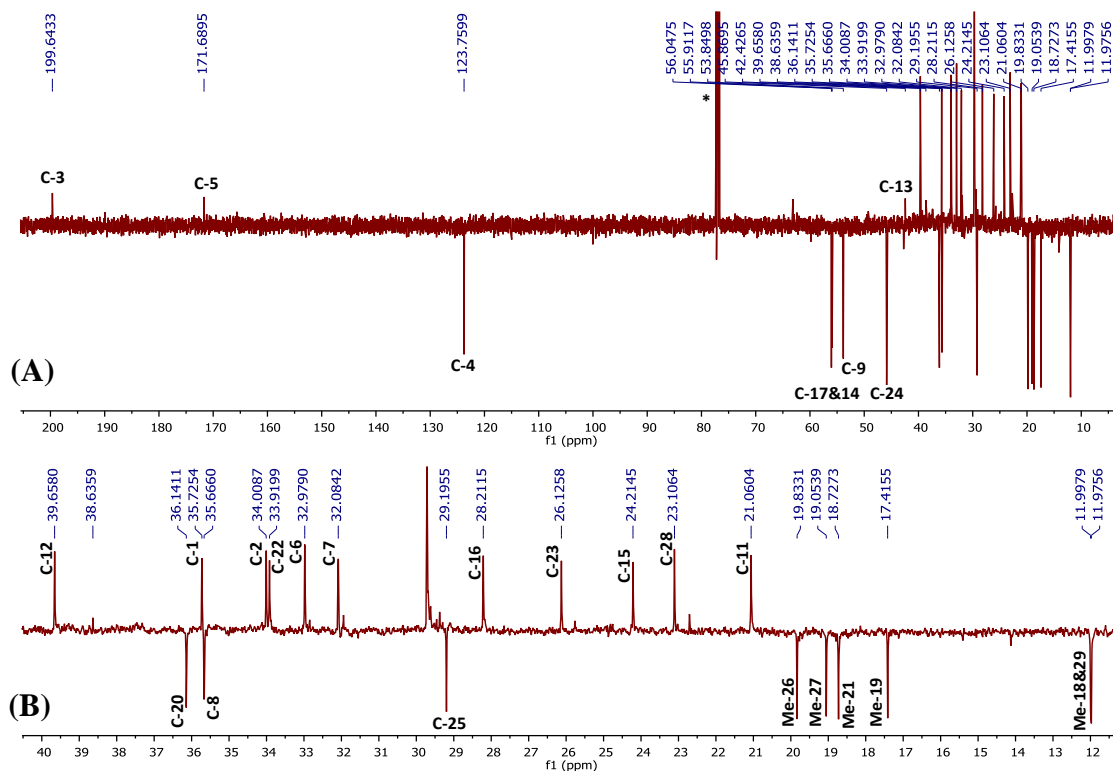


Figure 3.137: (A): Full DEPTq 135° ^{13}C NMR spectrum (100 MHz) of HM-18 in CDCl_3 (*); (B): Selected expansion in the aliphatic region

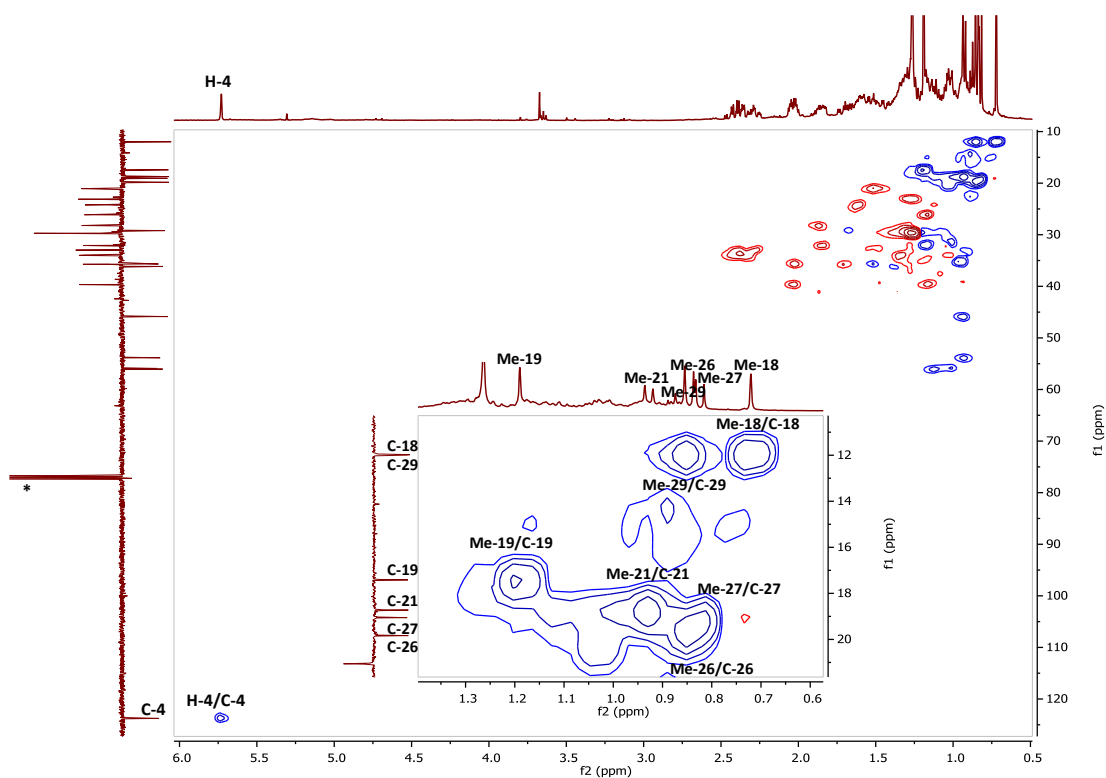


Figure 3.138: HSQC spectrum (400 MHz) of HM-18 in CDCl₃ (*) with selected expansion of the methyl groups

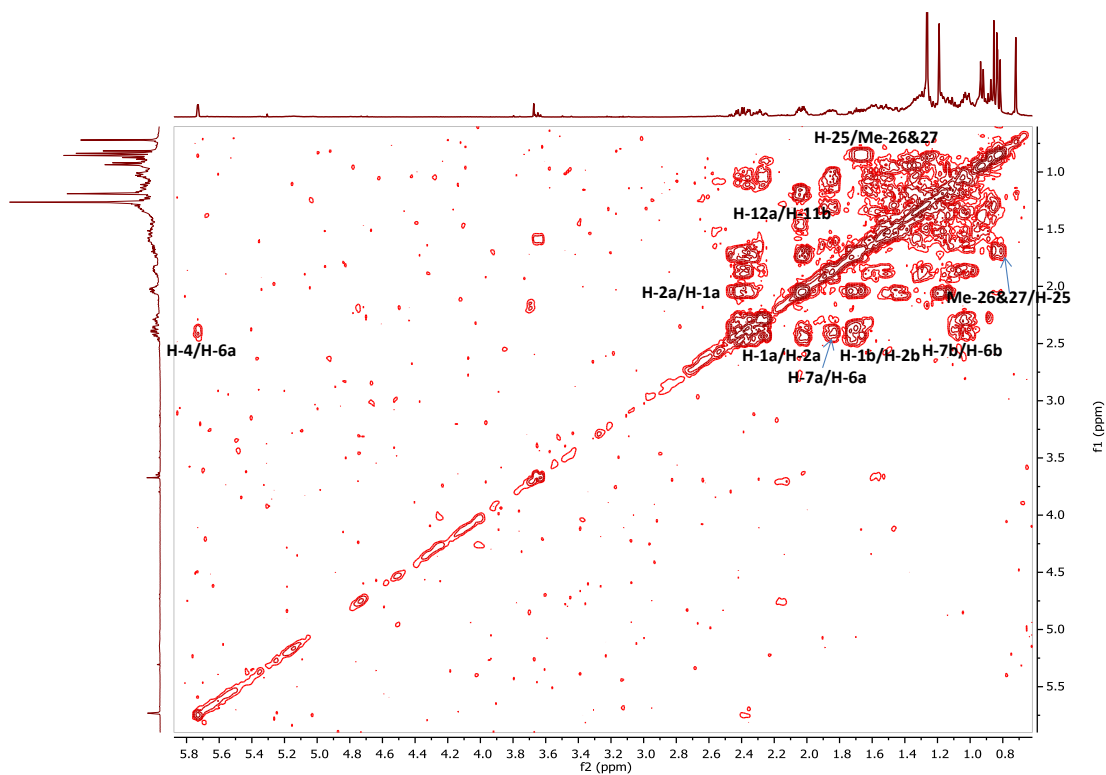
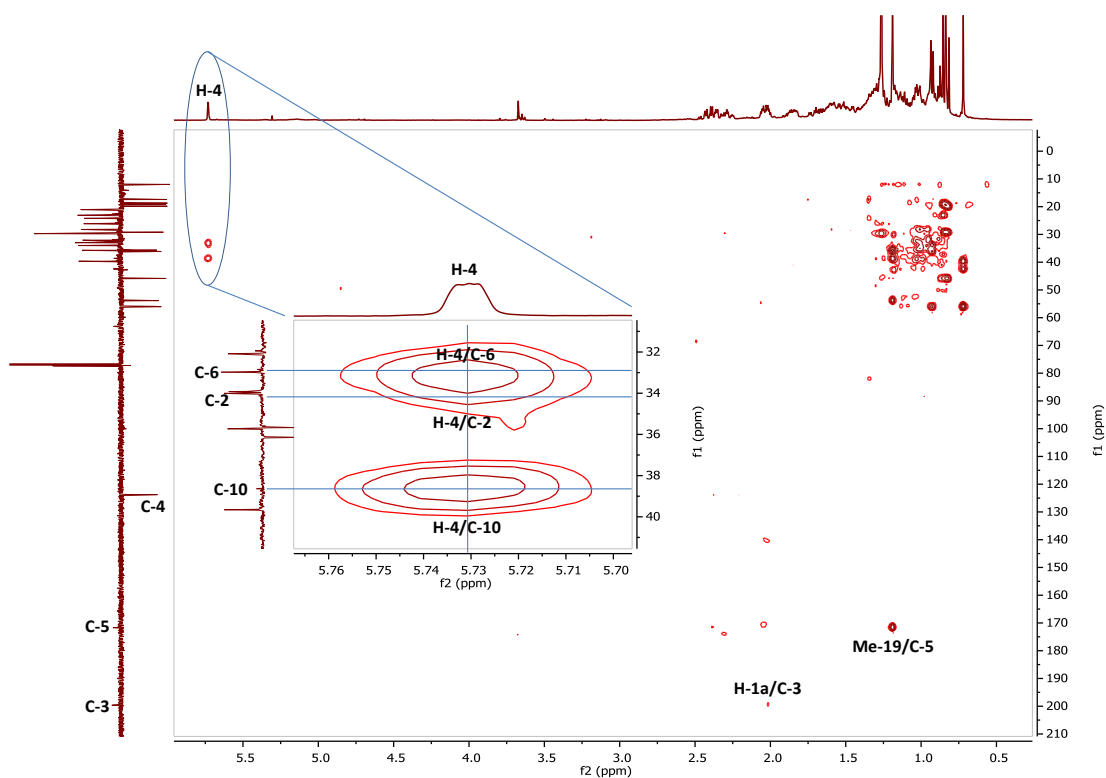
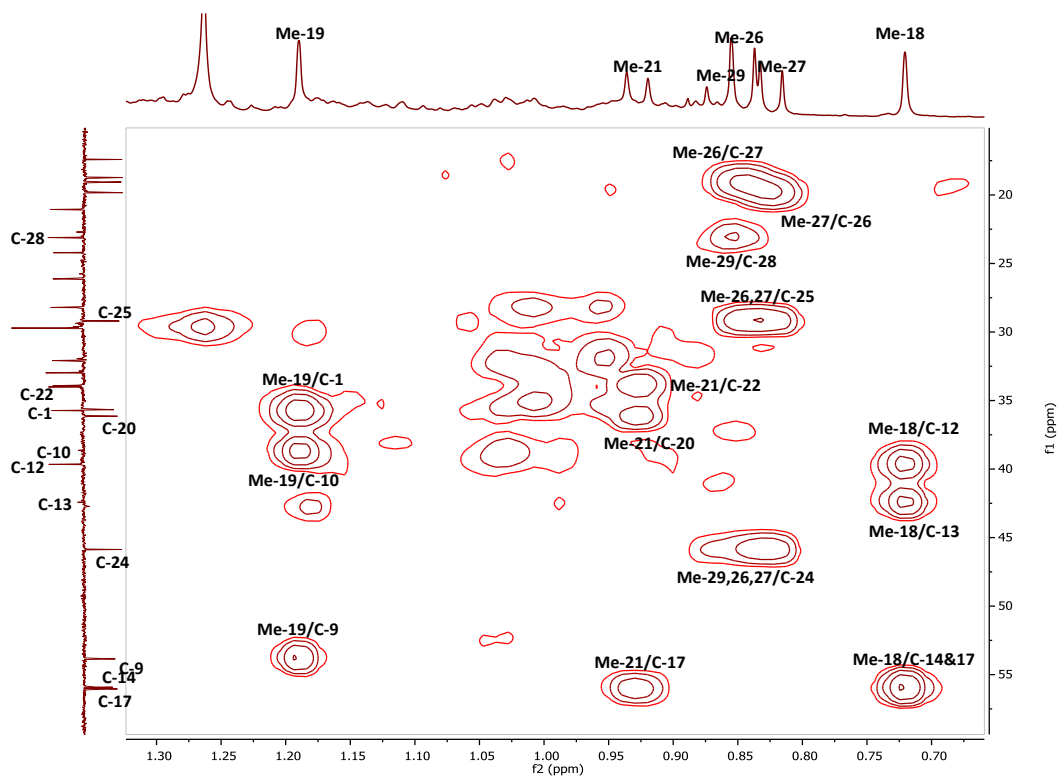


Figure 3.139: Full COSY spectrum (400 MHz) of HM-18 in CDCl₃



(A)



(B)

Figure 3.140: (A): HMBC spectrum (400 MHz) of HM-18 in CDCl_3 with selected expansion for the olefinic proton correlations; (B): Selected expansion for methyl groups

3.5 Simple phenolics

3.5.1 Characterisation of benzoic acid derivatives

3.5.1.1 Characterisation of HM-19 as 3, 4-dihydroxybenzoic acid (PA)

HM-19 was isolated from the EtOAc extract of the root bark by using Sephadex LH-20 as a brown amorphous solid. On TLC, the compound showed quenching under short UV (λ 254 nm) and appeared as brown spot after spraying with *p*-anisaldehyde-sulphuric acid reagent followed by heating. Its R_f was 0.2 on SiGel when eluted with the mobile phase 50% hexane in EtOAc.

The negative mode HRESI-MS spectrum showed a quasi-molecular ion $[M-H]^+$ at m/z 153.0193, suggesting a molecular formula of $C_7H_6O_4$ (DBE=5).

The 1H NMR spectrum (400 MHz, $(CD_3)_2CO$, Figure 3.142, Table 3.17 on p.246) clearly displayed three protons of an aromatic ABX pattern coupled to each other at δ_H 6.89 (1H, *d*, $J= 8.2$ Hz, H-5), 7.47 (1H, *dd*, $J= 8.2, 2.0$ Hz, H-6) and 7.53 (1H, *d*, $J= 2.0$ Hz, H-2). The 2D COSY experiment showed the strong vicinal coupling between the two proton signals at δ_H 6.89 and 7.47 indicating their adjacent position on the aromatic ring.

The DEPTq135 ^{13}C NMR spectrum (100 MHz, Figure 3.143) showed 7 carbon signals including a carbonyl at δ_C 167.6, three methines and three aromatic quaternaries where two of them were oxygen-bearing ones at δ_C 150.7 and 145.6. The chemical shifts of all hydrogen-bearing carbons were assigned from the HSQC spectrum.

In the HMBC spectrum (Figure 3.144), there were reciprocal 3J correlations from the two protons at δ_H 7.47 (H-6) and 7.53 (H-2) to each other's carbons. Each of these protons also gave 3J correlations to the carbonyl carbon at δ_C 167.6 (C-7) and to the oxygen-bearing carbon at δ_C 150.7 (C-4). 2J correlations to another oxygen-bearing carbon at δ_C 145.6 (C-3) were also observed from them. On the other hand, the doublet signal at δ_H 6.89 (H-5) gave 3J correlations to both of the quaternary carbons at δ_C 123.2 (C-1) and 145.6 (C-3), as well as 2J correlation to the carbon at δ_C 150.7 (C-4) and 4J correlations to the methine at 117.5 (C-2) and the carbonyl at δ_C 167.6 (C-7). These data along with the molecular formula justified the attachment of two hydroxyl groups at the positions-3 and -4 of the benzene ring.

Based on these findings, HM-19 was identified as 3,4-dihydroxybenzoic acid or protocatechuic acid (Figure 3.141). The ^1H , ^{13}C NMR data were in agreement with those published in literature (in CD_3OD) (Gutzeit *et al.*, 2006), where PA was isolated from the concentrated juice of sea buckthorn berries (*Hippophaë rhamnoides* L. ssp. *Rhamnoides*). This is the first report of the isolation of this compound from the root bark of *M. laevis*. It was previously isolated from the aerial parts of other plants such as *Thymus quinquecostatus* var. *japonica* (Lamiaceae) (Lee *et al.*, 2011), *Hedyosmum brasiliense* (Chloranthaceae) (Amoah *et al.*, 2013), and *Centaurea bracteata* Scop. (Asteraceae) (Flamini *et al.*, 2001). PA is also one of the phenolic compounds found in olive oil (Babich and Visioli, 2003).

Various studies have been carried out on PA and it was found to exhibit a variety of biological activities, which are more or less correlated with its antioxidant properties. The Syafni *et al.* (2012) and Chao and Yin (2009) studies reported the antibacterial activity of PA against food spoilage bacteria. While Li *et al.* (2011) and Tung *et al.* (2007) studies reported its potent antioxidant activity using different *in vitro* assays to identify the mechanism of action, which was found to be by both scavenging free radicals and by chelating metal transition ions. These studies suggested PA to be a useful agent in the food industry as a food preservative or as a natural antioxidant. An *in vivo* experimental study by Shi *et al.* (2006) proposed PA as a neuroprotective agent by reducing lipid peroxidative damage and increasing the activity of the endogenous antioxidants in the brain along with its effect in improving the cognition of aged rats. The *in vivo* anti-inflammatory and analgesic activities of PA were reported in Lende *et al.* (2011) experimental study on mice and rats. It significantly inhibited or restored different biological mediators in both acute and chronic rat models of inflammation with potency comparable to those of tested standard drugs. Another *in vivo* study carried out by Beytur *et al.* (2012) demonstrated the effectiveness of PA in preventing and treating the reproductive toxicity in rats due to the exposure to the environmental contaminant, 2,3,7,8-tetrachlorodibenzo-*p*-dioxin (TCDD). In the present study, a preliminary evaluation of the cytotoxicity and the anti-trypanosomal activity of HM-19 was performed (for further details see sections 4.1.1.2 and 4.2.2).

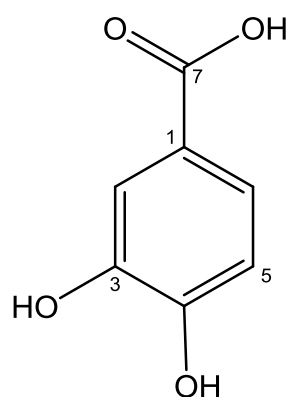


Figure 3.141: Structure of HM-19

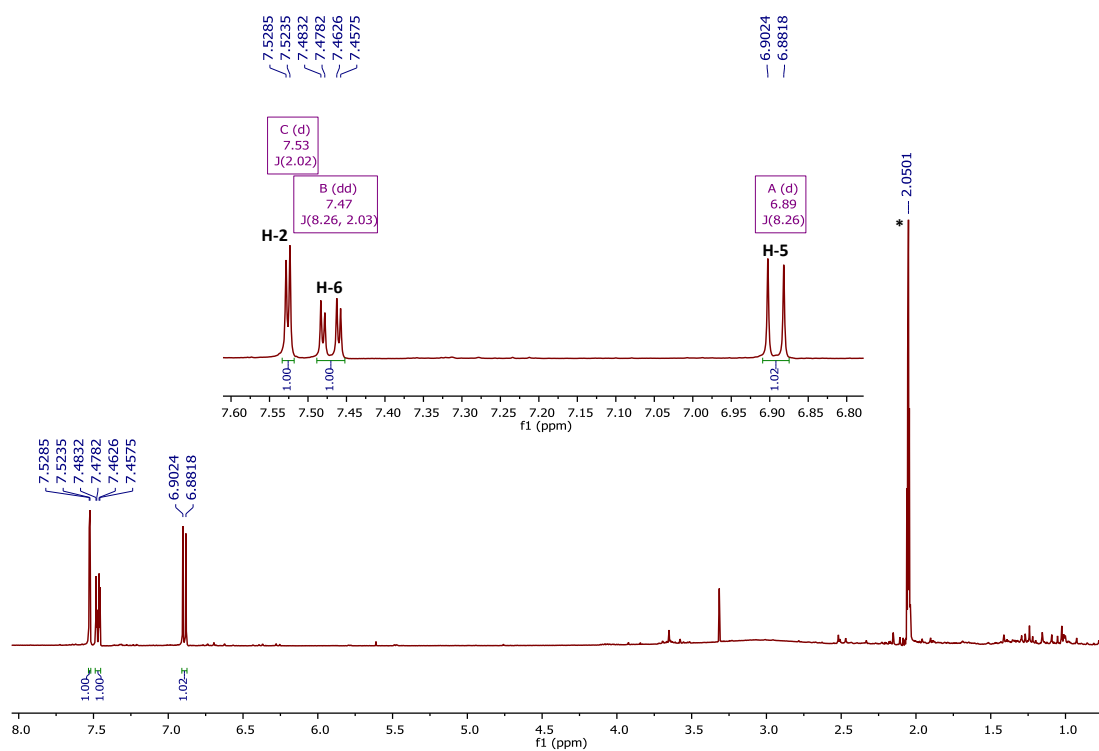


Figure 3.142: Full ^1H NMR spectrum (400 MHz) of HM-19 in $(\text{CD}_3)_2\text{CO}$; (*) $(\text{CH}_3)_2\text{CO}$ residue

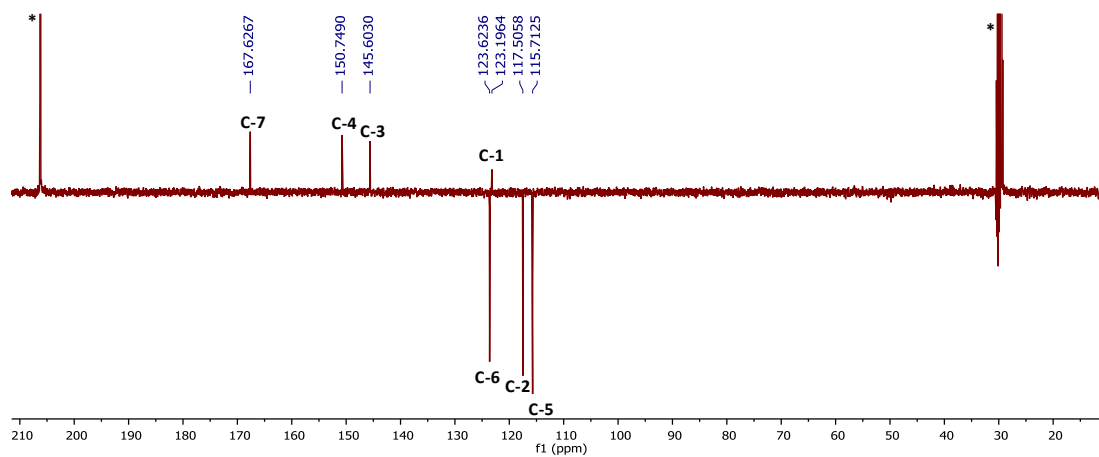


Figure 3.143: Full DEPTq ^{13}C NMR spectrum (100 MHz) of HM-19 in $(\text{CD}_3)_2\text{CO}$ (*)

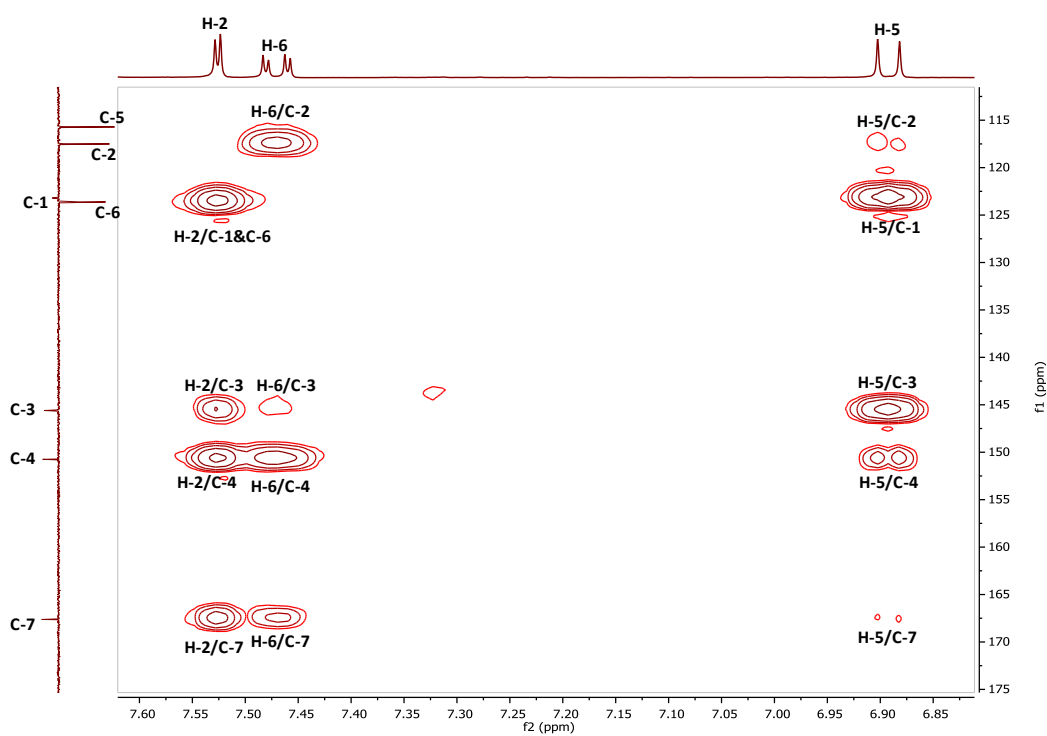


Figure 3.144: HMBC spectrum (400 MHz) of HM-19 in $(\text{CD}_3)_2\text{CO}$

3.5.2 Characterisation of benzaldehyde derivatives

3.5.2.1 Characterisation of HM-20 as *p*-hydroxybenzaldehyde (HBA)

HM-20 was isolated from the EtOAc of the stem bark as an amorphous brown solid. On TLC, the compound showed quenching under short UV (λ 254 nm) and appeared as brown spot after spraying with *p*-anisaldehyde-sulphuric acid reagent followed by heating, which then turned to bluish grey. Its R_f was 0.41 on SiGel when eluted with the mobile phase 50% hexane in EtOAc.

The negative mode HRESI-MS spectrum showed a quasi-molecular ion $[M-H]^+$ at m/z 121.0296, suggesting a molecular formula of $C_7H_6O_2$ (DBE=5).

HM-20 was separated by PTLC from its mixture with a triterpene compound, (HM-14) (see section 3.3.3.2). The structure elucidation was carried out using the same 1D and 2D NMR spectra for the mixture as there was no overlapping in the signals of the two compounds and due to the small quantity of the purified compound. However, the 1H NMR spectrum (Figure 3.146; B) confirmed the success of the separation process.

The 1H NMR spectrum (400 MHz, $CDCl_3$, Figure 3.146 ; A) revealed two signals at δ_H 6.97 (2H, *d*, $J=8.1$ Hz) and at δ_H 7.81 (2H, *d*, $J=8.1$ Hz), which indicated a 1,4-disubstituted aromatic ring. It also showed a signal at δ_H 9.87 (1H, *s*) which correlated with a carbonyl carbon at δ_C 190.8 indicating the existence of an aldehyde function. In the HMBC spectrum (Figure 3.148), the signal at δ_H 7.81(H-2 & 6) showed mutual 3J correlations to each other carbon at δ_C 132.3 (C-6 & 2) and to the carbonyl at δ_C 190.8 (C-7) as well as to the oxygen-bearing quaternary carbon at δ_C 161.6 (C-4). On the other hand, the signal at δ_H 6.97 (H-3 & 5) showed mutual 3J correlations to each other carbon at δ_C 115.9 (C-5 & 3) and to the quaternary carbon at δ_C 129.9 (C-1). Finally, the signal at δ_H 9.87 (H-7) gave 3J and 2J correlations to the methine carbons at δ_C 132.3 (C-6 & 2) and to the quaternary carbon at δ_C 129.9 (C-1), respectively.

Based on these results, HM-20 was identified as *p*-hydroxybenzaldehyde (HBA) (Figure 3.145). The spectral data were in agreement with those published in literature (Guo *et al.*, 2012). This compound was previously isolated from the root bark of *M. macrocarpa* "Chuchuguasa" by Tizkova *et al.* (2013), but is reported here for the first time from the stem bark of *M. laevis*.

HBA showed a weak antioxidant activity when tested as one of the major component of *Vanilla planifolia* extract using β -carotene-linoleate and DPPH *in vitro* assays by Shyamala *et al.* (2007). As an isolate from marine red alga *Laurencia papillosa* (Rhodomelaceae, Rhodophyta), its *in vitro* anti-malarial activity was assessed against *P. falciparum* and the results showed a weak yet a selective activity comparing to standard drugs (Wright *et al.*, 1996). Lim *et al.* (2008) *in vitro* and *in vivo* experimental study reported the anti-inflammatory, anti-angiogenic and anti-nociceptive activities of HBA by inhibiting the induction of the inflammatory mediators such as NO and cyclooxygenase-2 (COX-2) in dose-dependent manner. The Park *et al.* (2011) experimental study on the *Gastrodia elata* Blume water extract reported the ability of HBA, as major constituent, to reduce fat accumulation in the 3T3-L1 adipocytes by increasing fatty acid oxidation and to reduce insulin resistance by enhancing its action via increasing insulin-stimulated glucose uptake in a dose-dependent manner. Tao *et al.* (2006) study investigated the activity of HBA and its derivatives as inhibitors for the enzymes involved in the metabolism of γ -aminobutyric acid (GABA) which its elevated levels in brain tissues have therapeutic applications in neurological disorders. It was found that HBA worked as a competitive inhibitor and the presence of benzene ring along with a hydroxyl group at *para* position to a carbonyl function is the key feature for this activity. In the present study, a preliminary evaluation of the cytotoxicity and the anti-trypanosomal activity of HM-20 was performed (for further details see sections 4.1.2.2 and 4.2.2).

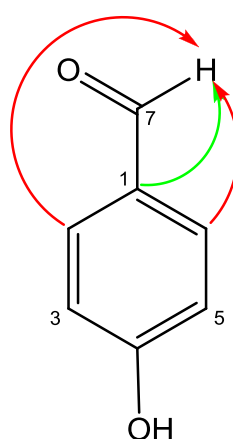


Figure 3.145: Structure of HM-20 with key HMBC correlations
 (\rightarrow) 3J (\rightarrow) 2J ^{13}C to 1H connectivity

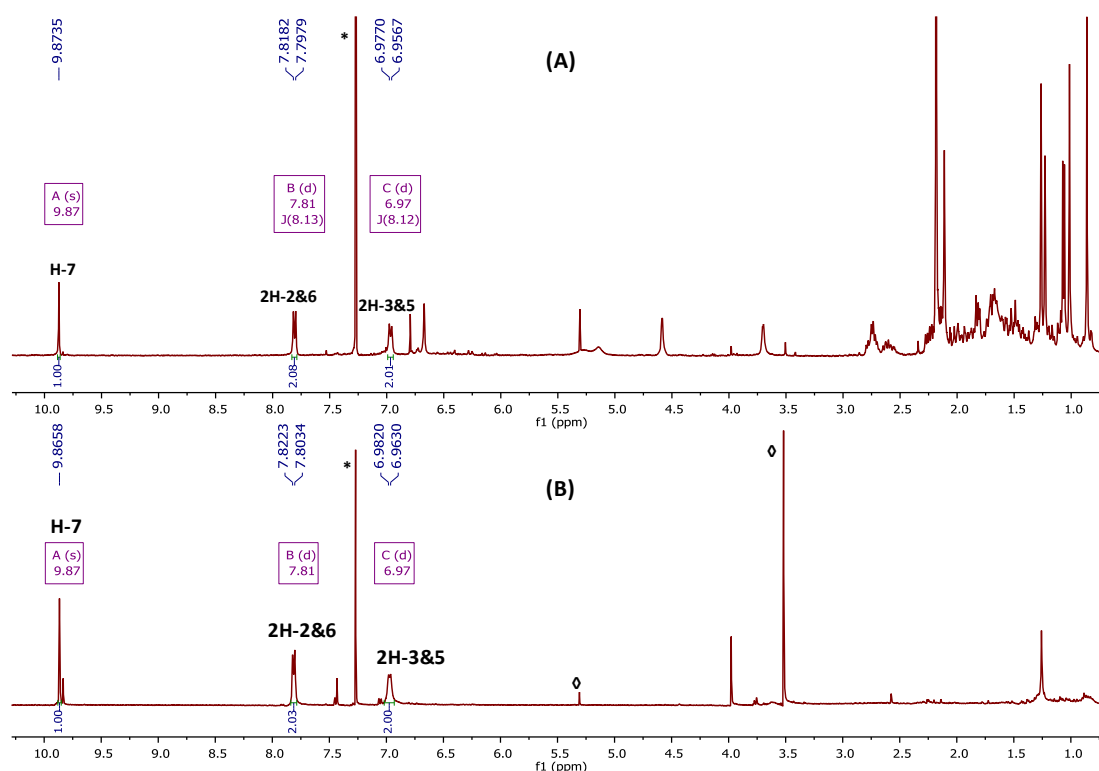


Figure 3.146: (A); ^1H NMR spectrum (400 MHz) of HM-20 in CDCl_3 in mixture, (B); ^1H NMR spectrum (400 MHz) of HM-20 in CDCl_3 after separation, (\diamond) Solvent impurity [MeOH & DCM]

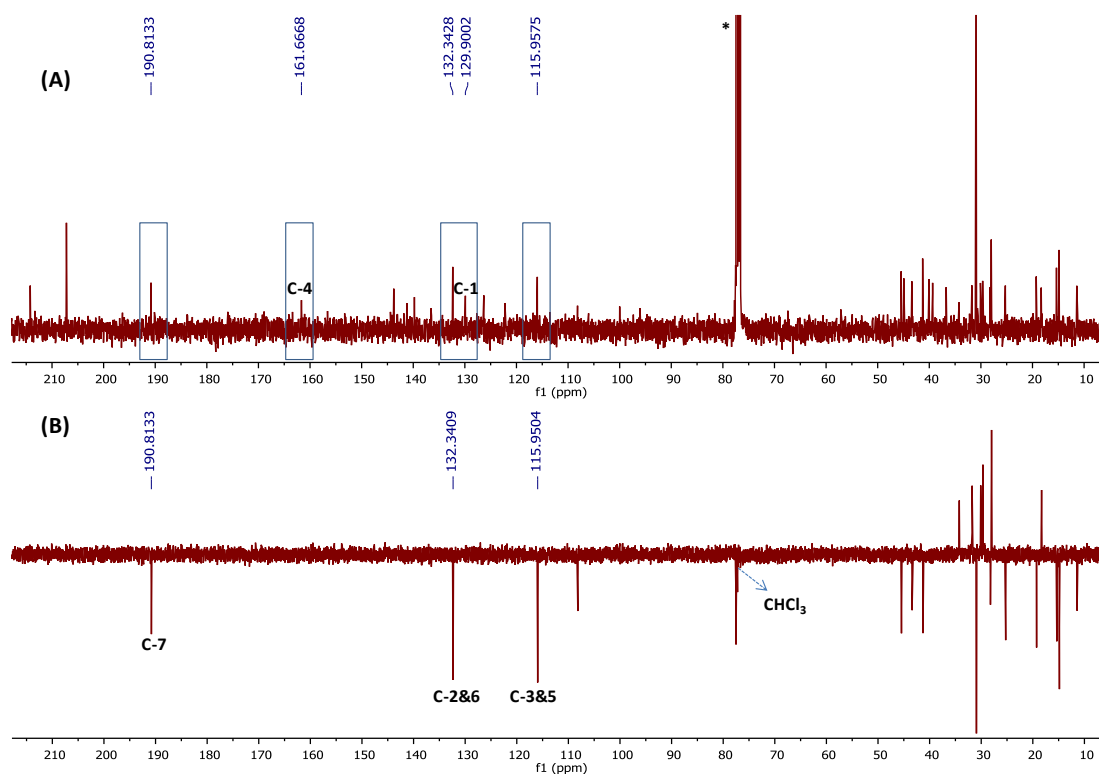


Figure 3.147: Full ^{13}C NMR (A) and DEPT 135 (B) spectra (100 MHz) of HM-20 in CDCl_3 (*) in mixture

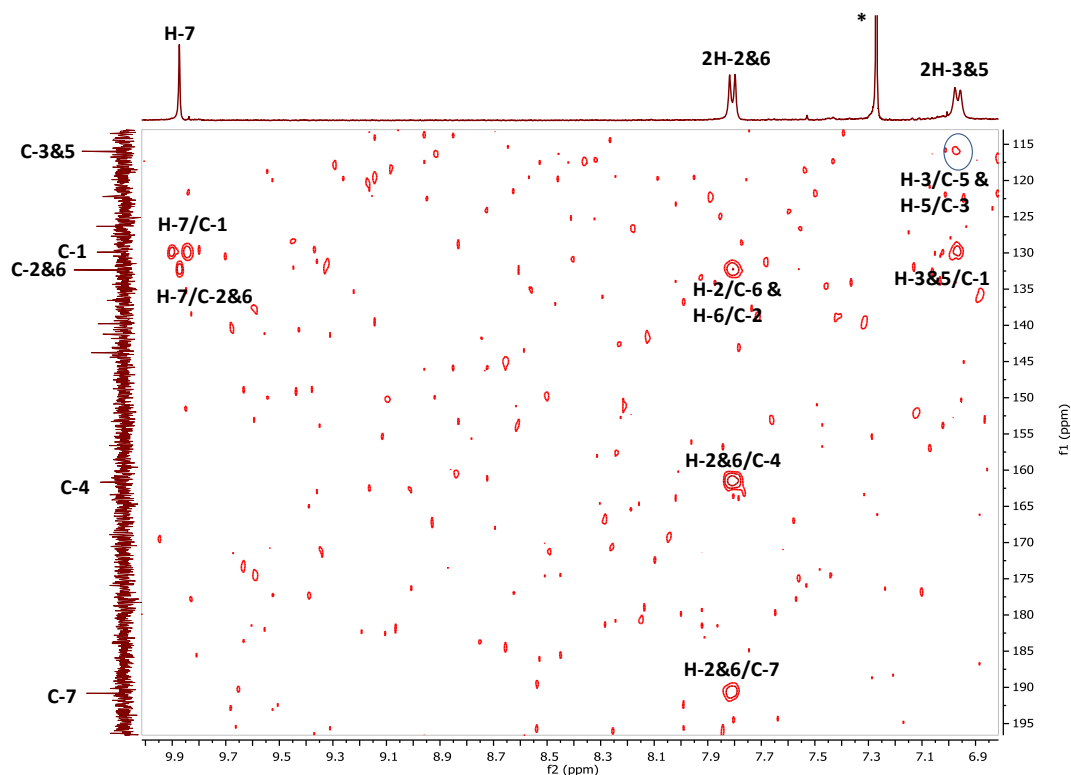


Figure 3.148: HMBC spectrum (400 MHz) of HM-20 in CDCl_3

Table 3.17: ^1H (400 MHz) and ^{13}C (100 MHz) NMR data of the isolated simple phenolics

Position	HM-19 (CD_3) $_2\text{CO}$		HM-20(CDCl_3)	
	δ_{H}	δ_{C}	δ_{H}	δ_{C}
1	-	123.2	-	129.9
2	7.53 (1H, <i>d</i> , <i>J</i> = 2.0 Hz)	117.5	7.81 (1H, <i>d</i> , <i>J</i> =8.1 Hz)	132.3
3	-	145.6	6.97 (1H, <i>d</i> , <i>J</i> =8.1 Hz)	115.9
4	-	150.7	-	161.6
5	6.89 (1H, <i>d</i> , <i>J</i> = 8.2 Hz)	115.7	6.97 (1H, <i>d</i> , <i>J</i> =8.1 Hz)	115.9
6	7.47 (1H, <i>dd</i> , <i>J</i> = 8.2, 2.0 Hz)	123.6	7.81 (1H, <i>d</i> , <i>J</i> =8.1 Hz)	132.3
7	-	167.6	9.87 (1H, <i>s</i>)	190.8

3.6 Isocoumarin

3.6.1 Characterisation of HM-21 as (\pm) mellein

HM-21 was isolated from the EtOAc of the stem bark as yellowish oil. On TLC, the compound showed quenching under short UV (λ 254 nm) and appeared as a purple spot after treatment with *p*-anisaldehyde-sulphuric acid reagent followed by heating. Its R_f was 0.61 on SiGel when eluted with the mobile phase 50% hexane in EtOAc. The negative mode HRESI-MS spectrum showed a quasi-molecular ion $[M-H]^+$ at m/z 177.0559, suggesting a molecular formula of $C_{10}H_{10}O_3$ (DBE=6).

The 1H NMR spectrum (400 MHz, $CDCl_3$, Figure 3.150, Table 3.18) revealed the presence of a sharp downfield singlet at δ_H 11.04 (1H, *s*), a doublet of doublet at δ_H 7.42 (1H, *dd*, $J= 8.4, 7.4$ Hz), a doublet at δ_H 6.90 (1H, *d*, $J= 8.4$ Hz), a doublet of quartet at δ_H 6.70 (1H, *dq*, $J= 7.4, 1.0$ Hz), a multiplet at δ_H 4.74 (1H, *m*), a doublet at δ_H 2.94 (2H, *d*, $J= 7.4$ Hz) and a doublet methyl at δ_H 1.54 (3H, *d*, $J= 6.4$ Hz).

In COSY spectrum (Figure 3.154), the methine proton at δ_H 4.74 showed vicinal coupling with both of the methyl at δ_H 1.54 and the methylene protons at δ_H 2.94 which justified their multiplicities. On the other hand, the methine proton at δ_H 7.42 coupled with both of the methine protons at δ_H 6.90 and 6.70, which indicated their positions in the same spin system and in a sequential order.

Since the molecular formula of this compound indicated its composition of ten carbons, and due to the low yields of it, the DEPTq135 ^{13}C NMR spectrum (100 MHz, Figure 3.151) only showed the presence of seven carbon signals including one quaternary at δ_C 139.4, three aromatic methines, one oxymethine at δ_C 76.1, one methylene and one methyl. Therefore, the carbon shifts of the three "missing" carbons were extracted from the HMBC experiment as they were two quaternaries and one carbonyl.

In the HMBC spectrum (Figure 3.153), the two aromatic methine protons at δ_H 6.70 and 6.90 showed 3J correlations to each other carbons and to an aromatic quaternary at δ_C 108.3. The most deshielded methine proton at δ_H 7.42, which according to the COSY analysis should be located in between the former two methines, showed 3J correlations to another aromatic quaternary at δ_C 139.4 and to a highly deshielded oxygen-bearing one at δ_C 162.2. This suggested a substructure

comprises of a tri-substituted aromatic ring A. Furthermore, the methine proton at δ_{H} 6.70 showed 3J correlation to the methylene carbon at δ_{C} 34.6, where in turn, the methylene protons at δ_{H} 2.94, corresponding to the latter carbon, gave 3J correlations to the former methine carbon at δ_{C} 117.9, to the aromatic quaternary at δ_{C} 108.3 and to the methyl at δ_{C} 20.8, as well as 2J correlations to the aromatic quaternary at δ_{C} 139.4 and to the oxymethine carbon at δ_{C} 76.1. Moreover, the sharp singlet at δ_{H} 11.04, which did not have any direct coupling with any carbon, indicated the presence of one hydrogen-bonded hydroxyl group. All these findings gave indications of the presence of a dihydroisocoumarin skeleton. In the HMBC spectrum, the hydroxyl group showed 3J and 2J correlations to the aromatic carbons at δ_{C} 116.2, 108.3 and 162.2, respectively, which were assigned in order as (C-6), (C-9) and (C-8). This confirmed its connectivity to the benzopyranone unit at position-8. Finally, the attachment site of the methyl group on (C-3) was determined by its 3J correlation to the methylene carbon at δ_{C} 34.6 (C-4) as well as 2J correlation to the oxymethine carbon at δ_{C} 76.1 (C-3). This was further confirmed from the NOESY spectrum (Figure 3.155), which showed that the methylene protons at δ_{H} 2.94 (2H-4) have correlations to the methyl group at δ_{H} 1.54 and to the methine proton at δ_{H} 6.70 (H-5).

Due to the very low yield of this compound, it was very difficult to assign the carbonyl group as it did not show in the DEPTq ^{13}C NMR spectrum. However, depending on the molecular formula which confirmed the presence of three oxygen atoms and by the complete analysis of the 1D and 2D NMR experiments and by comparison with literature, this compound was identified as 8-hydroxy-3-methyl-3,4-dihydroisocoumarin-1-one or (\pm) mellein (Figure 3.149). The spectral data were very consistent with the previous reports (Dimitriadis *et al.*, 1997; Flörke *et al.*, 2006). Both enantiomers of mellein occur in nature. It has been found in many fungal cultures (Hill, 1986) and several insects as part of their defence secretions (Gill, 1993) or as a communicative essence (i.e. trail pheromone) (Morgan, 2008). It was also isolated from plants such as *Celastrus rugosus* (Celastraceae) (Chang *et al.*, 2013). However, this is the first report of its isolation from *M. laevis*.

The less common stereoisomer, (*S*)-(+)-mellein or ochracin, was found to possess an insecticidal activity (Grove and Pople, 1979). (*R*)-(-)-mellein showed a weak to

moderate antimicrobial activity against a variety of organisms including Gram positive and negative bacteria, fungi and algae in agar diffusion test (Höller *et al.*, 1999; Krohn *et al.*, 1997; Sommart *et al.*, 2008). It also exhibited antiviral activity against hepatitis C virus (HCV) with an IC₅₀ value of 35 µM by inhibiting the viral protease NS3, which is responsible for the final stage of poly-protein processing during virus replication. At a concentration 200 µg/ml, it caused 100% mortality of *Artemia salina* larvae, i.e. possessing zootoxic activity (Parisi *et al.*, 1993). Further information about the biological activities of this compound is mentioned in sections 4.1.2.2 and 4.2.3.

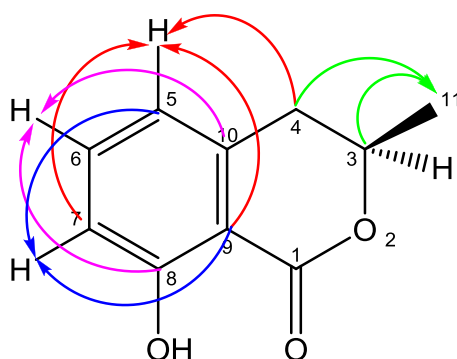


Figure 3.149: Structure of (R)-HM-21 with important HMBC correlations

Table 3.18: Comparison of ¹H (400 MHz) and ¹³C (100 MHz) NMR data of HM-21 and ¹H (300 MHz) and ¹³C (75 MHz) of (±) Mellein in CDCl₃ (Dimitriadis *et al.*, 1997)

Position	HM-21		(±) Mellein	
	δ _H	δ _C	δ _H	δ _C
1	-	†	-	169.9
2	-	-	-	-
3	4.74 (1H, <i>m</i>)	76.1	4.73 (1H, <i>m</i>)	76.1
4	2.94 (2H, <i>d</i> , <i>J</i> =7.4 Hz)	34.6	2.93 (2H, <i>d</i> , <i>J</i> =7.3 Hz)	34.6
5	6.70 (1H, <i>dq</i> , <i>J</i> =7.4, 1.0 Hz)	117.9	*6.69 (1H, <i>d</i> , <i>J</i> =7.3 Hz)	117.9
6	7.42 (1H, <i>dd</i> , <i>J</i> = 8.4,7.4 Hz)	136.1	7.41 (1H, <i>m</i>)	136.1
7	6.90 (1H, <i>d</i> , <i>J</i> =8.4 Hz)	116.2	*6.89 (1H, <i>d</i> , <i>J</i> =8.3 Hz)	117.0
8	-	162.2	-	162.1
9	-	108.3	-	108.2
10	-	139.4	-	139.3
11	1.54 (3H, <i>d</i> , <i>J</i> = 6.4 Hz)	20.8	1.53 (3H, <i>d</i> , <i>J</i> = 6.3 Hz)	20.8
8-OH	11.04 (1H, <i>s</i>)	-	11.03 (1H, <i>s</i>)	-

(†) Could not be assigned. (*) These protons were assigned in reverse order in the report.

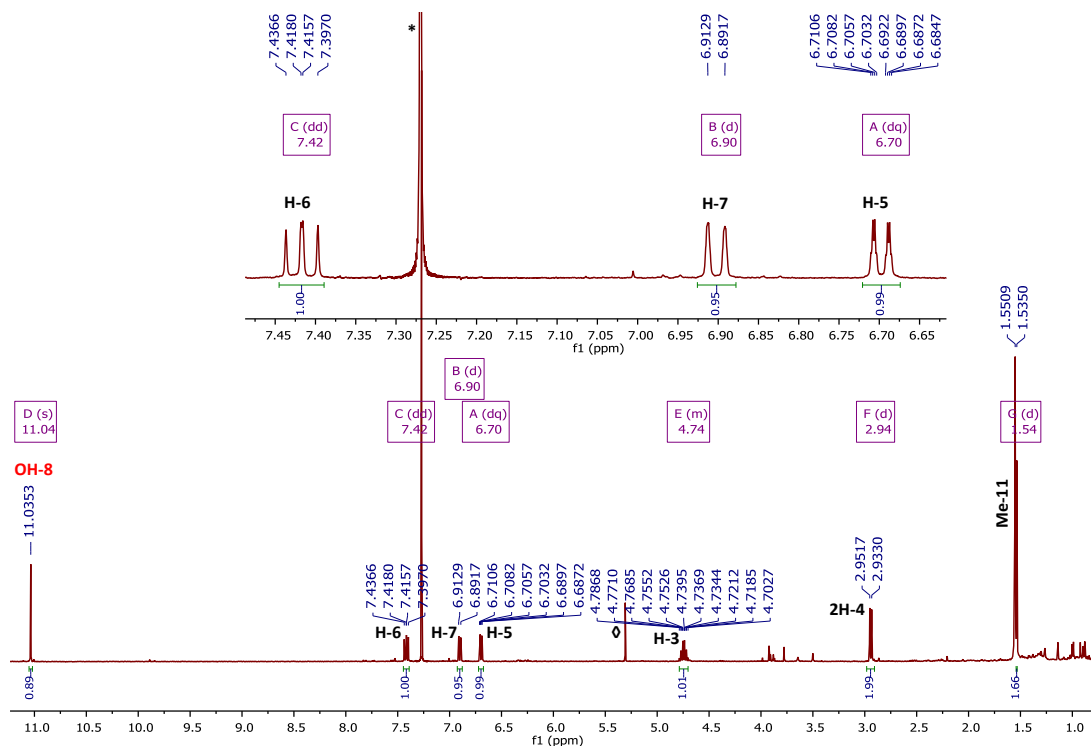


Figure 3.150: Full ^1H NMR spectrum (400 MHz) of HM-21 in CDCl_3 with selected expansion of the aromatic protons; (*) CHCl_3 residue, (\diamond); solvent impurity [DCM]

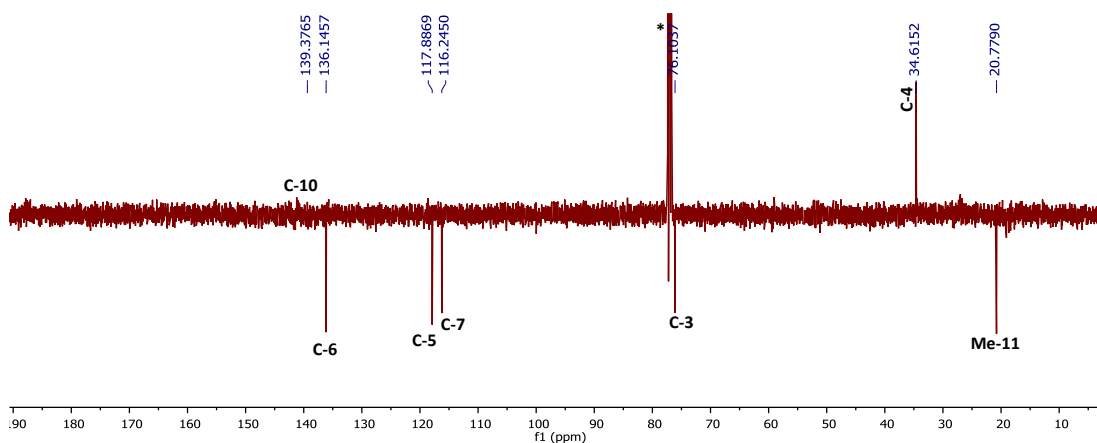


Figure 3.151: Full DEPTq ^{13}C 135 NMR spectrum (100 MHz) of HM-21 in CDCl_3 (*)

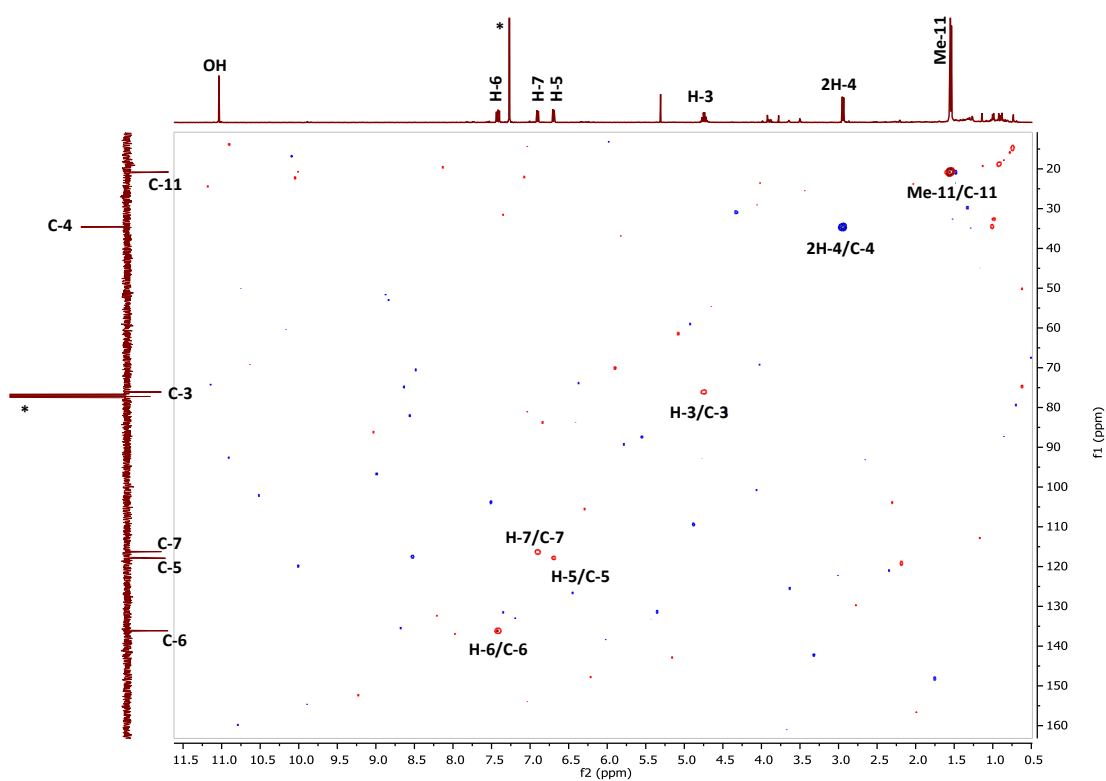


Figure 3.152: Full HSQC spectrum (400 MHz) of HM-21 in CDCl_3 (*)

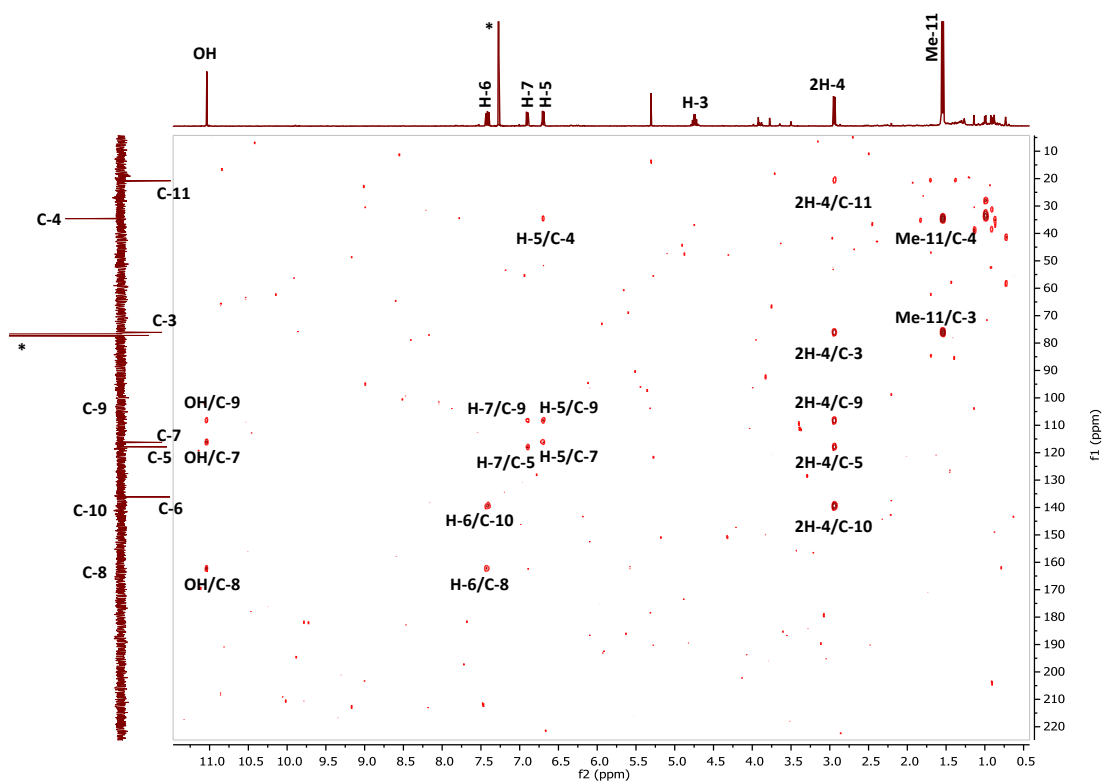


Figure 3.153: Full HMBC spectrum (400 MHz) of HM-21 in CDCl_3 (*)

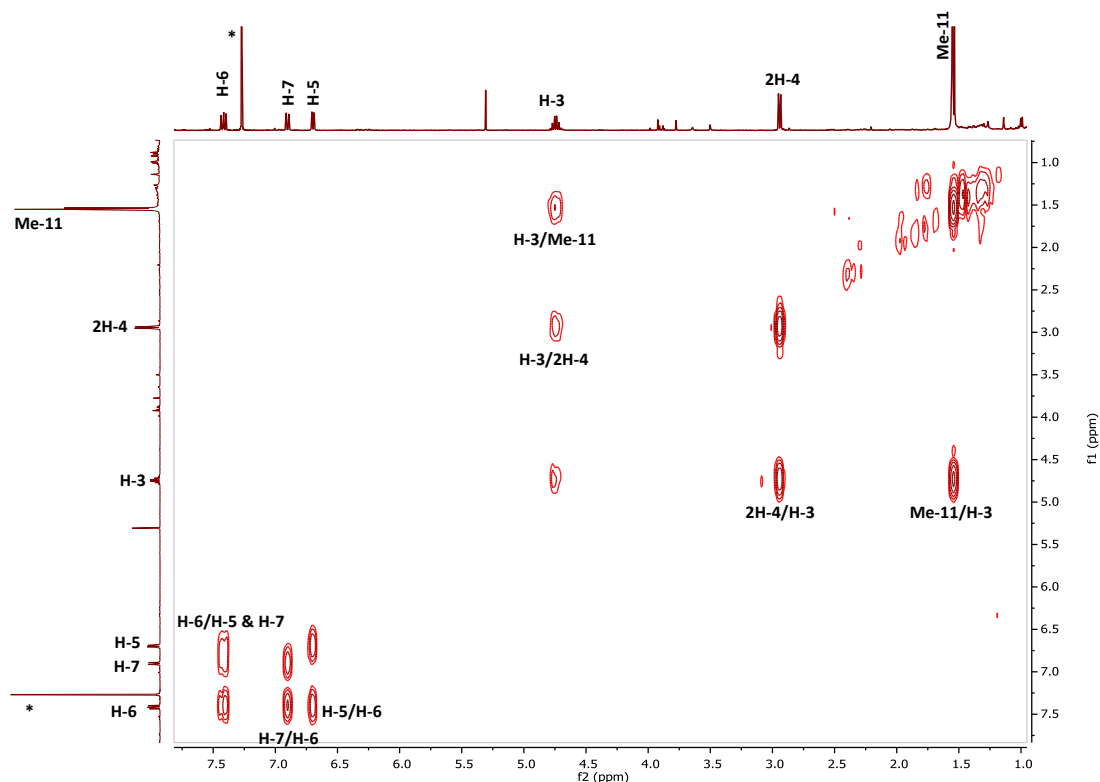


Figure 3.154: ^1H - ^1H COSY spectrum (400 MHz) of HM-21 in CDCl_3

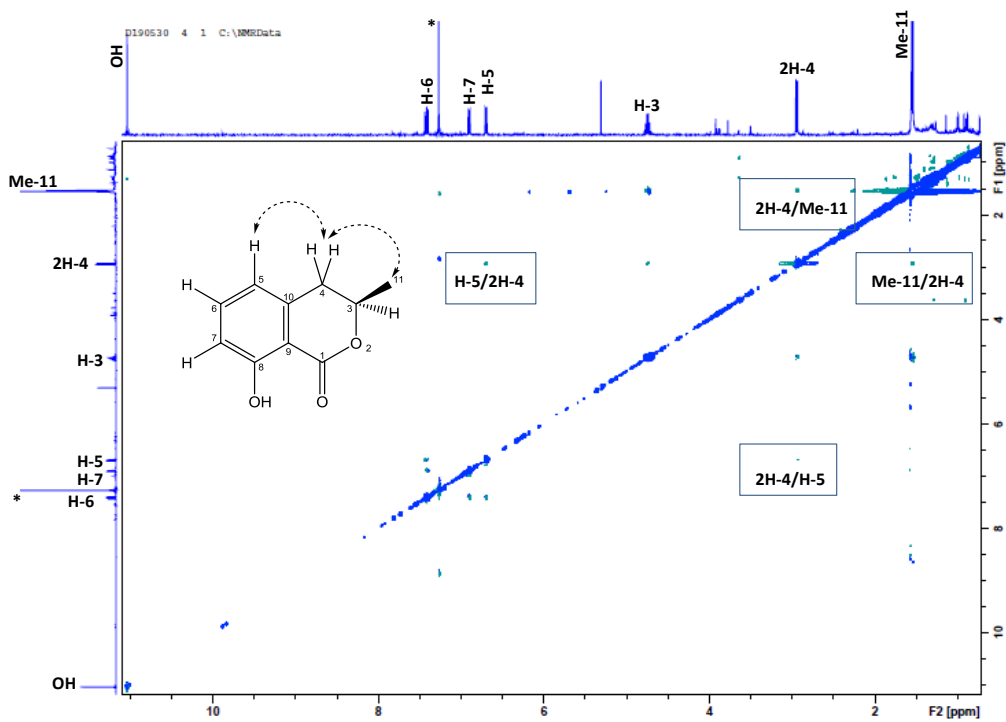


Figure 3.155: Full NOESY spectrum (400 MHz) in CDCl_3 using TopSpin 3.2 software and key NOE correlations of HM-21

3.7 General illustrative and supportive findings and overall conclusion

The two parts of the plant (about half kilogram each) produced a rubber-like substance after extraction, but with different yields, and mainly from the less polar extract. The major share came from the n-hexane extract of the root bark with 36 g (6.5% yield) compared to that of the stem bark with only 4 g (0.6% yield). The presence of this substance, which was identified as *trans*-1,4-polyisoprene (gutta-percha), is consistent with being one of the chemotaxonomic markers of the Celastraceae family (Hegnauer, 1966).

The colours of the crude extracts could be generally described as a gradient between red and brown with the exception of the EtOAc extract of the stem bark which gave a shade of greenish brownish colour. Furthermore, the initial and the most interesting sub-fractions generated from the partial fractionation of the n-hexane extract of the stem bark by VLC technique were greenish in colour.

The previous sections in this chapter discussed in depth the identification process of the compounds isolated from the root and stem barks of the plant *M. laevis*. All the compounds which were purified from the root bark have red or orange colour (the quinonemethides), while those which were found as majors in the n-hexane extract of the stem bark were white or colourless (friedelane-type triterpenes). Figure 3.156 shows a comparison between the crude extracts of both parts on TLC after elution with the mobile phase hexane-EtOAc (50:50%). The left image, shown in daylight after developing, illustrates the presence of the reddish coloured compounds (quinonemethides) as major components in columns A (MLH) and C (MLEt) from the root bark. While the right image after spraying with the reagent *p*-anisaldehyde-sulphuric acid and heating demonstrates the friedelane-type triterpenes as dominant components in column B (MLHs) from the stem bark.

These experimental observations and the physical findings provide scientific evidence which emphasises the previous studies about the biosynthetic pathway of these types of triterpenoids. As mentioned in section 1.5.3, Scheme 1.1, the Corsino *et al.* (2000) study on *M. aquifolium* signified that the friedelane-type triterpenes are putative precursors of the quinonemethide triterpenes, which are biosynthesised in the leaves and then translocated to the root bark where they are transformed to the cytotoxic quinonemethides. The latter triterpenoids then could undergo several

oxidation and rearrangement processes to form other classes of biogenetic congeners, see partial Scheme 3.1 (Gunatilaka, 1996).

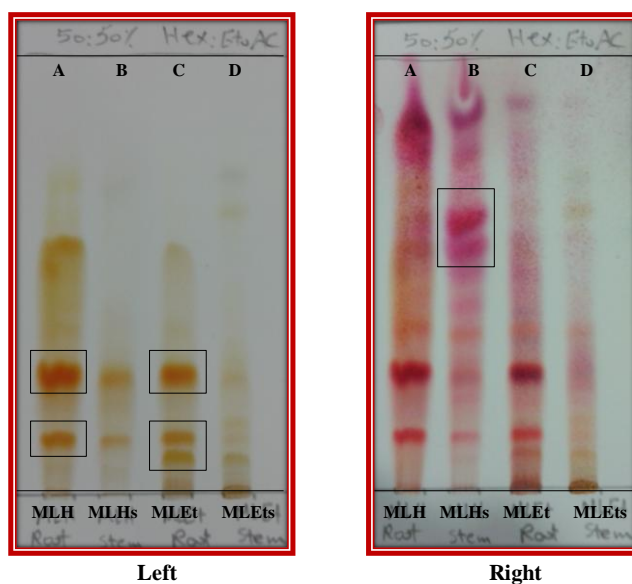
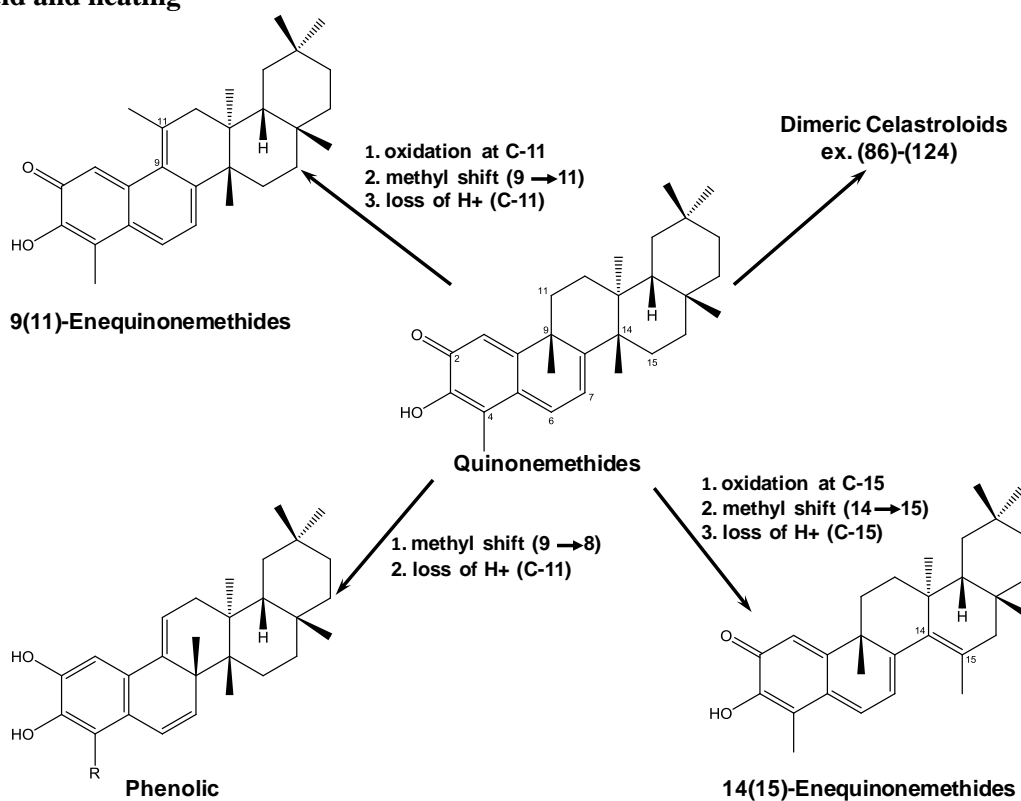


Figure 3.156: Comparison between root and stem bark extracts (A & C) and (B & D), respectively, on TLC. (Left); after developing with the mobile phase hexane-EtOAc (50:50%) as seen in daylight, (Right); after spraying with *p*-anisaldehyde-sulphuric acid and heating



Scheme 3.1: Some major classes of celastroloids and their structural (biogenetic) interrelationship (Gunatilaka, 1996)

CHAPTER IV

4. RESULTS AND DISCUSSION

PART II: BIOLOGICAL STUDIES

4.1 *In vitro* cytotoxicity assessment

The n-hexane, EtOAc and MeOH crude extracts of both the root and stem barks of *M. laevis* along with most of the isolated compounds were tested on A375 and Hs27 cell lines to determine their effects on the viability of these cells, using a resazurin assay (section 2.2.4.1.7). After 48 h of the addition of the samples, the cell viability was determined and EC₅₀ values were obtained (Table 4.2).

4.1.1 *Effects of crude extracts from the root bark of M. laevis on cell viability*

The effects of the crude extracts from the root bark were tested on viability of Hs27 and A375 cells. Dose response studies (100 to 3.125 µg/ml) were carried out in replicate (n=3 or 6).

As shown in Figure 4.1, both the n-hexane (MLH) and ethyl acetate (MLEt) extracts were toxic to the A375 melanoma cells as they produced significant ($P < 0.01$) reduction in viability compared to the control at all tested concentrations. On the Hs27 normal cells, both extracts caused significant ($P < 0.01$) reduction in the viability at concentrations ≥ 6.25 and ≥ 12.5 µg/ml for MLH and MLEt, respectively. However, at 3.125 µg/ml, both extracts were significantly toxic to the A375 cells but with no significant toxicity to the Hs27 cells. This could be an indicator of the potential selectivity to cancer cells as the difference in toxicity between the two cell lines was statistically significant ($P < 0.001$), though, this should be further investigated. On the other hand, the methanol extract (MLM) showed no toxicity to either cell line.

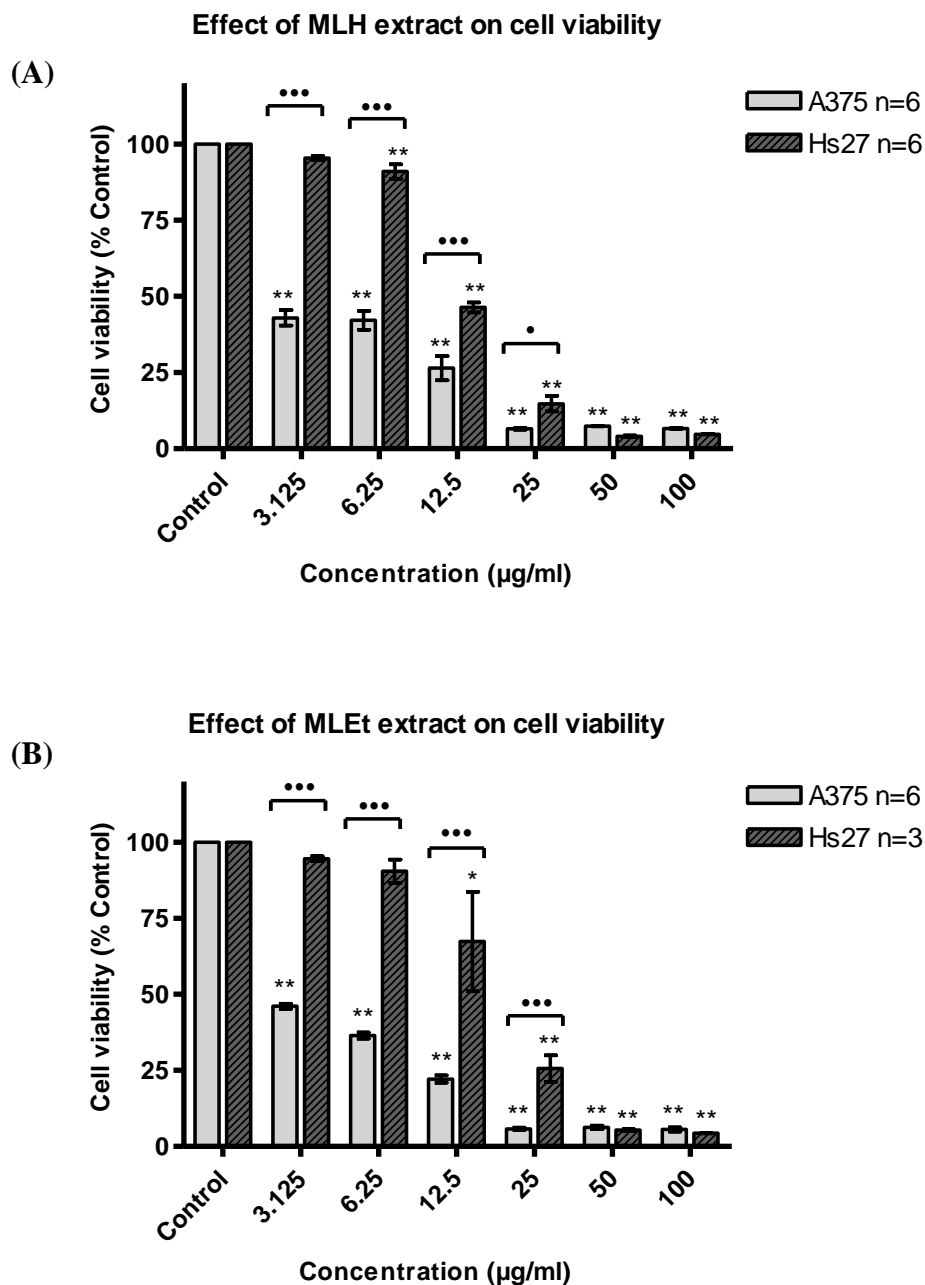


Figure 4.1: The cytotoxicity effect of n-hexane (A) and EtOAc (B) crude extracts from the root bark of *M. laevis* on A375 and Hs27 cell lines using a resazurin assay. Values are presented as a percentage of the untreated control (\pm SEM). The assays were performed in a 96-well plate using the same conditions to compare the effects on cell viability. The data were analysed by Dunnett post-test, * $P < 0.05$ & ** $P < 0.01$ vs. control, and by Bonferroni post-test, * $P < 0.05$ & *** $P < 0.001$ A375 vs. Hs27 cells.

4.1.1.1 Effects of constituents from the n-hexane extract (MLH) on cell viability

The four isolated celastroloids from the n-hexane extract of the root bark, including netzahualcoyondiol (HM-7), pristimerin (HM-10), netzahualcoyone (HM-8) and the new compound 22(α)-hydroxynetzahualcoyene (HM-9), showed high toxicity on both cell lines as they caused a highly significant ($P < 0.01$) reduction in cell viability at all tested concentrations compared to the control. The EC_{50} values were 1.7, 4.9 $\mu\text{g/ml}$ (3.5, 10.1 μM) for HM-7 and 0.04, 1.8 $\mu\text{g/ml}$ (0.08, 3.9 μM) for HM-10 on A375 and Hs27, respectively. Although HM-7 produced a small ($< 15\%$) but significant ($P < 0.01$) reduction in cell viability of Hs27 cells compared to the control at 3.125 $\mu\text{g/ml}$, the toxicity difference between the two cell lines was statistically significant ($P < 0.001$) as seen in Figure 4.2.

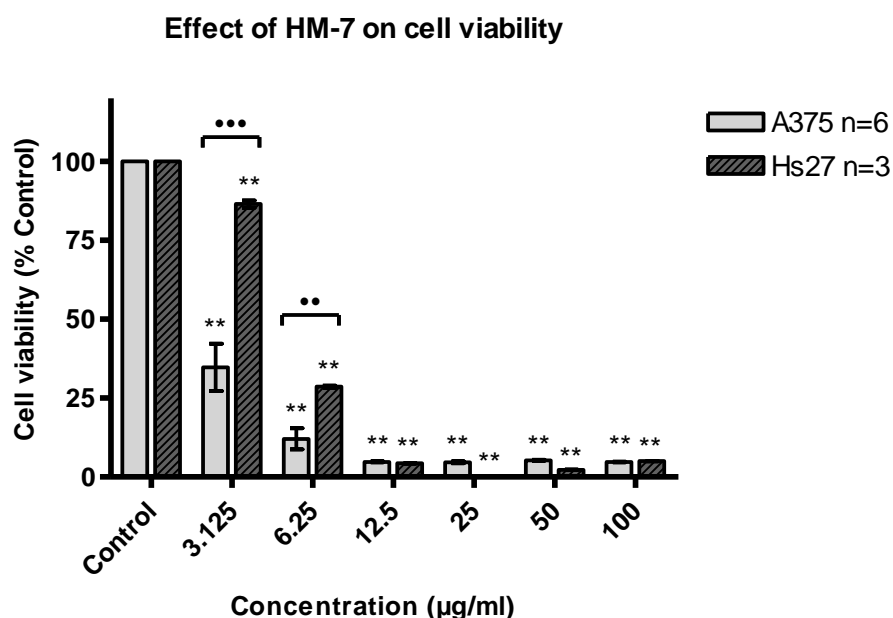


Figure 4.2: The cytotoxicity effect of netzahualcoyondiol (HM-7) on A375 and Hs27 cell lines using resazurin assay. Values are presented as a percentage of the untreated control (\pm SEM). The assays were performed in a 96-well plate using the same conditions to compare the effects on cell viability. The data were analysed by Dunnett post-test, $**P < 0.01$ vs. control, and by Bonferroni post-test, $**P < 0.01$ & $***P < 0.001$ A375 vs. Hs27 cells.

The cytostatic activity of HM-10, HM-7 and HM-8 against the HeLa cell line (Human Negroid cervix epitheloid carcinoma) was evaluated by Gonzales *et al.* (1988) and Gonzalez *et al.* (1977). All of them showed powerful activity with ID₅₀ of 0.3, 1 and 0.1 µg/ml (0.6, 2.0, 0.2 µM) respectively, and the latter being as active as the anticancer drug 6-mercaptopurine as cited by Gunatilaka (1996). It was found that these compounds stopped the formation of DNA, RNA and protein synthesis within a few minutes. Although a different cell line was used in the previous reports, the results regarding the median inhibitory concentration are relatively comparable with those generated in the present work.

A number of studies have reported the cytotoxicity of HM-10 against several cancer cell lines. Table 4.1 summarises these studies, which showed that pristimerin exhibits a broad spectrum inhibition on all the tested cancer cell lines. However, Costa *et al.* (2008) reported that this compound had poor selectivity on cancer cells as it was cytotoxic to human peripheral blood mononuclear cells (PBMC) with an IC₅₀ of 0.88 µM. In the current work, HM-10 showed potent but not selective activity on A375 and Hs27 cells. These findings seemed to correlate well with those reported in the literature regarding pristimerin cytotoxicity. In spite of the differences in the assays used for the cytotoxicity assessment in those studies, the results should still be comparable as it was found by Henriksson *et al.* (2006) when using *in vitro*-cultivated squamous cell carcinoma of the head and neck (SCCHN). Generally, the underlying mechanisms of the cytotoxic activity of the quinonemethide triterpenes involved interaction with DNA as a key feature (Gojman *et al.*, 1985; Setzer *et al.*, 2001).

Table 4.1: Cytotoxic activity of pristimerin on human tumour cell lines

Cell line	µg/ml (µM)	Assay	Reference(s)
L-1210 (lymphoid leukemia)*	0.36 (0.77) ^a	MTT	(O Shirota et al., 1994)
P-388 (lymphocytic leukemia)*	0.12 (0.25) ^a		
KB (epidermoid nasopharyngeal)	0.55 (1.18) ^a		
	0.1 (0.21) ^b	SRB	(Chang <i>et al.</i> , 2003)
A549 (lung cancer)	0.31 (0.66) ^b	SRB	(Chang <i>et al.</i> , 2003)
	(0.61) ^a	MTT	(Wu <i>et al.</i> , 2005)
MCF-7 (breast cancer)	0.14 (0.30) ^b	SRB	(Chang <i>et al.</i> , 2003)
	(0.42) ^a	MTT	(Wu <i>et al.</i> , 2005)
HCT-8 (colon cancer)	0.15 (0.32) ^b	SRB	(Chang <i>et al.</i> , 2003)
	0.69 (1.48) ^a	MTT	(Costa <i>et al.</i> , 2008)
KB-VIN (vincristine-resistant KB)	0.29 (0.62) ^b	SRB	(Chang <i>et al.</i> , 2003)
U-87-MG (glioblastoma)	0.17 (0.37) ^b		
PC-3 (prostate cancer)	0.23 (0.49) ^b		
1A9 (ovarian cancer)	0.1 (0.21) ^b		
PTX10 (ovarian cancer with β-tubulin mutation)	0.11 (0.24) ^b		
HepG2 , Hep3B (liver cancer)	(0.61) ^a	MTT	(Wu <i>et al.</i> , 2005)
HL-60 (promyelocytic leukemia)	0.61 (1.31) ^a	MTT	(Costa <i>et al.</i> , 2008)
K-562 (chronic myelocytic leukemia)	1.49 (3.20) ^a		
SF-295 (glioblastoma)	0.57 (1.22) ^a		
MDA/MB-435 (melanoma)	0.26 (0.55) ^a		
BxPC-3, PANC-1, AsPC-1 (pancreatic cancer)	(0.19-0.30) ^a	CCK-8	(Wang <i>et al.</i> , 2012)

(*): murine cells; (^a): IC₅₀; (^b): ED₅₀

sulforhodamine B (SRB) assay/ Cell Counting Kit-8 (CCK-8) assay

3-(4,5-dimethylthiazol-2-yl)-2,5-diphenyltetrazolium bromide (MTT) assay

The ¹HNMR spectrum of the MLH extract of the root bark revealed the presence of quinonemethide-type triterpenes as major constituents in addition to steroids and fats. Therefore, according to the aforementioned observations, the activity of this extract could be attributable to the combined effects of these quinonemethides. However, the activity observed for the isolated compounds was stronger than that for the MLH extract, suggesting that their activities might be decreased by the presence of other (non-purified) phytochemical(s) or the compounds acting antagonistically. These results, even being preliminary, provide some scientific basis for the ethnomedicinal use of *M. laevis* as an anti-tumour agent in skin cancer as reported by Gonzalez *et al.* (1982), who attributed this effect to the presence of similar derivatives such as

tingenone **65** and 22 β -hydroxytingenone **66**, which were isolated from the petroleum ether and chloroform extracts of the root bark.

4.1.1.2 *Effects of constituents from the EtOAc extract (MLEt) on cell viability*

Three compounds were isolated from the active EtOAc extract of the root bark, including HM-12, HM-15 and HM-19. Figure 4.3 shows their effects on the viability of A375 and Hs27 cell lines.

The new celastroid, 22(β)-hydroxycelastrol (HM-12), showed potent and significant ($P < 0.01$) toxicity to the A375 cells at all tested concentrations compared to the control with an EC_{50} of 2.1 $\mu\text{g/ml}$ (4.4 μM). On Hs27 cells, HM-12 caused a small ($< 20\%$), but significant ($P < 0.01$) reduction in cell viability at 6.25 $\mu\text{g/ml}$, while it was non-toxic at 3.125 $\mu\text{g/ml}$ and gave a higher EC_{50} value of 9.2 $\mu\text{g/ml}$ (19.8 μM). The cytotoxicity differences at the two aforementioned concentrations between the two cell lines were statistically significant ($P < 0.001$).

The new triterpene, methyl 2,3,22 α -trihydroxy-24,25-dinorfriedelan-1,3,5(10),6,8,14-hexaen-29-oate (HM-15), significantly ($P < 0.01$) decreased the number of viable A375 cells from 12.5 $\mu\text{g/ml}$ compared to the control, while it showed no significant reduction at 6.25 and 3.125 $\mu\text{g/ml}$ with an EC_{50} of 20.2 $\mu\text{g/ml}$ (43.5 μM). On the other hand, only at 100 $\mu\text{g/ml}$, HM-15 caused more than 50% reduction in the viable Hs27 cells compared to the control ($P < 0.01$), while it was non-toxic at concentrations ≤ 25 $\mu\text{g/ml}$ and gave an EC_{50} of 89.1 $\mu\text{g/ml}$ (191.9 μM). From 25 to 100 $\mu\text{g/ml}$ there were significant ($P < 0.001$) differences in cytotoxicity between the two cell lines. The above observations indicate that both HM-12 and HM-15 possess potential selective cytotoxicity to cancer cells with the former being relatively more potent.

Finally, the phenolic compound, protocatechuic acid (PA) (HM-19), showed significant ($P < 0.01$) toxicity to A375 cells from 6.25 $\mu\text{g/ml}$ compared to the control with an EC_{50} of 12.8 $\mu\text{g/ml}$ (83.1 μM), while it produced less but significant ($P < 0.01$) reduction in the Hs27 viability with a higher EC_{50} value of 62.4 $\mu\text{g/ml}$ (405.1 μM). There were statistically significant ($P < 0.001$) differences in cytotoxicity between the two cell lines starting from 6.25 $\mu\text{g/ml}$, particularly, at 50 $\mu\text{g/ml}$, PA caused 93% reduction in the number of viable A375 cells (c.f. 36% in Hs27 cells).

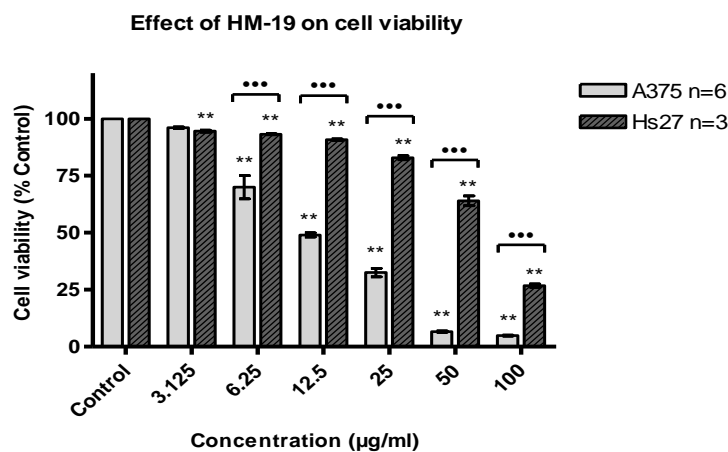
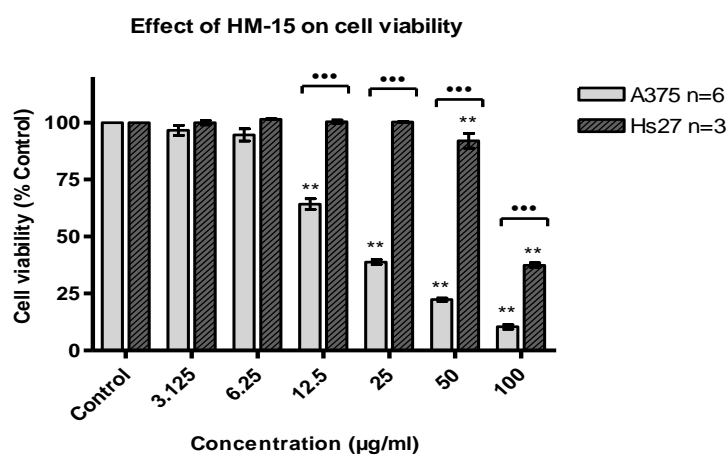
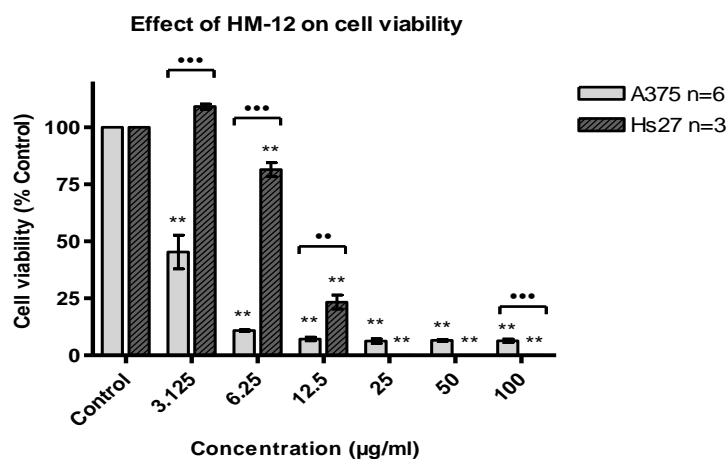


Figure 4.3: Cytotoxicity of isolated compounds from an EtOAc extract of the root bark of *M. laevis* on A375 and Hs27 cell lines using a resazurin assay. Values are presented as a percentage of the untreated control (\pm SEM). The assays were performed in a 96-well plate using the same conditions to compare the effects on cell viability. The data were analysed by Dunnett post-test, ** $P < 0.01$ vs. control, and by Bonferroni post-test, * $P < 0.001$ A375 vs. Hs27 cells.**

The activity of PA in the literature is controversial as it is uncertain whether the compound acts as an antioxidant and suppresses chemical-induced carcinogenesis or whether it induces oxidative stress and promotes tumour formation. *In vivo* trials found that its effect was dependent on the dose used and the time of exposure (Nakamura *et al.*, 2000). At low doses, PA acted as a chemopreventive agent, while at high doses it exhibited carcinogenic activity by enhancing the formation of tumours. An *in vitro* study on five cell lines derived from tissues in the human oral cavity including malignant and non-malignant cells using a neutral red assay showed that PA had no selective toxicity to malignant cells after 24h exposure (Babich *et al.*, 2002). PA in the range 2.5 to 25 mM showed midpoint cytotoxicity values (NR₅₀) from 15.5 to 23.3 mM. It was also reported that PA at elevated levels ≥ 10 mM loses its antioxidative properties and induces oxidative stress which is an important factor in promoting tumour formation.

It is difficult to compare the preliminary results obtained in the current work with those described in Babich *et al.* (2002), since it was found that the experimental design and the exposure duration were important factors in the cytotoxicity of PA. However, the concentrations used here (3.125 to 100 $\mu\text{g/ml}$ or 20.3 to 649.3 μM) fell far below those mentioned above which may justify the preferential anti-proliferative (inhibitory) effect exerted by PA (HM-19) on A375 cells.

The ¹HNMR spectrum of the MLEt extract of the root bark indicated the presence of phenolics and triterpenes under which the aforementioned compounds were classified, in addition to the presence of sterols, fats, triglycerides and tannins. The three isolated compounds from this extract were more polar compared to those isolated from the n-hexane extract. Generally, they all possessed cytotoxic activity against A375 cells at different concentrations; yet, lesser effects were shown on the Hs27 cells. Therefore, the activity of the MLEt extract could be attributable to their combined effects and/ or to those of the other non-purified phytochemical(s).

4.1.2 Effects of crude extracts from the stem bark of *M. laevis* on cell viability

The effects of the crude extracts from the stem bark were tested on the viability of Hs27 and A375 cells. As shown in Figure 4.4, from concentrations ≥ 12.5 $\mu\text{g/ml}$, both MLHs and MLEts extracts affected the viability of the melanoma cells, represented by a significant ($P < 0.01$) decrease in metabolic activity compared to the control. However, this effect was only significant ($P < 0.01$) on Hs27 cells at the highest tested concentration (100 $\mu\text{g/ml}$). At 25 and 50 $\mu\text{g/ml}$, both extracts showed no effects on Hs27 cells but exhibited statistically significant ($P < 0.001$) toxicity differences between the two cell lines. These observations suggest that a concentration range between 25-50 $\mu\text{g/ml}$ for both extracts could have a selective effect on the melanoma cells. On the other hand, the methanol extract (MLMs) of the stem bark showed no toxicity to either cell line.

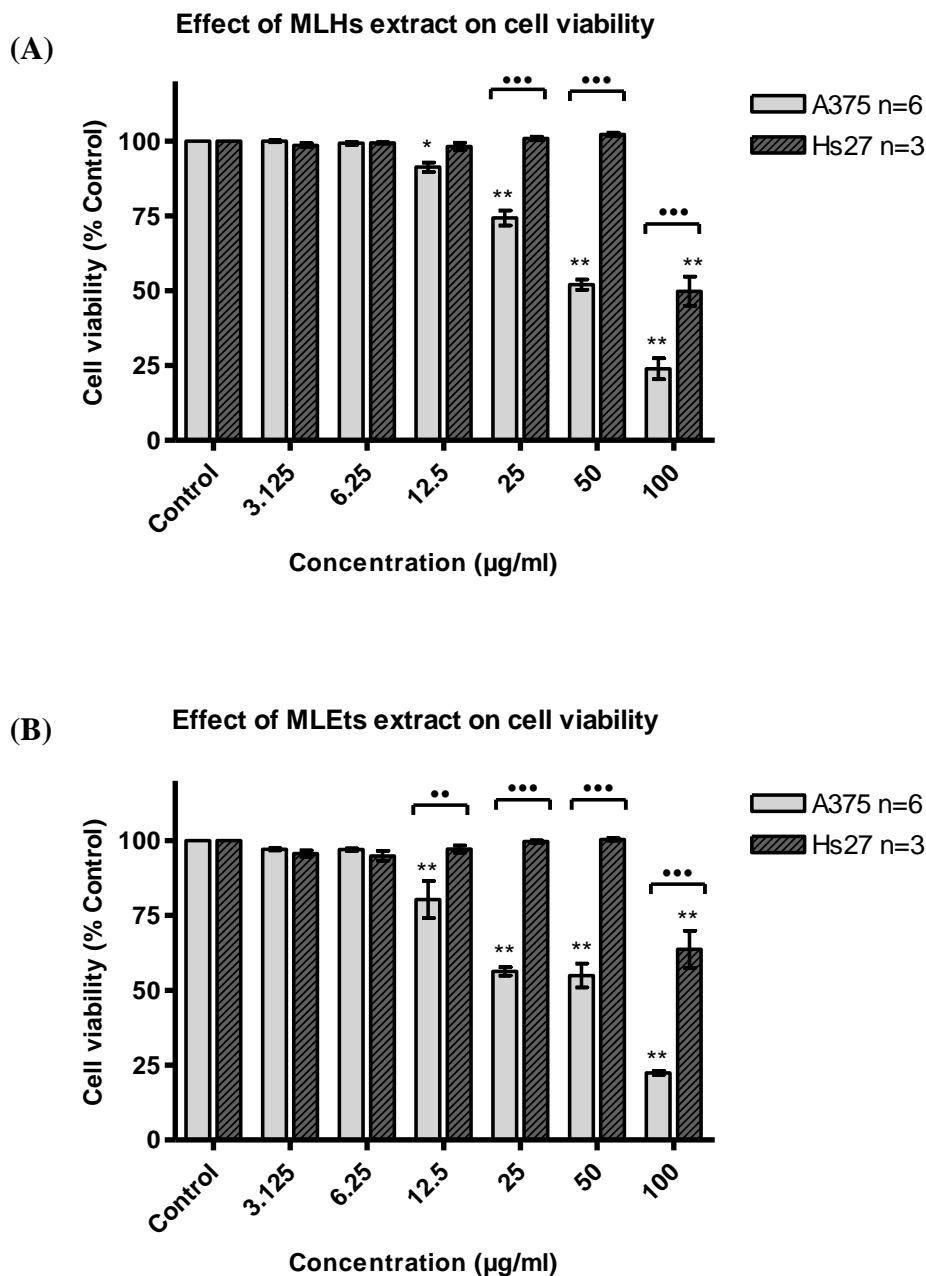


Figure 4.4: The cytotoxicity effect of n-hexane (A) and EtOAc (B) crude extracts from the stem bark of *M. laevis* on A375 and Hs27 cell lines using a resazurin assay. Values are presented as a percentage of the untreated control (\pm SEM). The assays were performed in a 96-well plate using the same conditions to compare the effects on cell viability. The data were analysed by Dunnett post-test, $*P < 0.05$ & $**P < 0.01$ vs. control, and by Bonferroni post-test, $**P < 0.01$ & $***P < 0.001$ A375 vs. Hs27 cells.

4.1.2.1 *Effects of constituents from the n-hexane extract (MLHs) on cell viability*

Nine compounds were isolated from the n-hexane extract of the stem bark of *M. laevis*. Canophyllol (HM-2) and friedelane-1,3-dione (HM-3) were relatively non-toxic to both cell lines with $EC_{50} > 100 \mu\text{g/ml}$. The new compound 15(β)-acetoxfriedelan-1,3-dione (HM-4), only tested on Hs27 cells, was also non-toxic. 28-hydroxyfriedelane-1,3-dione (HM-5) gave lower EC_{50} values of 84.2 and 79.7 $\mu\text{g/ml}$ (184.5 and 174.7 μM) on A375 and Hs27 cells, respectively. At 100 $\mu\text{g/ml}$, HM-5 produced an effective and significant ($P < 0.01$) reduction in the viability of both cell lines compared to the control as shown in Figure 4.5. The novel compound, 1,3-dioxocoredor-14,26-ene (HM-6), showed no effects on both cell lines even at the highest tested concentration.

HM-5 was previously tested for anti-tumour activity by Chávez *et al.* (1998) against P-388, A-549, HT-29 (human colon carcinoma) and MEL-28 (human melanoma) cell lines. No significant inhibitory activity was shown with an $IC_{50} > 10 \text{ mg/ml}$. The contradiction between the results in the present study and those obtained in the previous report might be due to the presence of an impurity (15%) in the sample used for screening as discussed earlier in section 3.3.1.4, therefore, the exerted inhibitory effect may in part be attributable to the minor unknown component directly or in combination with HM-5.

HM-3 has also been tested against human cancer cell lines U251(CNS), PC-3, K562, HCT-15 (colon), MCF-7, and SKLU-1(lung) using a SRB assay by Reyes *et al.* (2010) and was shown to be non-cytotoxic. In another study by Somwong *et al.* (2011), this compound was evaluated against other human cancer cell lines including SW620 (colon), CHAGO (lung), HepG2, BT474 (breast) and KATO-III (gastric) using a MTT assay and only showed significant activity against the SW620 cells with an IC_{50} of 2.02 μM compared to the positive control, doxorubicin (IC_{50} 0.18 μM). The results in the present work seem to correlate well with these reports as HM-3 was not toxic to A375 cells within the tested concentration range, and only at 100 $\mu\text{g/ml}$ it decreased the number of the viable cells by 12%. Therefore, HM-3 may possess selective activity against particular cell lines. This conclusion was also suggested by Ee *et al.* (2005) where this compound possessed selective strong inhibitory activity against the HeLa cell line with an IC_{50} of 4.6 $\mu\text{g/ml}$, while it was

not active against other screened cell lines at the highest tested concentration of 40 µg/ml.

While HM-2 showed no toxicity against both of the cell lines in this work, it showed a moderate activity on HL-60 with IC_{50} of 17.1 µM, a weak inhibitory effect on A549 and LLC (murine Lewis lung carcinoma) cancer cell lines and no activity on MCF-7 cancer cells when screened by Thao *et al.* (2010) using a MTT assay. Reyes-Chilpa *et al.* (2004) showed HM-2 had an inhibitory activity by only 7% and 13% compared to control against PC3 and U251 cancer cell lines, respectively, at a concentration of 31µM using a SRB assay, while it was non-toxic to K562 cells. Similarly to the previous compound HM-3, HM-2 could have a selective activity on particular cell lines rather than others, in addition to the effect of the purity level of the sample used for screening in these reports.

The two steroids β-sitosterol (HM-17) and stigmast-4-en-3-one (HM-18), isolated from the n-hexane extract of the stem bark, showed no activity on the normal Hs27 cells. While HM-17 was also not active on the melanoma A375 cells, HM-18 only showed an effect at the highest tested concentration with less than 25% reduction in cell viability compared to the control ($P < 0.01$), yet with an $EC_{50} > 100$ µg/ml.

The cytotoxicity of β-sitosterol has been evaluated on different cell lines in the literature and the results vary. Lin *et al.* (2012) showed that β-sitosterol exhibited moderate inhibitory activity towards HepG2, MCF-7 and HL-60 cancer cell lines with IC_{50} of 63.63, 51.74 and 70.47 µM, respectively, compared to cisplatin, the positive control, using a MTT assay. While Jackson *et al.* (2000) found that it was inactive on melanoma cell lines using a SRB assay. Luo *et al.* (2014) reported that both β-sitosterol and stigmast-4-en-3-one suppressed proliferation of PC3, Bcap-37 (breast) and MGC-803 (gastric) cancer cell lines to different extents using a MTT assay with IC_{50} values of 74.4, 58.2 and 43.8 µM for the former and 65.4, 79.3 and 56.9 µM for the latter. Stigmast-4-en-3-one also showed moderate cytotoxicity against HepG2, KB, LU-1, MCF-7, LNCaP (prostate), SW480 (colon), MKN7 (gastric), and HL-60 cancer cell lines with IC_{50} values ranging of 37.12-45.19 µg/ml (90-109.5µM) as reported by Dung *et al.* (2014). Generally, it seems that the preliminary results in the present work correlate well with Jackson and co-workers regarding the melanoma cells and it could be concluded that the potential anticancer

activity of these two steroids presents clearly towards some cell lines rather than others. Baskar *et al.* (2010) demonstrated that β -sitosterol induced apoptosis on COLO320DM cancer cells by its antioxidant activity with an IC_{50} of 266.2 μ M, and suppressed the expression of β -catenin and PCNA antigens (markers of proliferative activity in colon carcinogenesis), but with minimal toxicity to normal cells.

Similar to the celastrols from the n-hexane extract of the root bark (section 4.1.1.1), the isolated quinonemethide celastrol (HM-11) from the n-hexane extract of the stem bark also exhibited high and significant ($P < 0.01$) toxicity against A375 cells at all the tested concentrations compared to the control with an EC_{50} of 2.3 μ g/ml (5.1 μ M). However, it only caused an effective and significant ($P < 0.01$) reduction in the Hs27 cell viability from concentrations ≥ 12.5 μ g/ml compared to the control with an EC_{50} of 20 μ g/ml (44.4 μ M). From concentrations ≤ 6.25 μ g/ml, HM-11 seemed to possess selective activity against the melanoma cells only with statistically significant ($P < 0.001$) toxicity differences between the two cell lines as shown in Figure 4.5.

These results correlate well with those found by Ngassapa *et al.* (1994). Using a SRB assay, celastrol presented high cytotoxic activity against a series of cancer cell lines including P-388, HT-1080 (fibrosarcoma), KB, KB-V1, A431 (epidermoid carcinoma), U373 (glioblastoma), BC-1(breast), COL-2, LU-1, ZR-75-1 (hormone-dependant breast), LNCaP, and melanoma (MEL-2) with ED_{50} values ranging from 0.3 to 3.5 μ g/ml (0.7 to 7.8 μ M) and without any selectivity. A study by Morita *et al.* (2008) reported that celastrol, isolated from the bark of *M. chuchuhuasca*, showed potent inhibitory activity on the proliferation of RPMI8226 (human multiple myeloma) cells with an IC_{50} of 3.0 μ M using an *in vitro* tubulin polymerisation assay. It was indicated that in addition to the importance of the conjugated diosphenol function in ring A for the compound to be effective, the presence of a carboxylic acid function in ring E of the pentacyclic skeleton is favourable for tubulin binding, hence, more potentiality. The Nagase *et al.* (2003) study suggested that the anticancer activity could be due to apoptosis along with topoisomerase II inhibition.

Finally and as shown in Figure 4.5, the norfriedelane triterpene salaquinone A (HM-13), isolated from the n-hexane extract of the stem bark, exhibited high and

significant ($P < 0.01$) toxicity on A375 and Hs27 cells at all the tested concentrations compared to the control with EC_{50} values of 0.6 $\mu\text{g/ml}$ (1.4 μM) and 5.8 $\mu\text{g/ml}$ (12.8 μM), respectively. Nevertheless, at concentrations $\leq 6.25 \mu\text{g/ml}$, the toxicity differences between the two cell lines were significant ($P < 0.001$). There are no studies on the cytotoxicity activity of salaquinone A in the literature; therefore, the aforementioned preliminary findings are the first to be reported.

The ^1H NMR spectrum of the n-hexane extract of the stem bark (MLHs) indicated that the dominant types of compounds were mainly friedelane-type triterpenes as well as steroids. In general, the isolated compounds under these categories were found to be inactive within the tested range of concentrations, however, the minor components, HM-11 and HM-13 were found to be selective against the melanoma cells at the lowest tested concentration. Therefore, in view of these findings, the moderate and selective activity of MLHs could be attributable to the presence of these minor components and/ or to other unidentified phytochemical(s), or else to the possibility of inducing a synergistic effect with the major components.

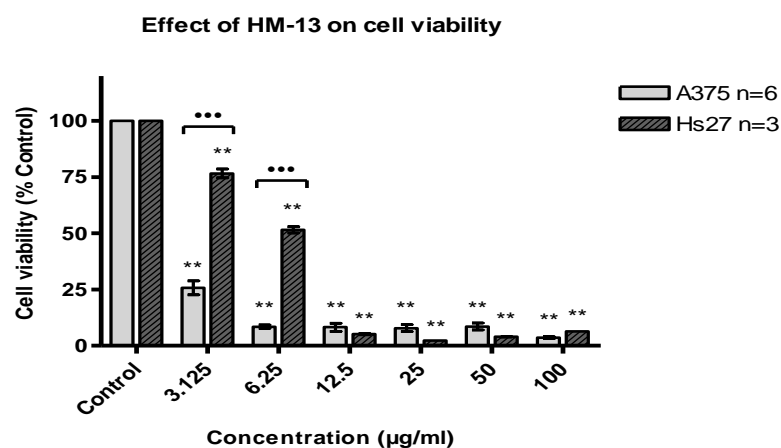
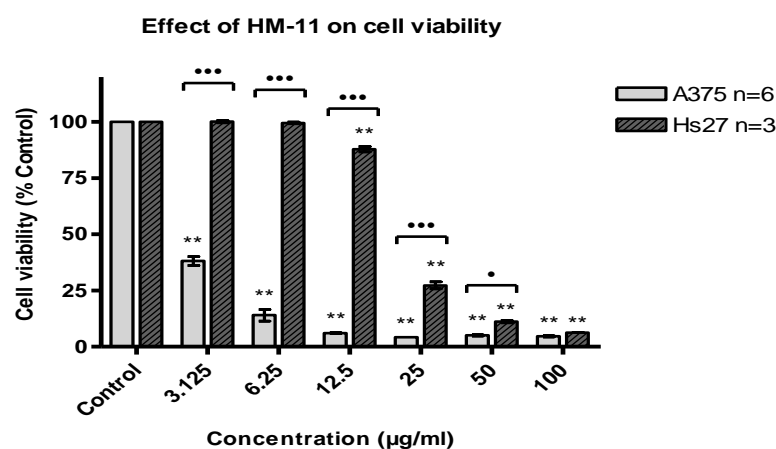
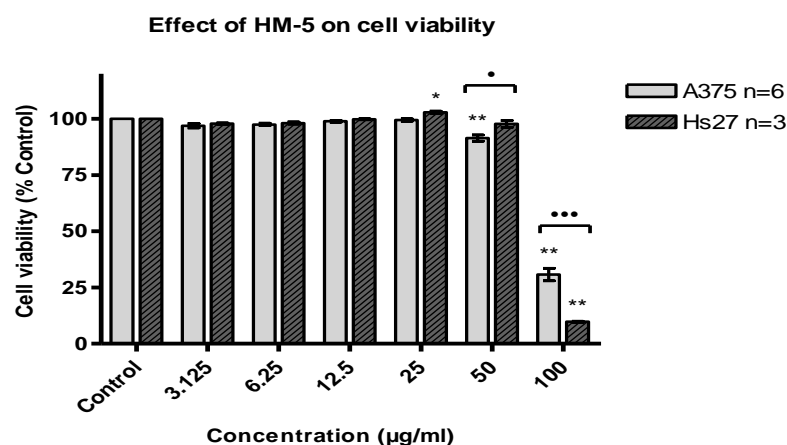


Figure 4.5: Cytotoxicity of some isolated compounds from n-hexane extract of the stem bark of *M. laevis* on A375 and Hs27 cell lines using a resazurin assay. Values are presented as a percentage of the untreated control (\pm SEM). The assays were performed in a 96-well plate using the same conditions to compare the effects on cell viability. The data were analysed by Dunnett post-test, * $P < 0.05$, ** $P < 0.01$ vs. control, and by Bonferroni post-test, * $P < 0.05$, *** $P < 0.001$ A375 vs. Hs27 cells.

4.1.2.2 *Effects of constituents from the EtOAc extract (MLEts) on cell viability*

From the EtOAc extract of the stem bark, only two out of four isolated compounds were tested for their cytotoxicity activity due to the small yields obtained.

The new nor-friedelane triterpene jujuborreal (HM-16), only caused small (< 25%) but significant ($P < 0.01$) reduction in the viability of the normal cells at 100 $\mu\text{g/ml}$ compared to the control with an $\text{EC}_{50} > 100 \mu\text{g/ml}$. However, from concentrations $\geq 25 \mu\text{g/ml}$, HM-16 exerted significant ($P < 0.01$) inhibitory effects on the melanoma cells compared to the control and a lower EC_{50} value of 41.9 $\mu\text{g/ml}$ (84.1 μM). There were significant ($P < 0.001$) cytotoxicity differences between the two cell lines from concentrations $\geq 50 \mu\text{g/ml}$; yet, no effect was shown on Hs27 cells at 50 $\mu\text{g/ml}$ (Figure 4.6). These observations suggest that this compound could be preferentially selective to melanoma cells and further tests need to be carried out on various cancer cells to confirm this anti-tumour activity.

The isolated phenolic compound *p*-hydroxybenzaldehyde (HM-20) also showed apparent selective activity against A375 cells with an EC_{50} of 21.6 $\mu\text{g/ml}$ (177 μM), except at the highest tested concentration where it significantly ($P < 0.01$) decreased the Hs27 viability to 60% compared to the control ($\text{EC}_{50} > 100 \mu\text{g/ml}$). At that particular concentration, the activity against A375 cells was the most potent (> 94% inhibition). Interestingly, at 50 $\mu\text{g/ml}$, there was significant ($P < 0.001$) difference in toxicity between the two cell lines, as HM-20 caused 87% inhibition in A375 cell viability but with no effect on Hs27 cells (Figure 4.6).

In a study by Rodrigues *et al.* (2014) on evaluating the cytotoxicity activity of commercial substituted benzaldehydes against SF-295, OVCAR-8 and HCT-116 human cancer cell lines using a MTT assay, *p*-hydroxybenzaldehyde was considered inactive against all three cell lines at the concentration of 5 $\mu\text{g/ml}$ with growth inhibition percentages of 48.77, 6.70 and 9.94 %, respectively. Their structure-activity relationship analysis indicated the importance of the presence of more than one hydroxyl group in the aromatic ring and at specific positions to show biological activity. The preliminary results presented in this work agree with those reported as HM-20 did not show activity on the melanoma cells at concentrations less than 12.5 $\mu\text{g/ml}$.

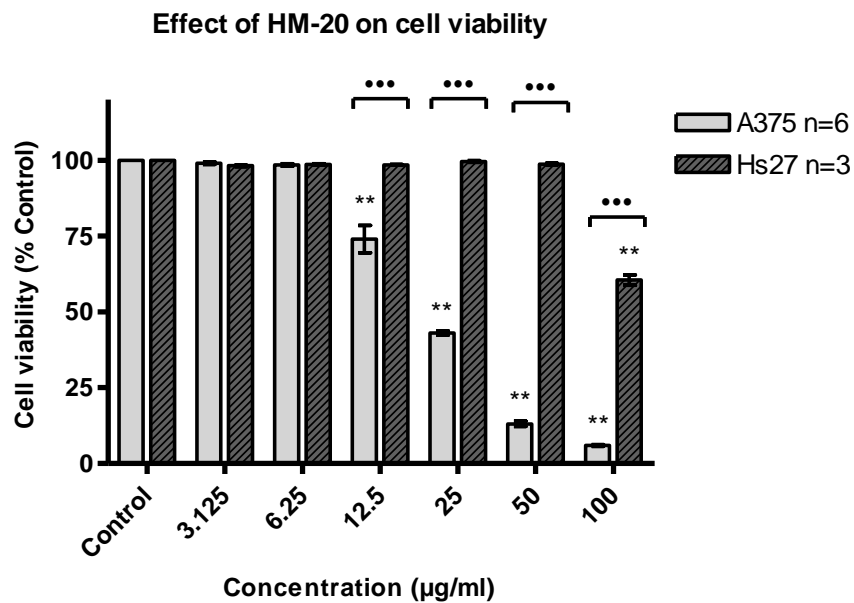
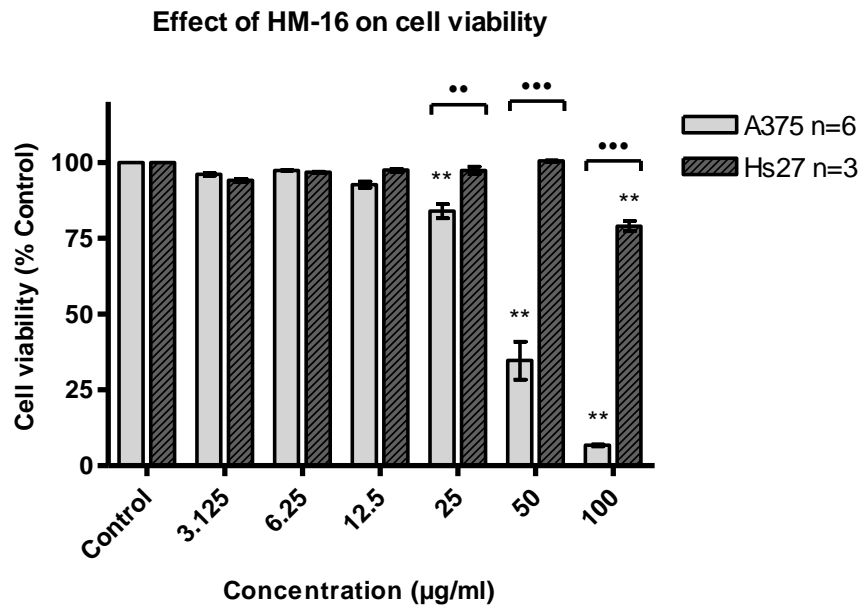


Figure 4.6: Cytotoxicity of some isolated compounds from an EtOAC extract of the stem bark of *M. laevis* on A375 and Hs27 cell lines using a resazurin assay. Values are presented as a percentage of the untreated control (\pm SEM). The assays were performed in a 96-well plate using the same conditions to compare the effects on cell viability. The data were analysed by Dunnett post-test, $P < 0.01$ vs. control, and by Bonferroni post-test, $**P < 0.01$, $***P < 0.001$ A375 vs. Hs27 cells.**

The nor-friedelane triterpene regeol A (HM-14) and the isocoumarin (\pm)-mellein (HM-21) were obtained in very small quantities, which prevented them from being tested for their cytotoxic activity. However, in a report by Montenegro *et al.* (2012), (*R*)-mellein, isolated from the fungus *Aspergillus* sp., was considered not toxic against HCT-8 and MDA-MB-435 cell lines with an $IC_{50} > 25 \mu\text{g/ml}$. (*R*)-mellein, isolated from *Celastrus rugosus* which belongs to the same family of the plant of the present study (Celastraceae), was also found to be non-toxic against SKOV3 (ovarian) and MGC-803 (gastric) tumour cell lines (Chang *et al.*, 2013). Regeol A was described by Nagase *et al.* (2003) as a celastrol derivative, which was used for a comparative evaluation of celastrol's effect to induce apoptosis in human leukemia HL-60 cells, although it was unable to induce DNA fragmentation.

The ^1H NMR spectrum of the EtOAc extract of the stem bark (MLEts) was not that informative as the signals were suppressed. However, the initial fractionation by VLC provided a general idea about the content of this extract. The most obvious signals in the spectra of the subsequent fractions were attributed to the presence of phenolic compounds, fats and steroids. Signals related to pheophytins, agarofuran sesquiterpene-type compounds and tannins were also detected. The *in vitro* and *in vivo* cytotoxicity of tannins was previously reported (Hong *et al.*, 2011; Sakagami *et al.*, 2000) and they were more active against a number of tumour cell lines compared with normal cells. In a study by Lv *et al.* (2014), the *in vitro* cytotoxicity of a number of dihydro- β -agarofuran sesquiterpene polyesters against some cancer cell lines was reported with moderate activity.

By considering all the above data, the moderate and more selective cytotoxic activity of the MLEts extract could therefore be attributed to its isolates as well as to the presence of other phytochemical(s).

Table 4.2: Summary of the cytotoxicity effects (EC₅₀ values) of crude extracts and their constituents from the root and stem bark of *M. laevis*

Sample Code	Hs27 cells, n=3 EC₅₀ µg/ml ± SEM (µM)	A375 cells, n=6 EC₅₀ µg/ml ± SEM (µM)
MLH	12.4 ± 0.4 (n=6)	2.9 ± 0.3
MLEt	16.5 ± 2.1	2.9 ± 0.1
MLM	NA	NA
MLHs	99.9 ± 2.1	51.1 ± 0.9
MLEts	104 ± 2.3	42.7 ± 3.5
MLMs	NA	NA
HM-2	NA	> 100
HM-3	> 100	> 100
HM-4	NA	-
HM-5	79.7 ± 3.9 (174.7)	84.2 ± 2.2 (184.5)
HM-6	NA	NA
HM-7	4.98 ± 0.03 (10.1)	1.7 ± 0.6 (3.5)
HM-8	ND*	ND*
HM-9	ND*	ND*
HM-10	1.8 ± ND (3.9)	0.04 ± 0.02 (0.08)
HM-11	20 ± 0.3 (44.4)	2.3 ± 0.1 (5.1)
HM-12	9.2 ± 0.4 (19.8)	2.1 ± 0.67 (4.4)
HM-13	5.8 ± 0.18 (12.8)	0.6 ± 0.2 (1.4)
HM-14	-	-
HM-15	89.1 ± 1.16 (191.9)	20.2 ± 0.8 (43.5)
HM-16	> 100	41.9 ± 3.05 (84.1)
HM-17	NA	NA
HM-18	NA	> 100
HM-19	62.4 ± 2.0 (405.1)	12.8 ± 0.57 (83.1)
HM-20	> 100	21.6 ± 0.88 (177)
HM-21	-	-

NA: not active, ND: not determined, ND*: not determined by software due to very low viability values at all tested concentrations ≈ 0, (-): not tested.

The highlighted compounds showed selectivity to A375 cells.

4.2 *In vitro* anti-trypanosomal activity assessment

Samples from the MLH, MLEt and MLM crude extracts of both the root and stem barks of *M. laevis* along with some fractions/ sub-fractions and some isolated compounds, were sent for *in vitro* anti-trypanosomal activity assessment. Due to technical issues, only preliminary screening at concentrations of 20 µg/ml (20 µM) and later at 5 µM was carried out on these samples to determine their *in vitro* activity against the bloodstream form of *Trypanosoma brucei brucei* S427 using an Alamar blue™ 96-well microplate assay.

4.2.1 *Anti-trypanosomal activity of crude extracts of M. laevis*

Results of the preliminary screening of *M. laevis* extracts along with some selected fractions against *T. b. brucei* are presented in Table 4.3. As shown in Figure 4.7, the MLH and MLEt extracts of the root and stem barks were found to be highly active at the tested concentration 20 µg/ml, as they caused more than 90% inhibition. The cell viability values were 0.6%, 1.8% for the n-hexane extracts and 1.5%, 2.8% for the ethyl acetate extracts of the stem and the root barks, respectively. The difference in the inhibitory effect of the MLM extracts of both parts was statistically significant ($P < 0.001$), however, they were considered not active at the tested concentration with cell viability more than 40 %.

**Preliminary screening of the crude extracts
against *Trypanosoma b. brucei* (S427) at 20 µg/ml**

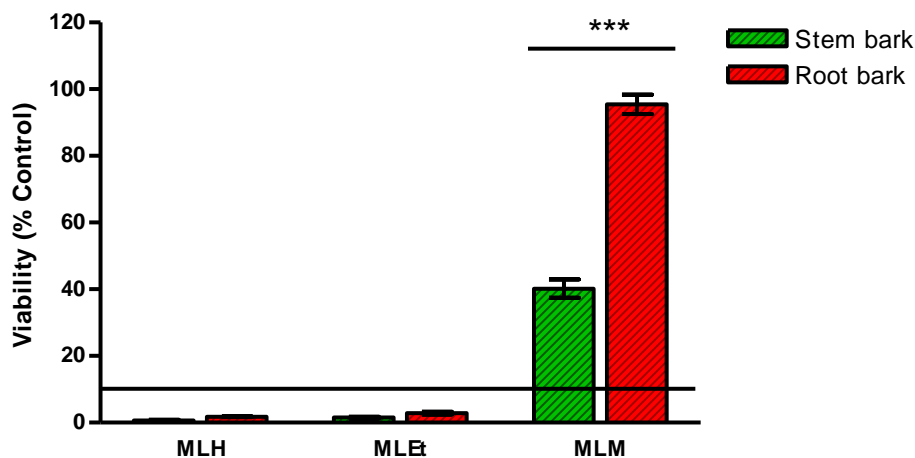


Figure 4.7: Preliminary screening results of the crude extracts from of the root and stem barks of *M. laevis* against *Trypanosoma b. brucei* (S427) blood stream forms using an Alamar blue assay. Values are presented as a percentage of the untreated control (\pm SEM), n=2. The data were analysed by Bonferroni post-test, *** $P < 0.001$ stem bark extracts vs. Root bark extracts.

Table 4.3: Anti-trypanosomal activities of the crude extracts and some fractions/ sub-fractions from the root and stem barks of *M. laevis* against *T. b. brucei* (S427)

Sample	Anti-trypanosomal activity (n=2)
	% of control \pm SEM (20 µg/ml)
MLHs	0.6 \pm 0.22
MLEts	1.5 \pm 0.28
MLMs	40.1 \pm 2.78
MLH	1.8 \pm 0.13
MLEt	2.8 \pm 0.41
MLM	95.4 \pm 2.95
HM-A	0.0 \pm 0.82
HM-B	-0.9 \pm 0.26
HM-C	-0.5 \pm 0.42
HM-D	0.3 \pm 0.24
HM-E	1.2 \pm 0.30

The highlighted samples were considered potentially active (i.e. Viability $<$ 10% of control's value).

4.2.2 *Anti-trypanosomal activity of some isolated compounds/ fractions*

Results of the preliminary screening of some isolated compounds from the root and stem barks of *M. laevis* against *T. b. brucei* at two selected concentrations (20 and 5 μM) are presented in Table 4.4.

All four isolated celastroloids from the n-hexane extract of the root bark, netzahualcoyondiol (HM-7), netzahualcoyone (HM-8), the new compound 22(α)-hydroxynetzahualcoyene (HM-9), and pristimerin (HM-10), showed high activity at both concentrations with cell viability values less than 4%, (Figure 4.8). In an early stage of this project, samples of HM-7 and HM-10 were screened for anti-trypanosomal activity following the same protocol and their MIC values were obtained as $< 0.19 \mu\text{g/ml}$ ($< 0.4 \mu\text{M}$). The anti-trypanosomal activity of HM-8, within a mixture of two compounds isolated from the root bark of *M. laevis*, was reported previously in a study by Igoli *et al.* (2011) with a MIC of $0.625 \mu\text{g/ml}$.

Dos Santos *et al.* (2013) described the anti-protozoal activity of two celastroloids isolated from the root bark of *M. ilicifolia*. One was pristimerin that showed potent activity compared to the positive control, benznidazole, with an IC_{50} of 0.3 nM against *T. cruzi* epimastigotes (extra cellular parasites), a species that causes Chagas' disease mostly in Latin America. Additionally, it exhibited marked *in vitro* leishmanicidal activity against promastigotes and amastigotes of *L. amazonensis* and *L. chagasi* with IC_{50} ranging from 0.05 to 0.88 nM. These data support the findings obtained in this work with respect to HM-10. The lower activity observed in the present study can be justified by the variation between strains and in the susceptibility to the compound due to differences in the composition of the plasma membrane of the extracellular and the intracellular forms of the parasite (Lião *et al.*, 2008). It was found that potential efficacy against the extracellular forms of the parasite could be relevant against the intracellular ones (Siqueira-Neto *et al.*, 2010). This suggests that this compound holds potential as an anti-trypanosomal drug lead.

From the EtOAc extract of the root bark, protocatechuic acid (PA) (HM-19) and the new celastrolid 22(β)-hydroxycelastrol (HM-12) were active at 20 μM with cell viability less than 4%. However at 5 μM , only HM-12 was still active with the same potency, while HM-19 became inactive (Figure 4.8).

Tasdemir *et al.* (2006) evaluated the activities of a number of flavonoids and phenolic compounds against trypanosomiasis and leishmaniasis. *In vitro*, PA was found to be only active against the bloodstream forms of *T. b. rhodesiense* STIB 900 with an IC₅₀ of 2.9 µg/ml (18.8 µM), while it was inactive against the trypomastigote forms of *T. cruzi* and *L. donovani* amastigotes. Another study supported these findings and found PA showed poor activity against the epimastigotes of *T. cruzi* with a MC₁₀₀ > 500 µg/ml (the minimum concentration which kills 100% after 48h incubation) (Reyes-Chilpa *et al.*, 2008).

From the n-hexane extract of the stem bark, only five isolated compounds were available at the time of screening. As shown in Figure 4.8, canophyllol (HM-2) and friedelane-1,3-dione (HM-3) along with stigmast-4-en-3-one (HM-18), were inactive at both tested concentrations. Celastrol (HM-11) and salaquinone A (HM-13) showed high activity at both tested concentrations with cell viability less than 2%. This is the first report in which the anti-trypanosomal activity of salaquinone A is mentioned.

These results seem to be in agreement with a study by Reyes-Chilpa *et al.* (2008), which reported that canophyllol was inactive against *T. cruzi* epimastigotes (MC₁₀₀ > 1000 µg/ml).

Stigmast-4-en-3-one was also evaluated for its *in vitro* anti-trypanosomal activity against *T. evansi* trypomastigotes by Nyunt *et al.* (2012) who found mild activity with an IC₅₀ of 62.8 µg/ml (150 µM). In the present work, this compound was inactive at 20 and 5 µM; hence, it might need higher concentrations to exhibit similar activity.

Liu *et al.* (2014) reported the inhibitory activity of celastrol, against *T. brucei* farnesyl pyrophosphate synthase (TbFPPS), an essential protein for parasite viability and an important target for anti-parasitic drug leads. Celastrol was used as a basis for a similarity search for multitarget inhibitors that could be used in the future for developing more potent analogues.

From the EtOAc extract of the stem bark, two compounds, regeol A (HM-14) and *p*-hydroxybenzaldehyde (HM-20) were screened for their anti-trypanosomal activity. Only the former was active at 20 µM with cell viability less than 2%, while it was inactive at 5 µM (Figure 4.8). This is the first report about the anti-parasitic activity of regeol A as there are no other studies in the literature.

p-hydroxybenzaldehyde was identified by GC/MS as one component of a sub-fraction from the dichloromethane extract of the marine red alga *Bostrychia tenella* J. Agardh (de Felício *et al.*, 2010). This sub-fraction showed moderate *in vitro* activity against *T. cruzi* trypomastigote forms (IC₅₀ of 36.5 µg/ml), while it was highly active against *L. amazonensis* promastigote forms (IC₅₀ of 4.3 µg/ml) compared to the positive controls, gentian violet and amphotericin B, respectively. The authors claimed that these activities might be due to the presence of *p*-hydroxybenzaldehyde and benzenoacetic acid, in the tested sub-fraction. However, these findings regarding the activity of *p*-hydroxybenzaldehyde should be explored more thoroughly in order to rely on them for the purpose of comparison with the results obtained in the present work, due to the presence of other components in the studied sub-fraction, which could also participate in the exerted activities.

Preliminary screening of the pure compounds against *Trypanosoma b. brucei* (S427)

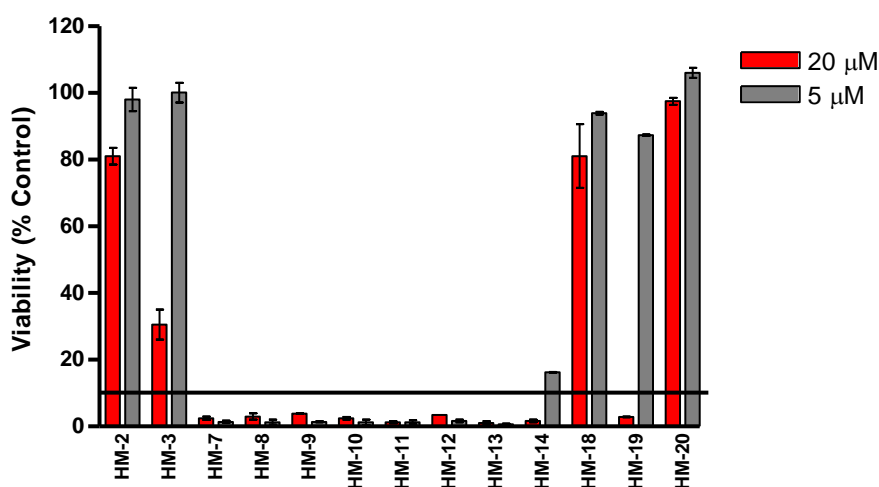


Figure 4.8: Preliminary screening of some isolated compounds from the extracts of the root and stem barks of *M. laevis* against *Trypanosoma b. brucei* (S427) blood stream forms at two concentrations (20 and 5 µM) using an Alamar blue assay. Values are presented as a percentage of the untreated control (\pm SEM), n=2.

Table 4.4: Preliminary screening of some isolated compounds from the root and stem barks of *M. laevis* against *T. b. brucei* (S427)

Sample	Anti-trypanosomal activity (n=2)	
	% of control \pm SEM (20 μ M)	% of control \pm SEM (5 μ M)
HM-2	81.0 \pm 2.48	98.0 \pm 3.55
HM-3	30.5 \pm 4.46	100.2 \pm 2.93
HM-7	2.4 \pm 0.51	1.3 \pm 0.35
HM-8	3.0 \pm 0.98	1.3 \pm 0.67
HM-9	3.8 \pm 0.09	1.4 \pm 0.15
HM-10	2.4 \pm 0.39	1.2 \pm 0.78
HM-11	1.2 \pm 0.27	1.2 \pm 0.63
HM-12	3.4 \pm 0.003	1.6 \pm 0.45
HM-13	1.1 \pm 0.45	0.7 \pm 0.19
HM-14	1.6 \pm 0.36	16.2 \pm 0.11
HM-18	81.1 \pm 9.60	93.9 \pm 0.36
HM-19	2.9 \pm 0.05	87.3 \pm 0.12
HM-20	97.5 \pm 1.06	106.1 \pm 1.46

The highlighted samples were considered potentially active (i.e. Viability < 10% of control's value).

Five selected fractions/sub-fractions (HM-A, B, C, D and E) were submitted for testing against *T. b. brucei*. The selection of these sub-fractions was dependent on their content as interesting targets for further separation and purification processes. They were either mixtures of already isolated compounds with unknowns or mixtures of unknown compounds. As presented in Table 4.3, the preliminary screening results of these samples at 20 μ g/ml were promising as they were all highly active.

The sub-fraction HM-A from the n-hexane extract of the root bark contained a mixture of three dihydroagarofuran sesquiterpenes in a ratio of 1.0:0.16:0.04. A proposed structure was suggested for the major component as explained later in section 5.2, Appendix II (A). In the literature, no studies were found on the anti-trypanosomal activity of these compounds. However, Cortés-Selva *et al.* (2005) examined a series of compounds under this class, and proved their ability to reverse the P-glycoprotein-dependent multidrug resistance (MDR) phenotype of *L. tropica* line and several human cancer cells (P-glycoprotein is an active protein of the cell

membrane which acts as a pump to reduce the intracellular accumulation of the drugs, hence, leading to a MDR phenotype). Another study by Santos *et al.* (2012) on macrolide sesquiterpene pyridine alkaloids, a major subclass of this group, reported them as potent anti-protozoan agents by testing them against *L. chagasi* and *T. cruzi*. To some extent, these findings support the preliminary results regarding these compounds as potential anti-trypanosomal drug leads.

The VLC fraction HM-B from the n-hexane extract of the stem bark contained the two friedelane triterpenes canophyllol (HM-2) and the new compound 15(β)-acetoxfriedelan-1,3-dione (HM-4) as major components in addition to β -sitosterol (HM-17) and unknowns. As discussed earlier, canophyllol (HM-2) was found to be inactive at 20 μ M (8.85 μ g/ml). β -sitosterol (HM-17) activity was not tested in this work, however, Kirmizibekmez *et al.* (2011) showed weak inhibition against *T. cruzi* (IC₅₀ of 35.4 μ g/ml, 85.4 μ M), while it was inactive against *T. b. rhodesiense* (IC₅₀ of 86.1 μ g/ml, 207.6 μ M). Therefore, and in view of the foregoing findings, the activity of this fraction could be related to the presence of the new compound (HM-4) alone or together with canophyllol if the latter possessed positive activity at higher concentration or to the other unknown phytochemical(s). The active sub-fraction HM-C, resulting from Sephadex chromatography of the previous fraction, contained HM-4 as a major component (> 80%). This eliminated the effect of canophyllol on the activity and narrowed down the possibilities to either the presence of HM-4 and/or to the minor unknowns. The purer sample of the new compound HM-4 was not available at the time of screening, thus, further tests are needed to confirm its activity.

The sub-fraction HM-D, resulting from PTLC of a fraction from the n-hexane extract of the stem bark, contained the two compounds friedelane-1,3-dione (HM-3) and the novel compound 1,3-dioxocorredor-14,26-ene (HM-6). HM-3 was considered inactive at 20 μ M (8.80 μ g/ml) and no reports were found about its anti-parasitic activity. This fraction was highly active at 20 μ g/ml, therefore, its activity could be due to the presence of the novel compound (HM-6) alone or to both compounds where HM-3 was present in sufficient concentration in this sample to promote positive activity.

Finally, the sub-fraction HM-E, resulting after a series of chromatographic fractionation of a VLC sample from the n-hexane extract of the stem bark, contained the compound 28-hydroxyfriedelane-1,3-dione (HM-5) as a major component in addition to minor unknowns. Since no reports were found about the activity of this compound in this domain, further tests need to be carried out on the purified compound to correlate the activity of this sample to it; otherwise it might be due to the presence of other unknown minor components.

4.2.3 Overall evaluation of the anti-trypanosomal activity of the crude extracts

Due to technical issues, it was not possible to test the rest of the purified compounds. Nevertheless, knowing that the celastroloids were the dominant class of compounds in both the n-hexane and EtOAc extracts of the root bark, and depending on the preliminary results of their associated isolated compounds, the high anti-trypanosomal activity of these extracts could be related to the presence of these compounds, yet, without underestimating the effects of the other non-purified phytochemical(s) such as the dihydroagarofuran sesquiterpenes.

The n-hexane and EtOAc extracts of the stem bark also possessed high anti-trypanosomal activity as explained in section 4.2.1. The dominant types of compounds in the n-hexane extract were mainly the friedelane-type triterpenes as well as steroids. The three tested compounds under the aforementioned classifications, canophyllol (HM-2), friedelane-1,3-dione (HM-3), and stigmast-4-en-3-one (HM-18), were inactive at 20 μ M (in the range of 8 to 9 μ g/ml depending on their molecular weight), yet, they might exert positive activity if present in sufficient concentrations within the extract's sample. The activity of the later isolated friedelane-type compounds including the new compound 15(β)-acetyoxyfriedelan-1,3-dione (HM-4), the known compound 28-hydroxyfriedelane-1,3-dione (HM-5), and the novel compound 1,3-dioxocorredor-14,26-ene (HM-6) were not tested. However, the activity of the fractions/ sub-fractions containing these compounds was evaluated as discussed earlier and the results were very promising. Moreover, the two minor components isolated from the n-hexane extract, celastrol (HM-11) and salaquinone A (HM-13) were found to be highly active at both tested concentrations. In conclusion, the activity of the n-hexane crude extract of the stem bark could be attributable to the

previous components and/ or to other non-purified phytochemical(s) without disregarding the possibility of the synergistic effect among these constituents.

The EtOAc extract of the stem bark mainly composed of phenolic compounds, fats, steroids in addition to pheophytins, agarofuran sesquiterpene type compounds and tannins, as explained earlier. Four compounds were isolated from this extract including the known nor-friedelane triterpene regeol A (HM-14), the new nor-friedelane triterpene jujuboreal (HM-16), the simple phenolic *p*-hydroxybenzaldehyde (HM-20) and the isocoumarin (\pm) mellein (HM-21). In addition to these compounds, a mixture of two other phenolics, identified as *p*-hydroxybenzoic acid: 3,4-dihydroxybenzaldehyde, was obtained (mentioned later in section 5.2). The preliminary results for regeol A (HM-14) and *p*-hydroxybenzaldehyde (HM-20) showed that only the former exhibited high activity at 20 μ M (\approx 8.8 μ g/ml). The other isolated compounds were not available at the time of screening. In the literature, *R*-(-)-mellein was found to possess *in vitro* anti-parasitic activity against *Schistosoma mansoni* adult worms with MC_{100} of 200 μ g/ml (Ramos *et al.*, 2013), while it was inactive when tested against the protozoan parasite, *Plasmodium falciparum*, at 10 μ g/ml (Sommart *et al.*, 2008). Similarly, the *in vitro* activity of *p*-hydroxybenzoic acid and 3,4-dihydroxybenzaldehyde against *S. mansoni* adult worms was evaluated by Alvarenga *et al.* (2012), who found that they only caused moderate reduction in the motor activity. Nevertheless, the benzoic acid derivatives appeared to have anti-malarial activity as reported by Verotta *et al.* (2001). The *in vivo* and *in vitro* anti-trypanosomal activities of the crude extracts of several plants were evaluated and their tannin content was linked to their efficacy (Adeyemi *et al.*, 2009; El-Ashmawy *et al.*, 2016; Ogbadoyi *et al.*, 2007). By considering all the aforementioned data, the anti-trypanosomal activity of the EtOAc extract of the stem bark could be attributed to the isolated compounds, although they were minor constituents, and to other phytochemicals such as tannins and agarofuran sesquiterpenes.

CHAPTER V

5. CONCLUSIONS AND FUTURE WORK

5.1 Summary of key findings

The present work aimed to carry out a phytochemical investigation on the Amazonian medicinal plant, *M. laevis* (Celastraceae). Soxhlet extractions of the plant materials (root and stem barks) using solvents of increasing polarity were performed. The fractionation of the resulting extracts and the subsequent purification using different chromatographic techniques led to the isolation of several triterpenoids, steroids and some phenolic derivatives. These types of natural components were expected to be found in this plant as a result of a literature search for the family Celastraceae and *Maytenus* species.

A total of thirteen compounds were isolated from the n-hexane and EtOAc extracts of the stem bark. Most of them were triterpenoids of friedelane and norfriedelane-types, in addition to steroids and simple phenolics. Three of these compounds appeared to be novel. One of them was identified with the aid of the X-ray crystallographic technique and is proposed to be the first of a new skeletal class of triterpenes for which the name *corredorane*^{*} was suggested. The novel compounds were given the trivial names 15(β)-acetyfriedelane-1,3-dione (HM-4), 1,3-dioxocorredor-14,26-ene^{*} (HM-6), and *jujuborreal*^{**} (HM-16). The isolated known compounds, friedelane-1,3-dione (HM-3), salaquinone A (HM-13), regeol A (HM-14), stigmast-4-en-3-one (HM-18) and (\pm) mellein (HM-21), are reported for the first time from "Chuchuguasa", *M. laevis*. With the exception of 28-hydroxyfriedelane-1,3-dione (HM-5), *p*-hydroxybenzaldehyde (HM-20), and celastrol (HM-11) being reported before as constituents of *M. macrocarpa* and *M. chuchuhuasca*, the relative species that are referred to as "Chuchuguasa"; this is also the first report of their isolation from *M. laevis*. Canophyllol (HM-2) and β -sitosterol (HM-17) were reported before from the bark of *M. laevis*.

When tested for cytotoxic activity on two cell lines A375 and Hs27, both n-hexane and EtOAc extracts of the stem bark showed moderate, but selective effects on the melanoma cells within a concentration range between 25-50 μ g/ml.

* These are named in memory of *Blanca M.V.de Corredor*, Anthropologist, Universidad Nacional de Colombia, without whose guidance and knowledge base this work would possibly have never been achieved. **The same applies to *Noé Rodríguez Jujuborre*, Muinane Cacique of Resguardo Guaimaraya, mid Caquetá region, Amazon tropical forest, Colombia.

The major components of the n-hexane extract, which is composed of the friedelane-type triterpenes and steroids, showed weak or no effects on the cell lines, while its minor components, such as celastrol (HM-11) and salaquinone A (HM-13), possessed strong and selective activity against A375 cells. Therefore, the inhibitory effect, particularly in A375 cells, produced by the n-hexane extract was suggested to be related to the presence of these minor components and/ or to those unidentified phytochemical(s). Only two of the four isolated compounds from the EtOAc extract were screened including the novel compound jujuborreal (HM-16) and *p*-hydroxybenzaldehyde (HM-20). They both demonstrated moderate but selective cytotoxicity to the A375 cells at particular concentrations, which suggested their contribution to the activity exerted by the EtOAc extract along with the effects of its other non-purified constituents.

Interestingly, the two aforementioned extracts showed very potent anti-trypanosomal activities against the parasitic protozoan *Trypanosoma b. brucei*, the cause of African trypanosomiasis in animals, at the preliminary concentration (20 µg/ml). Some of the isolated compounds, which were available at the time of screening, were tested along with some sub-fractions containing later purified compounds. The samples of the minor constituents such as celastrol (HM-11), salaquinone A (HM-13), and regeol A (HM-14), in addition to the tested sub-fractions were the most active ones as they showed very promising results. Accordingly, the strong observed anti-trypanosomal activities of the crude extracts were linked to these isolates, which could be acting synergistically.

From the n-hexane and EtOAc extracts of the root bark, a total of seven compounds were isolated. Among them, two new celastroloids and a new aromatic triterpene were identified and given the trivial names 22(α)-hydroxynetzahualcoyene (HM-9), 22(β)-hydroxycelastrol (HM-12), and methyl 2,3,22 α -trihydroxy-24,25-dinorfriedelan-1,3,5(10),6,8,14-hexaen-29-oate (HM-15). The isolated known compounds, netzahualcoyondiol (HM-7), netzahualcoyone (HM-8) and PA (HM-19), are reported for the first time from *M. laevis*. With the exception of pristimerin (HM-10) being isolated before from the botanically relative species *M. chuchuhuasca*, this is the first report of its isolation from *M. laevis*.

Both n-hexane and EtOAc crude extracts of the root bark presented cytotoxic activities against the two cell lines A375 and Hs27, but with preferable effects on the melanoma cells at the lowest tested concentration (3.125 µg/ ml). This provides some scientific support for the traditional use of *M. laevis* (the root bark in particular) as anti-tumour therapy in skin cancer. All the isolates from both extracts showed varying degrees of cytotoxicity on the two cell lines. Among them, the isolated celastroloids were the most potent; therefore, the effectiveness of the crude extracts was suggested to be mainly attributable to their presence. Additionally, both extracts exerted potent anti-trypanosomal activity at the preliminary concentration (20 µg/ ml). Their subsequent isolated compounds also gave promising results as they all maintained their efficacies even at the low concentration (5 µM).

The methanol extracts of both parts of *M. laevis* were found to be inactive in terms of potential anti-melanoma and anti-trypanosomal drugs. Furthermore, the phytochemical work on these extracts was limited due to the fact that the partial fractionation using VLC technique did not show interesting components that could be targeted for further separation and purification.

5.2 Recommendations for future work

- In addition to the previous isolated compounds, dihydro- β -agarofuran sesquiterpenes have been found in some fractions of the n-hexane extract of the root bark of *M. laevis*. One of the sub-fractions collected after repeated column chromatography contained a mixture of at least three of these compounds in a ratio of approximately 1.0:0.16:0.04. An attempt to identify the major compound by 1D and 2D NMR experiments along with LC-MS led to the proposed structure as clarified in Appendix II; (A), where a group of five esters, including three benzoyls, one nicotinoyl, and one acetyl, are involved. The fact that this type of compound includes polyester groups presents difficulties in determining their attachment sites on the main skeleton, hence, finalising its structure. However, it is positively believed that this compound could be new to literature if the nicotinoyl ester proved to be attached on position-2 instead of -1, otherwise, it will be a known compound, triptogelin A-10, that has been isolated before from *T. wilfordii* (Celastraceae) by Takaishi *et al* (1991). Further work

should be carried out in an attempt to purify this compound by Semi-Prep HPLC, as a possibility, as well as conducting more specific 2D NMR experiments such as J-resolved and/ or TOCSY which might help in dividing the overlapped proton signals and unambiguously finalise the structure.

- Considering that the essence of this work was to investigate the naturally occurring phytochemical components in this plant, it is worth mentioning that a mixture of two other phenolics was obtained from the EtOAc extract of the stem bark in a ratio of 1.0: 0.11. They were identified as *p*-hydroxybenzoic acid: 3,4-dihydroxybenzaldehyde, respectively, as clarified in Appendix II; (B). The lack of time as well as the small quantity of this mixture prevented trying to separate them, thus, this can be considered for future.
- The isolated compounds were tested for their effects on the viability of the melanoma and normal fibroblast cells to validate the traditional use of this plant in the treatment of skin cancer (as mentioned in section 1.5.2). However, more work will be required to be carried out on these cells and on other types of cancer cell lines using different protocols such as MTT assay with a different range of sample concentrations, especially for the quinonemethide compounds which exerted potent activity, even at the lowest tested concentration. Consequently, this will give more credibility and will determine whether these compounds possess any specific or selective effects on the tested cancer cells or their cytotoxicity effects are inclusive. It is also important to investigate the mechanism of action applied by the active compounds to determine whether the mode of cell death is apoptosis or necrosis by observing the morphological and the biochemical features of the cells.
- Depending on the availability of the *Trypanosoma b. brucei* parasite, the anti-trypanosomal activity (the MIC assay) should be continued on the given samples as well as on those that were isolated later. It will also be valuable to test these compounds on *T. cruzi*, the cause of Chagas disease or the American trypanosomiasis. Later, it will be interesting to carry out a structure activity relationship analysis (SAR), which may help for better understanding of the relationship between the exhibited bioactivity and the structure, and how it can be modified to obtain a desired or enhanced effect.

- A literature search showed that some of the isolated compounds exerted anti-inflammatory activity, which provides some scientific evidence for the traditional use of this plant for the treatment of arthritis and rheumatism. Some samples were already sent to be tested for their anti-inflammatory activity using U937 cell line; however, the results are not yet available.

5.3 Overall conclusion

Although considerable chemical work has been performed on the *Maytenus* species associated with Chuchuguasa (mainly the stem bark), there is some information so far about the chemistry of *M. laevis*, particularly those involving the root bark. This project proved that there is still a lot more to be discovered about this plant, its constituents and its use. The findings regarding the anti-trypanosomal activity are still initial, yet, they propose a new potential therapeutic use of *M. laevis* (the root and stem barks), which could lead to the discovery of powerful agents for the treatment of related parasitic diseases which are considered endemic in its habitat, such as Chagas disease (Dos Santos *et al.*, 2013).

Out of the twenty isolated compounds only four had been previously reported in other species called "Chuchuguasa" and two from actual *M. laevis* (bark). These were 28-hydroxyfriedelane-1,3-dione (HM-5, p.101, section 3.3.1.4), pristimerin (HM-10, p.157, section 3.3.2.4), celastrol (HM-11, p.166, section 3.3.2.5), p-hydroxybenzaldehyde (HM-20, p.243, section 3.5.2.1) and canophyllol (HM-2, p.70, section 3.3.1.1), β -sitosterol (HM-17, p.230, section 3.4.1), respectively.

This leads to some important questions; which part and what side of the plant possesses the active constituents? What is the preferable time for collection? If one does not take into account these factors, such as time of collection, part of the plant and its position on the plant, one could miss some important biologically active components as this thesis has shown. Nevertheless, the answers to these questions were already recognised by the true shamans "sabedores" who identified *M. laevis* and shared their in-depth knowledge on the positive energy held by this plant, particularly in its root bark, and its medicinal use within their societies. Therefore, all credit is humbly given to them and hope that the present work and what could generate from it in the future is of benefit to them, their communities and to science.

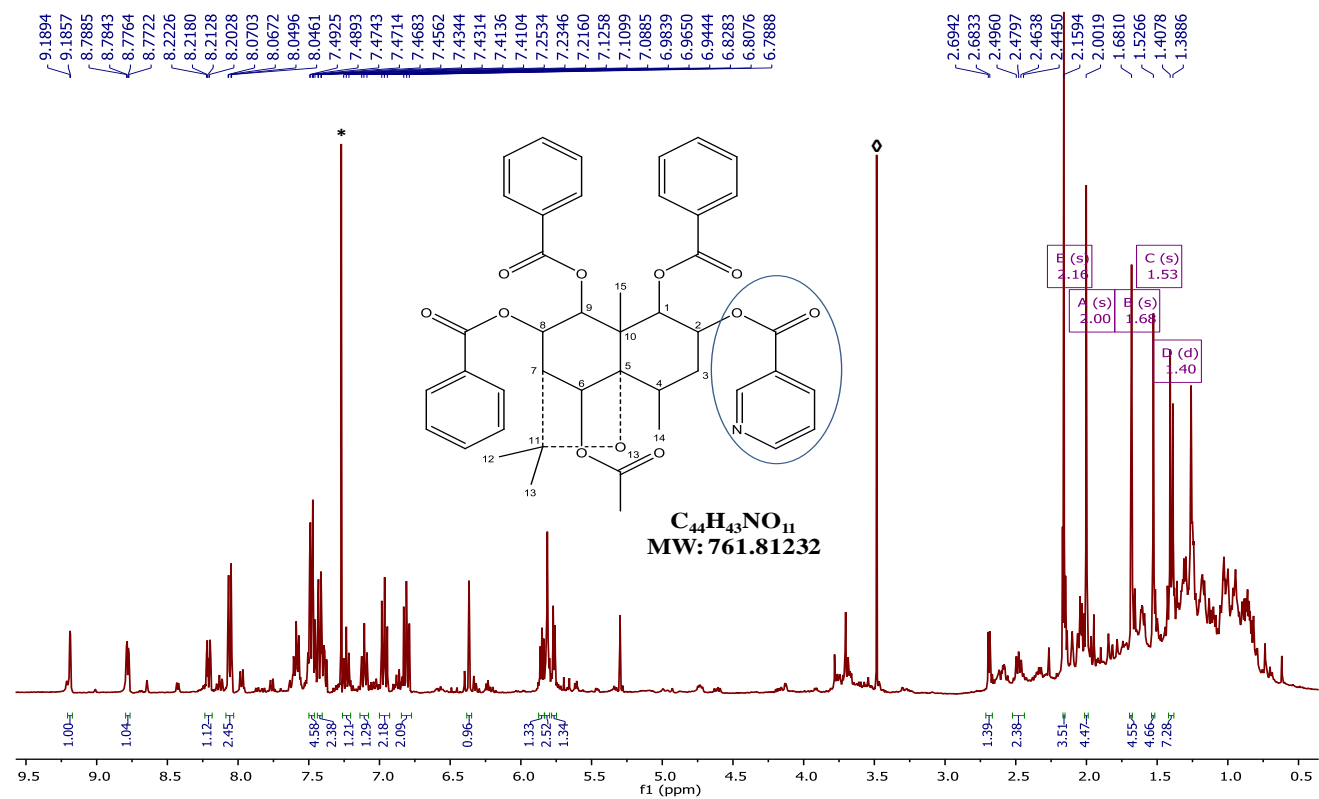
APPENDICES

Appendix I: Crystallographic Table

Crystal data	
Chemical formula	C ₃₀ H ₄₆ O ₂ ·CCl ₃ D
M_r	559.04
Crystal system, space group	Monoclinic, $P2_1$
Temperature (K)	123
a, b, c (Å)	13.976 (3), 6.3424 (10), 18.055 (3)
β (°)	111.481 (7)
V (Å ³)	1489.2 (4)
Z	2
Radiation type	Mo $K\alpha$
μ (mm ⁻¹)	0.33
Crystal size (mm)	0.5 × 0.4 × 0.3
Data collection	
Diffractometer	Bruker APEX-II CCD diffractometer
Absorption correction	Multi-scan (SADABS; Bruker, 2007)
T_{\min}, T_{\max}	0.641, 0.746
No. Of measured, independent and observed [$I > 2\sigma(I)$] reflections	12425, 6268, 4526
R_{int}	0.041
$(\sin \theta/\lambda)_{\text{max}}$ (Å ⁻¹)	0.645
Refinement	
$R[F^2 > 2\sigma(F^2)], wR(F^2), S$	0.059, 0.135, 1.04
No. of reflections	6268
No. of parameters	337
No. of restraints	1
H-atom treatment	H atoms treated by a mixture of independent and constrained refinement
$\Delta_{\text{max}}, \Delta_{\text{min}}$ (e Å ⁻³)	0.55, -0.42
Absolute structure	Flack x determined using 1514 quotients [(I+)-(I-)]/[(I+)+(I-)] (Parsons and Flack (2004), Acta Cryst. A60, s61).
Absolute structure parameter	0.02 (4)

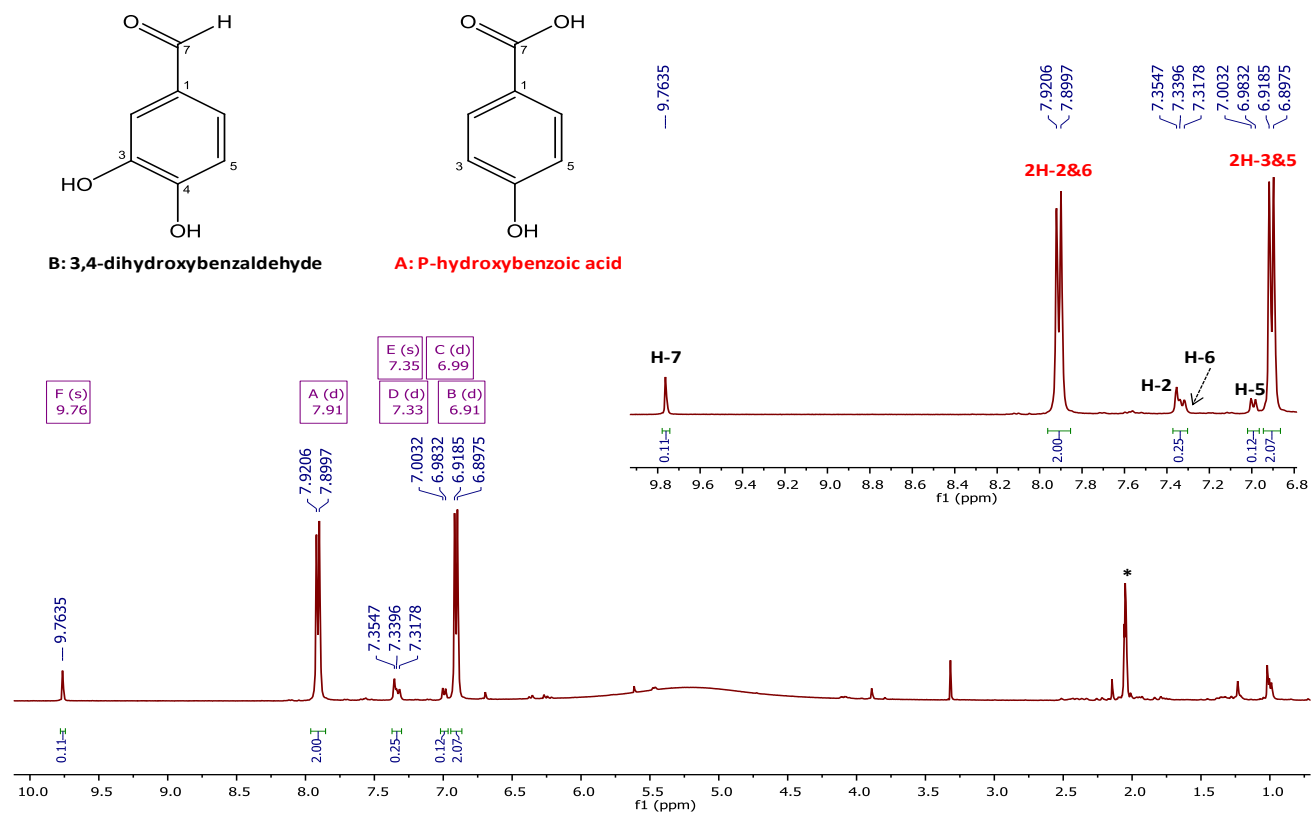
Data were given by Dr. Amit Delori/ Dr. Ian Oswald, SIPBS Department, Strathclyde University

Appendix II (A)



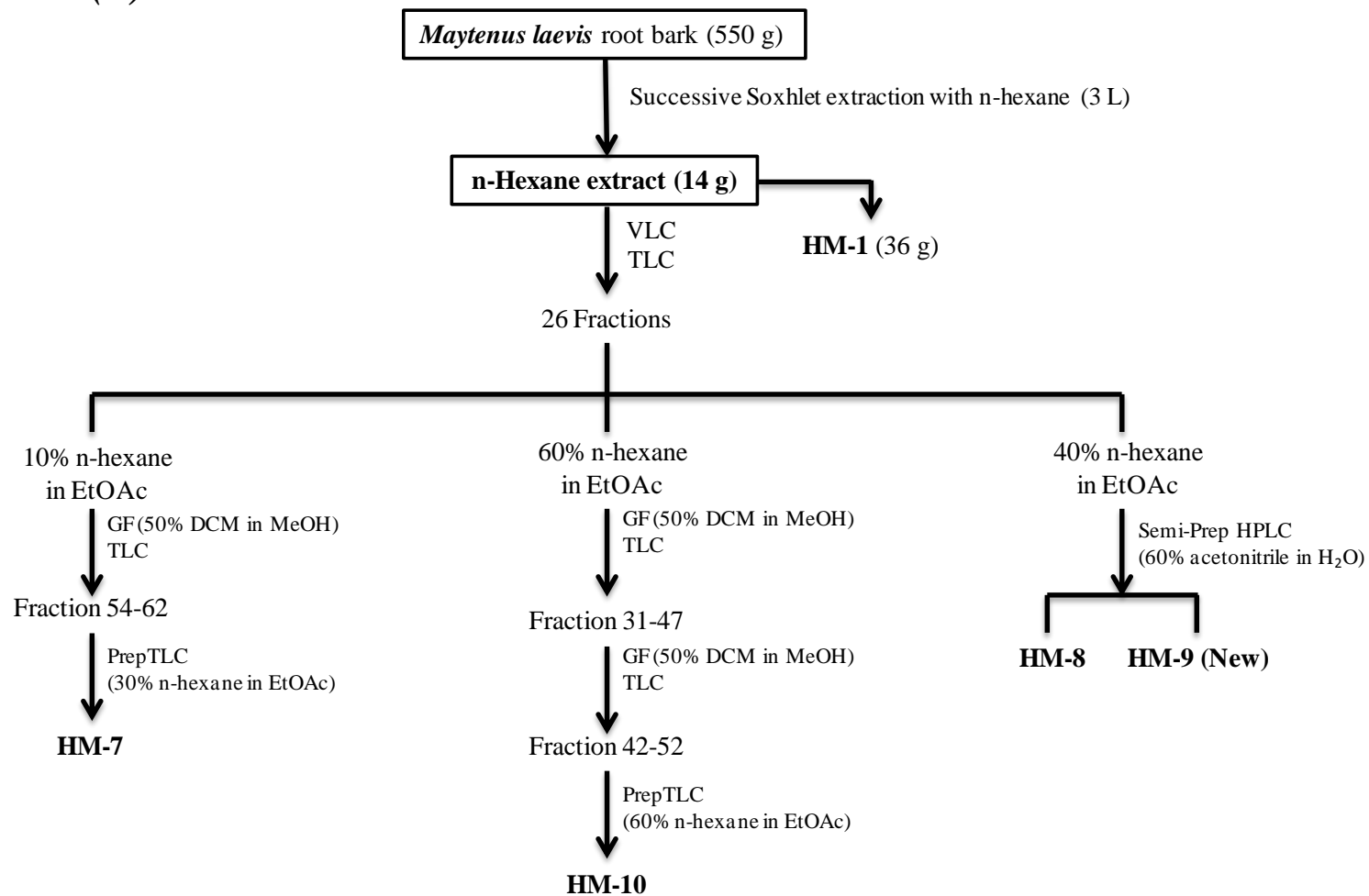
^1H NMR spectrum (400 MHz) of sesquiterpenes mixture in (CDCl_3) with the proposed structure of the major compound (*); CHCl_3 residue, (\diamond); solvent impurity (MeOH).

Appendix II (B)



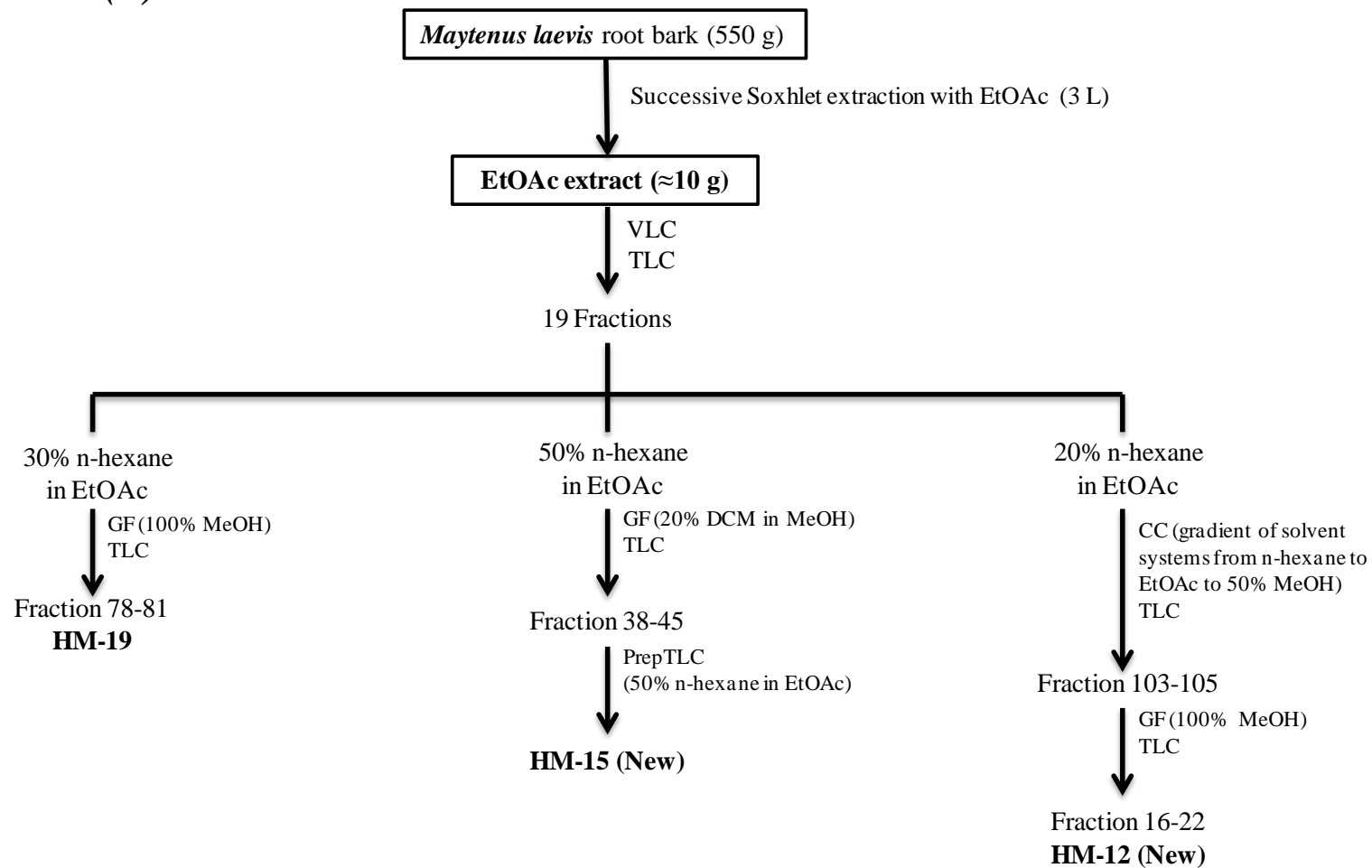
Full and expansion of ^1H NMR spectrum (400 MHz) of a phenolic mixture in $(\text{CD}_3)_2\text{CO}$ (*) and their structures

Appendix III (A)



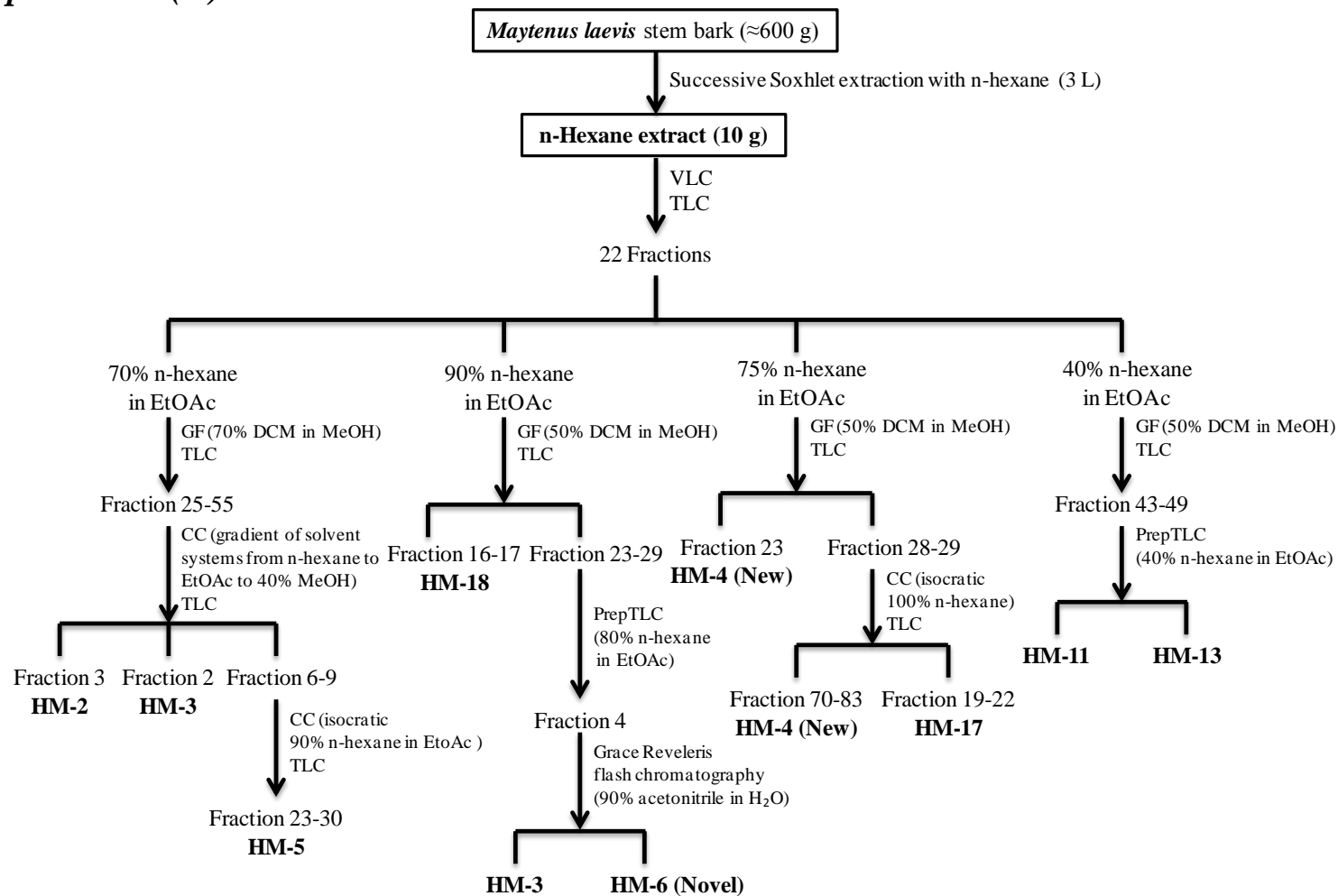
Isolation scheme of compounds from n-hexane extract of the root bark of *M. laevis*

Appendix III (B)



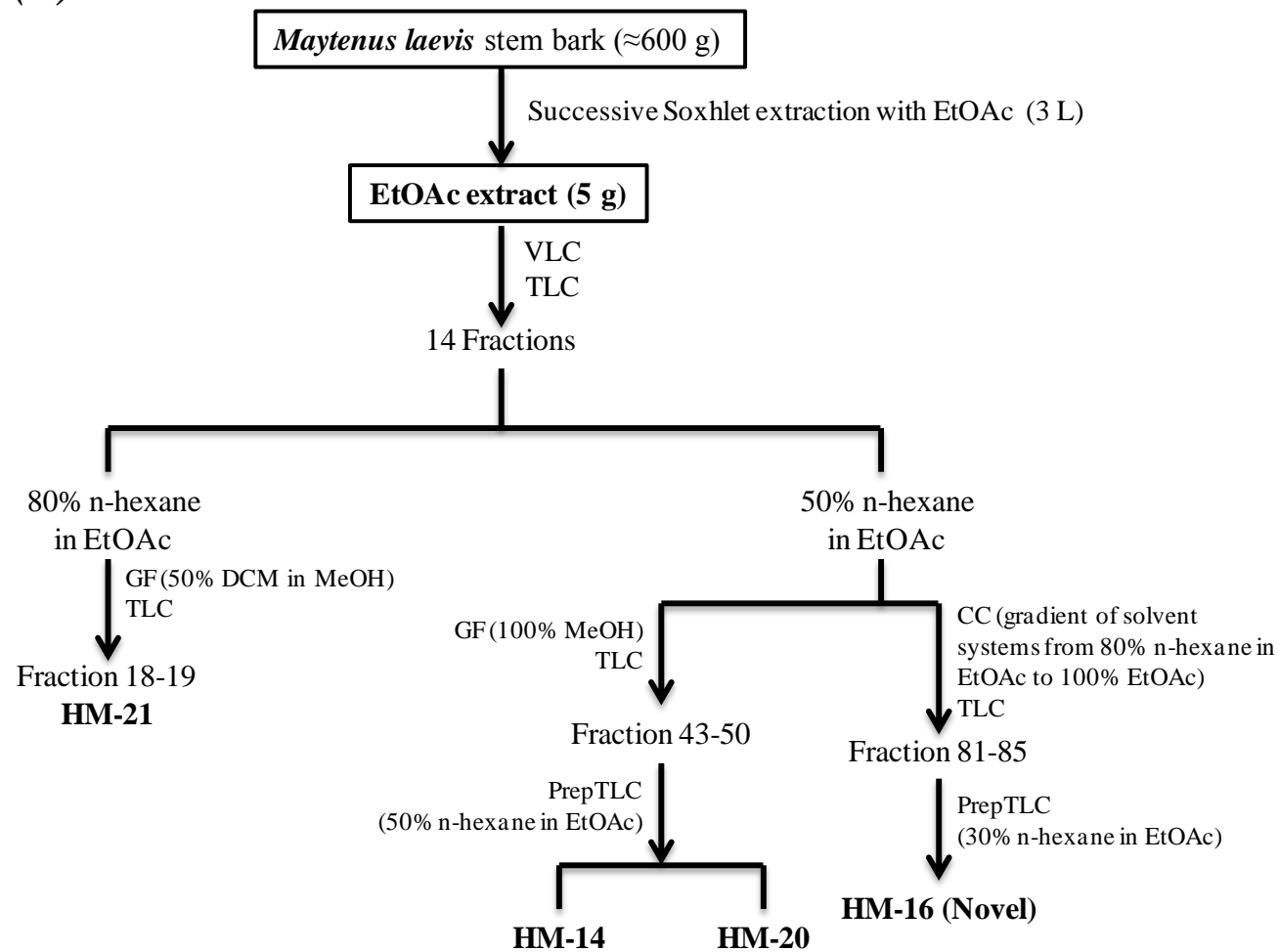
Isolation scheme of compounds from EtOAc extract of the root bark of *M. laevis*

Appendix III (C)



Isolation scheme of compounds from n-hexane extract of the stem bark of *M. laevis*

Appendix III (D)



Isolation scheme of compounds from EtOAc extract of the stem bark of *M. laevis*

Appendix IV

Serial codes of the isolated compounds and the crude extracts along with their original names as used in the lab, amounts and their molecular weights


Code/ Amount (mg)	Sample's name	Molecular weight
MLH, MLHs	MLH, MLHs	-
MLEt, MLEts	MLEt, MLEts	-
MLM, MLMs	MLM, MLMs	-
HM-1	MLHr	-
HM-2 (65)	MLHs-1	442.4
HM-3 (73)	MLHs-3	440.4
HM-4 (20)	MLHs-2	498.4
HM-5 (20)	MLHs-7	456.3
HM-6 (17)	MLHs-9	438.3
HM-7 (15.4)	MLH-1	494.3
HM-8 (23.7)	MLH-3	492.2
HM-9 (16.6)	MLH-4	478.3
HM-10 (24.7)	MLH-2	464.3
HM-11 (20)	MLHs-6	450.3
HM-12 (23.4)	MLEt-3	466.2
HM-13 (5)	MLHs-5	450.2
HM-14 (2)	MLEts-1	440.3
HM-15 (7.3)	MLEt-2A	464.2
HM-16 (4.2)	MLEts-4	498.3
HM-17 (8.5)	MLHs-8	414.7
HM-18 (5)	MLHs-4	412.4
HM-19 (4.8)	MLEt-1	154.01
HM-20 (5)	MLEts-2	122.02
HM-21 (1)	MLEts-3	178.05

• MLH, MLEt, MLM: n-hexane, ethyl acetate and methanol extracts of the root bark of *M. laevis*, respectively; MLHr: rubber-like substance.

• MLHs, MLEts, MLMs: n-hexane, ethyl acetate and methanol extracts of the stem bark of *M. laevis*, respectively.

Appendix V (A): POSTER PRESENTATION (2014)


TRENDS in NATURAL PRODUCTS RESEARCH CONFERENCE



Phytochemical Analysis of Medicinal Plants as a Source of Potential Anti-Parasitic Compounds

Hazar A. Mouad, John O. Igoli, Carol J. Clements, Ann M. Simpson, Valerie A. Ferro and Alexander I. Gray

Natural Product Laboratories, SIPBS, University of Strathclyde, Glasgow, Scotland



Introduction

- Parasitic diseases are a major global health problem with high endemicity in developing countries.
- About 7 to 8 million people worldwide are estimated to be infected with *Trypanosoma cruzi*, mostly in Latin America (WHO, 2013).
- More than 40 million cattle are threatened with Nagana (*T.b.brucei*)




Fig (1) - AMERICAN TRYPANOSOMIASIS
www.cdc.gov/dpdx/amti/

- Natural products and medicinal plants have continued to play a significant role in the search for new and potent anti-parasitic drugs with minimal side effects.
- Maytenus laevis* (Celastraceae), locally called Chuchugusa by indigenous communities in Colombia, S. America was chosen in this study in an attempt to screen crude extracts, fractions and isolated compounds from the root and stem bark for investigation of *in vitro* anti-parasitic activity.




Fig (2) a: Chuchugusa tree, b: the orange roots, c: leaves.

Materials & Methods

- Hot solvent extraction: Soxhlet apparatus (Fig. 3).
- Fractionation and purification: several chromatographic techniques were used such as VLC, CC, Sephadex LH-20, semi-preparative HPLC and PTLC (Figs. 3 & 4).
- Structure elucidation using:
NMR: ¹H, Dept q ¹³C, COSY, NOESY, HMBC, HSQC.
Mass Spectroscopy: HRESI-MS
- Anti-trypanosomal activity assay: using an Alamar blue™ 96 well microplate assay (Table 1).

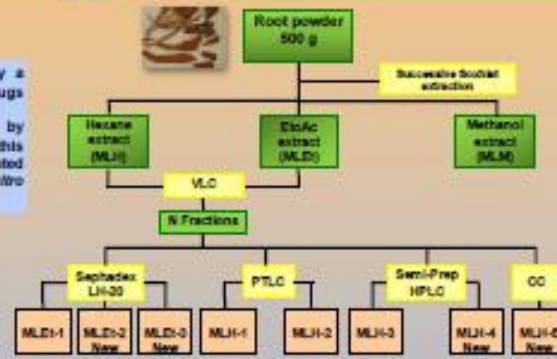


Fig (3) Fractionation scheme for *M. laevis* root bark

Results

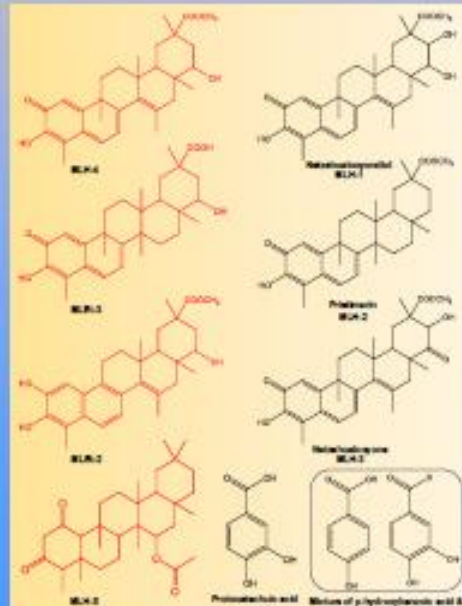


Fig (4) Comparison between stem and root bark extracts on TLC after developing (left) and under 266nm UV (right).

Sample code	20 µg/ml	
	Trypanosoma brucei Brucei 50/7	Trypanosoma brucei Brucei 94/7
MLH	% of control	
MLH	0.9	3.1
MLH	0.2	1.8
MLH	02.9	
MLE-1	0.2	3.1
MLE-1	0.2	<0.19
MLE-2	1.2	<0.19

Table (1) Anti-trypanosomal activity of some *M. laevis* samples

Conclusion

- The root bark of *M. laevis* gave four novel triterpenes, (MLH-4), (MLH-5), (MLE-2) and (MLE-3) along with three known quinonemethide triterpenes, netzahualcoyendiol (MLH-1), protiferments (MLH-2) and netzahualcoyone (MLH-3).
- Some phenolics such as protocatechuic acid (MLE-1) and a mixture of 3,4-dihydroxybenzaldehyde p-hydroxybenzoic acid were also isolated.
- So far, the preliminary phytochemical investigation of the stem bark appears quite different from that of the root bark.
- The quinonemethide triterpenes MLH-1 and 2 exhibited a marked *in vitro* trypanocidal activity.

References

- Das Neves, V.A., F.F.B., Leite, K.M., de Costa Nogueira, M., Nogueira, L.O., Martins, L., Nogueira, C.T., Gonçalves, M. & B. (2012). Antiparasitic activity of quinonemethide triterpenes from *Maytenus laevis* (Celastraceae). *Molecules* (Basel, Switzerland), 17(1), 100-112.
- Das, S., Das, M., Das, S., Das, S., Das, S., Das, S. (2012). The Alamar Blue assay to determine drug sensitivity of *Trypanosoma brucei* and *Trypanosoma evansi*. *Asia Trop. Med.* 1(2): 100-107.
- World Health Organization Media centre. (March 2013). Chagas disease (American trypanosomiasis) Fact sheet #103

Acknowledgements

- The SIPBS of the University of Strathclyde, S. America; Muebles Menchaca (2010) and the Rodriguez Aguilera (2010) and the ethnobotanical knowledge of the plant.
- NMR is funded through a PhD scholarship provided by Dundee University, UK.

Appendix V (B): BEST POSTER AWARD

TRENDS in NATURAL PRODUCTS RESEARCH
Young Scientists Meeting
Olomouc, Czech Republic
June 23 – 25, 2014



The Teva Award

This is to certify that

Hazar A. Mouad

Awarded the Prize from Teva Czech Industries for the Best Poster



Coche L. Juez

REFERENCES

- Abbas, J., Kardono, L., Hanafi, M., Kosela, S., Qin, G.-W., 2007. Canophyllol and Calaustralin From Two Indonesian Species of *Calophyllum*. Proceedings of The Henk Timmerman International Seminar on Pharmacochimistry 28–39.
- Abe, I., 2007. Enzymatic synthesis of cyclic triterpenes. Natural Product Reports 24, 1311–1331.
- Adeyemi, O.S., Akanji, M.A., Oguntoye, S. A., 2009. Ethanolic leaf extract of *Psidium guajava*: Phytochemical and trypanocidal activity in rats infected with *Trypanosoma brucei brucei*. Journal of Medicinal Plants 3, 420–423.
- Aguilar-Gonzalez, A.R., Mena-Rejón, G.J., Padilla-Montaña, N., Toscano, A., Quijano, L., 2005. Triterpenoids from *Hippocratea excelsa*. The crystal structure of 29-hydroxytaraxerol. Zeitschrift fur Naturforschung - Section B Journal of Chemical Sciences 60, 577–584.
- Akcos, Y., Ezer, N., Özçelik, B., Abbasoglu, U., 1998. Iridoid Glucosides From *Sideritis Lycia* Boiss. & Heldr. and its Antimicrobial Activites. Fabad Journal of Pharmaceutical Sciences 23, 99–103.
- Alexander-Lindo, R.L., Morrison, E.Y.S. a, Nair, M.G., 2004. Hypoglycaemic effect of stigmast-4-en-3-one and its corresponding alcohol from the bark of *Anacardium occidentale* (cashew). Phytotherapy Research 18, 403–7.
- Ali, M.S., Mahmud, S., Perveen, S., Ahmad, V.U., Rizwani, G.H., 1999. Epimers from the leaves of *Calophyllum inophyllum*. Phytochemistry 50, 1385–1389.
- Allison, A.C., Cacabelos, R., Lombardi, V.R.M., Álvarez, X.A., Vigo, C., 2001. Celastrol, a potent antioxidant and anti-inflammatory drug, as a possible treatment for Alzheimer's disease. Progress in Neuro-Psychopharmacology and Biological Psychiatry 25, 1341–1357.
- Alvarenga, T.A., Bêdo, T.R.F.O., Braguine, C.G., Gonçalves, U.O., Magalhães, L.G., Rodrigues, V., Gimenez, V.M.M., Groppo, M., Silva, M.L.A., Cunha, W.R., Januário, A.H., Pauletti, P.M., 2012. Evaluation of *Cuspidaria pulchra* and its Isolated Compounds Against *Schistosoma mansoni* Adult Worms. International Journal of Biotechnology for Wellness Industries 1, 122–127.
- Amoah, S.K.S., de Oliveira, F.L., da Cruz, A.C.H., de Souza, N.M., Campos, F.R., Barison, A., Biavatti, M.W., 2013. Sesquiterpene lactones from the leaves of *Hedyosmum brasiliense* (Chloranthaceae). Phytochemistry 87, 126–32.
- Anjaneyulu, A.S.R., Narayanarao, M., 1980. Elaeodendrol and elaeodendradiol, new nor-triterpenes from *Elaeodendron glaucum*. Phytochemistry 19, 1163–1169.
- Avilla, J., Teixidò, A., Velázquez, C., Alvarenga, N., Ferro, E., Canela, R., 2000. Insecticidal activity of *Maytenus* species (Celastraceae) nortriterpene quinone methides against codling moth, *Cydia pomonella* (L.) (Lepidoptera:

- Tortricidae). *Journal of Agricultural and Food Chemistry* 48, 88–92.
- Babich, H., Sedletcaia, A., Kenigsberg, B., 2002. *In vitro* cytotoxicity of protocatechuic acid to cultured human cells from oral tissue: involvement in oxidative stress. *Pharmacology & Toxicology* 91, 245–253.
- Babich, H., Visioli, F., 2003. *In vitro* cytotoxicity to human cells in culture of some phenolics from olive oil. *Farmaco* 58, 403–407.
- Barla, A., Birman, H., Kültür, Ş., Öksüz, S., 2006. Secondary Metabolites from *Euphorbia helioscopia* and their Vasodepressor Activity. *Turkish Journal of Chemistry* 30, 325–332.
- Baskar, A.A., Ignacimuthu, S., Paulraj, G.M., Al Numair, K.S., 2010. Chemopreventive potential of β -Sitosterol in experimental colon cancer model - an *In vitro* and *In vivo* study. *BMC Complementary and Alternative Medicine* 10, 1–10.
- Bessen, H.A., 1986. "Therapeutic and toxic effects of digitalis: William Withering. *Journal of Emergency Medicine* 4, 243–8.
- Betancor, C., Freire, R., Gonzalez, A.G., Salazar, J.A., Pascard, C., Prange, T., 1980. Three triterpenes and other terpenoids from *Catha cassinoides*. *Phytochemistry* 19, 1989–1993.
- Beytur, A., Ciftci, O., Aydin, M., Cakir, O., Timurkaan, N., Yilmaz, F., 2012. Protocatechuic acid prevents reproductive damage caused by 2,3,7,8-tetrachlorodibenzo-*p*-dioxin (TCDD) in male rats. *Andrologia* 44, 454–461.
- Bruni, R., Rossi, D., Muzzoli, M., Romagnoli, C., Paganetto, G., Besco, E., Choquecillo, F., Peralta, K., Lora, W.S., Sacchetti, G., 2006. Antimutagenic, antioxidant and antimicrobial properties of *Maytenus krukovii* bark. *Fitoterapia* 77, 538–45.
- Campos-López, E., Palacios, J., 1976. Microstructure of natural guayule rubber from 300-MHz nuclear magnetic resonance spectra. *Journal of Polymer Science: Polymer Chemistry Edition* 14, 1561–1563.
- Carvalho, P.R.F., Silva, D.H.S., Bolzani, V.S., Furlan, M., 2005. Antioxidant quinonemethide triterpenes from *Salacia campestris*. *Chemistry & Biodiversity* 2, 367–72.
- Caufield, C., 1986. *In the Rainforest, illustrate.* ed. University of Chicago Press, Chicago.
- Chang, F.-R., Hayashi, K.-I., Chen, I.-H., Liaw, C.-C., Bastow, K.F., Nakanishi, Y., Nozaki, H., Cragg, G.M., Wu, Y.-C., Lee, K.-H., 2003. Antitumor agents. 228. five new agarofurans, Reissantins A-E, and cytotoxic principles from *Reissantia*

- buchananii*. Journal of Natural Products 66, 1416–1420.
- Chang, R., Wang, C., Zeng, Q., Guan, B., Zhang, W., Jin, H., 2013. Chemical constituents of the stems of *Celastrus rugosus*. Archives of Pharmacal Research 36, 1291–301.
- Chao, C.-Y. and, Yin, M.-C., 2009. Antibacterial Effects of *Roselle Calyx* Extracts and Protocatechuic Acid in Ground Beef and Apple Juice. Foodborne Pathogens and Disease 6, 201–206.
- Chaturvedula, V.S.P., Prakash, I., 2012. Isolation of Stigmasterol and β -Sitosterol from the dichloromethane extract of *Rubus suavissimus*. International Current Pharmaceutical Journal 1, 239–242.
- Chávez, H., Callo, N., Estévez-Braun, A., Ravelo, A.G., González, A.G., 1999. Sesquiterpene polyol esters from the leaves of *Maytenus macrocarpa*. Journal of Natural Products 62, 1576–1577.
- Chávez, H., Estévez-Braun, A., Ravelo, A.G., González, A.G., 1998. Friedelane Triterpenoids from *Maytenus macrocarpa*. Journal of Natural Products 61, 82–85.
- Chávez, H., Estévez-Braun, A., Ravelo, Á.G., González, A.G., 1997. First examples of dammarane triterpenes isolated from Celastraceae. Tetrahedron 53, 6465–6472.
- Chávez, H., Rodríguez, G., Estévez-Braun, A., Ravelo, Á.G., Estévez-Reyes, R., González, A.G., Fdez-Puente, J.L., García-Grávalos, D., 2000. Macrocarpins A-D, new cytotoxic nor-triterpenes from *Maytenus macrocarpa*. Bioorganic and Medicinal Chemistry Letters 10, 759–762.
- Chen, K., Shi, Q., Kashiwada, Y., Zhang, D.-C., Hu, C.-Q., Jin, J.-Q., Nozaki, H., Kilkuskie, R.E., Tramontano, E., Cheng, Y.-C., McPhail, D.R., McPhail, A.T., Lee, K.-H., 1992. Anti-AIDS Agents, 6. Salaspermic Acid, an Anti-HIV Principle from *Tripterygium wilfordii*, and the Structure-activity Correlation with its Related Compounds. Journal of Natural Products 55, 340–346.
- Chen, Q., Saha, P., Kim, N.-G., Kim, J.K., 2015. Processing and characterization of electrospun trans-polyisoprene nanofibers. Journal of Polymer Engineering 35, 53–59.
- Chen, R.-C., Su, J.-H., Yang, S.-M., Li, J., Wang, T.-J., Zhou, H., 2002. Effect of isoverbascoside, a phenylpropanoid glycoside antioxidant, on proliferation and differentiation of human gastric cancer cell. Acta Pharmacologica Sinica 23, 997–1001.
- Chu, C.-W., Liu, C.-M., Chung, M.-I., Chen, C.-Y., 2015. Biofunctional Constituents from *Michelia compressa* var. *lanyuensis* with Anti-Melanogenic Properties.

- Claridge, T.D.W., 2008. High-Resolution NMR Techniques in Organic Chemistry, second ed. ed. Elsevier Ltd, Netherlands.
- Colas, R., 1937. Les plantes amazoniennes désignées sous le nom de “Chuchuhuasha”. Thèse, Imprimerie André Lesot, Paris.
- Coll, J.C., Bowden, B.F., 1986. The Application of Vacuum Liquid Chromatography to the Separation of Terpene Mixtures. *Journal of Natural Products* 49, 934–936.
- Cordell, G.A. (Ed.), 2003. *The Alkaloids: Chemistry and Biology*, First. ed. Academic Press, San Diego, California.
- Corredor de, B.M.V., Simpson, A., 2009. Traditional medicine used by ethnic groups in the Colombian Amazon tropical forest, South America. In: Steven B. Kayne (Ed.), *Traditional Medicine: A Global Perspective*. Pharmaceutical press, London, UK, pp. 65–81.
- Corsino, J., de Carvalho, P.R.F., Kato, M.J., Latorre, L.R., Oliveira, O.M.M., Araújo, A.R., Bolzani, V. da S., França, S.C., Pereira, A.M.S., Furlan, M., 2000. Biosynthesis of friedelane and quinonemethide triterpenoids is compartmentalized in *Maytenus aquifolium* and *Salacia campestris*. *Phytochemistry* 55, 741–748.
- Cortés-Selva, F., Jiménez, I.A., Muñoz-Martínez, F., Campillo, M., Bazzocchi, I.L., Pardo, L., Ravelo, A.G., Castanys, S., Gamarro, F., 2005. Dihydro- β -Agarofuran Sesquiterpenes: A New Class of Reversal Agents of the Multidrug Resistance Phenotype Mediated by P-Glycoprotein in the Protozoan Parasite *Leishmania*. *Current Pharmaceutical Design* 11, 3125–39.
- Costa, P.M. da, Ferreira, P.M.P., Bolzani, V. da S., Furlan, M., de Freitas Formenton Macedo dos Santos, V.A., Corsino, J., de Moraes, M.O., Costa-Lotufo, L.V., Montenegro, R.C., Pessoa, C., 2008. Antiproliferative activity of pristimerin isolated from *Maytenus ilicifolia* (Celastraceae) in human HL-60 cells. *Toxicology in Vitro* 22, 854–863.
- da Silva, G., Serrano, R., Silva, O., 2011. *Maytenus heterophylla* and *Maytenus senegalensis*, two traditional herbal medicines. *Journal of Natural Science, Biology, and Medicine* 2, 59–65.
- de Felício, R., de Albuquerque, S., Young, M.C.M., Yokoya, N.S., Deboni, H.M., 2010. Trypanocidal, leishmanicidal and antifungal potential from marine red alga *Bostrychia tenella* J. Agardh (Rhodomelaceae, Ceramiales). *Journal of Pharmaceutical and Biomedical Analysis* 52, 763–769.
- de Paiva Campello, J., Fonseca, S.F., Chang, C.-J., Wenkert, E., 1975. Terpenes of

Podocarpus lambertius. Phytochemistry 14, 243–248.

- DiCarlo, F.J., Haynes, L.J., Sliver, N.J., Phillips, and G.E., 1964. Protection of Mice Against Gram-Positive Bacteria with *Maytenus laevis* and Other RES Stimulants. Experimental Biology and Medicine 116, 195–197.
- Dimitriadis, C., Gill, M., Harte, M.F., 1997. The first stereospecific approach to both enantiomers of mellein. Tetrahedron Asymmetry 8, 2153–2158.
- Dos Santos, V. a F.F.M., Leite, K.M., da Costa Siqueira, M., Regasini, L.O., Martinez, I., Nogueira, C.T., Galuppo, M.K., Stolf, B.S., Pereira, A.M.S., Cicarelli, R.M.B., Furlan, M., Graminha, M. a S., 2013. Antiprotozoal activity of quinonemethide triterpenes from *Maytenus ilicifolia* (Celastraceae). Molecules (Basel, Switzerland) 18, 1053–62.
- Duan, H., Takaishi, Y., Bando, M., Kido, M., Imakura, Y., Lee, K., 1999. Novel sesquiterpene esters with alkaloid and monoterpene and related compounds from *Tripterygium hypoglaucum*: A new class of potent anti-HIV agents. Tetrahedron Letters 40, 2969–2972.
- Duan, H., Takaishi, Y., Momota, H., Ohmoto, Y., Taki, T., Jia, Y., Li, D., 2001. Immunosuppressive sesquiterpene alkaloids from *Tripterygium wilfordii*. Journal of Natural Products 64, 582–587.
- Duarte, L.E.A., 1979. Principales Plantas Utiles de la Amazonia Colombiana. Bogotá, Colombia.
- Duch, M.W., Grant, D.M., 1970. Carbon-13 Chemical Shift Studies of the 1,4-Polybutadienes and the 1,4-Polyisoprenes. Macromolecules 3.
- Duke, J.A., Vasquez, R., 1994. Amazonian ethnobotanical dictionary. CRC Press, Boca Raton.
- Dung, D.T., Ngo, V.Q., Yen, P.H., Hoang, L.T.A., Nguyen, X.N., Trang, D.T., Tho, P.T.T., Hang, D.T.T., Chau, V.M., Phan, V.K., 2014. Steroids from the sponge *Clathria vulpina* and their cytotoxic activities. Vietnam Journal of Chemistry 52, 559–563.
- Ee, G.C., Lim, C.K., Rahmat, A., Lee, H.L., 2005. Cytotoxic activities of chemical constituents from *Mesua daphnifolia*. Tropical Biomedicine 22, 99–102.
- El-Ashmawy, I.M., Al-Wabel, N.A., Bayad, A.E., 2016. *Achillea fragrantissima*, rich in flavonoids and tannins, potentiates the activity of diminazine acetate against *Trypanosoma evansi* in rats. Asian Pacific Journal of Tropical Medicine 1–7.
- Elhag, H., Mossa, J.S., El-olemy, M.M., 1999. Antimicrobial and Cytotoxic Activity of the Extracts of Khat Callus Cultures. In: Janick, J. (Ed.), Perspectives on

New Crops and New Uses. ASHS Press, Alexandria, VA, pp. 463–466.

- Evans, W.C., 2009. Trease and Evans Pharmacognosy, 16th ed. Elsevier Health Sciences.
- Farnsworth, N.R., 1988. Screening Plants for New Medicines. In: Wilson, E., Peter, F. (Eds.), Biodiversity. National Academies Press (US), Washington (DC), pp. 83–97.
- Ferchichi, L., Derbré, S., Mahmood, K., Touré, K., Guilet, D., Litaudon, M., Awang, K., Hadi, a. H. a, Le Ray, A.M., Richomme, P., 2012. Bioguided fractionation and isolation of natural inhibitors of advanced glycation end-products (AGEs) from *Calophyllum flavoramulum*. *Phytochemistry* 78, 98–106.
- Fernández, M.I., Pedro, J.R., Seoane, E., 1983. Constituents of a hexane extract of *Phoenix dactylifera*. *Phytochemistry* 22, 2087–2088.
- Fernando, H.C., Gunatilaka, A.A.L., Kumar, V., Weeratunga, G., Tezuka, Y., Kikuchi, T., 1988. Two new quinone-methides from *Cassine balaie*: Revised structure of balaenonol. *Tetrahedron Letters* 29, 387–390.
- Figueiredo, J.N., Rätz, B., Séquin, U., 1998. Novel quinone methides from *Salacia kraussii* with *in vitro* antimalarial activity. *Journal of Natural Products* 61, 718–723.
- Flamini, G., Antognoli, E., Morelli, I., 2001. Two flavonoids and other compounds from the aerial parts of *Centaurea bracteata* from Italy. *Phytochemistry* 57, 559–64.
- Flemming, K., Flemming, C., Graack, B., 1967. Strahlenresistenz bei pharmakologisch veränderter Phagozytoseaktivität des RES. *Strahlentherapie* 133, 280–287.
- Flörke, U., Krohn, K., Zia-Ullah, Hussain, H., 2006. An ortho-rhom-bic modification of (R)-(-)-8-hydr-oxy-3-methyl-3,4-dihydro-1H-2-benzopyran-1-one [(R)-(-)-mellein]. *Acta Crystallographica Section E* 62, o3539–o3541.
- Fujita, R., Duan, H., Takaishi, Y., 2000. Terpenoids from *Tripterygium hypoglaucum*. *Phytochemistry* 53, 715–722.
- Ganesan, A., 2008. “The impact of natural products upon modern drug discovery.” *Current Opinion in Chemical Biology* 12, 306–17.
- García-Barriga, H., 1974. Flora Medicinal de Colombia. Instituto de Ciencias Naturales, Bogotá, Colombia.
- Gaspar, E.M.M., das Neves, H.J.C., 1993. Steroidal constituents from mature wheat straw. *Phytochemistry* 34, 523–527.

- Gill, M., 1993. *The Chemistry of Natural Products*, 2nd editio. ed. London: Blackie A & P.
- Goijman, S., Turrens, J., Marini-Bettolo, G., Stoppani, A., 1985. Effect of tingenone, a quinonoid triterpene, on growth and macromolecule biosynthesis in *Trypanosoma cruzi*. *Experientia* 41, 646–8.
- Gonzales, A.G., Ravelo, A.G., Bazzocchi, I.L., Jimenes, J., Gonzales, C.M., Luis, J.G., Ferro, E.A., Gutierrez, A., Moujir, L., De las Heras, F.G., 1988. Biological study of triterpene quinones from Celastraceae. II Farmaco. Edizione scientifica 43, 501.
- González, A.G., Alvarenga, N.L., Ravelo, A.G., Bazzocchi, I.L., Ferro, E.A., Navarro, A.G., Moujir, L.M., 1996. Scutione, a new bioactive norquinonemethide triterpene from *Maytenus scutioides* (Celastraceae). *Bioorganic & Medicinal Chemistry* 4, 815–820.
- González, A.G., Bazzocchi, I.L., Moujir, L., Jiménez, I.A., 2000. Ethnobotanical uses of Celastraceae. Bioactive metabolites, *Studies in Natural Products Chemistry*, *Studies in Natural Products Chemistry*. Elsevier.
- Gonzalez, A.G., Bazzocchi, I.L., Ravelo, A.G., Luis, J.G., Dominguez, X.A., Vazquez, G., Cano, G., 1987. Triterpenes and triterpenoquinones of *Rzedowskia tolantoguensis* (Celastraceae). *Revista latinoamericana de química* Gonzalez 18, 83.
- Gonzalez, A.G., Darias, V., Boada, J., Alonso, G., 1977. Study of the cytostatic activity of iguesterin and related compounds. *Planta Medica* 32, 282–6.
- González, A.G., Ferro, E.A., Ravelo, A.G., 1987. Triterpenes From *Maytenus Horrida*. *Phytochemistry* 26, 2785–2788.
- González, A.G., Fraga, B.M., González, C.M., Ravelo, A.G., E., F., Dominguez, X.A., Martinez, M.A., Fayos, J., Perales, A., Rodríguez, M.L., 1983. X-Ray analysis of netzahualcoyone, A triterpene quinone from *Orthosphenia mexicana*. *Tetrahedron Letters* No. 24 3033–3036.
- González, A.G., J.J. Mendoza, Luis, J.G., Ravelo, A.G., Bazzocchi, I.L., 1989. New Epimeric Di-triterpene Quinone Ethers. Their Partial Synthesis and That of Netzahualcoyone from Pristimerin and DDQ. *Tetrahedron Letters* No. 7, 30, 863–866.
- González, A.G., Tincusi, B.M., Bazzocchi, I.L., Tokuda, H., Nishino, H., Konoshima, T., Jiménez, I.A., Ravelo, A.G., 2000. Anti-tumor promoting effects of sesquiterpenes from *Maytenus cuzcoina* (Celastraceae). *Bioorganic & Medicinal Chemistry* 8, 1773–1778.

- Gonzalez, J.G., Monache, G.D., Monache, F.D., Marini-Bettolò, G.B., 1982. Chuchuhuasha- A Drug Used In Folk Medicine In The Amazonian and Andean Areas. A Chemical Study of *Maytenus laevis*. *Journal of Ethnopharmacology* 5, 73–77.
- Goodman, M., 1967. Concepts of Polymer Stereochemistry. In: Allinger, N.L., Eliel, E.L. (Eds.), *Topics in Stereochemistry*. John Wiley & Sons, Inc., Hoboken, NJ, USA, p. 73.
- Gottlieb, H.E., Kotlyar, V., Nudelman, A., 1997. NMR Chemical Shifts of Common Laboratory Solvents as Trace Impurities. *Journal of Organic Chemistry* 62, 7512–7515.
- Graziose, R., Rojas-Silva, P., Rathinasabapathy, T., Dekock, C., Grace, M.H., Poulev, A., Ann Lila, M., Smith, P., Raskin, I., 2012. Antiparasitic compounds from *Cornus florida* L. with activities against *Plasmodium falciparum* and *Leishmania tarentolae*. *Journal of Ethnopharmacology* 142, 456–461.
- Grove, J.F., Pople, M., 1979. Metabolic Products of *Fusarium larvarum* Fuckel. The Fusarentins and the Absolute Configuration of Monocerin. *Journal of the Chemical Society, Perkin Transactions 1*, 2048–2051.
- Gunatilaka, A.A.L., 1996. Triterpenoid Quinonemethides and Related Compounds (Celastroloids). *Progress in the Chemistry of Organic Natural Products* 67, 1–123.
- Guo, J., Chen, J., Lin, L., Xu, F., 2012. Five chemical constituents of the ethyl acetate fraction from ethanol extract of semen litchi. *Journal of Medicinal Plants Research* 6, 168–170.
- Gupta, M.B., Nath, R., Srivastava, N., Shanker, K., Kishor, K., Bhargava, K.P., 1980. Anti-Inflammatory and Antipyretic Activities of β -Sitosterol. *Planta Medica* 39, 157–163.
- Gutzeit, D., Wray, V., Winterhalter, P., Jerz, G., 2006. Preparative Isolation and Purification of Flavonoids and Protocatechuic Acid from Sea Buckthorn Juice Concentrate (*Hippophaë rhamnoides* L. ssp. *rhamnoides*) by High-Speed Counter-Current Chromatography. *Chromatographia* 65, 1–7.
- Habsah, M., Ali, A.M., Lajis, N.H., Sukari, M.A., Yap, Y.H., Kikuzaki, H., Nakatani, N., 2005. Antitumour-promoting and cytotoxic constituents of *Etlingera elatior*. *Malaysian Journal of Medical Sciences* 12, 6–12.
- Harada, R., Kakisawa, H., Kobayashi, S., Musya, M., Nakanishi, K., Y. Takahashi, 1962. Structure of Pristimerin, A Quinonoid Triterpene. *Tetrahedron Letters* 14 603–607.
- Hegnauer, R., 1966. *Chemotaxonomie der Pflanzen*, 4th ed. Birkhäuser Basel.

- Henriksson, E., Kjellén, E., Wahlberg, P., Wennerberg, J., Kjellström, J.H., 2006. Differences in estimates of cisplatin-induced cell kill *in vitro* between colorimetric and cell count/colony assays. *In Vitro Cellular & Developmental Biology - Animal* 42, 320–323.
- Heywood, V.H., 1993. *Flowering Plants of the World*, 2, illustr. ed. Oxford University Press, New York.
- Hill, R., 1986. Naturally occurring isocoumarins. *Prog Chem Nat Prod* 49, 1–78.
- Höller, U., König, G.M., Wright, A.D., 1999. Three new metabolites from marine-derived fungi of the genera *Coniothyrium* and *Microsphaeropsis*. *Journal of Natural Products* 62, 114–118.
- Hong, L.S., Ibrahim, D., Kassim, J., 2011. Assessment of *in vivo* and *in vitro* cytotoxic activity of hydrolysable tannin extracted from *Rhizophora apiculata* barks. *World Journal of Microbiology and Biotechnology* 27, 2737–2740.
- Hussein, G., Miyashiro, H., Nakamura, N., Hattori, M., Kawahata, T., Otake, T., Kakiuchi, N., Shimotohno, K., 1999. Inhibitory effects of Sudanese plant extracts on HIV-1 replication and HIV-1 protease. *Phytotherapy Research* 13, 31–6.
- Hussein, G., Nakamura, N., Meselhy, M.R., Hattori, M., 1999. Phenolics from *Maytenus senegalensis*. *Phytochemistry* 50, 689–694.
- Igoli, J.O., Gray, A.I., Clements, C.J., Mouad, H.A., 2011. Anti-Trypanosomal Activity and Cytotoxicity of Some Compounds and Extracts from Nigerian Medicinal Plants. In: *Phytochemicals – Bioactivities and Impact on Health*. InTech, pp. 375–388.
- Itokawa, H., Shiota, O., Morita, H., Takeya, K., Litaka, Y., 1993. Isolation, Structural Elucidation and Conformational Analysis of Sesquiterpene Pyridine Alkaloids from *Maytenus ebenifolia* Reiss. X-Ray Molecular Structure of Ebenifoline W-I. *Journal of the Chemical Society, Perkin Transactions 1*, 11, 1247–1254.
- Iwagawa, T., Asai, H., Hase, T., Sako, S., Su, R., Hagiwara, N., Kim, M., 1990. Monoterpenoids from *Radermachia sinica*. *Phytochemistry* 29, 1913–1916.
- Jackson, S., Houghton, P., Retsas, S., Photiou, A., 2000. *In Vitro* Cytotoxicity of Norviburtinal and Isopinnatal from *Kigelia pinnata* Against Cancer Cell Lines. *Planta Medica* 66, 758–61.
- Jangruang, A., Sudta, P., Ratananukul, P., Suksamrarn, S., 2009. Chemical Constituents of the *Salacia verrucosa* Wight Stem. *SWU Journal of Science* 25.

- Jeller, A.H., Silva, D.H.S., Lião, L.M., Bolzani, V.D.S., Furlan, M., 2004. Antioxidant phenolic and quinonemethide triterpenes from *Cheiloclinium cognatum*. *Phytochemistry* 65, 1977–82.
- Jo, M., Nakamura, N., Kakiuchi, N., Komatsu, K., Qui, M., Shimotohno, K., Shimotohno, K., Hattori, M., 2006. Inhibitory effect of Yunnan traditional medicines on hepatitis C viral polymerase. *Journal of Natural Medicines* 60, 217–224.
- Jorge, R.M., Leite, J.P. V, Oliveira, A.B., Tagliati, C.A., 2004. Evaluation of antinociceptive, anti-inflammatory and antiulcerogenic activities of *Maytenus ilicifolia*. *Journal of Ethnopharmacology* 94, 93–100.
- Kanchanapoom, T., Kasai, R., Yamasaki, K., 2002. Phenolic glycosides from *Markhamia stipulata*. *Phytochemistry* 59, 557–563.
- Khalid, S.A., Friedrichsen, G.M., Christensen, S.B., Tahir, A. El, Sattic, G.M., 2007. Isolation and characterization of pristimerin as the antiplasmodial and antileishmanial agent of *Maytenus senegalensis* (Lam.) Exell. *ARKIVOC* 2007, 129–134.
- Kiaei, M., Kipiani, K., Petri, S., Chen, J., Calingasan, N., Beal, M., 2005. Celastrol Blocks Neuronal Cell Death and Extends Life in Transgenic Mouse Model of Amyotrophic Lateral Sclerosis. *Neurodegenerative Disease* 2, 246–254.
- Kim, D.Y., Park, J.W., Jeung, D., Ro, J.Y., 2009. Celastrol suppresses allergen-induced airway inflammation in a mouse allergic asthma model. *European Journal of Pharmacology* 612, 98–105.
- Kirmizibekmez, H., Atay, I., Kaiser, M., Brun, R., Cartagena, M.M., Carballeira, N.M., Yesilada, E., Tasdemir, D., 2011. Antiprotozoal Activity of *Melampyrum arvense* and its Metabolites. *Phytotherapy Research* 25, 142–146.
- Kishi, A., Morikawa, T., Matsuda, H., Yoshikawa, M., 2003. Structures of new friedelane- and norfriedelane-type triterpenes and polyacylated eudesmane-type sesquiterpene from *Salacia chinensis* LINN. (*S. prinoides* DC., Hippocrateaceae) and radical scavenging activities of principal constituents. *Chemical & Pharmaceutical Bulletin* 51, 1051–5.
- Kitani, Y., Zhu, S., Omote, T., Tanaka, K., Batkhuu, J., Sanchir, C., Fushimi, H., Mikage, M., Komatsu, K., 2009. “Molecular Analysis and Chemical Evaluation of *Ephedra* Plants in Mongolia.” *Biological and Pharmaceutical Bulletin* 32, 1235–1243.
- Klass, J., Tinto, W.F., Mclean, S., William F. Reynolds, 1992. Friedelane Triterpenoids From *Perzassa Compta*: Complete ^1H and ^{13}C Assignments By 2D NMR Spectroscopy. *Journal of Natural Products* 55, 1626–1630.

- Kloucek, P., Polesny, Z., Svobodova, B., Vlkova, E., Kokoska, L., 2005. Antibacterial screening of some Peruvian medicinal plants used in Calleria District. *Journal of Ethnopharmacology* 99, 309–312.
- Kloucek, P., Svobodova, B., Polesny, Z., Langrova, I., Smrcek, S., Kokoska, L., 2007. Antimicrobial activity of some medicinal barks used in Peruvian Amazon. *Journal of Ethnopharmacology* 111, 427–429.
- Kocór, M., Pyrek, J.S., Atal, C.K., Bedi, K.L., Sharma, B.R., 1973. Triterpenes of *Datura innoxia* Mill. Structure of daturadiol and daturaolone. *The Journal of Organic Chemistry* 38, 3685–3688.
- Kremmer, T. and Boross, L., 1979. *Gel chromatography: theory, methodology, applications*. Wiley.
- Krohn, K., Bahramsari, R., Flörke, U., Ludewig, K., Kliche-Spory, C., Michel, A., Aust, H.-J., Draeger, S., Schulz, B., Antus, S., 1997. Dihydroisocoumarins from fungi: Isolation, structure elucidation, circular dichroism and biological activity. *Phytochemistry* 45, 313–320.
- Kupchan, S.M., Komoda, Y., Court, W.A., Thomas, G.J., Smith, R.M., Karim, A., Gilmore, C.J., Haltiwanger, R.C., Bryan, R.F., 1972. Tumor inhibitors. LXXIII. Maytansine, a novel antileukemic ansa macrolide from *Maytenus ovatus*. *Journal of American Chemical Society* 94, 1354–1356.
- Kutney, J.P., Hewitt, G.M., Lee, G., Piotrowska, K., Roberts, M., Rettig, S.J., 1992. Studies with tissue cultures of the Chinese herbal plant, *Tripterygium wilfordii*. Isolation of metabolites of interest in rheumatoid arthritis, immunosuppression, and male contraceptive activity. *Canadian Journal of Chemistry* 70, 1455–1480.
- Lee, I.-C., Bae, J.-S., Kim, T., Kwon, O.J., Kim, T.H., 2011. Polyphenolic constituents from the aerial parts of *Thymus quinquecostatus* var. *japonica* collected on ulleung island. *Journal of the Korean Society for Applied Biological Chemistry* 54, 811–816.
- Lee, M.R., 2005. Curare: the South American arrow poison. *The journal of the Royal College of Physicians of Edinburgh* 35, 83–92.
- Lee, T.-H., Chiou, J.-L., Lee, C.-K., Kuo, Y.-H., 2005. Separation and Determination of Chemical Constituents in the Roots of *Rhus javanica* L. var. *roxburghiana*. *Journal of the Chinese Chemical Society* 52, 833–841.
- Lende, A.B., Kshirsagar, A.D., Deshpande, A.D., Muley, M.M., Patil, R.R., Bafna, P.A., Naik, S.R., 2011. Anti-inflammatory and analgesic activity of protocatechuic acid in rats and mice. *Inflammopharmacology* 19, 255–263.
- Li, X., Wang, X., Chen, D., Chen, S., 2011. Antioxidant activity and mechanism of protocatechuic acid *in vitro*. *Functional Foods in Health and Disease* 7, 232–

- Li, Y.-Z., Li, Z.-L., Yin, S.-L., Shi, G., Liu, M.-S., Jing, Y.-K., Hua, H.-M., 2010. Triterpenoids from *Calophyllum inophyllum* and their growth inhibitory effects on human leukemia HL-60 cells. *Fitoterapia* 81, 586–9.
- Lião, L.M., Silva, G.A., Monteiro, M.R., Albuquerque, S., 2008. Trypanocidal activity of quinonemethide triterpenoids from *Cheiloclinium cognatum* (Hippocrateaceae). *Zeitschrift fur Naturforschung - Section C Journal of Biosciences* 63, 207–210.
- Lim, E., Kang, H., Jung, H., Kim, K., Lim, C.-J., Park, E.-H., 2008. Anti-Inflammatory, Anti-Angiogenic and Anti-Nociceptive Activities of 4-Hydroxybenzaldehyde. *Biomolecules & Therapeutics* 16, 231–236.
- Lin, L., Gao, Q., Cui, C., Zhao, H., Fu, L., Chen, L., Yang, B., Luo, W., Zhao, M., 2012. Isolation and identification of ent-kaurane-type diterpenoids from *Rabdosia serra* (MAXIM.) HARA leaf and their inhibitory activities against HepG-2, MCF-7, and HL-60 cell lines. *Food Chemistry* 131, 1009–1014.
- Liu, Y.-L., Lindert, S., Zhu, W., Wang, K., McCammon, J.A., Oldfield, E., 2014. Taxodione and arenarone inhibit farnesyl diphosphate synthase by binding to the isopentenyl diphosphate site. *Proceedings of the National Academy of Sciences of the United States of America* 111, E2530–2539.
- López, R., Navarro, J. a., Montero, M.I., Vecht, K., Rodríguez, M., Polania, A., 2006. Manual de identificación de especies no maderables del corregimiento de Tarapacá, Colombia, First. ed. Instituto Amazónico de Investigaciones Científicas -SINCHI, Bogotá, D.C., Colombia.
- Luo, D.-Q., Wang, H., Tian, X., Shao, H.-J., Liu, J.-K., 2005. Antifungal properties of pristimerin and celastrol isolated from *Celastrus hypoleucus*. *Pest Management Science* 61, 85–90.
- Luo, H., Cai, Y., Peng, Z., Liu, T., Yang, S., 2014. Chemical composition and *in vitro* evaluation of the cytotoxic and antioxidant activities of supercritical carbon dioxide extracts of pitaya (dragon fruit) peel. *Chemistry Central Journal* 8, 1–7.
- Luo, X.-L., Shao, Q., Qu, H.-B., Cheng, Y.-Y., 2007. Simple method for determination of five terpenoids from different parts of *Tripterygium wilfordii* and its preparations by HPLC coupled with evaporative light scattering detection. *Journal of Separation Science* 30, 1284–91.
- Lv, C., Zheng, Z.-L., Miao, F., Geng, H.-L., Zhou, L., Liu, L.-P., 2014. New Dihydro- β -agarofuran Sesquiterpenes from *Parnassia wightiana* Wall: Isolation, Identification and Cytotoxicity against Cancer Cells. *International Journal of Molecular Sciences* 15, 11111–11125.

- Mabberley, D.J., 1993. The plant-book: a portable dictionary of the higher plants. Cambridge University Press, Cambridge, UK.
- Madrigal, R. V., Zilkowski, B.W., Jr., C.R.S., 1985. Structure-activity relationships among maytansinoids in their effect on the European corn borer, *Ostrinia nubilalis* (Hübner). *Journal of Chemical Ecology* 11, 501–506.
- Magalhães, C.G., Ferrari, F.C., Guimarães, D.A.S., Silva, G.D.F., Duarte, L.P., Figueiredo, R.C., Filho, S.A. V, 2011. *Maytenus salicifolia*: Triterpenes isolated from stems and antioxidant property of extracts from aerial parts. *Brazilian Journal of Pharmacognosy* 21, 415–419.
- Mahato, S.B., Kundu, A.P., 1994. Review Article Number 98 ¹³C NMR Spectra of Pentacyclic Triterpenoids-A Compilation and Some Salient Features. *Phytochemistry* 37, 1517–1575.
- Mandal, A.K., Abernathy, T., Nelluri, S.N., Stitzel, V., 1995. Is quinine effective and safe in leg cramps? *Journal of Clinical Pharmacology* 35, 588–93.
- Martinod, P., Paredes, A., Monache, F.D., Marini-Bettolo, G.B., 1976. Isolation of Tingenone and Pristimerin From *Maytenus Chuchuhuasca*. *Phytochemistry* 15, 562–563.
- Matsuda, H., Murakami, T., Yashiro, K., Yamahara, J., Yoshikawa, M., 1999. Antidiabetic principles of natural medicines. IV. Aldose reductase and α -glucosidase inhibitors from the roots of *Salacia oblonga* Wall. (Celastraceae): structure of a new friedelane-type triterpene, kotalagenin 16-acetate. *Chemical & Pharmaceutical Bulletin* 47, 1725–1729.
- Megalla, S., 1983. Rapid, economical qualitative method for separation of aflatoxins B-1, B-2 & G-1, G-2 by dry column chromatography. *Mycopathologia* 84, 45–7.
- Melo, A.M., Jardim, M.L., De Santana, C.F., Lacet, Y., Lobo, J., Gonçalves de Lima, O. Leoncio d' Albuquerque, I., 1974. Primeiras Observações do uso topico da primina, plumbagina e maitenina (tingenone) em pacientes portadores de câncer de pele. *Revista do Instituto de Antibioticos (Recife)* 14, 9–16.
- Miller, M.L., 1966. The Structure of Polymers, Polymer science and engineering series. Reinhold Publishing Corporation.
- Mitaine-Offer, A.-C., Hornebeck, W., Sauvain, M., Zèches-Hanrot, M., 2002. Triterpenes and phytosterols as human leucocyte elastase inhibitors. *Planta Medica* 68, 930–2.
- Mitchell, A.M., de Corredor, B.V., Gray, A.I., Corredor, A., 2010. Sabedores-sabedoras: Indigenous Methods of Recuperation, Preservation and Management

- of Forest Varzea, Amazonas – Colombia, Brazil, Peru, Ecuador. The International Journal of Environmental, Cultural, Economic and Social Sustainability 6, 128–165.
- Montenegro, T.G.C., Rodrigues, F.A.R., Jimenez, P.C., Angelim, A.L., Melo, V.M.M., Filho, E.R., De Oliveira, M.C.F., Costa-Lotufo, L. V., 2012. Cytotoxic activity of fungal strains isolated from the ascidian *Eudistoma vannamei*. Chemistry and Biodiversity 9, 2203–2209.
- Morgan, E.D., 2008. Chemical sorcery for sociality: exocrine secretions of ants (Hymenoptera: Formicidae). Myrmecological News 11, 79–90.
- Morikawa, T., Kishi, A., Pongpiriyadacha, Y., Matsuda, H., Yoshikawa, M., 2003. Structures of new friedelane-type triterpenes and eudesmane-type sesquiterpene and aldose reductase inhibitors from *Salacia chinensis*. Journal of Natural Products 66, 1191–6.
- Morimoto, S., Nonaka, G., Nishioka, I., Ezaki, N., Takizawa, N., 1985. Tannins and Related Compounds. XXIX. Seven New Methyl Derivatives of Flavan-3-ols and a 1, 3-Diarylpropan-2-ol from *Cinnamomum cassia*, *C. obtusifolium* and *Lindera umbellata* var. *membranacea*. Chemical & Pharmaceutical Bulletin 33, 2281–2286.
- Morita, H., Hirasawa, Y., Muto, A., Yoshida, T., Sekita, S., Shiota, O., 2008. Antimitotic quinoid triterpenes from *Maytenus chuchuhuasca*. Bioorganic & Medicinal Chemistry Letters 18, 1050–2.
- Mossi, A.J., Cansian, R.L., Carvalho, A.Z., Dariva, C., Oliveira, J.V., Mazutti, M., Filho, I.N., Echeverrigaray, S., 2004. Extraction and characterization of volatile compounds in *Maytenus ilicifolia*, using high-pressure CO₂. Fitoterapia 75, 168–78.
- Moujir, L., Gutiérrez-Navarro, A.M., González, A.G., Ravelo, A.G., Luis, J.G., 1991. Mode of action of netzahualcoyone. Antimicrobial Agents and Chemotherapy 35, 211–3.
- Moujir, L., Gutiérrez-Navarro, A.M., González, A.G., Ravelo, A.G., Luis, J.G., 1990. The Relationship Between Structure and Antimicrobial Activity in Quinones from the Celastraceae. Biochemical Systematics and Ecology 18, 25–28.
- Nagase, M., Oto, J., Sugiyama, S., Yube, K., Takaishi, Y., Sakato, N., 2003. Apoptosis induction in HL-60 cells and inhibition of topoisomerase II by triterpene celastrol. Bioscience, Biotechnology, and Biochemistry 67, 1883–7.
- Nakagawa, H., Takaishi, Y., Fujimoto, Y., Duque, C., Garzon, C., Sato, M., Okamoto, M., Oshikawa, T., Ahmed, S.U., 2004. Chemical constituents from the Colombian medicinal plant *Maytenus laevis*. Journal of Natural Products 67,

1919–24.

- Nakamura, Y., Torikai, K., Ohto, Y., Murakami, a, Tanaka, T., Ohigashi, H., 2000. A simple phenolic antioxidant protocatechuic acid enhances tumor promotion and oxidative stress in female ICR mouse skin: dose-and timing-dependent enhancement and involvement of bioactivation by tyrosinase. *Carcinogenesis* 21, 1899–907.
- Nakano, K., Maruyama, K., Murakami, K., Takaishi, Y., Tomimatsu, T., 1993. Iridoids from *Tabebuia avellaneda*. *Phytochemistry* 32, 371–373.
- Nakano, K., Oose, Y., Masuda, Y., Kamada, H., Takaishi, Y., 1997. A Diterpenoid and Triterpenes From Tissue Cultures of *Tripterygium wilfordii*. *Phytochemistry* 45, 293–296.
- Nakano, K., Oose, Y., Takaishi, Y., 1997. A Novel Epoxy-Triterpene and Nortriterpene From Callus Cultures of *Tripterygium Wilfordii*. *Phytochemistry* 46, 1179–1182.
- Newman, D., Fairfield, A., Bhattacharya, B., Grifo, F., Grupenhoff, J., 1997. The origins of prescription drugs. In: Rosenthal, F.G. and J. (Ed.), *Biodiversity and Human Health*. Island Press, Washington, DC, pp. 131–163.
- Newman, D.J., Cragg, G.M., 2012. Natural Products as Sources of New Drugs over the 30 Years from 1981-2010. *Journal of Natural Products* 75, 311–335.
- Ngassapa, O., Soejarto, D.D., Pezzuto, J.M., Farnsworth, N.R., 1994. Quinone-methide triterpenes and salaspermic acid from *Kokoona ochracea*. *Journal of Natural Products* 57, 1.
- Ngouamegne, E.T., Fongang, R.S., Ngouela, S., Boyom, F.F., Rohmer, M., Tsamo, E., Gut, J., Rosenthal, P.J., 2008. Endodesmiadiol, a friedelane triterpenoid, and other antiplasmodial compounds from *Endodesmia calophylloides*. *Chemical & Pharmaceutical Bulletin* 56, 374–377.
- Nirmal, S.A., Pal, S.C., Mandal, S.C., Patil, A.N., 2012. Analgesic and anti-inflammatory activity of β -sitosterol isolated from *Nyctanthes arbortristis* leaves. *Inflammopharmacology* 20, 219–224.
- Nishimura, H., Sasaki, H., Morota, T., Chin (Chen Zhengxiong), M., Mitsushashi, H., 1989. Six iridoid glycosides from *Rehmannia glutinosa*. *Phytochemistry* 28, 2705–2709.
- Nozaki, H., Suzuki, H., Hirayama, T., Kasai, R., Wu, R.-Y., Lee, K.-H., 1986. Antitumour Triterpenes of *Maytenus Diversifolia*. *Phytochemistry* 25, 479–485.
- Núñez, M.J., Guadaño, A., Jiménez, I. a, Ravelo, A.G., González-Coloma, A., Bazzocchi, I.L., 2004. Insecticidal sesquiterpene pyridine alkaloids from

- Maytenus chiapensis*. Journal of Natural Products 67, 14–8.
- Nyunt, K., Elkhateeb, A., Tosa, Y., Nabata, K., Katakura, K., Matsuura, H., 2012. Isolation of antitrypanosomal compounds from *Vitis repens*, a medicinal plant of Myanmar. Natural Product Communications 7, 609–10.
- Ogbadoyi, E.O., Abdulganiy, A.O., Adama, T.Z., Okogun, J.I., 2007. *In vivo* trypanocidal activity of *Annona senegalensis* Pers. leaf extract against *Trypanosoma brucei brucei*. Journal of Ethnopharmacology 112, 85–89.
- Olarte, J.C., 1976. Contribution al estudio de la flora colombiana. In: Seminario Latinoamericano de La Quimica de Los Productos Naturales,. Bogotá, p. 126.
- Parisi, A., Piattelli, M., Tringali, C., Lio, G.M.D., 1993. Identification of the Phytotoxin Mellein in Culture Fluids of *Phoma-Tracheiphila*. Phytochemistry 32, 865–867.
- Park, S., Kim, D.S., Kang, S., 2011. *Gastrodia elata* Blume water extracts improve insulin resistance by decreasing body fat in diet-induced obese rats: Vanillin and 4-hydroxybenzaldehyde are the bioactive candidates. European Journal of Nutrition 50, 107–118.
- Pateh, U.U., K., H.A., Garba, M., Iliya, I., Sule, I.M., Abubakar, M.S. and A.A.A., 2009. Isolation of Stigmasterol , β -Sitosterol and 2- Hydroxyhexadecanoic Acid Methyl Ester From The Rhizomes of *Stylochiton lancifolius* Pyer and Kotchy. Nigerian Journal of Pharmaceutical Sciences 8, 19–25.
- Paterson-Jones, J.C., 1983. The Polyisoprene Content of some South African Plants. Biomass 3, 225–234.
- Patra, A., Chaudhuri, S.K., 1987. Assignment of carbon-13 nuclear magnetic resonance spectra of some friedelanes. Magnetic Resonance in Chemistry 25, 95–100.
- Pereira, A., Pereira, P., Cerdeira, R., Rodrigues, D., Moraes, F., Moraes, J., França, S., 1993. Pharmacologically active compounds in plant tissue culture of *Maytenus ilicifolia* (Celastraceae). ISHS Acta Horticulturae 333, 205.
- Piacente, S., Dos Santos, L.C., Mahmood, N., Pizza, C., 2006. Triterpenes from *Maytenus macrocarpa* and evaluation of their anti-HIV activity. Natural Product Communications 1, 1073–1078.
- Piacente, S., Tommasi, N., Pizza, C., 1999. Laevisines A and B: two new sesquiterpene-pyridine alkaloids from *Maytenus laevis*. Journal of Natural Products 62, 161–3.
- Plotkin, M.J., 1993. Tales of a Shaman's Apprentice: An Ethnobotanist Searches for New Medicines in the Amazon Rain Forest, illustrate. ed. Penguin Books.

- Prakash, R., Gopikrishna, V., Kandaswamy, D., 2005. Gutta-percha – an untold story. *Endodontology* 17, 32–36.
- Ramos, H.P., Simão, M.R., de Souza, J.M., Magalhães, L.G., Rodrigues, V., Ambrósio, S.R., Said, S., 2013. Evaluation of dihydroisocoumarins produced by the endophytic fungus *Arthrinium* state of *Apiospora montagnei* against *Schistosoma mansoni*. *Natural Product Research* 27, 2240–2243.
- Räz, B., Iten, M., Grether-Bühler, Y., Kaminsky, R., Brun, R., 1997. The Alamar Blue assay to determine drug sensitivity of African trypanosomes (*T.b. rhodesiense* and *T.b. gambiense*) *in vitro*. *Acta tropica* 68, 139–47.
- Reyes, B.M., Ramírez-Apan, M.T., Toscano, R. a, Delgado, G., 2010. Triterpenes from *Garcia parviflora*. Cytotoxic evaluation of natural and semisynthetic friedelanes. *Journal of Natural Products* 73, 1839–45.
- Reyes, C.P., Muñoz-Martínez, F., Torrecillas, I.R., Mendoza, C.R., Gamarro, F., Bazzocchi, I.L., Núñez, M.J., Pardo, L., Castanys, S., Campillo, M., Jiménez, I. a, 2007. Biological evaluation, structure-activity relationships, and three-dimensional quantitative structure-activity relationship studies of dihydro-beta-agarofuran sesquiterpenes as modulators of P-glycoprotein-dependent multidrug resistance. *Journal of Medicinal Chemistry* 50, 4808–17.
- Reyes, C.P., Núñez, M.J., Jiménez, I.A., Busserolles, J., Alcaraz, M.J., Bazzocchi, I.L., 2006. Activity of lupane triterpenoids from *Maytenus* species as inhibitors of nitric oxide and prostaglandin E2. *Bioorganic and Medicinal Chemistry* 14, 1573–1579.
- Reyes-Chilpa, R., Estrada-muñiz, E., Ramírez Apan, T., Amekraz, B., Aumelas, A., Jankowski, C.K., Vázquez-Torres, M., 2004. Cytotoxic effects of mammea type coumarins from *Calophyllum brasiliense*. *Life Sciences* 75, 1635–1647.
- Reyes-Chilpa, R., Estrada-Muñiz, E., Vega-Avila, E., Abe, F., Kinjo, J., Hernández-Ortega, S., 2008. Trypanocidal constituents in plants. 7. Mammea-type coumarins. *Memorias do Instituto Oswaldo Cruz* 103, 431–436.
- Rodrigues, F.A.R., Oliveira, A.C.A., Cavalcanti, B.C., Costa, M.P., Pessoa, C., Pinheiro, A.C., de Souza, M.V.N., 2014. Cytotoxic Evaluation of Substituted Benzaldehydes. *European Chemical Bulletin* 3, 555–558.
- Sadasivam, K., Kumaresan, R., 2011. Antioxidant behavior of mearnsetin and myricetin flavonoid compounds - A DFT study. *Spectrochimica Acta - Part A: Molecular and Biomolecular Spectroscopy* 79, 282–293.
- Sagwan, S., Rao, D. V, Sharma, R.A., 2011. *Maytenus Emarginata* (Willd.): A Promising Drug For Cancer Therapy. *Asian Journal of Pharmaceutical and Clinical Research* 4.

- Sakagami, H., Jiang, Y., Kusama, K., Atsumi, T., Ueha, T., Toguchi, M., Iwakura, I., Satoh, K., Ito, H., Hatano, T., Yoshida, T., 2000. Cytotoxic activity of hydrolyzable tannins against human oral tumor cell lines--a possible mechanism. *Phytomedicine: International Journal of Phytotherapy and Phytopharmacology* 7, 39–47.
- Sangsuwon, C., Jiratchariyakul, W., U-Pratya, Y., Kummalue, T., 2013. Antiproliferative effect and the isolated compounds of *Pouzolzia indica*. *Evidence-based Complementary and Alternative Medicine* 2013, 1–9.
- Santos, V.A.F.F.M., Regasini, L.O., Nogueira, C.R., Passerini, G.D., Martinez, I., Bolzani, V.S., Graminha, M.A.S., Cicarelli, R.M.B., Furlan, M., 2012. Antiprotozoal sesquiterpene pyridine alkaloids from *Maytenus ilicifolia*. *Journal of Natural Products* 75, 991–995.
- Sanz-Biset, J., Campos-de-la-Cruz, J., Epiquién-Rivera, M.A., Cañigueral, S., 2009. A first survey on the medicinal plants of the Chazuta valley (Peruvian Amazon). *Journal of Ethnopharmacology* 122, 333–362.
- Sarker, S.D., Latif, Z., Gray, A.I. (Eds.), 2006. *Natural Products Isolation*, second ed. ed. Humana Press Inc, Totowa, New Jersey.
- Schultes, R.E., Raffauf, R.F., 1992. *The Healing Forest*. Dioscorides Press, Portland, Oregon.
- Sekar, K.V.S., Sneden, A.T., Flores, F.A., 1995. Mayteine and 6-Benzoyl-6-deacetyl-mayteine from *Maytenus krukovii*. *Planta Medica* 61, 390.
- Sen, A., Dhavan, P., Shukla, K.K., Singh, S., Tejavathi, G., 2012. Analysis of IR , NMR and Antimicrobial Activity of β -Sitosterol Isolated from *Momordica charantia*. *Science Secure Journal of Biotechnology (SSJBt)* 1, 9–13.
- Setzer, W., Holland, M., Bozeman, C., Rozmus, G., Setzer, M., Moriarity, D., Reeb, S., Vogler, B., Bates, R., Haber, W., 2001. Isolation and frontier molecular orbital investigation of bioactive quinone-methide triterpenoids from the bark of *Salacia petenensis*. *Planta Medica* 67, 65–9.
- Shaiq Ali, M., Mahmud, S., Perveen, S., Rizwani, G.H., Ahmad, V.U., 1999. screening for the antimicrobial properties of the leaves of *Calophyllum inophyllum* Linn (Guttiferae).pdf. *Journal of the Chemical Society of Pakistan* 21, 174–178.
- Shi, G.F., An, L.J., Jiang, B., Guan, S., Bao, Y.M., 2006. Alpinia protocatechuic acid protects against oxidative damage *in vitro* and reduces oxidative stress *in vivo*. *Neuroscience Letters* 403, 206–210.
- Shirota, O., Morita, H., Takeya, K., Itokawa, H., 1994. Cytotoxic aromatic

- triterpenes from *Maytenus ilicifolia* and *Maytenus chuchuhuasca*. *Journal of Natural Products* 57, 1675–1681.
- Shirota, O., Morita, H., Takeya, K., Itokawa, H., 1995. Structures of Xuxuarines , Stereoisomeric Triterpene Dimers from *Maytenus chuchuhuasca*. *Tetrahedron* 51, 1107–1120.
- Shirota, O., Morita, H., Takeya, K., Itokawa, H., 1997a. Revised structures of cangorosins, triterpene dimers from *Maytenus ilicifolia*. *Journal of Natural Products* 60, 111–115.
- Shirota, O., Morita, H., Takeya, K., Itokawa, H., 1997b. Five New Triterpene Dimers from *Maytenus chuchuhuasca*. *Journal of Natural Products* 60, 1100–1104.
- Shirota, O., Morita, H., Takeya, K., Itokawa, H., 1998. New Geometric and Stereoisomeric Triterpene Dimers from *Maytenus chuchuhuasca*. *Chemical & Pharmaceutical Bulletin* 46, 102–106.
- Shirota, O., Otsuka, A., Morita, H., Takeya, K., Itokawa, H., 1994. Sesquiterpene Pyridine Alkaloids from *Maytenus chuchuhuasca*. *Heterocycles* 38, 2219–2229.
- Shirota, O., Sekita, S., Satake, M., Morita, H., Takeya, K., Itokawa, H., 2004a. Two New Sesquiterpene Pyridine Alkaloids from *Maytenus chuchuhuasca*. *Heterocycles* 63, 1891–1896.
- Shirota, O., Sekita, S., Satake, M., Morita, H., Takeya, K., Itokawa, H., 2004b. Nine Regioisomeric and Stereoisomeric Triterpene Dimers from *Maytenus chuchuhuasca*. *Chemical & Pharmaceutical Bulletin* 52, 739–746.
- Shirota, O., Sekita, S., Satake, M., Morita, H., Takeya, K., Itokawa, H., 2004c. Nine new isoxuxuarine-type triterpene dimers from *Maytenus chuchuhuasca*. *Chemistry and Biodiversity* 1, 1296–1307.
- Shirota, O., Sekita, S., Satake, M., Morita, H., Takeya, K., Itokawa, H., 2004d. Two Cangorosin A Type Triterpene Dimers from *Maytenus chuchuhuasca*. *Chemical & Pharmaceutical Bulletin* 52, 1148–1150.
- Shirota, O., Tamemura, T., Morita, H., Takeya, K., Itokawa, H., 1996. Triterpenes from Brazilian medicinal plant “chuchuhuasi” (*Maytenus krukovii*). *Journal of Natural Products* 59, 1072–1075.
- Shyamala, B.N., Madhava Naidu, M., Sulochanamma, G., Srinivas, P., 2007. Studies on the antioxidant activities of natural vanilla extract and its constituent compounds through *in vitro* models. *Journal of Agricultural and Food Chemistry* 55, 7738–7743.
- Silva, G.D. de F., Duarte, L.P., Paes, H.C. da S., Sousa, J.R. De, Nonato, M.C., Portezani, P.J., Mascarenhas, Y.P., 1998. 3-Epiabruslactone A , a New

- Triterpene Lactone Isolated from *Austroplenckia populnea*. Journal of the Brazilian Chemical Society 9, 461–464.
- Simmons, M.P., Clevinger, C.C., Savolainen, V., Archer, R.H., Mathews, S., Doyle, J.J., 2001. Phylogeny of The Celastraceae Inferred From Phytochrome B Gene Sequence and Morphology. American Journal of Botany 88, 313–325.
- Siqueira-Neto, J.L., Song, O.R., Oh, H., Sohn, J.H., Yang, G., Nam, J., Jang, J., Cechetto, J., Lee, C.B., Moon, S., Genovesio, A., Chatelain, E., Christophe, T., Freitas-Junior, L.H., 2010. Antileishmanial high-throughput drug screening reveals drug candidates with new scaffolds. PLoS Neglected Tropical Diseases 4, 1–8.
- Smith-Kielland, I., Dornish, J.M., Malterud, K.E., Hvistendahl, G., Rømming, C., Bøckmann, O.C., Kolsaker, P., Stenstrøm, Y., Nordal, A., 1996. Cytotoxic Triterpenoids from the Leaves of *Euphorbia pulcherrima*. Planta Medica 62, 322–325.
- Solecki, R., 1975. “Shanidar IV. A neanderthal flower burial of Northern Iraq.” Science 190, 880–881.
- Sommat, U., Rukachaisirikul, V., Sukpondma, Y., Phongpaichit, S., Sakayaroj, J., Kirtikara, K., 2008. Hydronaphthalenones and a dihydroramulosin from the endophytic fungus PSU-N24. Chemical and Pharmaceutical Bulletin (Tokyo) 56, 1687–1690.
- Somwong, P., Suttisri, R., Buakeaw, A., 2011. A new 1,3-diketofriedelane triterpene from *Salacia verrucosa*. Fitoterapia 82, 1047–51.
- Sosa, S., Morelli, C.F., Tubaro, A., Cairolì, P., Speranza, G., Manitto, P., 2007. Anti-inflammatory activity of *Maytenus senegalensis* root extracts and of maytenoic acid. Phytomedicine: International Journal of Phytotherapy and Phytomedicine 14, 109–14.
- Sousa, J.R. DE, Silva, G.D.F., Pedersoli, J.L., Alves, R.J., 1990. Friedelane and Oleanane Triterpenoids From Bark Wood of *Austroplenckia populnea*. Phytochemistry 29, 3259–3261.
- Souza-Formigoni, M.L.O., Oliveira, M.G.M., Goldnadel Monteiro, M., Gomes da Silveira-Filho, N., Braz, S., Carlini, E.A., 1991. Antiulcerogenic effects of two *Maytenus* species in laboratory animals. Journal of Ethnopharmacology 34, 21–27.
- Still, W.C., Kahn, M., Mitra, A., 1978. Rapid chromatographic technique for preparative separations with moderate resolution. The Journal of Organic Chemistry 43, 2923–2925.
- Su, K., Gong, M., Zhou, J., 2009. Study on Chemical Composition of *Nauclea*

officinalis Leaves. International Journal of Chemistry 1, 77–82.

- Syafni, N., Putra, D.P., Arbain, D., 2012. 3, 4-Dihydroxybenzoic Acid and 3,4-Dihydroxybenzaldehyde From The Fern *Trichomanes Chinense* L.; Isolation, Antimicrobial and Antioxidant Properties. Indonesian Journal of Chemistry 12, 273–278.
- Tait, F., 2011. CHUCHUGUASI- A Photochemical Investigation of a Sample of Colombian *Maytenus laevis*. Strathclyde University.
- Takaishi, Y., Tokura, K., Tamai, S., Ujita, K., Nakano, K., Tomimatsu, T., 1991. Sesquiterpene Polyol Esters from *Tripterygium wilfordii* VAR. *Regelii*. Phytochemistry 30, 1567–1572.
- Takaishi, Y., Wariishi, N., Tateishi, H., Kawazoe, K., Nakano, K., Ono, Y., Tokuda, H., Nishino, H., Iwashima, A., 1997. Triterpenoid inhibitors of interleukin-1 secretion and tumour-promotion from *Tripterygium wilfordii* Var. *Regelii*. Phytochemistry 45, 969–974.
- Tao, Y.H., Yuan, Z., Tang, X.Q., Xu, H.B., Yang, X.L., 2006. Inhibition of GABA shunt enzymes' activity by 4-hydroxybenzaldehyde derivatives. Bioorganic and Medicinal Chemistry Letters 16, 592–595.
- Tasdemir, D., Kaiser, M., Brun, R., Yardley, V., Schmidt, T.J., Tosun, F., Rüedi, P., 2006. Antitrypanosomal and antileishmanial activities of flavonoids and their analogues: *in vitro*, *in vivo*, structure-activity relationship, and quantitative structure-activity relationship studies. Antimicrobial Agents and Chemotherapy 50, 1352–1364.
- Tewari, N.C., Ayengar, K.N.N., Srinivasa Rangaswami., 1974. Triterpenes of the Root-bark of *Salacia prenoides* DC. Journal of the Chemical Society, Perkin Transactions 1, 146–152.
- Tewtrakul, S., Tansakul, P., Daengrot, C., Ponglimanont, C., Karalai, C., 2010. Anti-inflammatory principles from *Heritiera littoralis* bark. Phytomedicine 17, 851–855.
- Thao, N.T.P., Hung, T.M., Lee, M.K., Kim, J.C., Min, B.S., Bae, K., 2010. Triterpenoids from *Camellia japonica* and their cytotoxic activity. Chemical & Pharmaceutical Bulletin 58, 121–124.
- Thuy, T.T., Cuong, N.H., Sung, T. Van, 2007. Triterpenes from *Celastrus hindsii* Benth. Journal of Chemistry 45, 373–376.
- Tizkova, K., Smejkal, K., Cvacka, J., 2013. Natural Compounds Isolated from *Maytenus macrocarpa* (Ruiz & Pav.) Briq. (Celastraceae). Planta Medica 79, 16.

- Torpocco, V., Chávez, H., Estévez-Braun, A., Ravelo, A.G., 2007. New dammarane triterpenes from *Maytenus macrocarpa*. *Chemical & Pharmaceutical Bulletin* 55, 812–814.
- Tung, Y.-T., Wu, J.-H., Kuo, Y.-H., Chang, S.-T., 2007. Antioxidant activities of natural phenolic compounds from *Acacia confusa* bark. *Bioresource Technology* 98, 1120–3.
- Ulloa-Urizar, G., Aguilar-Luis, M.A., De Lama-Odría, M. del C., Camarena-Lizarzaburu, J., del Valle Mendoza, J., 2015. Antibacterial activity of five Peruvian medicinal plants against *Pseudomonas aeruginosa*. *Asian Pacific Journal of Tropical Biomedicine* 5, 928–931.
- Urones, J.G., De Pascual Teresa, J., Marcos, I.S., Martín, D.D., 1987. Ent-isolariciresinol in *Reseda suffruticosa*. *Phytochemistry* 26, 1540–1541.
- Verotta, L., Dell'Agli, M., Giolito, a, Guerrini, M., Cabalion, P., Bosisio, E., 2001. *In vitro* antiplasmodial activity of extracts of *Tristanopsis* species and identification of the active constituents: ellagic acid and 3,4,5-trimethoxyphenyl-(6'-O-galloyl)-O-beta-D-glucopyranoside. *Journal of Natural Products* 64, 603–607.
- Viswanathan, N. Iyer, 1979. Salaspermic Acid, a New Triterpene Acid from *Salacia macrosperma* Wight. *Journal of the Chemical Society, Perkin Transactions 1* 349–352.
- Waldi, D., 1965. Spray Reagents for Thin-Layer Chromatography. In: Stahl, E. (Ed.), *In Thin Layer Chromatography A Laboratory Handbook*. Springer Berlin Heidelberg, pp. 483–502.
- Wang, K., Sun, C., Wu, X., Pan, Y., 2006. Novel Bioactive Dammarane Caffeoyl Esters from *Celastrus rosthornianus*. *Planta Medica* 72, 370–372.
- Wang, Y., Chen, W.-S., Wu, Z.-J., Xi, Z.-X., Chen, W., Zhao, G.-J., Li, X., Sun, L.-N., 2011. Chemical constituents from *Salacia amplifolia*. *Biochemical Systematics and Ecology* 39, 205–208.
- Wang, Y., Zhou, Y., Zhou, H., Jia, G., Liu, J., Han, B., Cheng, Z., Jiang, H., Pan, S., Sun, B., 2012. Pristimerin Causes G1 Arrest, Induces Apoptosis, and Enhances the Chemosensitivity to Gemcitabine in Pancreatic Cancer Cells. *PLoS ONE* 7, 1–12.
- Wang, Z., Guhling, O., Yao, R., Li, F., Yeats, T.H., Rose, J.K.C., Jetter, R., 2011. Two Oxidosqualene Cyclases Responsible for Biosynthesis of Tomato Fruit Cuticular Triterpenoids. *Plant Physiology* 155, 540–552.
- Weeratunga, G., Bohlin, L., Verpoorte, R., Kumar, V., 1985. Flavonoids from *Elaeodendron balae* root bark. *Phytochemistry* 24, 2093–2095.

- WHO, 2002. WHO Traditional Medicine Strategy 2002-2005. Geneva.
- WHO, 2013. WHO Traditional Medicine Strategy 2014-2023. Geneva.
- Williams, D.H., Fleming, I., 2008. Spectroscopic Methods in Organic Chemistry.
- Wright, A.D., Konig, G.M., Angerhofer, C.K., Greenidges, P., Linden, A., Desqueyroux-faundez, R., 1996. Antimalarial Activity: The Search for Marine-Derived Natural Products with Selective Antimalarial Activity. *Journal of Natural Products* 59, 710–716.
- Wu, C.-C., Chan, M.-L., Chen, W.-Y., Tsai, C.-Y., Chang, F.-R., Wu, Y.-C., 2005. Pristimerin induces caspase-dependent apoptosis in MDA-MB-231 cells via direct effects on mitochondria. *Molecular Cancer Therapeutics* 4, 1277–1285.
- Xie, Y., Ding, Z., Duan, W., Ye, Q., 2012. Isolation and purification of terpenoids from *Celastrus aculeatus* Merr. by high-speed counter-current chromatography. *Journal of Medicinal Plants Research* 6, 2520–2525.
- <http://www.sunfood.com/blog/newsletters/sunfood-president-got-stoned/> retrived on 11/07/2016